

UC Berkeley

UC Berkeley Electronic Theses and Dissertations

Title

Explorations of Computational Approaches to Chemical Reactions

Permalink

<https://escholarship.org/uc/item/45j4r9qq>

Author

Bertels, Luke Wilbert

Publication Date

2020

Peer reviewed|Thesis/dissertation

Explorations of Computational Approaches to Chemical Reactions

by

Luke W. Bertels

A dissertation submitted in partial satisfaction of the

requirements for the degree of

Doctor of Philosophy

in

Chemistry

in the

Graduate Division

of the

University of California, Berkeley

Committee in charge:

Professor Martin P. Head-Gordon, Chair

Professor Teresa L. Head-Gordon

Professor Jeffrey B. Neaton

Summer 2020

Explorations of Computational Approaches to Chemical Reactions

Copyright 2020
by
Luke W. Bertels

Abstract

Explorations of Computational Approaches to Chemical Reactions

by

Luke W. Bertels

Doctor of Philosophy in Chemistry

University of California, Berkeley

Professor Martin P. Head-Gordon, Chair

This thesis is concerned with the application, development, and assessment of computational approaches to treat chemical reactions from an electronic structure theory perspective. In Chapter 2, the recently developed density functional, ω B97X-V, and coupled cluster with single, double and perturbative triple excitations [CCSD(T)] are applied to study the reaction networks of excited state silicon atoms with allene and methylacetylene in the circumstellar envelope of carbon stars. In Chapter 3, another recently developed density functional, ω B97M-V, and CCSD(T) are used to benchmark the performance of the ReaxFF reactive force field as applied to hydrogen combustion systems. In Chapter 4, an extension of third-order Møller-Plesset perturbation theory (MP3) and regularized perturbation theory (κ -OOMP2) is developed and used to calculate thermochemistry, barrier heights, and noncovalent interaction energies. In Chapter 5, the use of κ -OOMP2 optimized orbitals is extended to CCSD(T) and used to investigate the vibrational frequencies of diatomic molecules.

For Mom.

You were always there cheering, even when it was painful, and I heard you every time.

Contents

Contents	ii
List of Figures	iv
List of Tables	ix
1 Introduction	1
1.1 The Schrödinger Equation	1
1.2 Hartree-Fock Theory	3
1.3 Correlated Wavefunction Methods	11
1.4 Density Functional Theory	18
1.5 Outline	27
2 Modeling of Gas Phase Formation of c-SiC₃ Molecules in the Circumstellar Medium of Carbon Stars	30
2.1 Introduction	30
2.2 Methods	31
2.3 Results and discussion	32
2.4 Conclusions	40
3 Benchmarking the Performance of the ReaxFF Reactive Force Field on Hydrogen Combustion Systems	43
3.1 Introduction	43
3.2 Computational Methods	45
3.3 Results and discussion	48
3.4 Conclusions	61
4 Third-Order Møller-Plesset Perturbation Theory Made Useful? Choice of Orbitals and Scaling Greatly Improves Accuracy	65
4.1 Introduction	65
4.2 Theory	68
4.3 Results	68
4.4 Conclusion	74

5 Polishing the gold standard: The role of orbital choice in CCSD(T) frequency prediction	76
5.1 Introduction	76
5.2 Computational Methods	79
5.3 Experimental Data Selection	79
5.4 Results and Discussion	80
5.5 Vibrational frequencies	80
5.6 Conclusions	92
Bibliography	94
A Additional Information: Modeling of Gas Phase Formation of c-SiC₃ Molecules in the Circumstellar Medium of Carbon Stars	122
A.1 Branching Ratio Calculations	122
A.2 Tables	123
A.3 Figures	220
B Additional Information: Benchmarking the Performance of the ReaxFF Reactive Force Field on Hydrogen Combustion Systems	222
B.1 Reactive Pathways	223
B.2 Intrinsic Reaction Coordinate Scans	226
C Additional Information: Third-Order Møller-Plesset Perturbation Theory Made Useful? Choice of Orbitals and Scaling Greatly Improves Accuracy	232
C.1 W4-11	232
C.2 RSE43	253
C.3 BH76RC	256
C.4 HTBH38	258
C.5 NHTBH38	260
C.6 TA13	262
C.7 A24	264
D Additional Information: Polishing the gold standard: The role of orbital choice in CCSD(T) frequency prediction	266
D.1 Equilibrium bond lengths	266
D.2 Species not included in the test set	276
D.3 Mean-field $\langle S^2 \rangle$ values	276
D.4 CCSD data	283

List of Figures

1.1	Schematic representation of the self-consistent field (SCF) procedure used to solve the Hartree-Fock equations.	9
2.1	A and B present laboratory angular distributions for the reactions of Si(¹ D) (blue) and SiH(X ² Π) (green) with allene and methylacetylene, respectively. The red curves represent the overall fit, solid circles represent experimental data points with one σ error bars, and CM denotes the center of mass angle. C and D present TOF spectra at select angles for the allene and methylacetylene systems, respectively. Here the blue curves represent reactions with Si(¹ D), the green curves reactions with SiH(X ² Π), the red curves the overall fit, and the open circles experimental data points. Atom colors: silicon (green), carbon (black), and hydrogen (light grey). Taken with permission from Ref. 93.	34
2.2	TOF spectra at m/z 68 (HD loss, SiC ₃ D ₂ ⁺ , blue) and 67 (D ₂ loss, SiC ₃ HD, red) taken at the respective CM angles for the reaction of Si(¹ D) with D3-methylacetylene. Taken with permission from Ref. 93.	34
2.3	CM translational energy distributions (A and B) and CM angular distributions (C and D) for the reactions of Si(¹ D) with allene (A and C) and methylacetylene (B and D) to yield SiC ₃ H ₂ species via molecular hydrogen elimination. The shaded areas denote acceptable fits for one σ errors in the laboratory data. Taken with permission from Ref. 93.	36
2.4	Simplified potential energy surface for the reactions of excited state silicon with methylacetylene and allene. Energies relative to separated reactants are given in units of kJ mol ⁻¹ . Pathways with barriers above the 30 kJ mol ⁻¹ collision energy are excluded. Atom colors: silicon (green), carbon (black), and hydrogen (light grey). Taken from Ref. 93.	37
2.5	Potential energy surface for the isomerization of low-energy SiC ₃ H ₂ isomers and dehydrogenation to yield SiC ₃ . Energies relative to the lowest energy SiC ₃ H ₂ isomer p1 are given in units of kJ mol ⁻¹ . The total internal energy on this scale for products of reaction I is 220 kJ mol ⁻¹ . Atom colors: silicon (green), carbon (black), and hydrogen (light grey). Taken from Ref. 93.	39

2.6	Modeled present-day fractional abundances relative to molecular hydrogen are plotted versus the radius of the circumstellar envelope of the carbon star IRC+10216. Species color: silicon tricarbonide (SiC_3)(blue), silicon tetracarbonide (SiC_4)(red), allene (H_2CCCH_2)(magenta), methylacetylene (CH_3CCH)(cyan), SiC_3H_2 (green). Taken from Ref. 93.	41
3.1	Time series of the kinetic temperature for a hydrogen-oxygen mixture that is initially stoichiometric at a temperature of 1250 K and pressure of 50 bar. . . .	47
3.2	Potential energy along the first $\text{H}_2 + \text{OH} \longrightarrow \text{H}_2\text{O} + \text{H}$ reactive pathway, extracted from a larger MD simulation. The parent simulation was run using ReaxFF with the HO2011 parameter set. The energies presented are relative to the energies of isolated H_2 and OH computed at the ReaxFF/HO2011 optimized geometries. The total time to complete this reaction path is 30 fs with a time step of 0.1 fs. . . .	51
3.3	Potential energy, atom energy, and the sum of all other energy contributions, in kcal mol^{-1} , for the first $\text{H}_2 + \text{OH} \longrightarrow \text{H}_2\text{O} + \text{H}$ reactive pathway, extracted from a larger MD simulation, are presented for the four ReaxFF parameter sets studied. The atom energy is the sum of the overcoordination and undercoordination energy contributions. The total time to complete this reaction path is 30 fs with a time step of 0.1 fs.	52
3.4	Potential energies along the $\text{H}_2 + \text{OH} \longrightarrow \text{H}_2\text{O} + \text{H}$ intrinsic reaction coordinate are presented for four ReaxFF parameter sets, $\omega\text{B97M-V}$, and CCSD(T) . Geometries along the reaction coordinate were calculated at the $\omega\text{B97M-V/cc-pVTZ}$ level of theory. The energies presented are relative to the energies of isolated H_2 and OH computed at the $\omega\text{B97M-V/cc-pVTZ}$ optimized geometries.	59
3.5	Potential energies along the $\text{H}_2\text{O}_2 + \text{OH} \longrightarrow \text{H}_2\text{O} + \text{HO}_2$ intrinsic reaction coordinate are presented for four ReaxFF parameter sets, $\omega\text{B97M-V}$, and CCSD(T) . Geometries along the reaction coordinate were calculated at the $\omega\text{B97M-V/cc-pVTZ}$ level of theory. The energies presented are relative to the energies of isolated H_2O_2 and OH computed at the $\omega\text{B97M-V/cc-pVTZ}$ optimized geometries.	59
3.6	Unrelaxed potential energy surfaces for the $\text{H}_2 + \text{OH} \longrightarrow \text{H}_2\text{O} + \text{H}$ reaction, in kcal mol^{-1} , are presented for $\omega\text{B97M-V}$ and four ReaxFF parameter sets. Here the $\text{HO}\cdots\text{H}\cdots\text{H}$ angle is linearized while all other geometric parameters are held fixed in the transition state configuration as optimized at the $\omega\text{B97M-V/cc-pVTZ}$ level of theory. The interatomic distances for points along the intrinsic reaction coordinate calculated at the $\omega\text{B97M-V/cc-pVTZ}$ level of theory are overlaid on each surface. The energies presented are relative to the energies of the isolated atoms.	60

- 3.7 Unrelaxed potential energy surfaces for the $\text{H}_2\text{O}_2 + \text{OH} \longrightarrow \text{H}_2\text{O} + \text{HO}_2$ reaction, in kcal mol^{-1} , are presented for $\omega\text{B97M-V}$ and four ReaxFF parameter sets. Here the $\text{HOO}\cdots\text{H}\cdots\text{OH}$ angle is linearized while all other geometric parameters are held fixed in the transition state configuration as optimized at the $\omega\text{B97M-V/cc-pVTZ}$ level of theory. The interatomic distances for points along the intrinsic reaction coordinate calculated at the $\omega\text{B97M-V/cc-pVTZ}$ level of theory are overlaid on each surface. The energies presented are relative to the energies of the isolated atoms. 62
- 4.1 Scans of the root mean square deviation on the non-MR subset of the W4-11 thermochemistry data set, in kcal mol^{-1} , for the scaled, two regularization parameter correlation energy functional given in Equation 4.5. We fix $\kappa = 1.45E_h^{-1}$. All calculations use the aVTZ basis; CCSD(T) is used for the reference values. 69
- 4.2 Scans of the root mean square deviation on the non-MR subset of the W4-11 thermochemical data set, in kcal mol^{-1} , for the regularized, second- and third-order correlation energy functional given in Equation 4.6. The optimal value of c_2 was found to be 1.0 for all κ_2 values plotted. SCF references were generated via κ -OOMP2 orbital optimization. The basis set used was aVTZ. Reference values are calculated at the CCSD(T)/aVTZ level of theory. 70
- 5.1 Box plots (overall, left, and enhanced, right) of the errors in corrected vibrational frequencies (in cm^{-1}) are presented. Red lines mark the median errors, boxes bound the central 50% of the data, whiskers enclose all data points within 1.5 times the inter-quartile range of the box edges, and points denote outlying data. 81
- 5.2 Box plots (overall, left, and enhanced, right) of the errors in corrected vibrational frequencies (in cm^{-1}) are presented for the pruned subset of species. Red lines mark the median errors, boxes bound the central 50% of the data, whiskers enclose all data points within 1.5 times the inter-quartile range of the box edges, and points denote outlying data. 91
- A.1 Complete potential energy surfaces involved in the reactions of electronically excited silicon atoms ($\text{Si}({}^1\text{D})$) with allene and methylacetylene. Relative energies are given in units of kJ mol^{-1} . Colors of the atoms: silicon (green), carbon (black) and hydrogen (light grey). Taken with permission from Ref. 93. 221
- A.2 Pathways exploited in the RRKM calculations to determine the branching ratios in the reactions of electronically excited silicon atoms ($\text{Si}({}^1\text{D})$) with methylacetylene, allene, and D3-methylacetylene. Relative energies are given in units of kJ mol^{-1} . Colors of the atoms: silicon (green), carbon (black) and hydrogen (light grey). Taken with permission from Ref. 93. 221

B.1	Potential energies, in kcal mol ⁻¹ , along the O + H ₂ + O ₂ → OH + HO ₂ reactive trajectory, extracted from a larger MD simulation. The parent simulation was run using ReaxFF with the HO2011 parameter set. The energies presented are relative to isolated O, H ₂ , and O ₂ at the ReaxFF/HO2011 optimized geometries.	223
B.2	Potential energies, in kcal mol ⁻¹ , along the O ₂ + H ₂ + HO ₂ → HO ₂ + H ₂ O ₂ reactive trajectory, extracted from a larger MD simulation. The parent simulation was run using ReaxFF with the HO2011 parameter set. The energies presented are relative to isolated O ₂ , H ₂ , and HO ₂ at the ReaxFF/HO2011 optimized geometries.	223
B.3	Potential energies, in kcal mol ⁻¹ , along the H ₂ + O ₂ → HO ₂ + H reactive trajectory, extracted from a larger MD simulation. The parent simulation was run using ReaxFF with the HO2011 parameter set. The energies presented are relative to isolated H ₂ and O ₂ at the ReaxFF/HO2011 optimized geometries.	224
B.4	Potential energies, in kcal mol ⁻¹ , along the H + O ₂ → HO ₂ reactive trajectory, extracted from a larger MD simulation. The parent simulation was run using ReaxFF with the HO2011 parameter set. The energies presented are relative to isolated H and O ₂ at the ReaxFF/HO2011 optimized geometries.	224
B.5	Potential energies, in kcal mol ⁻¹ , along the HO ₂ + H → 2 OH reactive trajectory, extracted from a larger MD simulation. The parent simulation was run using ReaxFF with the HO2011 parameter set. The energies presented are relative to isolated HO ₂ and H at the ReaxFF/HO2011 optimized geometries.	225
B.6	Potential energies, in kcal mol ⁻¹ , along the H ₂ + OH → H ₂ O + H reactive trajectory, extracted from a larger MD simulation. The parent simulation was run using ReaxFF with the HO2011 parameter set. The energies presented are relative to isolated H ₂ and OH at the ReaxFF/HO2011 optimized geometries.	225
B.7	Potential energies, in kcal mol ⁻¹ , along the H ₂ + OH → H ₂ O + H reactive trajectory, extracted from a larger MD simulation. The parent simulation was run using ReaxFF with the HO2011 parameter set. The energies presented are relative to isolated H ₂ and OH at the ReaxFF/HO2011 optimized geometries.	226
B.8	Potential energies, in kcal mol ⁻¹ , along the H + O ₂ → OH + O intrinsic reaction coordinate. The intrinsic reaction coordinate was calculated at the ωB97M-V/cc-pVTZ level of theory. The energies presented are relative to the energies of isolated H and O ₂ computed at the ωB97M-V/cc-pVTZ optimized geometries.	226
B.9	Potential energies, in kcal mol ⁻¹ , along the H ₂ + OH → H ₂ O + H intrinsic reaction coordinate. The intrinsic reaction coordinate was calculated at the ωB97M-V/cc-pVTZ level of theory. The energies presented are relative to the energies of isolated H ₂ and OH computed at the ωB97M-V/cc-pVTZ optimized geometries.	227
B.10	Potential energies, in kcal mol ⁻¹ , along the H ₂ O + O → 2 OH intrinsic reaction coordinate. The intrinsic reaction coordinate was calculated at the ωB97M-V/cc-pVTZ level of theory. The energies presented are relative to the energies of isolated H ₂ O and O computed at the ωB97M-V/cc-pVTZ optimized geometries.	227

- B.11 Potential energies, in kcal mol⁻¹, along the $\text{H} + \text{O}_2 \longrightarrow \text{HO}_2$ intrinsic reaction coordinate. The intrinsic reaction coordinate was calculated at the $\omega\text{B97M-V/cc-pVTZ}$ level of theory. The energies presented are relative to the energies of isolated H and O₂ computed at the $\omega\text{B97M-V/cc-pVTZ}$ optimized geometries. 228
- B.12 Potential energies, in kcal mol⁻¹, along the $\text{HO}_2 + \text{H} \longrightarrow \text{H}_2 + \text{O}_2$ intrinsic reaction coordinate. The intrinsic reaction coordinate was calculated at the $\omega\text{B97M-V/cc-pVTZ}$ level of theory. The energies presented are relative to the energies of isolated HO₂ and H computed at the $\omega\text{B97M-V/cc-pVTZ}$ optimized geometries. 228
- B.13 Potential energies, in kcal mol⁻¹, along the $\text{HO}_2 + \text{H} \longrightarrow 2\text{OH}$ intrinsic reaction coordinate. The intrinsic reaction coordinate was calculated at the $\omega\text{B97M-V/cc-pVTZ}$ level of theory. The energies presented are relative to the energies of isolated HO₂ and H computed at the $\omega\text{B97M-V/cc-pVTZ}$ optimized geometries. 229
- B.14 Potential energies, in kcal mol⁻¹, along the $2\text{HO}_2 \longrightarrow \text{H}_2\text{O}_2 + \text{O}_2$ intrinsic reaction coordinate. The intrinsic reaction coordinate was calculated at the $\omega\text{B97M-V/cc-pVTZ}$ level of theory. The energies presented are relative to the energies of two isolated HO₂ computed at the $\omega\text{B97M-V/cc-pVTZ}$ optimized geometries. 229
- B.15 Potential energies, in kcal mol⁻¹, along the $\text{H}_2\text{O}_2 + \text{H} \longrightarrow \text{H}_2\text{O} + \text{OH}$ intrinsic reaction coordinate. The intrinsic reaction coordinate was calculated at the $\omega\text{B97M-V/cc-pVTZ}$ level of theory. The energies presented are relative to the energies of isolated H₂O₂ and H computed at the $\omega\text{B97M-V/cc-pVTZ}$ optimized geometries. 230
- B.16 Potential energies, in kcal mol⁻¹, along the $\text{H}_2\text{O}_2 + \text{H} \longrightarrow \text{H}_2 + \text{HO}_2$ intrinsic reaction coordinate. The intrinsic reaction coordinate was calculated at the $\omega\text{B97M-V/cc-pVTZ}$ level of theory. The energies presented are relative to the energies of isolated H₂O₂ and H computed at the $\omega\text{B97M-V/cc-pVTZ}$ optimized geometries. 230
- B.17 Potential energies, in kcal mol⁻¹, along the $\text{H}_2\text{O}_2 + \text{O} \longrightarrow \text{HO}_2 + \text{OH}$ intrinsic reaction coordinate. The intrinsic reaction coordinate was calculated at the $\omega\text{B97M-V/cc-pVTZ}$ level of theory. The energies presented are relative to the energies of isolated H₂O₂ and O computed at the $\omega\text{B97M-V/cc-pVTZ}$ optimized geometries. 231
- B.18 Potential energies, in kcal mol⁻¹, along the $\text{H}_2\text{O}_2 + \text{OH} \longrightarrow \text{H}_2\text{O} + \text{HO}_2$ intrinsic reaction coordinate. The intrinsic reaction coordinate was calculated at the $\omega\text{B97M-V/cc-pVTZ}$ level of theory. The energies presented are relative to the energies of isolated H₂O₂ and OH computed at the $\omega\text{B97M-V/cc-pVTZ}$ optimized geometries. 231

List of Tables

3.1	Root mean square deviation, mean signed deviation, maximum absolute deviation, and non-parallelity error, in kcal mol ⁻¹ , are presented for a selection of reactive pathways extracted from larger MD simulations. CCSD(T)/CBS values were used as reference.	49
3.1	(continued)	50
3.2	Root mean square deviation, mean signed deviation, maximum absolute deviation, and non-parallelity error, in kcal/mol, are presented for a selection of intrinsic reaction coordinate scans of elementary reactions relevant to hydrogen combustion. Geometries along the reaction coordinate were calculated at the ω B97M-V/cc-pVTZ level of theory. CCSD(T)/CBS values were used as reference.	53
3.2	(continued)	54
3.2	(continued)	55
3.3	Reaction energy errors, forward reaction barrier height errors, and reverse reaction barrier height errors, in kcal mol ⁻¹ , are presented for a selection of intrinsic reaction coordinate scans of elementary reactions relevant to hydrogen combustion. Geometries along the reaction coordinate were calculated at the ω B97M-V/cc-pVTZ level of theory. CCSD(T)/CBS values were used as a reference and the reaction energies, forward reaction barriers, and reverse reaction barriers are reported, in kcal mol ⁻¹ . Infinitely separated reactants and products optimized at the ω B97M-V/cc-pVTZ level of theory are taken as the endpoints of the reaction paths.	56
3.3	(continued)	57
3.3	(continued)	58
4.1	Root mean square deviation, mean signed deviation, minimum deviation, and maximum deviation, in kcal mol ⁻¹ for the non-MR subset of the W4-11 set. All calculations use the aVTZ basis; CCSD(T) is used for the reference values. . . .	71
4.2	Root mean square deviation, mean signed deviation, minimum deviation, and maximum deviation, in kcal mol ⁻¹ , for the BH76RC set.	71
4.3	Root mean square deviation, mean signed deviation, minimum deviation, and maximum deviation, in kcal mol ⁻¹ , for the RSE43 set.	72

4.4	Root mean square deviation, mean signed deviation, minimum deviation, and maximum deviation, in kcal mol ⁻¹ , for the HTBH38 set.	72
4.5	Root mean square deviation, mean signed deviation, minimum deviation, and maximum deviation, in kcal mol ⁻¹ , for the NHTBH38 set.	73
4.6	Root mean square deviation, mean signed deviation, minimum deviation, and maximum deviation, in kcal mol ⁻¹ , for the TA13 set.	74
4.7	Root mean square deviation, mean signed deviation, minimum deviation, and maximum deviation, in kcal mol ⁻¹ , for the A24 set.	74
5.1	Root mean square deviations, mean signed deviations, most negative deviations, and most positive deviations (all in cm ⁻¹) for the predicted corrected vibrational frequencies of all species are summarized for the CCSD(T) methods utilizing different molecular orbital references.	81
5.2	Experimental vibrational frequencies (in cm ⁻¹) and errors (in cm ⁻¹) in the corrected vibrational frequencies for the 36 closed-shell species are presented in for the CCSD(T) methods utilizing different molecular orbitals. Root mean square deviations, mean signed deviations, most negative deviations, and most positive deviations (all in cm ⁻¹) for the set of species and subsets are also presented.	82
5.3	Experimental vibrational frequencies (in cm ⁻¹) and errors (in cm ⁻¹) in the corrected vibrational frequencies for the 59 open-shell species are presented in for the CCSD(T) methods utilizing different molecular orbitals. Root mean square deviations, mean signed deviations, most negative deviations, and most positive deviations (all in cm ⁻¹) for the set of species and subsets are presented.	85
5.4	Experimental vibrational frequencies (in cm ⁻¹), mean errors for the non-HF CCSD(T) methods (in cm ⁻¹), ranges of the errors for the non-HF CCSD(T) methods (in cm ⁻¹), and alternative experimental reported frequencies (in cm ⁻¹) are presented for species where the experimental results are in question.	88
5.5	Root mean square deviations, mean signed deviations, most negative deviations, and most positive deviations (all in cm ⁻¹) for the cropped subset of species are summarized for the CCSD(T) methods utilizing different molecular orbitals.	91
A.1	Reactants, products, intermediates, and transition state structures relevant to the reaction of electronically excited atomic silicon with methylacetylene and allene. Geometries were calculated at the ω B97X-V//cc-pVTZ level of theory; relative energies were calculated at the CCSD(T)//CBS level of theory.	124
A.2	Reactants, products, intermediates, and transition state structures relevant to the reaction of electronically excited atomic silicon with D3-methylacetylene. Geometries were calculated at the ω B97X-V//cc-pVTZ level of theory; relative energies were calculated at the CCSD(T)//CBS level of theory.	140
A.3	Exit transition state structures for the emission of H ₂ /HD/D ₂ , principle moments of inertia (AMU a_0^2), and angles of emission relative to the principal axes.	188

A.4	Products relevant to the reaction of electronically excited atomic silicon with methylacetylene and allene to form atomic hydrogen and SiC_3H_3 . Geometries were calculated at the $\omega\text{B97X-V//cc-pVTZ}$ level of theory; relative energies were calculated at the CCSD(T)//CBS level of theory.	195
A.5	Products relevant to the reaction of electronically excited atomic silicon with methylacetylene and allene to form methyl radical and SiC_2H . Geometries were calculated at the $\omega\text{B97X-V//cc-pVTZ}$ level of theory; relative energies were calculated at the CCSD(T)//CBS level of theory.	201
A.6	Reactants, products, and transition state structures relevant to the singlet SiC_2H_2 system. Geometries were calculated at the $\omega\text{B97X-V//cc-pVTZ}$ level of theory; relative energies were calculated at the CCSD(T)//CBS level of theory.	203
A.7	Excited states of six SiC_3H_2 isomers p1-p6 with excitation energies in the region of a Lyman- α photon.	208
A.8	Products relevant to the photodissociation of SiC_3H_2 to form atomic hydrogen and SiC_3H . Geometries were calculated at the $\omega\text{B97X-V//cc-pVTZ}$ level of theory; relative energies were calculated at the CCSD(T)//CBS level of theory.	215
A.9	Tunneling-corrected RRKM reaction rate constants, transition state imaginary frequencies, and reaction path degeneracies for the silicon–methylacetylene, silicon–allene, and silicon–D3-methylacetylene systems.	216
A.9	continued	217
A.9	continued	218
A.9	continued	219
A.9	continued	220
C.1	CCSD(T)/aVTZ energies (in kcal/mol) for the non-MR subset of the W4-11 set and errors for other methods	233
C.1	(continued)	234
C.1	(continued)	235
C.1	(continued)	236
C.1	(continued)	237
C.1	(continued)	238
C.1	(continued)	239
C.1	(continued)	240
C.1	(continued)	241
C.1	(continued)	242
C.1	(continued)	243
C.1	(continued)	244
C.1	(continued)	245
C.1	(continued)	246
C.1	(continued)	247
C.1	(continued)	248
C.1	(continued)	249

C.1 (continued)	250
C.1 (continued)	251
C.1 (continued)	252
C.2 CCSD(T)/aVTZ energies (in kcal/mol)for the RSE43 set and errors for other methods.	254
C.2 (continued)	255
C.3 CCSD(T)/aVTZ energies (in kcal/mol)for the BH76RC set and errors for other methods.	257
C.4 CCSD(T)/aVTZ barrier heights (in kcal/mol)for the HTHB38 set and errors for other methods.	259
C.5 CCSD(T)/aVTZ barrier heights (in kcal/mol)for the NHTHB38 set and errors for other methods.	261
C.6 CCSD(T)/aVTZ interaction energies (in kcal/mol)for the TA13 set and errors for other methods.	263
C.7 CCSD(T)/aVTZ interaction energies (in kcal/mol)for the TA13 set and errors for other methods.	265
D.1 Root mean square deviations, mean signed deviations, most negative deviation, and most positive deviations in the equilibrium bond lengths for all species are presented for the CCSD(T) methods utilizing different molecular orbital references.	266
D.2 Experimental equilibrium bond lengths (in Å) and errors in the computed bond lengths (in Å) for the closed-shell species are presented for the CCSD(T) methods utilizing different molecular orbitals. Root mean square deviations, mean signed deviations, most negative deviations, and most positive deviations (all in Å) for the set of species and subsets are presented. Experimental values were compiled by Huber and Herzberg[346].	267
D.3 Experimental equilibrium bond lengths (in Å) and errors in the computed bond lengths (in Å) for the open-shell species are presented for the CCSD(T) methods utilizing different molecular orbitals. Root mean square deviations, mean signed deviations, most negative deviations, and most positive deviations (all in Å) for the set of species and subsets are presented. Experimental values were compiled by Huber and Herzberg[346].	269
D.4 Root mean square deviations, mean signed deviations, most negative deviation, and most positive deviations in the equilibrium bond lengths for all species are presented for the CCSD methods utilizing different molecular orbital references.	271
D.5 Experimental equilibrium bond lengths (in Å) and errors in the computed bond lengths (in Å) for the closed-shell species are presented for the CCSD methods utilizing different molecular orbitals. Root mean square deviations, mean signed deviations, most negative deviations, and most positive deviations (all in Å) for the set of species and subsets are presented. Experimental values were compiled by Huber and Herzberg[346].	272

D.6	Experimental equilibrium bond lengths (in Å) and errors in the computed bond lengths (in Å) for the open-shell species are presented for the CCSD methods utilizing different molecular orbitals. Root mean square deviations, mean signed deviations, most negative deviations, and most positive deviations (all in Å) for the set of species and subsets are presented. Experimental values were compiled by Huber and Herzberg[346].	274
D.7	Species and experimental vibrational frequencies (in cm^{-1}) for which we were unable to compute a continuous PES with one or more of the methods surveyed. Experimental values were compiled by Huber and Herzberg[346].	276
D.8	Mean-field $\langle S^2 \rangle$ values for the reference methods at the CCSD(T) minimum energy points used in the fitting procedure.	277
D.9	Mean-field $\langle S^2 \rangle$ values for the reference methods at the CCSD minimum energy points used in the fitting procedure.	280
D.10	Experimental vibrational frequencies and errors in the corrected vibrational frequencies for the closed-shell species are presented in for the CCSD methods utilizing different molecular orbitals. Root mean square deviations, mean signed deviations, minimum deviations, and maximum deviations for the set of species and subsets are also presented.	284
D.11	Experimental vibrational frequencies and errors in the corrected vibrational frequencies for the open-shell species are presented in for the CCSD methods utilizing different molecular orbitals. Root mean square deviations, mean signed deviations, minimum deviations, and maximum deviations for the set of species and subsets are presented.	286

Acknowledgments

First and foremost I would like to thank Prof. Martin Head-Gordon for all he has done for me over the last six years. His welcoming nature pushed me over the edge when deciding to come to Berkeley for my graduate studies. He is incredibly knowledgeable and better yet can easily convey it to his students. Martin has always been available to give feedback and has been patient and understanding when the research has hit snags. I consider myself blessed to have had him as an advisor.

Secondly I'd like to thank all of the other professors that have helped me along my way. At the University of Chicago: Prof. Jack Cowan, whose phone call placed me in my undergraduate research group; Prof. David Mazziotti, my undergraduate research advisor who introduced me to the field of electronic structure theory and still lights up when we meet at conferences; and Prof. Laurie Butler, who despite having to wake me up in lecture was incredibly encouraging. At Berkeley, Prof. Teresa Head-Gordon has been both a supportive qualifying exam chair and enthusiastic collaborator who is quick to complement my contributions to our meetings. Prof. Ralf Kaiser, Prof. Igor Mezić, and Prof. Jason Green have all been enthusiastic collaborators who have helped connect my science to broader applications.

I'd like to acknowledge the National Science foundation for partially funding my graduated study through the NSF Graduate Research Fellowship Program DGE-1106400.

Next I'd to thank past and current members of the Head-Gordon group that I've had the pleasure of calling coworkers, collaborators, teammates, and friends. Beginning with the crew that ushered me in I'd especially like to thank David Stück for his Magic: the Gathering sales pitch during recruitment, Narbe Mardirossian for putting out a million small fires for me when I was starting up, keeping me company when I would work late, and introducing me to Cheese 'n Stuff, Julian Azar for always keeping things interesting, Paul Horn for passing the Cafe Strada mocha legacy down to me, Yuezhi Mao for his selflessness when helping other students, and Alec White for keeping the daily coffee trips on schedule. I thank Joonho Lee for being a font of knowledge of relevant literature, an crack programmer, and a truly loyal friend to me. Two of the chapters of this thesis build from his impressive additions to the field of electronic structure theory. I thank Srimukh Prasad for being a truly wonderful office mate, late night company, and lively target for pranks and other nonsense. I thank Matthias Loipersberger for being the most outgoing and least "German" German I've ever met and for his attempts to inspire me with motivational speeches from bodybuilders. To the newer members of the group thanks for indulging my sense of group traditions and my questionable sense of humor. I thank Abdul Aldossary for taking up my comedic mantle for the group and Elliot Rossomme for being a genuinely interesting person to discuss non-science topics with over lunch.

Will and Michael, you were better roommates that I deserved. Thanks for the Chinese buffet trips, odd caricatures, and game nights I showed up an hour late to. I also thank Alice Kunin, Julia Lazzari-Dean, and Kristen Wucherer who took care of me when the whole world seemed like threes and fours.

I thank Robinson Flaig, who after forging our friendship hiding together in a closet has never let me forget that he loves me and that I'm the family he's chosen. I hope despite my sarcasm you know that I love you too and just how important you are to me. I also thank Erin Sullivan, who has always been quick with a jab when I've gotten a bit too full of myself and ready to lift me up with kind words and a hot home cooked meal whenever I needed a pick-me-up. The two of you have been amazing friends to me throughout grad school. Berkeley would have been a much lonelier place without you in my life and I'm so excited to officiate your wedding next year. I'd like to thank Peter Waller and Mary Garner for opening up your lives to me, sharing Peter's wit and Mary's sneaky humor, and letting me officiate your wedding. I thank Mary for being my staunchest defender when I needed one the most and Peter for his constant dismay at how I manage my finances.

I thank the members of Bethlehem Lutheran Church, particularly Pastor Temesgen Dabsu, Siglinde Mitchell, and Gloria King, for helping me to grow in my faith and keep each week in perspective.

I thank my brothers, Zach, Josh, and Sam, for a lifetime of fun and an unbeatable reprieve from research when all together at home. I thank Zach for not overtaking me in his incredibly successful pursuit of a Ph. D., Josh for being the butt of jokes, and Sam for giving me the moniker "(Almost) Dr. Father Brother" after my becoming ordained.

I thank my father, Paul, for giving me updates about Dorsey that made it seem like I wasn't so far from home and for dispensing fatherly wisdom and common sense when called for. I thank my stepfather, Scott, who though our conversations were frequently handoffs to my mother was never shy about letting me know how proud he was of me.

Finally and most importantly I'd like to thank my mother, Sue, who has been my support system throughout graduate school. Thank you for talking me down from all the high-anxiety calls that twisted your stomach as much as mine. Even when things were their toughest you were always cheering me forward. I don't know if I could have done it without you and I'm so grateful for all that you do, even if I sometimes have a difficult time showing it.

Chapter 1

Introduction

Electronic structure theory is a subfield of chemistry (though at times its practice can resemble physics, computer science, and/or mathematics) that is concerned with modeling the motions of electrons and nuclei in molecules on the quantum scale and how these translate into observable chemical phenomena: reactivity, spectra, physical properties, etc. Though as theoretical chemists we are in possession of the exact laws that govern all chemical phenomena, however application of these laws to nontrivial systems requires the use of approximations. As chemistry occurs over broad domains in both space and time, one would desire a set of approximate methods that exist on a sliding scale from highly efficient treatment of large systems to highly accurate treatment of small model systems. In contrast to empirical science, which attempts to divine the physical laws through carefully planned observations, theoretical science begins from these laws to both elucidate observations and make predictions to be evaluated. In this sense, theorists and experimentalists complement each other: theoretical models give explanation to the observations of experiments while experiments demonstrate the reality (or lack thereof) of chemical model predictions.

In this thesis, we elucidate the reactivity of a chemical system using existing models to explain experimental observations, evaluate the performance of approximate models relative to more exact methods, and develop new modifications to existing models that improve upon their accuracy without altering the overall cost.

1.1 The Schrödinger Equation

In 1926 the physicist Erwin Schrödinger proposed an equation to describe the dynamics of a system of quantum particles:

$$i\hbar \frac{\partial}{\partial t} |\Psi\rangle = \hat{H} |\Psi\rangle, \quad (1.1)$$

where \hat{H} is the Hamiltonian operator and $|\Psi\rangle$ is the wavefunction representing the system. The time-independent form of this equation,

$$\hat{H} |\Psi_k\rangle = E_k |\Psi_k\rangle \quad (1.2)$$

is an eigenvalue equation where the wavefunction $|\Psi_k\rangle$ is an eigenfunction of \hat{H} with a corresponding energy eigenvalue E_k . While \hat{H} is related to the Hamiltonian in classical mechanics, in quantum mechanics the particles are described by a wavefunction that belongs to a multidimensional Hilbert space rather than points in phase space. For a system of n electrons and M nuclei, the molecular Hamiltonian, in atomic units (assumed throughout), is

$$\begin{aligned} \hat{H} = & \left(-\sum_A^M \frac{1}{2m_A} \hat{\nabla}_A^2 \right) + \left(-\sum_i^n \frac{1}{2} \hat{\nabla}_i^2 \right) + \left(\sum_A^M \sum_{B>A}^M \frac{Z_A Z_B}{|\hat{\mathbf{R}}_A - \hat{\mathbf{R}}_B|} \right) + \\ & \left(-\sum_i^n \sum_A^M \frac{Z_A}{|\hat{\mathbf{r}}_i - \hat{\mathbf{R}}_A|} \right) + \left(\sum_i^n \sum_{j>i}^n \frac{1}{|\hat{\mathbf{r}}_i - \hat{\mathbf{r}}_j|} \right), \end{aligned} \quad (1.3)$$

where m_A is the mass of nucleus A , Z_A and Z_B are the charges of nuclei A and B , respectively, $\hat{\mathbf{R}}_A$ and $\hat{\mathbf{R}}_B$ are the spatial coordinates of nuclei A and B , respectively, and $\hat{\mathbf{r}}_i$ and $\hat{\mathbf{r}}_j$ are the spatial coordinates of electrons i and j , respectively. Here the terms in the Hamiltonian are the nuclear kinetic energy operator (\hat{T}_N), the electronic kinetic energy operator (\hat{T}_e), the nuclei-nuclei Coulomb potential operator (\hat{V}_{NN}), the nuclei-electron Coulomb potential operator (\hat{V}_{Ne}), and the electron-electron Coulomb potential operator (\hat{V}_{ee}), respectively. The eigenfunctions of \hat{H} in position-space take the form $\Psi(\mathbf{r}, \mathbf{R})$ where $\mathbf{r} = \{\mathbf{r}_1, \mathbf{r}_2, \dots, \mathbf{r}_n\}$ and $\mathbf{R} = \{\mathbf{R}_1, \mathbf{R}_2, \dots, \mathbf{R}_M\}$. The squared modulus $|\Psi(\mathbf{r}, \mathbf{R})|^2$ gives the probability density of finding electron 1 at \mathbf{r}_1, \dots , electron n at \mathbf{r}_n , nucleus 1 at \mathbf{R}_1, \dots , and nucleus M at \mathbf{R}_M . Finding these wavefunctions therefore involves solving a $3n + 3M$ dimensional partial differential equation. While closed-form solutions exist for hydrogen-like atoms ($n = 1, M = 1$), the field of electronic structure theory relies on the use of careful approximations to simplify the system in question.

In order to reduce the dimensionality of the molecular Schrödinger equation, a popular approach is to apply the Born-Oppenheimer (BO) approximation where the nuclei are treated as fixed with respect to the electrons. This is rationalized by the observation that the nuclear motion, due to greater mass of nuclei ($m_p > 1800m_e$), occurs on a much longer timescale than electronic motion. Applying this approximation to Eq. 1.3, we see that the first term will go to zero and the third term will become a positive constant. This allows for the factorization of the wavefunction into an electronic term $\Psi_e(\mathbf{r}; \mathbf{R})$ that depends parametrically on the coordinates of the nuclei and a purely nuclear term $\Phi_N(\mathbf{R})$:

$$\Psi(\mathbf{r}, \mathbf{R}) = \Psi_e(\mathbf{r}; \mathbf{R})\Phi_N(\mathbf{R}). \quad (1.4)$$

With this reduction, the problem of interest becomes the electronic Schrödinger equation,

$$\hat{H}_e(\mathbf{R}) |\Psi_{e,k}(\mathbf{R})\rangle = E_{e,k}(\mathbf{R}) |\Psi_{e,k}(\mathbf{R})\rangle \quad (1.5)$$

$$\left(-\sum_i^n \frac{1}{2} \nabla_i^2 - \sum_i^n \sum_A^M \frac{Z_A}{|\mathbf{r}_i - \mathbf{R}_A|} + \sum_i^n \sum_{j>i}^n \frac{1}{|\mathbf{r}_i - \mathbf{r}_j|} \right) \Psi_{e,k}(\mathbf{r}; \mathbf{R}) = E_{e,k}(\mathbf{R}) \Psi_{e,k}(\mathbf{r}; \mathbf{R}), \quad (1.6)$$

where $|\Psi_{e,k}(\mathbf{R})\rangle$ is an electronic (eigen)state of the electronic Hamiltonian \hat{H}_e with electronic energy $E_{e,k}(\mathbf{R})$. The field of electronic structure theory is focused on finding accurate approximation solutions to this problem. Provided a solution to the electronic problem, one can define the corresponding BO potential energy surfaces (PES) on which the nuclei move:

$$V_k(\mathbf{R}) = E_{e,k}(\mathbf{R}) + V_{NN}(\mathbf{R}). \quad (1.7)$$

Accurate description of the ground state PES ($k = 0$) is a prominent aspect of many chapters in this thesis. It allows for a depiction of the energy change as systems move along reaction coordinates. The gradients of this potential energy are used to determine the forces for molecular dynamics simulations. One can also substitute Eqs. 1.4 and 1.7 into Eq. 1.2 to yield the BO nuclear Schrödinger equation:

$$[T_N + V_k(\mathbf{R})] \Phi_{K,k}(\mathbf{R}) = E_{K,k} \Phi_{K,k}(\mathbf{R}). \quad (1.8)$$

This equation has incorporated the BO approximation by neglecting the coupling of different electronic states by \hat{T}_N . This is valid when the electronic states are well-separated in energy for a given nuclear configuration, but can break down when the energies of two states become close. While one should be diligent about this issue, it is an appropriate approximation in the context of this thesis.

The nuclear Schrödinger equation is often neglected in electronic structure theory. A common approximation is to perform a second-order Taylor expansion of the PES at its extrema in order to model the nuclei as a set of coupled quantum harmonic oscillators. Normal mode analysis allows for computation of zero-point vibrational energies which are often used to correct zero-temperature electronic energy differences. In the context of molecular dynamics (MD) simulations, nuclei are often treated classically but approaches based on Feynman path integrals[1–5] and explicit quantum treatment of relevant light nuclei[6, 7] also are studied.

From here, we will focus on the electronic Schrödinger equation, leaving implicit the e subscript and \mathbf{R} dependence of the electronic Hamiltonian, wavefunction, and energy.

1.2 Hartree-Fock Theory

Despite much simplification, we are still left with a partial differential equation in $3n$ dimensions. A reasonable approximation to the ground state solution would be to minimize the expectation value of the Hamiltonian with a trial wavefunction $|\tilde{\Psi}\rangle$ parameterized by some coefficients \mathbf{C} . As the electronic Hamiltonian is a Hermitian operator, there exists a variational principle which guarantees this expectation value bounds the true ground state energy E_0 from above:

$$E_0 \leq \min_{\mathbf{C}} \frac{\langle \tilde{\Psi}(\mathbf{C}) | \hat{H} | \tilde{\Psi}(\mathbf{C}) \rangle}{\langle \tilde{\Psi}(\mathbf{C}) | \tilde{\Psi}(\mathbf{C}) \rangle} = \tilde{E}_0 \quad (1.9)$$

In order to determine a proper guess for the form of the wavefunction, one should consider the role of the permutation operator \hat{P}_{ij} , which exchanges electrons i and j . As electrons are indistinguishable, \hat{P}_{ij} commutes with \hat{H} and therefore the eigenfunctions of \hat{H} are also eigenvalues of \hat{P}_{ij} with eigenvalue p . Furthermore, applying the permutation operator twice will return the exact same wavefunction:

$$\hat{P}_{ij}\hat{P}_{ij}|\Psi_k\rangle = p^2|\Psi_k\rangle = |\Psi_k\rangle. \quad (1.10)$$

This eigenvalue p must be either 1, corresponding to bosonic particles with integer spin, or -1 , corresponding to fermionic particles with half-integer spin. As electrons are spin-1/2 particles and therefore fermions, the trial electronic wavefunction must be antisymmetric ($p = -1$) to particle exchange. The determinant of a square matrix is a mathematical object which obeys the property of antisymmetry with respect to exchange of two columns. Therefore a reasonable trial wavefunction is a Slater determinant, the determinant of a matrix where the rows index one-electron spin orbitals χ_i and columns index particle coordinates \mathbf{x}_j :

$$\Phi_S(\mathbf{x}_1, \mathbf{x}_2, \dots, \mathbf{x}_n) = \frac{1}{\sqrt{n!}} \det \begin{vmatrix} \chi_1(\mathbf{x}_1) & \chi_1(\mathbf{x}_2) & \cdots & \chi_1(\mathbf{x}_n) \\ \chi_2(\mathbf{x}_1) & \chi_2(\mathbf{x}_2) & \cdots & \chi_2(\mathbf{x}_n) \\ \vdots & \vdots & \ddots & \vdots \\ \chi_n(\mathbf{x}_1) & \chi_n(\mathbf{x}_2) & \cdots & \chi_n(\mathbf{x}_n) \end{vmatrix}. \quad (1.11)$$

We require the set of one-electron spin orbitals to be orthonormal to each other. These one-particle spin orbitals χ_i can be decomposed into a spatial orbital ψ_i and a spin component σ_i :

$$\chi_i(\mathbf{x}_j) = \psi_i(\mathbf{r}_j)\sigma_i(\omega_j). \quad (1.12)$$

Here \mathbf{r}_j and ω_j are the spatial coordinates and spin coordinate of electron j , respectively. Typically σ_i is chosen to be either α or β , the orthonormal eigenvectors of the one-particle spin operator projected along the z -axis \hat{s}_z with eigenvalues of $1/2$ and $-1/2$, respectively.

$$\langle \sigma(\omega_j) | \sigma'(\omega_j) \rangle = \delta_{\sigma,\sigma'} \quad (1.13)$$

$$\hat{s}_{z,j} |\alpha(\omega_j)\rangle = \frac{1}{2} |\alpha(\omega_j)\rangle \quad (1.14)$$

$$\hat{s}_{z,j} |\beta(\omega_j)\rangle = -\frac{1}{2} |\beta(\omega_j)\rangle \quad (1.15)$$

In practical calculations, the spatial orbitals are expanded in a finite basis $\{|\phi_\mu\rangle\}$ of N atom-centered orbitals (AOs).

$$|\psi_i(r)\rangle = \sum_{\mu}^N C_{\mu i} |\phi_\mu(r)\rangle \quad (1.16)$$

As σ_i can be either α or β , this yields a set of n occupied spin orbitals and $2N - n$ virtual (unoccupied) spin orbitals.

By taking this Slater determinant $|\Phi_S\rangle$ as a trial wavefunction and performing a variational optimization with respect to the wavefunction coefficients \mathbf{C} we have arrived at the Hartree-Fock (HF) approximation:

$$E_{\text{HF}} = \min_{\mathbf{C}} \langle \Phi_S | \hat{H} | \Phi_S \rangle. \quad (1.17)$$

The electronic Hamiltonian in Eq. 1.6 can be further split into one- and two-electron operators:

$$\hat{O}_1 = - \sum_i^n \frac{1}{2} \hat{\nabla}_i^2 - \sum_i^n \sum_A^M \frac{Z_A}{|\hat{\mathbf{r}}_i - \mathbf{R}_A|} = \sum_i^n \hat{h}(\mathbf{r}_i) \quad (1.18)$$

$$\hat{O}_2 = \sum_i^n \sum_{j>i}^n \frac{1}{|\hat{\mathbf{r}}_i - \hat{\mathbf{r}}_j|} = \sum_i^n \sum_{j>i}^n \frac{1}{\hat{r}_{ij}} \quad (1.19)$$

The expectation value in Eq. 1.17 can be evaluated using the Slater-Condon rules[8, 9] to yield the HF energy for a given Slater determinant:

$$E_{\text{HF}}[\Phi_S] = \sum_i^n \langle i | \hat{h} | i \rangle + \frac{1}{2} \sum_i^n \sum_j^n (\langle ij | ij \rangle - \langle ij | ji \rangle) \quad (1.20)$$

where

$$\langle i | \hat{h} | i \rangle = \int \chi_i^*(\mathbf{x}_1) h(\mathbf{r}_1) \chi_i(\mathbf{x}_1) d\mathbf{x}_1 \quad (1.21)$$

$$\langle ij | ij \rangle = \iint \chi_i^*(\mathbf{x}_1) \chi_j^*(\mathbf{x}_2) \frac{1}{r_{12}} \chi_i(\mathbf{x}_1) \chi_j(\mathbf{x}_2) d\mathbf{x}_1 d\mathbf{x}_2 \quad (1.22)$$

$$\langle ij | ji \rangle = \iint \chi_i^*(\mathbf{x}_1) \chi_j^*(\mathbf{x}_2) \frac{1}{r_{12}} \chi_j(\mathbf{x}_1) \chi_i(\mathbf{x}_2) d\mathbf{x}_1 d\mathbf{x}_2. \quad (1.23)$$

Eq. 1.22 represents the classical Coulomb interaction between two charge densities $|\chi_i(\mathbf{x}_1)|^2$ and $|\chi_j(\mathbf{x}_2)|^2$ while Eq. 1.23, the exchange integral, represents a purely quantum mechanical effect due to the antisymmetry constraint on the wavefunction.

Minimization of Eq. 1.20 with respect to the spin orbitals with the constraint that the spin orbitals are orthogonal can be achieved using the method of Lagrange multipliers.

$$\mathcal{L}[\{\chi_i\}] = E_{\text{HF}}[\{\chi_i\}] - \sum_i^n \sum_j^n \epsilon_{ij} (\langle \chi_i | \chi_j \rangle - \delta_{ij}) \quad (1.24)$$

Setting the variation of \mathcal{L} to zero leads to

$$\hat{f} |\chi_i\rangle = \sum_j^n \epsilon_{ij} |\chi_j\rangle. \quad (1.25)$$

The choice of the canonical orbitals which zero out the off-diagonal elements of ϵ_{ij} yields the Hartree-Fock equations,

$$\hat{f} |\chi_i\rangle = \epsilon_i |\chi_i\rangle, \quad i = 1, 2, \dots, n, \quad (1.26)$$

where the Fock operator,

$$\hat{f}(\mathbf{x}_1) = \hat{h}(\mathbf{r}_1) + \sum_j^n \int \chi_j^*(\mathbf{x}_2) \frac{1}{r_{12}} (1 - \hat{P}_{12}) \chi_j(\mathbf{x}_2) d\mathbf{x}_2, \quad (1.27)$$

include the mean-field potential that electron 1 experiences due to the other electrons. The Hartree-Fock wavefunction can then be considered a minimally-correlated approximation, as the only correlation between electrons comes from the antisymmetry constraint on the wavefunction.

Looking at Eq. 1.27, the Fock operator depends on the spin orbitals and therefore must be solved self-consistently within a basis. We begin by rewriting Eq. 1.26 in terms of spatial orbitals $\{\psi_{i,\sigma}\}$:

$$\hat{f}_\sigma |\psi_{i,\sigma}\rangle = \epsilon_{i,\sigma} |\psi_{i,\sigma}\rangle \quad (1.28)$$

where

$$\hat{f}_\sigma(\mathbf{r}_1) = \hat{h}(\mathbf{r}_1) + \sum_{\sigma' \in \{\alpha, \beta\}} \sum_j^{n_{\sigma'}} \int |\psi_{j,\sigma'}|^2 \frac{1}{r_{12}} d\mathbf{r}_2 - \sum_j^{n_\sigma} \int \psi_{j,\sigma}^* \frac{1}{r_{12}} \hat{P}_{12} \psi_{j,\sigma}(\mathbf{r}_2) d\mathbf{r}_2 \quad (1.29)$$

and $\sigma \in \{\alpha, \beta\}$ and n_σ is the number of electrons with spin component $|\sigma\rangle$. Here the Fock operator and spatial orbital are tagged with a spin label due to the action of the exchange operator on different spins. Revisiting Eq. 1.16, each spatial orbital is expanded in terms of the AO basis $\{\phi_\nu\}$:

$$|\psi_{i,\sigma}\rangle = \sum_\nu^N C_{\nu i, \sigma} |\phi_\nu\rangle. \quad (1.30)$$

Here the matrices \mathbf{C}_σ are the molecular orbital (MO) coefficient matrices. The basis functions $\{\phi_\nu\}$ are generally not orthogonal, with an overlap integral given by

$$S_{\mu\nu} = \langle \phi_\mu | \phi_\nu \rangle. \quad (1.31)$$

Substituting Eq. 1.30 into Eq. 1.28 and projecting with $\langle \phi_\mu |$ yields the Roothaan equation[10], a generalized matrix eigenvalue problem:

$$\langle \phi_\mu | \hat{f}_\sigma \sum_\nu^N |\phi_\nu\rangle C_{\nu i, \sigma} = \langle \phi_\mu | \sum_\nu^N |\phi_\nu\rangle C_{\nu i, \sigma} \epsilon_{i, \sigma} \quad (1.32)$$

$$\sum_\nu^N F_{\mu\nu, \sigma} C_{\nu i, \sigma} = \sum_\nu^N S_{\mu\nu} C_{\nu i, \sigma} \epsilon_i \quad (1.33)$$

$$\mathbf{F}_\sigma \mathbf{C}_\sigma = \mathbf{S} \mathbf{C}_\sigma \epsilon_\sigma. \quad (1.34)$$

where the Fock matrix elements in the AO basis are

$$F_{\mu\nu,\sigma} = h_{\mu\nu} + \sum_{\sigma' \in \{\alpha, \beta\}} \sum_j^{n_{\sigma'}} \langle \mu j_{\sigma'} | \nu j_{\sigma'} \rangle - \sum_j^{n_{\sigma}} \langle \mu j_{\sigma} | j_{\sigma} \mu \rangle. \quad (1.35)$$

The AO Fock matrix elements in Eq. 1.35 can be simplified via introduction of the one-particle density matrix (1-PDM). In HF theory, the real-space electron density $\rho(\mathbf{r})$ can be found by integrating the square of the wavefunction over all but one set of spatial coordinates:

$$\begin{aligned} \rho(\mathbf{r}_1) &= n \iint \cdots \int |\Phi_s(\mathbf{x}_1, \mathbf{x}_2, \dots, \mathbf{x}_n)|^2 d\omega_1 d\mathbf{x}_2 \dots d\mathbf{x}_n \\ &= \sum_{\sigma \in \{\alpha, \beta\}} \sum_i^{n_{\sigma}} |\psi_{i,\sigma}(\mathbf{r}_1)|^2. \end{aligned} \quad (1.36)$$

The spin-densities $\rho_{\sigma}(\mathbf{r})$ can be defined similarly. Transforming this into the AO basis using Eq.1.30 yields

$$\rho_{\sigma}(\mathbf{r}) = \sum_i^{n_{\sigma}} |\psi_{i,\sigma}(\mathbf{r})|^2 \quad (1.37)$$

$$= \sum_{\mu}^N \sum_{\nu}^N \sum_i^{n_{\sigma}} C_{\mu i, \sigma} C_{\nu i, \sigma}^* \phi_{\mu}(\mathbf{r}) \phi_{\nu}^*(\mathbf{r}) \quad (1.38)$$

$$= \sum_{\mu}^N \sum_{\nu}^N P_{\mu\nu, \sigma} \phi_{\mu}(\mathbf{r}) \phi_{\nu}^*(\mathbf{r}). \quad (1.39)$$

Here the 1-PDM for spin σ is given by

$$P_{\mu\nu, \sigma} = \sum_i^{n_{\sigma}} C_{\mu i, \sigma} C_{\nu i, \sigma}^*. \quad (1.40)$$

Incorporating Eq. 1.40 into Eq. 1.35 yields

$$F_{\mu\nu, \sigma} = h_{\mu\nu} + \sum_{\lambda}^N \sum_{\varsigma}^N \langle \mu \lambda | \nu \varsigma \rangle (P_{\lambda\varsigma, \alpha} + P_{\lambda\varsigma, \beta}) - \sum_{\lambda}^N \sum_{\varsigma}^N \langle \mu \lambda | \varsigma \nu \rangle P_{\lambda\varsigma, \sigma} \quad (1.41)$$

where one can define the Coulomb (\mathbf{J}) and exchange (\mathbf{K}) matrices as

$$J_{\mu\nu} = \sum_{\lambda}^N \sum_{\varsigma}^N \langle \mu \lambda | \nu \varsigma \rangle (P_{\lambda\varsigma, \alpha} + P_{\lambda\varsigma, \beta}) \quad (1.42)$$

$$K_{\mu\nu, \sigma} = \sum_{\lambda}^N \sum_{\varsigma}^N \langle \mu \lambda | \varsigma \nu \rangle P_{\lambda\varsigma, \sigma} \quad (1.43)$$

which are in turn contractions of the spin density matrices with the electron repulsion integrals (ERIs) in the AO basis. The Hartree-Fock energy, in terms of the spin density matrices is

$$E_{\text{HF}} = \frac{1}{2} (\text{Tr}[\mathbf{P}_\alpha(\mathbf{h} + \mathbf{F}_\alpha)] + \text{Tr}[\mathbf{P}_\beta(\mathbf{h} + \mathbf{F}_\beta)]). \quad (1.44)$$

The derivative of the Hartree-Fock energy with respect to a spin density matrix is the corresponding Fock matrix.

Eq. 1.41 and 1.44 provide the working equations for constructing a Fock matrix and evaluating the Hartree-Fock energy. In order to self-consistently solve the Roothaan equations, the generalized eigenvalue problem is transformed into a eigenvalue problem via orthogonalization of the AO basis. This is accomplished using the symmetric orthogonalization scheme of Löwdin[11]. Beginning with the Roothaan equation, we have

$$\mathbf{F}_\sigma \mathbf{C}_\sigma = \mathbf{S} \mathbf{C}_\sigma \epsilon_\sigma. \quad (1.45)$$

Let \mathbf{X} be the symmetric orthogonalizer of \mathbf{S} such that

$$\mathbf{X}^\dagger \mathbf{S} \mathbf{X} = \mathbf{I}, \quad (1.46)$$

$$\mathbf{X} = \mathbf{S}^{-1/2}. \quad (1.47)$$

Defining a transformed MO coefficient matrix \mathbf{C}'_σ and substituting into Eq. 1.45 yields

$$\mathbf{C}_\sigma = \mathbf{X} \mathbf{C}'_\sigma, \quad (1.48)$$

$$\mathbf{F}_\sigma \mathbf{X} \mathbf{C}'_\sigma = \mathbf{S} \mathbf{X} \mathbf{C}'_\sigma \epsilon_\sigma. \quad (1.49)$$

$$(1.50)$$

Finally, both sides of Eq. 1.49 are left-multiplied by the hermitian conjugate of the orthogonalizer and terms are grouped:

$$\mathbf{X}^\dagger \mathbf{F}_\sigma \mathbf{X} \mathbf{C}'_\sigma = \mathbf{X}^\dagger \mathbf{S} \mathbf{X} \mathbf{C}'_\sigma \epsilon_\sigma \quad (1.51)$$

$$\mathbf{X}^\dagger \mathbf{F}_\sigma \mathbf{X} = \mathbf{F}'_\sigma \quad (1.52)$$

$$\mathbf{F}'_\sigma \mathbf{C}'_\sigma = \mathbf{C}'_\sigma \epsilon_\sigma \quad (1.53)$$

Eq. 1.53 is now an eigenvalue problem that can be solved by diagonalizing the transformed Fock matrix \mathbf{F}'_σ . The eigenvectors \mathbf{C}'_σ can be back-transformed to \mathbf{C}_σ via Eq. 1.48, which can in turn be used to update the density matrix \mathbf{P}_σ via Eq. 1.40. As the Fock matrix depends explicitly on the MO coefficients, these equations must be solved iteratively, a process known as the self-consistent field method. Fig. 1.1 presents the Roothaan-Hall algorithm for SCF. Several methods[12–16], including direct inversion of the iterative subspace (DIIS)[17, 18] and geometric direct minimization (GDM)[19], have been proposed to accelerate convergence of the SCF procedure and are utilized throughout this thesis. The computational scaling of solving the HF equations is formally $\mathcal{O}(N^4)$, though algorithms which take advantage of the

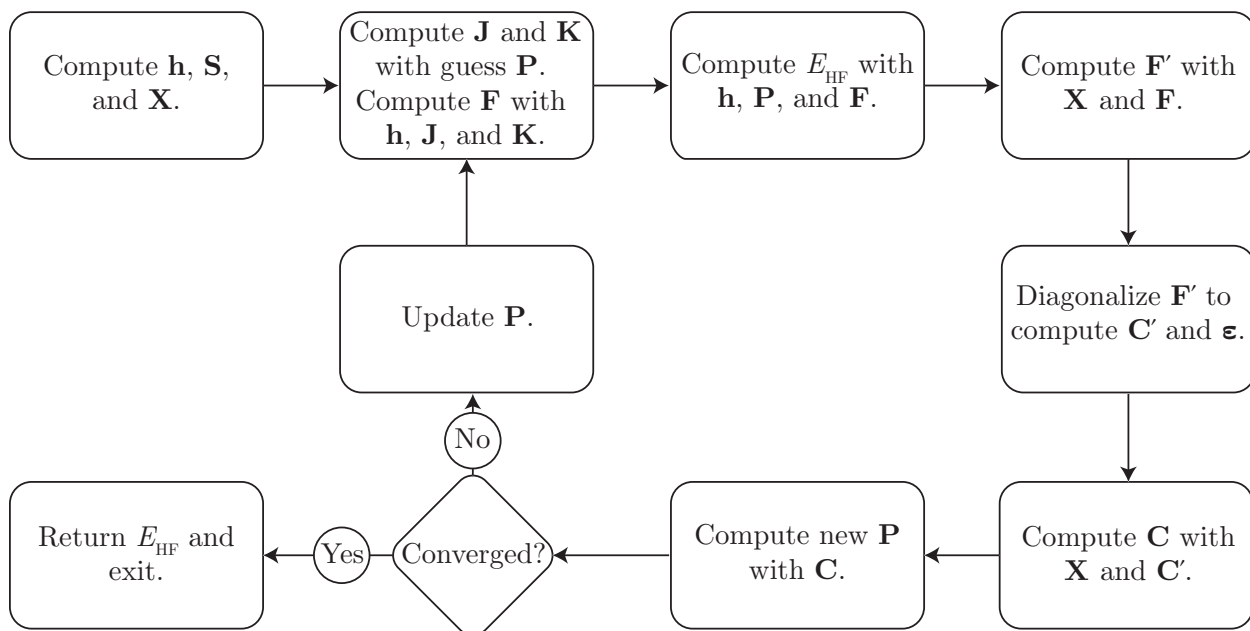


Figure 1.1: Schematic representation of the self-consistent field (SCF) procedure used to solve the Hartree-Fock equations.

sparsity of the ERIs reduce the asymptotic scaling to $\mathcal{O}(N^3)$ due to the diagonalization of the Fock matrix.

Throughout the derivations above, objects have been tagged with a spin index σ referring to the eigenstates of the one-particle operator \hat{s}_z , $|\alpha\rangle$ and $|\beta\rangle$. In doing so, we have assumed a common spin axis for all of the electrons in the system, making the wavefunction an eigenstate of the total spin operator projected along the z -axis, \hat{S}_z , where

$$\hat{S}_z = \sum_i^n \hat{s}_{z,i}. \quad (1.54)$$

As the molecular Hamiltonian commutes with \hat{S}_z , the exact wavefunction can be chosen to be an eigenstate of both operators with eigenvalue $(n_\alpha - n_\beta)/2$. Similarly, the square of the total spin operator, \hat{S}^2 , commutes with both \hat{H} and \hat{S}_z and therefore the exact wavefunction is expressible as an eigenstate of all three operators. Here

$$\hat{S}^2 = \hat{S}_x \hat{S}_x + \hat{S}_y \hat{S}_y + \hat{S}_z \hat{S}_z \quad (1.55)$$

$$= \hat{S}_+ \hat{S}_- - \hat{S}_z + \hat{S}_z \hat{S}_z \quad (1.56)$$

where

$$\hat{S}_+ = \sum_i^n \hat{s}_{+,i} \quad (1.57)$$

$$\hat{S}_- = \sum_i^n \hat{s}_{-,i} \quad (1.58)$$

and

$$\hat{s}_{+,i} |\alpha(\omega_i)\rangle = 0 \quad (1.59)$$

$$\hat{s}_{+,i} |\beta(\omega_i)\rangle = |\alpha(\omega_i)\rangle \quad (1.60)$$

$$\hat{s}_{-,i} |\alpha(\omega_i)\rangle = |\beta(\omega_i)\rangle \quad (1.61)$$

$$\hat{s}_{-,i} |\beta(\omega_i)\rangle = 0. \quad (1.62)$$

In this mutual eigenbasis, the eigenvalues of \hat{S}^2 are

$$\hat{S}^2 |\Psi\rangle = \left(\frac{n_\alpha - n_\beta}{2} \right) \left(\frac{n_\alpha - n_\beta}{2} + 1 \right) |\Psi\rangle. \quad (1.63)$$

For a Slater determinant wavefunction, the expectation value of \hat{S}^2 can be determined evaluated using the Slater-Condon rules[8, 9]:

$$\langle \Phi_s | \hat{S}^2 | \Phi_s \rangle = \langle \hat{S}^2 \rangle = \left(\frac{n_\alpha - n_\beta}{2} \right) \left(\frac{n_\alpha - n_\beta}{2} + 1 \right) + n_\beta - \sum_i^{n_\alpha} \sum_j^{n_\beta} |S_{ij}^{\alpha\beta}|^2 \quad (1.64)$$

where

$$S_{ij}^{\alpha\beta} = \langle \psi_{i,\alpha} | \psi_{j,\beta} \rangle \quad (1.65)$$

and $n_\alpha \geq n_\beta$. From Eq. 1.65, we see that restricting each α spin orbital to have a corresponding β spin orbital with the same spatial component leads the second and third terms to cancel. Therefore this approximation, referred to as restricted HF (RHF), leads to a wavefunction that is an eigenvalue of \hat{S}^2 . Conversely, unrestricted HF (UHF) allows the spatial components differ between α and β spin orbitals and therefore yields a wavefunction that is not a eigenstate of \hat{S}^2 . However, the variational nature of the HF energy functional states that additional constraints on an approximate wavefunction can only increase the energy. Therefore, there exists a tension between using an RHF ansatz in order to obtain an approximate wavefunction which shares the symmetries of the true wavefunction or a UHF ansatz in order to obtain a more accurate approximate energy, known in the field as the symmetry dilemma. While the works in this thesis give preference to the unrestricted approach, this symmetry dilemma plays an important role in Ch. 4 and 5 where orbital choice is examined in the context of methods built on top of HF. Additionally, one can consider other ansatz where the \hat{S}_z and/or complex-conjugation symmetries are broken by the approximate wavefunction to increase variational flexibility (general HF (GHF) and complex HF, respectively). These different classifications are categorized by Fukutome[20] and while interesting are not further explored in the context of this thesis.

1.3 Correlated Wavefunction Methods

In the previous section, the HF equations were derived by assuming a single Slater determinant wavefunction (Eq. 1.17). Pursuing this derivation led to the Roothaan equations (Eq. 1.34), a set of single-particle equations where the potential felt by each electron is the averaged field of the other electrons. In this sense, the electrons under the HF approximation are minimally correlated, with the only correlation arising from the antisymmetry conditions on the wavefunction. The energy contribution arising from the correlation between electrons in the exact ground state wavefunction is called the correlation energy and is given by

$$E_{\text{corr}} = E_0 - E_{\text{HF}} \quad (1.66)$$

The correlation energy for a given post-HF method is defined similarly as the difference between that method's total energy and E_{HF} .

For a system with n electrons and an AO basis of dimension N , the solution to the HF equations yields a set of $o = n$ occupied spin orbitals $\{\chi_i\}$ used to form the ground state wavefunction $|\Phi_0\rangle$ and $v = 2N - n$ virtual spin orbitals $\{\chi_a\}$ (As a point of notation, from here on occupied spin orbitals are indexed with $\{i, j, \dots\}$, virtual spin orbitals with $\{a, b, \dots\}$, and unspecified spin orbitals with $\{p, q, \dots\}$ and sums are condensed). With these pieces one can define a basis of orthonormal Slater determinants, the Fock space, created by excitations (replacing one or more occupied orbitals with virtual orbitals) from $|\Phi_0\rangle$. Within this Fock space, the creation operator, \hat{a}_p^\dagger , and annihilation operator, \hat{a}_q , creates an electron in χ_p and destroys an electron in χ_q , respectively. Excited determinants are formed via the action of excitation operators \hat{T}_x , which are grouped by level of excitation x , e.g.

$$\hat{T}_1 |\Phi_0\rangle = \sum_{ia} t_i^a \hat{a}_a^\dagger \hat{a}_i |\Phi_0\rangle = \sum_{ia} t_i^a |\Phi_i^a\rangle, \quad (1.67)$$

$$\hat{T}_2 |\Phi_0\rangle = \sum_{\substack{i < j \\ a < b}} t_{ij}^{ab} \hat{a}_a^\dagger \hat{a}_b^\dagger \hat{a}_j \hat{a}_i |\Phi_0\rangle = \sum_{\substack{i < j \\ a < b}} t_{ij}^{ab} |\Phi_{ij}^{ab}\rangle. \quad (1.68)$$

In the above example, $|\Phi_i^a\rangle$ is a singly-excited determinant with corresponding amplitude t_i^a and $|\Phi_{ij}^{ab}\rangle$ is a doubly-excited determinant with corresponding amplitude t_{ij}^{ab} . The Hamiltonian operator in this Fock space is given by

$$\hat{H} = \sum_{pq} h_{pq} \hat{a}_p^\dagger \hat{a}_q + \frac{1}{4} \sum_{pqrs} \langle pq || rs \rangle \hat{a}_p^\dagger \hat{a}_q^\dagger \hat{a}_s \hat{a}_r \quad (1.69)$$

where

$$h_{pq} = \int \chi_p^*(\mathbf{x}_1) h(\mathbf{r}_1) \chi_q(\mathbf{x}_1) d\mathbf{x}_1 \quad (1.70)$$

$$\langle pq || rs \rangle = \langle pq | rs \rangle - \langle pq | sr \rangle \quad (1.71)$$

$$\langle pq | rs \rangle = \iint \chi_p^*(\mathbf{x}_1) \chi_q^*(\mathbf{x}_2) \frac{1}{r_{12}} \chi_r(\mathbf{x}_1) \chi_s(\mathbf{x}_2) d\mathbf{x}_1 d\mathbf{x}_2 \quad (1.72)$$

are the MO one- and two-electron integrals.

Configuration Interaction Theory

Given this new basis of determinants, one might consider taking as a new trial wavefunction a linear combination of all possible Slater determinants, or configurations, in the Fock space:

$$|\Psi_{\text{FCI}}\rangle = \left(\hat{T}_0 + \hat{T}_1 + \hat{T}_2 + \dots + \hat{T}_n\right) |\Phi_0\rangle \quad (1.73)$$

$$= t_0 |\Phi_0\rangle + \sum_{ia} t_i^a |\Phi_i^a\rangle + \sum_{\substack{i,j>i \\ a,b>a}} t_{ij}^{ab} |\Phi_{ij}^{ab}\rangle + \dots \quad (1.74)$$

This approach, known as full configuration interaction (FCI), considers all possible excitation of all electrons and therefore completely spans the space given by the number of electrons and the choice of basis. Because of this completeness, the energies obtained by this method are exact within the corresponding basis set. Additionally, consideration of all possible configurations renders FCI invariant to changes in the reference state $|\Phi_0\rangle$. Solving for these t -amplitude coefficients is achieved by constructing the Hamiltonian matrix \mathbf{H} in the basis of configurations and solving for its eigenvalues and corresponding eigenvectors. While this in principle could be achieved through diagonalization, in practice approximate methods are often used to obtain the few lowest energy eigenstates due to the size of \mathbf{H} [21]. While this may seem like an ideal approach to incorporate correlation into a trial wavefunction, the total number of configurations (equivalent to the rank of \mathbf{H}) is $\binom{2N}{n}$ and therefore grows factorially with the size of the system, rendering the method intractable for all but the smallest systems.

Given this limitation, one could consider truncating the sum in Eq. 1.73, as each level of excitation x adds $\binom{o}{x}\binom{v}{x}$ configurations. For example, truncation after \hat{T}_2 would yield configuration interactions with single and double excitations (CISD) and inclusion of triply excited determinants through \hat{T}_3 would yield configuration interaction with single, double, and triple excitation (CISDT). As the full space of configurations these truncated configuration interaction (CI) methods are no longer independent of the choice of the reference $|\Phi_0\rangle$. This aspect is acceptable under the assumption that the reference determinant has a large overlap with the true wavefunction. A major weakness of truncated CI approaches, however, is the lack of size consistency. A method is size consistent if a calculation on a supersystem of non-interacting systems returns the same result as individual calculations on the subsystems. For example, if one were to imagine two non-interacting molecules, a doubly excited determinant on each molecule is accurately described by CISD in the subsystems whereas in the supersystem this effective quadruply excited determinant is excluded. Size consistency is an important property for methods used to study chemical reactivity, as reactants, intermediates, and products require equal treatment for accurate assessment of reaction thermodynamics.

Coupled Cluster Theory

Coupled cluster (CC) theory utilizes an exponential ansatz to parameterize the wavefunction:

$$|\Psi_{\text{CC}}\rangle = e^{(\hat{T}_1 + \hat{T}_2 + \dots)} |\Phi_0\rangle = e^{\hat{T}} |\Phi_0\rangle. \quad (1.75)$$

This wavefunction is equivalent to the FCI wavefunction when all excitations are included in the exponent. Unlike truncated CI, however, coupled cluster theory is size consistent with a truncated cluster operator \hat{T} . Considering coupled cluster with single and double excitation (CCSD)[22, 23], we see that expansion of the exponential leads to infinite-order excitations as products of single and double excitations,

$$|\Psi_{\text{CC}}\rangle = \left[1 + \hat{T}_1 + \hat{T}_2 + \frac{1}{2!} (\hat{T}_1\hat{T}_1 + \hat{T}_1\hat{T}_2 + \hat{T}_2\hat{T}_1 + \hat{T}_2\hat{T}_2) + \dots \right] |\Phi_0\rangle, \quad (1.76)$$

allowing for treatment of the effective quadruple and higher excitations lacking in previous example with CISD. This exponential form allows for separability of Hamiltonian in the limit of non-interacting systems.

While this new form of the wavefunction has provided a solution to the issue of size consistency, it comes at the cost of a variational approach to finding the t -amplitudes. Plugging Eq. 1.75 into Eq. 1.9 leads to a set of equations which do not truncate at finite order. In order to solve for the t -amplitudes one begins with the similar transformed Hamiltonian,

$$\bar{H} = e^{-\hat{T}} \hat{H} e^{\hat{T}}. \quad (1.77)$$

From here, the t -amplitudes and energy are determined via projected equations:

$$\langle \Phi_0 | \bar{H} | \Phi_0 \rangle = E_{\text{CC}} \quad (1.78)$$

$$\langle \Phi_i^a | \bar{H} | \Phi_0 \rangle = 0 \quad (1.79)$$

$$\langle \Phi_{ij}^{ab} | \bar{H} | \Phi_0 \rangle = 0 \quad (1.80)$$

$$\langle \Phi_{ij\dots}^{ab\dots} | \bar{H} | \Phi_0 \rangle = 0. \quad (1.81)$$

In these equations \bar{H} may be simplified using the Baker-Campbell-Hausdorff expansion as a linear combination of nested commutators of \hat{T} and \hat{H} ,

$$\bar{H} = \hat{H} + [\hat{H}, \hat{T}] + \frac{1}{2!} [[\hat{H}, \hat{T}], \hat{T}] + \frac{1}{3!} [[[[\hat{H}, \hat{T}], \hat{T}], \hat{T}]] + \dots, \quad (1.82)$$

which terminates after a finite number of terms. This termination can be rationalized by the observation that the Hamiltonian operator in the Fock space representation is given by Eq. 1.69 contains at most two de-excitation. These projected equations are nonlinear and must be iterated over to solve for the t -amplitudes and energy. The computational cost of CCSD is $\mathcal{O}(\sigma^2 v^4)$ per iteration and the inclusion of explicit triple excitations, CCSDT[24] has a cost of $\mathcal{O}(\sigma^3 v^5)$ per iteration. This high cost for the latter has inspired many approximations to treat the effects of the triples, most ubiquitous among them being CCSD(T)[25].

CCSD(T) is a non-iterative $\mathcal{O}(o^3v^4)$ method that gives a perturbative approximation to the triples amplitudes using the CCSD t_1 - and t_2 -amplitudes. For many computational chemists CCSD(T) is considered the "gold standard" in terms of the accuracy given the cost, though for practical applications with a reasonable basis set it is limited to a few tens of heavy (non-hydrogen) atoms (architecture dependent). This method is used extensively throughout this thesis to predict energies and barrier heights for reactions (Ch. 2 and 3) and benchmark more approximate levels of theory (Ch. 3 and 4). In Ch. 5, we investigate the role of the reference $|\Phi_0\rangle$ in predicting spectroscopic properties with CCSD(T).

More in-depth derivations and discussions of CC theory, including diagrammatic approaches to derive and represent the CC equations can be found in Refs. [26] and [27].

Perturbation Theory

Møller-Plesset (MP) theory offers another avenue to incorporate electron correlation based on Rayleigh-Schrödinger perturbation theory[28]. The Fock operator is taken as the zero-order Hamiltonian and the zero-order wavefunction is the HF ground state Slater determinant $|\Phi_0\rangle$. Expanding the \hat{H} , $|\Psi_{\text{MP}}\rangle$, and E_{MP}

$$\hat{H} = \hat{F} + \lambda\hat{V} \quad (1.83)$$

$$|\Psi_{\text{MP}}\rangle = |\Phi_0\rangle + \lambda|\Psi^{(1)}\rangle + \lambda^2|\Psi^{(2)}\rangle + \lambda^3|\Psi^{(3)}\rangle + \dots \quad (1.84)$$

$$E = E_{\text{MP}0} + \lambda E_{\text{MP}1} + \lambda^2 E_{\text{MP}2} + \lambda^3 E_{\text{MP}3} + \dots \quad (1.85)$$

Plugging Eq. 1.83–1.85 into the time-independent Schrödinger equation and separating by order in the perturbation λ yields

$$\hat{F}|\Phi_0\rangle = E_{\text{MP}0}|\Phi_0\rangle \quad (1.86)$$

$$\hat{F}|\Psi^{(1)}\rangle + \hat{V}|\Phi_0\rangle = E_{\text{MP}0}|\Psi^{(1)}\rangle + E_{\text{MP}1}|\Phi_0\rangle \quad (1.87)$$

$$\hat{F}|\Psi^{(2)}\rangle + \hat{V}|\Psi^{(1)}\rangle = E_{\text{MP}0}|\Psi^{(2)}\rangle + E_{\text{MP}1}|\Psi^{(1)}\rangle + E_{\text{MP}2}|\Phi_0\rangle \quad (1.88)$$

$$\hat{F}|\Psi^{(3)}\rangle + \hat{V}|\Psi^{(2)}\rangle = E_{\text{MP}0}|\Psi^{(3)}\rangle + E_{\text{MP}1}|\Psi^{(2)}\rangle + E_{\text{MP}2}|\Psi^{(1)}\rangle + E_{\text{MP}3}|\Phi_0\rangle \quad (1.89)$$

$$\vdots \quad (1.90)$$

By employing the convention of intermediate normalization:

$$\langle\Phi_0|\Psi_{\text{MP}}\rangle = 1, \quad (1.91)$$

these equations can be solved via projection with $\langle\Phi_0|$ to obtain energy contributions or with excited determinants to obtain higher-order wavefunction contributions.

The zeroth-order energy, $E_{\text{MP}0}$, is

$$E_{\text{MP}0} = \langle\Phi_0|\hat{F}|\Phi_0\rangle \quad (1.92)$$

$$= \sum_i \epsilon_i. \quad (1.93)$$

Here the occupied-occupied and virtual-virtual blocks of \mathbf{F} are assumed to be diagonal [(psuedo)canonical spin orbitals]. The first-order energy, E_{MP1} , is

$$E_{\text{MP1}} = \langle \Phi_0 | \hat{V} | \Phi_0 \rangle \quad (1.94)$$

$$= \langle \Phi_0 | \hat{H} - \hat{F} | \Phi_0 \rangle \quad (1.95)$$

$$= E_{\text{HF}} - \sum_i \epsilon_i. \quad (1.96)$$

We see that the total energy to first-order is E_{HF} . Turning to the first-order wavefunction contributions, we begin by expanding it in the basis of zeroth-order states:

$$|\Psi^{(1)}\rangle = \sum_{ia} t_i^a |\Phi_i^a\rangle + \sum_{\substack{i,j>i \\ a,b>a}} t_{ij}^{ab} |\Phi_{ij}^{ab}\rangle + \dots \quad (1.97)$$

Rearranging Eq. 1.87 and substituting in Eq. 1.97 yields

$$\left(\hat{F} - E_{\text{MP0}} \right) \left(\sum_{ia} t_i^a |\Phi_i^a\rangle + \sum_{\substack{i,j>i \\ a,b>a}} t_{ij}^{ab} |\Phi_{ij}^{ab}\rangle + \dots \right) = \left(E_{\text{MP1}} - \hat{V} \right) |\Phi_0\rangle. \quad (1.98)$$

At this point, the t -amplitudes can be solved for by left-projection with excited determinants. Looking at the right hand side, however, we notice that the $E_{\text{MP1}} |\Phi_0\rangle$ term becomes zero under this projection due to the orthogonality of the configuration space. Additionally, if HF orbitals are assumed, the occupied-virtual blocks of \mathbf{F} are zero, meaning that \hat{V} only couples states which are separated by two excitations. This means that only the t_2 -amplitudes are nonzero. Incorporating this into Eq. 1.98 and rearranging yields an expression for $|\Psi^{(1)}\rangle$:

$$\langle \Phi_{kl}^{cd} | \left(\hat{F} - E_{\text{MP0}} \right) \sum_{\substack{i<j \\ a<b}} t_{ij}^{ab} |\Phi_{ij}^{ab}\rangle = - \langle \Phi_{ij}^{ab} | \hat{V} | \Phi_0 \rangle \quad (1.99)$$

$$\left(\langle \Phi_{ij}^{ab} | \hat{F} | \Phi_{ij}^{ab} \rangle - E_{\text{MP0}} \right) t_{ij}^{ab} = - \langle \Phi_{ij}^{ab} | \hat{V} | \Phi_0 \rangle \quad (1.100)$$

$$t_{ij}^{ab} = - \frac{\langle ij || ab \rangle}{\epsilon_a + \epsilon_b - \epsilon_i - \epsilon_j} \quad (1.101)$$

$$|\Psi^{(1)}\rangle = - \sum_{\substack{i,j>i \\ a,b>a}} \frac{\langle ij || ab \rangle}{\epsilon_a + \epsilon_b - \epsilon_i - \epsilon_j} |\Phi_{ij}^{ab}\rangle. \quad (1.102)$$

The second-order energy, E_{MP2} , is found by left projecting $\langle \Phi_0 |$ on Eq. 1.88 and substituting

in Eq. 1.102:

$$E_{\text{MP2}} = \langle \Phi_0 | \hat{F} | \Psi^{(2)} \rangle + \langle \Phi_0 | \hat{V} | \Psi^{(1)} \rangle \quad (1.103)$$

$$= - \sum_{\substack{i < j \\ a < b}} \langle \Phi_0 | \hat{V} | \Psi^{(1)} \rangle \frac{\langle ij || ab \rangle}{\epsilon_a + \epsilon_b - \epsilon_i - \epsilon_j} \quad (1.104)$$

$$= - \sum_{\substack{i < j \\ a < b}} \frac{\langle ab || ij \rangle \langle ij || ab \rangle}{\epsilon_a + \epsilon_b - \epsilon_i - \epsilon_j} \quad (1.105)$$

$$= - \frac{1}{4} \sum_{ijab} \frac{|\langle ij || ab \rangle|^2}{\Delta_{ij}^{ab}}. \quad (1.106)$$

In this last expression, the prefactor of 1/4 arises to account for unrestricted of the bounds of the sum and Δ_{ij}^{ab} is the orbital energy difference $\epsilon_a + \epsilon_b - \epsilon_i - \epsilon_j$. The performance of the MP2 method lies between that of HF and CCSD and is generally accurate for closed-shell energies and properties. Computation of the energy has a cost of $\mathcal{O}(o^2v^2)$, however the computational bottleneck is the transformation of the ERIs from AO to MO, leading to an asymptotic cost of $\mathcal{O}(N^5)$. Use of the "resolution of the identity" (RI) decomposition for the two-electron integrals helps save on the memory requirements and allows for MP2 to treat systems of around 100 atoms with a moderate basis set[29, 30].

For open-shell systems, symmetry breaking in the reference can lead to poor accuracy for MP2[31–34]. A possible solution to this issue is orbital-optimized MP2 (OOMP2), where the MP2 total energy is optimized with respect to occupied-virtual rotations in the reference $|\Phi_0\rangle$ [35–37]. This is achieved through use of the Hylleraas functional, J_{H} [27, 38]:

$$J_{\text{H}}[\Psi^{(1)}] = \langle \Psi^{(1)} | \hat{F} - E_{\text{MP0}} | \Psi^{(1)} \rangle + \langle \Phi_0 | \hat{V} | \Psi^{(1)} \rangle + \langle \Psi^{(1)} | \hat{V} | \Phi_0 \rangle. \quad (1.107)$$

Writing this as a functional of the t -amplitudes and combining it with the total first-order energy leads to the MP2 Lagrangian which depends on a matrix Θ that parameterizes occupied-virtual rotation of the MO coefficients:

$$\mathcal{L}_{\text{MP2}}[\mathbf{t}, \Theta] = E_{\text{MP0}}[\Theta] + E_{\text{MP1}}[\Theta] + J_{\text{H}}[\mathbf{t}, \Theta]. \quad (1.108)$$

Setting the variation of Eq. 1.108 with respect to Θ to zero optimizes the orbitals in the reference state $|\Phi_0\rangle$ with respect to the overall MP2 energy. A thorough derivation of the working equations for OOMP2 is given in Ref. [39]. From the derivation of $|\Psi^{(1)}\rangle$, we observe that orbital optimization, which leads to nonzero F_{ia} , in principle results in a non-Brillouin singles contribution to the energy. In practice, however, this contribution is neglected for orbital-optimized methods as justified by [36]. While OOMP2 is able to address the limitations of MP2 with respect to open-shell systems it is not without its own limitations. From Eq. 1.106, we see that in the limit of $\Delta_{ij}^{ab} = 0$ the MP2 correlation energy diverges.

In order to remedy this, several methods have been developed to regularize the OOMP2 energy such that in the limit of $\Delta_{ij}^{ab} = 0$ does not diverge [39–41]. One particular method, κ -OOMP2[39], achieves this through an exponential regularization of the two-electron integrals:

$$E_{\kappa\text{-OOMP2}}(\kappa) = -\frac{1}{4} \sum_{ijab} \frac{|\langle ij||ab \rangle|^2}{\Delta_{ij}^{ab}} \left(1 - e^{-\kappa \Delta_{ij}^{ab}}\right)^2. \quad (1.109)$$

The ability of this method to remedy the failings of traditional OOMP2 has inspired its use in extensions seen in Ch. 4 and 5.

The third-order energy, E_{MP3} , can be found by projecting $\langle \Phi_0 |$ on Eq. 1.89:

$$E_{\text{MP3}} = \langle \Phi_0 | \hat{F} | \Psi^{(3)} \rangle + \langle \Phi_0 | \hat{V} | \Psi^{(2)} \rangle \quad (1.110)$$

The use of canonical HF orbitals eliminates the first term on the right hand side of Eq. 1.110, yielding

$$E_{\text{MP3}} = \langle \Phi_0 | \hat{V} | \Psi^{(2)} \rangle. \quad (1.111)$$

While this expression seems to require an expression for $|\Psi^{(2)}\rangle$ to evaluate, it can be rewritten using Wigner’s $2n + 1$ theorem, which states that corrections to the wavefunction to the n th order can be used to calculate the corrections to the energy up to the $(2n + 1)$ th order. Therefore, we may rewrite

$$E_{\text{MP3}} = \langle \Psi^{(1)} | \hat{V} | \Psi^{(1)} \rangle \quad (1.112)$$

$$= \sum_{\substack{i < j \\ a < b}} \sum_{\substack{k < l \\ c < d}} (t_{ij}^{ab})^* \langle \Phi_{ij}^{ab} | \hat{V} | \Phi_{kl}^{cd} \rangle t_{kl}^{cd}. \quad (1.113)$$

Recalling that \hat{V} couples states that differ by two spin orbitals, we are left with terms where $\langle \Phi_{ij}^{ab} |$ and $|\Phi_{kl}^{cd}\rangle$ share two occupied indices, two virtual indices, or one occupied and one virtual index:

$$\begin{aligned} E_{\text{MP3}} &= \frac{1}{8} \sum_{ijabcd} (t_{ij}^{ab})^* \langle ab||cd \rangle t_{ij}^{cd} \\ &\quad + \frac{1}{8} \sum_{ijklcd} (t_{ij}^{ab})^* \langle kl||ij \rangle t_{kl}^{ab} \\ &\quad - \sum_{ijkabc} (t_{ij}^{ab})^* \langle kb||ic \rangle t_{kj}^{ac}. \end{aligned} \quad (1.114)$$

Here the prefactors again arise to account for the redundancy after unrestricting the sums. This expression for E_{MP3} is therefore shown to be contractions of two t -amplitudes with two

electron integrals. Expanding Eq. 1.114 with Eq. 1.101 yields

$$\begin{aligned}
 E_{\text{MP3}} &= \frac{1}{8} \sum_{ijklcd} \frac{\langle ij||ab\rangle\langle ab||cd\rangle\langle cd||ij\rangle}{\Delta_{ij}^{ab}\Delta_{ij}^{cd}} \\
 &+ \frac{1}{8} \sum_{ijklcd} \frac{\langle ij||ab\rangle\langle kl||ij\rangle\langle ab||kl\rangle}{\Delta_{ij}^{ab}\Delta_{kl}^{ab}} \\
 &- \sum_{ijkabc} \frac{\langle ij||ab\rangle\langle kb||ic\rangle\langle ac||kj\rangle}{\Delta_{ij}^{ab}\Delta_{kj}^{ac}}.
 \end{aligned} \tag{1.115}$$

The cost to compute the terms in E_{MP3} are $\mathcal{O}(o^2v^4)$, $\mathcal{O}(o^4v^2)$, and $\mathcal{O}(o^3v^3)$, respectively. The convergence of the $\text{MP}x$ series for energies is slow in practice and not theoretically guaranteed and therefore higher-order methods than MP2 are traditionally disfavored relative to methods which scale similarly ($\mathcal{O}(o^2v^4)$ for MP3 vs iterative $\mathcal{O}(o^2v^4)$ for CCSD, for example). The development of a modified version of MP3 to improve upon this cost-benefit trade off is presented in Ch. 4.

1.4 Density Functional Theory

In the previous section we discussed the use of several correlated wavefunctions to improve upon the accuracy of HF for energies and properties at the cost of increased computational scaling and therefore limited system size. A method with similar computational scaling to HF that accounts for electron correlation is therefore an attractive proposition. Density functional theory (DFT) provides an answer to this proposition and has therefore become the most widely utilized electronic structure method in chemistry, physics, and material science.

Basic Principles

Returning to the electronic Schrödinger equation, we see that the exact ground state energy as a functional of the wavefunction is given by

$$E_0[\Psi_0] = \min_{\Psi} \langle \Psi | \hat{H} | \Psi \rangle. \tag{1.116}$$

The electronic Hamiltonian \hat{H} uniquely determines the ground state energy and properties of the system. \hat{H} , in turn, is uniquely determined by the total number of electrons n and the external potential $v_{\text{ext}}(\mathbf{r})$, which for a molecule is the field of the nuclei given by

$$v_{\text{ext}}(\mathbf{r}) = - \sum_A^M \frac{Z_A}{|\mathbf{r} - \mathbf{R}_A|}. \tag{1.117}$$

As the name density functional theory suggests, the premise of DFT is the ground state energy of a system is a functional of the real-space electron density $\rho(\mathbf{r})$,

$$E_0 = E_0[\rho(\mathbf{r})], \quad (1.118)$$

where

$$\rho(\mathbf{r}) = n \iint \cdots \int |\Psi(\mathbf{x}_1, \mathbf{x}_2, \dots, \mathbf{x}_n)|^2 d\omega_1 d\mathbf{x}_2 \dots d\mathbf{x}_n. \quad (1.119)$$

Given that the ground state energy E_0 is uniquely determined by n and $v_{\text{ext}}(\mathbf{r})$, Eq. 1.118 holds if $\rho(\mathbf{r})$ uniquely defines n and $v_{\text{ext}}(\mathbf{r})$. The fact $\rho(\mathbf{r})$ uniquely defines n is straightforward to demonstrate:

$$n = \int \rho(\mathbf{r}) d\mathbf{r} \quad (1.120)$$

Pierre Hohenberg and Walter Kohn published two important theorems in a 1964 article proving $\rho(\mathbf{r})$ uniquely defines $v_{\text{ext}}(\mathbf{r})$ [42]. The first of these (HK1) proves a one-to-one mapping between the ground state density and the external potential by contradiction. For two distinct Hamiltonians

$$\begin{aligned} \hat{H}^A &= \hat{T}_e + \hat{V}_{ee} + \hat{V}_{Ne}^A \\ \hat{H}^B &= \hat{T}_e + \hat{V}_{ee} + \hat{V}_{Ne}^B \end{aligned} \quad (1.121)$$

with corresponding ground state wavefunctions $|\Psi_0^A\rangle$ and $|\Psi_0^B\rangle$, suppose that the wavefunction of each gives the same density $\rho(\mathbf{r})$. Using Eq. 1.116 we may construct a statement of the variational principle for each Hamiltonian by measuring its expectation value with the wavefunction of the other:

$$\begin{aligned} \langle \Psi_0^A | \hat{H}^A | \Psi_0^A \rangle &< \langle \Psi_0^B | \hat{H}^A | \Psi_0^B \rangle \\ \langle \Psi_0^B | \hat{H}^B | \Psi_0^B \rangle &< \langle \Psi_0^A | \hat{H}^B | \Psi_0^A \rangle. \end{aligned} \quad (1.122)$$

Expanding \hat{H}^A and \hat{H}^B yields

$$\begin{aligned} \langle \Psi_0^A | \hat{T}_e + \hat{V}_{ee} + \hat{V}_{Ne}^A | \Psi_0^A \rangle &< \langle \Psi_0^B | \hat{T}_e + \hat{V}_{ee} + \hat{V}_{Ne}^A | \Psi_0^B \rangle \\ \langle \Psi_0^B | \hat{T}_e + \hat{V}_{ee} + \hat{V}_{Ne}^B | \Psi_0^B \rangle &< \langle \Psi_0^A | \hat{T}_e + \hat{V}_{ee} + \hat{V}_{Ne}^B | \Psi_0^A \rangle, \end{aligned} \quad (1.123)$$

$$\langle \Psi_0^A | \hat{T}_e + \hat{V}_{ee} | \Psi_0^A \rangle + \int v_{\text{ext}}^A(\mathbf{r})\rho(\mathbf{r})d\mathbf{r} < \langle \Psi_0^B | \hat{T}_e + \hat{V}_{ee} | \Psi_0^B \rangle + \int v_{\text{ext}}^A(\mathbf{r})\rho(\mathbf{r})d\mathbf{r} \quad (1.124)$$

$$\langle \Psi_0^B | \hat{T}_e + \hat{V}_{ee} | \Psi_0^B \rangle + \int v_{\text{ext}}^B(\mathbf{r})\rho(\mathbf{r})d\mathbf{r} < \langle \Psi_0^A | \hat{T}_e + \hat{V}_{ee} | \Psi_0^A \rangle + \int v_{\text{ext}}^B(\mathbf{r})\rho(\mathbf{r})d\mathbf{r},$$

$$\begin{aligned} \langle \Psi_0^A | \hat{T}_e + \hat{V}_{ee} | \Psi_0^A \rangle &< \langle \Psi_0^B | \hat{T}_e + \hat{V}_{ee} | \Psi_0^B \rangle \\ \langle \Psi_0^B | \hat{T}_e + \hat{V}_{ee} | \Psi_0^B \rangle &< \langle \Psi_0^A | \hat{T}_e + \hat{V}_{ee} | \Psi_0^A \rangle. \end{aligned} \quad (1.125)$$

Comparing the two inequalities in 1.125 demonstrates the contradiction, therefore there exists a one-to-one mapping between $\rho(\mathbf{r})$ and $v_{\text{ext}}(\mathbf{r})$. HKI therefore allows for the expression of E_0 as a functional of $\rho(\mathbf{r})$,

$$E_0[\rho(\mathbf{r})] = \langle \Psi_0 | \hat{T}_e + \hat{V}_{ee} | \Psi_0 \rangle + \int v_{\text{ext}}(\mathbf{r})\rho(\mathbf{r})d\mathbf{r} \quad (1.126)$$

$$= F_{\text{HK}}[\rho(\mathbf{r})] + \int v_{\text{ext}}(\mathbf{r})\rho(\mathbf{r})d\mathbf{r} \quad (1.127)$$

where $F_{\text{HK}}[\rho(\mathbf{r})]$ is the Hohenberg-Kohn functional and is independent of the external potential. The second Hohenberg-Kohn theorem (HKII) provides a variational principle with respect to a trial density $\tilde{\rho}(\mathbf{r})$:

$$E_0[\rho(\mathbf{r})] = E_{v_{\text{ext}}}[\rho(\mathbf{r})] < E_{v_{\text{ext}}}[\tilde{\rho}(\mathbf{r})] \quad (1.128)$$

To prove HKII, we begin by with a wavefunction $|\tilde{\Psi}_0\rangle$ that corresponds to the ground state wavefunction of a Hamiltonian \tilde{H} with external potential $\tilde{v}_{\text{ext}}(\mathbf{r})$ and corresponds to a density $\tilde{\rho}(\mathbf{r})$. Beginning from the Eq. 1.116, we take the expectation value of the Hamiltonian of interest with $|\tilde{\Psi}_0\rangle$:

$$\langle \Psi_0 | \hat{H} | \Psi_0 \rangle < \langle \tilde{\Psi}_0 | \hat{H} | \tilde{\Psi}_0 \rangle \quad (1.129)$$

$$F_{\text{HK}}[\rho(\mathbf{r})] + \int v_{\text{ext}}(\mathbf{r})\rho(\mathbf{r})d\mathbf{r} < F_{\text{HK}}[\tilde{\rho}(\mathbf{r})] + \int v_{\text{ext}}(\mathbf{r})\tilde{\rho}(\mathbf{r})d\mathbf{r} \quad (1.130)$$

$$E_0[\rho(\mathbf{r})] = E_{v_{\text{ext}}}[\rho(\mathbf{r})] < E_{v_{\text{ext}}}[\tilde{\rho}(\mathbf{r})] \quad (1.131)$$

HKII therefore states that the ground state energy is found via minimization with respect to trial densities $\tilde{\rho}(\mathbf{r})$. However, in the derivation of HKI and HKII, the density has been assumed to come from the ground state wavefunction corresponding to a Hamiltonian with a valid external potential; a condition known as v -representability. Unfortunately, the conditions that guarantee v -representability of a trial density $\tilde{\rho}(\mathbf{r})$ are unknown and therefore a search for a density that minimizes the energy functional may result in a non- v -representable density, invalidating the assumption of the variational principle.

The Levy constrained search formula, however, provides a loosening of the v -representability constraint via conversion to an n -representability constraint[43]. The n -representability conditions for a real-space density require the density to be continuous, positive semidefinite, integrate to n , and come from an antisymmetrized wavefunction. While the mapping of wavefunction to density is one-to-one via integration of the modulus squared, the inverse mapping from a n -representable density to an antisymmetrized wavefunction is (infinitely) many-to-one, that is many antisymmetrized wavefunctions integrate to the same density. For a given n -representable ground state density $\rho_n(\mathbf{r})$, the set of antisymmetrized wavefunctions which yield $\rho_n(\mathbf{r})$ by integration is $\{|\Psi_k^{\rho_n}\rangle\}$. Using one of these wavefunctions as a

trial wavefunction yields

$$\langle \Psi_0^{\rho_n} | \hat{H} | \Psi_0^{\rho_n} \rangle \leq \langle \Psi_k^{\rho_n} | \hat{H} | \Psi_k^{\rho_n} \rangle \quad (1.132)$$

$$\langle \Psi_0^{\rho_n} | \hat{T}_e + \hat{V}_{ee} | \Psi_0^{\rho_n} \rangle + \int v_{\text{ext}}(\mathbf{r}) \rho_n(\mathbf{r}) d\mathbf{r} \leq \quad (1.133)$$

$$\langle \Psi_k^{\rho_n} | \hat{T}_e + \hat{V}_{ee} | \Psi_k^{\rho_n} \rangle + \int v_{\text{ext}}(\mathbf{r}) \rho_n(\mathbf{r}) d\mathbf{r}$$

$$\langle \Psi_0^{\rho_n} | \hat{T}_e + \hat{V}_{ee} | \Psi_0^{\rho_n} \rangle \leq \langle \Psi_k^{\rho_n} | \hat{T}_e + \hat{V}_{ee} | \Psi_k^{\rho_n} \rangle. \quad (1.134)$$

For a given $\rho_n(\mathbf{r})$ we can then define a functional $F[\rho_n(\mathbf{r})]$ where

$$F[\rho_n(\mathbf{r})] = \min_{\{\Psi_k^{\rho_n}\}} \langle \Psi_k^{\rho_n} | \hat{T}_e + \hat{V}_{ee} | \Psi_k^{\rho_n} \rangle. \quad (1.135)$$

When $\rho_n(\mathbf{r}) = \rho(\mathbf{r})$, this functional is identical to $F_{\text{HK}}(\rho(\mathbf{r}))$. Having loosened the v -representability constraint, the energy functional for an n -representable density is given by

$$E[\rho_n(\mathbf{r})] = F[\rho_n(\mathbf{r})] + \int v_{\text{ext}}(\mathbf{r}) \rho_n(\mathbf{r}) d\mathbf{r} \quad (1.136)$$

and the ground state energy

$$E_0[\rho(\mathbf{r})] = \min_{\rho_n} E[\rho_n(\mathbf{r})] \quad (1.137)$$

can then be thought of as a double minimization where the inner minimization gives the ground state for a given n -representable density and the outer minimization minimizes over all n -representable densities.

Having established that the ground state energy can be written as a functional of the density, the next step is finding a representation for $E[\rho(\mathbf{r})]$. Decomposing the $F[\rho(\mathbf{r})]$ into its components yields

$$E[\rho(\mathbf{r})] = T_e[\rho(\mathbf{r})] + V_{ee}[\rho(\mathbf{r})] + \int v_{\text{ext}}(\mathbf{r}) \rho(\mathbf{r}) d\mathbf{r}. \quad (1.138)$$

The electron-electron interaction functional can further be broken down into classical ($J[\rho(\mathbf{r})]$) and non-classical ($K[\rho(\mathbf{r})]$) components:

$$J[\rho(\mathbf{r})] = \frac{1}{2} \iint \frac{\rho(\mathbf{r}) \rho(\mathbf{r}')}{|\mathbf{r} - \mathbf{r}'|} d\mathbf{r} d\mathbf{r}' \quad (1.139)$$

$$K[\rho(\mathbf{r})] = V_{ee}[\rho(\mathbf{r})] - J[\rho(\mathbf{r})]. \quad (1.140)$$

Plugging these definitions into Eq. 1.138 yields

$$E[\rho(\mathbf{r})] = T_e[\rho(\mathbf{r})] + \frac{1}{2} \iint \frac{\rho(\mathbf{r}) \rho(\mathbf{r}')}{|\mathbf{r} - \mathbf{r}'|} d\mathbf{r} d\mathbf{r}' + K[\rho(\mathbf{r})] + \int v_{\text{ext}}(\mathbf{r}) \rho(\mathbf{r}) d\mathbf{r}. \quad (1.141)$$

At this point $T_e[\rho(\mathbf{r})]$ and $K[\rho(\mathbf{r})]$ are the only terms without a known exact form and must therefore be approximated. An accurate approximate representation of $T_e[\rho(\mathbf{r})]$ is especially important for chemical applications as it's contribution is of the same magnitude as the energy. The Thomas-Fermi model[44, 45], which is exact for the uniform electron gas (UEG), has the following form for $T_e[\rho(\mathbf{r})]$:

$$T_e[\rho(\mathbf{r})] = \frac{3}{10} (3\pi^2)^{2/3} \int \rho(\mathbf{r})^{5/3} d\mathbf{r}. \quad (1.142)$$

Given the non-uniformity of the electron density within molecules, the Thomas-Fermi model understandably breaks down and is unable to properly describe chemical bonding. Accurate description of the kinetic energy functional is a yet unaccomplished task in the application of orbital-free DFT to the chemistry of atoms and molecules.

In 1965 Kohn and Sham[46] developed a method to circumvent the kinetic energy functional through the introduction of a Slater determinant of n spin orbitals. This Kohn-Sham (KS) determinant describes a fictitious non-interaction ($V_{ee} = 0$) system of electrons and integrates to give the same density $\rho(\mathbf{r})$ as the exact wavefunction. The kinetic energy $T_{e,\text{KS}}$, associated with the KS determinant is computed in a nearly identical fashion to the Hartree-Fock:

$$T_{e,\text{KS}} = \sum_i^n \left\langle \chi_i \left| -\frac{1}{2} \hat{\nabla}_i^2 \right| \chi_i \right\rangle. \quad (1.143)$$

$T_{e,\text{KS}}$ is a functional of $\rho(\mathbf{r})$ because the KS determinant is the solution to a modified Schrödinger equation whose external potential $v_{\text{ext}}(\mathbf{r})$ maps to $\rho(\mathbf{r})$. This allows us to write the exchange-correlation functional $E_{xc}[\rho(\mathbf{r})]$ as the sum of non-classical electron-electron interaction $K[\rho(\mathbf{r})]$ and the difference between the exact and KS kinetic energies:

$$E_{xc}[\rho(\mathbf{r})] = K[\rho(\mathbf{r})] + T_e[\rho(\mathbf{r})] - T_{e,\text{KS}}[\rho(\mathbf{r})]. \quad (1.144)$$

The overall KS energy functional is given by

$$E_{\text{KS}}[\rho(\mathbf{r})] = T_{e,\text{KS}}[\rho(\mathbf{r})] + J[\rho(\mathbf{r})] + \int v_{\text{ext}}(\mathbf{r})\rho(\mathbf{r})d\mathbf{r} + E_{xc}[\rho(\mathbf{r})]. \quad (1.145)$$

While Eq. 1.145 is formally exact, in practice approximations are made to the form of the exchange-correlation functional $E_{xc}[\rho(\mathbf{r})]$, which is further broken down into exchange ($E_x[\rho(\mathbf{r})]$) and correlation ($E_c[\rho(\mathbf{r})]$) functionals.

In analogy to the Hartree-Fock equations (Eq. 1.28), the Kohn-Sham equations can be recast as a set of effective one-electron equations

$$\hat{f}_\sigma^{\text{KS}} |\psi_{i,\sigma}\rangle = \epsilon_{i,\sigma} |\psi_{i,\sigma}\rangle \quad (1.146)$$

where the Fock operator is of the form

$$f_\sigma^{\text{KS}}(\mathbf{r}) = h(\mathbf{r}) + \sum_{\sigma' \in \{\alpha, \beta\}} \int \frac{\rho_{\sigma'}(\mathbf{r}')}{|\mathbf{r} - \mathbf{r}'|} d\mathbf{r}' + v_{xc,\sigma}(\mathbf{r}) \quad (1.147)$$

and the exchange-correlation potential

$$v_{xc,\sigma}(\mathbf{r}) = \frac{\delta E_{xc}[\rho_\alpha(\mathbf{r}), \rho_\beta(\mathbf{r})]}{\delta \rho_\sigma(\mathbf{r})} \quad (1.148)$$

is the functional derivative of the exchange-correlation energy with respect to the density. Expansion of Eq. 1.146 in a basis of AOs yields a generalized eigenvalue problem that is the KS equivalent of the Roothaan equations in HF theory (Eq. 1.34):

$$\mathbf{F}_\sigma^{\text{KS}} \mathbf{C}_\sigma = \mathbf{S} \mathbf{C}_\sigma \epsilon_\sigma \quad (1.149)$$

where

$$\mathbf{F}_\sigma = \mathbf{h} + \mathbf{J} + \mathbf{V}_{xc,\sigma} \quad (1.150)$$

and

$$V_{xc,\mu\nu,\sigma} = \langle \phi_\mu | \hat{v}_{xc,\sigma} | \phi_\nu \rangle. \quad (1.151)$$

The 1PDMs, \mathbf{P}_σ , for KS-DFT are defined identically to those for HF (Eq. 1.40) and bear an obvious connection to the spin densities $\rho_\sigma(\mathbf{r})$ (Eq. 1.39). The KS-DFT energy in terms of these density matrices is

$$E_{\text{KS}} = \text{Tr}[(\mathbf{P}_\alpha + \mathbf{P}_\beta)(\mathbf{h} + \mathbf{J})] + E_{xc}[\mathbf{P}_\alpha, \mathbf{P}_\beta]. \quad (1.152)$$

From this expression one notices that the Fock matrices \mathbf{F}_σ are the matrix derivative of E_{KS} with respect to the corresponding 1PDMs, \mathbf{P}_σ . The same SCF approach is used to optimize the KS orbitals and densities as are used in optimizing the HF orbitals, albeit with a modified Fock matrix build and energy computation. Generally speaking the quantities $E_{xc}[\mathbf{P}_\alpha, \mathbf{P}_\beta]$ and \mathbf{V}_{xc} are expressed as integrals over real-space evaluated via quadrature on a grid. The asymptotic computational scaling of KS-DFT is $\mathcal{O}(N^3)$ due to the diagonalization of \mathbf{F}_{xc} and can in principle be applied to systems of hundreds of atoms.

A more in-depth derivation of both Hohenberg-Kohn and Kohn-Sham DFT can be found in Ref. [47].

Modern Density Functional Theory

Over the last 30 years Kohn-Sham DFT (hereafter referred to as DFT unless specified) has become the most widely used tool in electronic structure theory. This has been accompanied by a proliferation of approximate exchange-correlation functionals, both by *ab initio* approaches, which design functionals to meet criteria of the exact exchange-correlation functional, and semi-empirical approaches, which fit a parameterized functional to higher-level computational or experimental data. The levels of approximation used in defining these functional are arranged in a hierarchy, originally referred as “Jacob’s Ladder” by Perdew[48], where ascending the ladder adds ingredients to the exchange-correlation functional and brings one closer to the “heaven” of chemical accuracy (typically thought of as errors less than 1

kcal mol⁻¹). Exchange-correlation functionals are split into an exchange functional E_x and a correlation functional E_c which assume the general forms

$$E_x = \sum_{\sigma \in \{\alpha, \beta\}} \int e_{x, \sigma}(\mathbf{r}) d\mathbf{r} \quad (1.153)$$

$$E_c = \int (\rho_\alpha(\mathbf{r}) + \rho_\beta(\mathbf{r})) \epsilon_c(\mathbf{r}) d\mathbf{r} \quad (1.154)$$

where $e_{x, \sigma}(\mathbf{r})$ is the exchange energy density for electrons of spin σ and $\epsilon_c(\mathbf{r})$ is the correlation energy per electron. From these definitions we observe that exchange interactions only occur between same-spin electrons while correlation interaction occur between both same-spin and opposite-spin electrons. From this point, in our notation we suppress the dependence of the spin-densities on the real-space coordinates \mathbf{r} .

Local spin-density approximation (LSDA) functionals occupy the first rung of Jacob's Ladder and are functionals of the spin-densities $\rho_\sigma(\mathbf{r})$

$$E_x^{\text{LSDA}}[\rho_\alpha, \rho_\beta] = \sum_{\sigma \in \{\alpha, \beta\}} \int e_{x, \sigma}(\rho_\sigma) d\mathbf{r} \quad (1.155)$$

$$E_c^{\text{LSDA}}[\rho_\alpha, \rho_\beta] = \int (\rho_\alpha + \rho_\beta) \epsilon_c(\rho_\alpha, \rho_\beta) d\mathbf{r}. \quad (1.156)$$

The LSDA exchange functional has an analytical form, known as the Slater-Dirac exchange functional E_x^{S} [49] that is exact for the UEG:

$$E_x^{\text{S}}[\rho_\alpha, \rho_\beta] = -C_x \sum_{\sigma \in \{\alpha, \beta\}} \int \rho_\sigma^{4/3} d\mathbf{r}. \quad (1.157)$$

The correlation functional for LSDA does not have an exact functional form and therefore approximations are made by fitting to quantum Monte-Carlo data[50], yielding among others the VWN5[51], PZ81[52], and PW92[53] correlation functionals. While able to predict binding behavior in molecules not captured by Thomas-Fermi DFT, LSDA has been shown to systematically overbind molecules relative to atoms. The inaccuracy of LSDA for describing molecular systems should come as little surprise, as the method is parameterized for the UEG and electrons in molecules are not uniformly distributed.

A method to improve upon the purely local nature of LSDA involves including information about the gradient of the spin densities $\nabla \rho_\sigma$ in order to better describe semi-local exchange and correlation effects. This generalized gradient approximation (GGA) is the second rung of Jacob's Ladder and has exchange and correlation functionals of the form

$$E_x^{\text{GGA}}[\rho_\alpha, \rho_\beta, |\nabla \rho_\alpha|^2, |\nabla \rho_\beta|^2] = \sum_{\sigma \in \{\alpha, \beta\}} \int e_{x, \sigma}(\rho_\sigma, |\nabla \rho_\sigma|^2) d\mathbf{r} \quad (1.158)$$

$$E_c^{\text{GGA}}[\rho_\alpha, \rho_\beta, |\nabla \rho_\alpha|^2, |\nabla \rho_\beta|^2, \nabla \rho_\alpha \cdot \nabla \rho_\beta] = \int (\rho_\alpha + \rho_\beta) \epsilon_c(\rho_\alpha, \rho_\beta, |\nabla \rho_\alpha|^2, |\nabla \rho_\beta|^2, \nabla \rho_\alpha \cdot \nabla \rho_\beta) d\mathbf{r}. \quad (1.159)$$

Popular GGA exchange-correlation functionals include the *ab initio* PBE (PBE exchange, PBE correlation)[54] and the semi-empirical BLYP (B88 exchange, LYP correlation)[55, 56].

Further improvement upon GGA exchange-correlation is achieved through the meta-generalized gradient approximation (meta-GGA), the third rung on Jacob's ladder. Increased semi-local information is included by incorporating either the kinetic energy spin-densities,

$$\tau_\sigma = \sum_i^{n_\sigma} |\nabla\psi_{\sigma,i}|^2 \quad (1.160)$$

or the Laplacians of the spin-densities $\nabla^2\rho_\sigma$ in the exchange and correlation functionals:

$$E_x^{\text{meta-GGA}}[\rho_\alpha, \rho_\beta, |\nabla\rho_\alpha|^2, |\nabla\rho_\beta|^2, \tau_\alpha, \tau_\beta] = \sum_{\sigma \in \{\alpha, \beta\}} \int e_{x,\sigma}(\rho_\sigma, |\nabla\rho_\sigma|^2, \tau_\sigma) d\mathbf{r} \quad (1.161)$$

$$E_c^{\text{meta-GGA}}[\rho_\alpha, \rho_\beta, |\nabla\rho_\alpha|^2, |\nabla\rho_\beta|^2, \nabla\rho_\alpha \cdot \nabla\rho_\beta, \tau_\alpha, \tau_\beta] = \int (\rho_\alpha + \rho_\beta) \epsilon_c(\rho_\alpha, \rho_\beta, |\nabla\rho_\alpha|^2, |\nabla\rho_\beta|^2, \nabla\rho_\alpha \cdot \nabla\rho_\beta, \tau_\alpha, \tau_\beta) d\mathbf{r}. \quad (1.162)$$

Popular meta-GGA exchange-correlation functionals include the *abinitio* TPSS[57] and SCAN[58] functionals and the semi-empirical M06-L[59] and MN15-L[60] functionals.

While the addition of terms into the exchange-correlation energy densities allows for more accurate treatment of chemical systems, semi-local density functionals exhibit three weakness that limit their universal applicability and accuracy: self-interaction error (SIE), poor treatment of long-range correlations, and failure to treat strongly correlated systems.

A simple to understand manifestation of SIE in DFT is seen when considering the neutral hydrogen atom. For this one electron system the exact electron-electron interaction term in the Hamiltonian, $\hat{V}_{ee} = \hat{J} + \hat{K}$, should be identically zero. Under the HF approximation, the Coulomb and exchange terms are equal in magnitude and opposite in sign and therefore cancel to give zero electron-electron interaction. For DFT, however, the non-classical part of \hat{V}_{ee} is folded into the exchange-correlation term and $J[\rho] + E_{xc}[\rho]$ is no longer identically zero. This means that the electrons in DFT "feel" themselves, contributing to the charge-delocalization error observed in DFT.

A possible solution to mediate this self-interaction error is the inclusion of some fraction of HF exact exchange, E_x^{HF} , into the exchange functional.

$$E_x^{\text{GH}} = c_x E_x^{\text{HF}} + (1 - c_x) E_x^{\text{DFT}} \quad (1.163)$$

These global hybrid (GH) density functional theory approaches belong to the fourth rung of Jacob's ladder and include explicit dependence on the occupied KS spin orbitals. Popular GH GGA exchange-correlation functionals include the B3LYP[61], B97[62], and PBE0[63] functionals, while popular GH meta-GGA exchange-correlation functionals include TPSSh[64], M06-2X[65], and MN15[66].

A more rigorous attempt at including HF exact exchange into the exchange functional is through the use of range-separated hybrid (RSH) functionals. In this approach, the Coulomb

interaction is separated into a long-range (lr) component and a short-range (sr) component through use of the error function and its complement, respectively:

$$\frac{1}{r_{12}} = \frac{\text{erf}(\omega r_{12})}{r_{12}} + \frac{\text{erfc}(\omega r_{12})}{r_{12}} \quad (1.164)$$

where the ω parameter determines how quickly the HF exact exchange ramps up. Within the RSH formalism the DFT exchange is similarly separated into long-range and short-range components; the long-range component usually being discarded such that the in the long-range SIE cancels. The semi-local nature of the DFT exchange makes it better suited for short range treatment, while a fraction of short-range HF exact exchange may also be included:

$$E_x^{\text{RSH}} = c_{x,\text{sr}} E_{x,\text{sr}}^{\text{HF}} + E_{x,\text{lr}}^{\text{HF}} + (1 - c_{x,\text{sr}}) E_{x,\text{sr}}^{\text{DFT}} \quad (1.165)$$

Popular examples of RSH exchange-correlation functionals include the CAM-B3LYP[67], ω B97X-D[68], and M11[69] functionals.

Addressing the lack of long-range correlations in DFT is necessary for application to weakly-bound systems. One proposed remedy for this issue is the use of dispersion-corrections that add an analytic potential function of the internuclear distance to the DFT energy. Grimme's empirical DFT-D methods[70–73] employ pre-computed coefficients for pairs of nuclei trained on higher levels of theory. The potential for the recent DFT-D4 dispersion correction[73] takes the form

$$E_{\text{D4}} = - \sum_{B>A} \sum_{k=6,8} s_k \frac{C_{AB}^{(k)}}{R_{AB}^k} f_{\text{damp},k}(R_{AB}) \quad (1.166)$$

where s_k is a functional dependent scaling factor, $C_{AB}^{(k)}$ are the pairwise coefficients, and $f_{\text{damp},k}(R_{AB})$ is a damping function that smoothly switches of the correction when the internuclear distance R_{AB} is small. Many forms of this damping function have been investigated[72–77]. The exchange-hole dipole moment (XDM) [78, 79] and Tkatchenko-Scheffler (TS) [80] compute these $C^{(k)}$ coefficients during a calculation from the electronic structure.

A less empirical method of introducing dispersion effects into DFT is the use of explicitly non-local correlation (NLC) functionals. These functionals couple the densities at points \mathbf{r} and \mathbf{r}' via the use of a NLC kernel $\Phi(\mathbf{r}, \mathbf{r}')$:

$$E_{\text{NLC}}[\rho] = \iint \rho(\mathbf{r}) \Phi(\mathbf{r}, \mathbf{r}') \rho(\mathbf{r}') d\mathbf{r} d\mathbf{r}'. \quad (1.167)$$

While E_{NLC} is expensive to evaluate due to the double quadrature, NLC functionals have seen increasing use, especially the two-parameter Vydrov-Van Voorhis kernel(VV10)[81]. Mardirossian and Head-Gordon have recently designed three minimally-parameterized semi-empirical functionals that are trained with this NLC functional: ω B97X-V[82], a RSH GGA, B97M-V[83], a semi-local meta-GGA, and ω B97M-V[84], a RSH meta-GGA. Extensive assessment of these and other functionals on an enormous composite database has demonstrated these functionals to be the best performing in their corresponding categories[85].

The accuracy of these functionals has inspired their employment in this thesis to characterize the critical points along reactive pathways (Ch. 2 and 3), to benchmark the performance of reactive molecular dynamics models (Ch. 3), and as generators of reference orbitals for correlated calculations (Ch. 5).

Double-hybrid DFT methods, the fifth rung of Jacob’s Ladder, provide a third way to incorporate missing correlation in semi-local DFT. The functionals incorporate a scaled second-order perturbative correction on top of the KS Slater determinant and therefore depend on the virtual KS spin orbitals $\{\chi_a\}$. Popular functionals in this rung include B2PLYP[86], XYG3[87], and ω B97M(2) [88].

Despite corrections to the SIE and dispersion, existing density functionals still struggle to describe strongly correlated systems. This is by virtue of the single-determinant nature of both HF and DFT to describe systems which are inherently multireference. In passing, we mention the use of Hubbard model-like correction[89, 90] and multiconfigurational[91, 92] attempts to solve these problems, though this is still an area where there is much to be improved.

1.5 Outline

Chapter 2

Mechanisms of formation of complex organosilicon molecules have remained elusive until recently, despite the ubiquity of such species in the circumstellar environments of carbon rich stars. These organosilicon molecules, among them precursors to silicon carbide grains, account for up to 80% of the carbon and silicon budgets in the interstellar medium as ejecta from the circumstellar shells. In this work we provide a combined computational, experimental, and modeling approach to study the synthesis of cyclic silicon tricarbon species (*c*-SiC₃), which has been observed in the circumstellar envelope of the asymptotic giant branch (AGB) star IRC+10216. Both experimental and computational approaches suggest reactions of hydrocarbons methylacetylene (CH₃CCH) and allene (H₂CCCH₂) with excited state silicon atoms (Si(¹D)), all species present in the inner envelope of IRC+10216, lead to the formation of SiC₃H₂ molecules via molecular hydrogen loss. Further computational studies suggest that these SiC₃H₂ molecules can undergo a photodissociation-mediated dehydrogenation to form bare *c*-SiC₃. This mechanism of the formation of silicon tricarbon via a two-step neutral-neutral reaction followed by photodissociation offers a competing explanation for the origin of organosilicon molecules in the circumstellar medium. This work has been published in *The Proceedings of the National Academy of Sciences of the United States of America*[93].

Chapter 3

A thorough understanding of the kinetics and dynamics of combusting mixtures is of considerable interest, especially in regimes beyond the reach of current experimental validation. The ReaxFF reactive force field method has provided a way to simulate large-scale systems of hydrogen combustion via a parameterized potential that can simulate bond breaking. This modeling approach has been applied to hydrogen combustion, as well as myriad other reactive chemical systems. In this work, we benchmark the performance of several common parameterizations of this potential against higher-level quantum mechanical (QM) approaches. We demonstrate instances where these parameterizations of the ReaxFF potential fail both quantitatively and qualitatively to describe reactive events relevant for hydrogen combustion systems. This work has been published in *The Journal of Physical Chemistry A*[94].

Chapter 4

We develop and test methods that include second and third-order perturbation theory (MP3) using orbitals obtained from regularized orbital-optimized second-order perturbation theory, κ -OOMP2, denoted as MP3: κ -OOMP2. Testing MP3: κ -OOMP2 shows RMS errors that are 1.7 to 5 times smaller than MP3 across 7 data sets. To do still better, empirical training of the scaling factors for the second- and third-order correlation energies and the regularization parameter on one of those data sets led to an unregularized scaled ($c_2 = 1.0$; $c_3 = 0.8$) denoted as MP2.8: κ -OOMP2. MP2.8: κ -OOMP2 yields significant additional improvement over MP3: κ -OOMP2 in 4 of 6 test data sets on thermochemistry, kinetics, and noncovalent interactions. Remarkably, these two methods outperform coupled cluster with singles and doubles in 5 of the 7 data sets considered, at greatly reduced cost (no $\mathcal{O}(N^6)$ iterations). This work has been in *The Journal of Physical Chemistry Letters*[95].

Chapter 5

While CCSD(T) with spin-restricted Hartree-Fock (RHF) orbitals has long been lauded for its ability to accurately describe closed-shell interactions, the performance of CCSD(T) on open-shell species is much more erratic, especially when using a spin-unrestricted HF (UHF) reference. Previous studies have shown improved treatment of open-shell systems when a non-HF set of molecular orbitals, like Brueckner or Kohn-Sham density functional theory (DFT) orbitals, is used as a reference. Inspired by the success of regularized orbital-optimized second-order Møller-Plesset perturbation theory (κ -OOMP2) orbitals as reference orbitals for MP3, we investigate the use of κ -OOMP2 orbitals and various DFT orbitals as reference orbitals for CCSD(T) calculations of the corrected ground-state harmonic vibrational frequencies of a set of 36 closed-shell (29 neutrals, 6 cations, 1 anion) and 59 open-shell diatomic species (38 neutrals, 15 cations, 6 anions). The aug-cc-pwCVTZ basis set is used for all calculations. The use of κ -OOMP2 orbitals in this context alleviates difficult cases observed for both UHF orbitals and OOMP2 orbitals. Removing 2 multireference systems and

12 systems with ambiguous experimental data leaves a pruned data set. Overall performance on the pruned data set highlights CCSD(T) with a B97 orbital reference (CCSD(T):B97), CCSD(T) with a κ -OOMP2 orbital reference (CCSD(T): κ -OOMP2), and CCSD(T) with a B97M-rV orbital reference (CCSD(T):B97M-rV) with RMSDs of 8.48 cm^{-1} and 8.50 cm^{-1} , and 8.75 cm^{-1} respectively, outperforming CCSD(T):UHF by nearly a factor of 5. Moreover, the performance on the closed- and open-shell subsets show these methods are able to treat open-shell and closed-shell systems with comparable accuracy and robustness. The use of κ -OOMP2 orbitals has also proven useful in diagnosing multireference character that can hinder the reliability of CCSD(T).

Chapter 2

Modeling of Gas Phase Formation of $c\text{-SiC}_3$ Molecules in the Circumstellar Medium of Carbon Stars

This chapter was adapted with permission from Yang T.; Bertels, L.; Dangi, B. B.; Li, X.; Head-Gordon, M.; Kaiser, R. I. Gas phase formation of $c\text{-SiC}_3$ molecules in the circumstellar envelope of carbon stars. *Proc. Natl. Acad. Sci. U.S.A.* **2019**, 116, 14471-14478.

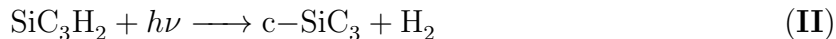
2.1 Introduction

Astronomical observations of the carbon-rich asymptotic giant branch (AGB) star IRC+10216 (CW Leo), coupled with astrochemical modeling and gas-phase reactions networks of ion-molecule[96–101] and neutral-neutral[99, 100, 102–106] reactions has furthered the understanding of the dynamic chemical environment of carbon-rich circumstellar envelopes. However for many silicon carbide species, including cyclic silicon dicarbide ($c\text{-SiC}_2$)[107], and bicyclic silicon tricarbonide ($c\text{-SiC}_3$), and linear silicon tetracarbide (SiC_4)[108], these modeling efforts underestimate their fractional abundance relative to observation by up to two orders of magnitude[109, 110]. From this discrepancy, it is clear that the mechanisms of organosilicon formation in the circumstellar medium are incomplete[110–112], despite the roles these molecules have in furnishing silicon and carbon in the interstellar medium[113, 114] and in the formation of silicon carbide grains.

Current astrochemical models propose that the initial carbon silicon coupling occurs in the inner envelope of carbon stars. In this region, shocks initiated by pulsations of the central star give rise to temperatures in excess of 3500 K[114] and generate metastable species such as silyldiyne radicals and excited state silicon atoms[115, 116]. These highly reactive fragments can then react with hydrocarbon molecules to form parent organosilicon species[115, 117]. From the inner envelope, stellar winds are proposed to drive these organosilicon species to the outer envelope. In this region, these parent organosilicon molecules can be photolyzed

to silicon carbides by the interstellar UV field, with carbon-hydrogen bonds (roughly 400 kJ mol⁻¹) being preferentially cleaved over silicon-carbon double bonds (450-550 kJ mol⁻¹). As these mechanisms have not been confirmed to date, deeper understanding of the molecular dynamics of circumstellar envelopes is required to concretely explain the genesis of interstellar silicon carbides.

In this work, we combine high-level *ab initio* calculations with crossed molecular beam experiments and astrochemical modeling to provide a mechanism for the formation of silicon tricarbide (*c*-SiC₃) observed in the circumstellar medium of the carbon star IRC+10216. The reaction of excited state silicon atoms (Si(¹D)) with methylacetylene (CH₃CCH) and allene (H₂CCCH₂) to form SiC₃H₂ isomers (reaction **I**) was explored computationally and experimentally under single collision conditions, mimicking the environment of the inner envelope of IRC+10216. Further photolysis of these parent SiC₃H₂ molecules in the outer envelope to form bicyclic silicon tricarbide (*c*-SiC₃) via dehydrogenation (reaction **II**) was explored computationally.



2.2 Methods

A detailed accounting of the materials and methods used in the experimental study can be found in Ref. 93.

Structures for the reactants, intermediates, and products were obtained via geometry optimizations and frequency calculations using the ω B97X-V [118] density functional and the cc-pVTZ basis set [119, 120]. This functional is known to be among the most accurate density functionals for thermochemistry and reaction barrier heights [85]. Transition state structures were calculated using the freezing string method [121] to generate an initial structure and Hessian which were then refined by a transition state search using the partitioned-rational function optimization eigenvector following method [122] and followed by a frequency calculation. These calculations were also carried out at the ω B97X-V/cc-pVTZ level of theory. Vibrational analysis was used to confirm that the minima have no imaginary frequencies and the transition states have only one imaginary frequency each, as well as to calculate harmonic zero-point energy corrections for the structures. Density functional theory calculations were all carried out using an ultra-fine integration grid consisting of 99 radial points and 590 angular points. To further improve the accuracy of the results for relative energies and barrier heights, single point energy calculations were performed at the minima and transition states. The objective was to approach the complete basis set (CBS) limit using coupled cluster with single, double, and perturbative triple excitations (CCSD(T)) [25]. To this end, CCSD(T)/cc-pVTZ calculations using a frozen core approximation were combined with second-order Møller-Plesset perturbation theory using the resolution of the identity approximation (RI-MP2) [29, 30], in larger basis sets. The working expression used for the

energy of a given structure was:

$$E(\text{CCSD(T)/CBS}) = E(\text{HF/cc-pV5Z}) + E^{\text{corr}}(\text{RI-MP2/CBS}_{3,4,5}) \\ + E^{\text{corr}}(\text{CCSD(T)/cc-pVTZ}) - E^{\text{corr}}(\text{RI-MP2/cc-pVTZ}) \\ + ZPE(\omega\text{B97X-V/cc-pVTZ}).$$

$E^{\text{corr}}(\text{RI-MP2/CBS}_{3,4,5})$ is the extrapolated RI-MP2 correlation energy using the cc-pVTZ, cc-pVQZ, and cc-pV5Z basis sets to fit

$$E^{\text{corr}}(\text{RI-MP2/cc-pVNZ}) = E^{\text{corr}}(\text{RI-MP2/CBS}_{3,4,5}) + AN^{-3},$$

where N denotes the cardinal number for the cc-pVNZ basis sets [123]. These CCSD(T)/CBS energies are typically accurate to about 3-4 kJ mol⁻¹. The energy of the silicon atom in the ¹D state was calculated by computing the energy of the atom on its triplet ground state and corrected with an experimentally derived triplet-singlet gap (75.4 kJ mol⁻¹) taken from the National Institute of Standards and Technology Atomic Spectra Database. Time-dependent density functional theory[124] calculations were also carried out on select SiC₃H₂ species to search for electronic excited states corresponding to the absorption of a Lyman- α photon. All calculations were performed using the Q-Chem suite of electronic structure programs [125]. For further analysis, the RRKM [126] rate constants for select dehydrogenation pathways of SiC₃H₄ isomers were approximated using a Beyer-Swinehart direct state counting algorithm [127] modified to include vibrational tunneling as suggested by Miller [128].

2.3 Results and discussion

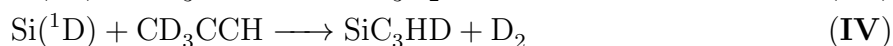
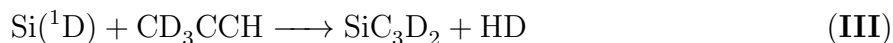
Experimental Results: Summary of Crossed Molecular Beam Studies

Laboratory Frame

The reactions of excited-state silicon atoms (Si(¹D)) with methylacetylene (CH₃CCH) and allene (H₂CCCH₂) were explored via molecular crossed beam experiments under single collision conditions at a collision energy of 30 ± 2 kJ mol⁻¹. The silicon source was generated via photolysis of 0.5% disilane seeded in helium. In addition to excited state silicon, this primary molecular beam also included ground state silicon (Si(³P)) and the silyldiyne radical (X²Π). Ground state silicon atoms do not react with the hydrocarbons explored here, while the reactions of the silyldiyne radical with allene and methylacetylene have been studied previously[129, 130]. These prior studies allow us to distinguish between signal arising from reactions of the silyldiyne radical and the excited-state silicon atom with methylacetylene and allene in the present study. Products of these reactions were ionized via electron impact (80 eV) and detected by a rotatable quadrupole mass-spectrometer, with time of flight (TOF) spectra gathered from analysis of the mass-to-charge ratios (*m/z*) and velocities of the ionized fragments[131].

For both the methylacetylene and allene systems reactive signals were observed at m/z of 68, 67, and 66, corresponding to SiC₃H₄⁺, SiC₃H₃⁺, and SiC₃H₂⁺, respectively. Previous studies have shown that the signal at m/z 68 originated from the reaction of methylacetylene and allene with the silyldyne radical (SiH(X²Π)) to form 2-methyl-1-silacycloprop-2-enylidene (*c*-SiC₃H₄) via an indirect scattering mechanism and atomic hydrogen ejection[129, 130]. For both reactions, scaling of the signal at m/z 67 reveals it to be indistinguishable from the signal at m/z 68, demonstrating that this signal arises from dissociative ionization of the SiC₃H₄ fragments. The reactive signal at m/z 66, however, is distinct from the signals at m/z 68 and 67, suggesting that this fragment does not arise solely from the dissociative ionization of SiC₃H₄ but also comes from the product(s) of indirect scattering reactions between excited state silicon atom and methylacetylene and allene, yielding SiC₃H₂ isomer(s) via molecular hydrogen elimination (reaction **I**). Fig. 2.4, taken from Ref. 93, presents the laboratory angle distribution and select TOF spectra for m/z 66 corresponding to SiC₃H₂⁺ for both the allene and methylacetylene reactions. The wide distributions and symmetries about the center-of-mass angles in both the methylacetylene and allene cases suggests indirect mechanisms involving SiC₃H₄ intermediates. The TOF spectra at m/z 66 can be fit to two channels in each case: a major channel comprising approximately 90% of the scattering signal accounting for the reactive scattering of Si(¹D) and C₃H₄ and a minor channel corresponding to the dissociative ionization of the SiC₃H₄ products of the SiH-C₃H₄ scattering dynamics explored previously[129, 130]. The laboratory angular distributions of the TOF spectra presented in Fig. 2.1 show a spread over 45° and a center-of-mass (CM) angle of 33° for both reactions. The near forward-backward symmetry of these distributions suggest these reactions occur via indirect scattering mechanisms involving SiC₃H₄ intermediates.

In order to further investigate the mechanism for molecular hydrogen loss in the Si(¹D)-C₃H₄ systems (reaction **I**), molecular cross beam experiments were carried out using partially deuterated D3-methylacetylene [CD₃CCH,(X¹A₁)]. These reactions can proceed either via HD loss to form SiC₃D₂ (reaction **III**) or via D₂ loss to form SiC₃HD (reaction **IV**), leading to TOF signals at m/z 68 and 67, respectively. With the exception of other isotopically substituted products (5.1% ²⁹Si, 3.3% ¹³C), these signals correspond exclusively to SiC₃D₂⁺ and SiC₃DH⁺, respectively. Fig. 2.2 presents the TOF spectra for both m/z 68 (blue) and 67 (red) ionized products of the reaction of Si(¹D) with D3-methylacetylene collected at the CM angle. These measurements predict a branching ratio of 60 ± 15% HD loss products and 40 ± 15% D₂ loss products. Therefore the reaction of Si(¹D) with D3-methylacetylene is seen to exhibit both HD and D₂ loss channels leading to distinct isomers. Similar analysis could not be performed with allene due to the chemical equivalency of all the hydrogen atoms in allene.



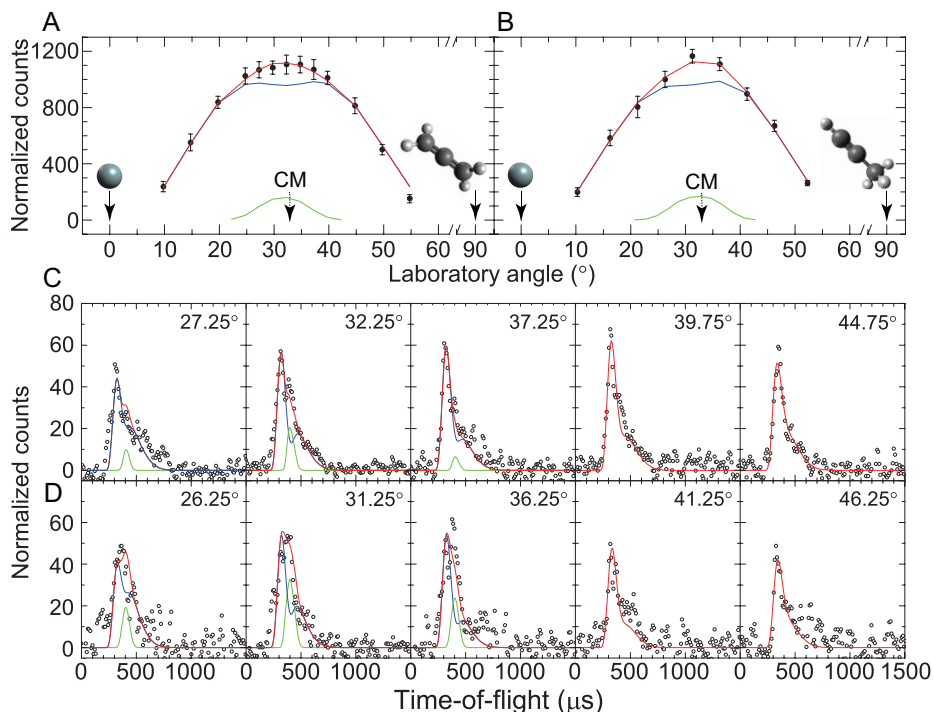


Figure 2.1: **A** and **B** present laboratory angular distributions for the reactions of Si(¹D) (blue) and SiH(X²Π) (green) with allene and methylacetylene, respectively. The red curves represent the overall fit, solid circles represent experimental data points with one σ error bars, and CM denotes the center of mass angle. **C** and **D** present TOF spectra at select angles for the allene and methylacetylene systems, respectively. Here the blue curves represent reactions with Si(¹D), the green curves reactions with SiH(X²Π), the red curves the overall fit, and the open circles experimental data points. Atom colors: silicon (green), carbon (black), and hydrogen (light grey). Taken with permission from Ref. 93.

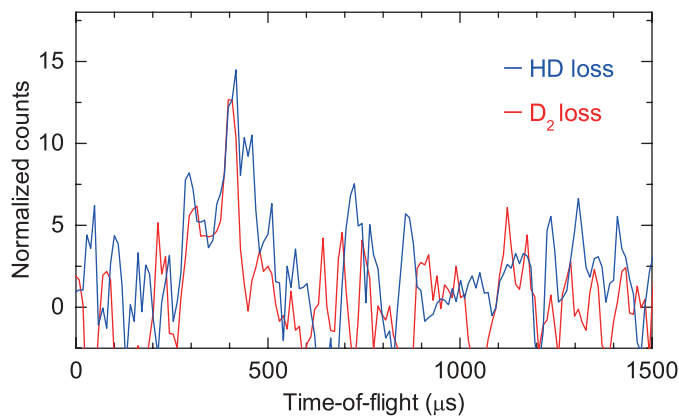


Figure 2.2: TOF spectra at m/z 68 (HD loss, SiC_3D_2^+ , blue) and 67 (D_2 loss, SiC_3HD , red) taken at the respective CM angles for the reaction of Si(¹D) with D₃-methylacetylene. Taken with permission from Ref. 93.

Center-of-Mass Frame

Interpretation of the raw TOF data suggests that the reactive scattering of excited state silicon atoms with allene and methylacetylene yields SiC₃H₂ molecules and molecular hydrogen. Deuterium-labeled experiments further show that in the case of methylacetylene there are multiple channels, including channels where the ejected hydrogen molecule is composed of hydrogen atoms from both the acetylenic and methyl groups. In order to probe the identity of these possible SiC₃H₂ products, the reaction dynamics of these systems was converted to the CM reference frame. CM translational energy distributions $P(E_T)$ and CM angular distributions $T(\theta)$ for the SiC₃H₂ plus molecular hydrogen exit channels are presented in Fig. 2.3. The maximum product translational energies for the Si(¹D)-allene and Si(¹D)-methylacetylene systems were found to be 218 ± 28 and 216 ± 26 kJ mol⁻¹, respectively. These maximum product translation energies are a sum of the initial collision energies and the reaction energies for products in their ground ro-vibrational states. This suggests then that the products of these Si(¹D)-C₃H₄ should be exoergic by 187 ± 31 kJ mol⁻¹. The broad peaks in the CM translational energy distributions centered at 50-80 kJ mol⁻¹ suggest molecular hydrogen loss from the SiC₃H₄ complexes occurs via a tight exit transition states and involves significant electron density rearrangement[132]. The wide distributions in the CM angular distributions suggests intermediate scattering dynamics where SiC₃H₄ intermediates persist with lifetimes comparable to or greater than the rotational period of the complex[133]. Both of these angular distributions are centered around 90°, suggesting a “sideways scattering” mechanism where the exit vector of the molecular hydrogen is nearly perpendicular to the rotation plane of the SiC₃H₄ transition state structures[133].

Electronic Structure Calculations for the Bimolecular Reactions

Molecular hydrogen loss channels

Having experimentally identified SiC₃H₂ isomers as the products of reactive scattering of excited state silicon with allene and methylacetylene, a computational approach was used to further elucidate the underlying reaction mechanisms and chemical dynamics. Reactants, products, intermediates, and transition state structures for species relevant to the reactions of electronically excited silicon atoms with allene, methylacetylene, and D3-methylacetylene are characterized in Tab. A.1-A.3 and summarized in Fig. 2.4, which presents zero-point corrected energies for species accessible within the experimental collision energy of 30 ± 2 kJ mol⁻¹ (a full version is presented in Fig. A.1). For both allene and methylacetylene, products **p1-p4** fall within the experimentally determined reaction energy window of 187 ± 31 kJ mol⁻¹.

The calculations predict the barrierless addition of Si(¹D) into the π electron density of the hydrocarbon. In the case of methylacetylene, this addition occurs via addition to the triple bond to yield [i1], the most stable of the SiC₃H₄ intermediate species. From [i1], the system can isomerize to [i2], [i4], [i5], and [i6] with barriers of 305, 188, 239, and 256 kJ mol⁻¹, respectively. Despite the lower barrier to [i4], rapid unimolecular dissociation to **p2**

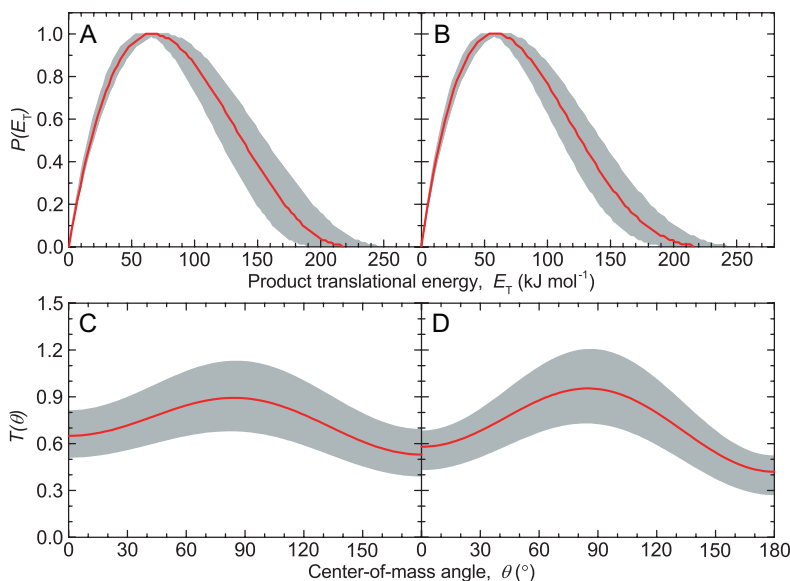


Figure 2.3: CM translational energy distributions (**A** and **B**) and CM angular distributions (**C** and **D**) for the reactions of Si(¹D) with allene (**A** and **C**) and methylacetylene (**B** and **D**) to yield SiC₃H₂ species via molecular hydrogen elimination. The shaded areas denote acceptable fits for one σ errors in the laboratory data. Taken with permission from Ref. 93.

via [i4]→[i13]→**p2** is stifled by a barrier of 260 kJ mol⁻¹ for the two-step process. Isomer [i5] can readily isomerize to [i2] with a barrier of 19 kJ mol⁻¹ or to [i9] with a barrier of 99 kJ mol⁻¹. From [i6], there is facile isomerization to [i9] and [i12] with barriers of 42 and 60 kJ mol⁻¹, respectively, and access to [i10] through a barrier of 143 kJ mol⁻¹. Most of the intermediates are thereby capable of interconverting, provided products are not too rapidly formed.

Qualitatively, this is confirmed by examining the exit barriers for molecular hydrogen loss to form SiC₃H₂. The most favorable exit transition states are the [i6]→**p4** transition state at -114 kJ mol⁻¹, i.e., a barrier of 188 kJ mol⁻¹, the [i9]→**p1** transition state at -89 kJ mol⁻¹ with barrier of 190 kJ mol⁻¹, and two [i12]→**p3** transition states at -71 and -76 kJ mol⁻¹ with barriers of 177 and 172 kJ mol⁻¹, but from a higher energy intermediate. Exit transition states to **p2** are much higher in energy, with energies of 7, -46, and -46 kJ mol⁻¹ for the [i1]→**p2**, [i6]→**p2**, and [i13]→**p2** transition states, respectively. Detailed prediction of branching ratios requires solving the coupled kinetic equations for all of these pathways, after applying Rice-Ramsperger-Kassel-Marcus (RRKM) theory to obtain the individual rate constants (Tab. A.9). The outcome for this network is a predicted product distribution of 38.2% **p1**, 0.6% **p2**, 11.1% **p3**, and 45.8% **p4**. The experimental results from the silicon-D₃-methylacetylene system, which reveal a branching ratio of 60±15% HD loss and 40±15% D₂ loss, allows for validation of the computed reaction network. Comparing the moderate exit barriers to the comparatively much smaller barriers to isomerization, significant isomerization is expected. Including all possible constitutional isomers in the reaction network, our RRKM

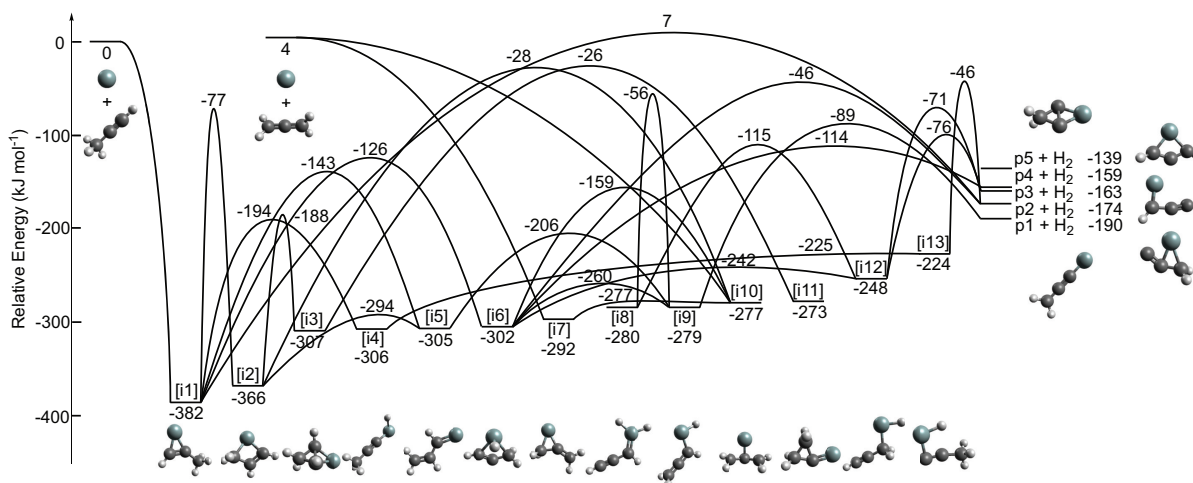


Figure 2.4: Simplified potential energy surface for the reactions of excited state silicon with methylacetylene and allene. Energies relative to separated reactants are given in units of kJ mol^{-1} . Pathways with barriers above the 30 kJ mol^{-1} collision energy are excluded. Atom colors: silicon (green), carbon (black), and hydrogen (light grey). Taken from Ref. 93.

calculations predict a product distribution of 56.8% HD loss and 43.2% D₂ loss. This result is in good agreement with experimental results and suggests that the energy landscape shown in Fig. 2.4 is faithfully capturing the critical aspects of the experimental dynamics observed for Si(¹D) with methylacetylene.

Turning next to the computational results for the reaction of Si(¹D) with allene, it is evident from Fig. 2.4 that the silicon atom can add barrierlessly to a C=C bond, yielding a 3-membered ring structure, [i7], or attack the central carbon atom to form the ring-opened isomer [i10]. There is virtually no barrier to ring-opening [i7] to yield [i10]. Intermediate [i10] provides access to the main intermediates already seen in silicon–methylacetylene system. For instance, the sequences [i10]→[i2]→[i1] and [i10]→[i6]→[i1] both access intermediate [i1], the initial encounter product for Si(¹D)-methylacetylene. Therefore, the initial collision complexes of the silicon–methylacetylene ([i1]) and silicon–allene ([i7]/[i10]) surfaces are effectively coupled via intermediates [i2] and [i6] with reaction pathways eventually leading to **p1–p4** via H₂ loss involving tight exit transition states located 45–167 kJ mol^{-1} above the energy of the separated products. The predicted product distribution for silicon–allene system is therefore very similar to that discussed above for the silicon–methylacetylene system: 38.7% **p1**, 0.5% **p2**, 11.3% **p3**, and 46.5% **p4**.

Atomic hydrogen and methyl loss channels

Having established that the molecular hydrogen loss channel leads predominantly to the formation of the 1-sila-1,2,3-butatrienylidene molecule ($\text{H}_2\text{C}=\text{C}=\text{C}=\text{Si}$; X¹A₁; **p1**) and the less stable 4-membered ring structure (*c*-SiCH=C=CH; X¹A₁; **p4**), the possibility of atomic hydrogen (H) and methyl (CH₃) loss channels were also investigated, though these channels

were not observed experimentally. For the atomic hydrogen loss channel, we located 22 SiC₃H₃ isomers (Tab. A.4). Six isomers—one acyclic (**n1**) and five cyclic molecules (**n2-n6**)—are energetically accessible under our experimental conditions at collision energies of 30±2 kJ mol⁻¹ holding overall reaction energies from -10 to 24 kJ mol⁻¹. For the methyl loss channels, four SiC₂H isomers could be identified (Tab. A.5), two of which were permitted under experimental conditions with overall reaction energies of -30 and -5 kJ mol⁻¹ for **m1** and **m2**, respectively. Statistical (RRKM) calculations were conducted to examine the branching ratios for the energetically accessible hydrogen atom and methyl loss channels (Tab. A.9) versus molecular hydrogen loss. These radical product channels were found to contribute only about 4% in total to the overall product stream for the silicon–methylacetylene system, and only 3% of the product stream for the silicon–allene system. These results bolster our experimental findings that the molecular hydrogen loss is the primary dissociation channel and also support the experimental non-detection of atomic hydrogen and methyl group loss channels.

Electronic Structure Calculations: Photodissociation of SiC₃H₂ to SiC₃

We have thus far concluded that the reactions of excited state silicon atom with allene and methylacetylene lead primarily to the formation of **p1** and **p4** under the experimental conditions. While these experiments are designed to mimic the conditions in the inner envelope of carbon stars, we also consider computationally the ejection of these SiC₃H₂ product species to the outer envelope, where subsequent photodissociation may occur to form silicon tricarbonide SiC₃ isomers including cyclic silicon tricarbonide (*c*-SiC₃), which has been astronomically observed. Reactants, products, and transition state structures for the isomerization and dehydrogenation reactions of SiC₃H₂ are characterized in Tab. A.6 and summarized in Fig. 2.5, where the zero-point corrected energies are presented relative to the most stable SiC₃H₂ isomer **p1**.

Under experimental conditions the total system energy is 220 kJ mol⁻¹ above **p1**, allowing for isomerization from **p1** to **p2** via ring closure, **p2** to **p5** via concerted ring opening and ring closure, **p4** to **p3** via ring opening, and **p3** to **p6** via two concerted ring closures, while leaving other the other isomerization channels and all of the dehydrogenation channels closed. Further activation of these species is required for dehydrogenation channels to be open, such as the absorption of a Lyman- α photon (10.2 eV or 984 kJ mol⁻¹ for hydrogen) from the interstellar UV field. As shown in Tab. A.7, **p1-p6** all have excited states with nonzero oscillator strength in the region of 10.2 eV, the species exhibiting the strongest absorption being **p2** (10.2 eV; $f = 0.20$) and **p4** (10.2 eV; $f = 0.25$). Following absorption and non-radiative relaxation to a vibrationally hot electronic ground state, these SiC₃H₂ species possess enough internal energy to surmount the barriers to isomerization and dehydrogenation via molecular hydrogen loss to SiC₃ species [1], [2], and [3].

In agreement with our results, previous computational studies predict that the bicyclic

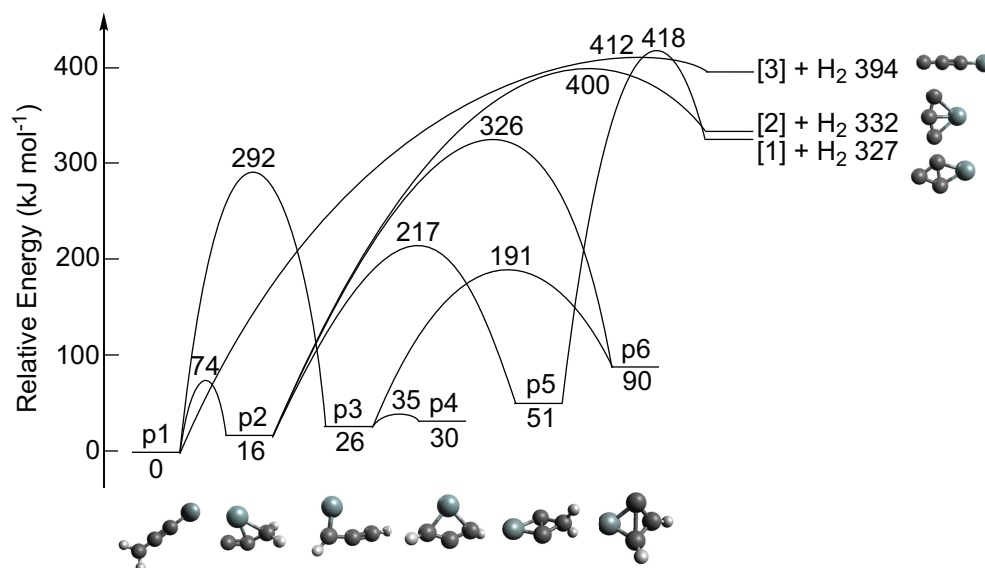


Figure 2.5: Potential energy surface for the isomerization of low-energy SiC₃H₂ isomers and dehydrogenation to yield SiC₃. Energies relative to the lowest energy SiC₃H₂ isomer **p1** are given in units of kJ mol⁻¹. The total internal energy on this scale for products of reaction **I** is 220 kJ mol⁻¹. Atom colors: silicon (green), carbon (black), and hydrogen (light grey). Taken from Ref. 93.

SiC₃ isomer **[1]** represents the thermodynamically most stable isomer on the singlet electronic surface, with the other bicyclic isomer **[2]** being 8-52 kJ mol⁻¹ higher in energy [134–143]. This lowest energy isomer **[1]** has been observed in the circumstellar envelope of IRC+10216. Previous studies of the linear isomers of SiC₃ have also predicted the carbon-terminal CSiCC to be approximately 318 kJ mol⁻¹ higher in energy than the silicon-terminal SiCCC on the triplet electronic surface (X³Σ⁻) [144].

We have also computationally investigated atomic hydrogen loss pathways from **p1**, **p2**, and **p5** as alternative photodissociation channels (Tab. A.8). These channels are endoergic by 387-410 kJ mol⁻¹ relative to **p1**. While these reaction energies are comparable to the molecular hydrogen loss barriers heights, the molecular hydrogen loss products are thermodynamically favored and the channels leading to them are enhanced by tunneling. We therefore suggest that molecular hydrogen loss to yield *c*-SiC₃ is the main dissociation channel.

Summary of Astrochemical Modeling

Following the combined computational and experimental conclusions that SiC₃H₂ species including **p1** and **p4** are formed via bimolecular reactions of excited state silicon atoms with allene and methylacetylene and further computational findings that these SiC₃H₂ species can form cyclic silicon tricarbonide (*c*-SiC₃) via molecular hydrogen-elimination photodissociation,

our co-authors used astrochemical modeling to relate these results to the circumstellar envelope of IRC+10216. This modeling seeks to account for the presence of other reactants and the overall reaction network not considered in the crossed beam experiments and electronic structure calculations. The simulations employed the chemical kinetic data from the RATE12 release of UMIST Database for Astrochemistry[110] with the addition of SiC₃H₂ reactivity proposed in this work and with work physical parameters taken from Li et. al[145]. Fractional abundances (measured relative to molecular hydrogen) of species are also taken from refs. 110 and 145.

Firstly, these modeling studies approximated the abundance of excited state silicon atoms in the inner envelope. Sources of Si(¹D) include photodissociation of silane (SiH₄)[146], silicon monoxide (SO), and silicon monosulfide (SiS)[114, 147], which have detected fractional abundances of 2.2×10^{-7} , 1.8×10^{-7} , and 1.3×10^{-6} , respectively, in the inner envelope of IRC+10218[110, 145]. For SiH₄, quantitative studies by Suto and Lee revealed that excited state silicon atom contributes 1.2% of the photodissociation yield for 106-160 nm photons[146]. These photodissociation channels could lead to up to 1% of the total budget of silicon, which peaks at a fractional abundance of 1.0×10^{-6} , to be excited state silicon atoms. These finding confirm that excited state silicon atoms required for our mechanisms are present in the circumstellar envelope of IRC+10216.

Results of the modeling study including the channels presented in this work are summarized in Fig. 2.6. The present-day fractional abundances of allene, methylacetylene, silicon tricarbon, and silicon tetracarbon all peak at a radius of 4×10^{16} cm with fractional abundances of 8×10^{-9} , 8×10^{-9} , 7×10^{-9} , and 2×10^{-10} , respectively[148]. From these fractional abundances it is clear that dissociation of silicon tetracarbon cannot be the dominant precursor of silicon tricarbon. The inclusion of the two-step mechanism proposed in this work has increased the modeled column density of silicon tricarbon by 80% versus previous modeling efforts. Since only Lyman- α photons were considered to photodissociate SiC₃H₂, this modeled fractional abundance of silicon tricarbon should be seen as a lower bound.

Finally, the modeling study predicts a fractional abundance of SiC₃H₂ to peak at a fractional abundance 10^{-10} relative to molecular hydrogen. At this abundance signal from these species should be observable in future searches to further confirm the proposed mechanisms.

2.4 Conclusions

Our combined computational and experimental approach for the bimolecular reactions of excited state silicon atom with allene and methylacetylene has revealed the indirect scattering mechanisms to form SiC₃H₂ products, including 1-sila-1,2,3-butatrienylidene (H₂C=C=C=Si; X¹A₁)(**p1**) among other isomers. These reactions begin with the barrierless addition of silicon into the π electron density of the carbon-carbon double bond(s) for allene and the carbon-carbon triple bond for methylacetylene, yielding distinct SiC₃H₄ species. The internal energy available to these intermediates allows for interconversion between several SiC₃H₄

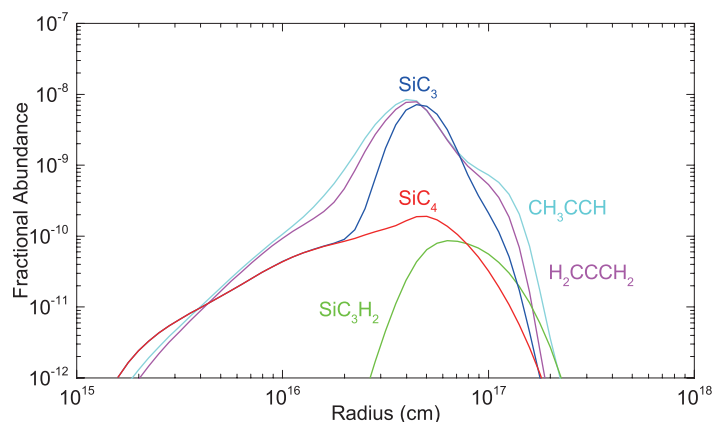


Figure 2.6: Modeled present-day fractional abundances relative to molecular hydrogen are plotted versus the radius of the circumstellar envelope of the carbon star IRC+10216. Species color: silicon tricarbonide (SiC₃)(blue), silicon tetracarbonide (SiC₄)(red), allene (H₂CCCH₂)(magenta), methylacetylene (CH₃CCH)(cyan), SiC₃H₂ (green). Taken from Ref. 93.

intermediate species before unimolecular decomposition via molecular hydrogen elimination. The computed reaction network was used to predict the product isomer distributions and provided excellent agreement with the the experimentally observed HD/D2 loss ratios observed in the experimental study of the silicon-D3-methylacetylene system. The experimental collision energy of 30 ± 2 kJ mol⁻¹ reflects the conditions in the circumstellar envelopes of carbon-rich stars undergoing shocks and pulsations of the stellar ejecta[114]. These SiC₃H₂ products of reaction **I** can then be transported from the inner envelope to the outer envelope via solar winds. We computationally studied the photolysis of SiC₃H₂ by the interstellar UV field to form cyclic silicon tricarbonide (*c*-SiC₃) via molecular hydrogen elimination (reaction **II**). These computational mechanisms were then integrated into an astrochemical kinetic model to draw conclusions about the observation and abundance of *c*-SiC₃ in the circumstellar envelope of IRC+10216.

These systems demonstrate excited-state neutral-neutral reactions in the inner circumstellar envelope to form SiC₃H₂ species which are then dehydrogenated by the interstellar UV field in the outer envelope to form cyclic silicon tricarbonide (*c*-SiC₃). While previous models have suggested photodissociation of silicon tetracarbonide (SiC₄) as the source of circumstellar silicon tricarbonide[99, 108, 149], the modeled fractional abundance of silicon tricarbonide in the circumstellar envelope of IRC+10216 exceeds that of silicon tetracarbonide by two orders of magnitude[110, 145]. The computations and astrochemical modeling in this work propose SiC₃H₂ species as important precursors of *c*-SiC₃. While the computational photodissociation study only considered Lyman- α photons as opposed to the wider interstellar UV field, this study serves as a proof-of-concept for the two-step mechanisms taking place in the inner and outer circumstellar envelopes. These mechanism for silicon carbide formation via neutral-neutral bimolecular reactions and subsequent dehydrogenation provide an alternative

to the conventional belief that silicon carbides could only be formed via high-temperature ion-molecule reactions or via photodissociation of larger silicon carbide molecules.

With the commission of the Atacama Large Millimeter/Submillimeter Array, the detection of novel organosilicon species will undoubtedly grow (including the 1-sila-1,2,3-butatrienyldiene, which has not yet been searched for in the envelope of IRC+10216). An understanding of the chemistry of these species will rely on combined computational, experimental, and astrochemical modeling efforts, helping to close the long-standing gap between observational and laboratory data.

Chapter 3

Benchmarking the Performance of the ReaxFF Reactive Force Field on Hydrogen Combustion Systems

Reprinted with permission from Bertels, L. W.; Newcomb, L. B.; Alaghemandi, M.; Green, J. R.; Head-Gordon, M. Benchmarking the Performance of the ReaxFF Reactive Force Field on Hydrogen Combustion Systems. *J. Phys. Chem. A* **2020**, 124, 5631–5645.

3.1 Introduction

Hydrogen combustion is a promising energy source for both space exploration[150] and cleaner terrestrial transportation[151–154]. Hydrogen is an attractive fuel in part because of its high energy density and lack of carbon-containing combustion products[155–157]. Such applications require understanding of how the chemistry of hydrogen and hydrogen combustion plays a role in storage, efficiency, and safety[150, 153, 158–162]. Furthermore, many of the elementary reactions relevant to hydrogen combustion are present in the combustion of other hydrogen-containing fuels[163].

Extensive effort has been made to model the reaction kinetics of hydrogen combustion under a variety of conditions with ample feedback from experimental studies. Mueller et al.[164] developed a model based on their experimental findings to accurately describe the kinetics below the second explosion limit. Li et al.[165], beginning from the mechanisms proposed by Mueller et al., updated the model by modifying reaction rates to better predict high-pressure flame speed experiments. O’Connaire et. al[166] also developed a new mechanism validated on flames speeds, ignition time delays, and species composition, also modifying reaction rates to better account for higher pressure experiments. Konnov[167], in updating the H_2/O_2 combustion mechanism, provided better analysis of the uncertainties in reaction rates and suggested the importance of $\text{HO}_2 + \text{H}$ reactions in accurately predicting ignition delays. Hong et. al.[168] proposed updates to reaction rates based on their UV and

IR measurements on high-temperature mixtures in shock tubes. Burke et al.[169] developed a model based on the Li mechanism that can push to more intermediate pressures towards the second extended explosion limit. To better treat high pressures, Shimuzi et al.[170], building on the work of Kitano et al.[171], further investigated the importance of $\text{HO}_2 + \text{H}$ reactions and called for more accurate rate constants to be determined for several reactions. The development of the ELTE mechanism by Varga et al.[172] involved a global optimization of parameters and considered all available direct and indirect measurements for evaluation. The authors also benchmarked the performance of a variety of previous models on their measurement set. An experimental study of laminar flames across a wide parameter range was complemented by quantum-chemical calculations of rate constants and shock tube data to develop the HP-Mech model and extract pressure-dependent reaction orders[173] Burke and Klippenstein[174], investigating the elementary reactions of hydrogen combustion via a *ab initio*-master equation, proposed inclusion of new three-body radical propagation and termination reactions. Recent work by Konnov[175], however, has suggested that new transport parameters suggested by Jasper et al.[176, 177] provided a better match to flame speeds than the inclusion of Burke and Klippenstein's new reactions. Experimental studies on the roles of impurities in shock tube data have also been recently performed[178]. Sabia et al.[179], in an experimental work to better quantify the role that different bath gases, has found existing models lacking for bath gases other than N_2 . In this work, the authors also highlight several existing challenges in the modeling of hydrogen combustion, including uncertainties in rate constants, unconsidered or excluded reaction mechanisms, and uncertainties relating to three-body effects. A more complete review of the history, current standings, and challenges of modeling H_2 combustion is given in the discussion of their work.[179]

Three of us[180–185] have recently developed and applied a method of reactive symbol sequences to the study of hydrogen combustion as an alternative route to analyze chemical kinetics. This framework avoids the ideas of elementary reactions and rate coefficients, both of which can be strongly dependent on modeling assumptions [186, 187]. Instead, reactive symbol sequences can be seen as a way to probe the emergent chemical processes present in combustion chemistry. Applied to reactive molecular dynamics (MD), this approach naturally includes important non-equilibrium fluctuations. Beginning with an all-atom potential function that depends only on the atomic positions, in principle also allows for a method to be predictive from the outset instead of relying on parameterization which is only relevant near the particular conditions on which it is trained.[188]

To generate the trajectories for this approach, one could, in principle, consider using *ab initio* MD simulations where energies and forces are determined using electronic structure theory methods. Examples of this include the nanoreactor studies in which pressure and temperature fluctuations are used to induce reactive events[189, 190]. Despite their accuracy for barrier heights and reaction energies, the high computational cost of these methods limits both the size and timescale of simulations.

Alternatively, empirical methods including reactive force fields[188, 191–196] and tight binding[197–199] offer a computationally more feasible approach to larger and longer simulations, though potentially with a loss of accuracy. The former allow for the nanosecond

scale simulations on thousands of atoms. Within the ReaxFF reactive force field[188], energies are determined via a combination of connection dependent terms based on bond orders and a polarizable charge description. These potentials depend on system-specific parameters which are trained against QM data, including reaction energies and barrier heights. ReaxFF potentials have been developed and applied to combustion reactions[200–216], including hydrocarbons, hydrogen[203, 212], and syngas[216]. The ReaxFF method has also been extensively applied to material science[217–232], catalysis[233–237], and other chemical systems[188, 238–246].

The reactive symbol sequence studies for hydrogen combustion cited above have utilized ReaxFF potentials in order to generate the trajectories required for their analysis. While ReaxFF potential are derived from fits to QM data, there are no reports available on assessment of ReaxFF parameterizations against independent test sets of QM data at combustion relevant atomic configurations. In this work, we benchmark the performance of several ReaxFF parameter sets on a set of trajectories and reactions relevant to the combustion of hydrogen. The predictive power of the ReaxFF method hinges on its fidelity to QM data, especially in conditions where experimental validation is difficult or impossible.

3.2 Computational Methods

ReaxFF Reactive Force Field Method

ReaxFF is an atomistic potential capable of describing reactive events. Bond breaking and formation are captured in ReaxFF via computed bond orders between pairs of atoms. Intramolecular bonded energy contributions are captured using potential functions that depend on these bond orders, which are determined by the interatomic distances. Nonbonded intermolecular interactions including Coulomb, dispersion, and polarization are computed between all pairs of atoms using geometry-dependent charge equilibration schemes and are damped at short range[247, 248]. Analytic forms for these potential functions can be found in the the supporting information of Chenoweth et al.[200]. The total potential is:

$$\begin{aligned} E_{\text{system}} = & E_{\text{bond}} + E_{\text{lp}} + E_{\text{over}} + E_{\text{under}} + E_{\text{val}} + E_{\text{tor}} \\ & + E_{\text{coa}} + E_{\text{conj}} + E_{\text{H-bond}} + E_{\text{vdW}} + E_{\text{coul}} + E_{\text{pol}} \end{aligned} \quad (3.1)$$

where E_{bond} , E_{lp} , E_{over} , E_{under} , E_{val} , E_{tor} , E_{coa} , E_{conj} , $E_{\text{H-bond}}$, E_{vdW} , E_{coul} , and E_{pol} , are the bond, lone pair, overcoordination, undercoordination, valence angle, torsional angle, three-body conjugation, four-body conjugation, hydrogen bond, van der Waals, Coulomb, and polarization energy contributions, respectively.

For a given class of chemical systems, parameters for these energy contributions were trained on a data set comprised of electronic structure theory calculations and experimental data. For the purposes of this work, we have selected four combustion-specific parameter sets of the ReaxFF force field to benchmark against high-level QM calculations.

1. The CHO2008 parameter set was developed in 2008 by Chenoweth, van Duin, and Goddard as a first parameterization of a ReaxFF potential for hydrocarbon oxidation[200].
2. The HO2011 parameter set was developed in 2011 by Agrawalla and van Duin specifically to simulate hydrogen combustion at high temperature and pressure[203].
3. The HO2014 parameter set was developed in 2014 by Cheng et al. as a reoptimization of the CHO2008 set for use in accelerated reactive molecular dynamics simulations[212].
4. The CHO2016 parameter set was developed in 2016 by Ashraf and van Duin as a systematic improvement of the CHO2008 to better capture small hydrocarbon oxidation and combustion initiation[216].

Our single-point calculations were performed using the `reax/c` package[249] as implemented in LAMMPS (<http://lammps.sandia.gov>)[250].

Molecular Dynamics Simulations

Molecular dynamics trajectories were calculated using the HO2011 parameter set[203] with the ReaxFF potential[200]. All trajectory simulations were carried out with constant particle number, volume, and energy (*NVE*) and utilized a time step of 0.1 fs and periodic boundary conditions.

We first considered a high-pressure simulation initialized with 66 H₂ molecules, 33 O₂ molecules, and an OH radical initiator at an initial pressure of 950 bar and an initial temperature of 1000 K (initial density $\rho_0 = 250 \text{ kg m}^{-3}$, stoichiometric ratio $\phi = 1$). These trajectories were allowed to evolve for 3 ns, at which point more than 80% of the reactants were converted to water[181]. This set of trajectories was calculated using the PuReMD-GPU simulation package[251]. This set of trajectories has already been reported and analyzed using reactive symbol sequences[181].

A larger, lower pressure simulation was also performed to better isolate bimolecular reactive events. This simulation was initialized with 320 H₂ molecules, 160 O₂ molecules, and 16 OH radical initiators at an initial pressure of 50 bar and an initial temperature of 1250 K ($\rho_0 = 5.9 \text{ kg m}^{-3}$, $\phi = 1$). This trajectory was allowed to evolve for approximately 70 ns, at which point the temperature had equilibrated and the reactants were nearly completely converted to water. The OH radicals were added to initiate the ignition of the reaction mixture. Figure 3.1 presents the kinetic temperature of this reacting mixture as a function of simulation time. This trajectory was calculated using the `reax/c` package[249] in LAMMPS[250].

From the simulated MD trajectories under these high and low pressure conditions, “reactive pathways” were extracted during the ignition events that characterize the combustion reaction at fixed energy [181]. These paths correspond to isolated elementary bi- and termolecular reaction events. Because they occur naturally during the course of ignition, the

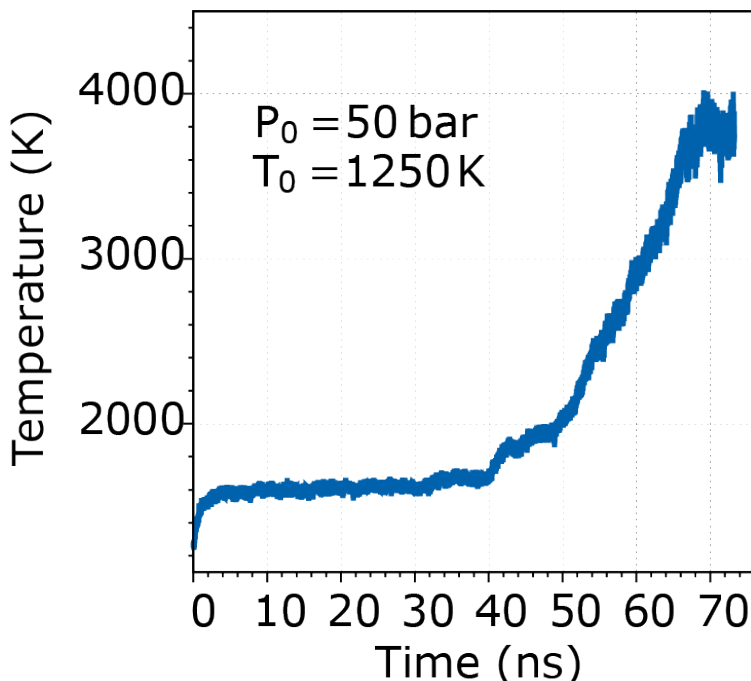


Figure 3.1: Time series of the kinetic temperature for a hydrogen-oxygen mixture that is initially stoichiometric at a temperature of 1250 K and pressure of 50 bar.

paths of these reactions through the transition state regions include oscillations about the spectator modes. These reactive paths are a point of comparison to minimum energy paths found via quantum-mechanical calculations.

Quantum-Mechanical Calculations

In order to benchmark the performance of the ReaxFF potential, QM calculations were performed using coupled cluster theory with single, double, and perturbative triple excitations [CCSD(T)][252] in the spin-unrestricted wave function formalism utilizing the frozen-core approximation and the cc-pVTZ basis set[119] and extrapolated to the complete basis set limit. The correlation energy was extrapolated with second-order Møller-Plesset perturbation theory using the resolution of the identity approximation (RI-MP2)[29, 30]. The expression for this overall extrapolated energy is

$$E(\text{CCSD(T)}/\text{CBS}) = E(\text{HF}/\text{cc-pV5Z}) + E^{\text{corr}}(\text{RI-MP2}/\text{CBS}_{3,4,5}) + E^{\text{corr}}(\text{CCSD(T)}/\text{cc-pVTZ}) - E^{\text{corr}}(\text{RI-MP2}/\text{cc-pVTZ}) \quad (3.2)$$

where $E^{\text{corr}}(\text{RI-MP2}/\text{CBS}_{3,4,5})$ is the extrapolated RI-MP2 correlation energy using the cc-pVTZ, cc-pVQZ, and cc-pV5Z basis sets[119] to fit

$$E^{\text{corr}}(\text{RI-MP2}/\text{cc-pVNZ}) = E^{\text{corr}}(\text{RI-MP2}/\text{CBS}_{3,4,5}) + AN^{-3} \quad (3.3)$$

and N is the cardinality of the cc-pVNZ basis set [123]. From comparisons between extrapolated CCSD(T) and composite Weizmann methods as well as evaluation of CCSD(T) for bond stretching, we predict errors in our benchmark calculations on the order of 1–4 kcal mol⁻¹[253–255].

As another point of comparison, QM calculations were also performed using the ω B97M-V[256] density functional in the spin-unrestricted wave function formalism with the cc-pVTZ basis set[119]. This functional has been ranked as one of the most accurate in a recent assessment of 200 density functionals on systems including thermochemistry and barrier heights.[85] All DFT calculations were carried out using an ultra-fine integration grid using 99 radial points and 590 angular points.

In addition to the reactive pathways harvested from MD simulations, intrinsic reaction coordinate scans for a subset of bimolecular reactions relevant to hydrogen combustion from Li et al.[165] were used for benchmarking systems. Structures for the products and reactants were computed via geometry optimization at the ω B97M-V/cc-pVTZ level of theory. Transition structures were computed using the freezing string method[121] to generate an approximate structure and Hessian, then refined by the partitioned-rational function optimization eigenvector following method (P-RFO)[122], also at the ω B97M-V/cc-pVTZ level of theory. Vibrational analysis was used to confirm that the minima have no imaginary frequencies and that the transition state structures have only one imaginary frequency. The reaction path on either side of the transition state structure was computed using the intrinsic reaction coordinate method[257–259]. All QM calculations were performed using the Q-Chem[125] package of electronic structure programs.

3.3 Results and discussion

Reactive Pathways

A collection of seven reactive pathways were harvested from larger MD simulations and are presented in order to benchmark the performance of ReaxFF against electronic structure theory calculations. By this, we mean that the coordinates of all spectator species are removed, leaving a relatively small subset of atoms undergoing chemical changes, whose relative energies can be tractably benchmarked. As the overall MD simulations were performed with the HO2011 parameter set, energies of the configurations along these pathways will be relative to energies of the isolated reactants at geometries optimized with ReaxFF using the HO2011 parameter set.

Two termolecular reactions were extracted from the high-pressure simulation ($N_{\text{H}_2,0} = 66$, $N_{\text{O}_2,0} = 33$, $N_{\text{OH},0} = 1$, $P_0 = 950$ bar, $T_0 = 1000$ K, $\rho_0 = 250$ kg m⁻³, $\phi = 1$). The first of these reactions is the near simultaneous cleaving of a hydrogen molecule by an oxygen atom and an oxygen molecule to yield a hydroxyl radical and a hydroperoxyl radical ($\text{O} + \text{H}_2 + \text{O}_2 \longrightarrow \text{OH} + \text{HO}_2$). For the *ab initio* calculations the ground state is a singlet. The second of these termolecular reactions is the cleaving of a hydrogen molecule by an

oxygen molecule and a hydroperoxyl radical to form a hydroperoxyl radical and hydrogen peroxide ($O_2 + H_2 + HO_2 \longrightarrow HO_2 + H_2O_2$). The ground state is a doublet for this reaction. Plots of the potential energy along the pathways for the methods surveyed are presented in Figures B.1–B.2.

In addition to these termolecular reactive pathways, five bimolecular reactive pathways were extracted from the 50 bar simulation ($N_{H_2,0} = 320$, $N_{O_2,0} = 160$, $N_{OH,0} = 16$, $P_0 = 50$ bar, $T_0 = 1250$ K, $\rho_0 = 5.9$ kg m⁻³, $\phi = 1$). The first of these is the initiation reaction between a hydrogen molecule and an oxygen molecule forming a hydroperoxyl radical and a hydrogen atom ($H_2 + O_2 \longrightarrow HO_2 + H$), which has a triplet ground state. The second is the reaction of a hydrogen atom and an oxygen molecule to form a hydroperoxyl radical ($H + O_2 \longrightarrow HO_2$), which has a doublet ground state. Third is the reaction of a hydroperoxyl radical and a hydrogen atom to form two hydroxyl radicals ($HO_2 + H \longrightarrow 2 OH$), occurring on the singlet surface. Fourth and fifth are both reactions of hydrogen molecules and hydroxyl radicals to form water and a hydrogen atom ($H_2 + OH \longrightarrow H_2O + H$), which have doublet ground states. Plots of the potential energy along the trajectories for the methods surveyed are presented in Figures 3.2,B.3–B.7.

Table 3.1: Root mean square deviation, mean signed deviation, maximum absolute deviation, and non-parallelity error, in kcal mol⁻¹, are presented for a selection of reactive pathways extracted from larger MD simulations. CCSD(T)/CBS values were used as reference.

Reaction	Method	RMSD	MSD	MAX	NPE
$O + H_2 + O_2 \longrightarrow OH + HO_2$	ω B97M-V	3.00	-2.51	-4.81	5.28
	CHO2008	59.54	-57.06	-77.33	53.70
	HO2011	41.55	-38.49	-58.41	57.93
	HO2014	28.18	-26.18	-45.20	32.14
	CHO2016	18.93	-10.78	-41.07	55.93
$O_2 + H_2 + HO_2 \longrightarrow HO_2 + H_2O_2$	ω B97M-V	2.02	0.74	4.38	7.33
	CHO2008	35.49	-33.70	-61.14	43.02
	HO2011	28.98	-24.46	-55.46	62.44
	HO2014	32.58	-29.67	-55.45	60.57
	CHO2016	16.86	-6.94	-37.15	58.38
$H_2 + O_2 \longrightarrow HO_2 + H$	ω B97M-V	1.21	-0.43	-2.77	3.91
	CHO2008	22.34	-19.36	-37.54	32.87
	HO2011	16.35	-13.51	-32.23	35.36
	HO2014	11.31	3.30	17.02	30.45
	CHO2016	8.40	-0.94	-18.31	34.08
$H + O_2 \longrightarrow HO_2$	ω B97M-V	2.17	1.57	4.79	5.10
	CHO2008	11.37	-10.63	-21.88	17.73
	HO2011	10.03	-1.21	15.43	30.85
	HO2014	12.60	-8.27	17.90	34.42
	CHO2016	8.63	-3.92	-14.17	26.69
$HO_2 + H \longrightarrow 2 OH$	ω B97M-V	4.11	3.68	6.00	6.43

Table 3.1: (continued)

Reaction	Method	RMSD	MSD	MAX	NPE
	CHO2008	18.06	5.64	26.88	53.42
	HO2011	8.55	2.43	-17.35	33.95
	HO2014	21.08	-4.21	-59.19	90.63
	CHO2016	14.80	-1.80	-38.68	58.01
$\text{H}_2 + \text{OH} \longrightarrow \text{H}_2\text{O} + \text{H}$	ω B97M-V	1.69	-0.50	-3.42	5.79
	CHO2008	14.66	-10.58	-28.76	33.98
	HO2011	8.29	-3.46	-20.16	32.29
	HO2014	8.27	-4.02	-15.89	24.25
	CHO2016	10.48	-4.62	-19.28	32.09
$\text{H}_2 + \text{OH} \longrightarrow \text{H}_2\text{O} + \text{H}$	ω B97M-V	1.94	0.03	3.11	5.47
	CHO2008	9.64	-4.75	-20.49	28.76
	HO2011	8.05	-2.24	-16.22	26.00
	HO2014	5.99	-1.60	-11.26	22.42
	CHO2016	8.72	7.61	16.81	28.94
All Pathways	Method	RMSD	MSD	MAX	NPE
	ω B97M-V	2.62	1.07	6.00	7.33
	CHO2008	18.32	-8.30	-77.33	53.70
	HO2011	12.46	-3.56	-58.41	62.44
	HO2014	15.10	-5.25	-59.19	90.63
	CHO2016	11.44	-2.59	-41.07	58.38

Table 3.1 presents the root mean square deviations (RMSD), mean signed deviation (MSD), maximum absolute deviation (MAX), and non-parallelity error (NPE), all in kcal mol⁻¹, for pathways extracted from MD simulations. Here, the non-parallelity error is defined as the difference between the maximum and minimum error along a reaction pathway. For the overall metrics, the modern density functional, ω B97M-V, unsurprisingly outperforms all of the surveyed ReaxFF methods by a factor of 4 for RMSDs, 2 for MSDs, 7 for MAXs, and 7 for NPEs. Of the ReaxFF methods, the CHO2016 parameter set outperforms the other parameter sets in terms of RMSDs, MSDs, and MAXs with values of 11.44 kcal mol⁻¹, -2.59 kcal mol⁻¹, and 41.07 kcal mol⁻¹, respectively. The next-best performing parameter set for these properties was HO2011, followed by HO2014 and CHO2008, respectively. The CHO2008 parameter set performs the best for NPEs with a value of 53.70 kcal mol⁻¹. The negative MSDs for all methods demonstrates a systematic overstabilization of configurations relative to isolated reactants. Furthermore, the NPEs in excess of 15 kcal mol⁻¹ and up to 90 kcal mol⁻¹ demonstrate that ReaxFF does not capture the shape of the potential energy surfaces along the reactive pathways.

As an example, Figure 3.2 presents the potential energy along the first $\text{H}_2 + \text{OH} \longrightarrow \text{H}_2\text{O} + \text{H}$ reactive pathway for the CCSD(T) reference, ω B97M-V, and four ReaxFF parameter sets. Like the others, this reactive pathway was sampled from a larger mixture undergoing

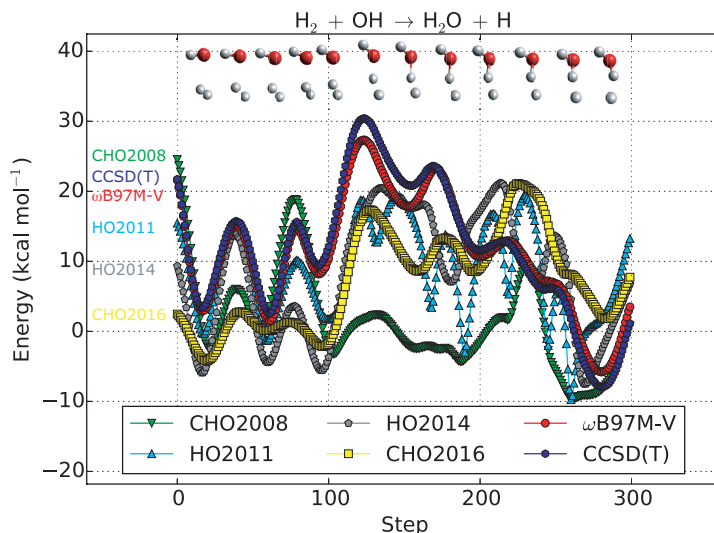


Figure 3.2: Potential energy along the first $\text{H}_2 + \text{OH} \longrightarrow \text{H}_2\text{O} + \text{H}$ reactive pathway, extracted from a larger MD simulation. The parent simulation was run using ReaxFF with the HO2011 parameter set. The energies presented are relative to the energies of isolated H_2 and OH computed at the ReaxFF/HO2011 optimized geometries. The total time to complete this reaction path is 30 fs with a time step of 0.1 fs.

ignition. This particular reactive path begins with the rotation of a H_2 molecule relative to an OH radical, followed attack by the OH radical and oscillation of the transferring H atom between the OH and H fragments until a H_2O molecule and H atom are left. Of the ReaxFF potentials, the HO2014 parameter set yields the best RMSD, MAX, and NPE of 8.27 kcal mol⁻¹, -15.89 kcal mol⁻¹, and 24.25 kcal mol⁻¹, respectively. The HO2011 parameter set yields the best MSD of -3.46 kcal mol⁻¹. Qualitatively, the positions of local minima and maxima for the HO2014 and CHO2016 parameter sets agree with the reference calculations, though the actual values at these extrema often differ by over 10 kcal mol⁻¹. The same can be said for the CHO2008 and HO2011 parameter sets in the first 100 time steps as well, however the CHO2008 parameter set significantly underestimates the barrier for hydrogen transfer. The HO2011 parameter set gives the most jarring performance qualitatively, with sharp features arising in the region of oscillation of H between OH and H.

In order to probe the origin of the sharp features in the HO2011 potential energy surface, we investigated the component-wise contributions to the potential energy. Figure 3.3 shows the overall potential energy, atom energy, and the difference, all in kcal mol⁻¹. Here the atom energy is defined as the sum of the overcoordination energy E_{over} and undercoordination energy E_{under} . For the HO2011 parameter set, the sharp features in the overall potential energy can be traced to the atom energy, whereas for all other parameter sets this contribution changes much more smoothly. In this term, positive contributions are seen to arise mainly from overcoordination of the transferring hydrogen atom whereas negative

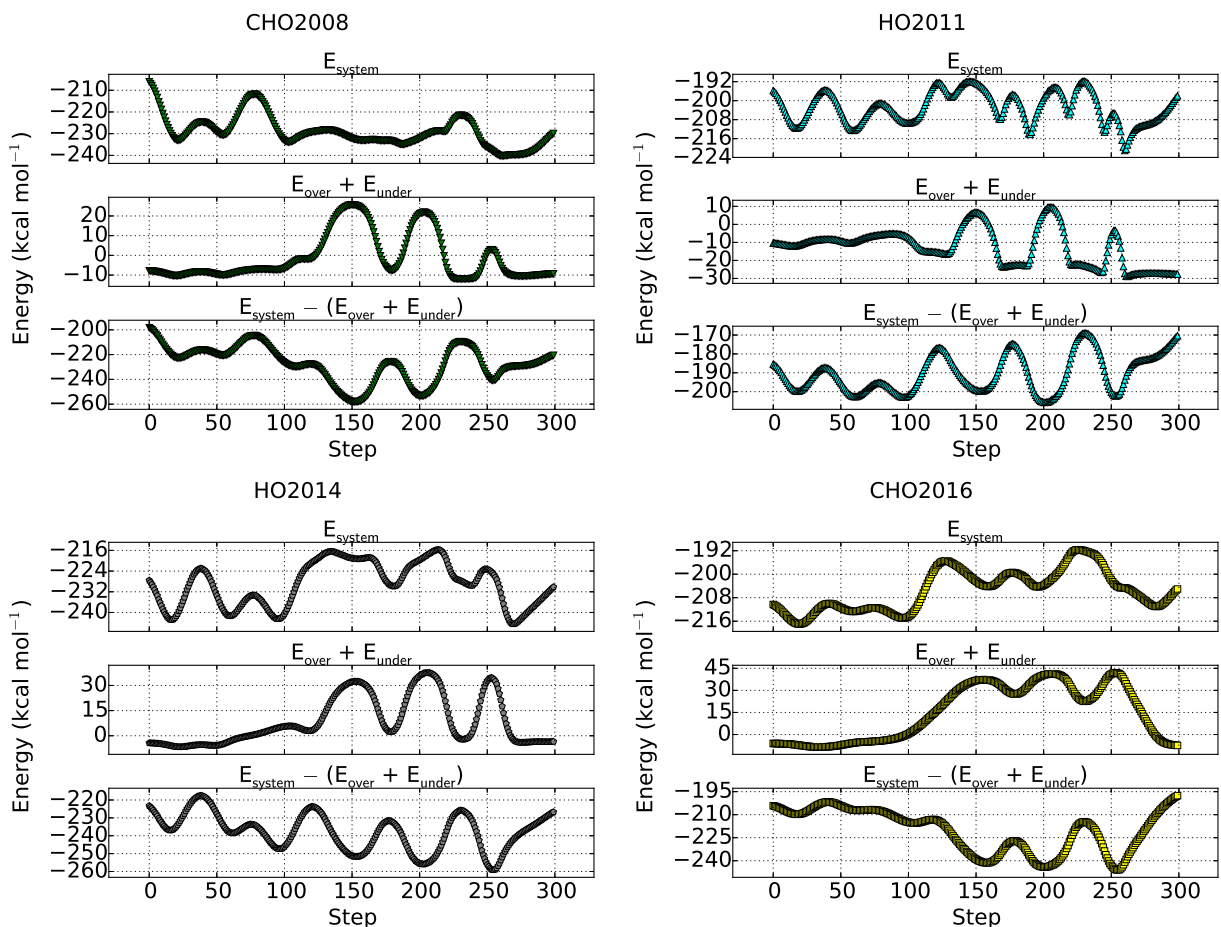


Figure 3.3: Potential energy, atom energy, and the sum of all other energy contributions, in kcal mol⁻¹, for the first $\text{H}_2 + \text{OH} \rightarrow \text{H}_2\text{O} + \text{H}$ reactive pathway, extracted from a larger MD simulation, are presented for the four ReaxFF parameter sets studied. The atom energy is the sum of the overcoordination and undercoordination energy contributions. The total time to complete this reaction path is 30 fs with a time step of 0.1 fs.

contributions arise from undercoordination of the OH radical in the entrance channel and H in the exit channel.

Intrinsic Reaction Coordinate Scans

We have calculated intrinsic reaction coordinate (IRC) scans for a subset of bimolecular reactions taken from Li et al.[165] as an additional set of systems on which to evaluate the performance of ReaxFF. These IRC scans were calculated at the $\omega\text{B97M-V/cc-pVTZ}$ level of theory. Energies of isolated reactant and product species were also calculated at the $\omega\text{B97M-V/cc-pVTZ}$ optimized geometries to present relative energies and compute reaction energies and barrier heights. Eleven scans are included (see Table 3.2 for the full list):

the radical attack of a hydrogen atom and an oxygen molecule to form a hydroxyl radical and an oxygen atom ($\text{H} + \text{O}_2 \longrightarrow \text{OH} + \text{O}$) on the quartet surface, the abstraction of hydrogen from a hydrogen molecule by a hydroxyl radical to form a water molecule and a hydrogen atom ($\text{H}_2 + \text{OH} \longrightarrow \text{H}_2\text{O} + \text{H}$) on the doublet surface, the abstraction of hydrogen from a water molecule by an oxygen atom to form two hydroxyl radicals ($\text{H}_2\text{O} + \text{O} \longrightarrow 2\text{OH}$) on the triplet surface, the formation of a hydroperoxyl radical from a hydrogen atom and an oxygen molecule ($\text{H} + \text{O}_2 \longrightarrow \text{HO}_2$) on the doublet surface, the abstraction of hydrogen from a hydroperoxyl radical by a hydrogen atom to form a hydrogen molecule and an oxygen molecule ($\text{HO}_2 + \text{H} \longrightarrow \text{H}_2 + \text{O}_2$) on the triplet surface, the radical attack of a hydrogen atom on a hydroperoxyl radical to form two hydroxyl radicals ($\text{HO}_2 + \text{H} \longrightarrow 2\text{OH}$) on the triplet surface, the abstraction of hydrogen from a hydroperoxyl radical by a second hydroperoxyl radical to form a hydrogen peroxide molecule and an oxygen molecule ($2\text{HO}_2 \longrightarrow \text{H}_2\text{O}_2 + \text{O}_2$) on the triplet surface, the radical attack of a hydrogen atom on a hydrogen peroxide molecule to form a water molecule and a hydroxyl radical ($\text{H}_2\text{O}_2 + \text{H} \longrightarrow \text{H}_2\text{O} + \text{OH}$) on the doublet surface, the abstraction of hydrogen from a hydrogen peroxide molecule by a hydrogen atom to form a hydrogen molecule and a hydroperoxyl radical ($\text{H}_2\text{O}_2 + \text{H} \longrightarrow \text{H}_2 + \text{HO}_2$) on the doublet surface, the abstraction of hydrogen from a hydrogen peroxide molecule by an oxygen atom to form a hydroperoxyl radical and a hydroxyl radical ($\text{H}_2\text{O}_2 + \text{O} \longrightarrow \text{HO}_2 + \text{OH}$) on the triplet surface, and the abstraction of hydrogen from a hydrogen peroxide molecule by a hydroxyl radical to form a water molecule and a hydroperoxyl radical ($\text{H}_2\text{O}_2 + \text{OH} \longrightarrow \text{H}_2\text{O} + \text{HO}_2$) on the doublet surface. Plots of the potential energy along the IRCs for the methods surveyed are presented in Figures 3.4,3.5,B.8–B.18.

Table 3.2: Root mean square deviation, mean signed deviation, maximum absolute deviation, and non-parallelity error, in kcal/mol, are presented for a selection of intrinsic reaction coordinate scans of elementary reactions relevant to hydrogen combustion. Geometries along the reaction coordinate were calculated at the $\omega\text{B97M-V/cc-pVTZ}$ level of theory. CCSD(T)/CBS values were used as reference.

Reaction	Method	RMSD	MSD	MAX	NPE
$\text{H} + \text{O}_2 \longrightarrow \text{OH} + \text{O}$	$\omega\text{B97M-V}$	1.52	1.36	2.85	2.33
	CHO2008	12.40	-9.37	-37.57	34.64
	HO2011	16.62	-12.14	-42.34	39.11
	HO2014	14.38	-0.96	33.47	45.50
	CHO2016	17.33	-12.77	-48.72	43.71
$\text{H}_2 + \text{OH} \longrightarrow \text{H}_2\text{O} + \text{H}$	$\omega\text{B97M-V}$	2.20	0.95	2.91	5.22
	CHO2008	6.40	2.22	-12.38	21.04
	HO2011	15.50	9.56	44.54	48.60
	HO2014	9.35	3.56	23.35	30.88
	CHO2016	9.24	5.54	16.31	23.16
$\text{H}_2\text{O} + \text{O} \longrightarrow 2\text{OH}$	$\omega\text{B97M-V}$	4.03	-3.51	-6.72	5.73
	CHO2008	28.88	-25.50	-53.15	42.86

Table 3.2: (continued)

Reaction	Method	RMSD	MSD	MAX	NPE
	HO2011	11.65	-4.05	23.24	39.46
	HO2014	17.63	-13.75	-31.44	36.48
	CHO2016	12.91	-10.61	-24.57	23.96
H + O ₂ → HO ₂	ωB97M-V	1.15	0.97	1.92	1.80
	CHO2008	10.25	-10.12	-14.06	6.76
	HO2011	9.40	-5.59	-14.17	21.20
	HO2014	14.92	-7.46	-21.49	36.32
	CHO2016	7.69	-2.68	-10.47	19.55
HO ₂ + H → H ₂ + O ₂	ωB97M-V	1.08	-0.40	-3.23	3.98
	CHO2008	10.03	4.98	19.05	31.95
	HO2011	5.18	-2.59	-11.57	15.35
	HO2014	21.36	-17.28	-32.82	33.26
	CHO2016	6.18	-1.29	12.06	19.38
HO ₂ + H → 2 OH	ωB97M-V	2.38	1.87	4.04	3.68
	CHO2008	11.84	-9.93	-28.12	26.36
	HO2011	16.17	-6.87	-36.94	47.49
	HO2014	25.91	-21.95	-38.11	34.65
	CHO2016	17.39	-11.83	-49.89	47.07
2 HO ₂ → H ₂ O ₂ + O ₂	ωB97M-V	1.97	-0.69	-4.27	5.93
	CHO2008	5.31	-2.69	-15.33	22.31
	HO2011	12.00	10.01	24.65	23.63
	HO2014	25.32	-9.90	-41.68	59.91
	CHO2016	11.75	4.01	20.44	31.80
H ₂ O ₂ + H → H ₂ O + OH	ωB97M-V	2.12	1.81	3.12	3.42
	CHO2008	3.81	1.83	11.49	12.53
	HO2011	12.96	9.26	19.18	20.57
	HO2014	16.97	5.62	41.82	50.24
	CHO2016	11.84	7.00	17.84	23.45
H ₂ O ₂ + H → H ₂ + HO ₂	ωB97M-V	2.65	-1.59	-4.87	5.84
	CHO2008	6.49	-1.64	-17.13	22.76
	HO2011	9.05	5.78	30.34	37.39
	HO2014	9.61	5.88	16.51	22.95
	CHO2016	4.90	1.15	-11.22	17.91
H ₂ O ₂ + O → HO ₂ + OH	ωB97M-V	3.86	-3.37	-7.71	6.77
	CHO2008	19.71	-17.65	-38.11	30.37
	HO2011	9.66	2.29	26.85	32.55
	HO2014	7.82	2.69	20.47	25.41
	CHO2016	4.50	1.09	7.78	13.85
H ₂ O ₂ + OH → H ₂ O + HO ₂	ωB97M-V	2.68	-2.49	-6.79	4.88

Table 3.2: (continued)

Reaction	Method	RMSD	MSD	MAX	NPE
	CHO2008	8.92	-3.27	-28.16	34.93
	HO2011	10.77	7.74	32.74	28.52
	HO2014	21.47	15.92	44.76	43.01
	CHO2016	13.27	8.13	22.78	25.31
All IRCs	Method	RMSD	MSD	MAX	NPE
	ω B97M-V	2.49	-0.42	-7.71	6.77
	CHO2008	12.47	-5.54	-53.15	42.86
	HO2011	12.36	1.78	44.54	48.60
	HO2014	18.30	-2.46	44.76	59.91
	CHO2016	11.79	-0.40	-49.89	47.07

Table 3.2 presents the RMSD, MSD, MAX, and NPE, all in kcal mol⁻¹, for the IRC scans. For the overall metrics, ω B97M-V again outperforms all of the surveyed ReaxFF methods by at least a factor of 4 for RMSDs, 5 for MAXs, and 6 for NPEs. Of the ReaxFF methods, the CHO2016 parameter set is shown to outperform all other parameter sets in terms of RMSDs with a value of 11.79 kcal mol⁻¹, followed closely by the HO2011 set the CHO2008 set, and finally the HO2014 set. For NPEs, the worst performances are 42.86 kcal mol⁻¹, 47.07 kcal mol⁻¹, 48.60 kcal mol⁻¹, and 59.91 kcal mol⁻¹ for the CHO2008 set, the CHO2016 set, the HO2011 set, and the HO2014 set, respectively. The lowest NPE for any of the ReaxFF parameter sets is 12.53 kcal mol⁻¹. This demonstrates the failure of ReaxFF to quantitatively replicate the shape of the CCSD(T) potential energy surface.

Table 3.3 presents the reaction energies, forward reaction barrier heights, and reverse reaction barrier heights for the IRC scans at the CCSD(T)/CBS level of theory and errors in these quantities for all other methods considered. For these calculations, forward and reverse barrier heights are measured as the difference between the maximum along the IRC and the isolated reactants or products at the ω B97M-V/cc-pVTZ optimized geometries, respectively. Reaction energies are computed as the difference between these isolated products and reactants. For both reaction energies and barrier heights ω B97M-V outperforms the best ReaxFF methods by a factor of 2 for reaction energy errors and a factor of 3 for barrier height errors. Of the ReaxFF parameter sets, the HO2011 set shows the best performance for reaction energies with an RMSD of 7.15 kcal mol⁻¹, followed by the CHO2016 set, the CHO2008 set, and the HO2014 set with RMSDs of 12.40 kcal mol⁻¹, 14.67 kcal mol⁻¹, and 25.09 kcal mol⁻¹, respectively. Turning to barrier heights, the performance of the ReaxFF methods is split, with the CHO2008 and CHO2016 parameter sets outperforming the HO2014 and HO2011 parameter sets by more than 8 kcal mol⁻¹. The CHO2008 parameter set is generally seen to underestimate the forward and reverse barriers and in many cases stabilizes configurations in the region of the ω B97M-V transition state, leading to a double-barrier potential energy surface. The CHO2016 parameter set shows a similar performance, both underestimating forward and reverse barriers and exhibiting multiple barriers on the potential energy surface.

For the HO2011 parameter set, forward and reverse barriers are seen to be overestimated on average. In particular, reaction barriers are strongly overestimated for hydrogen transfer reactions, with the exception of the $\text{HO}_2 + \text{H} \longrightarrow \text{H}_2 + \text{O}_2$ IRC scan. The HO2014 parameter set also overestimates both forward and reverse reaction barriers on average, with the performance being exacerbated by the poor performance on reaction energies.

Table 3.3: Reaction energy errors, forward reaction barrier height errors, and reverse reaction barrier height errors, in kcal mol^{-1} , are presented for a selection of intrinsic reaction coordinate scans of elementary reactions relevant to hydrogen combustion. Geometries along the reaction coordinate were calculated at the $\omega\text{B97M-V/cc-pVTZ}$ level of theory. CCSD(T)/CBS values were used as a reference and the reaction energies, forward reaction barriers, and reverse reaction barriers are reported, in kcal mol^{-1} . Infinitely separated reactants and products optimized at the $\omega\text{B97M-V/cc-pVTZ}$ level of theory are taken as the endpoints of the reaction paths.

Reaction	Method	ΔE	ΔE_f^\ddagger	ΔE_b^\ddagger
$\text{H} + \text{O}_2 \longrightarrow \text{OH} + \text{O}$	CCSD(T)/CBS	11.73	41.05	29.32
	$\omega\text{B97M-V}$	5.51	2.69	-2.82
	CHO2008	-17.22	-20.15	-2.92
	HO2011	6.43	-35.80	-42.23
	HO2014	-13.00	13.59	26.58
	CHO2016	-5.99	-33.38	-27.39
$\text{H}_2 + \text{OH} \longrightarrow \text{H}_2\text{O} + \text{H}$	CCSD(T)/CBS	-16.63	5.61	22.24
	$\omega\text{B97M-V}$	2.05	-2.31	-4.36
	CHO2008	8.55	3.27	-5.28
	HO2011	8.64	34.06	25.42
	HO2014	9.15	10.74	1.58
	CHO2016	13.62	2.72	-10.90
$\text{H}_2\text{O} + \text{O} \longrightarrow 2 \text{OH}$	CCSD(T)/CBS	19.00	22.05	3.06
	$\omega\text{B97M-V}$	-1.92	-6.65	-4.73
	CHO2008	-25.83	-32.91	-7.08
	HO2011	-13.82	21.44	35.26
	HO2014	-28.01	1.69	29.70
	CHO2016	-16.88	-13.76	3.12
$\text{H} + \text{O}_2 \longrightarrow \text{HO}_2$	CCSD(T)/CBS	-55.81	1.56	57.37
	$\omega\text{B97M-V}$	1.48	0.23	-1.25
	CHO2008	-14.25	-7.54	6.70
	HO2011	7.00	-7.98	-14.98
	HO2014	15.24	-16.32	-31.56
	CHO2016	5.61	-7.30	-12.91
$\text{HO}_2 + \text{H} \longrightarrow \text{H}_2 + \text{O}_2$	CCSD(T)/CBS	-54.12	2.62	56.74
	$\omega\text{B97M-V}$	-0.17	-0.95	-0.78
	CHO2008	18.37	-2.85	-21.21

Table 3.3: (continued)

Reaction	Method	ΔE	ΔE_f^\ddagger	ΔE_b^\ddagger
	HO2011	0.02	1.15	1.13
	HO2014	-13.89	-0.94	12.95
	CHO2016	-0.09	7.84	7.94
$\text{HO}_2 + \text{H} \longrightarrow 2 \text{OH}$	CCSD(T)/CBS	-40.02	14.42	54.43
	ω B97M-V	5.46	0.95	-4.52
	CHO2008	-16.15	-15.79	0.35
	HO2011	1.26	-15.54	-16.79
	HO2014	-45.75	-8.68	37.07
	CHO2016	-9.34	-16.70	-7.36
$2 \text{HO}_2 \longrightarrow \text{H}_2\text{O}_2 + \text{O}_2$	CCSD(T)/CBS	-39.20	0.29	39.49
	ω B97M-V	2.75	-4.00	-6.75
	CHO2008	10.76	-11.09	-21.84
	HO2011	-0.19	20.58	20.77
	HO2014	-38.29	17.53	55.81
	CHO2016	-10.53	17.04	27.57
$\text{H}_2\text{O}_2 + \text{H} \longrightarrow \text{H}_2\text{O} + \text{OH}$	CCSD(T)/CBS	-71.56	7.19	78.76
	ω B97M-V	4.59	0.08	-4.51
	CHO2008	0.01	10.06	10.05
	HO2011	10.10	2.00	-8.10
	HO2014	-12.20	29.67	41.87
	CHO2016	14.72	-5.41	-20.14
$\text{H}_2\text{O}_2 + \text{H} \longrightarrow \text{H}_2 + \text{HO}_2$	CCSD(T)/CBS	-14.92	10.24	25.16
	ω B97M-V	-2.92	-3.23	-0.31
	CHO2008	7.61	-9.55	-17.16
	HO2011	0.20	28.29	28.09
	HO2014	24.40	3.89	-20.51
	CHO2016	10.44	-2.17	-12.62
$\text{H}_2\text{O}_2 + \text{O} \longrightarrow \text{HO}_2 + \text{OH}$	CCSD(T)/CBS	-12.55	11.86	24.42
	ω B97M-V	-2.79	-7.29	-4.50
	CHO2008	-9.67	-21.31	-11.64
	HO2011	-4.98	24.35	29.33
	HO2014	5.54	10.19	4.65
	CHO2016	7.18	-2.10	-9.29
$\text{H}_2\text{O}_2 + \text{OH} \longrightarrow \text{H}_2\text{O} + \text{HO}_2$	CCSD(T)/CBS	-31.55	3.33	34.88
	ω B97M-V	-0.87	-5.69	-4.81
	CHO2008	16.16	-10.66	-26.82
	HO2011	8.84	26.29	17.46
	HO2014	33.55	25.20	-8.35
	CHO2016	24.06	1.77	-22.29

Table 3.3: (continued)

Reaction	Method	ΔE	ΔE_f^\ddagger	ΔE_b^\ddagger
RMSD	Method	ΔE	ΔE^\ddagger	
	ω B97M-V	3.25	4.00	
	CHO2008	14.67	15.08	
	HO2011	7.15	23.69	
	HO2014	25.09	23.45	
	CHO2016	12.40	15.24	

Figure 3.4 presents the potential energy along the $\text{H}_2 + \text{OH} \longrightarrow \text{H}_2\text{O} + \text{H}$ IRC for the CCSD(T) reference, ω B97M-V, and the four ReaxFF parameter sets. For the CHO2008 parameter set, we see a slightly overestimated barrier followed by a overstabilization of the configurations in the center of the scan. The HO2011 parameter set is seen to overestimate the forward and reverse barriers by 34 kcal mol⁻¹ and 25 kcal mol⁻¹, respectively. The HO2014 parameter set exhibits an exaggerated forward barrier and underestimates the stabilization in the product channel. The CHO2016 parameter set yields a comparatively good forward barrier but clearly overstabilizes configurations near the transition state leading to a second barrier.

Figure 3.5 presents the potential energy along the $\text{H}_2\text{O}_2 + \text{OH} \longrightarrow \text{H}_2\text{O} + \text{HO}_2$ IRC for the CCSD(T) reference, ω B97M-V, and the four ReaxFF parameter sets. Here the CHO2008 parameter set fails to predict a forward barrier to reaction and significantly overstabilizes configuration in the transition state regime. The HO2011 parameter set yields an exaggerated barrier that overestimates the forward barrier height by 26 kcal mol⁻¹ and the reverse barrier height by 17 kcal mol⁻¹. For the HO2014 parameter set the forward barrier is exaggerated nearly to the extent of the HO2011 parameter set and severely understabilizes the product channel, leading to a reaction energy error of 34 kcal mol⁻¹. The CHO2016 parameter set again gives a second barrier for this reaction and poorly reproduces the reaction barrier.

For both of the reactions presented above, Agrawalla and van Duin[203] show that the forward reactions should have no forward barrier with the HO2011 parameter set. In order to better elucidate the nature of the potential energy surfaces, Figures 3.6 and 3.7 present unrelaxed two-dimensional potential energy surfaces for the reactions $\text{H}_2 + \text{OH} \longrightarrow \text{H}_2\text{O} + \text{H}$ and $\text{H}_2\text{O}_2 + \text{OH} \longrightarrow \text{H}_2\text{O} + \text{HO}_2$, respectively. For these surfaces, the bonds which are breaking and forming are linearized while all other internal coordinates are held fixed in the configuration of the transition state calculated at the ω B97M-V/cc-pVTZ level of theory. The interatomic distance along the IRC for the bonds breaking and forming are superimposed in each plot to approximate the one-dimensional slices given in Figures 3.4 and 3.5.

Beginning with $\text{H}_2 + \text{OH} \longrightarrow \text{H}_2\text{O} + \text{H}$, the transition state structure as optimized with ω B97M-V has an HO–H bond length of 1.35 Å and a H–H bond length of 0.82 Å. The CHO2008 surface displays an entrance channel with a longer optimal H–H bond length and predicts a transition state structure to occur with a longer HO–H bond length and a longer H–H bond length. This surface also displays a well that extends to much shorter

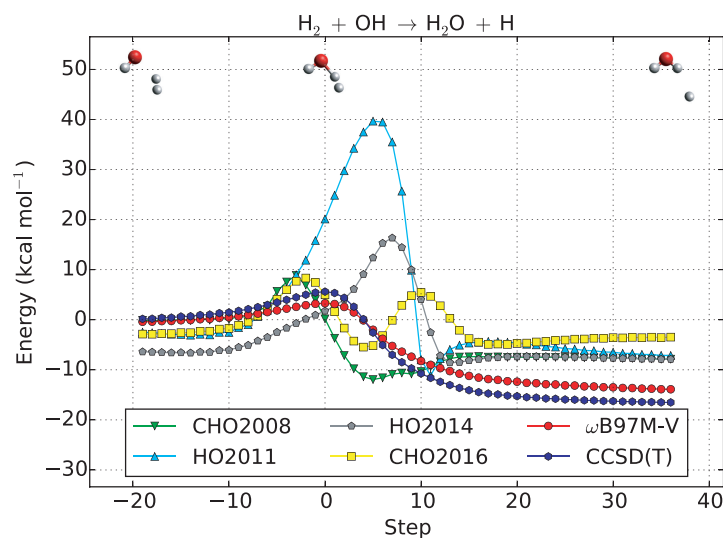


Figure 3.4: Potential energies along the $\text{H}_2 + \text{OH} \longrightarrow \text{H}_2\text{O} + \text{H}$ intrinsic reaction coordinate are presented for four ReaxFF parameter sets, $\omega\text{B97M-V}$, and CCSD(T). Geometries along the reaction coordinate were calculated at the $\omega\text{B97M-V/cc-pVTZ}$ level of theory. The energies presented are relative to the energies of isolated H_2 and OH computed at the $\omega\text{B97M-V/cc-pVTZ}$ optimized geometries.

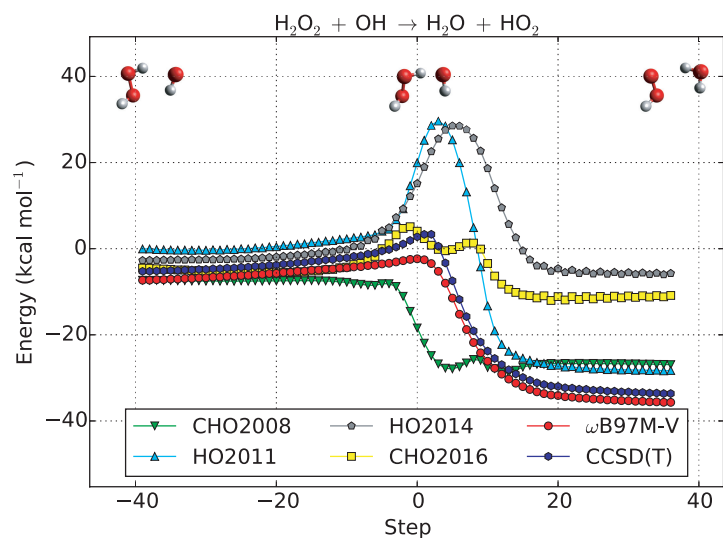


Figure 3.5: Potential energies along the $\text{H}_2\text{O}_2 + \text{OH} \longrightarrow \text{H}_2\text{O} + \text{HO}_2$ intrinsic reaction coordinate are presented for four ReaxFF parameter sets, $\omega\text{B97M-V}$, and CCSD(T). Geometries along the reaction coordinate were calculated at the $\omega\text{B97M-V/cc-pVTZ}$ level of theory. The energies presented are relative to the energies of isolated H_2O_2 and OH computed at the $\omega\text{B97M-V/cc-pVTZ}$ optimized geometries.

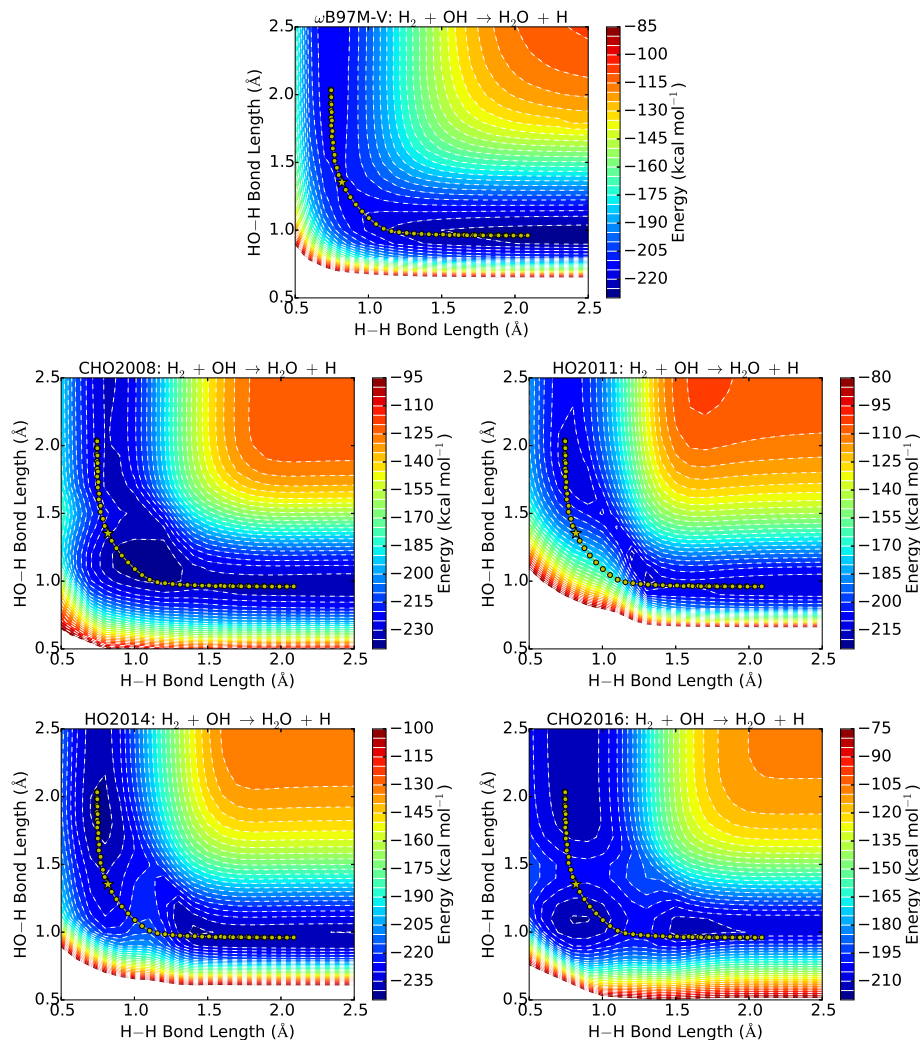


Figure 3.6: Unrelaxed potential energy surfaces for the $\text{H}_2 + \text{OH} \longrightarrow \text{H}_2\text{O} + \text{H}$ reaction, in kcal mol^{-1} , are presented for $\omega\text{B97M-V}$ and four ReaxFF parameter sets. Here the $\text{HO}\cdots\text{H}\cdots\text{H}$ angle is linearized while all other geometric parameters are held fixed in the transition state configuration as optimized at the $\omega\text{B97M-V/cc-pVTZ}$ level of theory. The interatomic distances for points along the intrinsic reaction coordinate calculated at the $\omega\text{B97M-V/cc-pVTZ}$ level of theory are overlaid on each surface. The energies presented are relative to the energies of the isolated atoms.

H–H bond lengths than the ω B97M-V surface. The HO2011 surface predicts a transition state structure with a longer H–H bond length. Following the IRC on the HO2011 surface elucidates the origin of the large errors in the barrier heights for this parameter set. The HO2014 surface predicts a transition state structure with a longer H–H bond length while the IRC skews toward a longer HO–H bond length, leading to an exaggerated barrier. The CHO2016 surface demonstrates the double barrier seen in Figure 3.4, with one transition state structure with a longer HO–H bond length and another with a longer H–H bond length. This surface also exhibits an exit channel with a slightly longer HO–H bond length than the ω B97M-V surface.

For $\text{H}_2\text{O}_2 + \text{OH} \longrightarrow \text{H}_2\text{O} + \text{HO}_2$, the transition state structure as optimized with ω B97M-V has an HOO–H bond length of 1.04 Å and a HO–H bond length of 1.37 Å. The CHO2008 surface exhibits a transition state structure with a longer HO–H bond length and a well in the region immediately after the ω B97M-V transition state. The HO2011 surface predicts a transition state structure with a longer HOO–H bond length, leading to an exaggeration of the barrier along the ω B97M-V IRC. This behavior is also seen in the HO2014 surface, though the HO2014 surface predicts a longer optimum HOO–H bond length in the entrance channel. The CHO2016 surface exhibits very little energy variation across the IRC, which misses a narrow well in the product channel. The IRC is also destabilized by a short HOO–H bond length in the region of the ω B97M-V transition state.

These two dimensional potential energy surfaces, coupled with the IRC scans, demonstrate failures of the ReaxFF methods to accurately model the QM methods. The ReaxFF potential show a general trend towards looser transition state structures. These differences can be expected to manifest themselves in MD simulations, where exaggerated barriers will prevent reactivity that would otherwise occur on the QM surfaces and under-estimated barriers will overrepresent other reactions.

3.4 Conclusions

We have benchmarked the performance of several ReaxFF methods against state-of-the-art DFT calculations and CCSD(T). The data sets included both reactive pathways extracted from MD simulations and IRC scans, reaction energies, and barrier heights computed with ω B97M-V. For the reactive pathways, the CHO2016 and HO2011 parameter sets had the best RMSDs (11 and 12 kcal mol⁻¹, respectively) while the average NPEs were similar across all methods surveyed (38 kcal mol⁻¹, 40 kcal mol⁻¹, 42 kcal mol⁻¹, and 42 kcal mol⁻¹ for CHO2008, HO2011, HO2014, and CHO2016, respectively). Along the reaction coordinate scans, the CHO2016, HO2011, and CHO2008 parameter sets exhibit similar performance on RMSDs (12 kcal mol⁻¹), while the average NPEs are favor CHO2008 and CHO2016 (26 kcal mol⁻¹ for CHO2008 and CHO2016; 32 kcal mol⁻¹ and 38 kcal mol⁻¹ for HO2011 and HO2014, respectively). While in principle the RMSDs are subject to systematic error, the NPEs serve as an independent metric.

While these results appear to be a condemnation of ReaxFF methods for these systems,

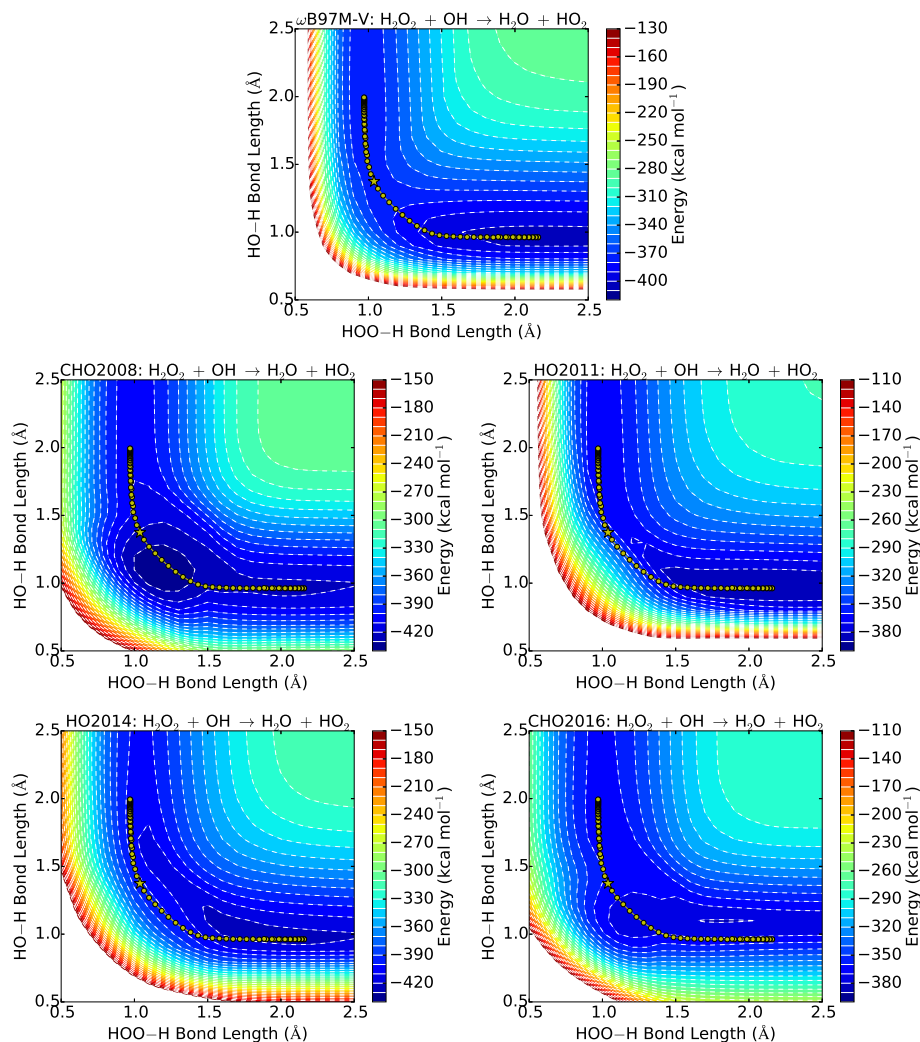


Figure 3.7: Unrelaxed potential energy surfaces for the $\text{H}_2\text{O}_2 + \text{OH} \longrightarrow \text{H}_2\text{O} + \text{HO}_2$ reaction, in kcal mol^{-1} , are presented for $\omega\text{B97M-V}$ and four ReaxFF parameter sets. Here the $\text{HOO}\cdots\text{H}\cdots\text{OH}$ angle is linearized while all other geometric parameters are held fixed in the transition state configuration as optimized at the $\omega\text{B97M-V/cc-pVTZ}$ level of theory. The interatomic distances for points along the intrinsic reaction coordinate calculated at the $\omega\text{B97M-V/cc-pVTZ}$ level of theory are overlaid on each surface. The energies presented are relative to the energies of the isolated atoms.

studies by both the developers[188, 200–204, 206, 207, 210, 212, 216–221, 223, 225–230, 232–246] and users[180–183, 205, 208, 209, 211, 213–215, 222, 224, 231] have demonstrated the utility of ReaxFF as an exploratory tool for atomistic simulation. We also acknowledge the difficulty of parameter training for the ReaxFF system. Our results here point to ways to improve the treatment of hydrogen combustion.

- Amount of training data: Training data for the hydrogen combustion potentials with ReaxFF has largely centered around bond stretches, angle distortions, heats of formation, and reaction barriers. As seen in the IRC scans, the transition state structures computed with DFT are often higher-energy structures on the ReaxFF potential energy surfaces. More geometric properties of transition state structures in the ReaxFF training set should in principle help to relieve this discrepancy. The variable performance of the various ReaxFF potentials on the reactive pathways suggest that inclusion of data points far from the minimum energy pathways would improve the overall fidelity of the method.
- Quality of training data: References 200, 203, and 216 all specify that the QM training data was generated at the B3LYP/6-311G** level of theory [56, 61, 260]. A recent review of DFT benchmarked the performance of over 200 functionals across diverse chemical systems, including hydrogen transfer and non-hydrogen transfer barrier heights. For these two test sets, B3LYP gave RMSDs of 4.89 kcal mol⁻¹ and 5.52 kcal mol⁻¹, respectively, while ω B97M-V gave RMSDs of 1.72 kcal mol⁻¹ and 1.98 kcal mol⁻¹, respectively.
- Optimization methods for parameter training: The ReaxFF parameter sets employed in this study were generated using the successive one-parameter parabolic extrapolation (SOPPE) approach[261], which is both tedious and subject to converging to local minima. As a more global optimization scheme, several studies beginning with Pahari and Chaturvedi in 2012[262] and Larrson, van Duin, and Hartke[263, 264] in 2013 have used genetic algorithms to optimize parameters for different ReaxFF potentials. More recently, a study of ReaxFF parameter optimization with Monte-Carlo and evolutionary algorithms has shown that care needs to be used when employing such methods and gives recommendations for initial guesses[265]. Machine learning approaches have also been applied recently to a parameter optimization scheme for ReaxFF[266]
- Overall form of the potential: Furman and Wales[267] recently published a letter in which a Taper corrections applied to bond order and bond length terms in ReaxFF are able to greatly reduce energy drifts seen in MD simulations on long timescales. Such corrections could in principle improve the sharp changes in the atom energy term seen in Figure 3.3. Currently work is also being done to replace the charge equilibration scheme in ReaxFF with a more advanced C-GeM model[268].

Overall, the benchmarking of ReaxFF potential for hydrogen combustion systems shows that there is room for improvement in order to more closely match QM potential energies,

energy differences important for thermochemistry, and energy barriers controlling chemical kinetics.

Chapter 4

Third-Order Møller-Plesset Perturbation Theory Made Useful? Choice of Orbitals and Scaling Greatly Improves Accuracy

Reprinted with permission from Bertels, L. W.; Lee, J.; Head-Gordon, M. Third-Order Møller-Plesset Perturbation Theory Made Useful? Choice of Orbitals and Scaling Greatly Improves Accuracy for Thermochemistry, Kinetics, and Intermolecular Interactions. *J. Phys. Chem. Lett.* **2019**, 10, 4170-4176.

4.1 Introduction

Single-reference second-order Møller-Plesset perturbation theory (MP2) is among the most popular correlated wavefunction methods in electronic structure theory, in part due to its economical $\mathcal{O}(N^5)$ scaling, where N is the basis set size.

$$E_{MP2} = -\frac{1}{4} \sum_{ijab} \frac{|\langle ij||ab \rangle|^2}{\Delta_{ij}^{ab}} \quad (4.1)$$

Equation (4.1) gives the correlation energy for MP2, where i, j, \dots represent occupied molecular orbitals, a, b, \dots represent virtual molecular orbitals, and $\Delta_{ij}^{ab} = \varepsilon_a + \varepsilon_b - \varepsilon_i - \varepsilon_j$ is the (non-negative) energy denominator. The resolution-of-identity (RI) technique applied to MP2 has allowed for a much more widespread use due to the reduction of the prefactor in the overall computational cost of the algorithm.[29, 30]

Orbital-optimized MP2 (OOMP2) methods were developed to improve the performance of MP2 for energies and other properties.[35–37]. For systems where the unrestricted Hartree-Fock (UHF) reference exhibits spin-contamination (artificial spin-symmetry breaking), the

use of these reference orbitals can lead to catastrophic performance of MP2.[31–34] OOMP2 can also be thought of as a relatively inexpensive way to approximate Brückner orbitals.[35] Orbital optimization at the MP2 level often reduces the level of spin-contamination and improves energetics.[35, 36, 269]

Despite the benefits of OOMP2 described above, there are several unsatisfying characteristics of the method that limit its applicability. Orbital optimization at the MP2 level can produce divergent energy contributions due to small energy denominators. This is often observed when stretching bonds and leads to significant underestimation of harmonic vibrational frequencies.[40] OOMP2 also often fails to continuously transition from spin-restricted (R) to spin-unrestricted (U) solutions even when the U solution is lower in energy.[270] A continuous R to U transition requires a Coulson-Fischer point where the lowest eigenvalue of the R to U stability Hessian becomes zero.[271] Resolution of this issue is necessary to reach the proper dissociation limit for bond-breaking curves.

Our group has attempted to remedy these issues of OOMP2 through use of regularization to prevent divergence of the energy due to small energy denominators. The first of these approaches was to shift the energy denominator by a constant factor, δ , so that $\Delta_{ij}^{ab} \leftarrow \Delta_{ij}^{ab} + \delta$. [40] This simple form was able to partially resolve the two issues with OOMP2 described above. The regularization parameter, δ , both prevents the energy expression from diverging and damps the correlation energy contribution from MP2, leading the method to more closely resemble the continuous R to U transition seen in the HF reference. Unfortunately, in the case of scaled opposite spin OOMP2 (SOS-OOMP2), Razban et al.[41] found the values of δ that could restore Coulson-Fischer points were very large and consequently led to poor performance on problems that are normally well-treated by MP2.

Recently, two of us[39] developed two new classes of orbital energy dependent regularizers for OOMP2, of which the most promising is denoted as κ -OOMP2. In κ -OOMP2, the matrix elements associated with small denominators are damped such that:

$$E_{MP2}(\kappa) = -\frac{1}{4} \sum_{ijab} \frac{|\langle ij || ab \rangle|^2}{\Delta_{ij}^{ab}} \left(1 - e^{-\kappa(\Delta_{ij}^{ab})}\right)^2 \quad (4.2)$$

Unlike the case of δ -OOMP2, for κ -OOMP2 the unregularized energy expression is recovered for large energy denominators, and in the limit of small energy denominators, the correlation energy contributions are zero. Regularization parameters of $\kappa \leq 1.5E_h^{-1}$ were found to restore Coulson-Fischer points for hydrogen, ethane, ethene, and ethyne bond-breaking curves. κ was trained on the W4-11 set to suggest a value for general application.[272] The result, $\kappa = 1.45E_h^{-1}$, proved robust to further testing on the RSE43[273] and TA13[274] sets, and defines κ -OOMP2 as a replacement for OOMP2. Complex restricted (cR) and complex general (cG) orbital extensions of κ -OOMP2 have also been used to interrogate singlet biradicaloids[275] and the nature of symmetry breaking in fullerenes[276], respectively.

The success and ubiquity of MP2 and OOMP2 have led several research groups to develop modified second-order methods aimed at improving energetics. Notable examples are spin-component-scaled MP2 (SCS-MP2)[277–282] and orbital optimized SCS-MP2 (SCS-OOMP2)[35, 36] methods, which weight correlation contributions coming from same-spin

and opposite-spin pairs of electrons differently. These techniques have also been applied to the second-order correlation contribution in several double-hybrid density functionals.[86, 88, 283–285] A subset of these methods, scaled-opposite-spin MP2 (SOS-MP2)[278, 280, 282] and SOS-OOMP2[35], are notable in that they can be implemented via an overall $\mathcal{O}(N^4)$ computational cost. Another example are the attenuated MP2 methods that partially cancel basis set superposition errors with errors in MP2 itself to yield improved intermolecular interaction energies in finite basis sets.[286–289] Density-fitting and Cholesky-decomposed variants of OOMP2 have also been developed to improve the computational efficiency of the method.[290]

Inclusion of higher-order terms in the perturbative expansion provides another approach to improve energetics from MP2.

$$\begin{aligned}
 E_{MP3} = & \frac{1}{8} \sum_{ijklcd} (t_{ij}^{ab})^* \langle ab || cd \rangle t_{ij}^{cd} \\
 & + \frac{1}{8} \sum_{ijklab} (t_{ij}^{ab})^* \langle kl || ij \rangle t_{kl}^{ab} \\
 & - \sum_{ijkabc} (t_{ij}^{ab})^* \langle kb || ic \rangle t_{kj}^{ac}
 \end{aligned} \tag{4.3}$$

Equation (4.3) gives the third-order Møller-Plesset (MP3) contribution to the correlation energy in the spin-orbital basis. MP3 formally scales as $\mathcal{O}(N^6)$ with basis set size, and describes the leading interaction of first-order pair-correlations, t_{ij}^{ab} , with each other. However, despite the higher compute cost, MP3 only modestly improves MP2 results (e.g. see data presented later). In passing we note that it is possible to utilize separable density fitting techniques such as tensor hypercontraction to achieve quartic scaling ($\mathcal{O}(N^4)$) MP3 (and also MP2) energy evaluation.[291]

Grimme[277] developed a spin-component scaled MP3 (SCS-MP3) method that improved ground state energies over SCS-MP2 for reaction energies, atomization energies, ionization energies, and stretched geometries. This method applied an overall third-order correlation energy scaling factor of 0.25 in addition to the scaling factors for same-spin and opposite-spin components. For weak noncovalent interactions, application of MP3 has failed to substantially improve binding energies as compared to MP2.[277, 281, 292–296] Hobza and coworkers[294–296] proposed scaling the third-order correlation energy to interpolate between the MP2 and MP3, leading to the development of MP2.5 and MP2.X, in order to improve binding energies for noncovalent interactions. Following these successes, Bozkaya and coworkers[269, 290, 297–299] developed OOMP3 and OOMP2.5 and evaluated the performance of these methods on thermochemistry, kinetics, and noncovalent interactions. OOMP2.5 was shown to outperform coupled cluster theory with single and double excitations (CCSD)[22, 23] on reaction energies and barrier heights [269] and perform comparably to coupled cluster with single, double, and perturbative triple excitations [CCSD(T)][25] for noncovalent interactions[290]. These are very promising results. Analytic gradients for OOMP3, OOMP2.5, and their density-fitting variants have also been introduced.[300, 301]

Following the recent success of regularized OOMP2 in treating inherent problems in OOMP2, we decided to explore the use of κ -OOMP2 orbitals at the MP3 level. At the same time, we wanted to see if κ regularization in MP3 could improve the overall energetics. Beginning from κ -OOMP2 would allow this method to avoid energy divergences caused by small energy denominators.[39]

4.2 Theory

In κ -OOMP2, damping of the two-electron integrals leads to the following expression for the t -amplitudes:

$$t_{ij}^{ab}(\kappa) = -\frac{\langle ab||ij\rangle}{\Delta_{ij}^{ab}} \left(1 - e^{-\kappa\Delta_{ij}^{ab}}\right). \quad (4.4)$$

Inserting Equation (4.4) into Equation (4.3) we arrive at a regularized third-order correlation energy expression, $E_{MP3}(\kappa)$. Our first candidate ansatz involved calculating the κ -OOMP2 energy and applying a scaled single-shot $E_{MP3}(\kappa)$ correction.

$$E_c(\kappa, \kappa_2, c_3) = E_{\kappa\text{-OOMP2}}(\kappa) + c_3 E_{MP3:\kappa\text{-OOMP2}}(\kappa_2) \quad (4.5)$$

As a second, alternative form, we considered using κ -OOMP2 (with $\kappa = 1.45E_h^{-1}$) as a method to generate molecular orbitals for use in correlated calculations containing second and third order energies which could then be independently regularized and/or scaled:

$$E_c(\kappa, \kappa_2, c_2, c_3) = c_2 E_{MP2:\kappa\text{-OOMP2}}(\kappa_2) + c_3 E_{MP3:\kappa\text{-OOMP2}}(\kappa_2) \quad (4.6)$$

In this second case the non-Brillouin singles contribution, $-\sum_{ia} f_{ia}^2/\Delta_i^a$, is included at second-order as κ -OOMP2 does not obey the Brillouin theorem. For simplicity (and ease of implementation), we do not include a non-Brillouin singles contribution at third-order.

We trained both energy functionals on the non-multireference (non-MR) subset of the W4-11 thermochemistry data set.[272] We excluded the MR points in the set from the training data because the single reference methods we are investigating should not be able to describe MR systems adequately. Both reference and training calculations were performed using the aug-cc-pVTZ (aVTZ) basis set [119, 120, 302] and the corresponding RI basis[303, 304] without the frozen core approximation. Reference data were computed using CCSD(T)[25]. All calculations were performed in a development version of Q-Chem[125].

4.3 Results

Figure 4.1 presents the root mean square deviations (RMSD) for scans of the κ_2 and c_3 parameters in the first model, as given by Equation 4.5. Overall, we see that stronger regularization at third-order (smaller κ_2) serves to lower the error on the training set. For $\kappa_2 = 1.00E_h^{-1}$, the optimal scaling parameter for the third-order regularized correlation

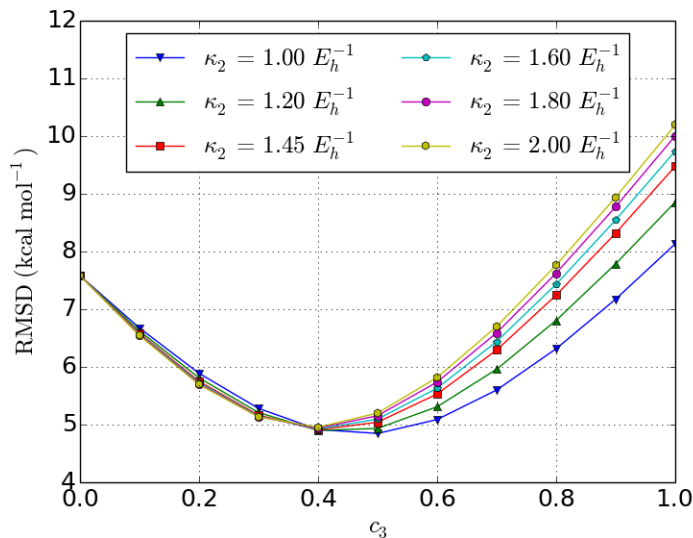


Figure 4.1: Scans of the root mean square deviation on the non-MR subset of the W4-11 thermochemistry data set, in kcal mol⁻¹, for the scaled, two regularization parameter correlation energy functional given in Equation 4.5. We fix $\kappa = 1.45E_h^{-1}$. All calculations use the aVTZ basis; CCSD(T) is used for the reference values.

energy is 0.5 for a RMSD of 4.85 kcal mol⁻¹. If instead one applies the same regularization parameter ($\kappa = 1.45E_h^{-1}$) at second- and third-order, we find an optimal scaling parameter for the third order correlation energy of $c_3 = 0.4$ with a RMSD of 4.91 kcal mol⁻¹. We note that $c_3 = 0.0$ corresponds to κ -OOMP2 with a RMSD of 7.58 kcal mol⁻¹. Inclusion of scaled, regularized third-order correlation energy contributions reduces the RMSD of κ -OOMP2 by more than 2.5 kcal mol⁻¹, which is useful but not dramatic.

Turning to the second form we considered, Figure 4.2 presents the RMSDs for scans of the κ_2 and c_3 parameters in Equation 4.6 with $c_2 = 1.0$ (the optimal value for all κ_2 values plotted). For this ansatz, we see that the error relative to CCSD(T)/aVTZ is driven down quite dramatically by weakening the regularization (increasing κ). Indeed, perhaps surprisingly, we find that computing energies with unregularized MP2 and scaled unregularized MP3 provides the lowest error. In this case, the optimal c_3 parameter was found to be 0.8 and yields a RMSD of only 1.59 kcal mol⁻¹, which is close to chemical accuracy. We also observe that increasing the regularization strength decreases the optimal fraction of regularized third-order correlation energy. Impressed with the performance on this set, we chose this method, which we denote as MP2.8: κ -OOMP2, as our candidate for further evaluation.

In order to assess the transferability of MP2.8: κ -OOMP2, we tested its performance on a series of benchmarks sets meant to encompass a variety of main group bonded and non-bonded interactions: the non-MR subset of the W4-11 set[272] (the training set), the BH76RC set[253, 305, 306], the RSE43 set[273, 307], the HTBH38 set[306], the NHTBH38 set[253], the TA13 set[274], and the A24 set[308]. We compare the performance of MP2.8: κ -

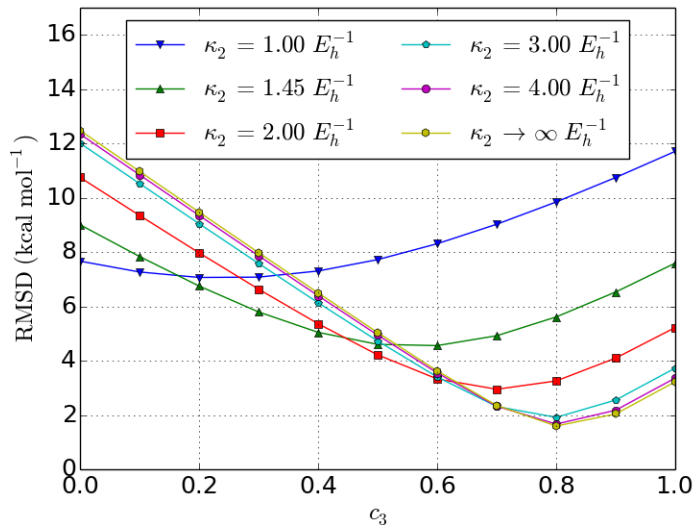


Figure 4.2: Scans of the root mean square deviation on the non-MR subset of the W4-11 thermochemical data set, in kcal mol^{-1} , for the regularized, second- and third-order correlation energy functional given in Equation 4.6. The optimal value of c_2 was found to be 1.0 for all κ_2 values plotted. SCF references were generated via κ -OOMP2 orbital optimization. The basis set used was aVTZ. Reference values are calculated at the CCSD(T)/aVTZ level of theory.

OOMP2 against an unscaled version of the method (MP3: κ -OOMP2), CCSD[22, 23], MP2.5[294], MP3, κ -OOMP2[39], OOMP2, and MP2. Details of the computations (aVTZ basis, CCSD(T) reference, no frozen core) are the same as given previously.

Table 4.1 presents the the RMSDs, mean signed deviations (MSD), minimum deviations (MIN), and maximum deviations (MAX), in kcal mol^{-1} , for the non-MR subset of the W4-11 set (the training set). This set includes atomization energies (TAE140), bond dissociation energies (BDE99), heavy atom transfer energies (HAT707), nucleophilic substitution reaction energies (SN13), and isomerization energies (ISOMERIZATION20).[272] We see that CCSD has a RMSD of $4.94 \text{ kcal mol}^{-1}$ and a MSD of $1.49 \text{ kcal mol}^{-1}$. MP2, MP2.5 and MP3 on top of UHF orbitals yields RMSDs of 11.99 , 8.97 , and $9.24 \text{ kcal mol}^{-1}$, respectively. The use of κ -OOMP2 optimized orbitals for the computation of the MP3 energy reduces the error over the use of UHF orbitals by a remarkably large factor of 3. MP2.8/ κ -OOMP2 yields a RMSD of $1.59 \text{ kcal mol}^{-1}$ and a MSD of $-0.45 \text{ kcal mol}^{-1}$, which is 6 times smaller than MP3. This is also an improvement on κ -OOMP2 by a factor of 4. Also remarkably, both third-order methods computed using κ -OOMP2 optimized orbitals outperform CCSD on this data set.

To validate the performance for thermochemistry outside of the training set, we tested MP2.8: κ -OOMP2 on the BH76RC[253, 305, 306] and RSE43[273, 307] sets. The BH76RC set contains reaction energies for 30 reactions involved in the HTBH38 and NHTBH38 sets.[253, 305, 306] On this set MP2.8: κ -OOMP2 outperforms all other methods surveyed with an

Method	RMSD	MSD	MIN	MAX
CCSD	4.94	1.49	-8.60	20.34
MP2.8: κ -OOMP2	1.59	-0.45	-5.83	5.24
MP3: κ -OOMP2	3.22	0.33	-8.12	14.63
MP2.5	8.97	-2.85	-40.24	24.87
MP3	9.24	-0.80	-38.57	31.66
κ -OOMP2	7.58	-3.14	-38.94	13.56
OOMP2	10.82	-3.50	-48.81	17.87
MP2	11.99	-4.90	-51.14	27.28

Table 4.1: Root mean square deviation, mean signed deviation, minimum deviation, and maximum deviation, in kcal mol⁻¹ for the non-MR subset of the W4-11 set. All calculations use the aVTZ basis; CCSD(T) is used for the reference values.

Method	RMSD	MSD	MIN	MAX
CCSD	1.905	-0.645	-7.175	1.977
MP2.8: κ -OOMP2	0.835	-0.143	-1.465	1.534
MP3: κ -OOMP2	1.574	-0.437	-6.213	1.228
MP2.5	4.625	-0.536	-21.407	9.904
MP3	4.511	-0.975	-21.604	4.232
κ -OOMP2	4.220	-0.276	-9.763	11.856
OOMP2	5.524	0.836	-10.010	20.496
MP2	6.341	-0.098	-21.211	15.577

Table 4.2: Root mean square deviation, mean signed deviation, minimum deviation, and maximum deviation, in kcal mol⁻¹, for the BH76RC set.

RMSD of 0.84 kcal mol⁻¹ and a MSD of -0.14 kcal mol⁻¹. MP3: κ -OOMP2 also performs very well. Of the $\mathcal{O}(N^5)$ methods, κ -OOMP2 provides the lowest RMSD while MP2 provides the lowest overall MSD. The largest absolute error using the canonical MP methods is for the $\text{H} + \text{F}_2 \longrightarrow \text{HF} + \text{H}$ reaction energy. This can be traced back to spin-contamination at the UHF level in the case of F_2 with a $\langle S^2 \rangle$ of 0.293. Both κ -OOMP2 and MP2.8: κ -OOMP2 show significant improvement on this case with errors of 1.425 kcal mol⁻¹ and 0.536 kcal mol⁻¹, respectively. MP2.8: κ -OOMP2 improves upon κ -OOMP2 in all but two cases in this set.

Table 4.3 contains benchmark results for the RSE43 set. The RSE43 set contains reaction energies for hydrogen abstraction from hydrocarbons by a methyl radical.[273, 307] For this set we see MP2.8: κ -OOMP2, with an RMSD of 0.63 kcal mol⁻¹ and a MSD of -0.54 kcal mol⁻¹, performs slightly worse than CCSD and MP3: κ -OOMP2. However the RMSD is still almost 4 times smaller than MP3. MP2.8: κ -OOMP2, MP3: κ -OOMP2, and OOMP2 all underestimate the reaction energies on average. For the $\mathcal{O}(N^5)$ methods, κ -OOMP2 outperforms OOMP2 and MP2 both in terms of RMSD and MSD. Several species in the set exhibit spin contamination, leading to failures of the canonical MP methods.

Method	RMSD	MSD	MIN	MAX
CCSD	0.446	0.316	-0.815	0.973
MP2.8: κ -OOMP2	0.634	-0.538	-1.726	0.050
MP3: κ -OOMP2	0.521	-0.416	-1.550	-0.002
MP2.5	3.234	1.907	0.061	12.899
MP3	2.433	1.563	0.109	9.361
κ -OOMP2	0.476	0.119	-0.964	1.020
OOMP2	0.922	-0.607	-2.261	0.478
MP2	4.099	2.252	-0.028	16.445

Table 4.3: Root mean square deviation, mean signed deviation, minimum deviation, and maximum deviation, in kcal mol⁻¹, for the RSE43 set.

Method	RMSD	MSD	MIN	MAX
CCSD	2.206	1.877	-0.782	4.146
MP2.8: κ -OOMP2	0.711	-0.120	-1.424	1.301
MP3: κ -OOMP2	0.730	0.346	-1.411	1.755
MP2.5	3.686	3.246	-0.273	7.323
MP3	3.883	3.506	0.695	7.214
κ -OOMP2	2.918	1.658	-1.434	9.558
OOMP2	3.479	-0.952	-7.152	8.566
MP2	4.044	2.986	-1.487	12.142

Table 4.4: Root mean square deviation, mean signed deviation, minimum deviation, and maximum deviation, in kcal mol⁻¹, for the HTBH38 set.

To evaluate the performance of MP2.8/ κ -OOMP2 on kinetics, we tested it on the HTBH38[306] and NHTBH38[253] data sets. The HTBH38 set contains forward and reverse barrier heights for 19 hydrogen transfer reactions.[306] Results for this set are presented in Table 4.4. On this set MP2.8: κ -OOMP2 (and MP3: κ -OOMP2) outperform the other methods surveyed with a RMSD of 0.71 kcal mol⁻¹ (and 0.73 kcal mol⁻¹), corresponding to chemical accuracy. The RMSDs are around 3 times smaller than that for CCSD. MP2, MP2.5, and MP3 overestimate the barrier heights in nearly all cases in the test set, with worst performances for the HF + H \longrightarrow H₂ + F, HF + H \longrightarrow H₂ + F, and OH + NH₃ \longrightarrow H₂O + NH₂ forward barriers, respectively. MP2.8: κ -OOMP2 improves significantly on these cases with barrier height errors of 0.24 kcal mol⁻¹ and -0.51 kcal mol⁻¹, respectively.

Assessment data for the NHTBH38[253] set are presented in Table 4.5. The NHTBH38 set contains forward and reverse barrier heights for 19 non-hydrogen transfer reactions. On this set, MP2.8: κ -OOMP2 outperforms all other methods surveyed (RMSD of 0.76 kcal mol⁻¹), with MP3: κ -OOMP2 performing second best. The reduction in RMSD relative to MP3 is more than a factor of 8 for MP2.8: κ -OOMP2. Remarkably, both methods improve substantially upon CCSD, with the improvement being more than a factor of 3 for MP2.8: κ -OOMP2. MP2, MP2.5, and MP3 all exhibit large errors in the barrier heights for the reactions

Method	RMSD	MSD	MIN	MAX
CCSD	2.534	2.067	0.132	7.646
MP2.8: κ -OOMP2	0.758	0.268	-0.949	1.579
MP3: κ -OOMP2	1.668	1.076	-0.718	7.175
MP2.5	6.590	4.763	-0.328	24.455
MP3	6.651	5.158	1.099	23.283
κ -OOMP2	2.766	1.553	-7.610	5.222
OOMP2	3.901	-1.650	-18.495	2.315
MP2	7.035	4.368	-2.676	25.627

Table 4.5: Root mean square deviation, mean signed deviation, minimum deviation, and maximum deviation, in kcal mol⁻¹, for the NHTBH38 set.

$\text{H} + \text{N}_2\text{O} \longrightarrow \text{OH} + \text{N}_2$, $\text{H} + \text{F}_2 \longrightarrow \text{HF} + \text{F}$, and $\text{CH}_3 + \text{ClF} \longrightarrow \text{CH}_3\text{F} + \text{Cl}$. For $\text{H} + \text{N}_2\text{O} \longrightarrow \text{OH} + \text{N}_2$ and $\text{CH}_3 + \text{ClF} \longrightarrow \text{CH}_3\text{F} + \text{Cl}$, both forward and reverse barriers are overestimated due to spin-contamination of the UHF reference for the transition state structures. The UHF reference $\langle S^2 \rangle$ values of 1.011 and 1.026, respectively, are corrected to mean-field $\langle S^2 \rangle$ values of 0.765 and 0.775, respectively, via the κ -OOMP2 orbital optimization procedure. For $\text{H} + \text{F}_2 \longrightarrow \text{HF} + \text{F}$, the reverse barriers are overestimated by more than 20 kcal mol⁻¹ with MP2, MP2.5, and MP3 while errors in the forward barriers are of similar magnitude to other systems in the data set. Significant spin-contamination is present in the UHF reference for both F_2 and the transition state structure, leading to a cancellation of errors in the forward barrier that is not seen in the reverse barrier. Orbital optimization with κ -OOMP2 helps to mitigate this spin-contamination, reducing the mean-field $\langle S^2 \rangle$ values of 0.293 and 1.212, respectively, to 0.000 and 0.767, respectively. For all three of these reactions MP2.8: κ -OOMP2 gives errors that are reduced by a factor of 5-10 relative to MP2, MP2.5, and MP3.

To round out the test suite we assessed the performance of MP2.8: κ -OOMP2 on two noncovalent interaction sets: the TA13 and A24 sets. The TA13 set contains 13 nonbonded interaction energies for radical closed-shell complexes.[274] We apply a counterpoise correction to these interaction energies to mitigate basis set superposition error (BSSE). Assessment data for the TA13 set is presented in Table 4.6. On this test set we see MP2.8: κ -OOMP2 performs almost as well as CCSD. MP2.8: κ -OOMP2 overbinds each interaction in the set, especially the H_2O -Al interaction which is overbound by 2.05 kcal mol⁻¹. Remarkably, κ -OOMP2 outperforms all methods surveyed on this set, with an RMSD of 0.35 kcal mol⁻¹. Table 4.7 presents the counterpoise-corrected results for the A24 set. The A24 set contains noncovalent interaction energies for 24 closed-shell small molecule complexes.[308] MP2.8: κ -OOMP2 outperforms all other methods with a RMSD of 0.08 kcal mol⁻¹ and a MSD of 0.01 kcal mol⁻¹. For MP2, MP2.5, and MP3, artifactual spin-contamination at the UHF level causes underbinding for the ethene-ethene and ethene-ethyne dimers. For the ethene dimer, the MP2, MP2.5, and MP3 errors are in excess of 2 kcal mol⁻¹ while MP2.8: κ -OOMP2 reduces this error to 0.04 kcal mol⁻¹.

Method	RMSD	MSD	MIN	MAX
CCSD	0.722	0.539	-0.259	1.470
MP2.8: κ -OOMP2	0.823	-0.459	-2.054	-0.011
MP3: κ -OOMP2	0.808	-0.442	-2.463	0.086
MP2.5	1.559	0.276	-3.888	3.708
MP3	1.435	0.391	-2.612	3.997
κ -OOMP2	0.350	-0.019	-0.589	0.650
OOMP2	0.789	-0.149	-1.938	1.370
MP2	1.791	0.160	-5.164	3.419

Table 4.6: Root mean square deviation, mean signed deviation, minimum deviation, and maximum deviation, in kcal mol⁻¹, for the TA13 set.

Method	RMSD	MSD	MIN	MAX
CCSD	0.247	0.226	0.093	0.429
MP2.8: κ -OOMP2	0.075	0.007	-0.169	0.233
MP3: κ -OOMP2	0.106	0.043	-0.113	0.373
MP2.5	0.492	0.132	-0.113	2.303
MP3	0.488	0.187	-0.010	2.203
κ -OOMP2	0.184	-0.045	-0.631	0.199
OOMP2	0.193	-0.131	-0.475	0.063
MP2	0.515	0.078	-0.441	2.403

Table 4.7: Root mean square deviation, mean signed deviation, minimum deviation, and maximum deviation, in kcal mol⁻¹, for the A24 set.

4.4 Conclusion

Considering all the data presented, let us summarize the main conclusions obtained from this work.

1. At the MP2 level the choice of orbitals matters considerably, as is well known. In our work, for all 7 data sets considered, orbital optimized MP2 (OO-MP2) yields lower RMSD than MP2 (using unrestricted orbitals when necessary). Regularization via $\kappa = 1.45$ has formal benefits in restoring Coulson-Fisher points. It also has practical benefits: κ -OOMP2 yields lower RMSD than OO-MP2 for all 7 data sets tested.
2. Use of κ -OOMP2 orbitals improves MP3 results to a surprising extent. MP3: κ -OOMP2 has lower RMSD than MP3 by factors ranging from 1.7 to more than 5 across the 7 data sets reported here. MP3: κ -OOMP2 is thus a far more robust method than MP3 itself, due to the reduced spin-contamination in κ -OOMP2 orbitals relative to HF orbitals.
3. Developing a semi-empirical variant based on scaling the MP2 and MP3 contributions yielded $c_2 = 1.0$ and $c_3 = 0.8$ based on the non-MR part of the W4-11 data set (no

regularization is preferred). In transferability tests, this MP2.8: κ -OOMP2 method improves over MP3: κ -OOMP2 in 4 of our 6 test sets, with the other two being very similar.

4. Remarkably, the results obtained with MP3: κ -OOMP2 and MP2.8: κ -OOMP2 produce lower RMSD than CCSD itself in 5 of the 7 data sets (the remaining two show no large failures). This indicates a level of performance that is beyond the physical content of MP3 theory, and involves some rather systematic cancellation of the effects due to connected triples.
5. These improved MP3 methods are single reference of course, and the data sets considered here are suitable for single reference methods. Much poorer performance must be expected for systems where strong correlations are in play (perhaps with the exception of biradicaloids[275])

The improved performance granted by the use of κ -OOMP2 optimized orbitals suggests future developments in electronic structure theory. It will be interesting to assess results across additional data sets, and explore the use of larger basis sets. We intend to explore scaled fourth-order perturbation approaches (MP4) and coupled cluster methods with κ -OOMP2 reference orbitals. The latter would be especially interesting in the context of nonvariational failures of CCSD(T). In a different direction, perhaps MP3 should be considered as an independent descriptor of electron correlation in double hybrid density functional theory, where MP2 is at present most widely used.[71, 88, 283–285] With the advances in integral compression techniques such as tensor hypercontraction, both MP2 and MP3 energy evaluations scale quartically with system size.[291] Incorporating this into the development of new double hybrid density functionals will be a promising future direction.

Chapter 5

Polishing the gold standard: The role of orbital choice in CCSD(T) frequency prediction

5.1 Introduction

Coupled cluster theory with single, double, and perturbative triple excitations [CCSD(T)][25] with spin-restricted Hartree-Fock (RHF) orbitals is considered the “gold standard” by many quantum chemists for its ability to routinely provide results approaching chemical accuracy for energies and properties of closed-shell species at a reasonable computational cost [309–311]. With the ability to achieve sub-kcal mol⁻¹ errors at a computational cost of $\mathcal{O}(N^7)$ and a memory cost of $\mathcal{O}(N^4)$, where N is the size of the basis, CCSD(T) strikes an advantageous accuracy-to-cost balance between coupled cluster theory with single and double excitations (CCSD)[22] ($\mathcal{O}(N^6)$ computational cost, $\mathcal{O}(N^4)$ memory cost) and explicit treatment of the triple excitations (CCSDT)[24] ($\mathcal{O}(N^8)$ computational cost, $\mathcal{O}(N^6)$ memory cost). For open-shell species, however, the performance of CCSD(T) (especially on top of spin-unrestricted HF (UHF) orbitals) is less clear. A study of bond lengths and frequencies of 33 small radical species by Byrd et. al[312] reported that CCSD(T) with a UHF reference (CCSD(T):UHF) shows little to no statistical improvement over CCSD[22] for geometries and frequencies. Beran et al.[313], in a study of harmonic vibrational frequencies of diatomic radicals, reported poor behaviour of CCSD(T):UHF for several species in the set including, CO⁺ and NO. Subsequent studies of these problem systems by Szalay et. al[314] investigated the source of this mixed performance. Stanton and Gauss[315] reviewed several potential factors leading to this discrepancy in describing open-shell species, including multireference (MR) character, spin-contamination, symmetry breaking, and instabilities and near-instabilities in the reference wavefunction. The use of restricted open-shell HF (ROHF) orbitals has been found to somewhat improve the performance on vibrational frequencies over UHF, though the former are prone to errors due to spatial symmetry breaking[315, 316]. While in the limit of full

configuration interaction the energy and properties are invariant to the choice of reference orbitals, any truncated approximate method will incur some level of orbital dependence.

Several strategies have been proposed as alternative references to UHF for CC calculations. The use of Brueckner orbitals in CC theory (BCC), which by definition have no singles contribution to the coupled cluster wavefunction, attempts to incorporate the most important electron correlations at the level of the reference[317–321]. BCC approaches have been known to preserve wavefunction symmetries as well, yielding more accurate properties[322–325]. In a similar vein, the molecular orbitals (MOs) can be directly optimized in the presence of CCD correlation energies as in the orbital-optimized coupled cluster doubles (OD) and orbital optimized coupled-cluster doubles and perturbative triples [OD(T)] approaches[326–328]. The use of OD(T) by Beran et al.[313] was shown to significantly suppress errors in the computed harmonic frequencies of CN, CO⁺, and NO compared to CCSD(T):UHF. Brueckner and/or optimized coupled cluster orbitals are costly to obtain; BCCD(T) and OD(T) typically are far more computationally expensive than CCSD(T) as orbital optimization is often more challenging than varying the singles amplitude. Given this steep computational cost, methods to approximate Brueckner or otherwise optimized orbitals at a lower cost are highly desirable.

One such approximate approach to incorporate correlation into the reference orbitals for a correlated calculation is the use of Kohn-Sham density functional theory (DFT) orbitals as a reference. The use of BLYP[55, 56] orbitals by Beran et al.[313] was shown to substantially improve the computed vibrational frequencies of radical diatomic species over UHF orbitals. More recently, Fang et al.[329] and Fang et al.[330] have demonstrated the efficacy of CCSD(T) with DFT orbitals in the prediction of thermodynamic properties of UCl₆ and several diatomic transition metal compounds, respectively. Aside from their use in CC calculations, DFT orbital references have been used successfully for excited state configuration interaction[331], as guiding functions in quantum Monte Carlo [332], and for second-order perturbation theory in the context of double-hybrid DFT[86]. In addition to their inexpensive computational cost ($\mathcal{O}(N^3)$), DFT orbitals offer improved stability against symmetry breaking compared to HF orbitals[333]. A connection between DFT orbitals and Brueckner orbitals has been proposed by several researchers as well[334–336].

Orbital-optimized second-order Møller-Plesset perturbation theory (OOMP2) and its variants offer another way to approximate higher-order orbital optimized-methods at a cost of $\mathcal{O}(N^5)$ per iteration[35, 36, 39]. Orbital optimization at the MP2 level, in addition to improving energetics, is often seen to reduce spin-contamination in the optimized reference[35, 36, 269]. Recently Haggag et al.[337] utilized OOMP2 reference orbitals for CC calculations on the triplet state of permanganate to combat spin contamination seen at the UHF level. Despite these benefits, OOMP2 exhibits three unsatisfying characteristics that limit its application: divergence in the cases of small orbital energy gaps[40], the loss of Coulson-Fischer points[271], and “artificial” symmetry restoration[276, 338]. The correlation energy

functional for MP2 is

$$E_{\text{MP2}} = -\frac{1}{4} \sum_{ijab} \frac{|\langle ij||ab \rangle|^2}{\Delta_{ij}^{ab}} \quad (5.1)$$

where $\Delta_{ij}^{ab} = \epsilon_a + \epsilon_b - \epsilon_i - \epsilon_j$ is the non-negative orbital energy denominator. This energy is seen to diverge in cases where the denominator becomes small, as can occur when stretching bonds. This behavior leads to poor performance of OOMP2 when predicting harmonic vibrational frequencies[40]. Secondly, OOMP2 often fails to continuously transition from restricted to unrestricted solutions even when the unrestricted solution is lower in energy[270]. Thirdly, OOMP2 has been shown in some cases to “artificially” restore spin-symmetry to systems where the spin symmetry breaking is an “essential” feature of the system due to MR character of the system[276, 338].

In order to address the problematic aspects of OOMP2, two of us developed κ -OOMP2, a regularized variant of OOMP2[39]. The κ -OOMP2 energy functional is given by

$$E_{\kappa\text{-OOMP2}}(\kappa) = -\frac{1}{4} \sum_{ijab} \frac{|\langle ij||ab \rangle|^2}{\Delta_{ij}^{ab}} \left(1 - e^{-\kappa \Delta_{ij}^{ab}}\right)^2, \quad (5.2)$$

where κ is a regularization parameter that damps contributions to the correlation energy when the orbital energy denominator becomes small. Regularization parameter values $\kappa \leq 1.5 E_h^{-1}$ were shown to restore Coulson-Fischer points for a series of bond-breaking curves[39]. Training of the regularization parameter on the W4-11 thermochemistry data set[272] led to an optimal κ value of $1.45 E_h^{-1}$ [39]. With this parameter value, κ -OOMP2 was able to outperform OOMP2 on the TA13 data set[274] of radical–closed-shell interaction energies[39]. Further application to symmetry breaking in fullerenes revealed the ability of κ -OOMP2 to distinguish between essential and artificial symmetry breaking[276, 338].

We recently developed a scaled variant of third-order MP theory (MP3) that utilizes κ -OOMP2 orbitals as a reference which we will denote as MP2.8: κ -OOMP2[95]. MP2.8: κ -OOMP2 and its unscaled version, MP3: κ -OOMP2, outperformed CCSD on five of the seven data sets investigated at the cost of a single $\mathcal{O}(N^6)$ iteration. The use of κ -OOMP2 orbitals strongly improves upon the performance of MP3 with UHF orbitals as well, especially in cases of spin-symmetry breaking.

Inspired by MP2.8: κ -OOMP2[95], the work of Beran et al.[313], and the success of κ -OOMP2 in treating radical species in the TA13 set[39] and in producing minimally spin-contaminated references for biradicaloid systems[275], in this work we explore the use of κ -OOMP2 orbitals as a reference for CCSD(T) computation of vibrational frequencies. Errors are calculated with respect to experimental values and compared against CCSD(T) with UHF orbitals, OOMP2 orbitals, and several flavors of DFT orbitals. This use of κ -OOMP2 orbitals as a reference for CCSD(T) was previously explored in the computation of spin-gaps in an iron porphyrin complex and showed an improvement over conventional CCSD(T) [339].

5.2 Computational Methods

We consider eight methods as generators of MOs for use as references: UHF, two OOMP2 methods (OOMP2[35–37] and κ -OOMP2[39]), and five density functionals (BLYP[55, 56], B97M-rV[340], B97[62], ω B97X-V[82], and ω B97M-V[256]). A regularization parameter value of $\kappa = 1.45E_h^{-1}$ was chosen for κ -OOMP2, as suggested by Lee and Head-Gordon[39]. Both the OOMP2 and κ -OOMP2 calculations were carried out using the resolution-of-the-identity (RI) approximation[29, 30]. The functionals B97M-rV, B97, ω B97X-V, and ω B97M-V were chosen on the basis of their performance in a recent benchmark of over 200 density functionals in which they were found to be the best performing meta-GGA, global hybrid GGA, range-separated hybrid GGA, and range-separated hybrid meta-GGA functionals, respectively[85]. The DFT calculations were performed using an ultra-fine integration grid of 99 radial points and 590 angular points per atom. Wavefunction stability analysis[270, 341] was performed on the UHF and DFT solutions to ensure that all orbitals used properly minimize their corresponding SCF energies. All unstable solutions (saddle points) were displaced and reoptimized to local minima. OOMP2 and κ -OOMP2 calculations were performed starting from a locally stable UHF solution. Both the reference calculations and CCSD(T) calculations were performed using unrestricted wavefunctions.

All calculations were performed with the aug-cc-pwCVTZ basis[119, 120, 302, 342, 343] set to capture the effects of core correlation. A core-valence basis set was utilized to account for the role of core-valence correlations in molecular property calculations. The use of the weighted, triple- ζ variant is justified by the faster convergence of properties to the complete basis set limit seen with cc-pwCVnZ over cc-pCVnZ[342]. Augmented functions were chosen to better treat the anions in the data set. The corresponding auxiliary basis set was utilized for the OOMP2 and κ -OOMP2 calculations (with cc-pwCVQZ-RI utilized for Li, Be, Na, and Mg)[303, 304, 344]. Atoms H-F have all electrons correlated and atoms Na-Cl utilize a frozen He core. All electronic structure calculations were performed using the Q-Chem package of electronic structure programs[125]. For a given reference, the corrected harmonic vibrational frequency was determined by fitting a quartic polynomial to seven equally-spaced points (0.005 Å between adjacent points) distributed near the minimum of the potential and applying Dunham analysis to the fitting coefficients to account for the effects of rotation[345]. Equilibrium bond lengths from the fitting procedure are reported in Tab. D.2 and D.3.

5.3 Experimental Data Selection

For simplicity and due to the lack of analytic first derivatives of the CCSD(T) energy with respect to nuclear displacements for non-HF references, we restricted the systems of study in this work to diatomic species for which the ground state potential energy surface can be determined via fitting to single point calculations. Beginning from all diatomics of row 2 and row 3 species (and hydrogen) for which Huber and Herzberg[346] report ground state frequencies, we include all species for which we were able to compute a smooth potential

energy surface about the corresponding equilibrium bond length for each method (excluded species are listed in Tab. D.7). The overall data set contains 36 closed-shell species (29 neutrals, 6 cations, 1 anion) and 59 open-shell species (38 neutrals, 15 cations, 6 anions; 46 doublets, 13 triplets). Among other species in this data set, we include all 12 species from Beran et al.[313] as well as several isovalent analogues of these species containing row 3 elements. Other notable inclusions are B_2 ($X^3\Sigma_g^-$) and C_2 ($X^1\Sigma_g^+$), both known to exhibit MR behavior in their ground states[272, 347], and F_2 ($X^1\Sigma_g^+$), a biradicaloid diamagnetic system known to be unbound at the UHF level of theory[348]. Where available, experimental frequencies were updated with data from Irikura[349]. Frequencies for OH^- , F_2^+ , and SO^+ were updated with more recent experimental data from Hotop et al.[350], Cormack et al.[351], and Milkman et al.[352], respectively.

5.4 Results and Discussion

5.5 Vibrational frequencies

Fig. 5.1 presents the errors in the corrected vibrational frequencies on the closed- and open-shell subsets for each method as box plots. In these plots, the boxed region represents data from the first to the third quartile of the distribution, a red line marks the median of the data, whiskers enclose all data within 1.5 times the inter-quartile distance of the upper and lower box edges, and points mark data lying outside of these regions. Tab. 5.1 presents the root mean square deviations (RMSD), mean signed deviations (MSD), most negative deviations (MIN), and most positive deviations (MAX), all in cm^{-1} , of the corrected vibrational frequencies from the experimental frequencies for the overall data set. $CCSD(T):\kappa$ -OOMP2 is seen to give the best overall performance in terms of RMSDs with a value of 17.66 cm^{-1} , reducing the RMSD for $CCSD(T):UHF$ by more than a factor of two. $CCSD(T):OOMP2$ is seen to perform slightly worse but still improves on the $CCSD(T):UHF$ RMSD by a factor of 2. The performance of the DFT orbital approaches is hindered by the presence of C_2 , representing the MIN value for all functionals tested. The MAX value, corresponding to PH^+ , is shared among all non-HF methods tested. On average the frequencies are slightly blue-shifted for $CCSD(T):UHF$ and slightly red-shifted for all other methods.

Closed-shell subset

Figure 5.1: Box plots (overall, left, and enhanced, right) of the errors in corrected vibrational frequencies (in cm^{-1}) are presented. Red lines mark the median errors, boxes bound the central 50% of the data, whiskers enclose all data points within 1.5 times the inter-quartile range of the box edges, and points denote outlying data.

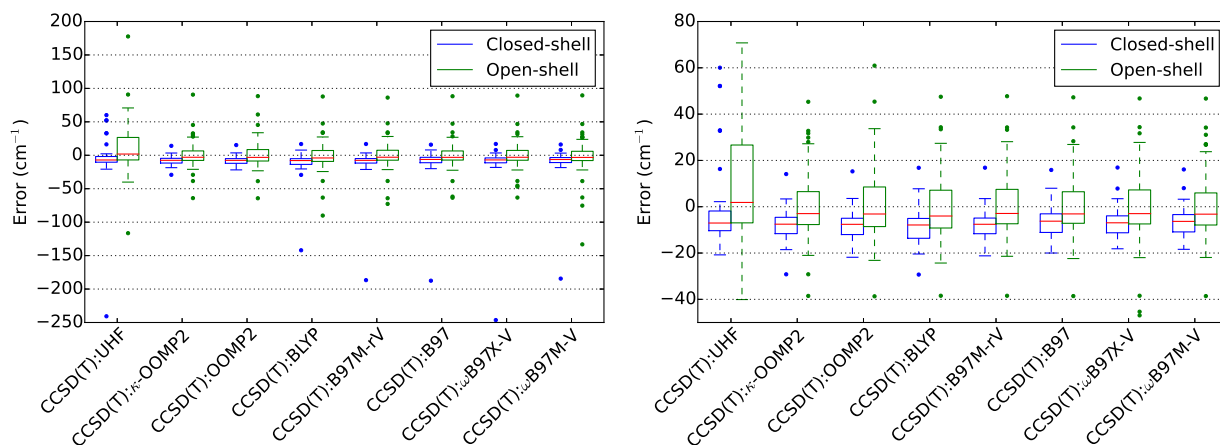


Table 5.1: Root mean square deviations, mean signed deviations, most negative deviations, and most positive deviations (all in cm^{-1}) for the predicted corrected vibrational frequencies of all species are summarized for the CCSD(T) methods utilizing different molecular orbital references.

	$\Delta(\text{CCSD(T):UHF})$	$\Delta(\text{CCSD(T):}\kappa\text{-OOMP2})$	$\Delta(\text{CCSD(T):OOMP2})$	$\Delta(\text{CCSD(T):BLYP})$	$\Delta(\text{CCSD(T):B97M-rV})$	$\Delta(\text{CCSD(T):B97})$	$\Delta(\text{CCSD(T):}\omega\text{B97X-V})$	$\Delta(\text{CCSD(T):}\omega\text{B97M-V})$
RMSD	41.05	17.66	18.82	24.75	26.75	26.35	31.19	29.77
MSD	4.35	-2.19	-1.80	-4.99	-4.36	-4.05	-4.71	-5.45
MIN	-240.71	-64.06	-64.26	-142.01	-186.68	-187.50	-246.37	-184.40
MAX	177.65	90.68	88.43	87.87	86.24	88.25	89.26	89.52

Table 5.2: Experimental vibrational frequencies (in cm^{-1}) and errors (in cm^{-1}) in the corrected vibrational frequencies for the 36 closed-shell species are presented in for the CCSD(T) methods utilizing different molecular orbitals. Root mean square deviations, mean signed deviations, most negative deviations, and most positive deviations (all in cm^{-1}) for the set of species and subsets are also presented.

Row 2- Row 2	Dimer	State	Expt.	$\Delta(\text{CCSD(T)})$ UHF	$\Delta(\text{CCSD(T)})$ κ -OOMP2	OOMP2	BLYP	$\Delta(\text{CCSD(T)})$ B97M-rV	$\Delta(\text{CCSD(T)})$ B97	$\Delta(\text{CCSD(T)})$ ω B97X-V	$\Delta(\text{CCSD(T)})$ ω B97M-V
	LiH	$X^1\Sigma^+$	1405.49805 ^a	-7.12	-8.81	-2.59	-8.41	-9.83	-2.50	-8.68	-6.13
	Li ₂	$X^1\Sigma^+$	351.4066 ^a	-11.40	-16.69	-16.52	-15.37	-13.54	-1.76	-16.24	-11.40
	LiF	$X^1\Sigma^+$	910.57272 ^a	-5.10	-5.60	-6.23	-6.96	-6.37	-6.23	-6.09	-6.07
	BeH ⁺	$X^1\Sigma^+$	2221.7 ^b	-11.81	-13.69	-12.35	-16.41	-13.93	-16.22	-11.43	-10.61
	BeO	$X^1\Sigma^+$	1487.32 ^b	-20.79	-17.36	-21.83	-20.41	-19.22	-20.00	-18.16	-18.40
	BH	$X^1\Sigma^+$	2366.7296 ^a	-2.51	0.49	-1.09	-1.00	-1.63	-1.02	-0.97	2.51
	BF	$X^1\Sigma^+$	1402.15865 ^a	-10.53	-12.64	-13.60	-15.41	-13.50	-13.60	-12.88	-13.02
	C ₂	$X^1\Sigma^+$	1855.0663 ^a	52.18	-29.19	-15.21	-142.01	-186.68	-187.50	-246.37	-184.40
	CO	$X^1\Sigma^+$	2169.75589 ^a	-16.15	-18.53	-19.25	-20.34	-18.52	-18.76	-18.10	-18.13
	N ₂	$X^1\Sigma^+$	2358.57 ^a	-4.81	-5.92	-6.09	-6.74	-5.86	-6.13	-5.77	-5.85
	NO ⁺	$X^1\Sigma^+$	2376.72 ^a	-7.36	-9.86	-9.73	-11.48	-10.19	-9.78	-9.70	-9.60
	OH ⁻	$X^1\Sigma^+$	3735.2 ^c	-0.73	-2.05	-6.68	-0.99	0.86	-0.98	0.55	-0.33
	HF	$X^1\Sigma^+$	4138.385 ^a	-7.04	-9.66	-8.96	-8.06	-7.40	-8.24	-7.48	-7.40
	F ₂	$X^1\Sigma^+$	916.929 ^a	60.05	3.10	3.57	3.20	3.06	3.00	2.93	2.73
	RMSD			23.32	13.29	11.97	39.74	51.03	51.14	66.67	50.25
	MSD			0.49	-10.46	-9.75	-19.31	-21.62	-20.69	-25.60	-20.44
	MIN			-20.79	-29.19	-21.83	-142.01	-186.68	-187.50	-246.37	-184.40
	MAX			60.05	3.10	3.57	3.20	3.06	3.00	2.93	2.73
Row 2- Row 3	Dimer	State	Expt.	$\Delta(\text{CCSD(T)})$ UHF	$\Delta(\text{CCSD(T)})$ κ -OOMP2	OOMP2	BLYP	$\Delta(\text{CCSD(T)})$ B97M-rV	$\Delta(\text{CCSD(T)})$ B97	$\Delta(\text{CCSD(T)})$ ω B97X-V	$\Delta(\text{CCSD(T)})$ ω B97M-V
	NaH	$X^1\Sigma^+$	1171.968 ^a	-8.85	-9.09	-9.02	7.76	-9.10	7.98	7.86	8.02
	NaLi	$X^1\Sigma^+$	256.5412 ^a	-1.17	-0.85	-3.97	-29.30	-1.75	-12.05	-1.76	-1.76
	NaF	$X^1\Sigma^+$	535.65805 ^a	-5.05	-5.43	-5.87	-6.35	-5.99	-5.62	-5.61	-5.57
	MgH ⁺	$X^1\Sigma^+$	1699.1 ^b	-10.18	-12.48	-12.48	-12.96	-11.67	-10.62	-11.98	-12.33
	AlH	$X^1\Sigma^+$	1682.37474 ^a	-15.37	-13.07	-12.95	-15.55	-21.21	-12.58	-16.38	-12.04
	AlF	$X^1\Sigma^+$	802.32447 ^a	-8.87	-9.64	-10.18	-11.23	-10.23	-10.19	-9.86	-9.95
	SH ⁺	$X^1\Sigma^+$	2157.17 ^a	-4.24	-1.20	-4.25	-1.28	-4.20	-2.62	-6.51	-2.32
	SiO	$X^1\Sigma^+$	1241.54388 ^a	-10.51	-11.60	-15.61	-14.30	-12.50	-12.45	-11.07	-11.14
	PN	$X^1\Sigma^+$	1336.948 ^a	33.01	-5.90	-7.60	-6.56	-5.54	-5.84	-5.45	-5.57
	BeS	$X^1\Sigma^+$	997.94 ^a	-240.71	-8.22	-8.10	-7.73	-8.00	-7.74	-7.96	-7.20
	CS	$X^1\Sigma^+$	1285.08 ^b	-5.98	-7.54	-9.54	-9.31	-8.00	-7.98	-6.94	-7.13
	NS ⁺	$X^1\Sigma^+$	1415 ^b	52.10	3.37	3.04	2.40	3.51	3.15	3.47	3.24
	HCl	$X^1\Sigma^+$	2990.9248 ^a	16.30	14.11	15.27	16.82	16.86	15.88	16.93	16.10
	LiCl	$X^1\Sigma^+$	642.95453 ^a	-7.45	-7.55	-7.57	-7.65	-7.58	-7.73	-7.49	-7.82
	BCl	$X^1\Sigma^+$	840.29472 ^a	-2.91	-2.44	-3.45	-4.81	-4.04	-3.51	-2.66	-2.84
	CCl ⁺	$X^1\Sigma^+$	1175 ^b	2.19	-4.74	-11.35	-9.69	-6.52	-6.24	-3.41	-3.94
	ClF	$X^1\Sigma^+$	783.4534 ^a	-7.29	-7.02	-6.99	-6.08	-5.87	-6.00	-6.31	-6.33
	RMSD			60.79	8.31	9.47	11.86	9.68	8.89	8.83	8.23
	MSD			-13.23	-5.25	-6.51	-6.81	-5.99	-4.95	-4.42	-4.03
	MIN			-240.71	-13.07	-15.61	-29.30	-21.21	-12.58	-16.38	-12.33

MAX	Dimer	State	Expt.	$\Delta(\text{CCSD(T)})$ UHF	$\Delta(\text{CCSD(T)})$ κ -OOMP2	14.11	15.27	16.82	16.86	15.88	16.93	16.10
Row 3- Row 3												
	NaCl	$X^1\Sigma^+$	364.6842 ^a	-5.25	-5.27	-5.29	-5.31	-5.31	-5.41	-5.31	-5.27	-5.29
	AlCl	$X^1\Sigma^+$	481.77466 ^a	-7.43	-7.38	-7.50	-7.88	-7.88	-7.70	-7.60	-7.44	-7.47
	SiS	$X^1\Sigma^+$	749.64559 ^a	-8.84	-8.35	-9.41	-9.62	-9.62	-9.05	-8.96	-8.42	-8.43
	P ₂	$X^1\Sigma^+$	780.77 ^a	32.77	-4.41	-4.67	-4.68	-4.68	-4.38	-4.48	-4.47	-4.52
	Cl ₂	$X^1\Sigma_g^+$	559.751 ^a	-11.83	-11.64	-11.69	-11.64	-11.64	-11.63	-11.59	-11.66	-11.63
	RMSD			16.58	7.84	8.14	8.25	8.06	8.06	8.01	7.87	7.88
	MSD			-0.11	-7.41	-7.71	-7.83	-7.64	-7.64	-7.59	-7.45	-7.47
	MIN			-11.83	-11.64	-11.69	-11.64	-11.63	-11.63	-11.59	-11.66	-11.63
	MAX			32.77	-4.41	-4.67	-4.68	-4.38	-4.38	-4.48	-4.47	-4.52
Closed- shell				$\Delta(\text{CCSD(T)})$ UHF	$\Delta(\text{CCSD(T)})$ κ -OOMP2	$\Delta(\text{CCSD(T)})$ OOMP2	$\Delta(\text{CCSD(T)})$ BLYP	$\Delta(\text{CCSD(T)})$ B97M-rV	$\Delta(\text{CCSD(T)})$ B97	$\Delta(\text{CCSD(T)})$ ω B97X-V	$\Delta(\text{CCSD(T)})$ ω B97M-V	
	RMSD			44.66	10.48	10.36	26.27	32.65	32.61	42.12	31.98	
	MSD			-6.07	-7.58	-7.94	-11.82	-12.30	-11.44	-13.08	-10.89	
	MIN			-240.71	-29.19	-21.83	-142.01	-186.68	-187.50	-246.37	-184.40	
	MAX			60.05	14.11	15.27	16.82	16.86	15.88	16.93	16.10	

^a From Ref. 349.

^b From Ref. 346.

^c From Ref. 350.

Tab. 5.2 presents the experimental vibrational frequencies, in cm^{-1} , and errors in the corrected vibrational frequencies, in cm^{-1} , for the 36 species in the closed-shell subset. We see that the use of OOMP2 or κ -OOMP2 orbitals is able to reduce the RMSD of UHF orbitals by a factor of 4 from 44.66 cm^{-1} to 10.36 and 10.48 cm^{-1} , respectively. The use of DFT orbitals is also seen to reduce the RMSD, with BLYP outperforming the other functionals and ω B97X-V improving the RMSD by only 2.5 cm^{-1} . On average, all methods are seen to red-shift the closed-shell frequencies by 5 - 12 cm^{-1} .

The performance of CCSD(T) with DFT orbitals is most negatively impacted for the C_2 system, with errors in excess of -100 cm^{-1} for each. This data point also represents a negative outlier for CCSD(T) with κ -OOMP2 orbitals and a positive outlier for CCSD(T) with UHF orbitals. Its significant MR character renders C_2 outside of the scope of the single-reference methods evaluated in this work[272, 347]. Judging from the mean-field $\langle S^2 \rangle$ values (Tab. D.8) for κ -OOMP2 and OOMP2 of 0.89140 and 0 , respectively, we observe that OOMP2 is “artificially” restoring symmetry in this case while the broken spin-symmetry of the κ -OOMP2 reference orbitals is diagnostic of a MR problem, consistent with the literature[272, 347]. Spin-symmetry breaking in κ -OOMP2 as a signal of MR character has been demonstrated earlier in a study of fullerenes by Lee and Head-Gordon[276]. Considering the other dimers in the closed-shell subset, CCSD(T) with UHF orbitals is seen to exhibit poor performance for F_2 , PN , BeS , NS^+ , and P_2 , especially given that all other methods have absolute errors below 10 cm^{-1} for these species. These errors can be attributed to spin contamination of the reference orbital set. For UHF, the mean field $\langle S^2 \rangle$ values for F_2 , PN , BeS , NS^+ , and P_2 are 0.31922 , 0.70716 , 1.01647 , 0.69154 , and 0.67604 , respectively while the mean-field $\langle S^2 \rangle$ values of κ -OOMP2, OOMP2, and the five DFT functionals for these species are all zero. The large error for BeS at the CCSD(T):UHF level can be traced to the character of the UHF wavefunction, which localizes nearly an entire electron’s spin density on each atomic center. The $\langle S^2 \rangle$ value of 1.01647 shows significant triplet contamination. In the absence of these symmetry-broken species (and MR C_2), the performance across the methods is largely equalized with RMSDs ranging from 9.5 to 12 cm^{-1} . The maximum error outlier for all non-HF references is attributed to HCl . NaLi is also an outlying case for CCSD(T):BLYP (-29.30 cm^{-1}).

Open-shell subset

Table 5.3: Experimental vibrational frequencies (in cm^{-1}) and errors (in cm^{-1}) in the corrected vibrational frequencies for the 59 open-shell species are presented in for the CCSD(T) methods utilizing different molecular orbitals. Root mean square deviations, mean signed deviations, most negative deviations, and most positive deviations (all in cm^{-1}) for the set of species and subsets are presented.

Row 2- Row 2	Dimer	State	Expt.	$\Delta(\text{CCSD(T)}): \Delta(\text{UHF})$	$\Delta(\text{CCSD(T)}): \Delta(\kappa\text{-OOMP2})$	$\Delta(\text{CCSD(T)}): \Delta(\text{OOMP2})$	BLYP	B97M-rV	B97	$\Delta(\text{CCSD(T)}): \Delta(\omega\text{B97X-V})$	$\Delta(\text{CCSD(T)}): \Delta(\omega\text{B97M-V})$
	LiO	$X^2\Pi_i$	814.62 ^a	-6.94	-7.10	-7.22	-8.16	-7.02	-7.04	-6.97	-6.94
	BeH	$X^2\Sigma^+$	2061.235 ^a	-5.15	-10.86	-3.14	-3.30	-7.48	-5.31	-4.56	-11.46
	BeF	$X^2\Sigma^+$	1247.36 ^b	9.50	8.85	8.47	7.42	8.23	8.30	8.61	8.42
	B ₂	$X^3\Sigma_g^-$	1051.3 ^b	-16.10	-29.18	-1.90	-90.13	-72.72	-61.76	-45.34	-75.26
	BN	$X^3\Pi$	1514.6 ^b	6.82	-8.55	-7.84	-7.27	-7.70	-7.12	-7.95	-8.55
	BO	$X^2\Sigma^+$	1885.286 ^a	-11.61	-21.02	-23.17	-24.32	-21.41	-22.38	-21.98	-21.92
	CH	$X^2\Pi_r$	2860.7508 ^a	-10.43	1.87	-1.66	-1.56	-0.88	-0.74	-0.33	-2.12
	C ₂ ⁻	$X^2\Sigma^+$	1781.189 ^a	-116.46	-6.89	-8.56	-7.90	-6.57	-4.75	-46.93	-133.20
	CN	$X^2\Sigma^+$	2068.648 ^a	54.67	-7.85	-10.32	-8.92	-7.36	-7.65	-7.05	-7.37
	CO ⁺	$X^2\Sigma^+$	2214.127 ^a	67.00	-16.90	-20.40	-19.77	-13.55	-16.29	-16.28	-16.00
	CF	$X^2\Pi_r$	1307.93 ^a	-3.10	-6.70	-8.59	-10.31	-7.35	-7.36	-6.36	-6.52
	NH	$X^3\Sigma^-$	3282.72 ^a	0.19	-1.75	-0.73	-1.66	-1.85	-0.93	-0.68	-0.93
	N ₂ ⁺	$X^2\Sigma^+$	2207.0115 ^a	70.77	-6.08	-7.18	-6.92	-4.96	-5.51	-4.79	-5.09
	NO	$X^2\Pi_r$	1904.1346 ^a	177.65	-6.77	-6.31	-7.80	-6.83	-7.09	-6.89	-6.90
	NF	$X^3\Sigma^-$	1141.37 ^a	-7.98	-10.86	-13.45	-14.29	-9.97	-10.40	-9.82	-9.56
	OH	$X^2\Pi_i$	3737.761 ^a	-10.03	-9.36	-10.91	-11.21	-9.13	-9.16	-8.56	-10.23
	OH ⁺	$X^3\Sigma^-$	3113.37 ^b	6.88	4.44	4.52	6.84	6.76	4.34	4.44	4.32
	O ₂	$X^3\Sigma_g^-$	1580.161 ^a	-4.57	-3.09	-3.11	-3.25	-3.05	-3.23	-3.22	-3.24
	O ₂ ⁺	$X^2\Pi_g$	1905.892 ^a	28.13	4.68	4.77	3.87	4.66	4.40	4.54	4.45
	O ₂ ⁻	$X^2\Pi_{g,i}$	1090 ^b	24.81	27.20	27.23	27.20	27.12	26.89	26.82	26.85
	OF	$X^2\Pi$	1053.0138 ^a	29.52	2.56	0.62	1.23	5.31	4.65	5.21	5.54
	HF ⁺	$X^2\Pi_i$	3090.5 ^b	26.49	27.97	29.45	27.38	28.07	26.44	26.44	26.78
	F ₂ ⁺	$X^2\Pi_{g,i}$	1104 ^d	-34.13	20.51	23.81	19.99	19.30	18.63	17.94	17.71
	F ₂ ⁻	$X^2\Sigma_u^+$	510 ^{b*}	-40.09	-64.06	-64.26	-63.25	-64.22	-63.46	-63.22	-63.09
	RMSD			51.77	18.77	18.44	25.78	23.00	21.46	21.76	35.74
	MSD			9.83	-4.96	-4.16	-8.17	-6.36	-6.11	-6.96	-12.26
	MIN			-116.46	-64.06	-64.26	-90.13	-72.72	-63.46	-63.22	-133.20
	MAX			177.65	27.97	29.45	27.38	28.07	26.89	26.82	26.85
Row 2- Row 3	Dimer	State	Expt.	$\Delta(\text{CCSD(T)}): \Delta(\text{UHF})$	$\Delta(\text{CCSD(T)}): \Delta(\kappa\text{-OOMP2})$	$\Delta(\text{CCSD(T)}): \Delta(\text{OOMP2})$	BLYP	B97M-rV	B97	$\Delta(\text{CCSD(T)}): \Delta(\omega\text{B97X-V})$	$\Delta(\text{CCSD(T)}): \Delta(\omega\text{B97M-V})$
	NaO	$X^2\Pi$	526 ^{b*}	-38.60	-38.52	-38.69	-38.45	-38.46	-38.58	-38.44	-38.59
	MgH	$X^2\Sigma^+$	1492.7763 ^a	-4.27	-2.49	-4.24	-5.69	-2.78	-0.51	-3.21	-4.82
	MgF	$X^2\Sigma^+$	711.69 ^b	0.08	-0.30	-0.66	-1.34	-0.93	-0.78	-0.50	-0.48
	AlH ⁺	$X^2\Sigma^+$	1620 ^b	24.02	29.86	21.80	34.31	28.10	28.30	27.77	19.42
	SiH	$X^2\Pi_r$	2042.5229 ^a	-12.95	-9.14	-9.12	-9.46	-7.06	-7.05	-12.62	-12.63
	SiF	$X^2\Pi_r$	837.32507 ^a	10.84	9.61	8.85	7.61	8.75	8.85	9.39	9.29
	PH	$X^3\Sigma^-$	2363.774 ^a	1.72	0.54	-1.71	1.43	-0.52	1.70	1.47	1.82
	PH ⁺	$X^2\Pi_r$	2299.6 ^b	90.81	90.68	88.43	87.87	86.24	88.25	89.26	89.52
	PH ⁻	$X^2\Pi_i$	2230 ^b	30.09	31.71	33.09	27.12	33.24	24.68	31.71	31.07

CP	$X^2\Sigma^+$	1239.79924 ^a	35.49	4.78	-7.69	-4.50	1.77	0.64	6.27	1.97
PO	$X^2\Pi_r$	1233.34 ^a	-3.47	-6.44	-8.11	-6.74	-5.69	-5.73	-5.24	-5.33
PO ⁻	$X^3\Sigma^-$	1000 ^b	34.68	32.77	30.68	33.46	34.26	34.26	34.36	34.19
PF	$X^3\Sigma^-$	846.75 ^a	-7.52	-8.36	-9.11	-10.09	-8.75	-8.78	-8.38	-8.48
PF ⁺	$X^2\Pi_r$	1053.25 ^b	-5.85	-7.91	-9.70	-11.04	-8.82	-8.66	-7.70	-7.83
HS	$X^2\Pi_i$	2696.2475 ^a	7.92	8.60	8.60	8.59	8.56	8.58	8.57	6.39
BS	$X^2\Sigma^+$	1179.91 ^a	1.85	-2.78	-4.02	-4.42	-3.32	-3.49	-3.09	-3.21
CS ⁺	$X^2\Sigma^+$	1384 ^b	30.28	-3.84	-13.40	-10.72	-2.47	-5.36	-2.25	-4.66
NS	$X^2\Pi_r$	1218.7 ^b	24.33	-3.17	-3.59	-4.01	-2.91	-2.67	-1.69	-2.36
SO	$X^3\Sigma^-$	1150.7913 ^a	2.02	-1.02	-2.19	0.40	1.28	0.91	0.86	0.82
SO ⁺	$X^2\Pi_r$	1306.778 ^e	21.21	0.55	-0.43	1.81	2.81	2.61	2.85	2.76
HCl ⁺	$X^2\Pi_i$	2673.69 ^a	26.52	23.76	23.84	23.45	24.90	23.34	24.97	23.78
LiCl ⁻	$X^2\Sigma^+$	480 ^b	26.79	27.15	26.71	27.08	27.11	26.71	27.15	27.04
BeCl	$X^2\Sigma^+$	846.7 ^b	-2.93	-2.97	-3.03	-3.26	-3.30	-3.10	-2.98	-3.02
CCl	$X^2\Pi$	876.89749 ^a	-6.99	-7.55	-10.06	-10.92	-9.15	-9.01	-7.69	-7.96
NCI	$X^3\Sigma^-$	827.95767 ^a	-11.14	-10.50	-12.85	-13.73	-11.79	-11.82	-10.95	-10.81
OCi	$X^2\Pi_i$	853.64268 ^a	-5.50	-4.64	-4.10	-4.86	-5.24	-5.15	-4.87	-4.87
ClF ⁺	$X^2\Pi$	870 ^b	50.44	45.33	45.39	47.50	47.73	47.24	46.76	46.72
RMSD			27.42	24.88	24.52	24.95	24.58	24.38	24.88	24.52
MSD			11.85	7.25	5.36	5.98	7.17	6.87	7.47	6.66
MIN			-38.60	-38.52	-38.69	-38.45	-38.46	-38.58	-38.44	-38.59
MAX			90.81	90.68	88.43	87.87	86.24	88.25	89.26	89.52
Row 3-Row 3	Dimer	Expt.	$\Delta(\text{CCSD(T)}; \text{UHF})$	$\Delta(\text{CCSD(T)}; \kappa\text{-OOMP2})$	$\Delta(\text{CCSD(T)}; \text{OOMP2})$	$\Delta(\text{CCSD(T)}; \text{BLYP})$	$\Delta(\text{CCSD(T)}; \text{B97M-rV})$	$\Delta(\text{CCSD(T)}; \text{B97})$	$\Delta(\text{CCSD(T)}; \omega\text{B97X-V})$	$\Delta(\text{CCSD(T)}; \omega\text{B97M-V})$
MgCl	$X^2\Sigma^+$	462.12 ^b	2.24	2.27	2.27	2.14	2.19	2.27	2.24	2.31
AlS	$X^2\Sigma^+$	617.1169 ^a	-8.83	-14.00	-16.97	-15.43	-15.34	-14.91	-13.45	-13.33
Si ₂	$X^3\Sigma^-$	510.98 ^a	-0.03	0.26	33.72	0.50	0.46	0.52	0.32	0.34
SiCl	$X^2\Pi_r$	535.59 ^a	-6.92	-6.88	-7.09	-7.63	-7.34	-7.19	-6.83	-6.91
P ₂ ⁺	$X^2\Pi_u$	672.2 ^a	33.88	8.27	60.95	8.56	8.68	8.56	8.25	8.27
PS	$X^2\Pi_r$	739.1 ^b	19.14	-5.46	-5.93	-5.94	-5.73	-5.64	-5.81	-5.71
S ₂	$X^3\Sigma^-$	725.7102 ^a	-7.69	-7.18	-7.44	-7.06	-7.05	-7.02	-7.17	-7.13
S ₂ ⁺	$X^2\Pi_{g,r}$	790 ^b	44.58	11.06	10.91	11.14	11.32	11.25	11.06	11.07
RMSD			21.48	8.07	25.99	8.54	8.52	8.37	7.97	7.95
MSD			9.55	-1.46	8.80	-1.71	-1.60	-1.52	-1.42	-1.39
MIN			-8.83	-14.00	-16.97	-15.43	-15.34	-14.91	-13.45	-13.33
MAX			44.58	11.06	60.95	11.14	11.32	11.25	11.06	11.07
Open-shell			$\Delta(\text{CCSD(T)}; \text{UHF})$	$\Delta(\text{CCSD(T)}; \kappa\text{-OOMP2})$	$\Delta(\text{CCSD(T)}; \text{OOMP2})$	$\Delta(\text{CCSD(T)}; \text{BLYP})$	$\Delta(\text{CCSD(T)}; \text{B97M-rV})$	$\Delta(\text{CCSD(T)}; \text{B97})$	$\Delta(\text{CCSD(T)}; \omega\text{B97X-V})$	$\Delta(\text{CCSD(T)}; \omega\text{B97M-V})$
RMSD			38.69	20.87	22.47	23.77	22.39	21.65	22.01	28.34
MSD			10.71	1.10	1.95	-0.82	0.48	0.45	-2.13	-2.13
MIN			-116.46	-64.06	-64.26	-90.13	-72.72	-63.46	-63.22	-133.20
MAX			177.65	90.68	88.43	87.87	86.24	88.25	89.26	89.52

^a From Ref. 349.

^b From Ref. 346.

^c From Ref. 351.

^e From Ref. 352.

* Theoretical results.

Tab. 5.3 presents the experimental vibrational frequencies, in cm^{-1} , and errors in the corrected vibrational frequencies, in cm^{-1} , for the 59 species in the open-shell subset. Turning to Fig. 5.1, the open-shell non-HF methods exhibit an increase in the number of outliers as compared to the closed-shell cases. Overall, CCSD(T) with κ -OOMP2 orbitals provides the best RMSD of all references (20.87 cm^{-1}), improving on the performance of CCSD(T) with UHF orbitals by nearly a factor of two (38.69 cm^{-1}). The use of OOMP2, BLYP, B97M-rV, B97, and ω B97X-V orbitals yields comparable performance to κ -OOMP2 orbitals ($22\text{-}24 \text{ cm}^{-1}$), while the overall performance of CCSD(T) with ω B97M-V orbitals falls between the other non-UHF references and the UHF reference (28.34 cm^{-1}). In terms of MSDs, CCSD(T) with UHF orbitals is seen to blue shift the open-shell frequencies by 11 cm^{-1} while the non-UHF methods yield little-to-no systemic shift in frequencies ($\pm 2 \text{ cm}^{-1}$). The performance of CCSD(T) with κ -OOMP2 or OOMP2 orbitals on the open-shell systems is a factor of two worse than for the closed-shell systems.

Looking at individual cases, errors in corrected vibrational frequencies for the triplet ground state of B_2 are seen to range from -1.90 cm^{-1} using OOMP2 orbitals to -90.13 cm^{-1} using BLYP orbitals. B_2 is another system which is known to exhibit MR character and therefore the varied and often poor performance of these single reference methods is to be expected[272]. Evidence of MR character is seen in the mean-field $\langle S^2 \rangle$ values, where the κ -OOMP2 and UHF orbitals both significantly break spin-symmetry ($\langle S^2 \rangle$ of 2.81206 and 2.90778, respectively; Tab. D.8). The DFT orbital references are also seen to significantly break spin-symmetry while the OOMP2 reference artificially restores spin-symmetry for this system.

In agreement with the work of Beran et al.[313] and Tentscher and Arey[316] the predictions of the frequencies of CN, NO, OF, and their isoelectronic and isovalent counterparts with CCSD(T) using a UHF reference yield sizeable errors. CN is isoelectronic to C_2^- , CO^+ , and N_2^+ and is isovalent to CP, CS^+ , and P_2^+ . CCSD(T) with UHF orbitals yields errors in the corrected frequencies of these species of 54.67 cm^{-1} , -116.46 cm^{-1} , 67.00 cm^{-1} , 70.77 cm^{-1} , 35.49 cm^{-1} , 30.28 cm^{-1} , and 33.88 cm^{-1} , respectively, while CCSD(T) with κ -OOMP2 orbitals improves these errors to -7.85 cm^{-1} , -6.89 cm^{-1} , -16.90 cm^{-1} , -6.08 cm^{-1} , 4.78 cm^{-1} , -3.84 cm^{-1} , and 8.27 cm^{-1} , respectively. In all of these cases but C_2^- these errors with UHF orbital references are accompanied by spin-symmetry breaking at the level of the reference with respective $\langle S^2 \rangle$ values of 1.15755, 0.75627, 0.96970, 1.23889, 1.61297, 1.47259, 1.16866 for UHF and 0.76257, 0.75579, 0.76730, 0.75334, 0.82118, 0.80770, 0.75476 for the κ -OOMP2 reference (Tab. D.8). The spin-symmetry restoration from the κ -OOMP2 (or OOMP2/DFT) orbitals is seen to dramatically improve the predicted frequencies for these systems with significant symmetry-breaking occurring at the UHF level. For C_2^- , the error in predicted frequency for CCSD(T) with UHF orbitals has the opposite sign of the other frequency errors in this isoelectronic/isovalent family of dimers and the UHF $\langle S^2 \rangle$ suggests little spin-contamination. Instead, UHF, ω B97X-V, and ω B97M-V are seen to favor broken-spatial-symmetry solutions for C_2^- , contributing to large errors in the predicted frequencies while κ -OOMP2, OOMP2, and the other density functionals preserve the spatial symmetry and yield much more reliable frequencies. For P_2^+ , CCSD(T):OOMP2 yields an error of

60.95 cm⁻¹, almost twice that of CCSD(T):UHF. The orbital optimization of the ground state at the OOMP2 level is shown to give preference to a higher symmetry orbital occupation where the π_{3p_x} and π_{3p_y} MOs are doubly-occupied and the σ_{3p_z} orbital is singly-occupied. The ground state for all other methods doubly occupies the σ_{3p_z} and singly-occupies one of the two π_{3p} orbitals, breaking the $D_{\infty h}$ symmetry of the molecule. The latter occupation, however, is the filling predicted by MO theory and yields reasonable frequencies in comparison to the experimental benchmark. This represents another example of essential symmetry breaking that is quelled by OOMP2.

NO is isoelectronic to O₂⁺ and isovalent to PO, NS, SO⁺, PS, and S₂⁺. CCSD(T) with UHF orbitals yields errors in the corrected frequencies of these species of 177.65 cm⁻¹, 28.13 cm⁻¹, -3.47 cm⁻¹, 24.33 cm⁻¹, 21.21 cm⁻¹, 19.14 cm⁻¹, and 44.58 cm⁻¹, respectively, while CCSD(T) with κ -OOMP2 orbitals yields error of -6.77 cm⁻¹, 4.68 cm⁻¹, -6.44 cm⁻¹, -3.17 cm⁻¹, 0.55 cm⁻¹, -5.46 cm⁻¹, and 11.06 cm⁻¹, respectively. NO represents the most positive outlier for CCSD(T) with UHF orbitals while the error for PO is the smallest of all the orbital references considered. Comparing the mean-field $\langle S^2 \rangle$ values between UHF and κ -OOMP2 for these species, O₂⁺ (1.12597 vs. 0.75272), NS (1.18951 vs. 0.75758), SO⁺ (1.18709 vs. 0.75583), PS (1.05380 vs. 0.76119), and S₂⁺ (1.23007 vs 0.75862) show significant spin-contamination at the UHF level while cases exhibiting the largest and smallest errors, NO (0.79621 vs. 0.75407) and PO (0.77298 vs. 0.75758), respectively, show little evidence of significant spin-contamination (Tab. D.8). These findings are consistent with those of Szalay et al.[314], which find that in these errors arise from instabilities in the doublet wavefunction. This discrepancy between NO and PO arises due to the instability in the PO UHF wavefunction occurring at a larger internuclear separation than the equilibrium bond length around which data was collected.

OF is isoelectronic to F₂⁺ and isovalent to OCl and ClF⁺. CCSD(T) with UHF orbitals yields errors in the corrected frequencies of these species of 29.52 cm⁻¹, -21.63 cm⁻¹, -5.50 cm⁻¹, and 50.44 cm⁻¹, respectively, while CCSD(T) with κ -OOMP2 orbitals yields error of 2.56 cm⁻¹, 33.01 cm⁻¹, -4.64 cm⁻¹, and 45.33 cm⁻¹, respectively. The errors for UHF and non-UHF orbitals for F₂⁺ are seen to differ by over 50 cm⁻¹ while for OCl and ClF the errors in the frequencies are in good agreement. Similarly to the cases of NO and PO, the UHF wavefunctions for OF, OCl, and ClF⁺ do not demonstrate signs of significant spin contamination ($\langle S^2 \rangle$ values of 0.77257, 0.77010, 0.76463, respectively; Tab. D.8).

Potential issues with experimental data

Table 5.4: Experimental vibrational frequencies (in cm⁻¹), mean errors for the non-HF CCSD(T) methods (in cm⁻¹), ranges of the errors for the non-HF CCSD(T) methods (in cm⁻¹), and alternative experimental reported frequencies (in cm⁻¹) are presented for species where the experimental results are in question.

Dimer	State	Current Expt. Frequency	Mean Non-HF Error	Non-HF Error Range	Alternative Expt. Frequency
-------	-------	-------------------------	-------------------	--------------------	-----------------------------

O_2^-	$X^2\Pi_{g,i}$	1090[346]	27.04	0.41	1090[353, 354] 1108 \pm 20[355] 1140[356] 1145[357]
HF ⁺	$X^2\Pi_i$	3090.5[346, 358, 359]	27.51	3.01	3061.8[360] 3118[313]* 3119[316]*
F ₂ ⁺	$X^2\Pi_{g,i}$	1104[351]	19.70	6.09	1091.5[361]
F ₂ ⁻	$X^2\Sigma_u^+$	510[346, 362]*	-63.65	1.17	
NaO	$X^2\Pi$	526[346]*	-38.53	0.25	504[363]* 547[364]
AlH ⁺	$X^2\Sigma^+$	1620[346, 365]	27.08	14.89	
PH ⁺	$X^2\Pi_r$	2299.6[346, 366]	88.61	4.44	2382.75[367]*
PH ⁻	$X^2\Pi_i$	2230[346]	30.37	8.56	2230 \pm 100[368]
PO ⁻	$X^3\Sigma^-$	1000[346]	33.43	3.68	1000 \pm 70[368]
HCl ⁺	$X^2\Pi_i$	2673.69[349]	24.00	1.63	2702.6[369]*
LiCl ⁻	$X^2\Sigma^+$	480[346]	26.99	0.44	480 \pm 80[370]
ClF ⁺	$X^2\Pi$	870[346]	46.67	2.40	870 \pm 30[371] 912 \pm 30[372]

* Theoretical results.

In the cases of ClF⁺ and PH⁺ the predicted frequencies for CCSD(T) with a UHF orbital reference and CCSD(T) with non-UHF orbital references differ significantly (more than 25 cm⁻¹) from the reported benchmark value while the CCSD(T) with non-UHF orbitals all yield predicted frequencies in agreement with each other. This observation is true of other molecules and ions in the open-shell set as well, as summarized in Tab. 5.4. In all of these cases except F₂⁺ and F₂⁻ the errors for CCSD(T) with UHF orbitals are consistent with the errors for CCSD(T) with non-HF orbitals. The agreement of all methods suggests that potentially inaccurate or imprecise experimental reference values should be revisited. For NaO[363, 364] and F₂⁻[362], the reference data given by Huber and Herzberg[346] are sourced from calculations performed at the HF level of theory; any of the CCSD(T) methods surveyed should be seen as a more accurate result for these systems. For another subset of these systems the error bars on the experimental values contain the frequencies calculated from this work (PH⁻: 2230 \pm 100 cm⁻¹[368], PO⁻: 1000 \pm 70 cm⁻¹[368], LiCl⁻: 480 \pm 80 cm⁻¹[370]). For ClF⁺, Huber and Herzberg[346] reference the DeKock et al.[371] who report a vibrational frequency of 870 \pm 30 cm⁻¹ while Anderson et al. [372] report a frequency of 912 \pm 30 cm⁻¹. Our calculations, which predict a ClF⁺ frequency of 917 cm⁻¹, more closely agree with the work of Anderson et al. Similarly, for O₂⁻ Huber and Herzberg[346] cite a value of 1090 cm⁻¹ based on the works of Boness and Schulz[353] and Linder and Schmidt[354] while also noting that Gray et al.[356] and Creighton and Lippincott[357] give values of 1140 cm⁻¹ and 1145 cm⁻¹, respectively. In a more recent study, Ervin et al.[355] give a value of 1108 \pm 20 cm⁻¹, which is in good agreement with our theoretical predictions of 1117 cm⁻¹. The most positive error point for many of the CCSD(T) method with non-UHF references, PH⁺, does not have much experimental data on its spectroscopic constants in the literature, with the value of 2299.6 cm⁻¹ tracing back to a study by Narasimham[366]. A recent modeling study by Reddy et al.[367] predicts a ground-state frequency of 2382.75 cm⁻¹, in good agreement with our calculated values of 2386–2390 cm⁻¹, suggesting that

further experimental study of this system is worthwhile. The experimental reference for F_2^+ was taken from Cormack et al.[351] while Yang et al.[361], consistent with Tentscher and Arey[316], suggest a value of 1091.5 cm^{-1} , further from our theoretical predictions. For HF^+ , the large-basis results from Beran et al.[313] and Tentscher and Arey[316] predict an error that agree with our error prediction of 28 cm^{-1} . These calculated frequencies are closer to the value originally reported by Gewurtz et al.[358] and Hovde et al.[359] of 3090.5 cm^{-1} adopted by Huber and Herzberg[346] than to the value of 3061.8 cm^{-1} proposed by Yenchu et al.[360]. Similarly, our predictions of the corrected vibrational frequency of HCl^+ are blue-shifted by approximately 24 cm^{-1} compared to the experimental reference value of 2673.69 cm^{-1} from Irikura[349]. A recent joint experimental and theoretical study of this system by Patanen et al.[369] has suggested a computed value of 2702.6 cm^{-1} , in much better agreement with our results. For AlH^+ , Huber and Herzberg[346] cite a 1934 study by Hoslt[365] to approximate the vibrational frequency, though a more precise value is desired for the point of comparison to our computed frequencies to better assess the error between the different reference methods.

Pruned subset

In order to draw more meaningful conclusions about the performance of CCSD(T) with κ -OOMP2 orbitals, we consider a subset of data points where the MR species (C_2 and B_2) and the species with ambiguous experimental values (Tab. 5.4) discussed above are excluded, leaving 35 closed-shell species (28 neutrals, 6 cations, 1 anion) and 46 open-shell species (36 neutrals, 9 cations, 1 anion; 35 doublets, 11 triplets). Tab. 5.5 presents the RMSDs, MSDs, MINs, and MAXs for the closed-shell species, open-shell species, and the overall pruned set. These data are presented graphically in Fig. 5.2. For the pruned data set CCSD(T):B97 and CCSD(T): κ -OOMP2 are seen to yield the best performance with RMSDs of 8.48 cm^{-1} and 8.50 cm^{-1} , respectively. The performances of CCSD(T): ω B97X-V and CCSD(T): ω B97M-V are hindered by C_2^- ; excluding this point brings the RMSDs for these methods to the same level as the other DFT-based methods.

Comparing Fig. 5.1 and Fig. 5.2, we see that the pruning procedure removed many of the outlier cases that were shared between all or nearly all of the methods surveyed. For CCSD(T):UHF, the remaining outlying points are the spin-contaminated points from the closed-shell subset (F_2 , PN, BeS, NS^+ , and P_2), and HCl, while the remaining open-shell outliers are NO, N_2^+ , CO^+ , and C_2^- . The range covered by the CCSD(T):UHF whiskers is larger by a factor of two than nearly all the other methods tested. For CCSD(T): κ -OOMP2, the pruning procedure leaves only one closed-shell and one open-shell outlier, HCl and BO, respectively. For CCSD(T):OOMP2, the remaining outliers in the closed-shell subset are HCl and BeO while the open-shell set has outliers P_2^+ , which has been previously discussed, Si_2 , which breaks spatial symmetry at the OOMP2 level, and BO. CCSD(T):BLYP has closed-shell outliers in NaLi, NaH, and HCl and an open-shell outlier in BO. CCSD(T):B97M-rV and CCSD(T):B97 both have HCl as an open-shell outlier and BO as a closed-shell outlier. CCSD(T): ω B97X-V has closed-shell outliers in HCl and NaH and open-shell outliers in C_2^-

Figure 5.2: Box plots (overall, left, and enhanced, right) of the errors in corrected vibrational frequencies (in cm^{-1}) are presented for the pruned subset of species. Red lines mark the median errors, boxes bound the central 50% of the data, whiskers enclose all data points within 1.5 times the inter-quartile range of the box edges, and points denote outlying data.

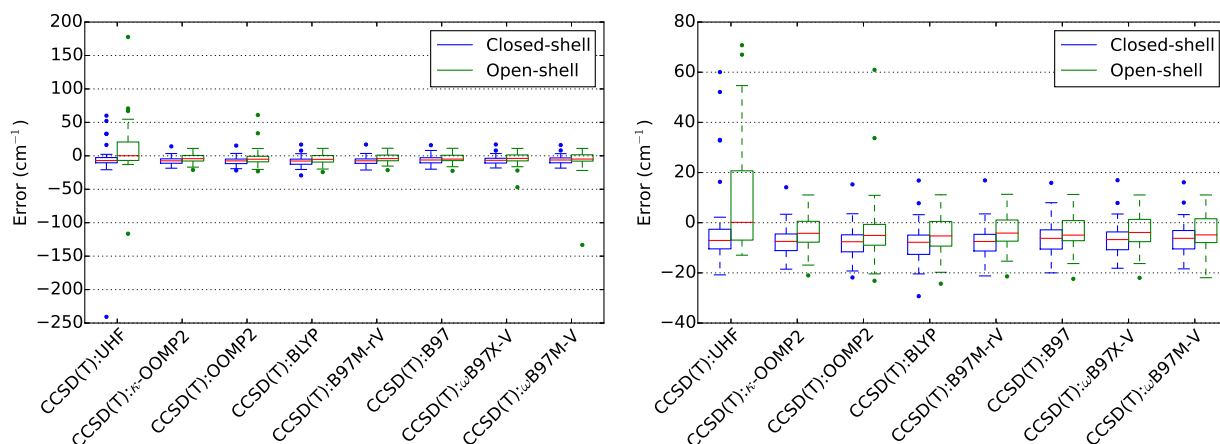


Table 5.5: Root mean square deviations, mean signed deviations, most negative deviations, and most positive deviations (all in cm^{-1}) for the cropped subset of species are summarized for the CCSD(T) methods utilizing different molecular orbitals.

Closed-shell pruned	$\Delta(\text{CCSD(T):UHF})$	$\Delta(\text{CCSD(T):}\kappa\text{-OOMP2})$	$\Delta(\text{CCSD(T):OOMP2})$	$\Delta(\text{CCSD(T):BLYP})$	$\Delta(\text{CCSD(T):B97M-rV})$	$\Delta(\text{CCSD(T):B97})$	$\Delta(\text{CCSD(T):}\omega\text{B97X-V})$	$\Delta(\text{CCSD(T):}\omega\text{B97M-V})$
RMSD	44.43	9.41	10.18	11.56	10.05	9.45	9.50	8.97
MSD	-7.74	-6.96	-7.73	-8.10	-7.32	-6.41	-6.41	-5.93
MIN	-240.71	-18.53	-21.83	-29.30	-21.21	-20.00	-18.16	-18.40
MAX	60.05	14.11	15.27	16.82	16.86	15.88	16.93	16.10
Open-shell pruned	$\Delta(\text{CCSD(T):UHF})$	$\Delta(\text{CCSD(T):}\kappa\text{-OOMP2})$	$\Delta(\text{CCSD(T):OOMP2})$	$\Delta(\text{CCSD(T):BLYP})$	$\Delta(\text{CCSD(T):B97M-rV})$	$\Delta(\text{CCSD(T):B97})$	$\Delta(\text{CCSD(T):}\omega\text{B97X-V})$	$\Delta(\text{CCSD(T):}\omega\text{B97M-V})$
RMSD	38.33	7.75	13.45	8.80	7.61	7.67	10.26	21.11
MSD	9.27	-3.48	-2.83	-4.61	-3.32	-3.35	-3.97	-6.34
MIN	-116.46	-21.02	-23.17	-24.32	-21.41	-22.38	-46.93	-133.20
MAX	177.65	11.06	60.95	11.14	11.32	11.25	11.06	11.07
Total pruned	$\Delta(\text{CCSD(T):UHF})$	$\Delta(\text{CCSD(T):}\kappa\text{-OOMP2})$	$\Delta(\text{CCSD(T):OOMP2})$	$\Delta(\text{CCSD(T):BLYP})$	$\Delta(\text{CCSD(T):B97M-rV})$	$\Delta(\text{CCSD(T):B97})$	$\Delta(\text{CCSD(T):}\omega\text{B97X-V})$	$\Delta(\text{CCSD(T):}\omega\text{B97M-V})$
RMSD	41.07	8.50	12.15	10.08	8.75	8.48	9.94	16.96
MSD	1.92	-4.98	-4.95	-6.11	-5.04	-4.67	-5.03	-6.17
MIN	-240.71	-21.02	-23.17	-29.30	-21.41	-22.38	-46.93	-133.20
MAX	177.65	14.11	60.95	16.82	16.86	15.88	16.93	16.10

and BO. CCSD(T): ω B97M-V also has HCl and NaH as closed-shell outliers and C_2^- as an open-shell outlier. The non-HF methods are seen to have their mean values red-shifted compared to experiments by 5-6 cm^{-1} .

5.6 Conclusions

We have evaluated the performance of CCSD(T) with different MO references to predict the vibrational frequencies of both closed-shell and open-shell diatomic molecules and ions. The at times problematic use of a UHF reference was compared against the use of κ -OOMP2, OOMP2, BLYP, B97M-rV, B97, ω B97X-V, and ω B97M-V molecular orbital references. Overall, CCSD(T):B97, CCSD(T): κ -OOMP2, and CCSD(T):B97M-rV yield RMSDs on the pruned overall data set of 8.48 cm^{-1} , 8.50 cm^{-1} , and 8.75 cm^{-1} , respectively, reducing the RMSD for CCSD(T):UHF by nearly a factor of 5. For the pruned closed- and open-shell subsets the associated RMSDs are 9.45 cm^{-1} and 7.67 cm^{-1} , respectively, 9.41 cm^{-1} and 7.75 cm^{-1} , respectively, and 10.05 and 7.61, respectively, for CCSD(T):B97, CCSD(T): κ -OOMP2, and CCSD(T):B97M-rV. The slightly degraded performance of the other non-HF MO references are skewed by one or two data points and otherwise rank competitively with the B97, κ -OOMP2, and B97M-rV. These outlying data points are seen to arise from spatial or spin-symmetry breaking or erroneous symmetry restoration. The effect of regularization in κ -OOMP2 is seen to prevent the symmetry issues seen in OOMP2.

A major practical limitation of these very promising non-HF CCSD(T) methods is the present lack of implemented analytic gradients, relegating the current application of these to systems with only a few atoms. One may develop an approach like that of Taube and Bartlett's FNO-CCSD(T)[373] for κ -OOMP2 and/or DFT orbitals. The success of the non-HF CCSD(T) methods in treating closed-shell and open-shell systems with the same accuracy speaks to the usefulness of such an implementation. Such approaches do not affect the overall asymptotic scaling and would extend the "black box" utility of CCSD(T) currently seen for closed-shell systems. Furthermore, the use of κ -OOMP2 as the generator of MOs also provides a diagnostic tool in the mean-field $\langle S^2 \rangle$ of the multireference character of the target system, informing the expected accuracy of the subsequent CCSD(T) results.

In order to assess errors relating to the computational treatment presented in this work we consider errors in the basis set and errors related to the approximate treatment of triple excitations. Peterson and Dunning[342] demonstrated a blue shift of computed harmonic frequencies for row 3 diatomic species of 2-15 cm^{-1} when going from the cc-pwCVTZ to cc-pwCV5Z. Provided this trend holds with the aug-cc-pwCVnZ basis sets the use of the aug-cc-pwCVQZ basis should help to correct the systematic red-shift seen for the non-HF CCSD(T) methods. For exact treatment of triples Tentscher and Arey[316] found CCSDT tends to red-shift in computed frequencies compared to CCSD(T). This effect is exacerbated for species where CCSD(T) with UHF orbitals is particularly poor (N_2^+ , CN) while for other species the shift was on the order of 5 cm^{-1} . We also note that CCSDT, free of the perturbative nature of CCSD(T), should be less sensitive to the choice of reference orbitals.

Further extension of this study approach to cases where DFT traditionally struggles would be of significant interest. In particular, extension to transition metals species and systems with significant charge separation is highly desirable to discriminate if CCSD(T):DFT is able to remedy the traditional failures of DFT. Additionally, the exponential regularization schemes of Lee and Head-Gordon[39] could be extended to the perturbative triples calculation in CCSD(T) as an attempt to handle cases of nonvariational failure in traditional CCSD(T).

Bibliography

- (1) Voth, G. A. Path-integral centroid methods in quantum statistical mechanics and dynamics. *Adv. Chem. Phys.* **2007**, 135–218.
- (2) Craig, I. R.; Manolopoulos, D. E. Quantum statistics and classical mechanics: Real time correlation functions from ring polymer molecular dynamics. *J. Chem. Phys.* **2004**, *121*, 3368–3373.
- (3) Trotter, H. F. On the product of semi-groups of operators. *Proc. Am. Math. Soc.* **1959**, *10*, 545–551.
- (4) Chandler, D.; Wolynes, P. G. Exploiting the isomorphism between quantum theory and classical statistical mechanics of polyatomic fluids. *J. Chem. Phys.* **1981**, *74*, 4078–4095.
- (5) Berne, B. J.; Thirumalai, D. On the simulation of quantum systems: path integral methods. *Annu. Rev. Phys. Chem.* **1986**, *37*, 401–424.
- (6) Webb, S. P.; Jordanov, T.; Hammes-Schiffer, S. Multiconfigurational nuclear-electronic orbital approach: Incorporation of nuclear quantum effects in electronic structure calculations. *J. Chem. Phys.* **2002**, *117*, 4106–4118.
- (7) Pak, M. V.; Chakraborty, A.; Hammes-Schiffer, S. Density functional theory treatment of electron correlation in the nuclear- electronic orbital approach. *J. Phys. Chem. A* **2007**, *111*, 4522–4526.
- (8) Slater, J. C. The theory of complex spectra. *Phys. Rev.* **1929**, *34*, 1293.
- (9) Condon, E. U. The theory of complex spectra. *Phys. Rev.* **1930**, *36*, 1121.
- (10) Roothaan, C. C. J. New developments in molecular orbital theory. *Rev. Mod. Phys.* **1951**, *23*, 69.
- (11) Löwdin, P.-O. On the non-orthogonality problem connected with the use of atomic wave functions in the theory of molecules and crystals. *J. Chem. Phys.* **1950**, *18*, 365–375.
- (12) Head-Gordon, M.; Pople, J. A. Optimization of wave function and geometry in the finite basis Hartree-Fock method. *J. Phys. Chem.* **1988**, *92*, 3063–3069.

- (13) Chaban, G.; Schmidt, M. W.; Gordon, M. S. Approximate second order method for orbital optimization of SCF and MCSCF wavefunctions. *Theo. Chem. Acc.* **1997**, *97*, 88–95.
- (14) Cancès, E.; Le Bris, C. Can we outperform the DIIS approach for electronic structure calculations? *Int. J. Quantum Chem.* **2000**, *79*, 82–90.
- (15) Kudin, K. N.; Scuseria, G. E.; Cancès, E. A black-box self-consistent field convergence algorithm: One step closer. *J. Chem. Phys.* **2002**, *116*, 8255–8261.
- (16) Hu, X.; Yang, W. Accelerating self-consistent field convergence with the augmented Roothaan–Hall energy function. *J. Chem. Phys.* **2010**, *132*, 054109.
- (17) Pulay, P. Convergence acceleration of iterative sequences. The case of SCF iteration. *Chem. Phys. Lett.* **1980**, *73*, 393–398.
- (18) Pulay, P. Improved SCF convergence acceleration. *J. Comput. Chem.* **1982**, *3*, 556–560.
- (19) Van Voorhis, T.; Head-Gordon, M. A geometric approach to direct minimization. *Mol. Phys.* **2002**, *100*, 1713–1721.
- (20) Fukutome, H. Unrestricted Hartree–Fock theory and its applications to molecules and chemical reactions. *Int. J. Quantum Chem.* **1981**, *20*, 955–1065.
- (21) Davidson, E. R. The iterative calculation of a few of the lowest eigenvalues and corresponding eigenvectors of large real-symmetric matrices. *J. Comput. Phys.* **1975**, *17*, 87–94.
- (22) Purvis, G. D.; Bartlett, R. J. A full coupled-cluster singles and doubles model: The inclusion of disconnected triples. *J. Chem. Phys.* **1982**, *76*, 1910–1918.
- (23) Scuseria, G. E.; Janssen, C. L.; Schaefer, H. F. An efficient reformulation of the closed-shell coupled cluster single and double excitation (CCSD) equations. *J. Chem. Phys.* **1988**, *89*, 7382–7387.
- (24) Noga, J.; Bartlett, R. J. The full CCSDT model for molecular electronic structure. *J. Chem. Phys.* **1987**, *86*, 7041–7050.
- (25) Raghavachari, K.; Trucks, G. W.; Pople, J. A.; Head-Gordon, M. A fifth-order perturbation comparison of electron correlation theories. *Chem. Phys. Lett.* **1989**, *157*, 479–483.
- (26) Crawford, T. D.; Schaefer III, H. F. In *Reviews in Computational Chemistry*, Lipkowitz, K. B., Boyd, D. B., Eds.; Wiley-VCH: New York, 2000; Vol. 14; Chapter 2, pp 33–136.
- (27) Shavitt, I.; Bartlett, R. J., *Many-Body Methods in Chemistry and Physics: MBPT and Coupled-Cluster Theory*; Cambridge University Press: New York, 2009.
- (28) Møller, C.; Plesset, M. S. Note on an approximation treatment for many-electron systems. *Phys. Rev.* **1934**, *46*, 618.

- (29) Feyereisen, M.; Fitzgerald, G.; Komornicki, A. Use of approximate integrals in *ab initio* theory. An application in MP2 energy calculations. *Chem. Phys. Lett.* **1993**, *208*, 359–363.
- (30) Bernholdt, D. E.; Harrison, R. J. Large-scale correlated electronic structure calculations: the RI-MP2 method on parallel computers. *Chem. Phys. Lett.* **1996**, *250*, 477–484.
- (31) Farnell, L.; Pople, J. A.; Radom, L. Structural predictions for open-shell systems: a comparative assessment of *ab initio* procedures. *J. Phys. Chem.* **1983**, *87*, 79–82.
- (32) Nobes, R. H.; Pople, J. A.; Radom, L.; Handy, N. C.; Knowles, P. J. Slow convergence of the Møller-Plesset perturbation series: the dissociation energy of hydrogen cyanide and the electron affinity of the cyano radical. *Chem. Phys. Lett.* **1987**, *138*, 481–485.
- (33) Gill, P. M. W.; Pople, J. A.; Radom, L.; Nobes, R. H. Why does unrestricted Møller-Plesset perturbation theory converge so slowly for spin-contaminated wave functions? *J. Chem. Phys.* **1988**, *89*, 7307–7314.
- (34) Jensen, F. A remarkable large effect of spin contamination on calculated vibrational frequencies. *Chem. Phys. Lett.* **1990**, *169*, 519–528.
- (35) Lochan, R. C.; Head-Gordon, M. Orbital-optimized opposite-spin scaled second-order correlation: An economical method to improve the description of open-shell molecules. *J. Chem. Phys.* **2007**, *126*, 164101.
- (36) Neese, F.; Schwabe, T.; Kossmann, S.; Schirmer, B.; Grimme, S. Assessment of Orbital-Optimized, Spin-Component Scaled Second-Order Many-Body Perturbation Theory for Thermochemistry and Kinetics. *J. Chem. Theory Comput.* **2009**, *5*, 3060–3073.
- (37) Bozkaya, U.; Turney, J. M.; Yamaguchi, Y.; Schaefer, H. F.; Sherrill, C. D. Quadratically convergent algorithm for orbital optimization in the orbital-optimized coupled-cluster doubles method and in orbital-optimized second-order Møller-Plesset perturbation theory. *J. Chem. Phys.* **2011**, *135*, 104103.
- (38) Hylleraas, E. A. Über den Grundterm der Zweielektronenprobleme von H^- , He, Li^+ , Be^{++} usw. *Z. Phys.* **1930**, *65*, 209–225.
- (39) Lee, J.; Head-Gordon, M. Regularized Orbital-Optimized Second-Order Møller-Plesset Perturbation Theory: A Reliable Fifth-Order-Scaling Electron Correlation Model with Orbital Energy Dependent Regularizers. *J. Chem. Theory Comput.* **2018**, *14*, 5203–5219.
- (40) Stück, D.; Head-Gordon, M. Regularized orbital-optimized second-order perturbation theory. *J. Chem. Phys.* **2013**, *139*, 244109.
- (41) Razban, R. M.; Stück, D.; Head-Gordon, M. Addressing first derivative discontinuities in orbital-optimised opposite-spin scaled second-order perturbation theory with regularisation. *Mol. Phys.* **2017**, *115*, 2102–2109.

- (42) Hohenberg, P.; Kohn, W. Inhomogeneous electron gas. *Phys. Rev.* **1964**, *136*, B864–B871.
- (43) Levy, M. Universal variational functionals of electron densities, first-order density matrices, and natural spin-orbitals and solution of the v-representability problem. *Proc. Natl. Acad. Sci. U.S.A.* **1979**, *76*, 6062–6065.
- (44) Thomas, L. H. The calculation of atomic fields. *Math. Proc. Camb. Philos. Soc* **1927**, *23*, 542–548.
- (45) Fermi, E. Statistical method to determine some properties of atoms. *Rend. Accad. Naz. Lincei* **1927**, *6*, 5.
- (46) Kohn, W.; Sham, L. J. Self-consistent equations including exchange and correlation effects. *Phys. Rev.* **1965**, *140*, A1133=A1138.
- (47) Parr, R. G.; Yang, W., *Density-Functional Theory of Atoms and Molecules*; Oxford University Press: New York, 1989.
- (48) Perdew, J. P.; Ruzsinszky, A.; Tao, J.; Staroverov, V. N.; Scuseria, G. E.; Csonka, G. I. Prescription for the design and selection of density functional approximations: More constraint satisfaction with fewer fits. *J. Chem. Phys.* **2005**, *123*, 062201.
- (49) Dirac, P. A. M. Note on exchange phenomena in the Thomas atom. **1930**, *26*, 376–385.
- (50) Ceperley, D. M.; Alder, B. J. Ground state of the electron gas by a stochastic method. *Phys. Rev. Lett.* **1980**, *45*, 566.
- (51) Vosko, S. H.; Wilk, L.; Nusair, M. Accurate spin-dependent electron liquid correlation energies for local spin density calculations: a critical analysis. *Can. J. Phys.* **1980**, *58*, 1200–1211.
- (52) Perdew, J. P.; Zunger, A. Self-interaction correction to density-functional approximations for many-electron systems. *Phys. Rev. B* **1981**, *23*, 5048.
- (53) Perdew, J. P.; Wang, Y. Accurate and simple analytic representation of the electron-gas correlation energy. *Phys. Rev. B* **1992**, *45*, 13244.
- (54) Perdew, J. P.; Burke, K.; Ernzerhof, M. Generalized gradient approximation made simple. *Phys. Rev. Lett.* **1996**, *77*, 3865.
- (55) Becke, A. D. Density-functional exchange-energy approximation with correct asymptotic behavior. *Phys. Rev. A* **1988**, *38*, 3098.
- (56) Lee, C.; Yang, W.; Parr, R. G. Development of the Colle-Salvetti correlation-energy formula into a functional of the electron density. *Phys. Rev. B* **1988**, *37*, 785.
- (57) Tao, J.; Perdew, J. P.; Staroverov, V. N.; Scuseria, G. E. Climbing the density functional ladder: Nonempirical meta-generalized gradient approximation designed for molecules and solids. *Phys. Rev. Lett.* **2003**, *91*, 146401.

- (58) Sun, J.; Ruzsinszky, A.; Perdew, J. P. Strongly constrained and appropriately normed semilocal density functional. *Phys. Rev. Lett.* **2015**, *115*, 036402.
- (59) Zhao, Y.; Truhlar, D. G. A new local density functional for main-group thermochemistry, transition metal bonding, thermochemical kinetics, and noncovalent interactions. *J. Chem. Phys.* **2006**, *125*, 194101.
- (60) Yu, H. S.; He, X.; Truhlar, D. G. MN15-L: A new local exchange–correlation functional for Kohn–Sham density functional theory with broad accuracy for atoms, molecules, and solids. *J. Chem. Theory Comput.* **2016**, *12*, 1280–1293.
- (61) Becke, A. D. Density-functional thermochemistry. III. The role of exact exchange. *J. Chem. Phys.* **1993**, *98*, 5648–5652.
- (62) Becke, A. D. Density-functional thermochemistry. V. Systematic optimization of exchange–correlation functionals. *J. Chem. Phys.* **1997**, *107*, 8554–8560.
- (63) Adamo, C.; Barone, V. Toward reliable density functional methods without adjustable parameters: The PBE0 model. *J. Chem. Phys.* **1999**, *110*, 6158–6170.
- (64) Sun, J.; Haunschild, R.; Xiao, B.; Bulik, I. W.; Scuseria, G. E.; Perdew, J. P. Semilocal and hybrid meta-generalized gradient approximations based on the understanding of the kinetic-energy-density dependence. *J. Chem. Phys.* **2013**, *138*, 044113.
- (65) Zhao, Y.; Truhlar, D. G. The M06 suite of density functionals for main group thermochemistry, thermochemical kinetics, noncovalent interactions, excited states, and transition elements: two new functionals and systematic testing of four M06-class functionals and 12 other functionals. *Theor. Chem. Acc.* **2008**, *120*, 215–241.
- (66) Haoyu, S. Y.; He, X.; Li, S. L.; Truhlar, D. G. MN15: A Kohn–Sham global-hybrid exchange–correlation density functional with broad accuracy for multi-reference and single-reference systems and noncovalent interactions. *Chem. Sci.* **2016**, *7*, 5032–5051.
- (67) Yanai, T.; Tew, D. P.; Handy, N. C. A new hybrid exchange–correlation functional using the Coulomb-attenuating method (CAM-B3LYP). *Chem. Phys. Lett.* **2004**, *393*, 51–57.
- (68) Chai, J.-D.; Head-Gordon, M. Long-range corrected hybrid density functionals with damped atom–atom dispersion corrections. *Phys. Chem. Chem. Phys.* **2008**, *10*, 6615–6620.
- (69) Peverati, R.; Truhlar, D. G. Improving the accuracy of hybrid meta-GGA density functionals by range separation. *J. Phys. Chem. Lett.* **2011**, *2*, 2810–2817.
- (70) Grimme, S. Accurate description of van der Waals complexes by density functional theory including empirical corrections. *J. Comput. Chem.* **2004**, *25*, 1463–1473.
- (71) Grimme, S. Semiempirical GGA-type density functional constructed with a long-range dispersion correction. *J. Comput. Chem.* **2006**, *27*, 1787–1799.

- (72) Grimme, S.; Antony, J.; Ehrlich, S.; Krieg, H. A consistent and accurate ab initio parametrization of density functional dispersion correction (DFT-D) for the 94 elements H-Pu. *J. Chem. Phys.* **2010**, *132*, 154104.
- (73) Caldeweyher, E.; Ehlert, S.; Hansen, A.; Neugebauer, H.; Spicher, S.; Bannwarth, C.; Grimme, S. A generally applicable atomic-charge dependent London dispersion correction. *J. Chem. Phys.* **2019**, *150*, 154122.
- (74) Grimme, S.; Ehrlich, S.; Goerigk, L. Effect of the damping function in dispersion corrected density functional theory. *J. Comput. Chem.* **2011**, *32*, 1456–1465.
- (75) Schröder, H.; Creon, A.; Schwabe, T. Reformulation of the D3 (Becke–Johnson) dispersion correction without resorting to higher than C_6 dispersion coefficients. *J. Chem. Theory Comput.* **2015**, *11*, 3163–3170.
- (76) Smith, D. G. A.; Burns, L. A.; Patkowski, K.; Sherrill, C. D. Revised damping parameters for the D3 dispersion correction to density functional theory. *J. Phys. Chem. Lett.* **2016**, *7*, 2197–2203.
- (77) Witte, J.; Mardirossian, N.; Neaton, J. B.; Head-Gordon, M. Assessing DFT-D3 damping functions across widely used density functionals: Can we do better? *J. Chem. Theory Comput.* **2017**, *13*, 2043–2052.
- (78) Becke, A. D.; Johnson, E. R. Exchange-hole dipole moment and the dispersion interaction. *J. Chem. Phys.* **2005**, *122*, 154104.
- (79) Becke, A. D.; Johnson, E. R. Exchange-hole dipole moment and the dispersion interaction revisited. *J. Chem. Phys.* **2007**, *127*, 154108.
- (80) Tkatchenko, A.; Scheffler, M. Accurate molecular van der Waals interactions from ground-state electron density and free-atom reference data. *Phys. Rev. Lett.* **2009**, *102*, 073005.
- (81) Vydrov, O. A.; Van Voorhis, T. Nonlocal van der Waals density functional: The simpler the better. *J. Chem. Phys.* **2010**, *133*, 244103.
- (82) Mardirossian, N.; Head-Gordon, M. ω B97X-V: A 10-parameter, range-separated hybrid, generalized gradient approximation density functional with nonlocal correlation, designed by a survival-of-the-fittest strategy. *Phys. Chem. Chem. Phys.* **2014**, *16*, 9904–9924.
- (83) Mardirossian, N.; Head-Gordon, M. Mapping the genome of meta-generalized gradient approximation density functionals: The search for B97M-V. *J. Chem. Phys.* **2015**, *142*, 074111.
- (84) Mardirossian, N.; Head-Gordon, M. ω B97M-V: A combinatorially optimized, range-separated hybrid, meta-GGA density functional with VV10 nonlocal correlation. *J. Chem. Phys.* **2016**, *144*, 214110.

- (85) Mardirossian, N.; Head-Gordon, M. Thirty years of density functional theory in computational chemistry: an overview and extensive assessment of 200 density functionals. *Mol. Phys.* **2017**, *115*, 2315–2372.
- (86) Grimme, S. Semiempirical hybrid density functional with perturbative second-order correlation. *J. Chem. Phys.* **2006**, *124*, 034108.
- (87) Zhang, Y.; Xu, X.; Goddard, W. A. Doubly hybrid density functional for accurate descriptions of nonbond interactions, thermochemistry, and thermochemical kinetics. *Proc. Natl. Acad. Sci. U.S.A.* **2009**, *106*, 4963–4968.
- (88) Mardirossian, N.; Head-Gordon, M. Survival of the most transferable at the top of Jacob’s ladder: Defining and testing the ω B97M (2) double hybrid density functional. *J. Chem. Phys.* **2018**, *148*, 241736.
- (89) Liechtenstein, A. I.; Anisimov, V. I.; Zaanen, J. Density-functional theory and strong interactions: Orbital ordering in Mott-Hubbard insulators. *Phys. Rev. B* **1995**, *52*, R5467.
- (90) Dudarev, S. L.; Botton, G. A.; Savrasov, S. Y.; Humphreys, C. J.; Sutton, A. P. Electron-energy-loss spectra and the structural stability of nickel oxide: An LSDA+U study. *Phys. Rev. B* **1998**, *57*, 1505.
- (91) Li Manni, G.; Carlson, R. K.; Luo, S.; Ma, D.; Olsen, J.; Truhlar, D. G.; Gagliardi, L. Multiconfiguration pair-density functional theory. *J. Chem. Theory Comput.* **2014**, *10*, 3669–3680.
- (92) Gagliardi, L.; Truhlar, D. G.; Li Manni, G.; Carlson, R. K.; Hoyer, C. E.; Bao, J. L. Multiconfiguration pair-density functional theory: A new way to treat strongly correlated systems. *Acc. Chem. Res.* **2017**, *50*, 66–73.
- (93) Yang, T.; Bertels, L.; Dangi, B. B.; Li, X.; Head-Gordon, M.; Kaiser, R. I. Gas phase formation of c-SiC₃ molecules in the circumstellar envelope of carbon stars. *Proc. Natl. Acad. Sci. U.S.A.* **2019**, *116*, 14471–14478.
- (94) Bertels, L. W.; Newcomb, L. B.; Alaghemandi, M.; Green, J. R.; Head-Gordon, M. Benchmarking the Performance of the ReaxFF Reactive Force Field on Hydrogen Combustion Systems. *J. Phys. Chem. A* **2020**, *124*, 5631–5645.
- (95) Bertels, L. W.; Lee, J.; Head-Gordon, M. Third-Order Møller–Plesset Perturbation Theory Made Useful? Choice of Orbitals and Scaling Greatly Improves Accuracy for Thermochemistry, Kinetics, and Intermolecular Interactions. *J. Phys. Chem. Lett.* **2019**, *10*, 4170–4176.
- (96) Millar, T. J.; Leung, C. M.; Herbst, E. How abundant are complex interstellar molecules? *Astron. Astrophys.* **1987**, *183*, 109–117.
- (97) Nejad, L. A. M.; Millar, T. J. Chemical modelling of molecular sources. *Astron. Astrophys.* **1987**, *183*, 279–286.

- (98) Bieging, J. H.; Rieu, N.-Q. Evidence for ion-molecular chemistry in the envelope of IRC+10216. *Astrophys. J.* **1988**, *329*, L107–L111.
- (99) Howe, D. A.; Millar, T. J. The formation of carbon chain molecules in IRC+10216. *Mon. Not. R. Astron. Soc.* **1990**, *244*, 444–449.
- (100) Millar, T. J.; Herbst, E.; Bettens, R. P. A. Large molecules in the envelope surrounding IRC+ 10216. *Mon. Not. R. Astron. Soc.* **2000**, *316*, 195–203.
- (101) McCarthy, M. C.; Gottlieb, C. A.; Gupta, H.; Thaddeus, P. Laboratory and astronomical identification of the negative molecular ion C_6H^- . *Astrophys. J.* **2006**, *652*, L141.
- (102) Cherchneff, I.; Glassgold, A. E. The formation of carbon chain molecules in IRC+10216. *Astrophys. J.* **1993**, *419*, L41.
- (103) Millar, T. J.; Herbst, E. A new chemical model of the circumstellar envelope surrounding IRC+10216. *Astron. Astrophys.* **1994**, *288*, 561–571.
- (104) Kaiser, R. I.; Stranges, D.; Lee, Y. T.; Suits, A. G. Neutral-neutral reactions in the interstellar medium. I. Formation of carbon hydride radicals via reaction of carbon atoms with unsaturated hydrocarbons. *Astrophys. J.* **1997**, *477*, 982.
- (105) Kaiser, R. I. Experimental investigation on the formation of carbon-bearing molecules in the interstellar medium via neutral- neutral reactions. *Chem. Rev.* **2002**, *102*, 1309–1358.
- (106) Wakelam, V.; Smith, I. W. M.; Herbst, E.; Troe, J.; Geppert, W.; Linnartz, H.; Öberg, K.; Roueff, E.; Agúndez, M.; Pernot, P.; Cuppen, H. M.; Loison, J. C.; Talbi, D. Reaction networks for interstellar chemical modelling: improvements and challenges. *Space Sci. Rev.* **2010**, *156*, 13–72.
- (107) Thaddeus, P.; Cummins, S. E.; Linke, R. A. Identification of the SiCC radical toward IRC+10216-The first molecular ring in an astronomical source. *Astrophys. J.* **1984**, *283*, L45–L48.
- (108) Ohishi, M.; Kaifu, N.; Kawaguchi, K.; Murakami, A.; Saito, S.; Yamamoto, S.; Ishikawa, S.-I.; Fujita, Y.; Shiratori, Y.; Irvine, W. M. Detection of a new circumstellar carbon chain molecule, C_4Si . *Astrophys. J.* **1989**, *345*, L83–L86.
- (109) MacKay, D. D. S.; Charnley, S. B. The silicon chemistry of IRC+10°216. *Mon. Not. R. Astron. Soc.* **1999**, *302*, 793–800.
- (110) McElroy, D.; Walsh, C.; Markwick, A. J.; Cordiner, M. A.; Smith, K.; Millar, T. J. The UMIST database for astrochemistry 2012. *Astron. Astrophys.* **2013**, *550*, A36.
- (111) Morata, O.; Herbst, E. Time-dependent models of dense PDRs with complex molecules. *Mon. Not. R. Astron. Soc.* **2008**, *390*, 1549–1561.
- (112) Wakelam, V. et al. A kinetic database for astrochemistry (KIDA). *Astrophys. J. Suppl. Ser.* **2012**, *199*, 21.

- (113) Marvel, K. B. No methane here. The HCN puzzle: Searching for CH₃OH and C₂H in oxygen-rich stars. *Astron. J.* **2005**, *130*, 261.
- (114) Ziurys, L. M. The chemistry in circumstellar envelopes of evolved stars: Following the origin of the elements to the origin of life. *Proc. Natl. Acad. Sci. U.S.A.* **2006**, *103*, 12274–12279.
- (115) Willacy, K.; Cherchneff, I. Silicon and sulphur chemistry in the inner wind of IRC+ 10216. *Astron. Astrophys.* **1998**, *330*, 676–684.
- (116) Agúndez, M.; Fonfría, J. P.; Cernicharo, J.; Kahane, C.; Daniel, F.; Guélin, M. Molecular abundances in the inner layers of IRC+ 10216. *Astron. Astrophys.* **2012**, *543*, A48.
- (117) Kaiser, R. I.; Krishtal, S. P.; Mebel, A. M.; Kostko, O.; Ahmed, M. An experimental and theoretical study of the ionization energies of SiC₂H_x ($x = 0, 1, 2$) isomers. *Astrophys. J.* **2012**, *761*, 178.
- (118) Mardirossian, N.; Head-Gordon, M. ω B97X-V: A 10-parameter, range-separated hybrid, generalized gradient approximation density functional with nonlocal correlation, designed by a survival-of-the-fittest strategy. *Phys. Chem. Chem. Phys.* **2014**, *16*, 9904–9924.
- (119) Dunning Jr, T. H. Gaussian basis sets for use in correlated molecular calculations. I. The atoms boron through neon and hydrogen. *J. Chem. Phys.* **1989**, *90*, 1007–1023.
- (120) Woon, D. E.; Dunning Jr, T. H. Gaussian basis sets for use in correlated molecular calculations. III. The atoms aluminum through argon. *J. Chem. Phys.* **1993**, *98*, 1358–1371.
- (121) Behn, A.; Zimmerman, P. M.; Bell, A. T.; Head-Gordon, M. Efficient exploration of reaction paths via a freezing string method. *J. Chem. Phys.* **2011**, *135*, 224108.
- (122) Baker, J. An algorithm for the location of transition states. *J. Comput. Chem.* **1986**, *7*, 385–395.
- (123) Halkier, A.; Helgaker, T.; Jørgensen, P.; Klopper, W.; Koch, H.; Olsen, J.; Wilson, A. K. Basis-set convergence in correlated calculations on Ne, N₂, and H₂O. *Chem. Phys. Lett.* **1998**, *286*, 243–252.
- (124) Runge, E.; Gross, E. K. U. Density-functional theory for time-dependent systems. *Phys. Rev. Lett.* **1984**, *52*, 997.
- (125) Shao, Y. et al. Advances in molecular quantum chemistry contained in the Q-Chem 4 program package. *Mol. Phys.* **2015**, *113*, 184–215.
- (126) Steinfeld, J. I.; Francisco, J. S.; Hase, W. L., *Chemical Kinetics and Dynamics*; Oxford University Press: Oxford, U.K., 1990.
- (127) Beyer, T.; Swinehart, D. F. Algorithm 448: number of multiply-restricted partitions. *Commun. ACM* **1973**, *16*, 379.

- (128) Miller, W. H. Tunneling corrections to unimolecular rate constants, with application to formaldehyde. *J. Am. Chem. Soc.* **1979**, *101*, 6810–6814.
- (129) Yang, T.; Dangi, B. B.; Maksyutenko, P.; Kaiser, R. I.; Bertels, L. W.; Head-Gordon, M. Combined experimental and theoretical study on the formation of the elusive 2-methyl-1-silacycloprop-2-enylidene molecule under single collision conditions via reactions of the silyldiyne radical (SiH; $X^2\Pi$) with Allene (H_2CCCH_2 ; X^1A_1) and D4-Allene (D_2CCCD_2 ; X^1A_1). *J. Phys. Chem. A* **2015**, *119*, 12562–12578.
- (130) Yang, T.; Dangi, B. B.; Kaiser, R. I.; Bertels, L. W.; Head-Gordon, M. A combined experimental and theoretical study on the formation of the 2-methyl-1-silacycloprop-2-enylidene molecule via the crossed beam reactions of the silyldiyne radical (SiH; $X^2\Pi$) with methylacetylene (CH_3CCH ; X^1A_1) and D4-methylacetylene (CD_3CCD ; X^1A_1). *J. Phys. Chem. A* **2016**, *120*, 4872–4883.
- (131) Gu, X.; Kaiser, R. I. Reaction dynamics of phenyl radicals in extreme environments: a crossed molecular beam study. *Acc. Chem. Res.* **2009**, *42*, 290–302.
- (132) Levine, R. D.; Bernstein, R. B., *Molecular Reaction Dynamics and Chemical Reactivity*; Oxford University Press: Oxford, U.K., 1987.
- (133) Miller, W. B.; Safron, S. A.; Herschbach, D. R. Exchange reactions of alkali atoms with alkali halides: A collision complex mechanism. *Discuss. Faraday Soc.* **1967**, *44*, 108–122.
- (134) McCarthy, M. C.; Apponi, A. J.; Thaddeus, P. Rhomboidal SiC_3 . *J. Chem. Phys.* **1999**, *110*, 10645–10648.
- (135) Apponi, A. J.; McCarthy, M. C.; Gottlieb, C. A.; Thaddeus, P. The rotational spectrum of rhomboidal SiC_3 . *J. Chem. Phys.* **1999**, *111*, 3911–3918.
- (136) McCarthy, M. C.; Apponi, A. J.; Gottlieb, C. A.; Thaddeus, P. Laboratory detection of five new linear silicon carbides: SiC_3 , SiC_5 , SiC_6 , SiC_7 , and SiC_8 . *Astrophys. J.* **2000**, *538*, 766.
- (137) Davico, G. E.; Schwartz, R. L.; Lineberger, W. C. Photoelectron spectroscopy of C_3Si and C_4Si_2 anions. *J. Chem. Phys.* **2001**, *115*, 1789–1794.
- (138) Stanton, J. F.; Gauss, J.; Christiansen, O. Equilibrium geometries of cyclic SiC_3 isomers. *J. Chem. Phys.* **2001**, *114*, 2993–2995.
- (139) Linguerri, R.; Rosmus, P.; Carter, S. Anharmonic vibrational levels of the two cyclic isomers of SiC_3 . *J. Chem. Phys.* **2006**, *125*, 034305.
- (140) Rintelman, J. M.; Gordon, M. S.; Fletcher, G. D.; Ivanic, J. A systematic multireference perturbation-theory study of the low-lying states of SiC_3 . *J. Chem. Phys.* **2006**, *124*, 034303.
- (141) Maclean, M. J.; Eichinger, P. C. H.; Wang, T.; Fitzgerald, M.; Bowie, J. H. A theoretical study of the cyclization processes of energized $CCCSi$ and $CCCP$. *The Journal of Physical Chemistry A* **2008**, *112*, 12714–12720.

- (142) Alberts, I. L.; Grev, R. S.; Schaefer III, H. F. Geometrical structures and vibrational frequencies of the energetically low-lying isomers of SiC₃. *J. Chem. Phys.* **1990**, *93*, 5046–5052.
- (143) Gomei, M.; Kishi, R.; Nakajima, A.; Iwata, S.; Kaya, K. Ab initio MO studies of neutral and anionic SiC_n clusters (n= 2–5). *J. Chem. Phys.* **1997**, *107*, 10051–10061.
- (144) Inostroza, N.; Hochlaf, M.; Senent, M. L.; Letelier, J. R. Ab initio characterization of linear C₃Si isomers. *Astron. Astrophys.* **2008**, *486*, 1047–1052.
- (145) Li, X.; Millar, T. J.; Walsh, C.; Heays, A. N.; Van Dishoeck, E. F. Photodissociation and chemistry of N₂ in the circumstellar envelope of carbon-rich AGB stars. *Astron. Astrophys.* **2014**, *568*, A111.
- (146) Suto, M.; Lee, L. C. Quantitative photoexcitation study of SiH₄ in vacuum ultraviolet. *J. Chem. Phys.* **1986**, *84*, 1160–1164.
- (147) Cherchneff, I. The inner wind of IRC+10216 revisited: new exotic chemistry and diagnostic for dust condensation in carbon stars. *Astron. Astrophys.* **2012**, *545*, A12.
- (148) Agúndez, M.; Fonfría, J. P.; Cernicharo, J.; Pardo, J. R.; Guélin, M. Detection of circumstellar CH₂CHCN, CH₂CN, CH₃CCH, and H₂CS. *Astron. Astrophys.* **2008**, *479*, 493–501.
- (149) Glassgold, A. E.; Mamon, G. A. In: University of Tokyo Press: Tokyo, Japan, 1992, pp 261–266.
- (150) Dawson, V. P.; Bowles, M. D., *Taming Liquid Hydrogen: The Centaur Upper Stage Rocket*; National Aeronautics and Space Administration, Office of External Relations: Washington, DC, 2004.
- (151) Schlapbach, L.; Züttel, A. Hydrogen-storage materials for mobile applications. *Nature* **2001**, *414*, 353–358.
- (152) Schlapbach, L. Technology: Hydrogen-fuelled vehicles. *Nature* **2009**, *460*, 809.
- (153) Verhelst, S.; Wallner, T. Hydrogen-fueled internal combustion engines. *Prog. Energy Combust. Sci.* **2009**, *35*, 490–527.
- (154) Chu, S.; Majumdar, A. Opportunities and challenges for a sustainable energy future. *Nature* **2012**, *488*, 294.
- (155) Marbán, G.; Valdás-Solís, T. Towards the hydrogen economy? *Int. J. Hydrog. Energy* **2007**, *32*, 1625–1637.
- (156) Midilli, A.; Dincer, I. Hydrogen as a renewable and sustainable solution in reducing global fossil fuel consumption. *Int. J. Hydrog. Energy* **2008**, *33*, 4209–4222.
- (157) Sánchez, A. L.; Williams, F. A. Recent advances in understanding of flammability characteristics of hydrogen. *Prog. Energy Combust. Sci.* **2014**, *41*, 1–55.

- (158) Palumbo, O.; Paolone, A.; Rispoli, P.; Cantelli, R. Novel materials for solid-state hydrogen storage: Anelastic spectroscopy studies. *Mater. Sci. Eng. A* **2009**, *521*, 134–138.
- (159) Petukhov, V. A.; Naboko, I. M.; Fortov, V. E. Explosion hazard of hydrogen–air mixtures in the large volumes. *Int. J. Hydrog. Energy* **2009**, *34*, 5924–5931.
- (160) Ray, I.; Chakraborty, T.; Roy, D.; Datta, A.; Mandal, B. K. Production, storage and properties of hydrogen as internal combustion engine fuel: a critical review. *Int. J. Emerging Technol. Adv. Eng.* **2013**, *3*, 119–125.
- (161) Verhelst, S. Recent progress in the use of hydrogen as a fuel for internal combustion engines. *Int. J. Hydrog. Energy* **2014**, *39*, 1071–1085.
- (162) Allendorf, M. D.; Hulvey, Z.; Gennett, T.; Ahmed, A.; Autrey, T.; Camp, J.; Cho, E. S.; Furukawa, H.; Haranczyk, M.; Head-Gordon, M., et al. An assessment of strategies for the development of solid-state adsorbents for vehicular hydrogen storage. *Energy Environ. Sci.* **2018**, *11*, 2784–2812.
- (163) Boivin, P.; Sánchez, A. L.; Williams, F. A. Analytical prediction of syngas induction times. *Combust. Flame* **2017**, *176*, 489–499.
- (164) Mueller, M. A.; Kim, T. J.; Yetter, R. A.; Dryer, F. L. Flow reactor studies and kinetic modeling of the H₂/O₂ reaction. *Int. J. Chem. Kinet.* **1999**, *31*, 113–125.
- (165) Li, J.; Zhao, Z.; Kazakov, A.; Dryer, F. L. An updated comprehensive kinetic model of hydrogen combustion. *Int. J. Chem. Kinet.* **2004**, *36*, 566–575.
- (166) O’Conaire, M.; Curran, H. J.; Simmie, J. M.; Pitz, W. J.; Westbrook, C. K. A comprehensive modeling study of hydrogen oxidation. *Int. J. Chem. Kinet.* **2004**, *36*, 603–622.
- (167) Konnov, A. A. Remaining uncertainties in the kinetic mechanism of hydrogen combustion. *Combust. Flame* **2008**, *152*, 507–528.
- (168) Hong, Z.; Davidson, D. F.; Hanson, R. K. An improved H₂/O₂ mechanism based on recent shock tube/laser absorption measurements. *Combust. Flame* **2011**, *158*, 633–644.
- (169) Burke, M. P.; Chaos, M.; Ju, Y.; Dryer, F. L.; Klippenstein, S. J. Comprehensive H₂/O₂ kinetic model for high-pressure combustion. *Int. J. Chem. Kinet.* **2012**, *44*, 444–474.
- (170) Shimizu, K.; Hibi, A.; Koshi, M.; Morii, Y.; Tsuboi, N. Updated kinetic mechanism for high-pressure hydrogen combustion. *J. Propul. Power* **2011**, *27*, 383–395.
- (171) Kitano, S.; Fukao, M.; Susa, A.; Tsuboi, N.; Hayashi, A.; Koshi, M. Spinning detonation and velocity deficit in small diameter tubes. *Proc. Combust. Inst.* **2009**, *32*, 2355–2362.

- (172) Varga, T.; Nagy, T.; Olm, C.; Zsély, I. G.; Pálvölgyi, R.; Valkó, É.; Vincze, G.; Cserhádi, M.; Curran, H.; Turányi, T. Optimization of a hydrogen combustion mechanism using both direct and indirect measurements. *Proc. Combust. Inst.* **2015**, *35*, 589–596.
- (173) Yang, S.; Yang, X.; Wu, F.; Ju, Y.; Law, C. K. Laminar flame speeds and kinetic modeling of H₂/O₂/diluent mixtures at sub-atmospheric and elevated pressures. *Proc. Combust. Inst.* **2017**, *36*, 491–498.
- (174) Burke, M. P.; Klippenstein, S. J. Ephemeral collision complexes mediate chemically termolecular transformations that affect system chemistry. *Nat. Chem.* **2017**, *9*, 1078–1082.
- (175) Konnov, A. A. Yet another kinetic mechanism for hydrogen combustion. *Combust. Flame* **2019**, *203*, 14–22.
- (176) Jasper, A. W.; Kamarchik, E.; Miller, J. A.; Klippenstein, S. J. First-principles binary diffusion coefficients for H, H₂, and four normal alkanes + N₂. *J. Chem. Phys.* **2014**, *141*, 124313.
- (177) Jasper, A. W.; Miller, J. A. Lennard–Jones parameters for combustion and chemical kinetics modeling from full-dimensional intermolecular potentials. *Combust. Flame* **2014**, *161*, 101–110.
- (178) Mulvihill, C. R.; Petersen, E. L. Concerning shock-tube ignition delay times: an experimental investigation of impurities in the H₂/O₂ system and beyond. *Proc. Combust. Inst.* **2019**, *37*, 259–266.
- (179) Sabia, P.; de Joannon, M. On H₂–O₂ oxidation in several bath gases. *Int. J. Hydrog. Energy* **2020**, *45*, 8151–8167.
- (180) Alaghemandi, M.; Green, J. R. Reactive symbol sequences for a model of hydrogen combustion. *Phys. Chem. Chem. Phys.* **2016**, *18*, 2810–2817.
- (181) Alaghemandi, M.; Newcomb, L. B.; Green, J. R. Ignition in an atomistic model of hydrogen oxidation. *J. Phys. Chem. A* **2017**, *121*, 1686–1692.
- (182) Nicholson, S. B.; Alaghemandi, M.; Green, J. R. Learning the mechanisms of chemical disequilibria. *J. Chem. Phys.* **2016**, *145*, 084112.
- (183) Nicholson, S. B.; Alaghemandi, M.; Green, J. R. Effects of temperature and mass conservation on the typical chemical sequences of hydrogen oxidation. *J. Chem. Phys.* **2018**, *148*, 044102.
- (184) Newcomb, L. B.; Alaghemandi, M.; Green, J. R. Nonequilibrium phase coexistence and criticality near the second explosion limit of hydrogen combustion. *J. Chem. Phys.* **2017**, *147*, 034108.
- (185) Newcomb, L. B.; Marucci, M. E.; Green, J. R. Explosion limits of hydrogen–oxygen mixtures from nonequilibrium critical points. *Phys. Chem. Chem. Phys.* **2018**, *20*, 15746–15752.

- (186) Warnatz, J. In *Symp. (Int.) Combust.* 1992; Vol. 24, pp 553–579.
- (187) Van de Vijver, R.; Vandewiele, N. M.; Bhoorasingh, P. L.; Slakman, B. L.; Seyedzadeh Khanshan, F.; Carstensen, H.-H.; Reyniers, M.-F.; Marin, G. B.; West, R. H.; Van Geem, K. M. Automatic Mechanism and Kinetic Model Generation for Gas-and Solution-Phase Processes: A Perspective on Best Practices, Recent Advances, and Future Challenges. *Int. J. Chem. Kinet.* **2015**, *47*, 199–231.
- (188) Van Duin, A. C.; Dasgupta, S.; Lorant, F.; Goddard, W. A. ReaxFF: a reactive force field for hydrocarbons. *J. Phys. Chem. A* **2001**, *105*, 9396–9409.
- (189) Wang, L.-P.; Titov, A.; McGibbon, R.; Liu, F.; Pande, V. S.; Martínez, T. J. Discovering chemistry with an ab initio nanoreactor. *Nat. Chem.* **2014**, *6*, 1044.
- (190) Martínez, T. J. Ab Initio Reactive Computer Aided Molecular Design. *Acc. Chem. Res.* **2017**, *50*, 652–656.
- (191) Brenner, D. W. Empirical potential for hydrocarbons for use in simulating the chemical vapor deposition of diamond films. *Phys. Rev. B* **1990**, *42*, 9458.
- (192) Brenner, D. W.; Shenderova, O. A.; Harrison, J. A.; Stuart, S. J.; Ni, B.; Sinnott, S. B. A second-generation reactive empirical bond order (REBO) potential energy expression for hydrocarbons. *J. Phys. Condens. Matter* **2002**, *14*, 783.
- (193) Yu, J.; Sinnott, S. B.; Phillpot, S. R. Charge optimized many-body potential for the Si/SiO₂ system. *Phys. Rev. B* **2007**, *75*, 085311.
- (194) Zhao, M.; Iron, M. A.; Staszewski, P.; Schultz, N. E.; Valero, R.; Truhlar, D. G. Valence–bond order (VBO): A new approach to modeling reactive potential energy surfaces for complex systems, materials, and nanoparticles. *J. Chem. Theory Comput.* **2009**, *5*, 594–604.
- (195) Shan, T.-R.; Devine, B. D.; Hawkins, J. M.; Asthagiri, A.; Phillpot, S. R.; Sinnott, S. B. Second-generation charge-optimized many-body potential for Si/SiO₂ and amorphous silica. *Phys. Rev. B* **2010**, *82*, 235302.
- (196) Nouranian, S.; Tschopp, M. A.; Gwaltney, S. R.; Baskes, M. I.; Horstemeyer, M. F. An interatomic potential for saturated hydrocarbons based on the modified embedded-atom method. *Phys. Chem. Chem. Phys.* **2014**, *16*, 6233–6249.
- (197) Slater, J. C.; Koster, G. F. Simplified LCAO method for the periodic potential problem. *Phys. Rev.* **1954**, *94*, 1498.
- (198) Andersen, O. K.; Jepsen, O. Explicit, first-principles tight-binding theory. *Phys. Rev. Lett.* **1984**, *53*, 2571.
- (199) Bannwarth, C.; Ehlert, S.; Grimme, S. GFN2-xTB—An accurate and broadly parametrized self-consistent tight-binding quantum chemical method with multipole electrostatics and density-dependent dispersion contributions. *J. Chem. Theory Comput.* **2019**, *15*, 1652–1671.

- (200) Chenoweth, K.; Van Duin, A. C. T.; Goddard, W. A. ReaxFF reactive force field for molecular dynamics simulations of hydrocarbon oxidation. *J. Phys. Chem. A* **2008**, *112*, 1040–1053.
- (201) Chenoweth, K.; Van Duin, A. C. T.; Dasgupta, S.; Goddard III, W. A. Initiation mechanisms and kinetics of pyrolysis and combustion of JP-10 hydrocarbon jet fuel. *J. Phys. Chem. A* **2009**, *113*, 1740–1746.
- (202) Weismiller, M. R.; van Duin, A. C. T.; Lee, J.; Yetter, R. A. ReaxFF Reactive Force Field Development and Applications for Molecular Dynamics Simulations of Ammonia Borane Dehydrogenation and Combustion. *J. Phys. Chem. A* **2010**, *114*, 5485–5492.
- (203) Agrawalla, S.; Van Duin, A. C. T. Development and application of a ReaxFF reactive force field for hydrogen combustion. *J. Phys. Chem. A* **2011**, *115*, 960–972.
- (204) Liu, L.; Bai, C.; Sun, H.; Goddard III, W. A. Mechanism and kinetics for the initial steps of pyrolysis and combustion of 1, 6-dicyclopropane-2, 4-hexyne from ReaxFF reactive dynamics. *J. Phys. Chem. A* **2011**, *115*, 4941–4950.
- (205) Wang, Q.-D.; Wang, J.-B.; Li, J.-Q.; Tan, N.-X.; Li, X.-Y. Reactive molecular dynamics simulation and chemical kinetic modeling of pyrolysis and combustion of n-dodecane. *Combust. Flame* **2011**, *158*, 217–226.
- (206) Qian, H.-J.; Van Duin, A. C. T.; Morokuma, K.; Irle, S. Reactive molecular dynamics simulation of fullerene combustion synthesis: ReaxFF vs DFTB potentials. *J. Chem. Theory Comput.* **2011**, *7*, 2040–2048.
- (207) Castro-Marcano, F.; Kamat, A. M.; Russo Jr, M. F.; van Duin, A. C. T.; Mathews, J. P. Combustion of an Illinois No. 6 coal char simulated using an atomistic char representation and the ReaxFF reactive force field. *Combust. Flame* **2012**, *159*, 1272–1285.
- (208) Cheng, X.-M.; Wang, Q.-D.; Li, J.-Q.; Wang, J.-B.; Li, X.-Y. ReaxFF molecular dynamics simulations of oxidation of toluene at high temperatures. *J. Phys. Chem. A* **2012**, *116*, 9811–9818.
- (209) Guo, F.; Cheng, X.; Zhang, H. ReaxFF molecular dynamics study of initial mechanism of JP-10 combustion. *Combust. Sci. Technol.* **2012**, *184*, 1233–1243.
- (210) Castro-Marcano, F.; van Duin, A. C. T. Comparison of thermal and catalytic cracking of 1-heptene from ReaxFF reactive molecular dynamics simulations. *Combust. Flame* **2013**, *160*, 766–775.
- (211) Beste, A. ReaxFF study of the oxidation of lignin model compounds for the most common linkages in softwood in view of carbon fiber production. *J. Phys. Chem. A* **2014**, *118*, 803–814.

- (212) Cheng, T.; Jaramillo-Botero, A.; Goddard III, W. A.; Sun, H. Adaptive accelerated ReaxFF reactive dynamics with validation from simulating hydrogen combustion. *J. Amer. Chem. Soc.* **2014**, *136*, 9434–9442.
- (213) He, Z.; Li, X.-B.; Liu, L.-M.; Zhu, W. The intrinsic mechanism of methane oxidation under explosion condition: A combined ReaxFF and DFT study. *Fuel* **2014**, *124*, 85–90.
- (214) Bharti, A.; Banerjee, T. Reactive force field simulation studies on the combustion behavior of n-octanol. *Fuel Process. Technol.* **2016**, *152*, 132–139.
- (215) Zhang, T.; Li, X.; Qiao, X.; Zheng, M.; Guo, L.; Song, W.; Lin, W. Initial mechanisms for an overall behavior of lignin pyrolysis through large-scale ReaxFF molecular dynamics simulations. *Energy Fuels* **2016**, *30*, 3140–3150.
- (216) Ashraf, C.; van Duin, A. C. T. Extension of the ReaxFF Combustion Force Field toward Syngas Combustion and Initial Oxidation Kinetics. *J. Phys. Chem. A* **2017**, *121*, 1051–1068.
- (217) Strachan, A.; van Duin, A. C. T.; Chakraborty, D.; Dasgupta, S.; Goddard III, W. A. Shock waves in high-energy materials: The initial chemical events in nitramine RDX. *Phys. Rev. Lett.* **2003**, *91*, 098301.
- (218) Strachan, A.; Kober, E. M.; Van Duin, A. C. T.; Oxgaard, J.; Goddard III, W. A. Thermal decomposition of RDX from reactive molecular dynamics. *J. Chem. Phys.* **2005**, *122*, 054502.
- (219) Buehler, M. J.; Van Duin, A. C. T.; Goddard III, W. A. Multiparadigm modeling of dynamical crack propagation in silicon using a reactive force field. *Phys. Rev. Lett.* **2006**, *96*, 095505.
- (220) Ludwig, J.; Vlachos, D. G.; Van Duin, A. C. T.; Goddard, W. A. Dynamics of the dissociation of hydrogen on stepped platinum surfaces using the ReaxFF reactive force field. *J. Phys. Chem. B* **2006**, *110*, 4274–4282.
- (221) Nomura, K.-i.; Kalia, R. K.; Nakano, A.; Vashishta, P.; Van Duin, A. C. T.; Goddard III, W. A. Dynamic transition in the structure of an energetic crystal during chemical reactions at shock front prior to detonation. *Phys. Rev. Lett.* **2007**, *99*, 148303.
- (222) Bagri, A.; Mattevi, C.; Acik, M.; Chabal, Y. J.; Chhowalla, M.; Shenoy, V. B. Structural evolution during the reduction of chemically derived graphene oxide. *Nat. Chem.* **2010**, *2*, 581–587.
- (223) LaBrosse, M. R.; Johnson, J. K.; Van Duin, A. C. T. Development of a transferable reactive force field for cobalt. *J. Phys. Chem. A* **2010**, *114*, 5855–5861.
- (224) Ganesh, P.; Kent, P. R. C.; Mochalin, V. Formation, characterization, and dynamics of onion-like carbon structures for electrical energy storage from nanodiamonds using reactive force fields. *J. Appl. Phys.* **2011**, *110*, 073506.

- (225) Srinivasan, S. G.; van Duin, A. C. T. Molecular-Dynamics-Based Study of the Collisions of Hyperthermal Atomic Oxygen with Graphene Using the ReaxFF Reactive Force Field. *J. Phys. Chem. A* **2011**, *115*, 13269–13280.
- (226) Huang, X.; Yang, H.; Van Duin, A. C. T.; Hsia, K. J.; Zhang, S. Chemomechanics control of tearing paths in graphene. *Phys. Rev. B* **2012**, *85*, 195453.
- (227) Islam, M. M.; Ostadhosseini, A.; Borodin, O.; Yeates, A. T.; Tipton, W. W.; Hennig, R. G.; Kumar, N.; van Duin, A. C. T. ReaxFF molecular dynamics simulations on lithiated sulfur cathode materials. *Phys. Chem. Chem. Phys.* **2015**, *17*, 3383–3393.
- (228) Ostadhosseini, A.; Cubuk, E. D.; Tritsarlis, G. A.; Kaxiras, E.; Zhang, S.; van Duin, A. C. T. Stress effects on the initial lithiation of crystalline silicon nanowires: reactive molecular dynamics simulations using ReaxFF. *Phys. Chem. Chem. Phys.* **2015**, *17*, 3832–3840.
- (229) Srinivasan, S. G.; van Duin, A. C. T.; Ganesh, P. Development of a ReaxFF potential for carbon condensed phases and its application to the thermal fragmentation of a large fullerene. *J. Phys. Chem. A* **2015**, *119*, 571–580.
- (230) Verners, O.; van Duin, A. C. T. Comparative molecular dynamics study of fcc-Ni nanoplate stress corrosion in water. *Surf. Sci.* **2015**, *633*, 94–101.
- (231) Wood, M. A.; Cherukara, M. J.; Kober, E. M.; Strachan, A. Ultrafast chemistry under nonequilibrium conditions and the shock to deflagration transition at the nanoscale. *J. Phys. Chem. C* **2015**, *119*, 22008–22015.
- (232) Zou, C.; Shin, Y. K.; van Duin, A. C. T.; Fang, H.; Liu, Z.-K. Molecular dynamics simulations of the effects of vacancies on nickel self-diffusion, oxygen diffusion and oxidation initiation in nickel, using the ReaxFF reactive force field. *Acta Mater.* **2015**, *83*, 102–112.
- (233) Nielson, K. D.; Van Duin, A. C. T.; Oxgaard, J.; Deng, W.-Q.; Goddard, W. A. Development of the ReaxFF reactive force field for describing transition metal catalyzed reactions, with application to the initial stages of the catalytic formation of carbon nanotubes. *J. Phys. Chem. A* **2005**, *109*, 493–499.
- (234) Goddard, W. A.; Van Duin, A.; Chenoweth, K.; Cheng, M.-J.; Pudar, S.; Oxgaard, J.; Merinov, B.; Jang, Y. H.; Persson, P. Development of the ReaxFF reactive force field for mechanistic studies of catalytic selective oxidation processes on BiMoO_x. *Top. Catal.* **2006**, *38*, 93.
- (235) Mueller, J. E.; Van Duin, A. C. T.; Goddard III, W. A. Development and validation of ReaxFF reactive force field for hydrocarbon chemistry catalyzed by nickel. *J. Phys. Chem. C* **2010**, *114*, 4939–4949.
- (236) Zou, C.; Van Duin, A. Investigation of complex iron surface catalytic chemistry using the ReaxFF reactive force field method. *JOM* **2012**, *64*, 1426–1437.

- (237) Shin, Y. K.; Kwak, H.; Vasenkov, A. V.; Sengupta, D.; van Duin, A. C. T. Development of a ReaxFF reactive force field for Fe/Cr/O/S and application to oxidation of butane over a pyrite-covered Cr_2O_3 catalyst. *ACS Catal.* **2015**, *5*, 7226–7236.
- (238) Zhang, Q.; Çağın, T.; Van Duin, A.; Goddard III, W. A.; Qi, Y.; Hector Jr, L. G. Adhesion and nonwetting-wetting transition in the Al/ α - Al_2O_3 interface. *Phys. Rev. B* **2004**, *69*, 045423.
- (239) Chenoweth, K.; Cheung, S.; Van Duin, A. C. T.; Goddard, W. A.; Kober, E. M. Simulations on the thermal decomposition of a poly (dimethylsiloxane) polymer using the ReaxFF reactive force field. *J. Am. Chem. Soc.* **2005**, *127*, 7192–7202.
- (240) Cheung, S.; Deng, W.-Q.; Van Duin, A. C. T.; Goddard, W. A. ReaxFF_{MgH} reactive force field for magnesium hydride systems. *J. Phys. Chem. A* **2005**, *109*, 851–859.
- (241) Van Duin, A. C. T.; Zeiri, Y.; Dubnikova, F.; Kosloff, R.; Goddard III, W. A. Atomistic-scale simulations of the initial chemical events in the thermal initiation of triacetoneperoxide. *J. Am. Chem. Soc.* **2005**, *127*, 11053–11062.
- (242) Goddard III, W.; Merinov, B.; Van Duin, A.; Jacob, T.; Blanco, M.; Molinero, V.; Jang, S. S.; Jang, Y. H. Multi-paradigm multi-scale simulations for fuel cell catalysts and membranes. *Mol. Simulat.* **2006**, *32*, 251–268.
- (243) Hong, S.; van Duin, A. C. T. Molecular dynamics simulations of the oxidation of aluminum nanoparticles using the ReaxFF reactive force field. *J. Phys. Chem. C* **2015**, *119*, 17876–17886.
- (244) Verlackt, C.; Neyts, E. C.; Jacob, T.; Fantauzzi, D.; Golkaram, M.; Shin, Y. K.; van Duin, A. C. T.; Bogaerts, A. Atomic-scale insight into the interactions between hydroxyl radicals and DNA in solution using the ReaxFF reactive force field. *New J. Phys.* **2015**, *17*, 103005.
- (245) Yeon, J.; van Duin, A. C. T. ReaxFF molecular dynamics simulations of hydroxylation kinetics for amorphous and nano-silica structure, and its relations with atomic strain energy. *J. Phys. Chem. C* **2015**, *120*, 305–317.
- (246) Yue, D.-C.; Ma, T.-B.; Hu, Y.-Z.; Yeon, J.; van Duin, A. C. T.; Wang, H.; Luo, J. Tribochemical mechanism of amorphous silica asperities in aqueous environment: A Reactive Molecular Dynamics Study. *Langmuir* **2015**, *31*, 1429–1436.
- (247) Mortier, W. J.; Ghosh, S. K.; Shankar, S. Electronegativity-equalization method for the calculation of atomic charges in molecules. *J. Am. Chem. Soc.* **1986**, *108*, 4315–4320.
- (248) Rappe, A. K.; Goddard III, W. A. Charge equilibration for molecular dynamics simulations. *J. Phys. Chem.* **1991**, *95*, 3358–3363.
- (249) Aktulga, H. M.; Fogarty, J. C.; Pandit, S. A.; Grama, A. Y. Parallel reactive molecular dynamics: Numerical methods and algorithmic techniques. *Parallel Comput.* **2012**, *38*, 245–259.

- (250) Plimpton, S. Fast parallel algorithms for short-range molecular dynamics. *J. Comput. Phys.* **1995**, *117*, 1–19.
- (251) Kylasa, S. B.; Aktulga, H. M.; Grama, A. Y. PuReMD-GPU: A reactive molecular dynamics simulation package for GPUs. *J. Comput. Phys.* **2014**, *272*, 343–359.
- (252) Raghavachari, K.; Trucks, G. W.; Pople, J. A.; Head-Gordon, M. A fifth-order perturbation comparison of electron correlation theories. *Chem. Phys. Lett.* **1989**, *157*, 479–483.
- (253) Zhao, Y.; González-García, N.; Truhlar, D. G. Benchmark database of barrier heights for heavy atom transfer, nucleophilic substitution, association, and unimolecular reactions and its use to test theoretical methods. *J. Phys. Chem. A* **2005**, *109*, 2012–2018.
- (254) Karton, A.; Sylvetsky, N.; Martin, J. M. L. W4-17: A diverse and high-confidence dataset of atomization energies for benchmarking high-level electronic structure methods. *J. Comput. Chem.* **2017**, *38*, 2063–2075.
- (255) Yarkony, D., *Modern Electronic Structure Theory*; World Scientific: New Jersey, 1995; Vol. 2.
- (256) Mardirossian, N.; Head-Gordon, M. ω B97M-V: A combinatorially optimized, range-separated hybrid, meta-GGA density functional with VV10 nonlocal correlation. *J. Chem. Phys.* **2016**, *144*, 214110.
- (257) Fukui, K. Formulation of the reaction coordinate. *J. Phys. Chem.* **1970**, *74*, 4161–4163.
- (258) Ishida, K.; Morokuma, K.; Komornicki, A. The intrinsic reaction coordinate. An ab initio calculation for $\text{HNC} \longrightarrow \text{HCN}$ and $\text{H}^- + \text{CH}_4 \longrightarrow \text{CH}_4 + \text{H}^-$. *J. Chem. Phys.* **1977**, *66*, 2153–2156.
- (259) Schmidt, M. W.; Gordon, M. S.; Dupuis, M. The intrinsic reaction coordinate and the rotational barrier in silaethylene. *J. Am. Chem. Soc.* **1985**, *107*, 2585–2589.
- (260) Krishnan, R. B. J. S.; Binkley, J. S.; Seeger, R.; Pople, J. A. Self-consistent molecular orbital methods. XX. A basis set for correlated wave functions. *J. Chem. Phys.* **1980**, *72*, 650–654.
- (261) Van Duin, A. C. T.; Baas, J. M. A.; Van De Graaf, B. Delft molecular mechanics: a new approach to hydrocarbon force fields. Inclusion of a geometry-dependent charge calculation. *J. Chem. Soc. Faraday Trans.* **1994**, *90*, 2881–2895.
- (262) Pahari, P.; Chaturvedi, S. Determination of best-fit potential parameters for a reactive force field using a genetic algorithm. *J. Mol. Model.* **2012**, *18*, 1049–1061.
- (263) Larsson, H. R.; Hartke, B. Fitting reactive force fields using genetic algorithms. *Comput. Method Mater. Sci.* **2013**, *13*.
- (264) Larsson, H. R.; Van Duin, A. C. T.; Hartke, B. Global optimization of parameters in the reactive force field ReaxFF for SiOH. *J. Comput. Chem.* **2013**, *34*, 2178–2189.

- (265) Shchygol, G.; Yakovlev, A.; Trnka, T.; van Duin, A. C. T.; Verstraelen, T. ReaxFF Parameter Optimization with Monte-Carlo and Evolutionary Algorithms: Guidelines and Insights. *J. Chem. Theory Comput.* **2019**, *15*, 6799–6812.
- (266) Nakata, H.; Bai, S. Development of a new parameter optimization scheme for a reactive force field based on a machine learning approach. *J. Comput. Chem.* **2019**, *40*, 2000–2012.
- (267) Furman, D.; Wales, D. J. Transforming the Accuracy and Numerical Stability of ReaxFF Reactive Force Fields. *J. Phys. Chem. Lett.* **2019**, *10*, 7215–7223.
- (268) Leven, I.; Head-Gordon, T. C-GeM: Coarse-Grained Electron Model for Predicting the Electrostatic Potential in Molecules. *J. Phys. Chem. Lett.* **2019**, *10*, 6820–6826.
- (269) Soydaş, E.; Bozkaya, U. Assessment of Orbital-Optimized MP2.5 for Thermochemistry and Kinetics: Dramatic Failures of Standard Perturbation Theory Approaches for Aromatic Bond Dissociation Energies and Barrier Heights of Radical Reactions. *J. Chem. Theory Comput.* **2015**, *11*, 1564–1573.
- (270) Sharada, S. M.; Stück, D.; Sundstrom, E. J.; Bell, A. T.; Head-Gordon, M. Wavefunction stability analysis without analytical electronic Hessians: application to orbital-optimised second-order Møller-Plesset theory and VV10-containing density functionals. *Mol. Phys.* **2015**, *113*, 1802–1808.
- (271) Coulson, C. A.; Fischer, I. XXXIV. Notes on the molecular orbital treatment of the hydrogen molecule. *Philos. Mag.* **1949**, *40*, 386–393.
- (272) Karton, A.; Daon, S.; Martin, J. M. W4-11: A high-confidence benchmark dataset for computational thermochemistry derived from first-principles W4 data. *Chem. Phys. Lett.* **2011**, *510*, 165–178.
- (273) Zipse, H. In *Radicals in Synthesis I*, Gansäuer, A., Ed.; Springer Berlin Heidelberg: Berlin, Heidelberg, 2006, pp 163–189.
- (274) Tentscher, P. R.; Arey, J. S. Binding in Radical-Solvent Binary Complexes: Benchmark Energies and Performance of Approximate Methods. *J. Chem. Theory Comput.* **2013**, *9*, 1568–1579.
- (275) Lee, J.; Head-Gordon, M. Two single-reference approaches to singlet biradicaloid problems: Complex, restricted orbitals and approximate spin-projection combined with regularized orbital-optimized Møller-Plesset perturbation theory. *J. Chem. Phys.* **2019**, *150*, 244106.
- (276) Lee, J.; Head-Gordon, M. Distinguishing artificial and essential symmetry breaking in a single determinant: approach and application to the C₆₀, C₃₆, and C₂₀ fullerenes. *Phys. Chem. Chem. Phys.* **2019**, *21*, 4763–4778.
- (277) Grimme, S. Improved second-order Møller-Plesset perturbation theory by separate scaling of parallel- and antiparallel-spin pair correlation energies. *J. Chem. Phys.* **2003**, *118*, 9095–9102.

- (278) Jung, Y.; Lochan, R. C.; Dutoi, A. D.; Head-Gordon, M. Scaled opposite-spin second order Møller–Plesset correlation energy: An economical electronic structure method. *J. Chem. Phys.* **2004**, *121*, 9793–9802.
- (279) Grimme, S. Accurate Calculation of the Heats of Formation for Large Main Group Compounds with Spin-Component Scaled MP2 Methods. *J. Phys. Chem. A* **2005**, *109*, 3067–3077.
- (280) Lochan, R. C.; Jung, Y.; Head-Gordon, M. Scaled Opposite Spin Second Order Møller-Plesset Theory with Improved Physical Description of Long-Range Dispersion Interactions. *J. Phys. Chem. A* **2005**, *109*, 7598–7605.
- (281) Distasio Jr., R. A.; Head-Gordon, M. Optimized spin-component scaled second-order Møller-Plesset perturbation theory for intermolecular interaction energies. *Mol. Phys.* **2007**, *105*, 1073–1083.
- (282) Lochan, R. C.; Shao, Y.; Head-Gordon, M. Quartic-Scaling Analytical Energy Gradient of Scaled Opposite-Spin Second-Order Møller-Plesset Perturbation Theory. *J. Chem. Theory Comput.* **2007**, *3*, 988–1003.
- (283) Chai, J.-D.; Head-Gordon, M. Long-range corrected double-hybrid density functionals. *J. Chem. Phys.* **2009**, *131*, 174105.
- (284) Kozuch, S.; Martin, J. M. L. DSD-PBEP86: in search of the best double-hybrid DFT with spin-component scaled MP2 and dispersion corrections. *Phys. Chem. Chem. Phys.* **2011**, *13*, 20104–20107.
- (285) Najibi, A.; Goerigk, L. A Comprehensive Assessment of the Effectiveness of Orbital Optimization in Double-Hybrid Density Functionals in the Treatment of Thermochemistry, Kinetics, and Noncovalent Interactions. *J. Phys. Chem. A* **2018**, *122*, 5610–5624.
- (286) Goldey, M.; Head-Gordon, M. Attenuating Away the Errors in Inter- and Intramolecular Interactions from Second-Order Møller-Plesset Calculations in the Small Aug-cc-pVDZ Basis Set. *J. Phys. Chem. Lett.* **2012**, *3*, 3592–3598.
- (287) Goldey, M.; Dutoi, A.; Head-Gordon, M. Attenuated second-order Møller-Plesset perturbation theory: performance within the aug-cc-pVTZ basis. *Phys. Chem. Chem. Phys.* **2013**, *15*, 15869–15875.
- (288) Goldey, M.; Head-Gordon, M. Separate Electronic Attenuation Allowing a Spin-Component-Scaled Second-Order Møller-Plesset Theory to Be Effective for Both Thermochemistry and Noncovalent Interactions. *J. Phys. Chem. B* **2014**, *118*, 6519–6525.
- (289) Goldey, M. B.; Belzunces, B.; Head-Gordon, M. Attenuated MP2 with a Long-Range Dispersion Correction for Treating Nonbonded Interactions. *J. Chem. Theor. Comput.* **2015**, *11*, 4159–4168.

- (290) Bozkaya, U.; Sherrill, C. D. Orbital-optimized MP2.5 and its analytic gradients: Approaching CCSD(T) quality for noncovalent interactions. *J. Chem. Phys.* **2014**, *141*, 204105.
- (291) Hohenstein, E. G.; Parrish, R. M.; Martínez, T. J. Tensor hypercontraction density fitting. I. Quartic scaling second- and third-order Møller-Plesset perturbation theory. *J. Chem. Phys.* **2012**, *137*, 044103.
- (292) Gráfová, L.; Pitoňák, M.; Řezáč, J.; Hobza, P. Comparative Study of Selected Wave Function and Density Functional Methods for Noncovalent Interaction Energy Calculations Using the Extended S22 Data Set. *J. Chem. Theory Comput.* **2010**, *6*, 2365–2376.
- (293) Riley, K. E.; Platts, J. A.; Řezáč, J.; Hobza, P.; Hill, J. G. Assessment of the Performance of MP2 and MP2 Variants for the Treatment of Noncovalent Interactions. *J. Phys. Chem. A* **2012**, *116*, 4159–4169.
- (294) Pitoňák, M.; Neogrady, P.; Černý, J.; Grimme, S.; Hobza, P. Scaled MP3 Noncovalent Interaction Energies Agree Closely with Accurate CCSD(T) Benchmark Data. *ChemPhysChem* **2009**, *10*, 282–289.
- (295) Riley, K. E.; Řezáč, J.; Hobza, P. The performance of MP2.5 and MP2.X methods for nonequilibrium geometries of molecular complexes. *Phys. Chem. Chem. Phys.* **2012**, *14*, 13187–13193.
- (296) Sedlak, R.; Riley, K. E.; Řezáč, J.; Pitoňák, M.; Hobza, P. MP2.5 and MP2.X: Approaching CCSD(T) Quality Description of Noncovalent Interaction at the Cost of a Single CCSD Iteration. *ChemPhysChem* **2013**, *14*, 698–707.
- (297) Bozkaya, U. Orbital-optimized third-order Møller-Plesset perturbation theory and its spin-component and spin-opposite scaled variants: Application to symmetry breaking problems. *J. Chem. Phys.* **2011**, *135*, 224103.
- (298) Soydaş, E.; Bozkaya, U. Assessment of Orbital-Optimized Third-Order Møller-Plesset Perturbation Theory and Its Spin-Component and Spin-Opposite Scaled Variants for Thermochemistry and Kinetics. *J. Chem. Theory Comput.* **2013**, *9*, 1452–1460.
- (299) Bozkaya, U. Orbital-Optimized MP3 and MP2.5 with Density-Fitting and Cholesky Decomposition Approximations. *J. Chem. Theory Comput.* **2016**, *12*, 1179–1188.
- (300) Bozkaya, U. Analytic energy gradients for the orbital-optimized third-order Møller-Plesset perturbation theory. *J. Chem. Phys.* **2013**, *139*, 104116.
- (301) Bozkaya, U. Analytic energy gradients for orbital-optimized MP3 and MP2.5 with the density-fitting approximation: An efficient implementation. *J. Comput. Chem.* **2018**, *39*, 351–360.
- (302) Kendall, R. A.; Dunning, T. H.; Harrison, R. J. Electron affinities of the first-row atoms revisited. Systematic basis sets and wave functions. *J. Chem. Phys.* **1992**, *96*, 6796–6806.

- (303) Weigend, F.; Köhn, A.; Hättig, C. Efficient use of the correlation consistent basis sets in resolution of the identity MP2 calculations. *J. Chem. Phys.* **2002**, *116*, 3175–3183.
- (304) Hättig, C. Optimization of auxiliary basis sets for RI-MP2 and RI-CC2 calculations: Core-valence and quintuple- ζ basis sets for H to Ar and QZVPP basis sets for Li to Kr. *Phys. Chem. Chem. Phys.* **2005**, *7*, 59–66.
- (305) Goerigk, L.; Grimme, S. A General Database for Main Group Thermochemistry, Kinetics, and Noncovalent Interactions: Assessment of Common and Reparameterized (meta-)GGA Density Functionals. *J. Chem. Theory Comput.* **2010**, *6*, 107–126.
- (306) Zhao, Y.; Lynch, B. J.; Truhlar, D. G. Multi-coefficient extrapolated density functional theory for thermochemistry and thermochemical kinetics. *Phys. Chem. Chem. Phys.* **2005**, *7*, 43–52.
- (307) Goerigk, L.; Hansen, A.; Bauer, C.; Ehrlich, S.; Najibi, A.; Grimme, S. A look at the density functional theory zoo with the advanced GMTKN55 database for general main group thermochemistry, kinetics and noncovalent interactions. *Phys. Chem. Chem. Phys.* **2017**, *19*, 32184–32215.
- (308) Řezáč, J.; Hobza, P. Describing Noncovalent Interactions beyond the Common Approximations: How Accurate Is the "Gold Standard", CCSD(T) at the Complete Basis Set Limit? *J. Chem. Theory Comput.* **2013**, *9*, 2151–2155.
- (309) Thomas, J. R.; DeLeeuw, B. J.; Vacek, G.; Crawford, T. D.; Yamaguchi, Y.; Schaefer III, H. F. The balance between theoretical method and basis set quality: A systematic study of equilibrium geometries, dipole moments, harmonic vibrational frequencies, and infrared intensities. *J. Chem. Phys.* **1993**, *99*, 403–416.
- (310) Helgaker, T.; Gauss, J.; Jørgensen, P.; Olsen, J. The prediction of molecular equilibrium structures by the standard electronic wave functions. *J. Chem. Phys.* **1997**, *106*, 6430–6440.
- (311) Bak, K. L.; Gauss, J.; Jørgensen, P.; Olsen, J.; Helgaker, T.; Stanton, J. F. The accurate determination of molecular equilibrium structures. *J. Chem. Phys.* **2001**, *114*, 6548–6556.
- (312) Byrd, E. F.; Sherrill, C. D.; Head-Gordon, M. The theoretical prediction of molecular radical species: a systematic study of equilibrium geometries and harmonic vibrational frequencies. *J. Phys. Chem. A* **2001**, *105*, 9736–9747.
- (313) Beran, G. J. O.; Gwaltney, S. R.; Head-Gordon, M. Approaching closed-shell accuracy for radicals using coupled cluster theory with perturbative triple substitutions. *Phys. Chem. Chem. Phys.* **2003**, *5*, 2488–2493.
- (314) Szalay, P. G.; Vázquez, J.; Simmons, C.; Stanton, J. F. Triplet instability in doublet systems. *J. Chem. Phys.* **2004**, *121*, 7624–7631.

- (315) Stanton, J. F.; Gauss, J. A Discussion of Some Problems Associated with the Quantum Mechanical Treatment of Open-Shell Molecules. *Adv. Chem. Phys.* **2003**, *125*, 101–146.
- (316) Tentscher, P. R.; Arey, J. S. Geometries and vibrational frequencies of small radicals: Performance of coupled cluster and more approximate methods. *J. Chem. Theory Comput.* **2012**, *8*, 2165–2179.
- (317) Brueckner, K. A. Nuclear saturation and two-body forces. II. Tensor forces. *Phys. Rev.* **1954**, *96*, 508.
- (318) Nesbet, R. K. Brueckner's Theory and the Method of Superposition of Configurations. *Phys. Rev.* **1958**, *109*, 1632.
- (319) Dykstra, C. E. An examination of the Brueckner condition for the selection of molecular orbitals in correlated wavefunctions. *Chem. Phys. Lett.* **1977**, *45*, 466–469.
- (320) Handy, N. C.; Pople, J. A.; Head-Gordon, M.; Raghavachari, K.; Trucks, G. W. Size-consistent Brueckner theory limited to double substitutions. *Chem. Phys. Lett.* **1989**, *164*, 185–192.
- (321) Hampel, C.; Peterson, K. A.; Werner, H.-J. A comparison of the efficiency and accuracy of the quadratic configuration interaction (QCISD), coupled cluster (CCSD), and Brueckner coupled cluster (BCCD) methods. *Chem. Phys. Lett.* **1992**, *190*, 1–12.
- (322) Stanton, J. F.; Gauss, J.; Bartlett, R. J. On the choice of orbitals for symmetry breaking problems with application to NO_3 . *J. Chem. Phys.* **1992**, *97*, 5554–5559.
- (323) Barnes, L. A.; Lindh, R. Symmetry breaking in O_4^+ : An application of the Brueckner coupled-cluster method. *Chem. Phys. Lett.* **1994**, *223*, 207–214.
- (324) Xie, Y.; Allen, W. D.; Yamaguchi, Y.; Schaefer III, H. F. Is the oxywater radical cation more stable than neutral oxywater? *J. Chem. Phys.* **1996**, *104*, 7615–7623.
- (325) Crawford, T. D.; Stanton, J. F.; Szalay, P. G.; Schaefer III, H. F. The \tilde{C}^2A_2 excited state of NO_2 : Evidence for a C_s equilibrium structure and a failure of some spin-restricted reference wavefunctions. *J. Chem. Phys.* **1997**, *107*, 2525–2528.
- (326) Scuseria, G. E.; Schaefer III, H. F. The optimization of molecular orbitals for coupled cluster wavefunctions. *Chem. Phys. Lett.* **1987**, *142*, 354–358.
- (327) Krylov, A. I.; Sherrill, C. D.; Byrd, E. F.; Head-Gordon, M. Size-consistent wave functions for nondynamical correlation energy: The valence active space optimized orbital coupled-cluster doubles model. *J. Chem. Phys.* **1998**, *109*, 10669–10678.
- (328) Van Voorhis, T.; Head-Gordon, M. The quadratic coupled cluster doubles model. *Chem. Phys. Lett.* **2000**, *330*, 585–594.
- (329) Fang, Z.; Lee, Z.; Peterson, K. A.; Dixon, D. A. Use of Improved Orbitals for CCSD(T) Calculations for Predicting Heats of Formation of Group IV and Group VI Metal Oxide Monomers and Dimers and UCl_6 . *J. Chem. Theory Comput.* **2016**, *12*, 3583–3592.

- (330) Fang, Z.; Vasiliu, M.; Peterson, K. A.; Dixon, D. A. Prediction of bond dissociation energies/heats of formation for diatomic transition metal compounds: CCSD(T) works. *J. Chem. Theory Comput.* **2017**, *13*, 1057–1066.
- (331) Bouř, P. Configuration interaction with Kohn–Sham orbitals and their relation to excited electronic states. *Chem. Phys. Lett.* **2001**, *345*, 331–337.
- (332) Needs, R. J.; Kent, P. R. C.; Porter, A. R.; Towler, M. D.; Rajagopal, G. Quantum Monte Carlo calculations for ground and excited states. *Int. J. Quantum Chem.* **2002**, *86*, 218–225.
- (333) Sherrill, C. D.; Lee, M. S.; Head-Gordon, M. On the performance of density functional theory for symmetry-breaking problems. *Chem. Phys. Lett.* **1999**, *302*, 425–430.
- (334) Scuseria, G. E. On the connections between Brueckner–coupled-cluster, density-dependent Hartree–Fock, and density functional theory. *Int. J. Quantum Chem.* **1995**, *55*, 165–171.
- (335) Heßelmann, A.; Jansen, G. First-order intermolecular interaction energies from Kohn–Sham orbitals. *Chem. Phys. Lett.* **2002**, *357*, 464–470.
- (336) Lindgren, I.; Salomonson, S. Brueckner orbitals and density-functional theory. *Int. J. Quantum Chem.* **2002**, *90*, 294–308.
- (337) Haggag, O. S.; Malakar, P.; Pokhilko, P.; Stanton, J. F.; Krylov, A. I.; Ruhman, S. The elusive dynamics of aqueous permanganate photochemistry. *Phys. Chem. Chem. Phys.* **2020**, *22*, 10043–10055.
- (338) Lee, J. Postmodern Electronic Structure Theory., Ph.D. Thesis, University of California, Berkeley, 2019.
- (339) Lee, J.; Malone, F. D.; Morales, M. A. Utilizing essential symmetry breaking in auxiliary-field quantum Monte Carlo: Application to the spin gaps of the C₃₆ fullerene and an iron porphyrin model complex. *J. Chem. Theory Comput.* **2020**, *16*, 3019–3027.
- (340) Mardirossian, N.; Ruiz Pestana, L.; Womack, J. C.; Skylaris, C.-K.; Head-Gordon, T.; Head-Gordon, M. Use of the rVV10 nonlocal correlation functional in the B97M-V density functional: defining B97M-rV and related functionals. *J. Phys. Chem. Lett.* **2017**, *8*, 35–40.
- (341) Seeger, R.; Pople, J. A. Self-consistent molecular orbital methods. XVIII. Constraints and stability in Hartree–Fock theory. *J. Chem. Phys.* **1977**, *66*, 3045–3050.
- (342) Peterson, K. A.; Dunning Jr, T. H. Accurate correlation consistent basis sets for molecular core–valence correlation effects: The second row atoms Al–Ar, and the first row atoms B–Ne revisited. *J. Chem. Phys.* **2002**, *117*, 10548–10560.

- (343) Prascher, B. P.; Woon, D. E.; Peterson, K. A.; Dunning, T. H.; Wilson, A. K. Gaussian basis sets for use in correlated molecular calculations. VII. Valence, core-valence, and scalar relativistic basis sets for Li, Be, Na, and Mg. *Theor. Chem. Acc.* **2011**, *128*, 69–82.
- (344) Hill, J. G.; Peterson, K. A. Correlation consistent basis sets for explicitly correlated wavefunctions: valence and core-valence basis sets for Li, Be, Na, and Mg. *Phys. Chem. Chem. Phys.* **2010**, *12*, 10460–10468.
- (345) Dunham, J. L. The energy levels of a rotating vibrator. *Phys. Rev.* **1932**, *41*, 721.
- (346) Huber, K. P.; Herzberg, G. H. In *NIST Chemistry WebBook, NIST Standard Reference Database Number 69*, Linstrom, P., Mallard, W., Eds., data prepared by Jean W. Gallagher and Russell D. Johnson, III; National Institute of Standards and Technology: Gaithersburg MD, 20899, 1979.
- (347) Watts, J. D.; Bartlett, R. J. Coupled-cluster calculations on the C₂ molecule and the C₂⁺ and C₂⁻ molecular ions. *J. Chem. Phys.* **1992**, *96*, 6073–6084.
- (348) Purwanto, W.; Al-Saidi, W.; Krakauer, H.; Zhang, S. Eliminating spin contamination in auxiliary-field quantum Monte Carlo: Realistic potential energy curve of F₂. *J. Chem. Phys.* **2008**, *128*, 114309.
- (349) Irikura, K. K. Experimental Vibrational Zero-Point Energies: Diatomic Molecules. *J. Phys. Chem. Ref. Data* **2007**, *36*, 389–397.
- (350) Hotop, H.; Patterson, T.; Lineberger, W. High resolution photodetachment study of OH⁻ and OD⁻ in the threshold region 7000–6450 Å. *J. Chem. Phys.* **1974**, *60*, 1806–1812.
- (351) Cormack, A. J.; Yench, A. J.; Donovan, R. J.; Lawley, K. P.; Hopkirk, A.; King, G. C. High-resolution threshold photoelectron spectroscopy of molecular fluorine. *Chem. Phys.* **1996**, *213*, 439–448.
- (352) Milkman, I. W.; Choi, J. C.; Hardwick, J. L.; Moseley, J. T. High-resolution studies of the A²Π-X²Π system of rotationally cooled SO⁺. *J. Mol. Spectrosc.* **1988**, *130*, 20–32.
- (353) Boness, M. J. W.; Schulz, G. J. Structure of O₂. *Phys. Rev. A* **1970**, *2*, 2182.
- (354) Linder, F.; Schmidt, H. Experimental study of low energy e-O₂ collision processes. *Z. Naturforsch. A* **1971**, *26*, 1617–1625.
- (355) Ervin, K. M.; Anusiewicz, I.; Skurski, P.; Simons, J.; Lineberger, W. C. The only stable state of O₂⁻ is the X²Π_g ground state and it (still!) has an adiabatic electron detachment energy of 0.45 eV. *J. Phys. Chem. A* **2003**, *107*, 8521–8529.
- (356) Gray, R. L.; Haselton, H. H.; Krause Jr, D.; Soltysik, E. A. Vibrational structure in electron scattering by O₂. *Chem. Phys. Lett.* **1972**, *13*, 51–53.
- (357) Creighton, J. A.; Lippincott, E. R. Vibrational frequency and dissociation energy of the superoxide ion. *J. Chem. Phys.* **1964**, *40*, 1779–1780.

- (358) Gewurtz, S.; Lew, H.; Flainek, P. The electronic spectrum of HF^+ . *Can. J. Phys.* **1975**, *53*, 1097–1108.
- (359) Hovde, D. C.; Keim, E. R.; Saykally, R. J. Velocity modulation laser spectroscopy of molecular ions: The hyperfine-resolved rovibrational spectrum of HF^+ . *Mol. Phys.* **1989**, *68*, 599–607.
- (360) Yench, A. J.; Cormack, A. J.; Donovan, R. J.; Hopkirk, A.; King, G. C. Threshold photoelectron spectroscopy of HF and DF in the outer valence ionization region. *J. Phys. B: At., Mol. Opt. Phys.* **1999**, *32*, 2539.
- (361) Yang, J.; Hao, Y.; Li, J.; Zhou, C.; Mo, Y. A combined zero electronic kinetic energy spectroscopy and ion-pair dissociation imaging study of the $\text{F}_2^+(X^2\Pi_g)$ structure. *J. Chem. Phys.* **2005**, *122*, 134308.
- (362) Gilbert, T. L.; Wahl, A. C. Single-Configuration Wavefunctions and Potential Curves for Low-Lying States of He_2^+ , Ne_2^+ , Ar_2^+ , F_2^- , Cl_2^- and the Ground State of Cl_2 . *J. Chem. Phys.* **1971**, *55*, 5247–5261.
- (363) O'Hare, P. A. G.; Wahl, A. C. Thermochemical and Theoretical Investigations of the Sodium-Oxygen System. II. Properties of NaO and Its Ions from Hartree-Fock Molecular Orbital Studies. *J. Chem. Phys.* **1972**, *56*, 4516–4525.
- (364) So, S. P.; Richards, W. G. The electronic ground states of alkali monoxides. *Chem. Phys. Lett.* **1975**, *32*, 227–230.
- (365) Holst, W. Über das Bandenspektrum des ionisierten Aluminiumhydrides. *Z. Phys.* **1934**, *89*, 40–49.
- (366) Narasimham, N. A. The Emission Spectrum of the PH^+ molecule. *Can. J. Phys.* **1957**, *35*, 901–911.
- (367) Reddy, R.; Ahammed, Y. N.; Rao, A. S.; Rao, T. V. R. Dissociation energies of PH and PH^+ . *J. Quant. Spectrosc. Radiat. Transf.* **1995**, *54*, 1035–1038.
- (368) Zittel, P. F.; Lineberger, W. C. Laser photoelectron spectrometry of PO^- , PH^- , and PH_2^- . *J. Chem. Phys.* **1976**, *65*, 1236–1243.
- (369) Patanen, M.; Nicolas, C.; Linguerri, R.; Simoes, G.; Travnikova, O.; Liu, X.-J.; Hochlaf, M.; Bozek, J. D.; Miron, C. High-Resolution Photoelectron Spectroscopy with Angular Selectivity-A Tool To Probe Valence-Rydberg States and Couplings in HCl^+ . *J. Phys. Chem. A* **2014**, *118*, 4975–4981.
- (370) Carlsten, J. L.; Peterson, J. R.; Lineberger, W. C. Binding of an electron by the field of a molecular dipole— LiCl^- . *Chem. Phys. Lett.* **1976**, *37*, 5–8.
- (371) DeKock, R. L.; Higginson, B. R.; Lloyd, D. R.; Breeze, A.; Cruickshank, D. W. J.; Armstrong, D. R. Photoelectron spectra of halides: V. Experimental and theoretical study of the electronic structures of ClF , ClF_3 , BrF and BrF_3 . *Mol. Phys.* **1972**, *24*, 1059–1072.

- (372) Anderson, C. P.; Mamantov, G.; Bull, W.; Grimm, F. A.; Carver, J. C.; Carlson, T. A. Photoelectron spectrum of chlorine monofluoride. *Chem. Phys. Lett.* **1971**, *12*, 137–139.
- (373) Taube, A. G.; Bartlett, R. J. Frozen natural orbital coupled-cluster theory: Forces and application to decomposition of nitroethane. *J. Chem. Phys.* **2008**, *128*, 164101.

Appendix A

Additional Information: Modeling of Gas Phase Formation of c -SiC₃ Molecules in the Circumstellar Medium of Carbon Stars

A.1 Branching Ratio Calculations

We performed RRKM calculations[126] via direct counting of vibrational states[127] to determine the unimolecular reaction rate constants for the silicon–methylacetylene, silicon–allene, and silicon–D3-methylacetylene systems. We also applied a tunneling correction to the reaction rates by approximating the barriers as Eckart potentials[128]. These rate constants were used to form the coupled systems of equations for each network, which was then solved and evaluated in the longtime limit to extract branching ratios. For the silicon–methylacetylene system, the trimmed reaction network of reactions considered in the RRKM calculations is given in Fig. S3. For this system our network began with a unit population in isomer [i1] and no population in any other isomers, corresponding to the entrance channel for this reaction. Using the tunneling-corrected rates, we predicted a branching ratio of 38.2% **p1**, 0.6% **p2**, 11.1% **p3**, and 45.8% **p4**. For the silicon–allene system, the same reaction network and rates were used as in the silicon–methylacetylene case. For this system, however, our network began with unit population in isomer [i7]. While we observed that the silicon–allene system has entrance channels leading to both isomers [i7] and [i10], we note that all flux out of isomer [i7] into the reaction network must proceed through [i10] according to our network. Using the tunneling-corrected rates, we predicted a branching ratio of 38.7% **p1**, 0.5% **p2**, 11.3% **p3**, and 46.5% **p4**.

Comparison of the silicon–methylacetylene and silicon–allene branching ratios shows similar branching ratios for each product. While the reaction rates show the fastest isomerization from [i1] to be [i1]→[i4], exit from this channel is stifled by the high barrier to form product

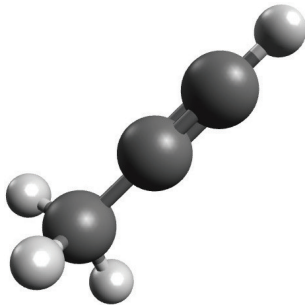
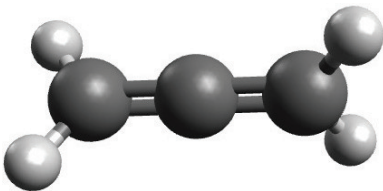
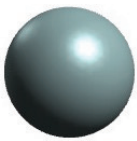
p2 going through intermediate [i13]. This allows for the other channels out of [i1] to be expressed, particularly [i1]→[i5] and [i1]→[i6]. Both of these channels can eventually lead to isomers [i6], [i9], and [i12], from which we see much lower overall barriers to for products **p4**, **p1**, and **p3**, respectively. Starting from isomer [i7], we predict fast isomerization to [i10], which then preferentially isomerizes to [i6] over [i2]. From [i6] we have facile isomerization to isomers [i9] and [i12] via ring opening. These computational results corroborate the experimental results for these systems, where the product translational energy distributions of the silicon–methylacetylene and silicon–allene systems are nearly identical.


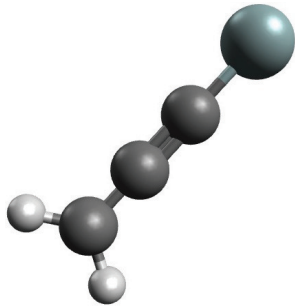
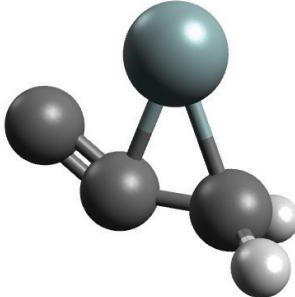
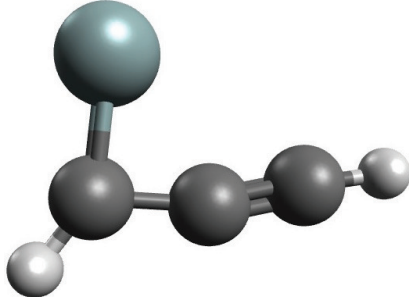
We also examined the branching ratios for hydrogen atom and methyl loss in the silicon–methylacetylene and silicon–allene systems. These channels were found to contribute negligibly (4.2% for methylacetylene, 2.9% for allene) to the overall product stream, corroborating the experimental findings. Specifically, when considering the silicon–methylacetylene and silicon–allene networks, we included exits to atomic hydrogen loss products **n1**, **n2**, **n3**, **n4**, and **n6** and methyl loss product **m2**. For the silicon–methylacetylene system, we predicted branching ratio of 3.9% **n1**, 0.06% **n2**, 0.02% **n3**, 0.01% **n4**, 0.01% **n6**, and 0.2% **m2**. For the silicon–allene system, we predicted branching ratio of 2.7% **n1**, 0.03% **n2**, 0.02% **n3**, 0.01% **n4**, 0.004% **n6**, and 0.1% **m2**. These lower branching ratios are due to the higher barriers for hydrogen atom or methyl loss when compared to the more favorable molecular hydrogen loss channels.

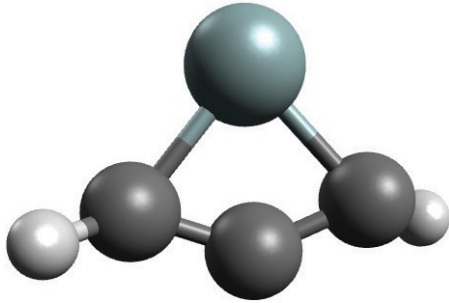
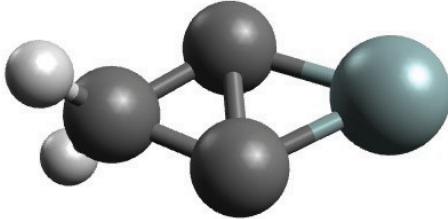
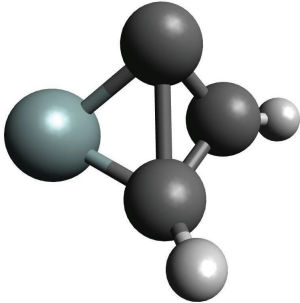
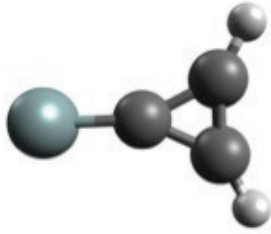
For the silicon–D3-methylacetylene system, we begin from the same reaction network as in the non-deuterated case. From here, we expanded the reaction network to include all possible constitutional isomers for each corresponding non-deuterated isomer to account for the potential of hydrogen-deuterium scrambling. Hydrogen-deuterium scrambling reaction can occur for the [i2]↔[i3], [i2]↔[i10], [i6]↔[i10], and [i6]→[i9]→[i8]→[i12]→[i6] reactions. We further included the [i2]→[i2] and [i2]→[i3] reactions in our reaction network. Using the tunneling-corrected rates, we predicted a branching ratio of 21.7% **p1a** + HD, 11.0% **p1b** + D₂, 0.3% **p2a** + HD, 0.01% **p2b** + D₂, 0.01% **p2c** + D₂, 2.6% **p3a** + D₂, 1.8% **p3b** + D₂, 5.2% **p3c** + HD, 27.7% **p4a** + D₂, and 29.5% **p4b** + HD. Therefore, we predicted a total branching ratio of 56.8% HD loss products and 43.2% D₂ loss products. These values are in good agreement with the experimental findings of 60 ± 15% HD loss and 40 ± 15% D₂ loss. Furthermore, this corroborates the non-deuterated results, which utilize the same general reaction network framework. Reaction rate constants, imaginary transition state frequencies, and reaction path degeneracies are reported in Table A.9.

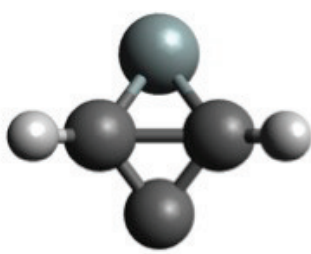

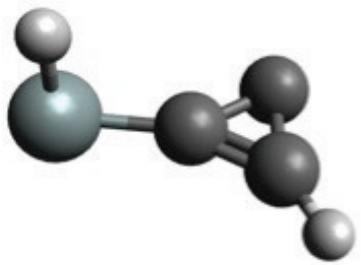
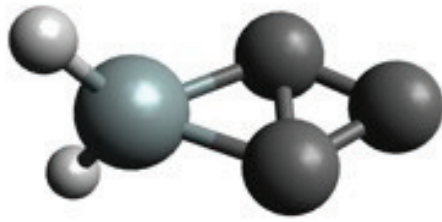
A.2 Tables

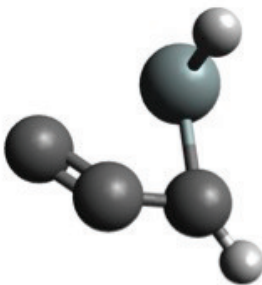
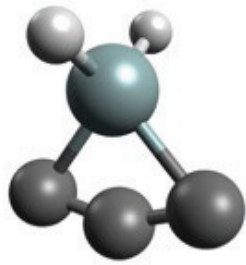
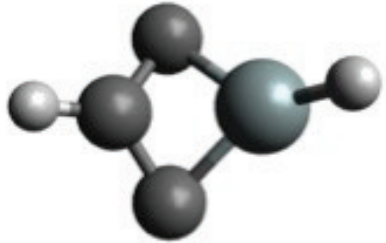
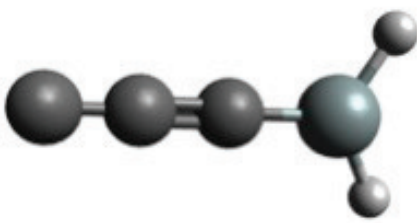
Table A.1: Reactants, products, intermediates, and transition state structures relevant to the reaction of electronically excited atomic silicon with methylacetylene and allene. Geometries were calculated at the $\omega\text{B97X-V//cc-pVTZ}$ level of theory; relative energies were calculated at the CCSD(T)//CBS level of theory.

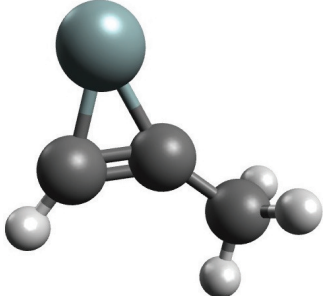
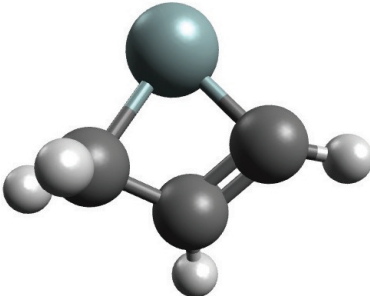
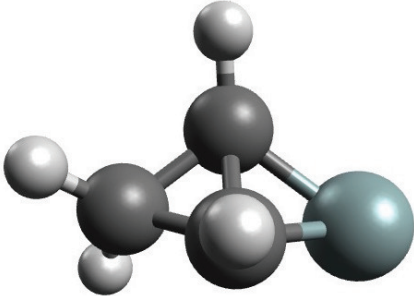
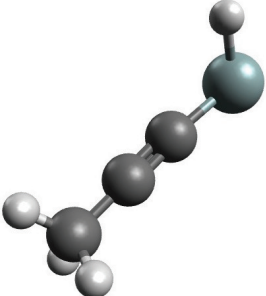
Reactants							
CH_3CCH				CH_2CCH_2			
							
0.0 kJ mol^{-1}				3.9 kJ mol^{-1}			
$\text{C}_{3v}^{-1}\text{A}_1$				$\text{D}_{2d}^{-1}\text{A}_1$			
C	-1.919449	1.519750	0.000000	C	-7.512217	1.836332	0.000036
C	-0.721221	1.524736	0.000000	C	-6.210183	1.823559	0.000153
C	-3.382029	1.513693	0.000000	C	-4.908232	1.810798	0.000267
H	0.343441	1.529181	0.000000	H	-8.068002	1.984399	-0.919492
H	-3.768514	1.986640	-0.905294	H	-8.070971	1.698436	0.919347
H	-3.768812	2.058826	0.863618	H	-4.360016	0.885485	-0.140011
H	-3.762327	0.490833	0.041676	H	-4.342009	2.725331	0.139709
Si							
							
—							
^1D							
Si	0.000000	0.000000	0.000000				

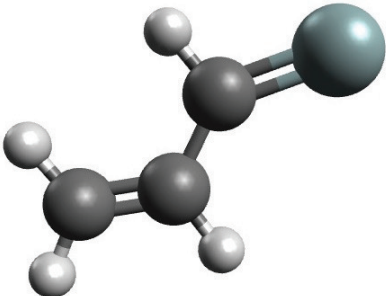
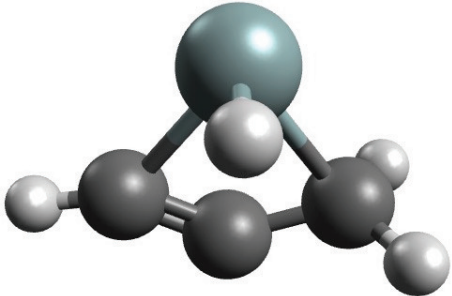
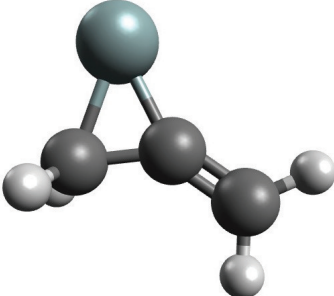
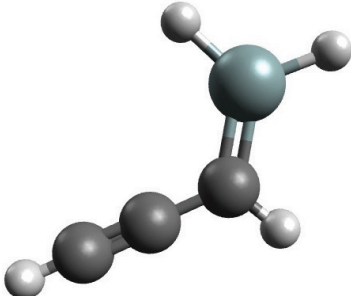
Products									
H_2				p1					
									
—				-189.6 kJ mol ⁻¹					
$D_{\infty\text{h}}^{-1}\Sigma$				$C_{2\text{v}}^{-1}\text{A}_1$					
H	0.003216	0.000000	0.000000	Si	-2.667415	2.191276	0.000000		
H	0.746784	0.000000	0.000000	C	-0.985018	2.220382	0.000000		
				C	0.298405	2.242563	0.000000		
				C	1.607796	2.265203	0.000000		
				H	2.142021	3.207971	0.000000		
				H	2.174299	1.341470	0.000000		
p2				p3					
									
-173.9 kJ mol ⁻¹				-163.4 kJ mol ⁻¹					
$C_s^{-1}\text{A}'$				$C_s^{-1}\text{A}'$					
Si	-3.530077	0.607099	0.333008	Si	-1.440031	2.135965	1.571949		
C	-2.115964	1.751749	-0.167586	C	-1.258585	1.493357	-0.509032		
C	-1.762971	0.449585	-0.634584	C	-1.918764	2.648067	0.002796		
C	-2.980050	2.474570	0.443216	C	-0.632564	0.456668	-0.644013		
H	-0.954113	-0.065250	-0.122807	H	-2.429665	3.372178	-0.610959		
H	-1.792019	0.273905	-1.706863	H	-0.091486	-0.444116	-0.815669		

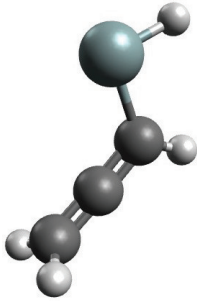
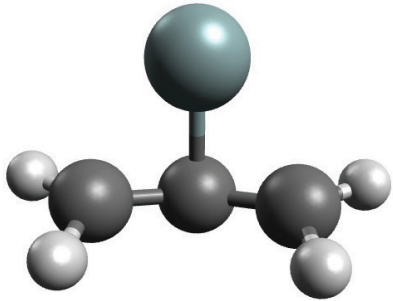
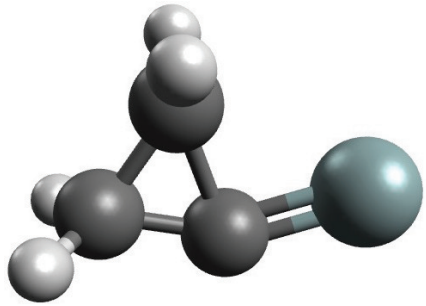
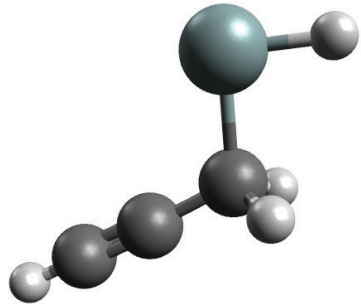
p4				p5			
							
-159.3 kJ mol ⁻¹				-138.6 kJ mol ⁻¹			
$C_{2v}^{-1}A_1$				$C_{2v}^{-1}A_1$			
Si	0.015583	1.421694	0.441321	Si	-0.153925	2.791130	0.597108
C	-1.710909	1.657474	1.228824	C	-0.701267	1.901637	-0.854814
C	-1.833196	1.452865	-0.080188	C	-1.470675	0.643621	-0.899626
C	-1.051473	1.232997	-1.134185	C	-1.079103	1.277031	0.374194
H	-2.213088	1.188068	2.060067	H	-0.958764	-0.265564	-1.204780
H	-1.030405	1.710504	-2.101157	H	-2.515112	0.686694	-1.198739
p6				p7			
							
-99.8 kJ mol ⁻¹				-83.5 kJ mol ⁻¹			
$C_1^{-1}A$				$C_{2v}^{-1}A_1$			
Si	0.000000	0.000000	0.000000	Si	0.000000	0.000000	0.000000
C	0.000000	0.000000	1.806628	C	0.000000	0.000000	1.719212
C	-1.286808	0.627089	1.815653	C	0.639430	0.000000	3.039625
C	-0.765193	1.502612	0.924959	C	-0.652963	-0.004736	3.033189
H	0.697327	0.000000	2.637474	H	1.582650	0.005577	3.557070
H	-2.217623	0.494213	2.353974	H	-1.601967	-0.006606	3.539526

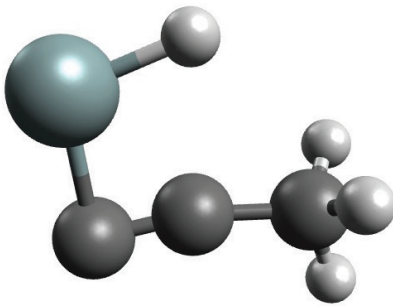
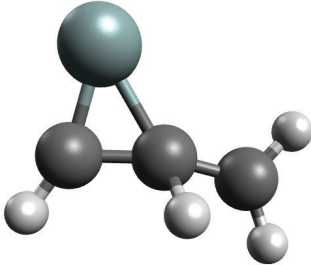
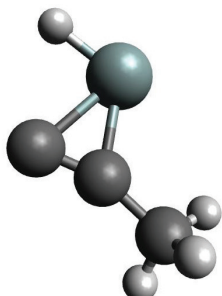
p8				p9			
							
-70.6 kJ mol ⁻¹				-62.1 kJ mol ⁻¹			
C _s ⁻¹ A'				C _s ⁻¹ A'			
Si	0.000000	0.000000	0.000000	Si	0.000000	0.000000	0.000000
C	0.000000	0.000000	1.843287	C	1.937037	0.000000	-0.025559
C	-1.401563	-0.160952	2.078228	C	2.673224	1.126057	-0.140369
C	-0.973371	-1.112994	1.101537	C	1.353436	1.386523	-0.023475
H	-1.159475	-2.178800	1.178760	H	0.000000	0.000000	1.517171
H	0.745816	0.000000	2.630932	H	3.661304	1.544024	-0.241081
p10				p11			
							
-6.0 kJ mol ⁻¹				26.5 kJ mol ⁻¹			
C ₁ ⁻¹ A				C _{2v} ⁻¹ A ₁			
Si	0.000000	0.000000	0.000000	Si	0.000000	0.000000	0.000000
C	1.834756	0.000000	-0.012712	C	-1.406915	-0.732528	-0.876099
C	3.087703	0.481614	-0.103968	C	-2.436321	0.000674	-1.517362
C	2.999800	-0.889315	-0.084047	C	-1.406701	0.733908	-0.875881
H	0.000000	0.000000	1.519674	H	0.000000	0.000000	1.472112
H	3.675556	1.385395	-0.152491	H	1.321012	0.000000	-0.649666

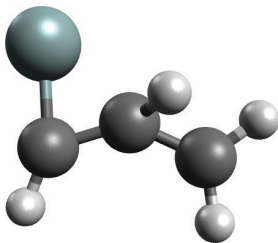
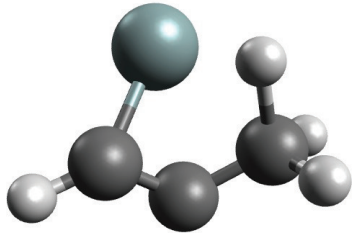
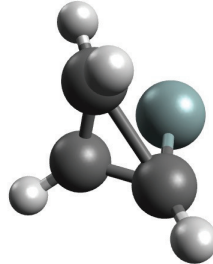
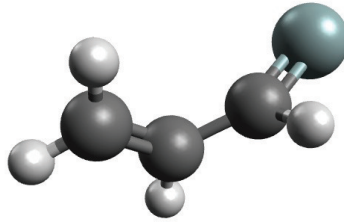
p12				p13			
							
58.7 kJ mol ⁻¹				82.7 kJ mol ⁻¹			
C ₁ ⁻¹ A				C _{2v} ⁻¹ A ₁			
Si	0.000000	0.000000	0.000000	Si	0.000000	0.000000	0.000000
C	1.906751	0.000000	-0.088904	C	-1.604147	-0.000599	-0.965813
C	1.719817	-1.323251	-0.158049	C	-1.321163	1.286223	-0.796186
C	0.828888	-2.195636	-0.498761	C	-1.319392	-1.286995	-0.795253
H	0.000000	0.000000	1.522410	H	0.000000	0.000000	1.471313
H	2.826815	0.569597	-0.151117	H	1.299958	0.000000	-0.689114
p14				p15			
							
127.8 kJ mol ⁻¹				147.4 kJ mol ⁻¹			
C _s ⁻¹ A'				C _{2v} ⁻¹ A ₁			
Si	0.000000	0.000000	0.000000	Si	0.000000	0.000000	0.000000
C	1.264017	0.000000	-1.312498	C	-1.482108	0.004467	-0.835693
C	0.536426	-1.228541	-1.454983	C	-2.602584	0.005168	-1.467455
C	-0.859350	-0.926376	-1.313170	C	-3.727678	0.003497	-2.101864
H	0.000000	0.000000	1.476786	H	0.000000	0.000000	1.469804
H	0.950336	-2.176678	-1.791926	H	1.257655	0.000000	-0.760691

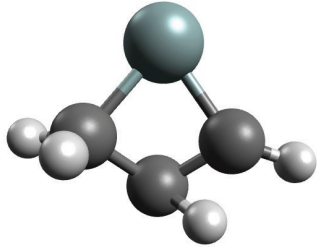
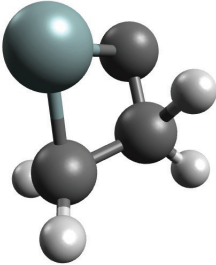
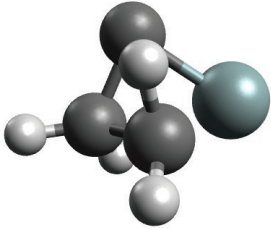
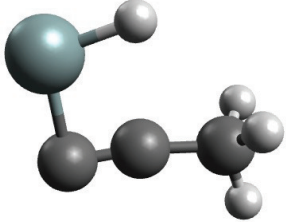
Intermediates											
[i1]					[i2]						
											
-381.9 kJ mol ⁻¹					-366.5 kJ mol ⁻¹						
C _s ⁻¹ A'					C ₁ ⁻¹ A						
Si	-1.656605	1.891479	-0.619303	Si	1.217161	2.092109	-0.478041	Si	1.217161	2.092109	-0.478041
C	-3.043502	0.820878	-0.149821	C	-0.718085	2.105551	-0.106733	C	-0.718085	2.105551	-0.106733
C	-1.887126	0.137774	-0.160470	C	0.896350	0.503330	0.378512	C	0.896350	0.503330	0.378512
C	-1.441882	-1.256744	0.108866	C	-0.384938	0.659690	-0.076621	C	-0.384938	0.659690	-0.076621
H	-2.267948	-1.914363	0.393239	H	-1.435881	2.452625	-0.849645	H	-1.435881	2.452625	-0.849645
H	-0.951711	-1.667938	-0.777728	H	-0.927003	2.520049	0.875808	H	-0.927003	2.520049	0.875808
H	-0.695679	-1.260617	0.907968	H	-1.014639	-0.115450	-0.520096	H	-1.014639	-0.115450	-0.520096
H	-4.076299	0.569772	0.067786	H	1.393630	-0.440136	0.568491	H	1.393630	-0.440136	0.568491
[i3]					[i4]						
											
-307.0 kJ mol ⁻¹					-306.5 kJ mol ⁻¹						
C _s ⁻¹ A'					C ₁ ⁻¹ A						
Si	-2.584650	2.826243	0.102164	Si	2.269227	0.314672	0.012013	Si	2.269227	0.314672	0.012013
C	-1.277255	1.533566	0.133824	C	0.446698	0.519161	0.002884	C	0.446698	0.519161	0.002884
C	-2.614644	1.183903	0.928846	C	-0.767059	0.515702	-0.005318	C	-0.767059	0.515702	-0.005318
C	-1.976747	0.221766	-0.020795	C	-2.225868	0.529673	-0.008062	C	-2.225868	0.529673	-0.008062
H	-1.488341	-0.647336	0.417639	H	2.557659	1.810564	-0.006117	H	2.557659	1.810564	-0.006117
H	-2.696767	0.944785	1.983522	H	-2.625510	-0.364956	-0.490733	H	-2.625510	-0.364956	-0.490733
H	-2.476241	-0.001272	-0.958483	H	-2.607844	1.412410	-0.525637	H	-2.607844	1.412410	-0.525637
H	-0.273455	1.579469	0.542808	H	-2.593502	0.553573	1.020967	H	-2.593502	0.553573	1.020967

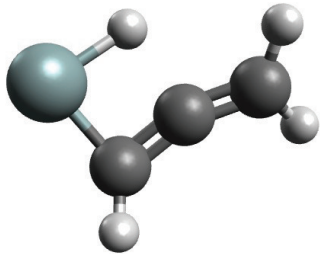
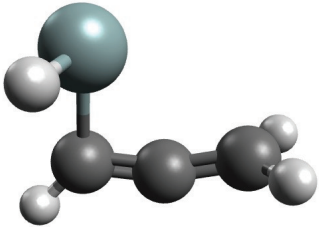
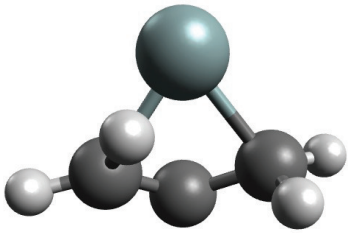
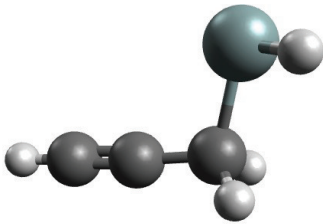
[i5]				[i6]			
							
-305.2 kJ mol ⁻¹				-301.9 kJ mol ⁻¹			
$C_s^{-1}A'$				$C_1^{-1}A$			
Si	-2.791074	1.331229	0.575045	Si	1.271276	2.401422	0.597200
C	0.041883	1.957213	0.098223	C	-0.676445	2.076496	-0.045615
C	1.276133	1.530665	-0.176961	C	1.201685	0.439514	-0.022520
C	-1.134334	1.101465	0.199981	C	0.071228	0.921046	-0.285832
H	-0.109806	3.022058	0.263830	H	1.712703	2.984364	-0.742591
H	2.111404	2.219175	-0.232581	H	-0.965219	2.689118	-0.894417
H	1.481749	0.478866	-0.350967	H	-1.396336	2.031078	0.765002
H	-0.944290	0.035021	0.000428	H	1.843949	-0.418828	-0.047808
[i7]				[i8]			
							
-292.0 kJ mol ⁻¹				-280.5 kJ mol ⁻¹			
$C_s^{-1}A'$				$C_s^{-1}A'$			
Si	-0.002314	3.177910	-0.169760	Si	-2.123430	2.732956	0.435983
C	-0.649663	1.369072	-0.142375	C	-0.578881	1.995631	0.420032
C	0.826543	1.531957	-0.066304	C	-0.360326	0.594266	0.333811
C	1.909821	0.771693	0.020207	C	-0.179590	-0.593207	0.258429
H	-1.073424	0.953192	-1.057167	H	-2.265622	4.199834	0.528920
H	-1.173338	1.016264	0.746817	H	-3.379454	1.961598	0.360797
H	1.853963	-0.315790	0.055069	H	0.306230	2.623143	0.479257
H	2.902621	1.211905	0.059823	H	-0.015456	-1.642789	0.191810

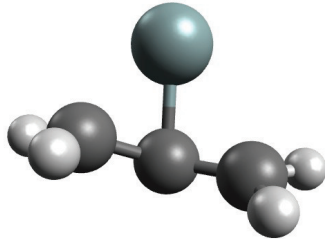
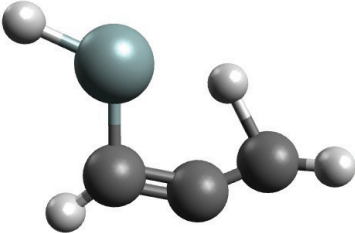
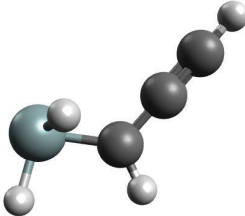
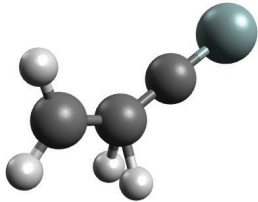
[i9]				[i10]			
							
-279.4 kJ mol ⁻¹				-277.3 kJ mol ⁻¹			
C _s ⁻¹ A'				C _s ⁻¹ A'			
Si	-0.948677	2.863727	0.654535	Si	-0.333163	1.486867	-0.671031
C	-1.217505	1.006333	0.704275	C	-0.144820	0.334917	0.683483
C	-0.284681	0.271592	0.142353	C	-1.419478	-0.081122	0.274337
C	0.670871	-0.400535	-0.428995	C	1.062694	0.035706	0.040856
H	-2.235815	3.206243	1.405402	H	-1.610019	-1.027212	-0.240233
H	-2.068992	0.501898	1.155645	H	-2.282879	0.366410	0.756404
H	1.531568	-0.731501	0.140907	H	1.241688	-0.893852	-0.506956
H	0.619686	-0.645957	-1.483673	H	1.954699	0.571689	0.349342
[i11]				[i12]			
							
-273.3 kJ mol ⁻¹				-247.9 kJ mol ⁻¹			
C _s ⁻¹ A'				C _s ⁻¹ A'			
Si	1.409563	2.464346	0.895067	Si	-0.980308	2.921623	1.046459
C	-0.674602	1.916613	-0.147441	C	-1.407690	1.314359	0.084885
C	0.532533	1.098713	0.523749	C	-0.359350	0.302722	0.082071
C	-0.611275	0.405511	-0.024987	C	0.531367	-0.500595	0.106582
H	-0.564797	2.315714	-1.149586	H	-2.336725	3.551344	0.727266
H	-1.405816	2.412592	0.481019	H	-1.671387	1.607227	-0.940700
H	-0.477705	-0.147527	-0.951107	H	-2.336671	0.913777	0.513390
H	-1.312873	-0.051284	0.668184	H	1.315662	-1.220461	0.122189

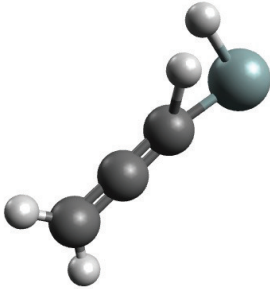
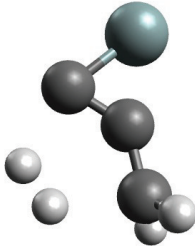
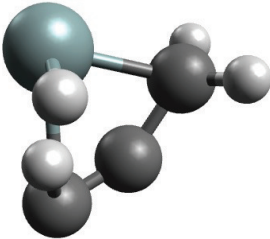
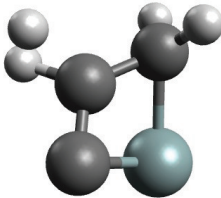
[i13]			
			
-224.0 kJ mol ⁻¹			
C _s ⁻¹ A'			
Si	-1.688737	2.624682	0.616789
C	-0.244907	1.218317	-0.220340
C	1.218639	1.272651	-0.343790
C	-1.465384	0.927557	-0.237325
H	-0.260660	3.204713	0.754427
H	1.524821	2.129620	-0.945098
H	1.687125	1.351436	0.638071
H	1.564998	0.357273	-0.829223
Transition State Structures			
[i1]→[i2]		[i1]→[i4]	
			
-77.0 kJ mol ⁻¹		-194.1 kJ mol ⁻¹	
C ₁ ⁻¹ A		C ₁ ⁻¹ A	
Si	0.387656	1.918057	-0.868165
C	0.507204	-1.109474	-0.273582
C	-0.001009	0.171130	-0.093798
C	-0.892669	1.297958	0.108223
H	1.347937	-1.296852	-0.939211
H	0.177136	-0.265142	0.972772
H	0.170559	-1.954642	0.325094
H	-1.765240	1.299326	0.746709
Si	-2.122577	1.493357	-0.465731
C	-3.577778	0.142016	0.174868
C	-2.426216	-0.379803	0.065365
C	-1.341337	-1.393100	0.060616
H	-1.737882	-2.337896	-0.315266
H	-0.507637	-1.078652	-0.566987
H	-0.973850	-1.547956	1.076886
H	-3.309526	2.412152	-0.373543

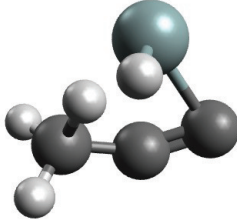
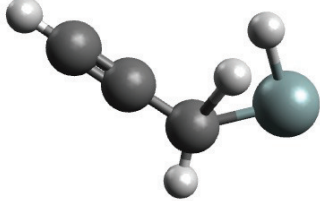
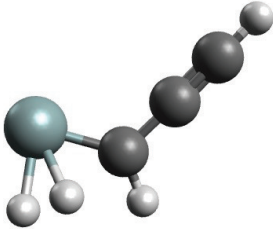
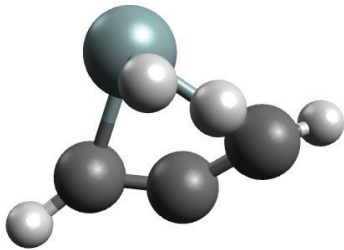
[i1]→[i5]				[i1]→[i6]			
							
-142.6 kJ mol ⁻¹				-125.8 kJ mol ⁻¹			
C ₁ ⁻¹ A				C ₁ ⁻¹ A			
Si	0.485782	2.153579	-0.469008	Si	0.778035	1.356341	0.013393
C	0.332198	-1.132452	-0.095064	C	-1.041349	0.972089	0.089159
C	0.161878	0.240941	-0.155304	C	-0.726348	-0.144886	-0.571048
C	-0.869881	1.190140	0.041691	C	0.465469	-0.839573	-0.180070
H	1.058802	-0.010869	0.587659	H	0.248932	-1.572742	0.597463
H	-0.474833	-1.810179	0.181935	H	1.180352	-1.204148	-0.916275
H	1.295799	-1.572078	-0.331053	H	1.081984	-0.069503	0.844891
H	-1.919433	1.016042	0.235748	H	-1.980789	1.508295	0.137363
[i2]→[i3]				[i2]→[i5]			
							
-188.1 kJ mol ⁻¹				-294.1 kJ mol ⁻¹			
C ₁ ⁻¹ A				C ₁ ⁻¹ A			
Si	-2.150053	2.178667	0.625370	Si	0.342188	2.735051	-0.130811
C	-0.578457	1.585315	-0.456669	C	0.391241	-1.205372	-0.299825
C	-1.232877	0.355972	-0.039025	C	0.039692	-0.188254	0.478770
C	-0.432102	1.821019	0.963102	C	-0.308252	1.168082	-0.001663
H	0.445188	1.756078	1.604662	H	0.000480	-0.344895	1.555941
H	0.020532	1.864829	-1.311772	H	0.632717	-2.174234	0.123862
H	-0.716789	-0.405155	0.544939	H	0.451087	-1.098752	-1.378354
H	-2.145988	-0.008539	-0.518207	H	-1.322618	1.262237	-0.434147

[i2]→[i10]				[i2]→[i11]			
							
-27.6 kJ mol ⁻¹				8.3 kJ mol ⁻¹			
C ₁ ⁻¹ A				C ₁ ⁻¹ A			
Si	0.728857	1.050351	-1.035226	Si	0.711581	1.120945	-1.147132
C	0.745086	-0.738470	-0.340304	C	0.472146	-0.659767	-0.443763
C	0.053676	-0.073521	0.854344	C	-0.426581	0.126484	0.507436
C	-0.693567	0.957443	0.165361	C	0.185285	1.423246	0.742216
H	1.677882	-1.260348	-0.131790	H	-1.131751	-0.376092	1.184455
H	0.063165	-1.398234	-0.873462	H	1.329286	-1.008742	0.132221
H	-1.158678	-0.176597	0.686967	H	0.056519	-1.475193	-1.037839
H	-1.402374	1.604957	0.677393	H	-1.169658	0.875873	-0.033549
[i3]→[i11]				[i4]→[i13]			
							
-25.7 kJ mol ⁻¹				-224.8 kJ mol ⁻¹			
C ₁ ⁻¹ A				C _s ⁻¹ A'			
Si	-2.117498	2.386481	0.331886	Si	-1.742300	2.701762	0.558436
C	-1.109699	0.390124	0.271138	C	-1.453027	0.995062	-0.232032
C	-0.453814	1.674840	-0.208502	C	-0.226982	1.212635	-0.272076
C	-1.026002	1.305652	1.486479	C	1.233250	1.262100	-0.377354
H	-2.106608	0.234772	-0.198696	H	-0.321943	3.146011	0.987967
H	0.243508	1.734296	-1.034771	H	1.549669	2.031502	-1.083304
H	-0.560203	-0.548099	0.270135	H	1.675869	1.477113	0.596678
H	0.211278	1.873915	0.737564	H	1.597521	0.293445	-0.727392

[i5]→[i9]				[i6]→[i9]			
							
-206.4 kJ mol ⁻¹				-259.9 kJ mol ⁻¹			
C ₁ ⁻¹ A				C ₁ ⁻¹ A			
Si	-1.992862	2.228890	0.527181	Si	1.820646	2.497868	0.585175
C	-1.168691	0.701841	0.088179	C	1.254585	0.742483	0.074294
C	0.014708	1.354943	0.010861	C	0.032876	1.141174	-0.073976
C	1.299058	1.583736	-0.198471	C	-1.054450	1.887589	-0.083800
H	-0.660165	2.892930	0.016175	H	2.460246	2.819309	-0.774176
H	-1.325198	-0.327819	0.375544	H	1.690241	-0.197006	-0.235942
H	1.802093	2.476996	0.142678	H	-1.294651	2.500444	-0.946357
H	1.862043	0.843052	-0.756205	H	-1.774537	1.839849	0.726578
[i6]→[i10]				[i6]→[i12]			
							
-159.1 kJ mol ⁻¹				-241.9 kJ mol ⁻¹			
C ₁ ⁻¹ A				C ₁ ⁻¹ A			
Si	1.108893	2.428844	0.896755	Si	0.852609	1.635684	0.581065
C	1.254157	0.804122	-0.190514	C	-0.565860	0.423002	0.059391
C	-0.047399	0.766331	0.066469	C	0.001882	-0.919555	0.000234
C	-0.677368	2.066019	0.073662	C	0.544992	-1.989473	-0.037835
H	2.054356	0.150676	-0.497980	H	0.555684	2.682867	-0.493235
H	1.608219	2.139909	-0.662094	H	-1.048992	0.683920	-0.883382
H	-0.645862	2.587746	-0.883451	H	-1.329382	0.463880	0.848535
H	-1.601289	2.227878	0.621898	H	1.001958	-2.950630	-0.071481

[i7]→[i10]				[i8]→[i9]			
							
-276.7 kJ mol ⁻¹				-56.0 kJ mol ⁻¹			
C ₁ ⁻¹ A				C ₁ ⁻¹ A			
Si	-1.965407	2.054224	0.949023	Si	1.041061	0.917892	0.436916
C	-2.941031	0.741834	-0.252682	C	0.760892	-0.738193	-0.161392
C	-1.529983	0.959789	-0.397630	C	-0.609128	-0.750344	-0.306514
C	-0.519325	0.330323	0.274811	C	-1.670823	-0.094074	-0.212414
H	-3.585322	1.284613	-0.938932	H	2.501462	1.265763	0.648959
H	-3.363470	-0.192898	0.123519	H	-0.818889	0.943557	0.334551
H	-0.582867	-0.703830	0.623728	H	1.411713	-1.596634	-0.075037
H	0.457528	0.798760	0.345200	H	-2.618347	0.185964	-0.624789
[i8]→[i12]				[i5]→p1			
							
-115.2 kJ mol ⁻¹				36.0 kJ mol ⁻¹			
C ₁ ⁻¹ A				C _s ⁻¹ A'			
Si	-2.521663	2.463165	1.136938	Si	-2.989127	-0.912311	-0.067647
C	-0.857503	2.002660	0.565118	C	-1.436574	-0.366039	-0.033811
C	-0.462648	0.671903	0.277186	C	-0.145854	0.096600	-0.001158
C	-0.127979	-0.463490	0.061318	C	1.148919	-0.335722	0.029154
H	-0.053439	2.725894	0.410733	H	1.968519	0.370590	0.051314
H	0.166755	-1.470185	-0.125512	H	1.364749	-1.396295	0.033802
H	-2.334378	3.957638	1.028947	H	-0.052376	1.252833	0.469567
H	-2.405675	1.983846	-0.345689	H	-0.028713	1.251089	-0.470006

[i9]→p1				[i1]→p2			
							
-88.7 kJ mol ⁻¹				7.0 kJ mol ⁻¹			
C ₁ ⁻¹ A				C _s ⁻¹ A'			
Si	-0.744770	2.157892	1.133843	Si	0.528665	2.400596	-0.746415
C	-0.117447	0.739329	0.301978	C	0.638969	-0.741790	0.047537
C	0.508868	-0.265289	-0.184605	C	0.334217	0.578629	-0.236986
C	1.137912	-1.291212	-0.706981	C	-0.782728	1.293996	-0.211915
H	2.192710	-1.451493	-0.511820	H	1.142678	-0.981263	0.980498
H	0.620937	-2.000203	-1.344227	H	0.810919	-1.435189	-0.771673
H	-1.537155	0.742156	0.712436	H	-1.559747	-0.175915	0.315690
H	-2.215299	1.527879	0.692674	H	-1.065292	-0.900941	0.410427
[i6]→p2				[i11]→p2			
							
-46.2 kJ mol ⁻¹				98.6 kJ mol ⁻¹			
C ₁ ⁻¹ A				C ₁ ⁻¹ A			
Si	1.178923	2.205371	0.803390	Si	0.042413	-0.714013	0.848100
C	-0.641206	2.137118	-0.050763	C	-0.717668	0.642379	-0.366158
C	-0.130702	0.814244	0.053579	C	0.748846	0.531954	-0.607018
C	0.888991	0.086553	0.200705	C	1.444960	-0.634113	-0.453494
H	-0.835280	2.504167	-1.054512	H	-1.128405	1.560574	0.057494
H	-1.380706	2.457777	0.683302	H	-1.303184	0.282882	-1.207928
H	1.725043	1.088245	-0.475804	H	1.486648	1.537155	-0.404833
H	1.923344	2.086626	-0.687100	H	1.243355	1.496133	-1.295948

[i13]→p2				[i12]→p3			
							
-45.6 kJ mol ⁻¹				-70.6 kJ mol ⁻¹			
C ₁ ⁻¹ A				C ₁ ⁻¹ A			
Si	-0.830773	0.883817	0.953003	Si	-1.151997	1.718947	0.728726
C	-1.811287	-0.696687	0.301549	C	-0.793552	-0.036891	0.485201
C	-0.590983	-0.923847	0.102221	C	0.356363	-0.744575	0.018188
C	0.749568	-0.461799	-0.040845	C	1.337204	-1.326892	-0.364743
H	1.185475	-0.546441	-1.038520	H	-1.597641	-0.704860	0.800559
H	1.455315	-0.696271	0.749183	H	2.205962	-1.845464	-0.696218
H	0.271987	0.942873	-0.437740	H	-0.463884	1.036474	-0.582223
H	-0.545547	1.525644	-0.576927	H	0.061553	1.931814	-0.358027
[i12]→p3'				[i6]→p4			
							
-76.3 kJ mol ⁻¹				-114.2 kJ mol ⁻¹			
C ₁ ⁻¹ A				C ₁ ⁻¹ A			
Si	-1.555112	0.642765	0.911988	Si	0.831125	0.640403	0.777373
C	0.049390	0.418870	0.114001	C	-1.185225	0.266693	0.157410
C	0.581034	-0.893905	-0.073288	C	-0.415827	-0.797532	0.102736
C	1.006592	-2.011224	-0.207659	C	0.854625	-1.135711	0.195070
H	0.726733	1.208649	-0.209397	H	-2.051331	0.445181	0.777573
H	1.387736	-2.997804	-0.330653	H	1.482402	-1.878498	-0.264555
H	-1.435106	2.141508	0.235326	H	-0.203090	1.162708	-0.807825
H	-1.002771	1.445970	-0.426216	H	0.676107	1.295027	-0.933420

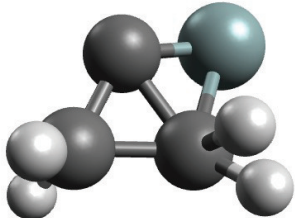
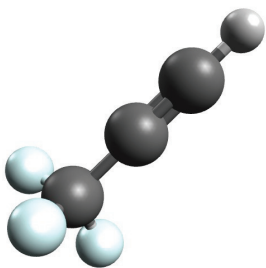
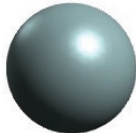
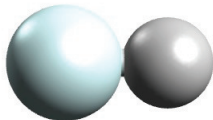
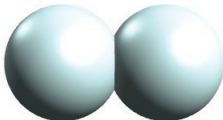
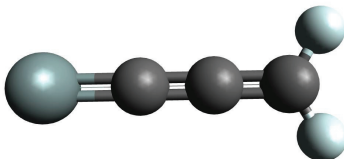
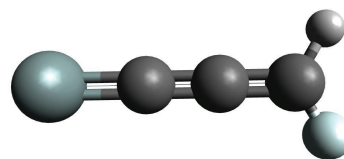
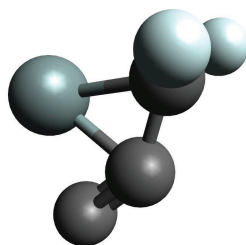
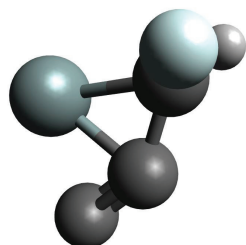
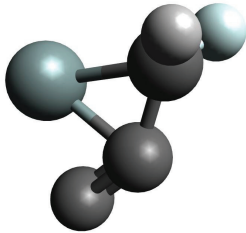
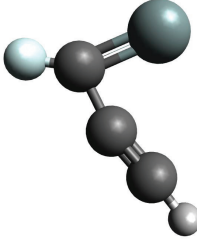
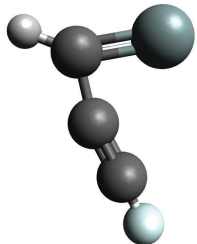
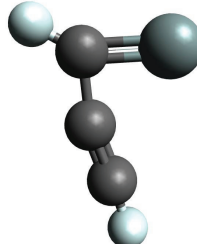
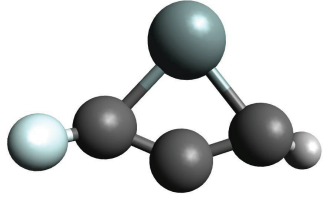
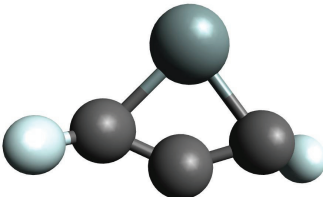
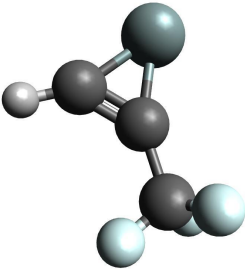
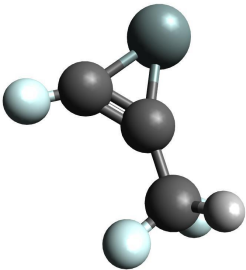
[i11]→p5			
			
66.7 kJ mol ⁻¹			
C ₁ ⁻¹ A			
Si	-0.987538	1.955490	-0.108967
C	0.391227	0.544056	-0.099353
C	-0.222777	-0.796271	-0.455253
C	-1.149070	0.247028	-0.031728
H	-0.029086	-1.630912	0.222284
H	-0.176856	-1.062271	-1.507519
H	1.344670	0.560033	0.664829
H	0.776750	0.207977	1.273359

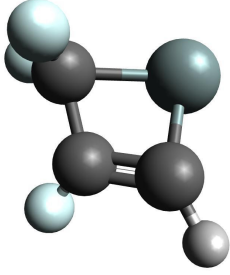
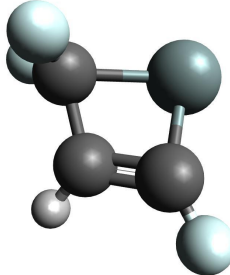
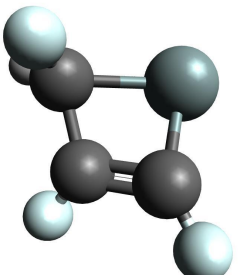
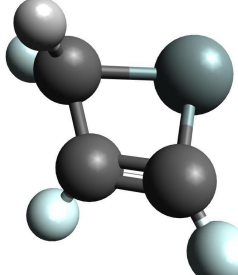
Table A.2: Reactants, products, intermediates, and transition state structures relevant to the reaction of electronically excited atomic silicon with D3-methylacetylene. Geometries were calculated at the $\omega\text{B97X-V//cc-pVTZ}$ level of theory; relative energies were calculated at the CCSD(T)//CBS level of theory.

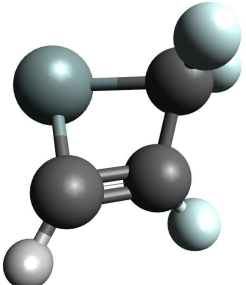
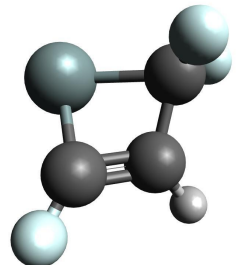
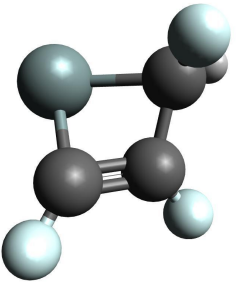
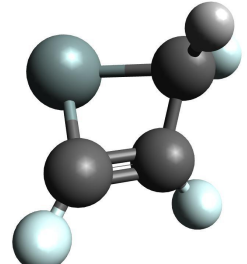
Reactants							
CD ₃ CCH				Si			
							
0.0 kJ mol ⁻¹				—			
C _{3v} ⁻¹ A ₁				¹ D			
C	-1.919449	1.519750	0.000000	Si	0.000000	0.000000	0.000000
C	-0.721221	1.524736	0.000000				
C	-3.382029	1.513693	0.000000				
H	0.343441	1.529181	0.000000				
D	-3.768514	1.986640	-0.905294				
D	-3.768812	2.058826	0.863618				
D	-3.762327	0.490833	0.041676				
Products							
HD				D ₂			
							
—				—			
C _{∞v} ⁻¹ Σ				D _{∞h} ⁻¹ Σ			
D	0.003216	0.000000	0.000000	D	0.003216	0.000000	0.000000
H	0.746784	0.000000	0.000000	D	0.746784	0.000000	0.000000

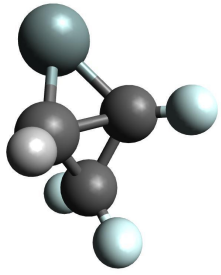
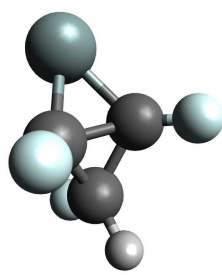
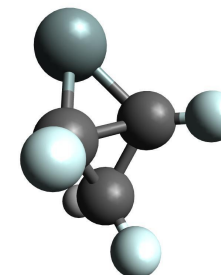
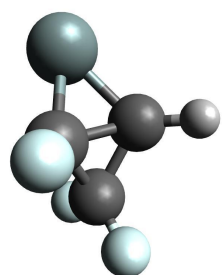
p1a				p1b			
							
-183.1 kJ mol ⁻¹				-179.8 kJ mol ⁻¹			
$C_{2v}^{-1}A_1$				$C_s^{-1}A'$			
Si	-2.667415	2.191276	0.000000	Si	-2.667415	2.191276	0.000000
C	-0.985018	2.220382	0.000000	C	-0.985018	2.220382	0.000000
C	0.298405	2.242563	0.000000	C	0.298405	2.242563	0.000000
C	1.607796	2.265203	0.000000	C	1.607796	2.265203	0.000000
D	2.142021	3.207971	0.000000	H	2.142021	3.207971	0.000000
D	2.174299	1.341470	0.000000	D	2.174299	1.341470	0.000000
p2a				p2b			
							
-169.2 kJ mol ⁻¹				-165.1 kJ mol ⁻¹			
$C_s^{-1}A'$				$C_1^{-1}A$			
Si	-3.530077	0.607099	0.333008	Si	-3.530077	0.607099	0.333008
C	-2.115964	1.751749	-0.167586	C	-2.115964	1.751749	-0.167586
C	-1.762971	0.449585	-0.634584	C	-1.762971	0.449585	-0.634584
C	-2.980050	2.474570	0.443216	C	-2.980050	2.474570	0.443216
D	-0.954113	-0.065250	-0.122807	H	-0.954113	-0.065250	-0.122807
D	-1.792019	0.273905	-1.706863	D	-1.792019	0.273905	-1.706863

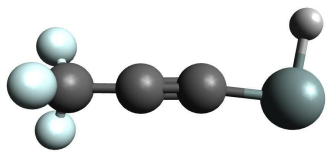
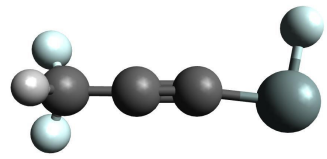
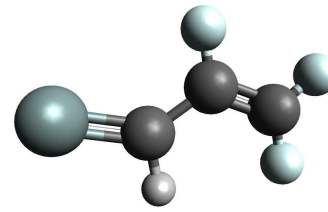
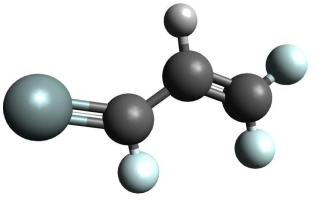
p2c				p3a			
							
-165.1 kJ mol ⁻¹				-154.0 kJ mol ⁻¹			
$C_1^{-1}A$				$C_s^{-1}A'$			
Si	-3.530077	0.607099	0.333008	Si	-1.440031	2.135965	1.571949
C	-2.115964	1.751749	-0.167586	C	-1.258585	1.493357	-0.509032
C	-1.762971	0.449585	-0.634584	C	-1.918764	2.648067	0.002796
C	-2.980050	2.474570	0.443216	C	-0.632564	0.456668	-0.644013
D	-0.954113	-0.065250	-0.122807	D	-2.429665	3.372178	-0.610959
H	-1.792019	0.273905	-1.706863	H	-0.091486	-0.444116	-0.815669
p3b				p3c			
							
-153.5 kJ mol ⁻¹				-157.0 kJ mol ⁻¹			
$C_s^{-1}A'$				$C_s^{-1}A'$			
Si	-1.440031	2.135965	1.571949	Si	-1.440031	2.135965	1.571949
C	-1.258585	1.493357	-0.509032	C	-1.258585	1.493357	-0.509032
C	-1.918764	2.648067	0.002796	C	-1.918764	2.648067	0.002796
C	-0.632564	0.456668	-0.644013	C	-0.632564	0.456668	-0.644013
H	-2.429665	3.372178	-0.610959	D	-2.429665	3.372178	-0.610959
D	-0.091486	-0.444116	-0.815669	D	-0.091486	-0.444116	-0.815669

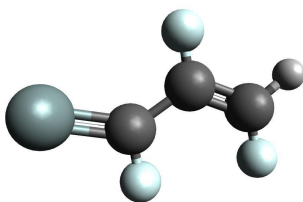
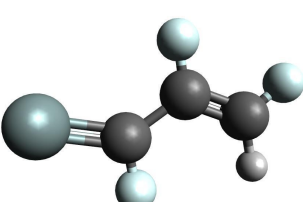
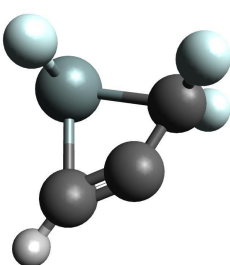
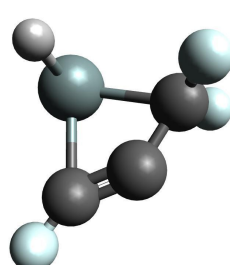
p4a				p4b			
							
-149.7 kJ mol ⁻¹				-153.1 kJ mol ⁻¹			
C ₁ ⁻¹ A				C ₂ ⁻¹ A ₁			
Si	0.015583	1.421694	0.441321	Si	0.015583	1.421694	0.441321
C	-1.710909	1.657474	1.228824	C	-1.710909	1.657474	1.228824
C	-1.833196	1.452865	-0.080188	C	-1.833196	1.452865	-0.080188
C	-1.051473	1.232997	-1.134185	C	-1.051473	1.232997	-1.134185
H	-2.213088	1.188068	2.060067	D	-2.213088	1.188068	2.060067
D	-1.030405	1.710504	-2.101157	D	-1.030405	1.710504	-2.101157
Intermediates							
[i1a]				[i1b]			
							
-381.9 kJ mol ⁻¹				-381.2 kJ mol ⁻¹			
C _s ⁻¹ A'				C ₁ ⁻¹ A			
Si	-1.656605	1.891479	-0.619303	Si	-1.656605	1.891479	-0.619303
C	-3.043502	0.820878	-0.149821	C	-3.043502	0.820878	-0.149821
C	-1.887126	0.137774	-0.160470	C	-1.887126	0.137774	-0.160470
C	-1.441882	-1.256744	0.108866	C	-1.441882	-1.256744	0.108866
D	-2.267948	-1.914363	0.393239	D	-2.267948	-1.914363	0.393239
D	-0.951711	-1.667938	-0.777728	D	-0.951711	-1.667938	-0.777728
D	-0.695679	-1.260617	0.907968	H	-0.695679	-1.260617	0.907968
H	-4.076299	0.569772	0.067786	D	-4.076299	0.569772	0.067786

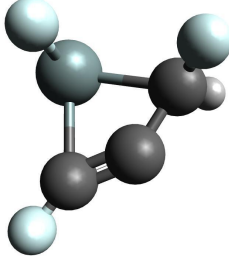
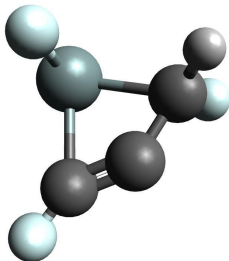
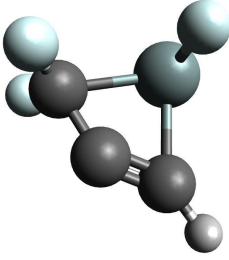
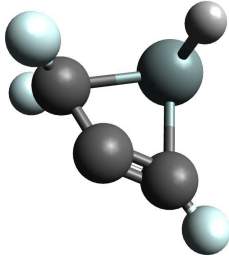
[i2a]				[i2b]			
							
-366.5 kJ mol ⁻¹				-366.5 kJ mol ⁻¹			
C ₁ ⁻¹ A				C ₁ ⁻¹ A			
Si	1.217161	2.092109	-0.478041	Si	1.217161	2.092109	-0.478041
C	-0.718085	2.105551	-0.106733	C	-0.718085	2.105551	-0.106733
C	0.896350	0.503330	0.378512	C	0.896350	0.503330	0.378512
C	-0.384938	0.659690	-0.076621	C	-0.384938	0.659690	-0.076621
D	-1.435881	2.452625	-0.849645	D	-1.435881	2.452625	-0.849645
D	-0.927003	2.520049	0.875808	D	-0.927003	2.520049	0.875808
D	-1.014639	-0.115450	-0.520096	H	-1.014639	-0.115450	-0.520096
H	1.393630	-0.440136	0.568491	D	1.393630	-0.440136	0.568491
[i2c]				i2d			
							
-366.2 kJ mol ⁻¹				-366.2 kJ mol ⁻¹			
C ₁ ⁻¹ A				C ₁ ⁻¹ A			
Si	1.217161	2.092109	-0.478041	Si	1.217161	2.092109	-0.478041
C	-0.718085	2.105551	-0.106733	C	-0.718085	2.105551	-0.106733
C	0.896350	0.503330	0.378512	C	0.896350	0.503330	0.378512
C	-0.384938	0.659690	-0.076621	C	-0.384938	0.659690	-0.076621
H	-1.435881	2.452625	-0.849645	D	-1.435881	2.452625	-0.849645
D	-0.927003	2.520049	0.875808	H	-0.927003	2.520049	0.875808
D	-1.014639	-0.115450	-0.520096	D	-1.014639	-0.115450	-0.520096
D	1.393630	-0.440136	0.568491	D	1.393630	-0.440136	0.568491

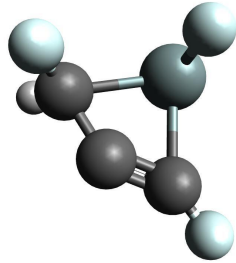
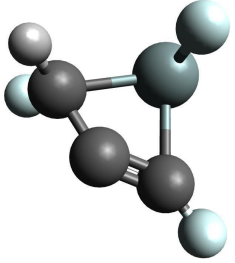
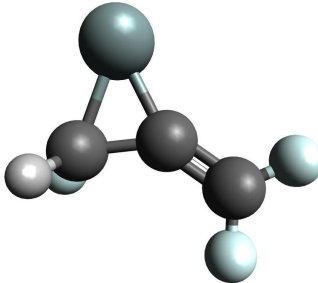
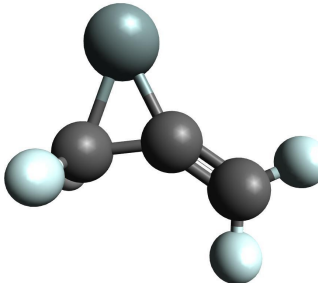
[i2e]				[i2f]			
							
-366.5 kJ mol ⁻¹				-366.5 kJ mol ⁻¹			
C ₁ ⁻¹ A				C ₁ ⁻¹ A			
Si	-1.217161	2.092109	-0.478041	Si	-1.217161	2.092109	-0.478041
C	0.718085	2.105551	-0.106733	C	0.718085	2.105551	-0.106733
C	-0.896350	0.503330	0.378512	C	-0.896350	0.503330	0.378512
C	0.384938	0.659690	-0.076621	C	0.384938	0.659690	-0.076621
D	1.435881	2.452625	-0.849645	D	1.435881	2.452625	-0.849645
D	0.927003	2.520049	0.875808	D	0.927003	2.520049	0.875808
D	1.014639	-0.115450	-0.520096	H	1.014639	-0.115450	-0.520096
H	-1.393630	-0.440136	0.568491	D	-1.393630	-0.440136	0.568491
[i2g]				[i2h]			
							
-366.2 kJ mol ⁻¹				-366.2 kJ mol ⁻¹			
C ₁ ⁻¹ A				C ₁ ⁻¹ A			
Si	-1.217161	2.092109	-0.478041	Si	-1.217161	2.092109	-0.478041
C	0.718085	2.105551	-0.106733	C	0.718085	2.105551	-0.106733
C	-0.896350	0.503330	0.378512	C	-0.896350	0.503330	0.378512
C	0.384938	0.659690	-0.076621	C	0.384938	0.659690	-0.076621
H	1.435881	2.452625	-0.849645	D	1.435881	2.452625	-0.849645
D	0.927003	2.520049	0.875808	H	0.927003	2.520049	0.875808
D	1.014639	-0.115450	-0.520096	D	1.014639	-0.115450	-0.520096
D	-1.393630	-0.440136	0.568491	D	-1.393630	-0.440136	0.568491

[i3a]				[i3b]			
							
-307.7 kJ mol ⁻¹				-307.3 kJ mol ⁻¹			
$C_1^{-1}A$				$C_s^{-1}A'$			
Si	-2.584650	2.826243	0.102164	Si	-2.584650	2.826243	0.102164
C	-1.277255	1.533566	0.133824	C	-1.277255	1.533566	0.133824
C	-2.614644	1.183903	0.928846	C	-2.614644	1.183903	0.928846
C	-1.976747	0.221766	-0.020795	C	-1.976747	0.221766	-0.020795
D	-1.488341	-0.647336	0.417639	H	-1.488341	-0.647336	0.417639
H	-2.696767	0.944785	1.983522	D	-2.696767	0.944785	1.983522
D	-2.476241	-0.001272	-0.958483	D	-2.476241	-0.001272	-0.958483
D	-0.273455	1.579469	0.542808	D	-0.273455	1.579469	0.542808
[i3c]				[i3d]			
							
-307.2 kJ kJ mol ⁻¹				-307.7 kJ mol ⁻¹			
$C_s^{-1}A'$				$C_1^{-1}A$			
Si	-2.584650	2.826243	0.102164	Si	-2.584650	2.826243	0.102164
C	-1.277255	1.533566	0.133824	C	-1.277255	1.533566	0.133824
C	-2.614644	1.183903	0.928846	C	-2.614644	1.183903	0.928846
C	-1.976747	0.221766	-0.020795	C	-1.976747	0.221766	-0.020795
D	-1.488341	-0.647336	0.417639	D	-1.488341	-0.647336	0.417639
D	-2.696767	0.944785	1.983522	D	-2.696767	0.944785	1.983522
H	-2.476241	-0.001272	-0.958483	D	-2.476241	-0.001272	-0.958483
D	-0.273455	1.579469	0.542808	H	-0.273455	1.579469	0.542808

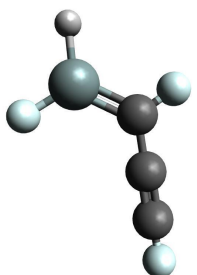
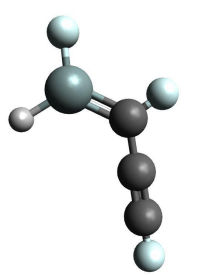
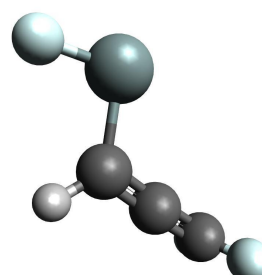
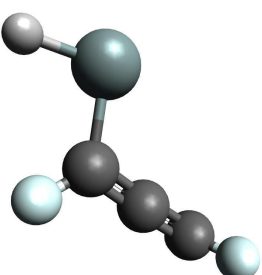
[i4a]				[i4b]			
							
-306.4 kJ mol ⁻¹				-302.8 kJ mol ⁻¹			
C ₁ ⁻¹ A				C ₁ ⁻¹ A			
Si	2.269227	0.314672	0.012013	Si	2.269227	0.314672	0.012013
C	0.446698	0.519161	0.002884	C	0.446698	0.519161	0.002884
C	-0.767059	0.515702	-0.005318	C	-0.767059	0.515702	-0.005318
C	-2.225868	0.529673	-0.008062	C	-2.225868	0.529673	-0.008062
H	2.557659	1.810564	-0.006117	D	2.557659	1.810564	-0.006117
D	-2.625510	-0.364956	-0.490733	D	-2.625510	-0.364956	-0.490733
D	-2.607844	1.412410	-0.525637	D	-2.607844	1.412410	-0.525637
D	-2.593502	0.553573	1.020967	H	-2.593502	0.553573	1.020967
[i5a]				[i5b]			
							
-305.2 kJ mol ⁻¹				-304.1 kJ mol ⁻¹			
C _s ⁻¹ A'				C _s ⁻¹ A'			
Si	-2.791074	1.331229	0.575045	Si	-2.791074	1.331229	0.575045
C	0.041883	1.957213	0.098223	C	0.041883	1.957213	0.098223
C	1.276133	1.530665	-0.176961	C	1.276133	1.530665	-0.176961
C	-1.134334	1.101465	0.199981	C	-1.134334	1.101465	0.199981
D	-0.109806	3.022058	0.263830	H	-0.109806	3.022058	0.263830
D	2.111404	2.219175	-0.232581	D	2.111404	2.219175	-0.232581
D	1.481749	0.478866	-0.350967	D	1.481749	0.478866	-0.350967
H	-0.944290	0.035021	0.000428	D	-0.944290	0.035021	0.000428

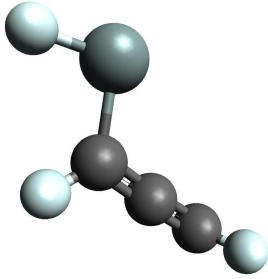
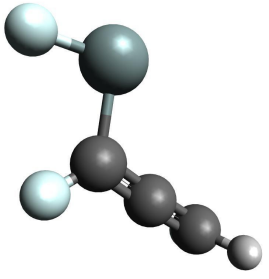
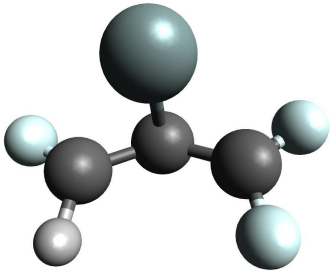
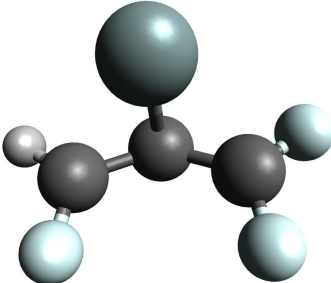
[i5c]				[i5d]			
							
-304.3 kJ mol ⁻¹				-304.4 kJ mol ⁻¹			
C _s ⁻¹ A'				C _s ⁻¹ A'			
Si	-2.791074	1.331229	0.575045	Si	-2.791074	1.331229	0.575045
C	0.041883	1.957213	0.098223	C	0.041883	1.957213	0.098223
C	1.276133	1.530665	-0.176961	C	1.276133	1.530665	-0.176961
C	-1.134334	1.101465	0.199981	C	-1.134334	1.101465	0.199981
D	-0.109806	3.022058	0.263830	D	-0.109806	3.022058	0.263830
H	2.111404	2.219175	-0.232581	D	2.111404	2.219175	-0.232581
D	1.481749	0.478866	-0.350967	H	1.481749	0.478866	-0.350967
D	-0.944290	0.035021	0.000428	D	-0.944290	0.035021	0.000428
[i6a]				[i6b]			
							
-299.6 kJ mol ⁻¹				-301.5 kJ mol ⁻¹			
C ₁ ⁻¹ A				C ₁ ⁻¹ A			
Si	1.271276	2.401422	0.597200	Si	1.271276	2.401422	0.597200
C	-0.676445	2.076496	-0.045615	C	-0.676445	2.076496	-0.045615
C	1.201685	0.439514	-0.022520	C	1.201685	0.439514	-0.022520
C	0.071228	0.921046	-0.285832	C	0.071228	0.921046	-0.285832
D	1.712703	2.984364	-0.742591	H	1.712703	2.984364	-0.742591
D	-0.965219	2.689118	-0.894417	D	-0.965219	2.689118	-0.894417
D	-1.396336	2.031078	0.765002	D	-1.396336	2.031078	0.765002
H	1.843949	-0.418828	-0.047808	D	1.843949	-0.418828	-0.047808

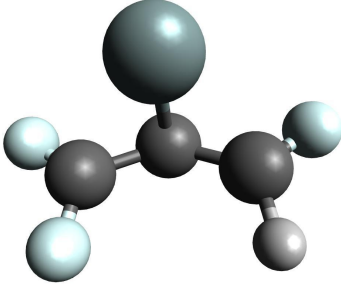
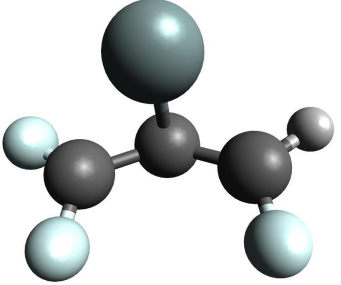
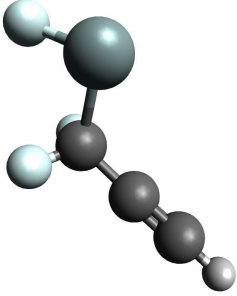
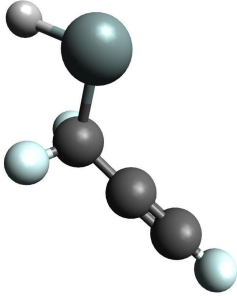
[i6c]				[i6d]			
							
-298.9 kJ mol ⁻¹				-299.0 kJ mol ⁻¹			
C ₁ ⁻¹ A				C ₁ ⁻¹ A			
Si	1.271276	2.401422	0.597200	Si	1.271276	2.401422	0.597200
C	-0.676445	2.076496	-0.045615	C	-0.676445	2.076496	-0.045615
C	1.201685	0.439514	-0.022520	C	1.201685	0.439514	-0.022520
C	0.071228	0.921046	-0.285832	C	0.071228	0.921046	-0.285832
D	1.712703	2.984364	-0.742591	D	1.712703	2.984364	-0.742591
D	-0.965219	2.689118	-0.894417	H	-0.965219	2.689118	-0.894417
H	-1.396336	2.031078	0.765002	D	-1.396336	2.031078	0.765002
D	1.843949	-0.418828	-0.047808	D	1.843949	-0.418828	-0.047808
[i6e]				[i6f]			
							
-299.6 kJ mol ⁻¹				-301.5 kJ mol ⁻¹			
C ₁ ⁻¹ A				C ₁ ⁻¹ A			
Si	-1.271276	2.401422	0.597200	Si	-1.271276	2.401422	0.597200
C	0.676445	2.076496	-0.045615	C	0.676445	2.076496	-0.045615
C	-1.201685	0.439514	-0.022520	C	-1.201685	0.439514	-0.022520
C	-0.071228	0.921046	-0.285832	C	-0.071228	0.921046	-0.285832
D	-1.712703	2.984364	-0.742591	H	-1.712703	2.984364	-0.742591
D	0.965219	2.689118	-0.894417	D	0.965219	2.689118	-0.894417
D	1.396336	2.031078	0.765002	D	1.396336	2.031078	0.765002
H	-1.843949	-0.418828	-0.047808	D	-1.843949	-0.418828	-0.047808

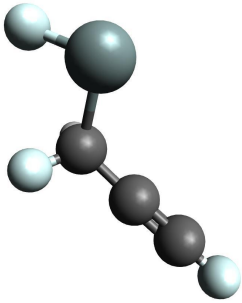
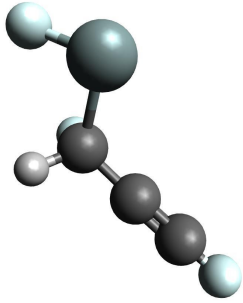
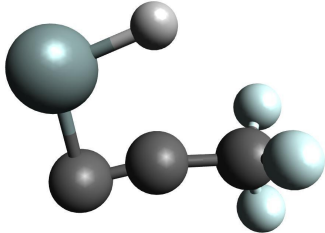
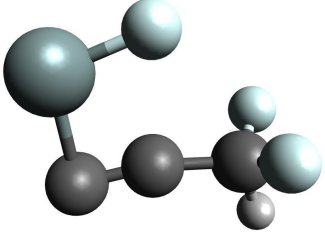
[i6g]				[i6h]			
							
-298.9 kJ mol ⁻¹				-299.0 kJ mol ⁻¹			
C ₁ ⁻¹ A				C ₁ ⁻¹ A			
Si	-1.271276	2.401422	0.597200	Si	-1.271276	2.401422	0.597200
C	0.676445	2.076496	-0.045615	C	0.676445	2.076496	-0.045615
C	-1.201685	0.439514	-0.022520	C	-1.201685	0.439514	-0.022520
C	-0.071228	0.921046	-0.285832	C	-0.071228	0.921046	-0.285832
D	-1.712703	2.984364	-0.742591	D	-1.712703	2.984364	-0.742591
D	0.965219	2.689118	-0.894417	H	0.965219	2.689118	-0.894417
H	1.396336	2.031078	0.765002	D	1.396336	2.031078	0.765002
D	-1.843949	-0.418828	-0.047808	D	-1.843949	-0.418828	-0.047808
[i7a]				[i7b]			
							
-291.2 kJ mol ⁻¹				-291.2 kJ mol ⁻¹			
C ₁ ⁻¹ A				C ₁ ⁻¹ A			
Si	-0.002314	3.177910	-0.169760	Si	-0.002314	3.177910	-0.169760
C	-0.649663	1.369072	-0.142375	C	-0.649663	1.369072	-0.142375
C	0.826543	1.531957	-0.066304	C	0.826543	1.531957	-0.066304
C	1.909821	0.771693	0.020207	C	1.909821	0.771693	0.020207
D	-1.073424	0.953192	-1.057167	H	-1.073424	0.953192	-1.057167
H	-1.173338	1.016264	0.746817	D	-1.173338	1.016264	0.746817
D	1.853963	-0.315790	0.055069	D	1.853963	-0.315790	0.055069
D	2.902621	1.211905	0.059823	D	2.902621	1.211905	0.059823

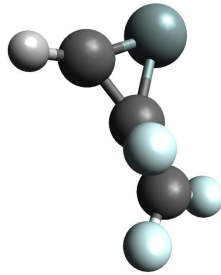
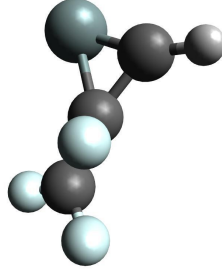
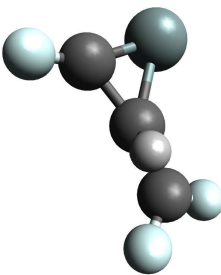
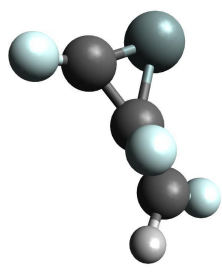
[i7c]				[i7d]			
-290.9 kJ mol ⁻¹				-291.1 kJ mol ⁻¹			
C _s ⁻¹ A'				C _s ⁻¹ A'			
Si	-0.002314	3.177910	-0.169760	Si	-0.002314	3.177910	-0.169760
C	-0.649663	1.369072	-0.142375	C	-0.649663	1.369072	-0.142375
C	0.826543	1.531957	-0.066304	C	0.826543	1.531957	-0.066304
C	1.909821	0.771693	0.020207	C	1.909821	0.771693	0.020207
D	-1.073424	0.953192	-1.057167	D	-1.073424	0.953192	-1.057167
D	-1.173338	1.016264	0.746817	D	-1.173338	1.016264	0.746817
D	1.853963	-0.315790	0.055069	H	1.853963	-0.315790	0.055069
H	2.902621	1.211905	0.059823	D	2.902621	1.211905	0.059823
[i8a]				[i8b]			
-275.2 kJ mol ⁻¹				-274.7 kJ mol ⁻¹			
C _s ⁻¹ A'				C _s ⁻¹ A'			
Si	-2.123430	2.732956	0.435983	Si	-2.123430	2.732956	0.435983
C	-0.578881	1.995631	0.420032	C	-0.578881	1.995631	0.420032
C	-0.360326	0.594266	0.333811	C	-0.360326	0.594266	0.333811
C	-0.179590	-0.593207	0.258429	C	-0.179590	-0.593207	0.258429
D	-2.265622	4.199834	0.528920	D	-2.265622	4.199834	0.528920
D	-3.379454	1.961598	0.360797	D	-3.379454	1.961598	0.360797
D	0.306230	2.623143	0.479257	H	0.306230	2.623143	0.479257
H	-0.015456	-1.642789	0.191810	D	-0.015456	-1.642789	0.191810

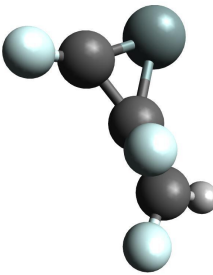
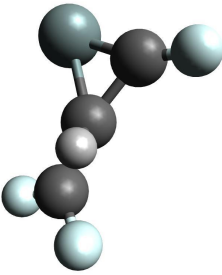
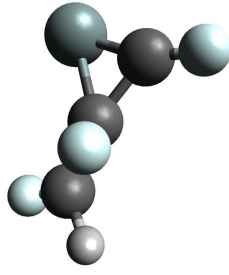
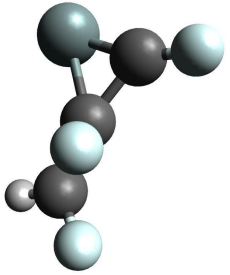
[i8c]				[i8d]			
							
-276.8 kJ mol ⁻¹				-276.9 kJ mol ⁻¹			
$C_s^{-1}A'$				$C_s^{-1}A'$			
Si	-2.123430	2.732956	0.435983	Si	-2.123430	2.732956	0.435983
C	-0.578881	1.995631	0.420032	C	-0.578881	1.995631	0.420032
C	-0.360326	0.594266	0.333811	C	-0.360326	0.594266	0.333811
C	-0.179590	-0.593207	0.258429	C	-0.179590	-0.593207	0.258429
H	-2.265622	4.199834	0.528920	D	-2.265622	4.199834	0.528920
D	-3.379454	1.961598	0.360797	H	-3.379454	1.961598	0.360797
D	0.306230	2.623143	0.479257	D	0.306230	2.623143	0.479257
D	-0.015456	-1.642789	0.191810	D	-0.015456	-1.642789	0.191810
[i9a]				[i9b]			
							
-275.3 kJ mol ⁻¹				-278.3 kJ mol ⁻¹			
$C_s^{-1}A'$				$C_s^{-1}A'$			
Si	-0.948677	2.863727	0.654535	Si	-0.948677	2.863727	0.654535
C	-1.217505	1.006333	0.704275	C	-1.217505	1.006333	0.704275
C	-0.284681	0.271592	0.142353	C	-0.284681	0.271592	0.142353
C	0.670871	-0.400535	-0.428995	C	0.670871	-0.400535	-0.428995
D	-2.235815	3.206243	1.405402	H	-2.235815	3.206243	1.405402
H	-2.068992	0.501898	1.155645	D	-2.068992	0.501898	1.155645
D	1.531568	-0.731501	0.140907	D	1.531568	-0.731501	0.140907
D	0.619686	-0.645957	-1.483673	D	0.619686	-0.645957	-1.483673

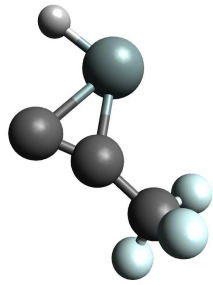
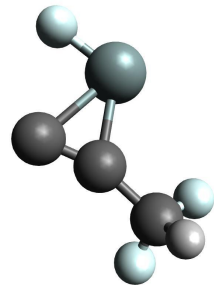
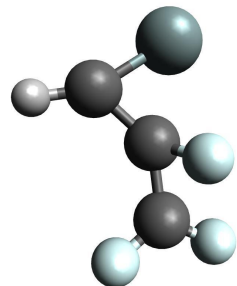
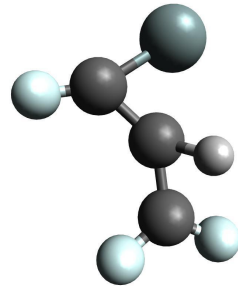
[i9c]				[i9d]			
							
-275.4 kJ mol ⁻¹				-275.4 kJ mol ⁻¹			
C ₁ ⁻¹ A				C ₁ ⁻¹ A			
Si	-0.948677	2.863727	0.654535	Si	-0.948677	2.863727	0.654535
C	-1.217505	1.006333	0.704275	C	-1.217505	1.006333	0.704275
C	-0.284681	0.271592	0.142353	C	-0.284681	0.271592	0.142353
C	0.670871	-0.400535	-0.428995	C	0.670871	-0.400535	-0.428995
D	-2.235815	3.206243	1.405402	D	-2.235815	3.206243	1.405402
D	-2.068992	0.501898	1.155645	D	-2.068992	0.501898	1.155645
D	1.531568	-0.731501	0.140907	H	1.531568	-0.731501	0.140907
H	0.619686	-0.645957	-1.483673	D	0.619686	-0.645957	-1.483673
[i10a]				[i10b]			
							
-277.4 kJ mol ⁻¹				-277.1 kJ mol ⁻¹			
C ₁ ⁻¹ A				C ₁ ⁻¹ A			
Si	-0.333163	1.486867	-0.671031	Si	-0.333163	1.486867	-0.671031
C	-0.144820	0.334917	0.683483	C	-0.144820	0.334917	0.683483
C	-1.419478	-0.081122	0.274337	C	-1.419478	-0.081122	0.274337
C	1.062694	0.035706	0.040856	C	1.062694	0.035706	0.040856
H	-1.610019	-1.027212	-0.240233	D	-1.610019	-1.027212	-0.240233
D	-2.282879	0.366410	0.756404	H	-2.282879	0.366410	0.756404
D	1.241688	-0.893852	-0.506956	D	1.241688	-0.893852	-0.506956
D	1.954699	0.571689	0.349342	D	1.954699	0.571689	0.349342

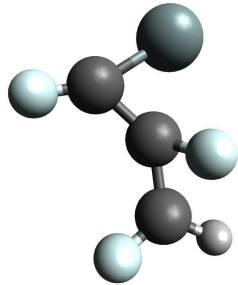
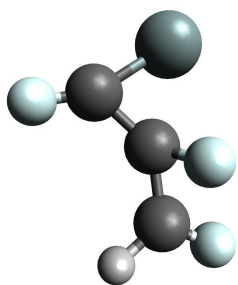
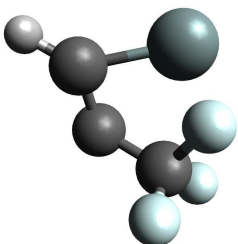
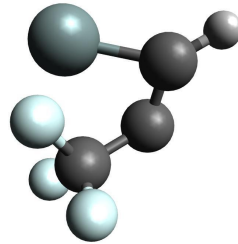
[i10c]				[i10d]			
							
-277.4 kJ mol ⁻¹				-277.1 kJ mol ⁻¹			
C ₁ ⁻¹ A				C ₁ ⁻¹ A			
Si	-0.333163	1.486867	-0.671031	Si	-0.333163	1.486867	-0.671031
C	-0.144820	0.334917	0.683483	C	-0.144820	0.334917	0.683483
C	-1.419478	-0.081122	0.274337	C	-1.419478	-0.081122	0.274337
C	1.062694	0.035706	0.040856	C	1.062694	0.035706	0.040856
D	-1.610019	-1.027212	-0.240233	D	-1.610019	-1.027212	-0.240233
D	-2.282879	0.366410	0.756404	D	-2.282879	0.366410	0.756404
H	1.241688	-0.893852	-0.506956	D	1.241688	-0.893852	-0.506956
D	1.954699	0.571689	0.349342	H	1.954699	0.571689	0.349342
[i12a]				[i12b]			
							
-244.3 kJ mol ⁻¹				-246.7 kJ mol ⁻¹			
C _s ⁻¹ A'				C _s ⁻¹ A'			
Si	-0.980308	2.921623	1.046459	Si	-0.980308	2.921623	1.046459
C	-1.407690	1.314359	0.084885	C	-1.407690	1.314359	0.084885
C	-0.359350	0.302722	0.082071	C	-0.359350	0.302722	0.082071
C	0.531367	-0.500595	0.106582	C	0.531367	-0.500595	0.106582
D	-2.336725	3.551344	0.727266	H	-2.336725	3.551344	0.727266
D	-1.671387	1.607227	-0.940700	D	-1.671387	1.607227	-0.940700
D	-2.336671	0.913777	0.513390	D	-2.336671	0.913777	0.513390
H	1.315662	-1.220461	0.122189	D	1.315662	-1.220461	0.122189

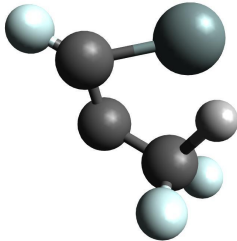
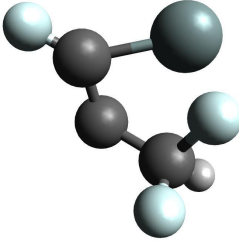
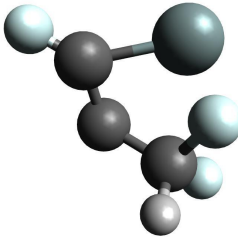
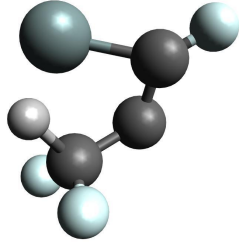
[i12c]				[i12d]			
							
-243.7 kJ mol ⁻¹				-243.7 kJ mol ⁻¹			
C ₁ ⁻¹ A				C ₁ ⁻¹ A			
Si	-0.980308	2.921623	1.046459	Si	-0.980308	2.921623	1.046459
C	-1.407690	1.314359	0.084885	C	-1.407690	1.314359	0.084885
C	-0.359350	0.302722	0.082071	C	-0.359350	0.302722	0.082071
C	0.531367	-0.500595	0.106582	C	0.531367	-0.500595	0.106582
D	-2.336725	3.551344	0.727266	D	-2.336725	3.551344	0.727266
H	-1.671387	1.607227	-0.940700	D	-1.671387	1.607227	-0.940700
D	-2.336671	0.913777	0.513390	H	-2.336671	0.913777	0.513390
D	1.315662	-1.220461	0.122189	D	1.315662	-1.220461	0.122189
[i13a]				[i13b]			
							
-224.2 kJ mol ⁻¹				-220.8 kJ mol ⁻¹			
C _s ⁻¹ A'				C _s ⁻¹ A'			
Si	-1.688737	2.624682	0.616789	Si	-1.688737	2.624682	0.616789
C	-0.244907	1.218317	-0.220340	C	-0.244907	1.218317	-0.220340
C	1.218639	1.272651	-0.343790	C	1.218639	1.272651	-0.343790
C	-1.465384	0.927557	-0.237325	C	-1.465384	0.927557	-0.237325
H	-0.260660	3.204713	0.754427	D	-0.260660	3.204713	0.754427
D	1.524821	2.129620	-0.945098	D	1.524821	2.129620	-0.945098
D	1.687125	1.351436	0.638071	D	1.687125	1.351436	0.638071
D	1.564998	0.357273	-0.829223	H	1.564998	0.357273	-0.829223

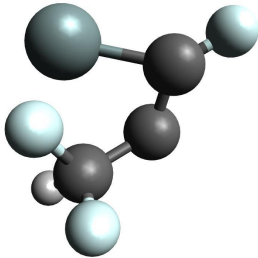
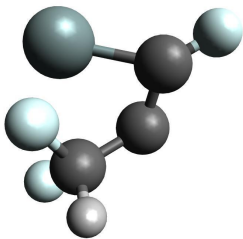
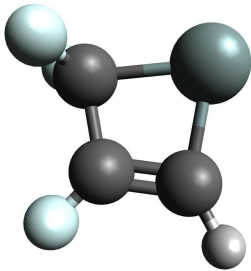
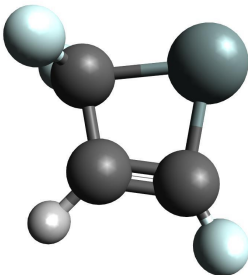
Transition State Structures											
[i1a]→[i2a]					[i1a]→[i2e]						
											
-75.0 kJ mol ⁻¹					-75.0 kJ mol ⁻¹						
C ₁ ⁻¹ A					C ₁ ⁻¹ A						
Si	0.387656	1.918057	-0.868165	Si	-0.387656	1.918057	-0.868165	Si	0.387656	1.918057	-0.868165
C	0.507204	-1.109474	-0.273582	C	-0.507204	-1.109474	-0.273582	C	0.507204	-1.109474	-0.273582
C	-0.001009	0.171130	-0.093798	C	0.001009	0.171130	-0.093798	C	-0.001009	0.171130	-0.093798
C	-0.892669	1.297958	0.108223	C	0.892669	1.297958	0.108223	C	-0.892669	1.297958	0.108223
D	1.347937	-1.296852	-0.939211	D	-1.347937	-1.296852	-0.939211	D	1.347937	-1.296852	-0.939211
D	0.177136	-0.265142	0.972772	D	-0.177136	-0.265142	0.972772	D	0.177136	-0.265142	0.972772
D	0.170559	-1.954642	0.325094	D	-0.170559	-1.954642	0.325094	D	0.170559	-1.954642	0.325094
H	-1.765240	1.299326	0.746709	H	1.765240	1.299326	0.746709	H	-1.765240	1.299326	0.746709
[i1b]→[i2b]					[i2b]→[i2c]						
											
-76.5 kJ mol ⁻¹					-74.7 kJ mol ⁻¹						
C ₁ ⁻¹ A					C ₁ ⁻¹ A						
Si	0.387656	1.918057	-0.868165	Si	0.387656	1.918057	-0.868165	Si	0.387656	1.918057	-0.868165
C	0.507204	-1.109474	-0.273582	C	0.507204	-1.109474	-0.273582	C	0.507204	-1.109474	-0.273582
C	-0.001009	0.171130	-0.093798	C	-0.001009	0.171130	-0.093798	C	-0.001009	0.171130	-0.093798
C	-0.892669	1.297958	0.108223	C	-0.892669	1.297958	0.108223	C	-0.892669	1.297958	0.108223
D	1.347937	-1.296852	-0.939211	D	1.347937	-1.296852	-0.939211	D	1.347937	-1.296852	-0.939211
H	0.177136	-0.265142	0.972772	D	0.177136	-0.265142	0.972772	D	0.177136	-0.265142	0.972772
D	0.170559	-1.954642	0.325094	H	0.170559	-1.954642	0.325094	H	0.170559	-1.954642	0.325094
D	-1.765240	1.299326	0.746709	D	-1.765240	1.299326	0.746709	D	-1.765240	1.299326	0.746709

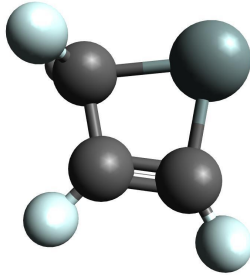
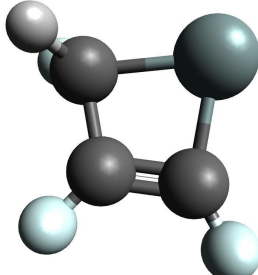
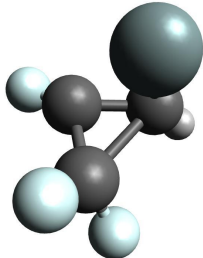
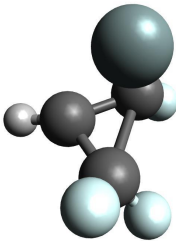
[i1b]→[i2d]				[i1b]→[i2f]			
							
-74.5 kJ mol ⁻¹				-76.5 kJ mol ⁻¹			
C ₁ ⁻¹ A				C ₁ ⁻¹ A			
Si	0.387656	1.918057	-0.868165	Si	-0.387656	1.918057	-0.868165
C	0.507204	-1.109474	-0.273582	C	-0.507204	-1.109474	-0.273582
C	-0.001009	0.171130	-0.093798	C	0.001009	0.171130	-0.093798
C	-0.892669	1.297958	0.108223	C	0.892669	1.297958	0.108223
H	1.347937	-1.296852	-0.939211	D	-1.347937	-1.296852	-0.939211
D	0.177136	-0.265142	0.972772	H	-0.177136	-0.265142	0.972772
D	0.170559	-1.954642	0.325094	D	-0.170559	-1.954642	0.325094
D	-1.765240	1.299326	0.746709	D	1.765240	1.299326	0.746709
[i1b]→[i2g]				[i1b]→[i2h]			
							
-74.7 kJ mol ⁻¹				-74.5 kJ mol ⁻¹			
C ₁ ⁻¹ A				C ₁ ⁻¹ A			
Si	-0.387656	1.918057	-0.868165	Si	-0.387656	1.918057	-0.868165
C	-0.507204	-1.109474	-0.273582	C	-0.507204	-1.109474	-0.273582
C	0.001009	0.171130	-0.093798	C	0.001009	0.171130	-0.093798
C	0.892669	1.297958	0.108223	C	0.892669	1.297958	0.108223
D	-1.347937	-1.296852	-0.939211	H	-1.347937	-1.296852	-0.939211
D	-0.177136	-0.265142	0.972772	D	-0.177136	-0.265142	0.972772
H	-0.170559	-1.954642	0.325094	D	-0.170559	-1.954642	0.325094
D	1.765240	1.299326	0.746709	D	1.765240	1.299326	0.746709

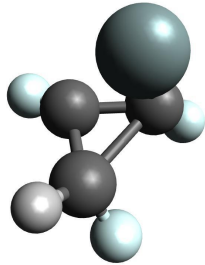
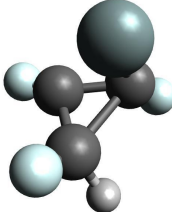
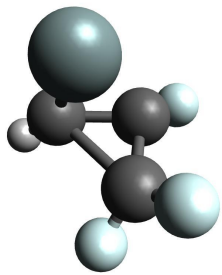
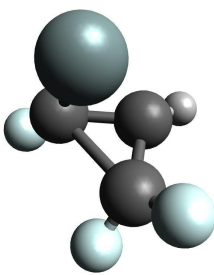
[i1a]→[i4a]				[i1b]→[i4b]			
							
-194.4 kJ mol ⁻¹				-190.8 kJ mol ⁻¹			
C ₁ ⁻¹ A				C ₁ ⁻¹ A			
Si	-2.122577	1.493357	-0.465731	Si	-2.122577	1.493357	-0.465731
C	-3.577778	0.142016	0.174868	C	-3.577778	0.142016	0.174868
C	-2.426216	-0.379803	0.065365	C	-2.426216	-0.379803	0.065365
C	-1.341337	-1.393100	0.060616	C	-1.341337	-1.393100	0.060616
D	-1.737882	-2.337896	-0.315266	D	-1.737882	-2.337896	-0.315266
D	-0.507637	-1.078652	-0.566987	D	-0.507637	-1.078652	-0.566987
D	-0.973850	-1.547956	1.076886	H	-0.973850	-1.547956	1.076886
H	-3.309526	2.412152	-0.373543	D	-3.309526	2.412152	-0.373543
[i1a]→[i5a]				[i1b]→[i5b]			
							
-140.2 kJ mol ⁻¹				-141.9 kJ mol ⁻¹			
C ₁ ⁻¹ A				C ₁ ⁻¹ A			
Si	0.485782	2.153579	-0.469008	Si	0.485782	2.153579	-0.469008
C	0.332198	-1.132452	-0.095064	C	0.332198	-1.132452	-0.095064
C	0.161878	0.240941	-0.155304	C	0.161878	0.240941	-0.155304
C	-0.869881	1.190140	0.041691	C	-0.869881	1.190140	0.041691
D	1.058802	-0.010869	0.587659	H	1.058802	-0.010869	0.587659
D	-0.474833	-1.810179	0.181935	D	-0.474833	-1.810179	0.181935
D	1.295799	-1.572078	-0.331053	D	1.295799	-1.572078	-0.331053
H	-1.919433	1.016042	0.235748	D	-1.919433	1.016042	0.235748

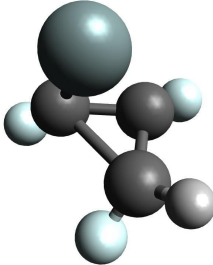
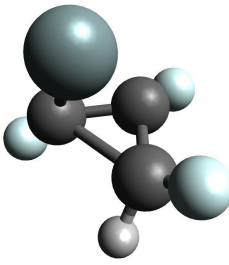
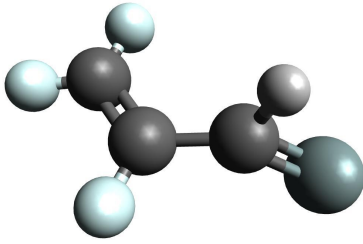
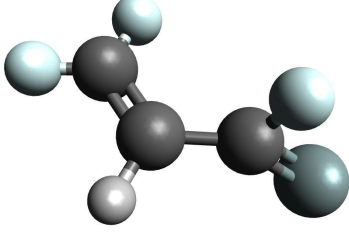
[i1b]→[i5c]				[i1b]→[i5d]			
							
-139.5 kJ mol ⁻¹				-139.8 kJ mol ⁻¹			
C ₁ ⁻¹ A				C ₁ ⁻¹ A			
Si	0.485782	2.153579	-0.469008	Si	0.485782	2.153579	-0.469008
C	0.332198	-1.132452	-0.095064	C	0.332198	-1.132452	-0.095064
C	0.161878	0.240941	-0.155304	C	0.161878	0.240941	-0.155304
C	-0.869881	1.190140	0.041691	C	-0.869881	1.190140	0.041691
D	1.058802	-0.010869	0.587659	D	1.058802	-0.010869	0.587659
D	-0.474833	-1.810179	0.181935	H	-0.474833	-1.810179	0.181935
H	1.295799	-1.572078	-0.331053	D	1.295799	-1.572078	-0.331053
D	-1.919433	1.016042	0.235748	D	-1.919433	1.016042	0.235748
[i1a]→[i6a]				[i1a]→[i6e]			
							
-122.9 kJ mol ⁻¹				-122.9 kJ mol ⁻¹			
C ₁ ⁻¹ A				C ₁ ⁻¹ A			
Si	0.778035	1.356341	0.013393	Si	-0.778035	1.356341	0.013393
C	-1.041349	0.972089	0.089159	C	1.041349	0.972089	0.089159
C	-0.726348	-0.144886	-0.571048	C	0.726348	-0.144886	-0.571048
C	0.465469	-0.839573	-0.180070	C	-0.465469	-0.839573	-0.180070
D	0.248932	-1.572742	0.597463	D	-0.248932	-1.572742	0.597463
D	1.180352	-1.204148	-0.916275	D	-1.180352	-1.204148	-0.916275
D	1.081984	-0.069503	0.844891	D	-1.081984	-0.069503	0.844891
H	-1.980789	1.508295	0.137363	H	1.980789	1.508295	0.137363

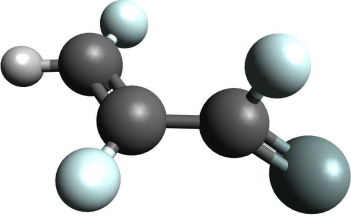
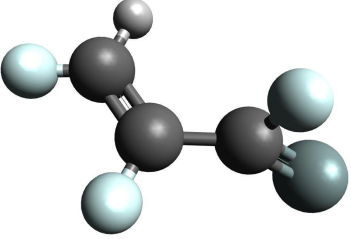
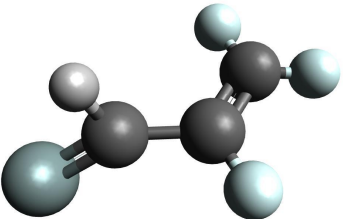
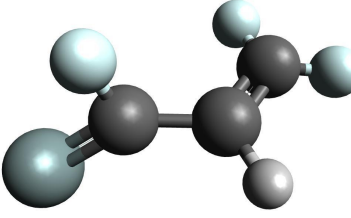
[i1b]→[i6b]				[i1b]→[i6c]			
							
-125.8 kJ mol ⁻¹				-122.4 kJ mol ⁻¹			
C ₁ ⁻¹ A				C ₁ ⁻¹ A			
Si	0.778035	1.356341	0.013393	Si	0.778035	1.356341	0.013393
C	-1.041349	0.972089	0.089159	C	-1.041349	0.972089	0.089159
C	-0.726348	-0.144886	-0.571048	C	-0.726348	-0.144886	-0.571048
C	0.465469	-0.839573	-0.180070	C	0.465469	-0.839573	-0.180070
D	0.248932	-1.572742	0.597463	D	0.248932	-1.572742	0.597463
D	1.180352	-1.204148	-0.916275	H	1.180352	-1.204148	-0.916275
H	1.081984	-0.069503	0.844891	D	1.081984	-0.069503	0.844891
D	-1.980789	1.508295	0.137363	D	-1.980789	1.508295	0.137363
[i1b]→[i6d]				[i1b]→[i6f]			
							
-122.4 kJ mol ⁻¹				-125.8 kJ mol ⁻¹			
C ₁ ⁻¹ A				C ₁ ⁻¹ A			
Si	0.778035	1.356341	0.013393	Si	-0.778035	1.356341	0.013393
C	-1.041349	0.972089	0.089159	C	1.041349	0.972089	0.089159
C	-0.726348	-0.144886	-0.571048	C	0.726348	-0.144886	-0.571048
C	0.465469	-0.839573	-0.180070	C	-0.465469	-0.839573	-0.180070
H	0.248932	-1.572742	0.597463	D	-0.248932	-1.572742	0.597463
D	1.180352	-1.204148	-0.916275	D	-1.180352	-1.204148	-0.916275
D	1.081984	-0.069503	0.844891	H	-1.081984	-0.069503	0.844891
D	-1.980789	1.508295	0.137363	D	1.980789	1.508295	0.137363

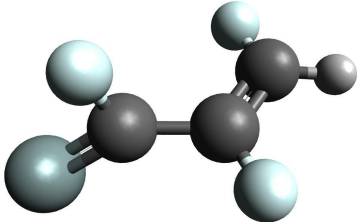
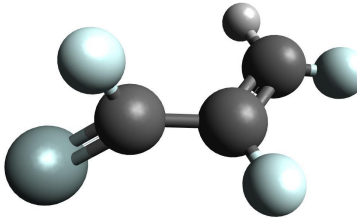
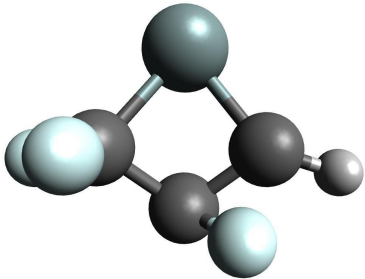
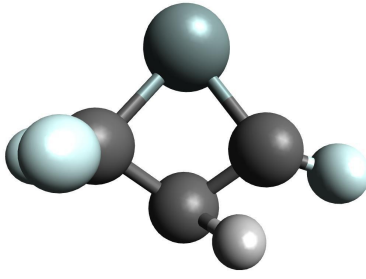
[i1b]→[i6g]				[i1b]→[i6h]			
							
-122.4 kJ mol ⁻¹				-122.4 kJ mol ⁻¹			
C ₁ ⁻¹ A				C ₁ ⁻¹ A			
Si	-0.778035	1.356341	0.013393	Si	-0.778035	1.356341	0.013393
C	1.041349	0.972089	0.089159	C	1.041349	0.972089	0.089159
C	0.726348	-0.144886	-0.571048	C	0.726348	-0.144886	-0.571048
C	-0.465469	-0.839573	-0.180070	C	-0.465469	-0.839573	-0.180070
D	-0.248932	-1.572742	0.597463	H	-0.248932	-1.572742	0.597463
H	-1.180352	-1.204148	-0.916275	D	-1.180352	-1.204148	-0.916275
D	-1.081984	-0.069503	0.844891	D	-1.081984	-0.069503	0.844891
D	1.980789	1.508295	0.137363	D	1.980789	1.508295	0.137363
[i2a]→[i2e]				[i2b]→[i2f]			
							
-343.8 kJ mol ⁻¹				-344.1 kJ mol ⁻¹			
C _s ⁻¹ A'				C _s ⁻¹ A'			
Si	1.278722	2.298406	-0.055446	Si	1.278722	2.298406	-0.055446
C	-0.670175	2.114670	-0.122843	C	-0.670175	2.114670	-0.122843
C	0.931362	0.457675	0.076046	C	0.931362	0.457675	0.076046
C	-0.403313	0.629572	0.008121	C	-0.403313	0.629572	0.008121
D	-1.163674	2.406338	-1.054805	D	-1.163674	2.406338	-1.054805
D	-1.238437	2.548998	0.705255	D	-1.238437	2.548998	0.705255
D	-1.174293	-0.147915	0.038856	H	-1.174293	-0.147915	0.038856
H	1.448755	-0.490942	0.172710	D	1.448755	-0.490942	0.172710

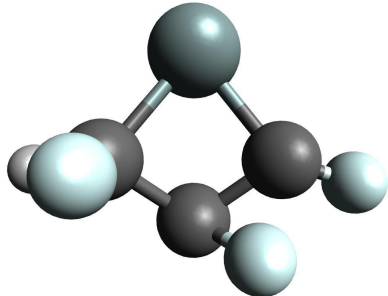
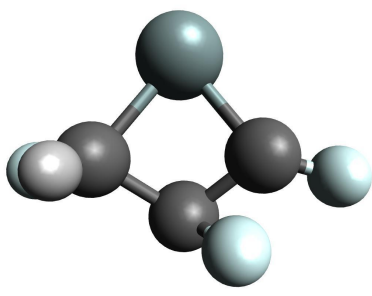
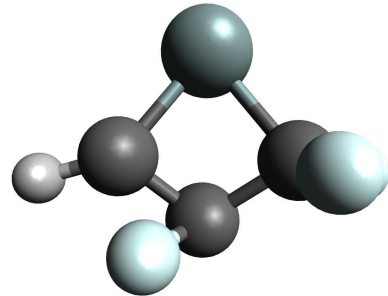
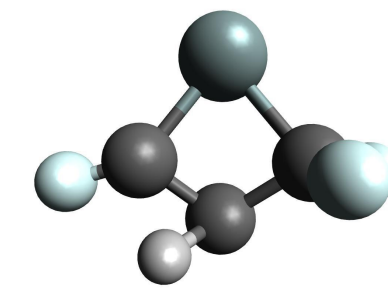
[i2c]→[i2h]				[i2d]→[i2g]			
							
-343.7 kJ mol ⁻¹				-343.7 kJ mol ⁻¹			
C ₁ ⁻¹ A				C ₁ ⁻¹ A			
Si	1.278722	2.298406	-0.055446	Si	1.278722	2.298406	-0.055446
C	-0.670175	2.114670	-0.122843	C	-0.670175	2.114670	-0.122843
C	0.931362	0.457675	0.076046	C	0.931362	0.457675	0.076046
C	-0.403313	0.629572	0.008121	C	-0.403313	0.629572	0.008121
H	-1.163674	2.406338	-1.054805	D	-1.163674	2.406338	-1.054805
D	-1.238437	2.548998	0.705255	H	-1.238437	2.548998	0.705255
D	-1.174293	-0.147915	0.038856	D	-1.174293	-0.147915	0.038856
D	1.448755	-0.490942	0.172710	D	1.448755	-0.490942	0.172710
[i2a]→[i3a]				[i2b]→[i3d]			
							
-187.7 kJ mol ⁻¹				-187.3 kJ mol ⁻¹			
C ₁ ⁻¹ A				C ₁ ⁻¹ A			
Si	-2.150053	2.178667	0.625370	Si	-2.150053	2.178667	0.625370
C	-0.578457	1.585315	-0.456669	C	-0.578457	1.585315	-0.456669
C	-1.232877	0.355972	-0.039025	C	-1.232877	0.355972	-0.039025
C	-0.432102	1.821019	0.963102	C	-0.432102	1.821019	0.963102
H	0.445188	1.756078	1.604662	D	0.445188	1.756078	1.604662
D	0.020532	1.864829	-1.311772	H	0.020532	1.864829	-1.311772
D	-0.716789	-0.405155	0.544939	D	-0.716789	-0.405155	0.544939
D	-2.145988	-0.008539	-0.518207	D	-2.145988	-0.008539	-0.518207

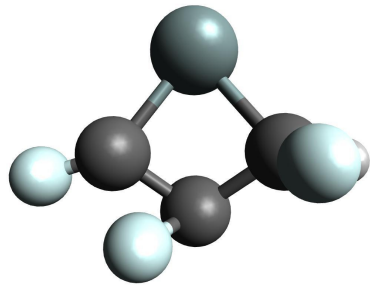
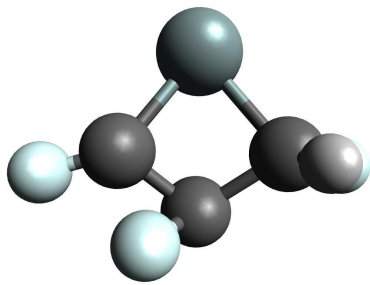
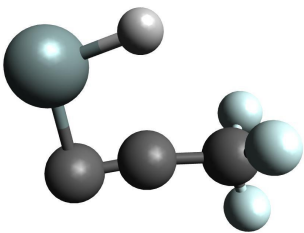
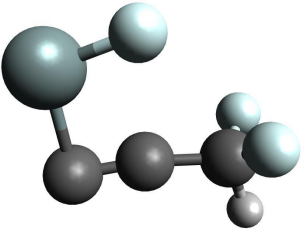
[i2c]→[i3c]				[i2d]→[i3b]			
							
-187.5 kJ mol ⁻¹				-187.0 kJ mol ⁻¹			
C ₁ ⁻¹ A				C ₁ ⁻¹ A			
Si	-2.150053	2.178667	0.625370	Si	-2.150053	2.178667	0.625370
C	-0.578457	1.585315	-0.456669	C	-0.578457	1.585315	-0.456669
C	-1.232877	0.355972	-0.039025	C	-1.232877	0.355972	-0.039025
C	-0.432102	1.821019	0.963102	C	-0.432102	1.821019	0.963102
D	0.445188	1.756078	1.604662	D	0.445188	1.756078	1.604662
D	0.020532	1.864829	-1.311772	D	0.020532	1.864829	-1.311772
D	-0.716789	-0.405155	0.544939	H	-0.716789	-0.405155	0.544939
H	-2.145988	-0.008539	-0.518207	D	-2.145988	-0.008539	-0.518207
[i2e]→[i3d]				[i2f]→[i3a]			
							
-187.7 kJ mol ⁻¹				-187.3 kJ mol ⁻¹			
C ₁ ⁻¹ A				C ₁ ⁻¹ A			
Si	2.150053	2.178667	0.625370	Si	2.150053	2.178667	0.625370
C	0.578457	1.585315	-0.456669	C	0.578457	1.585315	-0.456669
C	1.232877	0.355972	-0.039025	C	1.232877	0.355972	-0.039025
C	0.432102	1.821019	0.963102	C	0.432102	1.821019	0.963102
H	-0.445188	1.756078	1.604662	D	-0.445188	1.756078	1.604662
D	-0.020532	1.864829	-1.311772	H	-0.020532	1.864829	-1.311772
D	0.716789	-0.405155	0.544939	D	0.716789	-0.405155	0.544939
D	2.145988	-0.008539	-0.518207	D	2.145988	-0.008539	-0.518207

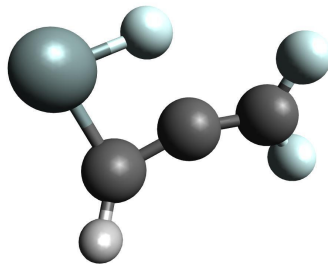
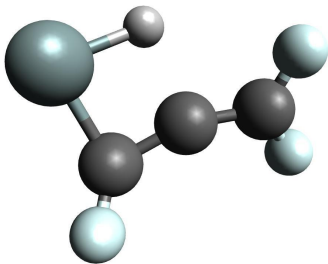
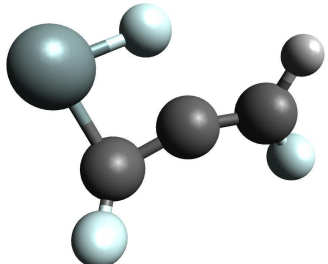
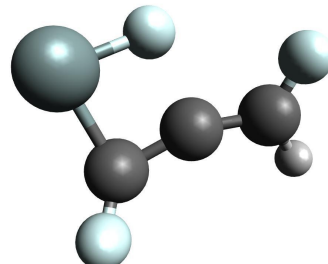
[i2g]→[i3c]				[i2h]→[i3b]			
							
-187.5 kJ mol ⁻¹				-187.0 kJ mol ⁻¹			
C ₁ ⁻¹ A				C ₁ ⁻¹ A			
Si	2.150053	2.178667	0.625370	Si	2.150053	2.178667	0.625370
C	0.578457	1.585315	-0.456669	C	0.578457	1.585315	-0.456669
C	1.232877	0.355972	-0.039025	C	1.232877	0.355972	-0.039025
C	0.432102	1.821019	0.963102	C	0.432102	1.821019	0.963102
D	-0.445188	1.756078	1.604662	D	-0.445188	1.756078	1.604662
D	-0.020532	1.864829	-1.311772	D	-0.020532	1.864829	-1.311772
D	0.716789	-0.405155	0.544939	H	0.716789	-0.405155	0.544939
H	2.145988	-0.008539	-0.518207	D	2.145988	-0.008539	-0.518207
[i2a]→[i5a]				[i2b]→[i5b]			
							
-294.0 kJ mol ⁻¹				-292.4 kJ mol ⁻¹			
C ₁ ⁻¹ A				C ₁ ⁻¹ A			
Si	0.342188	2.735051	-0.130811	Si	0.342188	2.735051	-0.130811
C	0.391241	-1.205372	-0.299825	C	0.391241	-1.205372	-0.299825
C	0.039692	-0.188254	0.478770	C	0.039692	-0.188254	0.478770
C	-0.308252	1.168082	-0.001663	C	-0.308252	1.168082	-0.001663
D	0.000480	-0.344895	1.555941	H	0.000480	-0.344895	1.555941
D	0.632717	-2.174234	0.123862	D	0.632717	-2.174234	0.123862
D	0.451087	-1.098752	-1.378354	D	0.451087	-1.098752	-1.378354
H	-1.322618	1.262237	-0.434147	D	-1.322618	1.262237	-0.434147

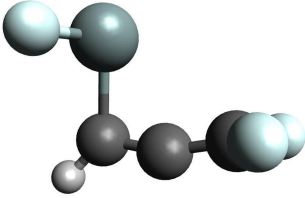
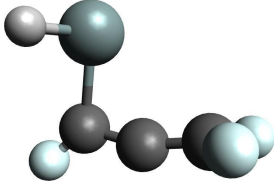
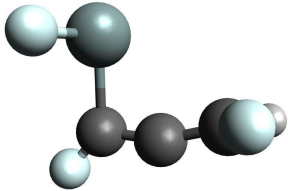
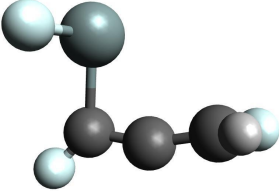
[i2c]→[i5c]				[i2d]→[i5d]			
							
-292.4 kJ mol ⁻¹				-292.5 kJ mol ⁻¹			
C ₁ ⁻¹ A				C ₁ ⁻¹ A			
Si	0.342188	2.735051	-0.130811	Si	0.342188	2.735051	-0.130811
C	0.391241	-1.205372	-0.299825	C	0.391241	-1.205372	-0.299825
C	0.039692	-0.188254	0.478770	C	0.039692	-0.188254	0.478770
C	-0.308252	1.168082	-0.001663	C	-0.308252	1.168082	-0.001663
D	0.000480	-0.344895	1.555941	D	0.000480	-0.344895	1.555941
H	0.632717	-2.174234	0.123862	D	0.632717	-2.174234	0.123862
D	0.451087	-1.098752	-1.378354	H	0.451087	-1.098752	-1.378354
D	-1.322618	1.262237	-0.434147	D	-1.322618	1.262237	-0.434147
[i2e]→[i5a]				[i2f]→[i5b]			
							
-294.0 kJ mol ⁻¹				-292.4 kJ mol ⁻¹			
C ₁ ⁻¹ A				C ₁ ⁻¹ A			
Si	-0.342188	2.735051	-0.130811	Si	-0.342188	2.735051	-0.130811
C	-0.391241	-1.205372	-0.299825	C	-0.391241	-1.205372	-0.299825
C	-0.039692	-0.188254	0.478770	C	-0.039692	-0.188254	0.478770
C	0.308252	1.168082	-0.001663	C	0.308252	1.168082	-0.001663
D	-0.000480	-0.344895	1.555941	H	-0.000480	-0.344895	1.555941
D	-0.632717	-2.174234	0.123862	D	-0.632717	-2.174234	0.123862
D	-0.451087	-1.098752	-1.378354	D	-0.451087	-1.098752	-1.378354
H	1.322618	1.262237	-0.434147	D	1.322618	1.262237	-0.434147

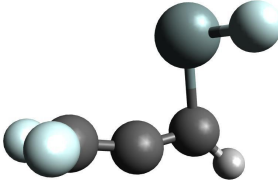
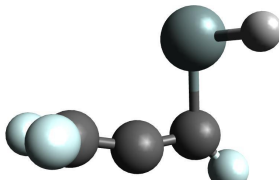
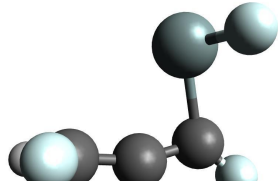
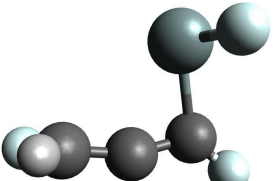
[i2g]→[i5c]				[i2h]→[i5d]			
							
-292.4 kJ mol ⁻¹				-292.5 kJ mol ⁻¹			
C ₁ ⁻¹ A				C ₁ ⁻¹ A			
Si	-0.342188	2.735051	-0.130811	Si	-0.342188	2.735051	-0.130811
C	-0.391241	-1.205372	-0.299825	C	-0.391241	-1.205372	-0.299825
C	-0.039692	-0.188254	0.478770	C	-0.039692	-0.188254	0.478770
C	0.308252	1.168082	-0.001663	C	0.308252	1.168082	-0.001663
D	-0.000480	-0.344895	1.555941	D	-0.000480	-0.344895	1.555941
H	-0.632717	-2.174234	0.123862	D	-0.632717	-2.174234	0.123862
D	-0.451087	-1.098752	-1.378354	H	-0.451087	-1.098752	-1.378354
D	1.322618	1.262237	-0.434147	D	1.322618	1.262237	-0.434147
[i2a]→[i10d]				[i2b]→[i10c]			
							
-25.2 kJ mol ⁻¹				-27.6 kJ mol ⁻¹			
C ₁ ⁻¹ A				C ₁ ⁻¹ A			
Si	0.728857	1.050351	-1.035226	Si	0.728857	1.050351	-1.035226
C	0.745086	-0.738470	-0.340304	C	0.745086	-0.738470	-0.340304
C	0.053676	-0.073521	0.854344	C	0.053676	-0.073521	0.854344
C	-0.693567	0.957443	0.165361	C	-0.693567	0.957443	0.165361
D	1.677882	-1.260348	-0.131790	D	1.677882	-1.260348	-0.131790
D	0.063165	-1.398234	-0.873462	D	0.063165	-1.398234	-0.873462
D	-1.158678	-0.176597	0.686967	H	-1.158678	-0.176597	0.686967
H	-1.402374	1.604957	0.677393	D	-1.402374	1.604957	0.677393

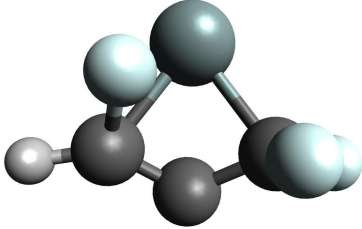
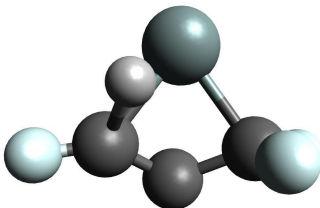
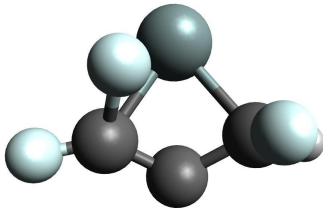
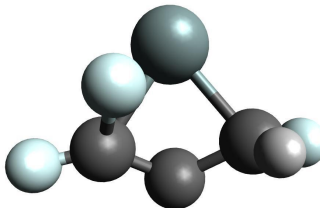
[i2c]→[i10b]				[i2d]→[i10a]			
							
-25.0 kJ mol ⁻¹				-25.3 kJ mol ⁻¹			
C ₁ ⁻¹ A				C ₁ ⁻¹ A			
Si	0.728857	1.050351	-1.035226	Si	0.728857	1.050351	-1.035226
C	0.745086	-0.738470	-0.340304	C	0.745086	-0.738470	-0.340304
C	0.053676	-0.073521	0.854344	C	0.053676	-0.073521	0.854344
C	-0.693567	0.957443	0.165361	C	-0.693567	0.957443	0.165361
H	1.677882	-1.260348	-0.131790	D	1.677882	-1.260348	-0.131790
D	0.063165	-1.398234	-0.873462	H	0.063165	-1.398234	-0.873462
D	-1.158678	-0.176597	0.686967	D	-1.158678	-0.176597	0.686967
D	-1.402374	1.604957	0.677393	D	-1.402374	1.604957	0.677393
[i2e]→[i10b]				[i2f]→[i10a]			
							
-25.2 kJ mol ⁻¹				-27.6 kJ mol ⁻¹			
C ₁ ⁻¹ A				C ₁ ⁻¹ A			
Si	-0.728857	1.050351	-1.035226	Si	-0.728857	1.050351	-1.035226
C	-0.745086	-0.738470	-0.340304	C	-0.745086	-0.738470	-0.340304
C	-0.053676	-0.073521	0.854344	C	-0.053676	-0.073521	0.854344
C	0.693567	0.957443	0.165361	C	0.693567	0.957443	0.165361
D	-1.677882	-1.260348	-0.131790	D	-1.677882	-1.260348	-0.131790
D	-0.063165	-1.398234	-0.873462	D	-0.063165	-1.398234	-0.873462
D	1.158678	-0.176597	0.686967	H	1.158678	-0.176597	0.686967
H	1.402374	1.604957	0.677393	D	1.402374	1.604957	0.677393

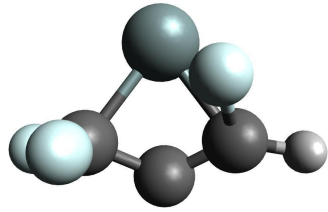
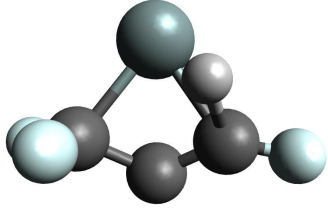
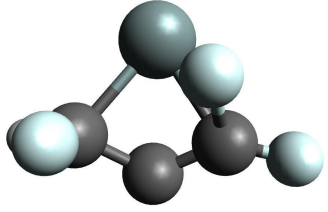
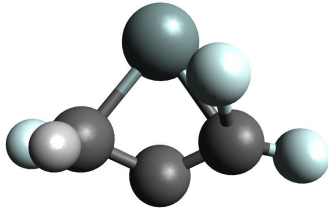
[i2g]→[i10d]				[i2h]→[i10c]			
							
-25.0 kJ mol ⁻¹				-25.3 kJ mol ⁻¹			
C ₁ ⁻¹ A				C ₁ ⁻¹ A			
Si	-0.728857	1.050351	-1.035226	Si	-0.728857	1.050351	-1.035226
C	-0.745086	-0.738470	-0.340304	C	-0.745086	-0.738470	-0.340304
C	-0.053676	-0.073521	0.854344	C	-0.053676	-0.073521	0.854344
C	0.693567	0.957443	0.165361	C	0.693567	0.957443	0.165361
H	-1.677882	-1.260348	-0.131790	D	-1.677882	-1.260348	-0.131790
D	-0.063165	-1.398234	-0.873462	H	-0.063165	-1.398234	-0.873462
D	1.158678	-0.176597	0.686967	D	1.158678	-0.176597	0.686967
D	1.402374	1.604957	0.677393	D	1.402374	1.604957	0.677393
[i4a]→[i13a]				[i4b]→[i13b]			
							
-224.9 kJ mol ⁻¹				-221.4 kJ mol ⁻¹			
C _s ⁻¹ A'				C _s ⁻¹ A'			
Si	-1.742300	2.701762	0.558436	Si	-1.742300	2.701762	0.558436
C	-1.453027	0.995062	-0.232032	C	-1.453027	0.995062	-0.232032
C	-0.226982	1.212635	-0.272076	C	-0.226982	1.212635	-0.272076
C	1.233250	1.262100	-0.377354	C	1.233250	1.262100	-0.377354
H	-0.321943	3.146011	0.987967	D	-0.321943	3.146011	0.987967
D	1.549669	2.031502	-1.083304	D	1.549669	2.031502	-1.083304
D	1.675869	1.477113	0.596678	D	1.675869	1.477113	0.596678
D	1.597521	0.293445	-0.727392	H	1.597521	0.293445	-0.727392

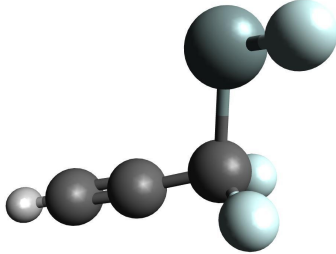
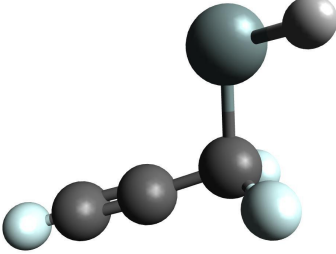
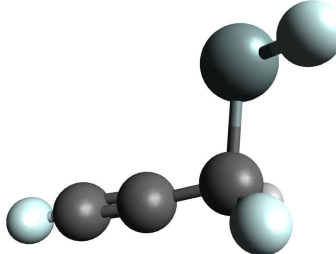
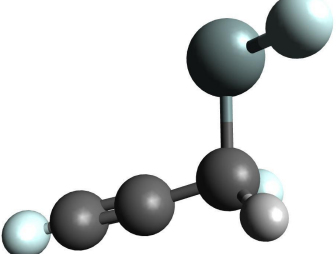
[i5a]→[i9a]				[i5b]→[i9b]			
							
-202.5 kJ mol ⁻¹				-205.3 kJ mol ⁻¹			
C ₁ ⁻¹ A				C ₁ ⁻¹ A			
Si	-1.992862	2.228890	0.527181	Si	-1.992862	2.228890	0.527181
C	-1.168691	0.701841	0.088179	C	-1.168691	0.701841	0.088179
C	0.014708	1.354943	0.010861	C	0.014708	1.354943	0.010861
C	1.299058	1.583736	-0.198471	C	1.299058	1.583736	-0.198471
D	-0.660165	2.892930	0.016175	H	-0.660165	2.892930	0.016175
H	-1.325198	-0.327819	0.375544	D	-1.325198	-0.327819	0.375544
D	1.802093	2.476996	0.142678	D	1.802093	2.476996	0.142678
D	1.862043	0.843052	-0.756205	D	1.862043	0.843052	-0.756205
[i5c]→[i9d]				[i5d]→[i9c]			
							
-202.3 kJ mol ⁻¹				-202.5 kJ mol ⁻¹			
C ₁ ⁻¹ A				C ₁ ⁻¹ A			
Si	-1.992862	2.228890	0.527181	Si	-1.992862	2.228890	0.527181
C	-1.168691	0.701841	0.088179	C	-1.168691	0.701841	0.088179
C	0.014708	1.354943	0.010861	C	0.014708	1.354943	0.010861
C	1.299058	1.583736	-0.198471	C	1.299058	1.583736	-0.198471
D	-0.660165	2.892930	0.016175	D	-0.660165	2.892930	0.016175
D	-1.325198	-0.327819	0.375544	D	-1.325198	-0.327819	0.375544
H	1.802093	2.476996	0.142678	D	1.802093	2.476996	0.142678
D	1.862043	0.843052	-0.756205	H	1.862043	0.843052	-0.756205

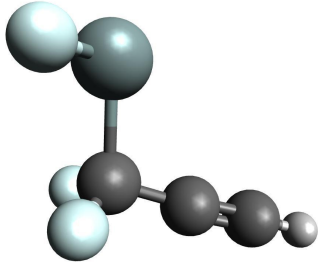
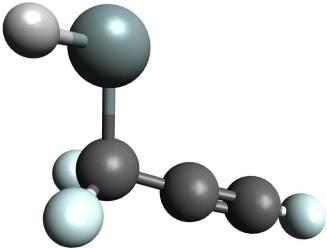
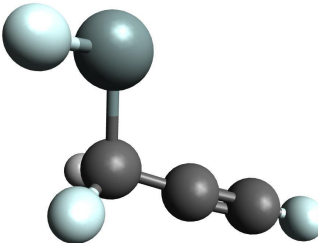
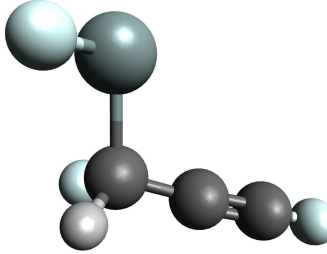
[i6a]→[i9a]				[i6b]→[i9b]			
							
-256.0 kJ mol ⁻¹				-258.8 kJ mol ⁻¹			
C ₁ ⁻¹ A				C ₁ ⁻¹ A			
Si	1.820646	2.497868	0.585175	Si	1.820646	2.497868	0.585175
C	1.254585	0.742483	0.074294	C	1.254585	0.742483	0.074294
C	0.032876	1.141174	-0.073976	C	0.032876	1.141174	-0.073976
C	-1.054450	1.887589	-0.083800	C	-1.054450	1.887589	-0.083800
D	2.460246	2.819309	-0.774176	H	2.460246	2.819309	-0.774176
H	1.690241	-0.197006	-0.235942	D	1.690241	-0.197006	-0.235942
D	-1.294651	2.500444	-0.946357	D	-1.294651	2.500444	-0.946357
D	-1.774537	1.839849	0.726578	D	-1.774537	1.839849	0.726578
[i6c]→[i9c]				[i6d]→[i9d]			
							
-255.8 kJ mol ⁻¹				-255.7 kJ mol ⁻¹			
C ₁ ⁻¹ A				C ₁ ⁻¹ A			
Si	1.820646	2.497868	0.585175	Si	1.820646	2.497868	0.585175
C	1.254585	0.742483	0.074294	C	1.254585	0.742483	0.074294
C	0.032876	1.141174	-0.073976	C	0.032876	1.141174	-0.073976
C	-1.054450	1.887589	-0.083800	C	-1.054450	1.887589	-0.083800
D	2.460246	2.819309	-0.774176	D	2.460246	2.819309	-0.774176
D	1.690241	-0.197006	-0.235942	D	1.690241	-0.197006	-0.235942
D	-1.294651	2.500444	-0.946357	H	-1.294651	2.500444	-0.946357
H	-1.774537	1.839849	0.726578	D	-1.774537	1.839849	0.726578

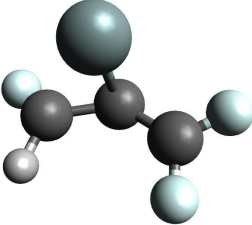
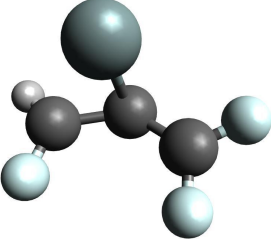
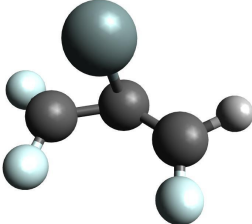
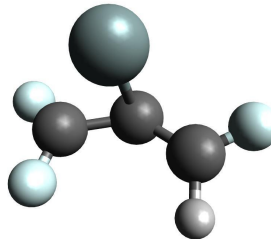
[i6e]→[i9a]				[i6f]→[i9b]			
							
-256.0 kJ mol ⁻¹				-258.8 kJ mol ⁻¹			
C ₁ ⁻¹ A				C ₁ ⁻¹ A			
Si	-1.820646	2.497868	0.585175	Si	-1.820646	2.497868	0.585175
C	-1.254585	0.742483	0.074294	C	-1.254585	0.742483	0.074294
C	-0.032876	1.141174	-0.073976	C	-0.032876	1.141174	-0.073976
C	1.054450	1.887589	-0.083800	C	1.054450	1.887589	-0.083800
D	-2.460246	2.819309	-0.774176	H	-2.460246	2.819309	-0.774176
H	-1.690241	-0.197006	-0.235942	D	-1.690241	-0.197006	-0.235942
D	1.294651	2.500444	-0.946357	D	1.294651	2.500444	-0.946357
D	1.774537	1.839849	0.726578	D	1.774537	1.839849	0.726578
[i6g]→[i9d]				[i6h]→[i9c]			
							
-255.8 kJ mol ⁻¹				-255.7 kJ mol ⁻¹			
C ₁ ⁻¹ A				C ₁ ⁻¹ A			
Si	-1.820646	2.497868	0.585175	Si	-1.820646	2.497868	0.585175
C	-1.254585	0.742483	0.074294	C	-1.254585	0.742483	0.074294
C	-0.032876	1.141174	-0.073976	C	-0.032876	1.141174	-0.073976
C	1.054450	1.887589	-0.083800	C	1.054450	1.887589	-0.083800
D	-2.460246	2.819309	-0.774176	D	-2.460246	2.819309	-0.774176
D	-1.690241	-0.197006	-0.235942	D	-1.690241	-0.197006	-0.235942
D	1.294651	2.500444	-0.946357	H	1.294651	2.500444	-0.946357
H	1.774537	1.839849	0.726578	D	1.774537	1.839849	0.726578

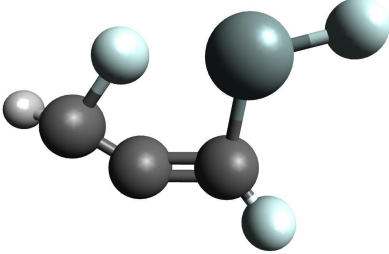
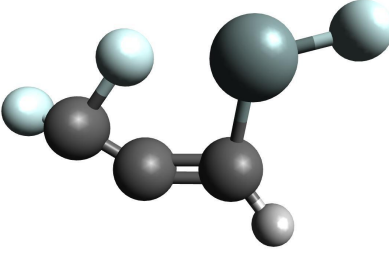
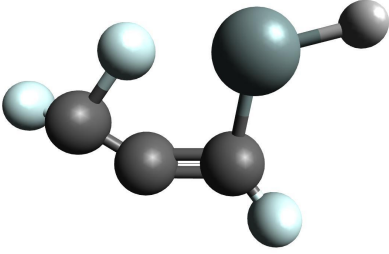
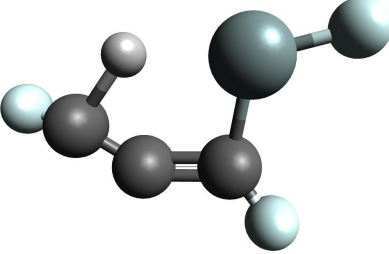
[i6a]→[i10b]				[i6b]→[i10a]			
							
-155.7 kJ mol ⁻¹				-158.9 kJ mol ⁻¹			
C ₁ ⁻¹ A				C ₁ ⁻¹ A			
Si	1.108893	2.428844	0.896755	Si	1.108893	2.428844	0.896755
C	1.254157	0.804122	-0.190514	C	1.254157	0.804122	-0.190514
C	-0.047399	0.766331	0.066469	C	-0.047399	0.766331	0.066469
C	-0.677368	2.066019	0.073662	C	-0.677368	2.066019	0.073662
H	2.054356	0.150676	-0.497980	D	2.054356	0.150676	-0.497980
D	1.608219	2.139909	-0.662094	H	1.608219	2.139909	-0.662094
D	-0.645862	2.587746	-0.883451	D	-0.645862	2.587746	-0.883451
D	-1.601289	2.227878	0.621898	D	-1.601289	2.227878	0.621898
[i6c]→[i10d]				[i6d]→[i10c]			
							
-155.4 kJ mol ⁻¹				-155.7 kJ mol ⁻¹			
C ₁ ⁻¹ A				C ₁ ⁻¹ A			
Si	1.108893	2.428844	0.896755	Si	1.108893	2.428844	0.896755
C	1.254157	0.804122	-0.190514	C	1.254157	0.804122	-0.190514
C	-0.047399	0.766331	0.066469	C	-0.047399	0.766331	0.066469
C	-0.677368	2.066019	0.073662	C	-0.677368	2.066019	0.073662
D	2.054356	0.150676	-0.497980	D	2.054356	0.150676	-0.497980
D	1.608219	2.139909	-0.662094	D	1.608219	2.139909	-0.662094
D	-0.645862	2.587746	-0.883451	H	-0.645862	2.587746	-0.883451
H	-1.601289	2.227878	0.621898	D	-1.601289	2.227878	0.621898

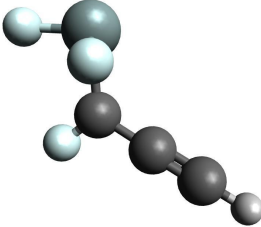
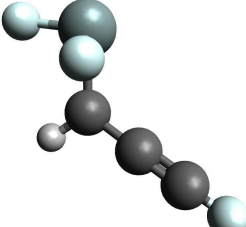
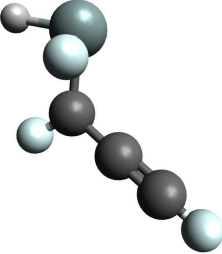
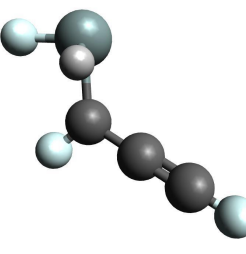
[i6e]→[i10d]				[i6f]→[i10c]			
							
-155.7 kJ mol ⁻¹				-158.9 kJ mol ⁻¹			
C ₁ ⁻¹ A				C ₁ ⁻¹ A			
Si	-1.108893	2.428844	0.896755	Si	-1.108893	2.428844	0.896755
C	-1.254157	0.804122	-0.190514	C	-1.254157	0.804122	-0.190514
C	0.047399	0.766331	0.066469	C	0.047399	0.766331	0.066469
C	0.677368	2.066019	0.073662	C	0.677368	2.066019	0.073662
H	-2.054356	0.150676	-0.497980	D	-2.054356	0.150676	-0.497980
D	-1.608219	2.139909	-0.662094	H	-1.608219	2.139909	-0.662094
D	0.645862	2.587746	-0.883451	D	0.645862	2.587746	-0.883451
D	1.601289	2.227878	0.621898	D	1.601289	2.227878	0.621898
[i6g]→[i10b]				[i6h]→[i10a]			
							
-155.4 kJ mol ⁻¹				-155.7 kJ mol ⁻¹			
C ₁ ⁻¹ A				C ₁ ⁻¹ A			
Si	-1.108893	2.428844	0.896755	Si	-1.108893	2.428844	0.896755
C	-1.254157	0.804122	-0.190514	C	-1.254157	0.804122	-0.190514
C	0.047399	0.766331	0.066469	C	0.047399	0.766331	0.066469
C	0.677368	2.066019	0.073662	C	0.677368	2.066019	0.073662
D	-2.054356	0.150676	-0.497980	D	-2.054356	0.150676	-0.497980
D	-1.608219	2.139909	-0.662094	D	-1.608219	2.139909	-0.662094
D	0.645862	2.587746	-0.883451	H	0.645862	2.587746	-0.883451
H	1.601289	2.227878	0.621898	D	1.601289	2.227878	0.621898

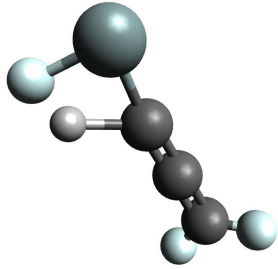
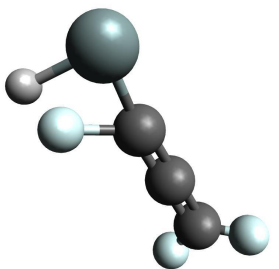
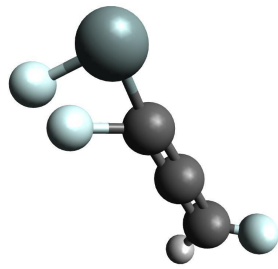
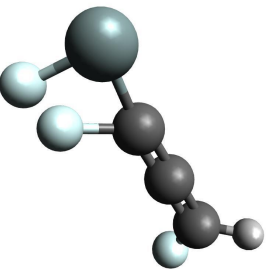
[i6a]→[i12a]				[i6b]→[i12b]			
							
-238.3 kJ mol ⁻¹				-241.1 kJ mol ⁻¹			
C ₁ ⁻¹ A				C ₁ ⁻¹ A			
Si	0.852609	1.635684	0.581065	Si	0.852609	1.635684	0.581065
C	-0.565860	0.423002	0.059391	C	-0.565860	0.423002	0.059391
C	0.001882	-0.919555	0.000234	C	0.001882	-0.919555	0.000234
C	0.544992	-1.989473	-0.037835	C	0.544992	-1.989473	-0.037835
D	0.555684	2.682867	-0.493235	H	0.555684	2.682867	-0.493235
D	-1.048992	0.683920	-0.883382	D	-1.048992	0.683920	-0.883382
D	-1.329382	0.463880	0.848535	D	-1.329382	0.463880	0.848535
H	1.001958	-2.950630	-0.071481	D	1.001958	-2.950630	-0.071481
[i6c]→[i12d]				[i6d]→[i12c]			
							
-237.7 kJ mol ⁻¹				-237.4 kJ mol ⁻¹			
C ₁ ⁻¹ A				C ₁ ⁻¹ A			
Si	0.852609	1.635684	0.581065	Si	0.852609	1.635684	0.581065
C	-0.565860	0.423002	0.059391	C	-0.565860	0.423002	0.059391
C	0.001882	-0.919555	0.000234	C	0.001882	-0.919555	0.000234
C	0.544992	-1.989473	-0.037835	C	0.544992	-1.989473	-0.037835
D	0.555684	2.682867	-0.493235	D	0.555684	2.682867	-0.493235
D	-1.048992	0.683920	-0.883382	H	-1.048992	0.683920	-0.883382
H	-1.329382	0.463880	0.848535	D	-1.329382	0.463880	0.848535
D	1.001958	-2.950630	-0.071481	D	1.001958	-2.950630	-0.071481

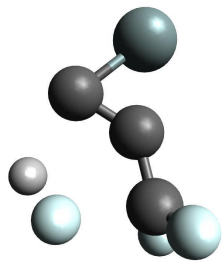
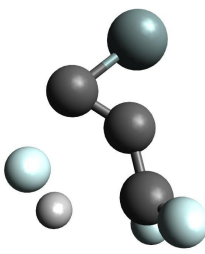
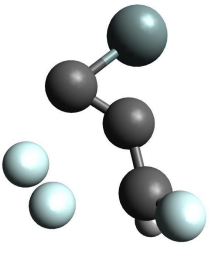
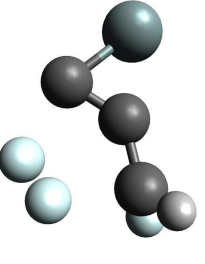
[i6e] → [i12a]				[i6f] → [i12b]			
							
-238.3 kJ mol ⁻¹				-241.1 kJ mol ⁻¹			
C ₁ ⁻¹ A				C ₁ ⁻¹ A			
Si	-0.852609	1.635684	0.581065	Si	-0.852609	1.635684	0.581065
C	0.565860	0.423002	0.059391	C	0.565860	0.423002	0.059391
C	-0.001882	-0.919555	0.000234	C	-0.001882	-0.919555	0.000234
C	-0.544992	-1.989473	-0.037835	C	-0.544992	-1.989473	-0.037835
D	-0.555684	2.682867	-0.493235	H	-0.555684	2.682867	-0.493235
D	1.048992	0.683920	-0.883382	D	1.048992	0.683920	-0.883382
D	1.329382	0.463880	0.848535	D	1.329382	0.463880	0.848535
H	-1.001958	-2.950630	-0.071481	D	-1.001958	-2.950630	-0.071481
[i6g] → [i12c]				[i6h] → [i12d]			
							
-237.7 kJ mol ⁻¹				-237.4 kJ mol ⁻¹			
C ₁ ⁻¹ A				C ₁ ⁻¹ A			
Si	-0.852609	1.635684	0.581065	Si	-0.852609	1.635684	0.581065
C	0.565860	0.423002	0.059391	C	0.565860	0.423002	0.059391
C	-0.001882	-0.919555	0.000234	C	-0.001882	-0.919555	0.000234
C	-0.544992	-1.989473	-0.037835	C	-0.544992	-1.989473	-0.037835
D	-0.555684	2.682867	-0.493235	D	-0.555684	2.682867	-0.493235
D	1.048992	0.683920	-0.883382	H	1.048992	0.683920	-0.883382
H	1.329382	0.463880	0.848535	D	1.329382	0.463880	0.848535
D	-1.001958	-2.950630	-0.071481	D	-1.001958	-2.950630	-0.071481

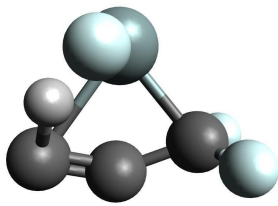
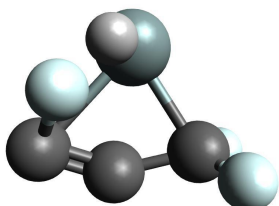
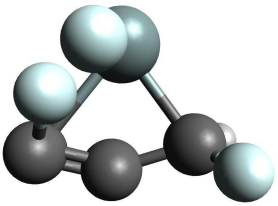
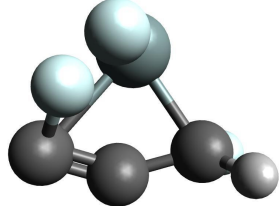
[i7a]→[i10a]				[i7b]→[i10b]			
							
-276.6 kJ mol ⁻¹				-276.4 kJ mol ⁻¹			
C ₁ ⁻¹ A				C ₁ ⁻¹ A			
Si	-1.965407	2.054224	0.949023	Si	-1.965407	2.054224	0.949023
C	-2.941031	0.741834	-0.252682	C	-2.941031	0.741834	-0.252682
C	-1.529983	0.959789	-0.397630	C	-1.529983	0.959789	-0.397630
C	-0.519325	0.330323	0.274811	C	-0.519325	0.330323	0.274811
D	-3.585322	1.284613	-0.938932	H	-3.585322	1.284613	-0.938932
H	-3.363470	-0.192898	0.123519	D	-3.363470	-0.192898	0.123519
D	-0.582867	-0.703830	0.623728	D	-0.582867	-0.703830	0.623728
D	0.457528	0.798760	0.345200	D	0.457528	0.798760	0.345200
[i7c]→[i10d]				[i7d]→[i10c]			
							
-276.4 kJ mol ⁻¹				-276.7 kJ mol ⁻¹			
C ₁ ⁻¹ A				C ₁ ⁻¹ A			
Si	-1.965407	2.054224	0.949023	Si	-1.965407	2.054224	0.949023
C	-2.941031	0.741834	-0.252682	C	-2.941031	0.741834	-0.252682
C	-1.529983	0.959789	-0.397630	C	-1.529983	0.959789	-0.397630
C	-0.519325	0.330323	0.274811	C	-0.519325	0.330323	0.274811
D	-3.585322	1.284613	-0.938932	D	-3.585322	1.284613	-0.938932
D	-3.363470	-0.192898	0.123519	D	-3.363470	-0.192898	0.123519
D	-0.582867	-0.703830	0.623728	H	-0.582867	-0.703830	0.623728
H	0.457528	0.798760	0.345200	D	0.457528	0.798760	0.345200

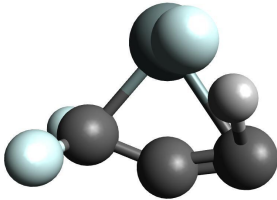
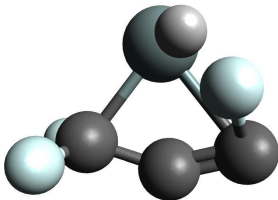
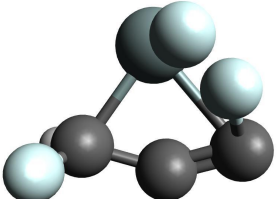
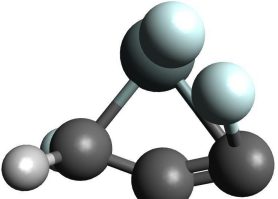
[i8a]→[i9d]				[i8b]→[i9a]			
							
-47.9 kJ mol ⁻¹				-47.6 kJ mol ⁻¹			
C ₁ ⁻¹ A				C ₁ ⁻¹ A			
Si	1.041061	0.917892	0.436916	Si	1.041061	0.917892	0.436916
C	0.760892	-0.738193	-0.161392	C	0.760892	-0.738193	-0.161392
C	-0.609128	-0.750344	-0.306514	C	-0.609128	-0.750344	-0.306514
C	-1.670823	-0.094074	-0.212414	C	-1.670823	-0.094074	-0.212414
D	2.501462	1.265763	0.648959	D	2.501462	1.265763	0.648959
D	-0.818889	0.943557	0.334551	D	-0.818889	0.943557	0.334551
D	1.411713	-1.596634	-0.075037	H	1.411713	-1.596634	-0.075037
H	-2.618347	0.185964	-0.624789	D	-2.618347	0.185964	-0.624789
[i8c]→[i9b]				[i8d]→[i9c]			
							
-50.0 kJ mol ⁻¹				-51.4 kJ mol ⁻¹			
C ₁ ⁻¹ A				C ₁ ⁻¹ A			
Si	1.041061	0.917892	0.436916	Si	1.041061	0.917892	0.436916
C	0.760892	-0.738193	-0.161392	C	0.760892	-0.738193	-0.161392
C	-0.609128	-0.750344	-0.306514	C	-0.609128	-0.750344	-0.306514
C	-1.670823	-0.094074	-0.212414	C	-1.670823	-0.094074	-0.212414
H	2.501462	1.265763	0.648959	D	2.501462	1.265763	0.648959
D	-0.818889	0.943557	0.334551	H	-0.818889	0.943557	0.334551
D	1.411713	-1.596634	-0.075037	D	1.411713	-1.596634	-0.075037
D	-2.618347	0.185964	-0.624789	D	-2.618347	0.185964	-0.624789

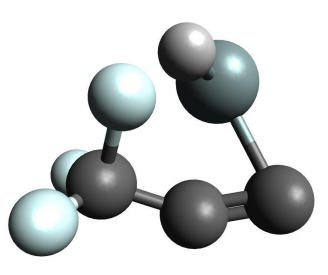
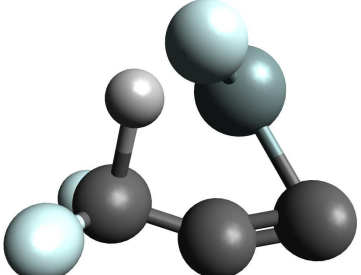
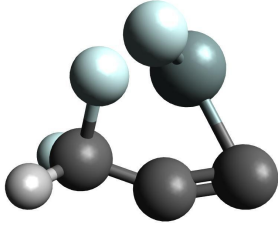
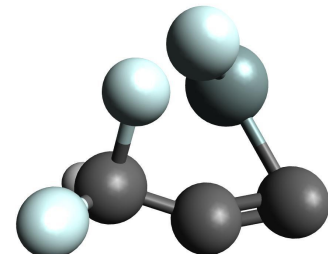
[i8a]→[i12a]				[i8b]→[i12c]			
							
-108.7 kJ mol ⁻¹				-108.2 kJ mol ⁻¹			
C ₁ ⁻¹ A				C ₁ ⁻¹ A			
Si	-2.521663	2.463165	1.136938	Si	-2.521663	2.463165	1.136938
C	-0.857503	2.002660	0.565118	C	-0.857503	2.002660	0.565118
C	-0.462648	0.671903	0.277186	C	-0.462648	0.671903	0.277186
C	-0.127979	-0.463490	0.061318	C	-0.127979	-0.463490	0.061318
D	-0.053439	2.725894	0.410733	H	-0.053439	2.725894	0.410733
H	0.166755	-1.470185	-0.125512	D	0.166755	-1.470185	-0.125512
D	-2.334378	3.957638	1.028947	D	-2.334378	3.957638	1.028947
D	-2.405675	1.983846	-0.345689	D	-2.405675	1.983846	-0.345689
[i8c]→[i12b]				[i8d]→[i12d]			
							
-110.5 kJ mol ⁻¹				-111.6 kJ mol ⁻¹			
C ₁ ⁻¹ A				C ₁ ⁻¹ A			
Si	-2.521663	2.463165	1.136938	Si	-2.521663	2.463165	1.136938
C	-0.857503	2.002660	0.565118	C	-0.857503	2.002660	0.565118
C	-0.462648	0.671903	0.277186	C	-0.462648	0.671903	0.277186
C	-0.127979	-0.463490	0.061318	C	-0.127979	-0.463490	0.061318
D	-0.053439	2.725894	0.410733	D	-0.053439	2.725894	0.410733
D	0.166755	-1.470185	-0.125512	D	0.166755	-1.470185	-0.125512
H	-2.334378	3.957638	1.028947	D	-2.334378	3.957638	1.028947
D	-2.405675	1.983846	-0.345689	H	-2.405675	1.983846	-0.345689

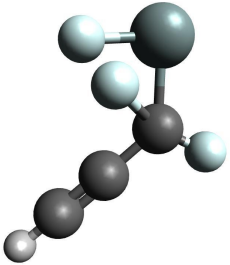
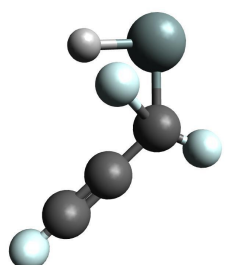
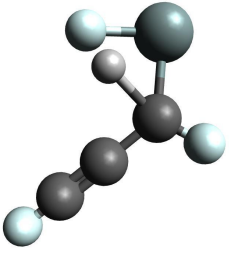
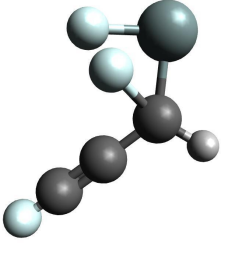
[i9a]→p1a				[i9b]→p1a			
							
-84.8 kJ mol ⁻¹				-83.8 kJ mol ⁻¹			
C ₁ ⁻¹ A				C ₁ ⁻¹ A			
Si	-0.744770	2.157892	1.133843	Si	-0.744770	2.157892	1.133843
C	-0.117447	0.739329	0.301978	C	-0.117447	0.739329	0.301978
C	0.508868	-0.265289	-0.184605	C	0.508868	-0.265289	-0.184605
C	1.137912	-1.291212	-0.706981	C	1.137912	-1.291212	-0.706981
D	2.192710	-1.451493	-0.511820	D	2.192710	-1.451493	-0.511820
D	0.620937	-2.000203	-1.344227	D	0.620937	-2.000203	-1.344227
H	-1.537155	0.742156	0.712436	D	-1.537155	0.742156	0.712436
D	-2.215299	1.527879	0.692674	H	-2.215299	1.527879	0.692674
[i9c]→p1b				[i9d]→p1b			
							
-81.1 kJ mol ⁻¹				-81.1 kJ mol ⁻¹			
C ₁ ⁻¹ A				C ₁ ⁻¹ A			
Si	-0.744770	2.157892	1.133843	Si	-0.744770	2.157892	1.133843
C	-0.117447	0.739329	0.301978	C	-0.117447	0.739329	0.301978
C	0.508868	-0.265289	-0.184605	C	0.508868	-0.265289	-0.184605
C	1.137912	-1.291212	-0.706981	C	1.137912	-1.291212	-0.706981
D	2.192710	-1.451493	-0.511820	H	2.192710	-1.451493	-0.511820
H	0.620937	-2.000203	-1.344227	D	0.620937	-2.000203	-1.344227
D	-1.537155	0.742156	0.712436	D	-1.537155	0.742156	0.712436
D	-2.215299	1.527879	0.692674	D	-2.215299	1.527879	0.692674

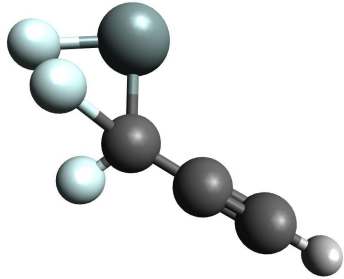
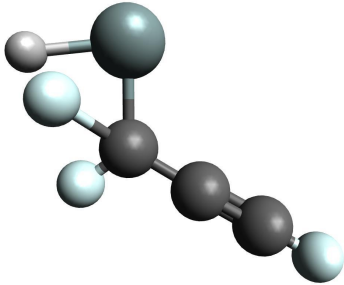
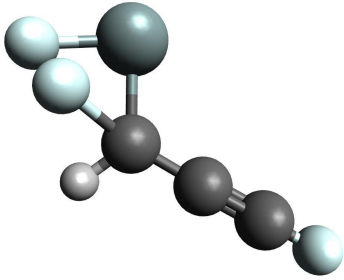
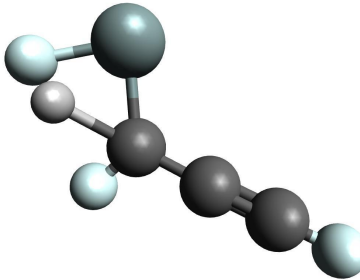
[i1a]→p2a				[i1b]→p2a			
							
10.8 kJ mol ⁻¹				11.0 kJ mol ⁻¹			
C _s ⁻¹ A'				C _s ⁻¹ A'			
Si	0.528665	2.400596	-0.746415	Si	0.528665	2.400596	-0.746415
C	0.638969	-0.741790	0.047537	C	0.638969	-0.741790	0.047537
C	0.334217	0.578629	-0.236986	C	0.334217	0.578629	-0.236986
C	-0.782728	1.293996	-0.211915	C	-0.782728	1.293996	-0.211915
D	1.142678	-0.981263	0.980498	D	1.142678	-0.981263	0.980498
D	0.810919	-1.435189	-0.771673	D	0.810919	-1.435189	-0.771673
H	-1.559747	-0.175915	0.315690	D	-1.559747	-0.175915	0.315690
D	-1.065292	-0.900941	0.410427	H	-1.065292	-0.900941	0.410427
[i1b]→p2b				[i1b]→p2c			
							
13.9 kJ mol ⁻¹				13.9 kJ mol ⁻¹			
C ₁ ⁻¹ A				C ₁ ⁻¹ A			
Si	0.528665	2.400596	-0.746415	Si	0.528665	2.400596	-0.746415
C	0.638969	-0.741790	0.047537	C	0.638969	-0.741790	0.047537
C	0.334217	0.578629	-0.236986	C	0.334217	0.578629	-0.236986
C	-0.782728	1.293996	-0.211915	C	-0.782728	1.293996	-0.211915
D	1.142678	-0.981263	0.980498	H	1.142678	-0.981263	0.980498
H	0.810919	-1.435189	-0.771673	D	0.810919	-1.435189	-0.771673
D	-1.559747	-0.175915	0.315690	D	-1.559747	-0.175915	0.315690
D	-1.065292	-0.900941	0.410427	D	-1.065292	-0.900941	0.410427

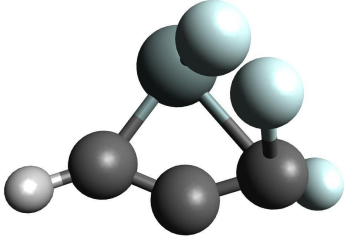
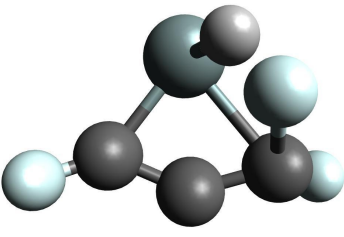
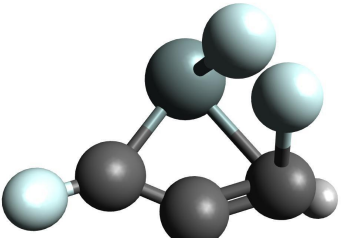
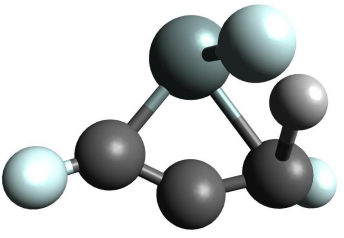
[i6a]→p2a				[i6b]→p2a			
							
-43.5 kJ mol ⁻¹				-41.9 kJ mol ⁻¹			
C ₁ ⁻¹ A				C ₁ ⁻¹ A			
Si	1.178923	2.205371	0.803390	Si	1.178923	2.205371	0.803390
C	-0.641206	2.137118	-0.050763	C	-0.641206	2.137118	-0.050763
C	-0.130702	0.814244	0.053579	C	-0.130702	0.814244	0.053579
C	0.888991	0.086553	0.200705	C	0.888991	0.086553	0.200705
D	-0.835280	2.504167	-1.054512	D	-0.835280	2.504167	-1.054512
D	-1.380706	2.457777	0.683302	D	-1.380706	2.457777	0.683302
H	1.725043	1.088245	-0.475804	D	1.725043	1.088245	-0.475804
D	1.923344	2.086626	-0.687100	H	1.923344	2.086626	-0.687100
[i6c]→p2b				[i6d]→p2c			
							
-39.4 kJ mol ⁻¹				-39.4 kJ mol ⁻¹			
C ₁ ⁻¹ A				C ₁ ⁻¹ A			
Si	1.178923	2.205371	0.803390	Si	1.178923	2.205371	0.803390
C	-0.641206	2.137118	-0.050763	C	-0.641206	2.137118	-0.050763
C	-0.130702	0.814244	0.053579	C	-0.130702	0.814244	0.053579
C	0.888991	0.086553	0.200705	C	0.888991	0.086553	0.200705
D	-0.835280	2.504167	-1.054512	H	-0.835280	2.504167	-1.054512
H	-1.380706	2.457777	0.683302	D	-1.380706	2.457777	0.683302
D	1.725043	1.088245	-0.475804	D	1.725043	1.088245	-0.475804
D	1.923344	2.086626	-0.687100	D	1.923344	2.086626	-0.687100

[i6e]→p2a				[i6f]→p2a			
							
-43.5 kJ mol ⁻¹				-41.9 kJ mol ⁻¹			
C ₁ ⁻¹ A				C ₁ ⁻¹ A			
Si	-1.178923	2.205371	0.803390	Si	-1.178923	2.205371	0.803390
C	0.641206	2.137118	-0.050763	C	0.641206	2.137118	-0.050763
C	0.130702	0.814244	0.053579	C	0.130702	0.814244	0.053579
C	-0.888991	0.086553	0.200705	C	-0.888991	0.086553	0.200705
D	0.835280	2.504167	-1.054512	D	0.835280	2.504167	-1.054512
D	1.380706	2.457777	0.683302	D	1.380706	2.457777	0.683302
H	-1.725043	1.088245	-0.475804	D	-1.725043	1.088245	-0.475804
D	-1.923344	2.086626	-0.687100	H	-1.923344	2.086626	-0.687100
[i6g]→p2c				[i6h]→p2b			
							
-39.4 kJ mol ⁻¹				-39.4 kJ mol ⁻¹			
C ₁ ⁻¹ A				C ₁ ⁻¹ A			
Si	-1.178923	2.205371	0.803390	Si	-1.178923	2.205371	0.803390
C	0.641206	2.137118	-0.050763	C	0.641206	2.137118	-0.050763
C	0.130702	0.814244	0.053579	C	0.130702	0.814244	0.053579
C	-0.888991	0.086553	0.200705	C	-0.888991	0.086553	0.200705
D	0.835280	2.504167	-1.054512	H	0.835280	2.504167	-1.054512
H	1.380706	2.457777	0.683302	D	1.380706	2.457777	0.683302
D	-1.725043	1.088245	-0.475804	D	-1.725043	1.088245	-0.475804
D	-1.923344	2.086626	-0.687100	D	-1.923344	2.086626	-0.687100

[i13a]→p2a				[i13b]→p2a			
							
-42.3 kJ mol ⁻¹				-43.1 kJ mol ⁻¹			
C ₁ ⁻¹ A				C ₁ ⁻¹ A			
Si	-0.830773	0.883817	0.953003	Si	-0.830773	0.883817	0.953003
C	-1.811287	-0.696687	0.301549	C	-1.811287	-0.696687	0.301549
C	-0.590983	-0.923847	0.102221	C	-0.590983	-0.923847	0.102221
C	0.749568	-0.461799	-0.040845	C	0.749568	-0.461799	-0.040845
D	1.185475	-0.546441	-1.038520	D	1.185475	-0.546441	-1.038520
D	1.455315	-0.696271	0.749183	D	1.455315	-0.696271	0.749183
D	0.271987	0.942873	-0.437740	H	0.271987	0.942873	-0.437740
H	-0.545547	1.525644	-0.576927	D	-0.545547	1.525644	-0.576927
[i13b]→p2b				[i13b]→p2c			
							
-39.9 kJ mol ⁻¹				-39.7 kJ mol ⁻¹			
C ₁ ⁻¹ A				C ₁ ⁻¹ A			
Si	-0.830773	0.883817	0.953003	Si	-0.830773	0.883817	0.953003
C	-1.811287	-0.696687	0.301549	C	-1.811287	-0.696687	0.301549
C	-0.590983	-0.923847	0.102221	C	-0.590983	-0.923847	0.102221
C	0.749568	-0.461799	-0.040845	C	0.749568	-0.461799	-0.040845
H	1.185475	-0.546441	-1.038520	D	1.185475	-0.546441	-1.038520
D	1.455315	-0.696271	0.749183	H	1.455315	-0.696271	0.749183
D	0.271987	0.942873	-0.437740	D	0.271987	0.942873	-0.437740
D	-0.545547	1.525644	-0.576927	D	-0.545547	1.525644	-0.576927

[i12a]→p3a				[i12b]→p3c			
							
-64.2 kJ mol ⁻¹				-66.3 kJ mol ⁻¹			
C ₁ ⁻¹ A				C ₁ ⁻¹ A			
Si	-1.151997	1.718947	0.728726	Si	-1.151997	1.718947	0.728726
C	-0.793552	-0.036891	0.485201	C	-0.793552	-0.036891	0.485201
C	0.356363	-0.744575	0.018188	C	0.356363	-0.744575	0.018188
C	1.337204	-1.326892	-0.364743	C	1.337204	-1.326892	-0.364743
D	-1.597641	-0.704860	0.800559	D	-1.597641	-0.704860	0.800559
H	2.205962	-1.845464	-0.696218	D	2.205962	-1.845464	-0.696218
D	-0.463884	1.036474	-0.582223	D	-0.463884	1.036474	-0.582223
D	0.061553	1.931814	-0.358027	H	0.061553	1.931814	-0.358027
[i12c]→p3c				[i12d]→p3b			
							
-66.8 kJ mol ⁻¹				-63.6 kJ mol ⁻¹			
C ₁ ⁻¹ A				C ₁ ⁻¹ A			
Si	-1.151997	1.718947	0.728726	Si	-1.151997	1.718947	0.728726
C	-0.793552	-0.036891	0.485201	C	-0.793552	-0.036891	0.485201
C	0.356363	-0.744575	0.018188	C	0.356363	-0.744575	0.018188
C	1.337204	-1.326892	-0.364743	C	1.337204	-1.326892	-0.364743
D	-1.597641	-0.704860	0.800559	H	-1.597641	-0.704860	0.800559
D	2.205962	-1.845464	-0.696218	D	2.205962	-1.845464	-0.696218
H	-0.463884	1.036474	-0.582223	D	-0.463884	1.036474	-0.582223
D	0.061553	1.931814	-0.358027	D	0.061553	1.931814	-0.358027

[i12a]→p3a'				[i12b]→p3c'			
							
-69.9 kJ mol ⁻¹				-71.9 kJ mol ⁻¹			
C ₁ ⁻¹ A				C ₁ ⁻¹ A			
Si	-1.555112	0.642765	0.911988	Si	-1.555112	0.642765	0.911988
C	0.049390	0.418870	0.114001	C	0.049390	0.418870	0.114001
C	0.581034	-0.893905	-0.073288	C	0.581034	-0.893905	-0.073288
C	1.006592	-2.011224	-0.207659	C	1.006592	-2.011224	-0.207659
D	0.726733	1.208649	-0.209397	D	0.726733	1.208649	-0.209397
H	1.387736	-2.997804	-0.330653	D	1.387736	-2.997804	-0.330653
D	-1.435106	2.141508	0.235326	H	-1.435106	2.141508	0.235326
D	-1.002771	1.445970	-0.426216	D	-1.002771	1.445970	-0.426216
[i12c]→p3b'				[i12d]→p3c'			
							
-69.2 kJ mol ⁻¹				-72.6 kJ mol ⁻¹			
C ₁ ⁻¹ A				C ₁ ⁻¹ A			
Si	-1.555112	0.642765	0.911988	Si	-1.555112	0.642765	0.911988
C	0.049390	0.418870	0.114001	C	0.049390	0.418870	0.114001
C	0.581034	-0.893905	-0.073288	C	0.581034	-0.893905	-0.073288
C	1.006592	-2.011224	-0.207659	C	1.006592	-2.011224	-0.207659
H	0.726733	1.208649	-0.209397	D	0.726733	1.208649	-0.209397
D	1.387736	-2.997804	-0.330653	D	1.387736	-2.997804	-0.330653
D	-1.435106	2.141508	0.235326	D	-1.435106	2.141508	0.235326
D	-1.002771	1.445970	-0.426216	H	-1.002771	1.445970	-0.426216

[i6a]→p4a				[i6b]→p4b			
							
-107.7 kJ mol ⁻¹				-109.7 kJ mol ⁻¹			
C ₁ ⁻¹ A				C ₁ ⁻¹ A			
Si	0.831125	0.640403	0.777373	Si	0.831125	0.640403	0.777373
C	-1.185225	0.266693	0.157410	C	-1.185225	0.266693	0.157410
C	-0.415827	-0.797532	0.102736	C	-0.415827	-0.797532	0.102736
C	0.854625	-1.135711	0.195070	C	0.854625	-1.135711	0.195070
D	-2.051331	0.445181	0.777573	D	-2.051331	0.445181	0.777573
H	1.482402	-1.878498	-0.264555	D	1.482402	-1.878498	-0.264555
D	-0.203090	1.162708	-0.807825	D	-0.203090	1.162708	-0.807825
D	0.676107	1.295027	-0.933420	H	0.676107	1.295027	-0.933420
[i6c]→p4a				[i6d]→p4b			
							
-107.7 kJ mol ⁻¹				-110.6 kJ mol ⁻¹			
C ₁ ⁻¹ A				C ₁ ⁻¹ A			
Si	0.831125	0.640403	0.777373	Si	0.831125	0.640403	0.777373
C	-1.185225	0.266693	0.157410	C	-1.185225	0.266693	0.157410
C	-0.415827	-0.797532	0.102736	C	-0.415827	-0.797532	0.102736
C	0.854625	-1.135711	0.195070	C	0.854625	-1.135711	0.195070
H	-2.051331	0.445181	0.777573	D	-2.051331	0.445181	0.777573
D	1.482402	-1.878498	-0.264555	D	1.482402	-1.878498	-0.264555
D	-0.203090	1.162708	-0.807825	H	-0.203090	1.162708	-0.807825
D	0.676107	1.295027	-0.933420	D	0.676107	1.295027	-0.933420

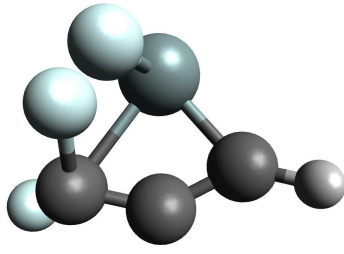
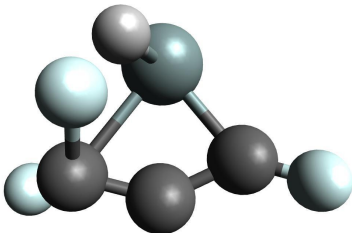
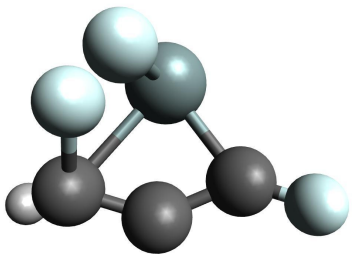
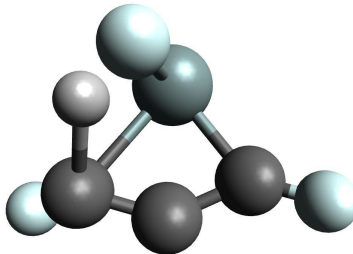
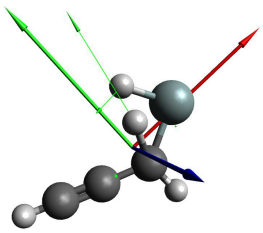
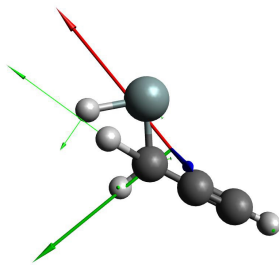
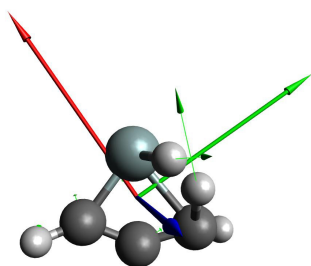
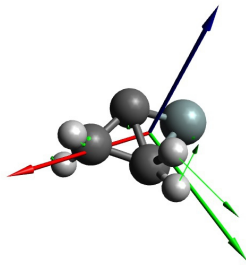
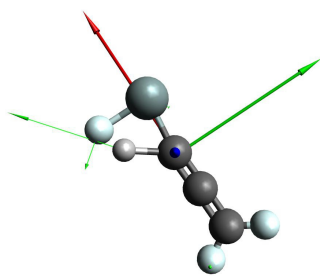
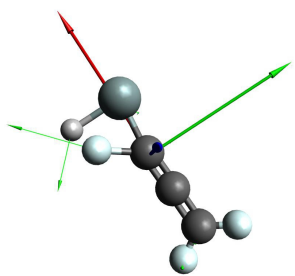
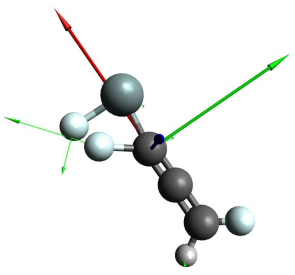
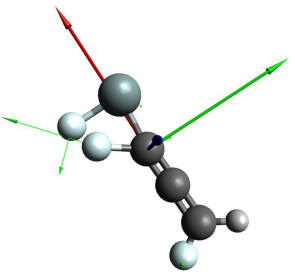
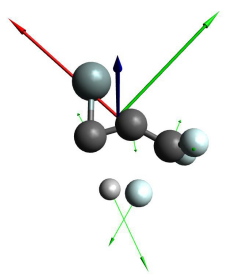
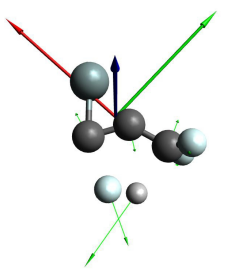
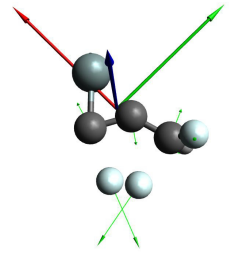
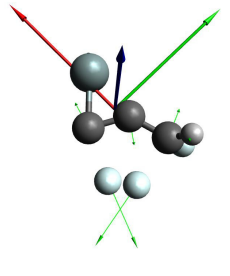
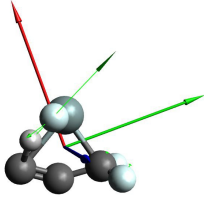
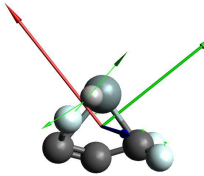
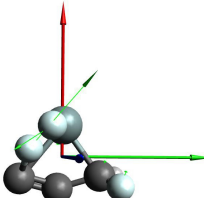
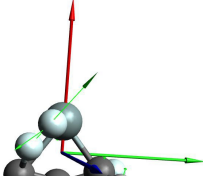
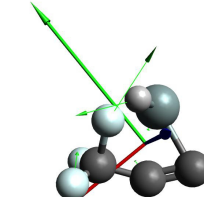
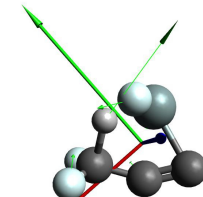
[i6e]→p4a				[i6f]→p4b			
							
-107.7 kJ mol ⁻¹				-109.7 kJ mol ⁻¹			
C ₁ ⁻¹ A				C ₁ ⁻¹ A			
Si	-0.831125	0.640403	0.777373	Si	-0.831125	0.640403	0.777373
C	1.185225	0.266693	0.157410	C	1.185225	0.266693	0.157410
C	0.415827	-0.797532	0.102736	C	0.415827	-0.797532	0.102736
C	-0.854625	-1.135711	0.195070	C	-0.854625	-1.135711	0.195070
D	2.051331	0.445181	0.777573	D	2.051331	0.445181	0.777573
H	-1.482402	-1.878498	-0.264555	D	-1.482402	-1.878498	-0.264555
D	0.203090	1.162708	-0.807825	D	0.203090	1.162708	-0.807825
D	-0.676107	1.295027	-0.933420	H	-0.676107	1.295027	-0.933420
[i6g]→p4a				[i6h]→p4b			
							
-107.7 kJ mol ⁻¹				-110.6 kJ mol ⁻¹			
C ₁ ⁻¹ A				C ₁ ⁻¹ A			
Si	-0.831125	0.640403	0.777373	Si	-0.831125	0.640403	0.777373
C	1.185225	0.266693	0.157410	C	1.185225	0.266693	0.157410
C	0.415827	-0.797532	0.102736	C	0.415827	-0.797532	0.102736
C	-0.854625	-1.135711	0.195070	C	-0.854625	-1.135711	0.195070
H	2.051331	0.445181	0.777573	D	2.051331	0.445181	0.777573
D	-1.482402	-1.878498	-0.264555	D	-1.482402	-1.878498	-0.264555
D	0.203090	1.162708	-0.807825	H	0.203090	1.162708	-0.807825
D	-0.676107	1.295027	-0.933420	D	-0.676107	1.295027	-0.933420

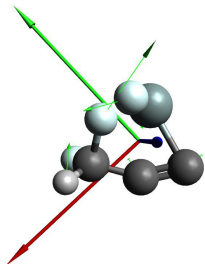
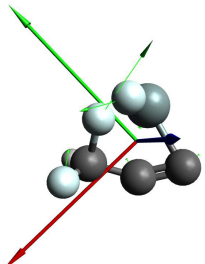
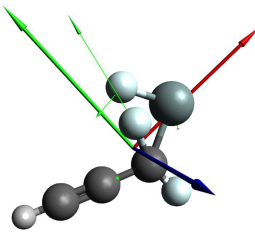
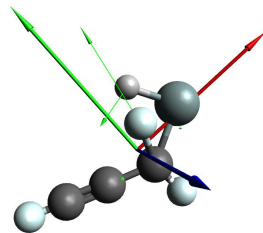
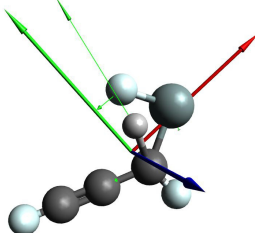
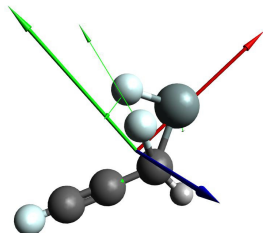
Table A.3: Exit transition state structures for the emission of $\text{H}_2/\text{HD}/\text{D}_2$, principle moments of inertia (AMU a_0^2), and angles of emission relative to the principal axes.

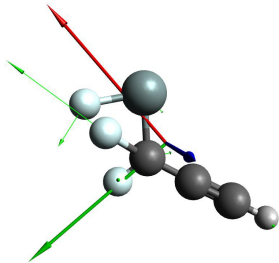
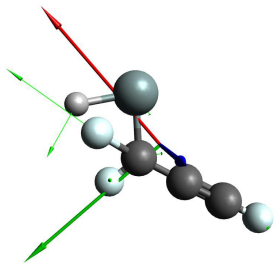
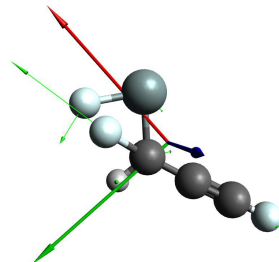
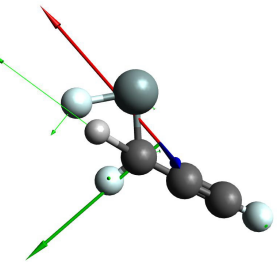
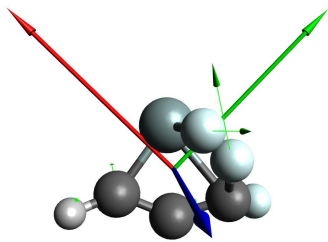
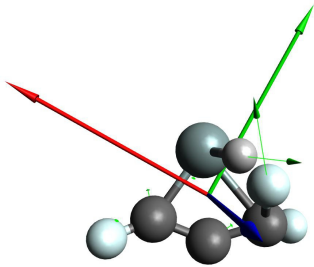
$[\text{i}5] \rightarrow \text{p}1$		$[\text{i}9] \rightarrow \text{p}1$	
35.6	111.4°	22.4	118.1°
704.3	158.6°	748.2	28.1°
736.8	90.1°	768.9	90.1°
$[\text{i}1] \rightarrow \text{p}2$		$[\text{i}6] \rightarrow \text{p}2$	
90.8	128.3°	187.7	63.2°
418.3	141.7°	215.7	96.5°
418.3	90.0°	364.0	27.7°
$[\text{i}11] \rightarrow \text{p}2$		$[\text{i}13] \rightarrow \text{p}2$	
175.7	146.1°	171.1	109.3°
215.1	83.4°	238.0	80.4°
356.6	56.9°	373.2	21.7°

[i12]→p3		[i12]→p3'	
			
50.2	95.2°	66.2	33.2°
647.7	11.0°	598.2	58.0°
690.1	99.7°	658.3	98.0°
[i6]→p4		[i11]→p5	
			
176.8	67.9°	89.0	107.6°
212.0	84.3°	341.2	65.3°
349.2	22.9°	395.7	31.1°
[i9a]→p1a		[i9b]→p1a	
			
37.1	115.9°	34.5	121.4°
828.8	25.9°	820.3	31.4°
863.6	91.5°	851.5	89.8°

[i9c] → p1b		[i9d] → p1b	
			
39.6	119.3°	39.0	117.9°
797.2	29.3°	798.2	27.9°
833.9	89.4°	834.4	88.9°
[i1a] → p2a		[i1b] → p2a	
			
107.3	127.8°	113.0	127.4°
479.7	142.2°	470.7	142.6°
562.6	90.0°	559.4	90.0°
[i1b] → p2b		[i1b] → p2c	
			
113.0	129.9°	113.0	129.9°
465.0	140.1°	465.0	140.1°
560.2	89.2°	560.2	90.8°

[i6a]→p2a		[i6b]→p2a	
			
225.7	74.3°	224.2	78.7°
236.0	71.9°	230.1	61.5°
394.3	24.3°	395.3	31.0°
[i6c]→p2b		[i6d]→p2c	
			
220.3	65.9°	221.4	63.6°
234.8	76.6°	231.7	82.0°
385.0	28.0°	387.0	27.8°
[i13a]→p2a		[i13b]→p2a	
			
188.4	110.6°	192.1	104.7°
274.5	76.1°	278.9	77.3°
409.4	25.2°	408.6	19.6°

[i13b]→p2b		[i13b]→p2c	
			
196.5	110.3°	192.9	106.4°
264.0	75.7°	268.0	73.8°
396.0	25.3°	400.9	23.4°
[i12a]→p3a		[i12b]→p3c	
			
73.6	95.1°	66.5	93.0°
653.7	8.4°	692.6	8.8°
713.5	96.7°	746.0	98.2°
[i12c]→p3c		[i12d]→p3b	
			
71.2	98.5°	64.2	95.8°
692.5	12.0°	695.3	9.0°
754.7	98.3°	746.0	96.8°

[i12a]→p3a'		[i12b]→p3c'	
			
87.9	31.9°	86.2	28.7°
625.2	59.0°	646.4	62.4°
701.9	96.7°	721.8	97.1°
[i12c]→p3b'		[i12d]→p3c'	
			
78.4	30.7°	84.1	34.6°
665.6	60.2°	657.3	56.5°
733.4	96.9°	734.1	97.7°
[i6a]→p4a		[i6b]→p4b	
			
204.1	69.2°	206.1	71.0°
244.8	76.1°	241.3	73.8°
374.4	25.3°	390.5	25.4°

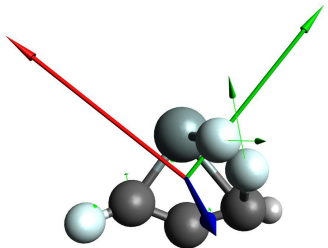
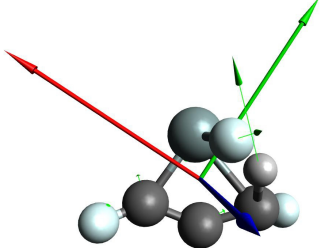
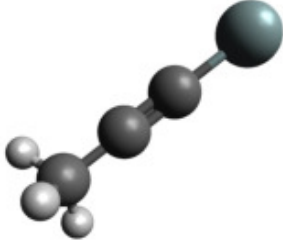
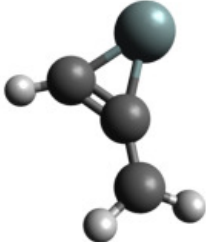
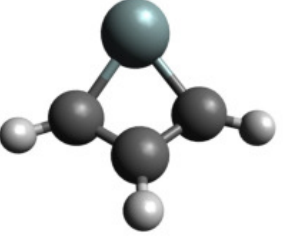
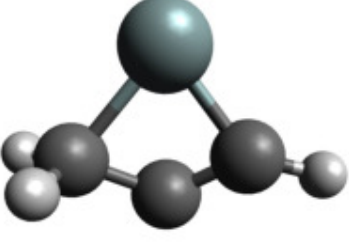

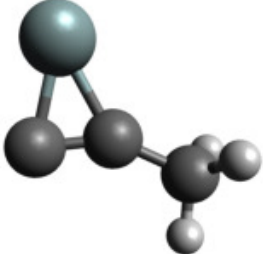
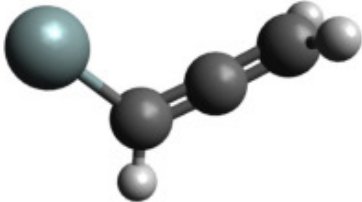
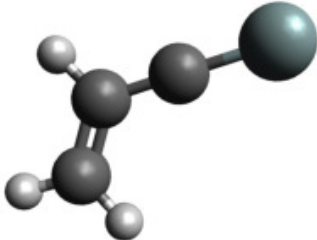
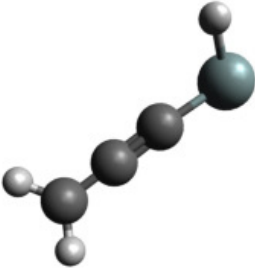
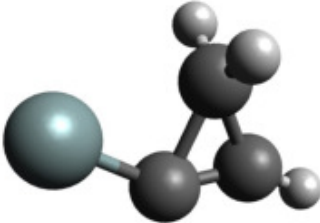
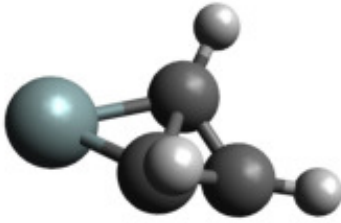
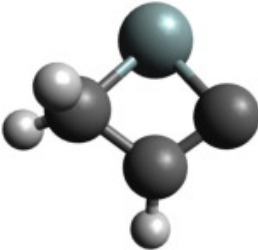
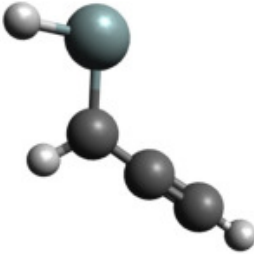

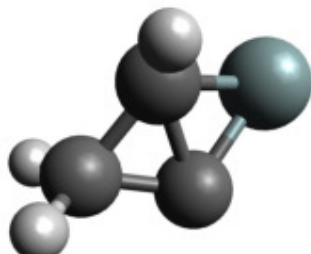
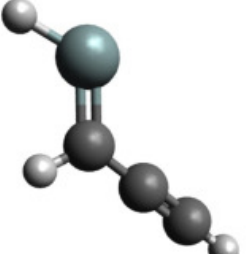
[i6c] → p4a		[i6d] → p4b	
			
216.4	72.3°	210.3	70.7°
231.5	74.5°	242.8	76.8°
376.2	23.9°	389.9	23.7°


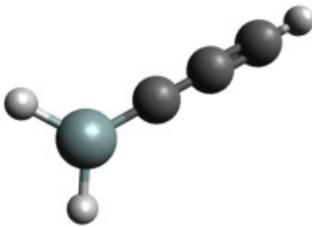
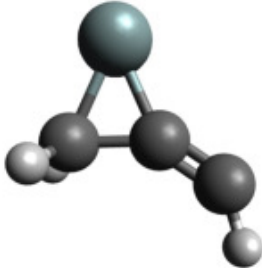
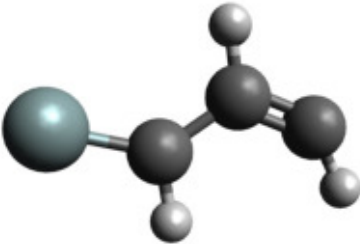
Table A.4: Products relevant to the reaction of electronically excited atomic silicon with methylacetylene and allene to form atomic hydrogen and SiC_3H_3 . Geometries were calculated at the $\omega\text{B97X-V//cc-pVTZ}$ level of theory; relative energies were calculated at the CCSD(T)//CBS level of theory.

n1				n2			
							
-10.0 kJ mol ⁻¹				3.9 kJ mol ⁻¹			
$C_{3v}^{-2}A_1$				$C_s^{-2}A'$			
Si	2.256938	0.386814	-0.000054	Si	-1.648670	1.864824	-0.639004
C	0.452597	0.445576	0.001238	C	-3.059962	0.865119	-0.096199
C	-0.767469	0.480303	0.004880	C	-1.956341	0.083084	-0.283303
C	-2.224034	0.526369	0.004637	C	-1.616436	-1.271962	-0.143675
H	-2.643608	-0.348009	-0.498856	H	-2.264110	-1.960263	0.392886
H	-2.561104	1.418906	-0.528946	H	-0.692145	-1.662759	-0.553724
H	-2.617180	0.570276	1.023216	H	-4.087409	0.662816	0.185587
n3				n4			
							
7.0 kJ mol ⁻¹				11.4 kJ mol ⁻¹			
$C_s^{-2}A'$				$C_1^{-2}A$			
Si	1.265159	2.162075	-0.444465	Si	1.208012	2.089231	-0.448538
C	-0.607874	2.024234	-0.328499	C	-0.745936	2.116845	-0.093209
C	0.896654	0.500285	0.357941	C	0.910530	0.446506	0.329165
C	-0.395785	0.642838	-0.176604	C	-0.351043	0.718990	-0.018821
H	-1.518838	2.509970	-0.653582	H	-1.431207	2.427755	-0.878519
H	-1.060126	-0.160934	-0.504981	H	-0.968549	2.572982	0.868603
H	1.374406	-0.420749	0.666057	H	1.419426	-0.479092	0.553088

n5				n6			
							
11.5 kJ mol ⁻¹				24.4 kJ mol ⁻¹			
$C_s^{-2}A'$				$C_s^{-2}A'$			
Si	-0.357120	1.246352	-0.941397	Si	-1.573453	1.860263	-0.624254
C	-0.224659	-0.413295	0.358340	C	-3.053427	0.877832	-0.162194
C	-1.552969	-0.035456	0.272406	C	-2.014789	0.087378	-0.128936
C	0.911547	-0.089182	-0.083811	C	-1.441504	-1.261433	0.109938
H	-2.226882	-0.652993	-0.312865	H	-2.222907	-1.968179	0.399486
H	-1.995601	0.484661	1.115990	H	-0.947918	-1.627458	-0.792862
H	1.959706	-0.318373	-0.071805	H	-0.690455	-1.217933	0.901573
n7				n8			
							
33.1 kJ mol ⁻¹				45.1 kJ mol ⁻¹			
$C_s^{-2}A'$				$C_s^{-2}A'$			
Si	-2.187581	1.634287	1.295559	Si	-2.654104	0.750695	0.461772
C	0.051611	1.182614	-0.115557	C	0.054200	2.167105	0.127665
C	1.314261	1.492673	-0.038176	C	1.204947	1.500096	-0.166927
C	-1.232532	0.906849	-0.142409	C	-1.174983	1.525933	0.279596
H	1.718281	2.306210	-0.630132	H	0.101347	3.249863	0.248999
H	1.982839	0.942873	0.614082	H	2.148416	2.023473	-0.279824
H	-1.605409	0.188127	-0.870198	H	1.196132	0.423506	-0.294711

n9				n10			
							
62.1 kJ mol ⁻¹				72.1 kJ mol ⁻¹			
$C_1\text{-}^2A$				$C_s\text{-}^2A'$			
Si	-2.291802	2.588971	1.004979	Si	1.258456	2.565463	1.003571
C	0.397110	1.552862	0.026512	C	-0.623501	1.956099	-0.193860
C	1.610713	1.062007	-0.294224	C	0.616569	1.034679	0.382244
C	-0.724745	2.021162	0.301926	C	-0.361129	0.485074	-0.277162
H	-2.437580	3.782829	0.074313	H	-0.481565	2.545990	-1.097167
H	2.447989	1.727500	-0.468446	H	-1.405388	2.291595	0.484508
H	1.769210	-0.006354	-0.382326	H	-0.795541	-0.412938	-0.675421
n11				n12			
							
80.2 kJ mol ⁻¹				92.2 kJ mol ⁻¹			
$C_s\text{-}^2A'$				$C_1\text{-}^2A$			
Si	-2.574063	2.832638	0.123250	Si	1.209442	2.097470	-0.530517
C	-1.238260	1.527070	0.101728	C	-0.698444	2.114228	-0.082086
C	-2.654502	1.156447	0.943789	C	0.871270	0.519741	0.408493
C	-1.892585	0.264449	0.139078	C	-0.386726	0.642348	-0.077667
H	-1.517244	-0.732291	0.331673	H	-1.404686	2.446373	-0.846667
H	-2.823994	0.955161	2.000984	H	-0.946638	2.519689	0.893844
H	-0.211210	1.638921	0.447506	H	-1.011254	-0.121945	-0.542215

n13				n14			
							
95.3 kJ mol ⁻¹				96.2 kJ mol ⁻¹			
$C_1^{-2}A$				$C_s^{-2}A'$			
Si	-0.985382	2.986144	1.021451	Si	1.266892	2.417929	0.545124
C	-1.112970	1.510143	-0.086940	C	-0.513422	2.108452	-0.345251
C	-0.249537	0.428763	0.000560	C	1.220128	0.475897	0.012334
C	0.510002	-0.511322	0.124227	C	0.113298	0.965102	-0.496432
H	-2.442307	3.405788	0.874610	H	2.016603	2.947139	-0.672214
H	-1.803839	1.493576	-0.929501	H	-1.434786	2.608535	-0.574972
H	1.175602	-1.336872	0.224343	H	1.790465	-0.429923	0.089828
n15				n16			
							
100.5 kJ mol ⁻¹				103.4 kJ mol ⁻¹			
$C_s^{-2}A'$				$C_1^{-2}A$			
Si	-1.190224	2.801061	0.833141	Si	1.193399	2.298845	0.391243
C	-1.168840	1.085298	0.732883	C	-0.704840	2.116248	-0.023680
C	-0.098546	0.262454	0.301977	C	1.226452	0.404007	-0.057734
C	0.810323	-0.436603	-0.063699	C	0.069526	0.893913	-0.211514
H	-2.431565	3.480292	1.319383	H	1.934239	3.126046	-0.613101
H	-2.086989	0.582431	1.037028	H	-1.095714	2.589399	-0.921264
H	1.612611	-1.057174	-0.386591	H	-1.404169	2.114579	0.807277

n17				n18			
							
108.7 kJ mol ⁻¹				117.5 kJ mol ⁻¹			
C ₁ ⁻² A				C _{2v} ⁻² A ₁			
Si	-2.464141	2.945399	0.274357	Si	-2.311951	2.797319	0.436930
C	-1.402738	1.539986	0.017239	C	-1.347058	1.427980	0.366860
C	-2.656658	1.177833	0.870404	C	-0.579950	0.339258	0.311177
C	-1.964943	0.185393	-0.030971	C	0.125545	-0.661917	0.259982
H	-1.409247	-0.612469	0.460416	H	-1.741994	4.155135	0.537058
H	-2.744651	0.954547	1.933667	H	-3.785613	2.721926	0.402298
H	-2.472267	-0.129035	-0.938397	H	0.738262	-1.531412	0.215476
n19				n20			
							
142.3 kJ mol ⁻¹				162.9 kJ mol ⁻¹			
C _s ⁻² A'				C _s ⁻² A'			
Si	0.043742	3.154114	-0.166368	Si	-2.830058	1.396545	0.563817
C	-0.724823	1.416847	-0.148213	C	0.020435	1.929632	0.104027
C	0.785745	1.448685	-0.065657	C	1.226258	1.487302	-0.182331
C	1.844977	0.723600	0.018307	C	-1.178048	1.088902	0.213717
H	-1.148970	1.007794	-1.064990	H	-0.107872	2.998903	0.273833
H	-1.249067	1.071020	0.742447	H	1.697174	0.537596	-0.400024
H	2.139985	-0.317762	0.070963	H	-1.007629	0.017638	0.036540

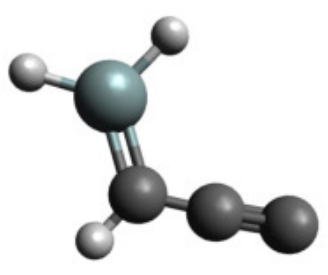
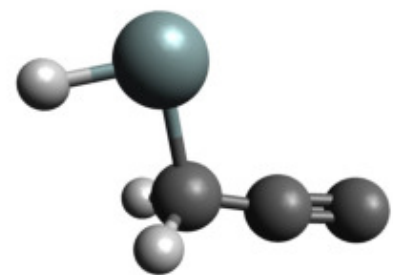
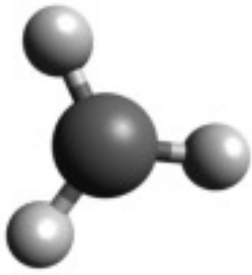
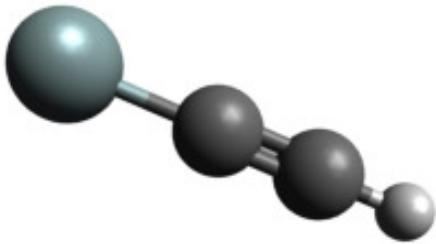
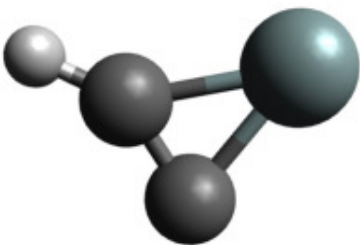
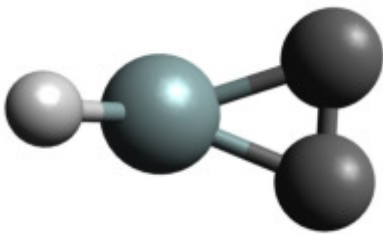
n21				n22			
							
221.1 kJ mol ⁻¹				303.6 kJ mol ⁻¹			
$C_s^{-2}A'$				$C_s^{-2}A'$			
Si	-2.111813	2.725963	0.436207	Si	-0.952202	2.895186	1.046884
C	-0.502023	2.028434	0.423706	C	-1.442045	1.273467	0.049434
C	-0.381293	0.665379	0.337252	C	-0.404343	0.306776	0.063506
C	-0.337798	-0.605402	0.255140	C	0.600189	-0.477548	0.149868
H	-2.333611	4.183554	0.526784	H	-2.310437	3.508799	0.720181
H	-3.302425	1.864084	0.355458	H	-1.683793	1.658231	-0.950735
H	0.387891	2.652209	0.482682	H	-2.368134	0.945547	0.540814

Table A.5: Products relevant to the reaction of electronically excited atomic silicon with methylacetylene and allene to form methyl radical and SiC_2H . Geometries were calculated at the $\omega\text{B97X-V//cc-pVTZ}$ level of theory; relative energies were calculated at the CCSD(T)//CBS level of theory.

CH_3				m1			
							
—				-30.0 kJ mol ⁻¹			
$\text{D}_{3\text{h}}^{-2}\text{A}_2''$				$\text{C}_{\infty\text{v}}^{-2}\text{II}$			
C	-0.951849	0.641383	0.030228	Si	-2.442919	0.826756	0.000000
H	0.066970	0.283748	-0.012939	C	-0.664513	1.191684	0.000000
H	-1.461269	0.932347	-0.877290	C	0.527499	1.436282	0.000000
H	-1.461264	0.707991	0.980921	H	1.572824	1.650730	0.000000
m2				m3			
							
-5.0 kJ mol ⁻¹				144.5 kJ mol ⁻¹			
$\text{C}_s^{-2}\text{A}'$				$\text{C}_s^{-2}\text{A}'$			
Si	-0.263369	1.916480	0.123746	Si	-0.098748	1.527158	-0.929747
C	1.306779	2.912456	-0.144538	C	-0.713212	0.293539	0.287855
C	1.559669	1.640124	-0.007267	C	0.539217	0.390597	0.368126
H	1.692598	3.909459	-0.305242	H	-0.233597	3.003472	-0.658751

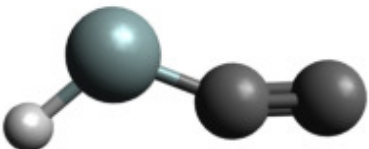
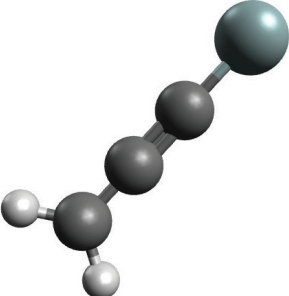
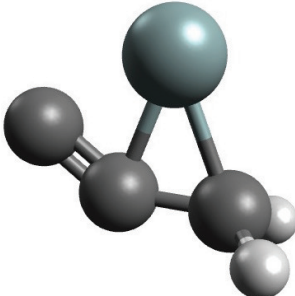
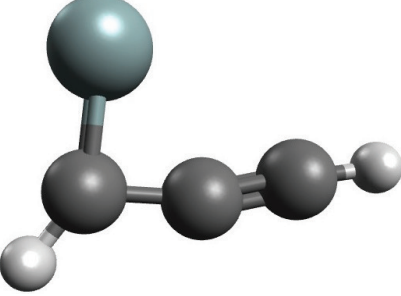
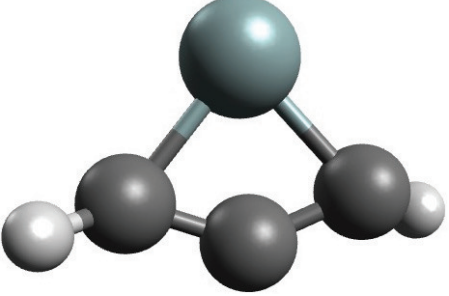
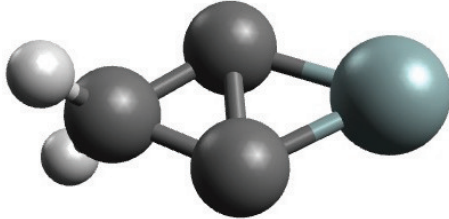
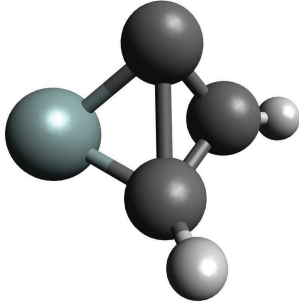
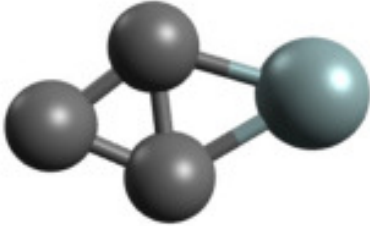

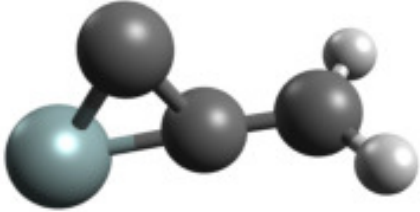
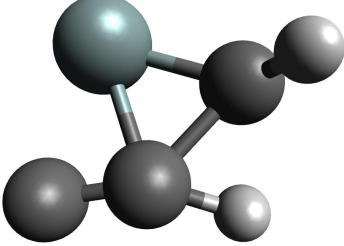
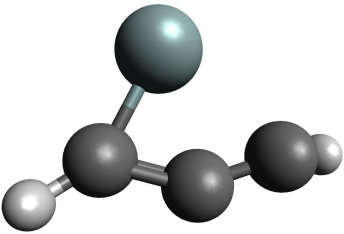
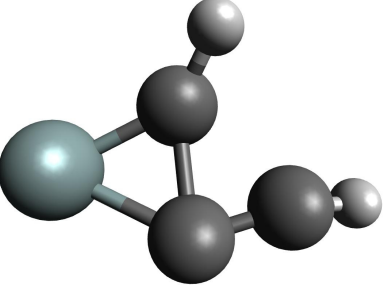
m4			
			
159.2 kJ mol ⁻¹			
C _s ⁻² A'			
Si	-1.052457	2.186941	0.048100
C	0.478917	1.465532	0.044356
C	1.698811	1.296828	-0.287872
H	-2.136410	1.624032	0.921397

Table A.6: Reactants, products, and transition state structures relevant to the singlet SiC_2H_2 system. Geometries were calculated at the $\omega\text{B97X-V//cc-pVTZ}$ level of theory; relative energies were calculated at the CCSD(T)//CBS level of theory.

Reactants							
p1			p2				
							
0 kJ mol^{-1}			15.7 kJ mol^{-1}				
$C_{2v}^{-1}A_1$			$C_s^{-1}A'$				
Si	-2.667415	2.191276	0.000000	Si	-3.530077	0.607099	0.333008
C	-0.985018	2.220382	0.000000	C	-2.115964	1.751749	-0.167586
C	0.298405	2.242563	0.000000	C	-1.762971	0.449585	-0.634584
C	1.607796	2.265203	0.000000	C	-2.980050	2.474570	0.443216
H	2.142021	3.207971	0.000000	H	-0.954113	-0.065250	-0.122807
H	2.174299	1.341470	0.000000	H	-1.792019	0.273905	-1.706863
p3			p4				
							
26.2 kJ mol^{-1}			30.3 kJ mol^{-1}				
$C_s^{-1}A'$			$C_s^{-1}A'$				
Si	-1.497455	1.581760	-1.469801	Si	0.015583	1.421694	0.441321
C	-1.339958	2.070906	0.170228	C	-1.710909	1.657474	1.228824
C	0.014251	1.630794	0.108585	C	-1.833196	1.452865	-0.080188
C	1.093044	1.182725	-0.237854	C	-1.051473	1.232997	-1.134185
H	-1.794955	2.499942	1.048186	H	-2.213088	1.188068	2.060067
H	2.054975	0.801432	-0.489589	H	-1.030405	1.710504	-2.101157

p5				p6			
							
51.0 kJ mol ⁻¹				89.8 kJ mol ⁻¹			
C _{2v} ⁻¹ A ₁				C ₁ ⁻¹ A			
Si	-0.153925	2.791130	0.597108	Si	0.000000	0.000000	0.000000
C	-0.701267	1.901637	-0.854814	C	0.000000	0.000000	1.806628
C	-1.470675	0.643621	-0.899626	C	-1.286808	0.627089	1.815653
C	-1.079103	1.277031	0.374194	C	-0.765193	1.502612	0.924959
H	-0.958764	-0.265564	-1.204780	H	0.697327	0.000000	2.637474
H	-2.515112	0.686694	-1.198739	H	-2.217623	0.494213	2.353974
Products							
[1]				[2]			
							
327.1 kJ mol ⁻¹				332.4 kJ mol ⁻¹			
C _{2v} ⁻¹ A ₁				C _{2v} ⁻¹ A ₁			
Si	-3.475749	2.641607	0.512311	Si	-3.427362	1.625193	1.036789
C	-2.415184	1.166612	0.747246	C	-2.211335	0.501827	-0.133135
C	-2.016023	1.994725	-0.385703	C	-2.242047	1.804914	-0.422423
C	-1.293928	0.804610	-0.061731	C	-2.684682	3.045589	-0.204463

p2→p5				p2→p6			
							
216.6 kJ mol ⁻¹				326.5 kJ mol ⁻¹			
$C_s^{-1}A'$				$C_1^{-1}A$			
Si	-1.747415	2.192117	0.631384	Si	-0.055032	1.783261	0.075704
C	-0.726407	2.290059	-0.882772	C	-1.168897	0.125688	-0.408579
C	0.016254	2.219441	0.409350	C	-1.787386	1.063113	0.218017
C	1.348831	2.236480	0.302214	C	-1.427514	2.444367	1.067918
H	1.899910	3.173627	0.295983	H	-2.035607	3.266860	0.681532
H	1.914855	1.315559	0.186033	H	-2.549883	1.381730	1.028390
p3→p4				p3→p6			
							
34.8 kJ mol ⁻¹				190.5 kJ mol ⁻¹			
$C_1^{-1}A$				$C_1^{-1}A$			
Si	-1.069242	1.492753	-1.390925	Si	-1.913929	1.504303	-1.242424
C	-1.320148	1.984111	0.282526	C	-0.837758	2.188007	-0.048120
C	0.040325	1.733392	0.253700	C	-0.271626	0.758029	-0.566567
C	1.042599	1.415660	-0.447969	C	0.707158	1.171608	0.093043
H	-1.929010	2.506285	0.997954	H	-0.902898	2.598930	0.949658
H	1.756851	0.623631	-0.570277	H	1.716663	1.490465	0.251411

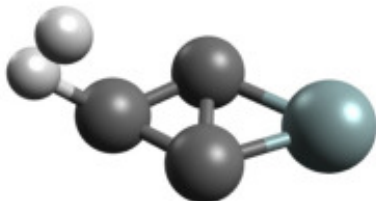
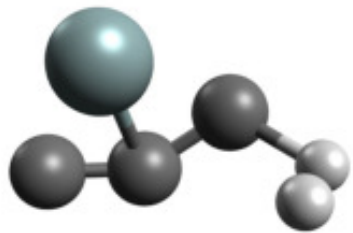
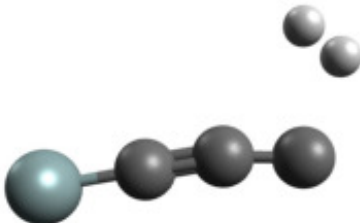
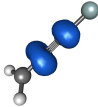
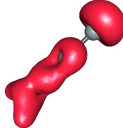
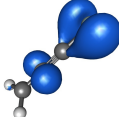
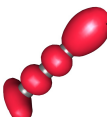

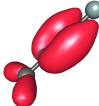
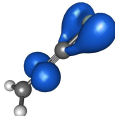
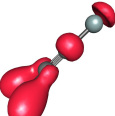
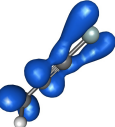
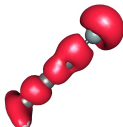
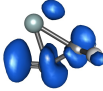

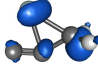
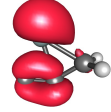
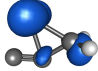

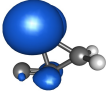
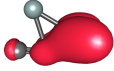
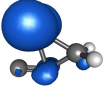

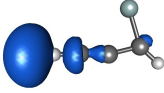
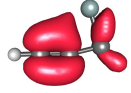
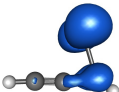
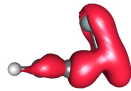
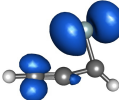
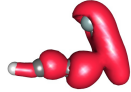
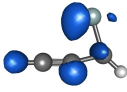
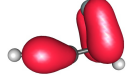
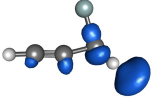
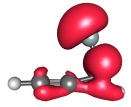
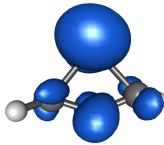
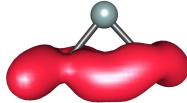
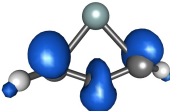

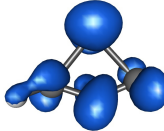
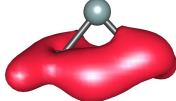
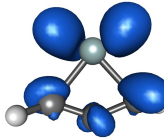
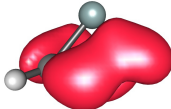
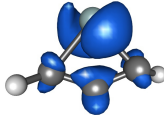
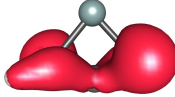
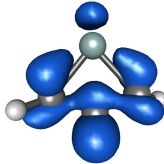
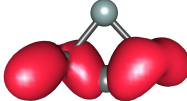
p5→[1]				p2→[2]			
							
417.8 kJ mol ⁻¹				400.4 kJ mol ⁻¹			
$C_s^{-1}A'$				$C_1^{-1}A$			
Si	-0.467866	3.174918	0.595550	Si	-3.654008	0.659771	0.202068
C	-0.477089	2.021651	-0.792545	C	-3.156407	2.579324	0.092405
C	-0.673171	0.590493	-0.708054	C	-2.151736	1.771052	-0.080262
C	-0.877286	1.422661	0.457992	C	-1.646692	0.497172	0.138953
H	-1.559940	-0.070334	-1.308318	H	-1.557132	-0.024346	-1.630107
H	-2.249902	0.491914	-1.259838	H	-1.044179	-0.140306	-1.013032
p1→[3]				→			
							
412.5 kJ mol ⁻¹							
$C_s^{-1}A'$							
Si	-1.284546	0.614725	0.341830				
C	0.280930	-0.071001	0.309093				
C	1.457679	-0.594085	0.274620				
C	2.575093	-1.242370	0.051990				
H	3.725873	-0.775049	1.241686				
H	3.408591	-0.262386	1.718808				

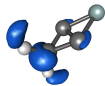
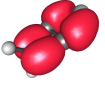
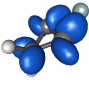
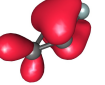
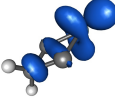
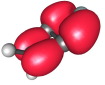
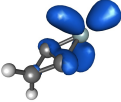
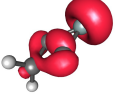
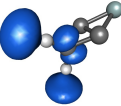
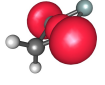
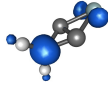
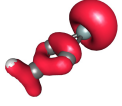
Table A.7: Excited states of six SiC_3H_2 isomers **p1-p6** with excitation energies in the region of a Lyman- α photon.

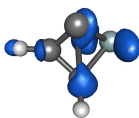
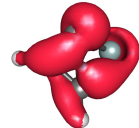
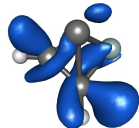
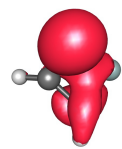
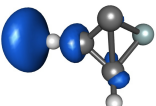
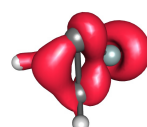
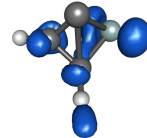

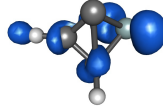

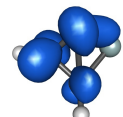

p1						
State	Excitation Energy (eV)	Oscillator Strength	Sym	Major Amplitudes	Attachment Density	Detachment Density
42	9.865	5.61×10^{-2}	1A_1	$2b_2 \rightarrow 4b_2 = 0.300$ $2b_1 \rightarrow 5b_1 = -0.199$ $11a_1 \rightarrow 12a_1 = -0.440$ $11a_1 \rightarrow 13a_1 = -0.179$ $3b_2 \rightarrow 5b_2 = -0.277$ $3b_1 \rightarrow 5b_1 = -0.196$		
46	10.074	1.99×10^{-4}	1B_2	$9a_1 \rightarrow 4b_2 = 0.225$ $10a_1 \rightarrow 4b_2 = 0.617$		
47	10.175	6.77×10^{-2}	1B_2	$3b_2 \rightarrow 13a_1 = 0.675$		
50	10.430	0.177	1A_1	$2b_2 \rightarrow 4b_2 = 0.546$ $11a_1 \rightarrow 12a_1 = 0.225$ $11a_1 \rightarrow 14a_1 = -0.190$ $3b_2 \rightarrow 5b_2 = 0.165$ $3b_1 \rightarrow 5b_1 = 0.161$		
52	10.544	2.45×10^{-2}	1B_1	$10a_1 \rightarrow 4b_1 = 0.454$ $11a_1 \rightarrow 5b_1 = -0.440$ $3b_1 \rightarrow 6b_1 = -0.257$		

p2						
State	Excitation Energy (eV)	Oscillator Strength	Sym	Major Amplitudes	Attachment Density	Detachment Density
46	10.029	0.538	$^1A'$	$12a' \rightarrow 17a' = 0.375$ $3a'' \rightarrow 5a'' = 0.313$ $13a' \rightarrow 17a' = -0.369$		
49	10.207	0.203	$1A'$	$13a' \rightarrow 18a' = 0.633$		
50	10.320	1.04×10^{-3}	$1A''$	$11a' \rightarrow 4a'' = -0.365$ $3a' \rightarrow 17a' = -0.159$ $3a'' \rightarrow 18a' = 0.553$		
51	10.436	0.235	$^1A'$	$2a'' \rightarrow 4a'' = 0.637$		
52	10.588	0.182	$^1A''$	$11a' \rightarrow 4a'' = 0.566$ $3a'' \rightarrow 18a' = 0.371$		

p3						
State	Excitation Energy (eV)	Oscillator Strength	Sym	Major Amplitudes	Attachment Density	Detachment Density
48	9.879	1.30×10^{-2}	$^1A'$	$13a' \rightarrow 18a' = 0.574$ $14a' \rightarrow 18a' = -0.343$		
49	9.957	1.08×10^{-2}	$^1A''$	$12a' \rightarrow 4a'' = 0.612$ $3a'' \rightarrow 20a' = -0.279$		
50	10.007	0.178	$^1A'$	$12a' \rightarrow 15a' = 0.620$		
51	10.220	1.81×10^{-2}	$^1A''$	$3a'' \rightarrow 21a' = 0.650$		
55	10.678	0.120	$^1A'$	$14a' \rightarrow 18a' = 0.195$ $14a' \rightarrow 19a' = 0.580$		

p4						
State	Excitation Energy (eV)	Oscillator Strength	Sym	Major Amplitudes	Attachment Density	Detachment Density
43	9.826	2.49×10^{-2}	1A	$5b \rightarrow 8b = 0.534$ $6b \rightarrow 9b = -0.237$ $6b \rightarrow 10b = -0.348$		
44	9.889	0.895	1B	$7b \rightarrow 11a = 0.163$ $7b \rightarrow 12a = 0.560$ $9a \rightarrow 9b = 0.249$ $10a \rightarrow 10b = -0.177$		
47	10.207	0.248	1A	$8a \rightarrow 11a = 0.169$ $5b \rightarrow 8b = 0.384$ $6b \rightarrow 9b = 0.231$ $6b \rightarrow 10b = 0.426$ $9a \rightarrow 11a = 0.164$		
50	10.422	5.62×10^{-2}	1A	$6b \rightarrow 9b = 0.575$ $6b \rightarrow 10b = -0.320$		
52	10.507	0.147	1B	$8a \rightarrow 8b = -0.168$ $5b \rightarrow 11a = -0.251$ $10a \rightarrow 12b = 0.602$		
53	10.598	5.95×10^{-3}	1B	$5b \rightarrow 11a = 0.618$ $10a \rightarrow 12b = 0.259$		

p5						
State	Excitation Energy (eV)	Oscillator Strength	Sym	Major Amplitudes	Attachment Density	Detachment Density
40	9.778	1.17×10^{-2}	1B_2	$4b_2 \rightarrow 11a_1 = 0.621$ $4b_2 \rightarrow 12a_1 = -0.264$		
41	9.848	5.06×10^{-7}	1A_2	$3b_1 \rightarrow 6b_2 = 0.678$		
42	9.909	1.32×10^{-2}	1B_2	$4b_2 \rightarrow 11a_1 = 0.259$ $4b_2 \rightarrow 12a_1 = 0.636$		
44	10.025	0.499	1A_1	$9a_1 \rightarrow 11a_1 = -0.155$ $9a_1 \rightarrow 12a_1 = 0.659$		
46	10.156	1.17×10^{-2}	1B_1	$9a_1 \rightarrow 5b_1 = 0.208$ $10a_1 \rightarrow 5b_1 = 0.666$		
50	10.468	0.436	1A_1	$9a_1 \rightarrow 11a_1 = 0.589$ $9a_1 \rightarrow 13a_1 = 0.154$ $3b_1 \rightarrow 5b_1 = 0.201$ $10a_1 \rightarrow 11a_1 = -0.155$ $10a_1 \rightarrow 13a_1 = -0.186$		

p6						
State	Excitation Energy (eV)	Oscillator Strength	Sym	Major Amplitudes	Attachment Density	Detachment Density
45	9.801	0.158	1A	15a \rightarrow 22a = 0.554 16a \rightarrow 23a = 0.291 16a \rightarrow 24a = 0.195		
47	9.857	5.58×10^{-2}	1A	17a \rightarrow 25a = 0.673		
49	9.991	4.45×10^{-2}	1A	13a \rightarrow 18a = 0.167 15a \rightarrow 22a = -0.286 16a \rightarrow 22a = 0.162 16a \rightarrow 23a = 0.572		
51	10.154	4.37×10^{-2}	1A	13a \rightarrow 18a = 0.410 15a \rightarrow 23a = 0.228 16a \rightarrow 22a = 0.160 16a \rightarrow 23a = -0.201 16a \rightarrow 24a = 0.382		
53	10.236	0.187	1A	13a \rightarrow 18a = -0.451 15a \rightarrow 23a = 0.367 16a \rightarrow 24a = 0.259		
54	10.292	2.07×10^{-2}	1A	13a \rightarrow 19a = 0.573 15a \rightarrow 23a = 0.321		

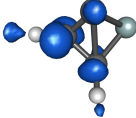

57	10.338	5.44×10^{-2}	^1A	$13\text{a} \rightarrow 19\text{a} = 0.317$ $15\text{a} \rightarrow 23\text{a} = -0.403$ $16\text{a} \rightarrow 24\text{a} = 0.381$		
----	--------	-----------------------	--------------	--	--	---

Table A.8: Products relevant to the photodissociation of SiC_3H_2 to form atomic hydrogen and SiC_3H . Geometries were calculated at the $\omega\text{B97X-V//cc-pVTZ}$ level of theory; relative energies were calculated at the CCSD(T)//CBS level of theory.

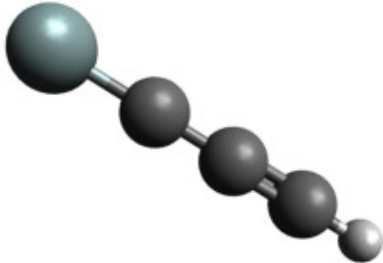
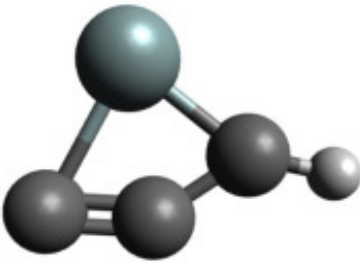
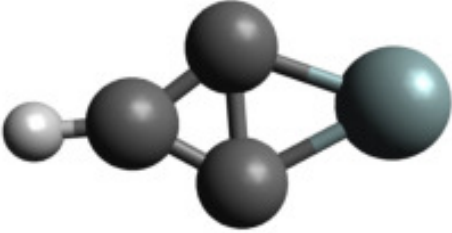
1				2			
							
386.9 kJ mol ⁻¹				399.7 kJ mol ⁻¹			
$C_{\infty v}^{-2}\Pi$				$C_s^{-2}A'$			
Si	-0.151031	2.995567	0.000000	Si	0.160190	2.314648	0.000000
C	-0.284810	1.318339	0.000000	C	1.981786	2.002412	0.000000
C	-0.391670	-0.020999	0.000000	C	1.341367	0.789581	0.000000
C	-0.488903	-1.239734	0.000000	C	0.164322	0.230650	0.000000
H	-0.573593	-2.301281	0.000000	H	3.012843	2.311956	0.000000
3							
							
409.7 kJ mol ⁻¹							
$C_{2v}^{-2}A_1$							
Si	0.375572	2.261711	0.000000				
C	-0.388292	0.542499	0.000000				
C	1.102760	0.526660	0.000000				
C	0.345057	-0.611559	0.000000				
H	0.333627	-1.686713	0.000000				

Table A.9: Tunneling-corrected RRKM reaction rate constants, transition state imaginary frequencies, and reaction path degeneracies for the silicon–methylacetylene, silicon–allene, and silicon–D3-methylacetylene systems.

Reaction	k_f (s^{-1})	k_b (s^{-1})	ω_b (cm^{-1})	Forward Reaction Path Degeneracy	Backwards Reaction Path Degeneracy
[i1]→[i2]	3.74×10^6	5.64×10^7	1235	2	1
[i1]→[i4]	1.37×10^{11}	5.67×10^{10}	168	2	2
[i1]→[i5]	3.44×10^8	2.88×10^9	1399	2	2
[i1]→[i6]	6.03×10^7	1.39×10^9	1018	2	1
[i2]→[i5]	8.55×10^{12}	4.76×10^{12}	190	1	2
[i2]→[i10]	2.78×10^5	1.52×10^6	1207	1	2
[i4]→[i13]	1.45×10^{11}	6.54×10^{12}	203	2	2
[i5]→[i9]	1.04×10^{11}	2.38×10^{11}	883	2	2
[i6]→[i9]	4.62×10^{12}	3.83×10^{12}	240	1	2
[i6]→[i10]	1.16×10^{10}	4.13×10^{10}	989	1	2
[i6]→[i12]	3.73×10^{12}	3.22×10^{12}	217	1	2
[i7]→[i10]	7.49×10^{11}	3.28×10^{12}	124	2	2
[i8]→[i9]	2.05×10^7	5.54×10^7	1532	2	2
[i8]→[i12]	2.11×10^9	5.95×10^9	1082	2	2
[i9]→ p1	1.36×10^9		1470	2	
[i1]→ p2	4.81×10^2		1225	1	
[i6]→ p2	8.41×10^6		1429	1	
[i13]→ p2	1.09×10^7		1399	2	
[i12]→ p3	1.65×10^8		1475	2	
[i12]→ p3'	2.49×10^8		1424	2	
[i6]→ p4	1.97×10^9		908	1	
[i1]→ n2	1.47×10^5			1	
[i13]→ n6	1.39×10^5			1	
[i1]→ n6	6.58×10^3			1	
[i2]→ n3	4.94×10^5			1	
[i2]→ n4	7.54×10^4			1	
[i4]→ n1	4.11×10^6			1	
[i6]→ n4	2.32×10^5			1	
[i1]→ m2	5.40×10^5			1	

Table A.9: continued

Reaction	k_f (s^{-1})	k_b (s^{-1})	ω_b (cm^{-1})	Forward Reaction Path Degeneracy	Backwards Reaction Path Degeneracy
[i1a]→[i2a]	1.28×10^6	1.93×10^7	977	1	1
[i1b]→[i2b]	1.56×10^6	2.33×10^7	1184	1	1
[i1b]→[i2c]	1.34×10^6	1.99×10^7	1006	1	1
[i1b]→[i2d]	1.35×10^6	2.01×10^7	1000	1	1
[i1a]→[i2e]	1.28×10^6	1.93×10^7	977	1	1
[i1b]→[i2f]	1.56×10^6	2.33×10^7	1184	1	1
[i1b]→[i2g]	1.34×10^6	1.99×10^7	1006	1	1
[i1b]→[i2h]	1.35×10^6	2.01×10^7	1000	1	1
[i1a]→[i4a]	9.67×10^{10}	4.35×10^{10}	166	2	2
[i1b]→[i4b]	9.27×10^{10}	5.44×10^{10}	152	2	2
[i1a]→[i5a]	1.49×10^8	1.48×10^9	1063	2	2
[i1b]→[i5b]	2.00×10^8	1.93×10^9	1371	2	2
[i1b]→[i5c]	1.57×10^8	1.58×10^9	1075	2	2
[i1b]→[i5d]	1.53×10^8	1.51×10^9	1078	2	2
[i1a]→[i6a]	2.58×10^7	6.60×10^8	801	1	1
[i1b]→[i6b]	3.44×10^7	8.92×10^8	993	1	1
[i1b]→[i6c]	2.50×10^7	6.49×10^8	803	1	1
[i1b]→[i6d]	2.53×10^7	6.55×10^8	816	1	1
[i1a]→[i6e]	2.58×10^7	6.60×10^8	801	1	1
[i1b]→[i6f]	3.44×10^7	8.92×10^8	993	1	1
[i1b]→[i6g]	2.50×10^7	6.49×10^8	803	1	1
[i1b]→[i6h]	2.53×10^7	6.55×10^8	816	1	1
[i2a]→[i2e]	3.64×10^{12}	3.64×10^{12}	227	1	1
[i2b]→[i2f]	3.98×10^{12}	3.98×10^{12}	249	1	1
[i2c]→[i2h]	3.65×10^{12}	3.68×10^{12}	229	1	1
[i2d]→[i2g]	3.68×10^{12}	3.65×10^{12}	229	1	1
[i2a]→[i3a]	9.68×10^9	1.04×10^{11}	587	1	1
[i2b]→[i3d]	8.81×10^9	9.40×10^{10}	551	1	1
[i2c]→[i3c]	9.22×10^9	1.02×10^{11}	589	1	1
[i2d]→[i3b]	9.12×10^9	1.01×10^{11}	566	1	1
[i2e]→[i3d]	9.68×10^9	1.04×10^{11}	587	1	1
[i2f]→[i3a]	8.81×10^9	9.40×10^{10}	551	1	1
[i2g]→[i3c]	9.22×10^9	1.02×10^{11}	589	1	1
[i2d]→[i3b]	9.12×10^9	1.01×10^{11}	566	1	1
[i2a]→[i5a]	6.86×10^{12}	4.52×10^{12}	177	1	1
[i2b]→[i5b]	6.17×10^{12}	3.98×10^{12}	161	1	1

Table A.9: continued

Reaction	k_f (s^{-1})	k_b (s^{-1})	ω_b (cm^{-1})	Forward Reaction Path Degeneracy	Backwards Reaction Path Degeneracy
[i2c] → [i5c]	5.79×10^{12}	3.93×10^{12}	155	1	1
[i2d] → [i5d]	6.08×10^{12}	4.00×10^{12}	160	1	1
[i2e] → [i5a]	6.86×10^{12}	4.52×10^{12}	177	1	1
[i2f] → [i5b]	6.17×10^{12}	3.98×10^{12}	161	1	1
[i2g] → [i5c]	5.79×10^{12}	3.93×10^{12}	155	1	1
[i2h] → [i5d]	6.08×10^{12}	4.00×10^{12}	160	1	1
[i2a] → [i10d]	5.41×10^4	3.34×10^5	912	1	1
[i2b] → [i10c]	9.27×10^4	5.70×10^5	1195	1	1
[i2c] → [i10b]	5.41×10^4	3.34×10^5	903	1	1
[i2d] → [i10a]	5.28×10^4	3.26×10^5	903	1	1
[i2e] → [i10b]	5.41×10^4	3.34×10^5	912	1	1
[i2f] → [i10a]	9.27×10^4	5.70×10^5	1195	1	1
[i2g] → [i10d]	5.41×10^4	3.34×10^5	903	1	1
[i2h] → [i10c]	5.28×10^4	3.26×10^5	903	1	1
[i4a] → [i13a]	1.16×10^{11}	6.46×10^{12}	202	2	2
[i4b] → [i13b]	1.28×10^{11}	5.47×10^{12}	171	2	2
[i5a] → [i9a]	7.40×10^{10}	7.21×10^{10}	706	2	2
[i5b] → [i9b]	8.26×10^{10}	8.19×10^{10}	832	2	2
[i5c] → [i9d]	7.22×10^{10}	6.91×10^{10}	706	2	2
[i5d] → [i9c]	7.01×10^{10}	6.89×10^{10}	716	2	2
[i6a] → [i9a]	3.40×10^{12}	1.29×10^{12}	199	1	1
[i6b] → [i9b]	4.04×10^{12}	1.49×10^{12}	224	1	1
[i6c] → [i9c]	3.61×10^{12}	1.34×10^{12}	205	1	1
[i6d] → [i9d]	3.47×10^{12}	1.29×10^{12}	197	1	1
[i6e] → [i9a]	3.40×10^{12}	1.29×10^{12}	199	1	1
[i6f] → [i9b]	4.04×10^{12}	1.49×10^{12}	224	1	1
[i6g] → [i9d]	3.61×10^{12}	1.34×10^{12}	205	1	1
[i6h] → [i9c]	3.47×10^{12}	1.29×10^{12}	197	1	1
[i6a] → [i10b]	6.54×10^9	2.39×10^{10}	795	1	1
[i6b] → [i10a]	8.57×10^9	3.05×10^{10}	980	1	1
[i6c] → [i10d]	6.42×10^9	2.26×10^{10}	794	1	1
[i6d] → [i10c]	6.65×10^9	2.36×10^{10}	794	1	1
[i6e] → [i10d]	6.54×10^9	2.39×10^{10}	795	1	1
[i6f] → [i10c]	8.57×10^9	3.05×10^{10}	980	1	1
[i6g] → [i10b]	6.42×10^9	2.26×10^{10}	794	1	1
[i6h] → [i10a]	6.65×10^9	2.36×10^{10}	794	1	1

Table A.9: continued

Reaction	k_f (s^{-1})	k_b (s^{-1})	ω_b (cm^{-1})	Forward Reaction Path Degeneracy	Backwards Reaction Path Degeneracy
[i6a]→[i12a]	2.39×10^{12}	2.39×10^{12}	163	1	1
[i6b]→[i12b]	3.32×10^{12}	3.10×10^{12}	213	1	1
[i6c]→[i12d]	2.52×10^{12}	2.39×10^{12}	163	1	1
[i6d]→[i12c]	2.42×10^{12}	2.29×10^{12}	163	1	1
[i6e]→[i12a]	2.39×10^{12}	2.39×10^{12}	163	1	1
[i6f]→[i12b]	3.32×10^{12}	3.10×10^{12}	213	1	1
[i6g]→[i12c]	2.52×10^{12}	2.39×10^{12}	163	1	1
[i6h]→[i12d]	2.42×10^{12}	2.29×10^{12}	163	1	1
[i7a]→[i10a]	6.96×10^{11}	3.07×10^{12}	116	2	2
[i7b]→[i10b]	7.04×10^{11}	3.09×10^{12}	116	2	2
[i7c]→[i10d]	6.86×10^{11}	3.08×10^{12}	117	2	2
[i7d]→[i10c]	7.29×10^{11}	3.21×10^{12}	123	2	2
[i8a]→[i9d]	4.65×10^6	5.06×10^6	1134	2	2
[i8b]→[i9c]	7.22×10^6	8.24×10^6	1498	2	2
[i8c]→[i9b]	5.32×10^6	5.90×10^6	1148	2	2
[i8d]→[i9a]	4.54×10^6	5.21×10^6	1134	2	2
[i8a]→[i12a]	8.84×10^8	2.51×10^9	789	2	2
[i8b]→[i12c]	8.48×10^8	2.46×10^9	811	2	2
[i8c]→[i12b]	8.72×10^8	2.45×10^9	794	2	2
[i8d]→[i12d]	1.23×10^9	3.63×10^9	1058	2	2
[i9a]→ p1a	2.29×10^8		1403	2	
[i9b]→ p1a	1.84×10^8		1118	2	
[i9c]→ p1b	1.43×10^8		1064	2	
[i9d]→ p1b	1.44×10^8		1064	2	
[i1a]→ p2a	4.83×10^1		1104	1	
[i1b]→ p2a	4.93×10^1		1105	1	
[i1b]→ p2b	1.42×10^1		980	1	
[i1b]→ p2c	1.42×10^1		980	1	
[i6a]→ p2a	2.67×10^6		1372	1	
[i6b]→ p2a	2.12×10^6		1080	1	
[i6c]→ p2b	1.57×10^6		1032	1	
[i6d]→ p2c	1.58×10^6		1032	1	
[i6e]→ p2a	2.67×10^6		1372	1	
[i6f]→ p2a	2.12×10^6		1080	1	
[i6g]→ p2c	1.57×10^6		1032	1	
[i6h]→ p2b	1.58×10^6		1032	1	

Table A.9: continued

Reaction	k_f (s^{-1})	k_b (s^{-1})	ω_b (cm^{-1})	Forward Reaction Path Degeneracy	Backwards Reaction Path Degeneracy
[i13a]→ p2a	3.10×10^6		1067	2	
[i13b]→ p2a	4.78×10^6		1327	2	
[i13b]→ p2b	2.65×10^6		1030	2	
[i13b]→ p2c	2.65×10^6		1024	2	
[i12a]→ p3a	4.26×10^7		1060	2	
[i12b]→ p3c	5.00×10^7		1111	2	
[i12c]→ p3c	6.76×10^7		1409	2	
[i12d]→ p3b	4.61×10^7		1076	2	
[i12a]→ p3a'	7.47×10^7		1023	2	
[i12b]→ p3c'	8.62×10^7		1071	2	
[i12c]→ p3b'	7.30×10^7		1034	2	
[i12d]→ p3c'	1.19×10^8		1364	2	
[i6a]→ p4a	7.46×10^8		675	1	
[i6b]→ p4b	8.81×10^8		720	1	
[i6c]→ p4a	7.71×10^8		679	1	
[i6d]→ p4b	1.05×10^9		837	1	
[i6e]→ p4a	7.46×10^8		675	1	
[i6f]→ p4b	8.81×10^8		720	1	
[i6g]→ p4a	7.71×10^8		679	1	
[i6h]→ p4b	1.05×10^9		837	1	

A.3 Figures

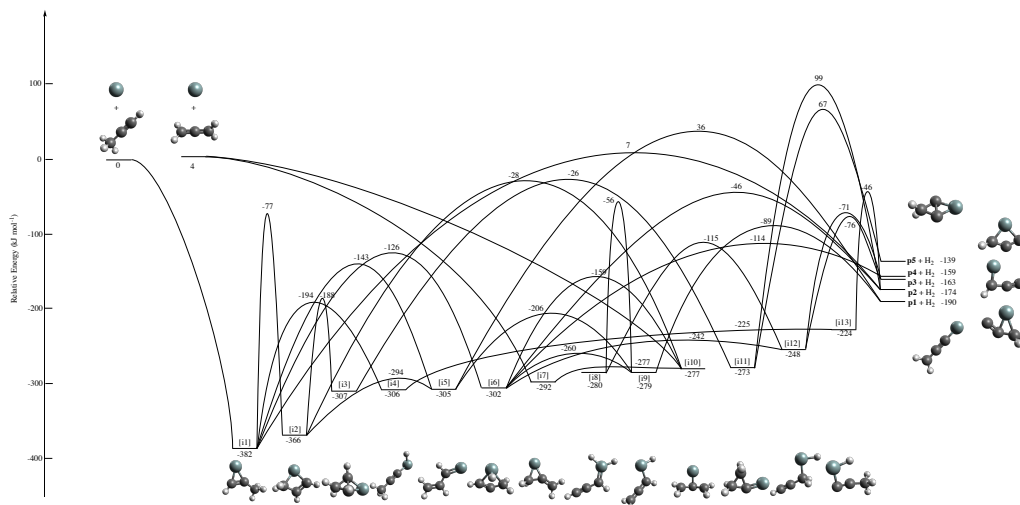


Figure A.1: Complete potential energy surfaces involved in the reactions of electronically excited silicon atoms (Si^1D) with allene and methylacetylene. Relative energies are given in units of kJ mol^{-1} . Colors of the atoms: silicon (green), carbon (black) and hydrogen (light grey). Taken with permission from Ref. 93.

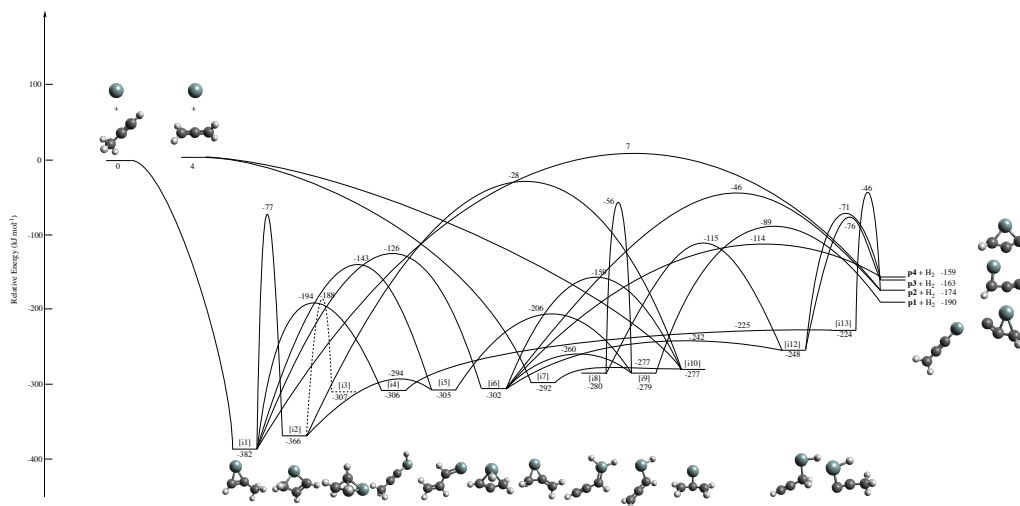


Figure A.2: Pathways exploited in the RRKM calculations to determine the branching ratios in the reactions of electronically excited silicon atoms (Si^1D) with methylacetylene, allene, and D3-methylacetylene. Relative energies are given in units of kJ mol^{-1} . Colors of the atoms: silicon (green), carbon (black) and hydrogen (light grey). Taken with permission from Ref. 93.

Appendix B

Additional Information: Benchmarking the Performance of the ReaxFF Reactive Force Field on Hydrogen Combustion Systems

B.1 Reactive Pathways

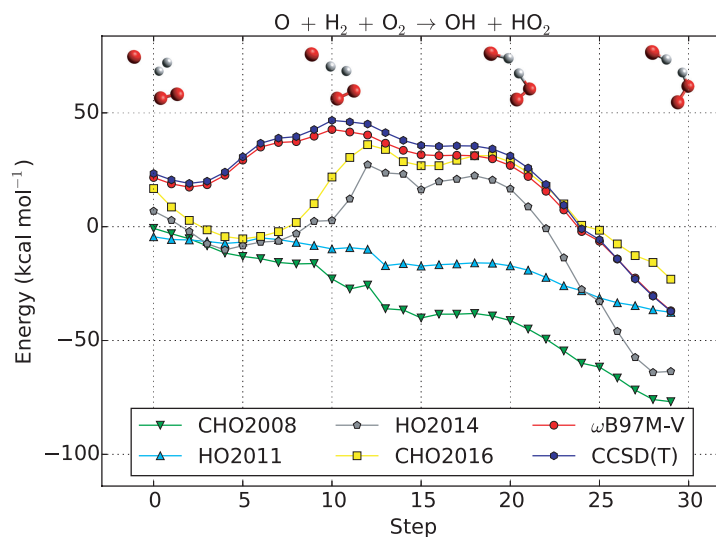


Figure B.1: Potential energies, in kcal mol^{-1} , along the $O + H_2 + O_2 \rightarrow OH + HO_2$ reactive trajectory, extracted from a larger MD simulation. The parent simulation was run using ReaxFF with the HO2011 parameter set. The energies presented are relative to isolated O, H_2 , and O_2 at the ReaxFF/HO2011 optimized geometries.

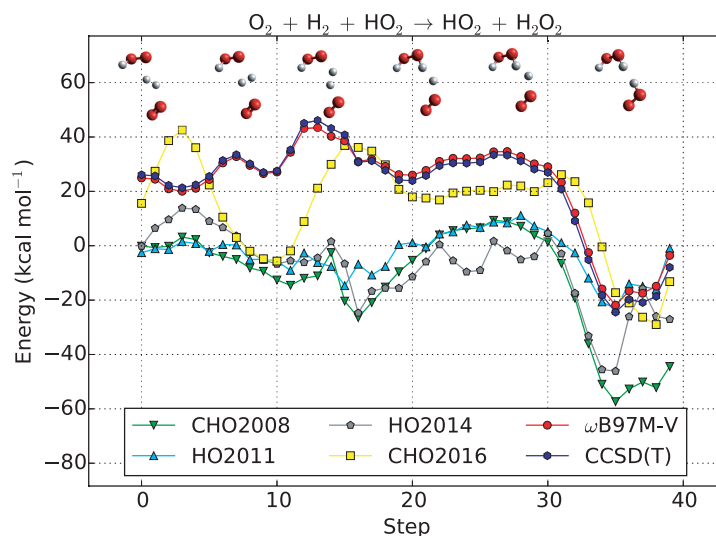


Figure B.2: Potential energies, in kcal mol^{-1} , along the $O_2 + H_2 + HO_2 \rightarrow HO_2 + H_2O_2$ reactive trajectory, extracted from a larger MD simulation. The parent simulation was run using ReaxFF with the HO2011 parameter set. The energies presented are relative to isolated O_2 , H_2 , and HO_2 at the ReaxFF/HO2011 optimized geometries.

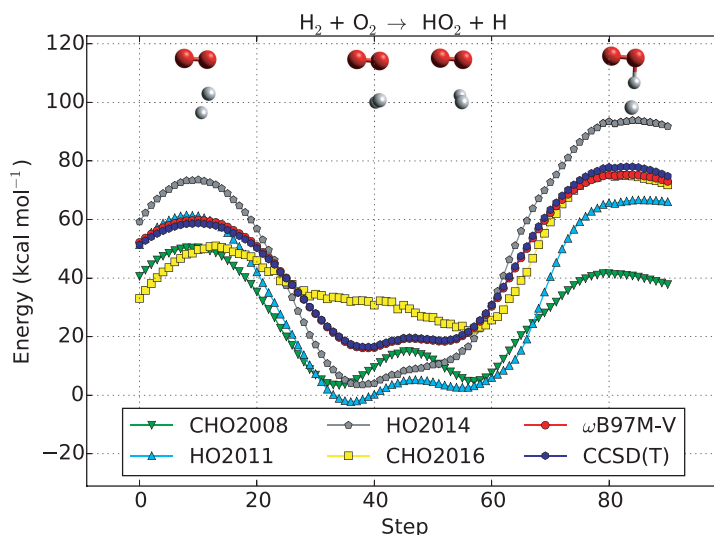


Figure B.3: Potential energies, in kcal mol^{-1} , along the $\text{H}_2 + \text{O}_2 \longrightarrow \text{HO}_2 + \text{H}$ reactive trajectory, extracted from a larger MD simulation. The parent simulation was run using ReaxFF with the HO2011 parameter set. The energies presented are relative to isolated H_2 and O_2 at the ReaxFF/HO2011 optimized geometries.

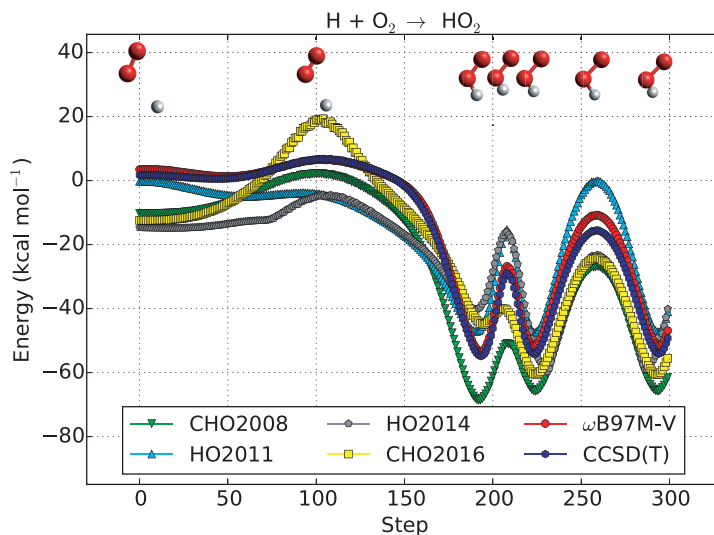


Figure B.4: Potential energies, in kcal mol^{-1} , along the $\text{H} + \text{O}_2 \longrightarrow \text{HO}_2$ reactive trajectory, extracted from a larger MD simulation. The parent simulation was run using ReaxFF with the HO2011 parameter set. The energies presented are relative to isolated H and O_2 at the ReaxFF/HO2011 optimized geometries.

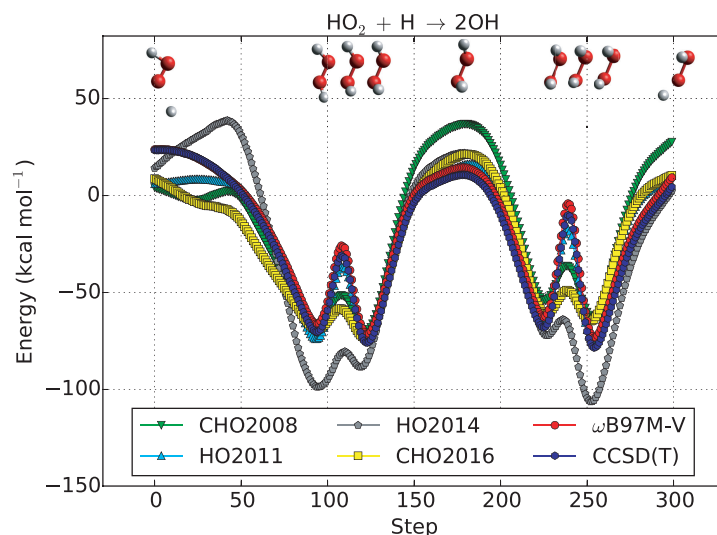


Figure B.5: Potential energies, in kcal mol^{-1} , along the $\text{HO}_2 + \text{H} \longrightarrow 2\text{OH}$ reactive trajectory, extracted from a larger MD simulation. The parent simulation was run using ReaxFF with the HO2011 parameter set. The energies presented are relative to isolated HO_2 and H at the ReaxFF/HO2011 optimized geometries.

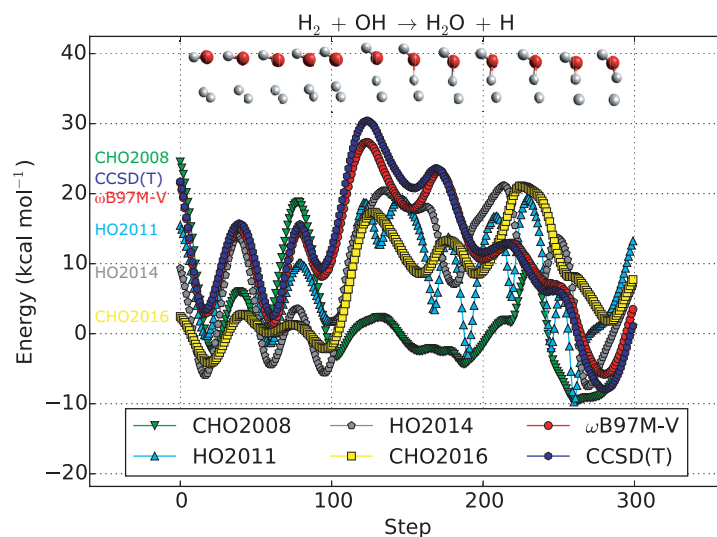


Figure B.6: Potential energies, in kcal mol^{-1} , along the $\text{H}_2 + \text{OH} \longrightarrow \text{H}_2\text{O} + \text{H}$ reactive trajectory, extracted from a larger MD simulation. The parent simulation was run using ReaxFF with the HO2011 parameter set. The energies presented are relative to isolated H_2 and OH at the ReaxFF/HO2011 optimized geometries.

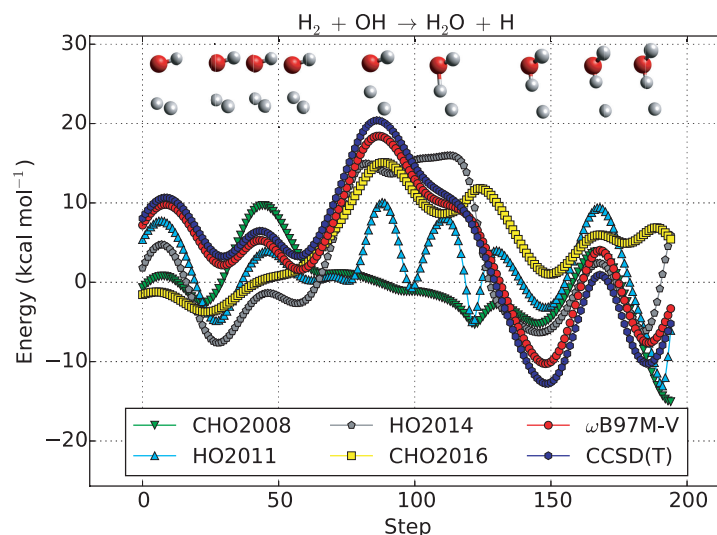


Figure B.7: Potential energies, in kcal mol^{-1} , along the $\text{H}_2 + \text{OH} \longrightarrow \text{H}_2\text{O} + \text{H}$ reactive trajectory, extracted from a larger MD simulation. The parent simulation was run using ReaxFF with the HO2011 parameter set. The energies presented are relative to isolated H_2 and OH at the ReaxFF/HO2011 optimized geometries.

B.2 Intrinsic Reaction Coordinate Scans

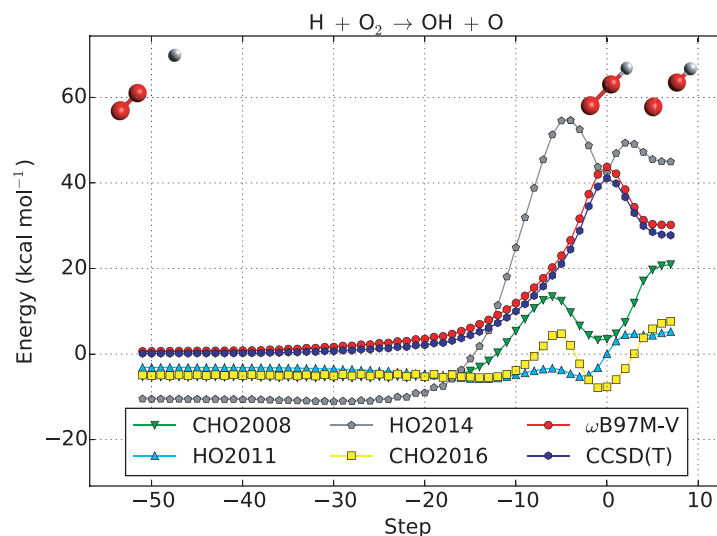


Figure B.8: Potential energies, in kcal mol^{-1} , along the $\text{H} + \text{O}_2 \longrightarrow \text{OH} + \text{O}$ intrinsic reaction coordinate. The intrinsic reaction coordinate was calculated at the $\omega\text{B97M-V/cc-pVTZ}$ level of theory. The energies presented are relative to the energies of isolated H and O_2 computed at the $\omega\text{B97M-V/cc-pVTZ}$ optimized geometries.

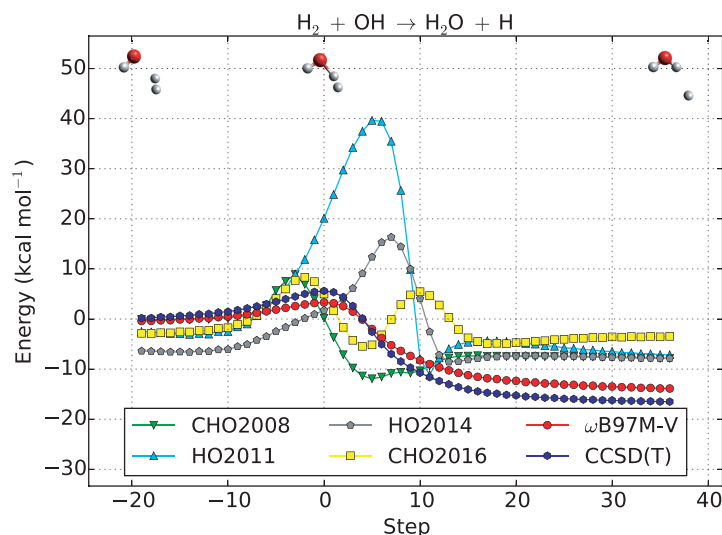


Figure B.9: Potential energies, in kcal mol^{-1} , along the $\text{H}_2 + \text{OH} \longrightarrow \text{H}_2\text{O} + \text{H}$ intrinsic reaction coordinate. The intrinsic reaction coordinate was calculated at the $\omega\text{B97M-V/cc-pVTZ}$ level of theory. The energies presented are relative to the energies of isolated H_2 and OH computed at the $\omega\text{B97M-V/cc-pVTZ}$ optimized geometries.

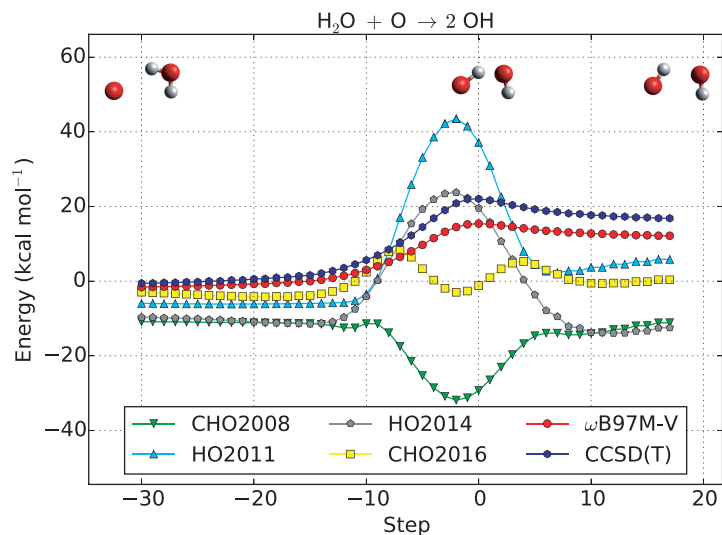


Figure B.10: Potential energies, in kcal mol^{-1} , along the $\text{H}_2\text{O} + \text{O} \longrightarrow 2\text{OH}$ intrinsic reaction coordinate. The intrinsic reaction coordinate was calculated at the $\omega\text{B97M-V/cc-pVTZ}$ level of theory. The energies presented are relative to the energies of isolated H_2O and O computed at the $\omega\text{B97M-V/cc-pVTZ}$ optimized geometries.

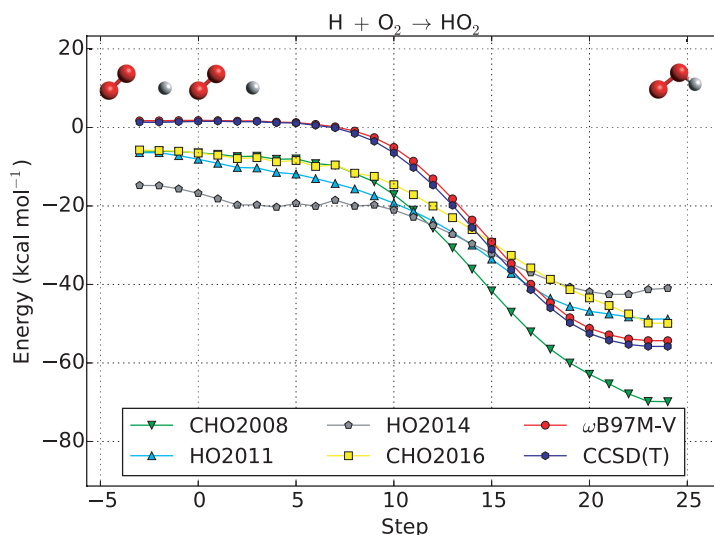


Figure B.11: Potential energies, in kcal mol^{-1} , along the $\text{H} + \text{O}_2 \longrightarrow \text{HO}_2$ intrinsic reaction coordinate. The intrinsic reaction coordinate was calculated at the $\omega\text{B97M-V/cc-pVTZ}$ level of theory. The energies presented are relative to the energies of isolated H and O_2 computed at the $\omega\text{B97M-V/cc-pVTZ}$ optimized geometries.

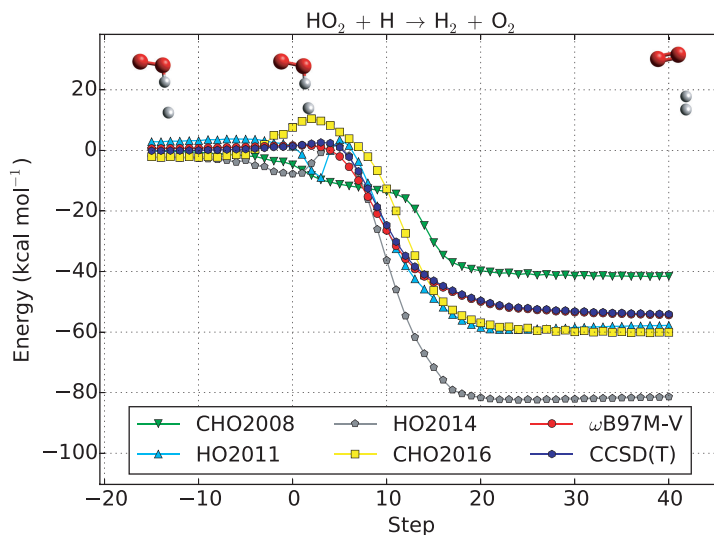


Figure B.12: Potential energies, in kcal mol^{-1} , along the $\text{HO}_2 + \text{H} \longrightarrow \text{H}_2 + \text{O}_2$ intrinsic reaction coordinate. The intrinsic reaction coordinate was calculated at the $\omega\text{B97M-V/cc-pVTZ}$ level of theory. The energies presented are relative to the energies of isolated HO_2 and H computed at the $\omega\text{B97M-V/cc-pVTZ}$ optimized geometries.

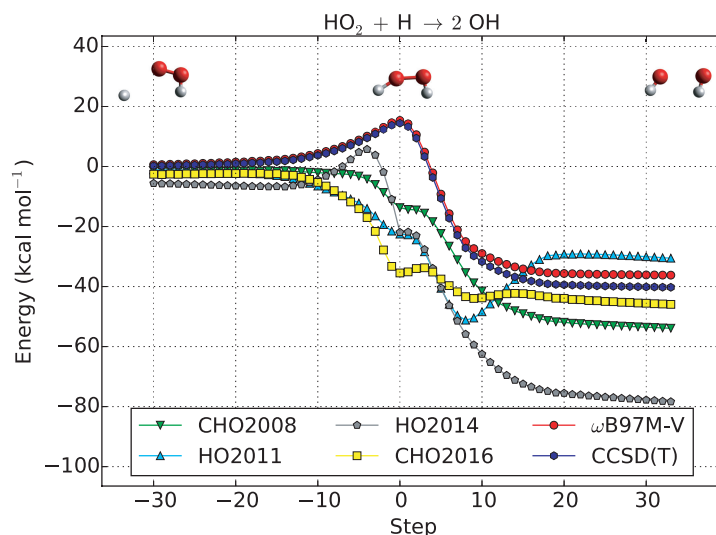


Figure B.13: Potential energies, in kcal mol^{-1} , along the $\text{HO}_2 + \text{H} \longrightarrow 2 \text{OH}$ intrinsic reaction coordinate. The intrinsic reaction coordinate was calculated at the $\omega\text{B97M-V/cc-pVTZ}$ level of theory. The energies presented are relative to the energies of isolated HO_2 and H computed at the $\omega\text{B97M-V/cc-pVTZ}$ optimized geometries.

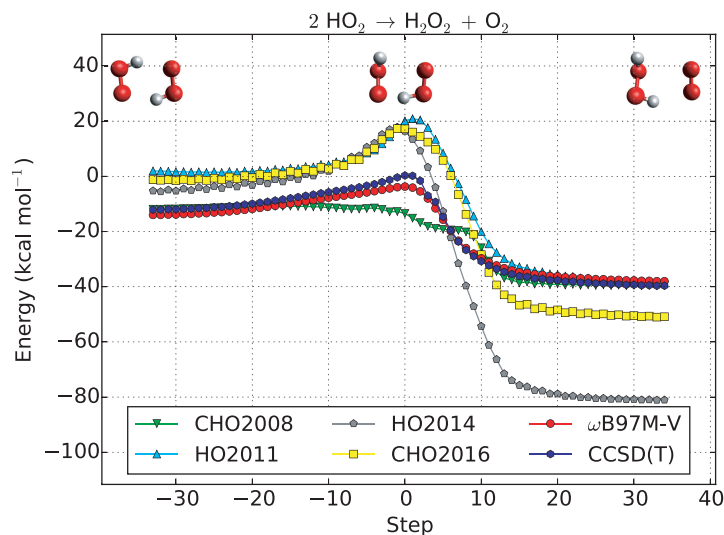


Figure B.14: Potential energies, in kcal mol^{-1} , along the $2 \text{HO}_2 \longrightarrow \text{H}_2\text{O}_2 + \text{O}_2$ intrinsic reaction coordinate. The intrinsic reaction coordinate was calculated at the $\omega\text{B97M-V/cc-pVTZ}$ level of theory. The energies presented are relative to the energies of two isolated HO_2 computed at the $\omega\text{B97M-V/cc-pVTZ}$ optimized geometries.

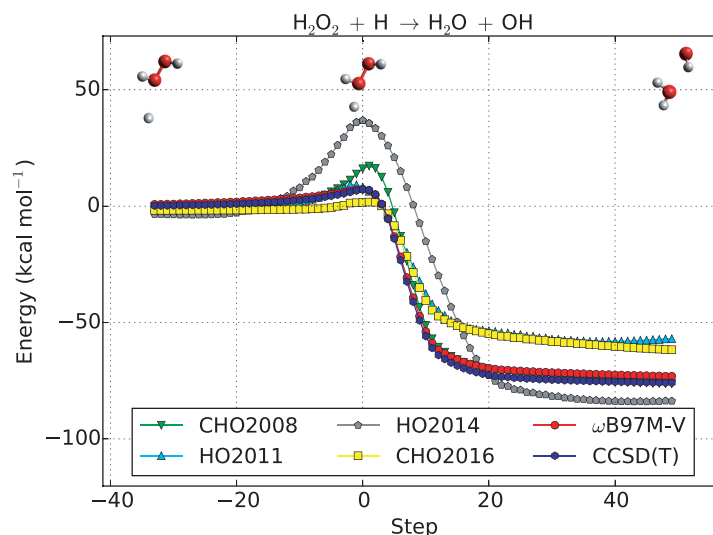


Figure B.15: Potential energies, in kcal mol^{-1} , along the $\text{H}_2\text{O}_2 + \text{H} \longrightarrow \text{H}_2\text{O} + \text{OH}$ intrinsic reaction coordinate. The intrinsic reaction coordinate was calculated at the $\omega\text{B97M-V/cc-pVTZ}$ level of theory. The energies presented are relative to the energies of isolated H_2O_2 and H computed at the $\omega\text{B97M-V/cc-pVTZ}$ optimized geometries.

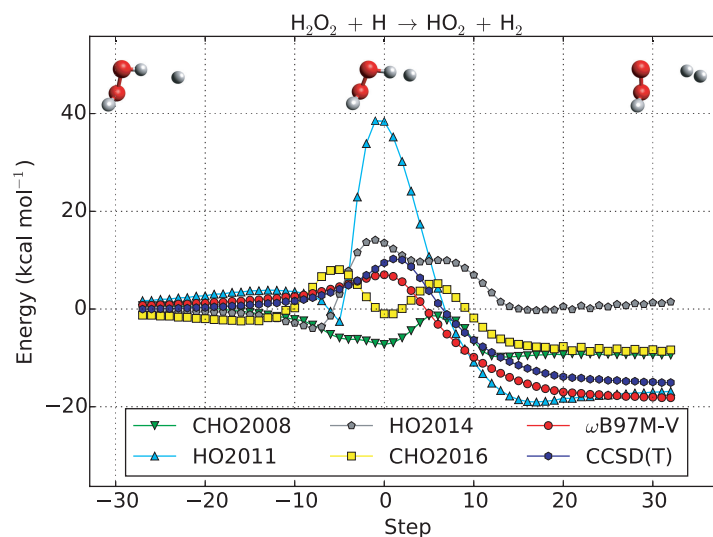


Figure B.16: Potential energies, in kcal mol^{-1} , along the $\text{H}_2\text{O}_2 + \text{H} \longrightarrow \text{H}_2 + \text{HO}_2$ intrinsic reaction coordinate. The intrinsic reaction coordinate was calculated at the $\omega\text{B97M-V/cc-pVTZ}$ level of theory. The energies presented are relative to the energies of isolated H_2O_2 and H computed at the $\omega\text{B97M-V/cc-pVTZ}$ optimized geometries.

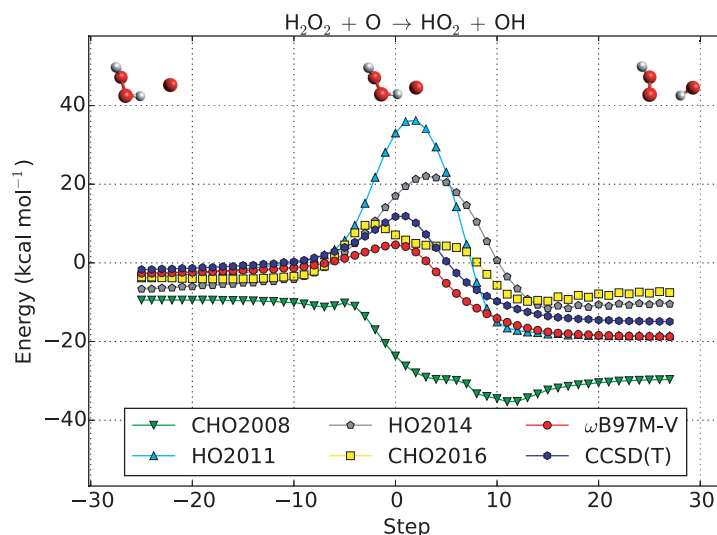


Figure B.17: Potential energies, in kcal mol^{-1} , along the $\text{H}_2\text{O}_2 + \text{O} \longrightarrow \text{HO}_2 + \text{OH}$ intrinsic reaction coordinate. The intrinsic reaction coordinate was calculated at the $\omega\text{B97M-V/cc-pVTZ}$ level of theory. The energies presented are relative to the energies of isolated H_2O_2 and O computed at the $\omega\text{B97M-V/cc-pVTZ}$ optimized geometries.

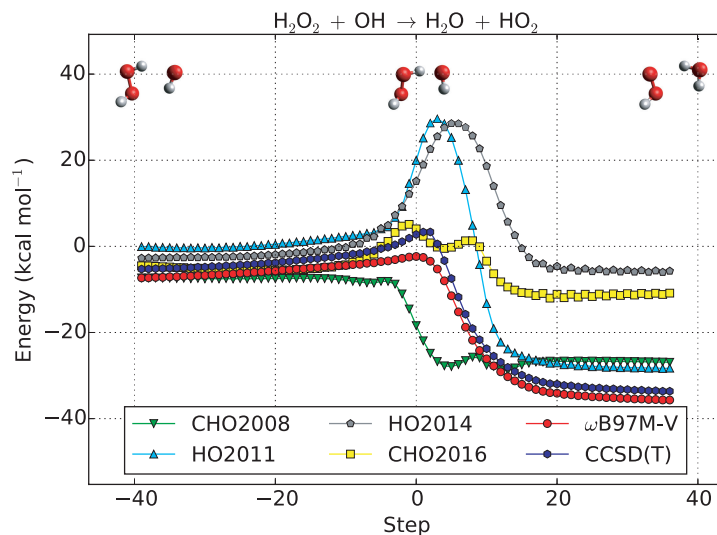


Figure B.18: Potential energies, in kcal mol^{-1} , along the $\text{H}_2\text{O}_2 + \text{OH} \longrightarrow \text{H}_2\text{O} + \text{HO}_2$ intrinsic reaction coordinate. The intrinsic reaction coordinate was calculated at the $\omega\text{B97M-V/cc-pVTZ}$ level of theory. The energies presented are relative to the energies of isolated H_2O_2 and OH computed at the $\omega\text{B97M-V/cc-pVTZ}$ optimized geometries.

Appendix C

Additional Information: Third-Order Møller-Plesset Perturbation Theory Made Useful? Choice of Orbitals and Scaling Greatly Improves Accuracy

C.1 W4-11

Table C.1 presents CCSD(T) reaction energies for the non-multireference (non-MR) subset of the W4-11 set in kcal mol⁻¹ and errors for other methods. All calculations were performed with the aVTZ basis set and the corresponding RI basis was used for the MP2, OOMP2, and κ -OOMP2 calculations. For this set, we did not use the RI approximation for the CCSD(T), CCSD, or MP3 contributions.

Table C.1: CCSD(T)/aVTZ energies (in kcal/mol) for the non-MR subset of the W4-11 set and errors for other methods

Reaction	CCSD(T)	$\Delta(\text{CCSD})$	$\Delta(\text{MP2.8}\kappa\text{-OOMP2})$	$\Delta(\text{MP3}\kappa\text{-OOMP2})$	$\Delta(\text{MP2.5})$	$\Delta(\text{MP3})$	$\Delta(\kappa\text{-OOMP2})$	$\Delta(\text{OOMP2})$	$\Delta(\text{MP2})$
2H \rightarrow H ₂	-108.55	0.00	1.90	1.20	3.04	1.30	5.64	4.74	4.78
Al + 3H \rightarrow AlH ₃	-214.45	0.18	1.73	0.74	3.15	0.65	4.43	5.74	5.64
Al + H \rightarrow AlH	-73.97	0.29	1.42	0.93	4.97	3.96	4.65	3.41	5.98
Si + 4H \rightarrow SiH ₄	-324.46	0.91	2.74	1.46	5.13	1.91	7.73	8.01	8.34
B + 3H \rightarrow BH ₃	-282.54	0.76	-0.97	-1.70	0.18	-1.69	0.84	2.04	2.04
B + H \rightarrow BH	-85.81	0.56	1.86	1.42	6.93	6.58	4.21	3.34	7.29
C + 2H \rightarrow ³ CH ₂	-192.08	0.89	-1.01	-1.23	0.05	-0.53	0.20	0.14	0.63
Si + H \rightarrow SiH	-73.58	0.44	1.61	1.15	3.41	2.32	4.20	3.55	4.50
2Si + 6H \rightarrow Si ₂ H ₆	-536.29	2.95	3.57	1.83	7.43	2.96	11.80	10.85	11.90
C + 3H \rightarrow CH ₃	-308.24	1.77	-0.15	-0.59	1.24	0.04	2.83	1.96	2.44
C + 4H \rightarrow CH ₄	-420.43	2.76	0.42	-0.02	1.94	0.68	4.46	2.65	3.19
2B + 6H \rightarrow B ₂ H ₆	-611.16	4.26	-2.59	-3.61	0.14	-2.62	1.42	2.07	2.89
Si + 3H + F \rightarrow SiH ₃ F	-379.79	2.95	1.10	2.61	0.97	4.02	-4.79	-3.65	-2.09
P + 3H \rightarrow PH ₃	-240.35	2.05	3.19	2.18	6.03	3.43	10.37	7.59	8.63
2C + 6H \rightarrow C ₂ H ₆	-714.06	6.09	-0.58	-0.45	1.04	0.96	2.85	-0.11	1.12
3C + 8H \rightarrow propane	-1010.13	9.65	-1.58	-0.77	0.10	1.42	1.04	-3.27	-1.21
C + 2H \rightarrow ¹ CH ₂	-181.88	1.23	0.04	-0.40	2.06	0.98	2.88	2.12	3.14
C + H \rightarrow CH	-84.78	0.94	1.15	0.68	5.91	5.17	4.19	3.20	6.65
2H + S \rightarrow H ₂ S	-181.88	2.31	1.38	1.17	1.93	1.28	5.67	2.31	2.57
H + S \rightarrow HS	-86.56	1.08	0.87	0.66	1.48	0.91	3.30	1.80	2.05
2C + 5H + F \rightarrow C ₂ H ₅ F	-722.71	8.49	-1.57	1.00	-1.36	3.92	-6.63	-9.48	-6.64
C + N + 5H \rightarrow CH ₃ NH ₂	-580.56	6.93	1.05	2.12	1.87	3.93	2.22	-1.93	-0.18
C + 3H + F \rightarrow CH ₃ F	-422.88	5.00	-0.39	1.55	-0.54	3.51	-4.79	-6.46	-4.58
3C + 6H \rightarrow propene	-863.23	10.67	-2.29	-0.54	-1.38	2.21	-0.61	-7.50	-4.98
N + 3H \rightarrow NH ₃	-295.48	3.67	1.86	2.40	2.36	3.37	3.64	0.38	1.35
2C + O + 6H \rightarrow ethanol	-811.22	10.01	-0.82	2.00	-1.15	4.70	-5.38	-9.91	-6.99
C + N + 4H \rightarrow CH ₃ NH	-473.50	5.81	0.19	0.71	2.93	3.57	3.10	-0.29	2.30
2C + 4H \rightarrow C ₂ H ₄	-564.36	7.09	-1.19	-0.18	-0.24	1.83	1.57	-3.99	-2.32
C + O + 4H \rightarrow methanol	-512.19	6.48	0.26	2.40	-0.25	4.23	-3.46	-6.73	-4.73
H + Cl \rightarrow HCl	-106.39	1.52	0.37	0.60	-0.08	0.40	1.44	-0.54	-0.57
N + 2H \rightarrow NH ₂	-180.84	2.33	1.50	1.41	2.90	2.49	4.57	2.42	3.31
N + H \rightarrow NH	-82.32	1.06	0.94	0.65	2.38	1.63	3.46	2.46	3.14
C + N + 4H \rightarrow CH ₂ NH ₂	-480.36	6.48	-0.05	1.24	1.68	4.18	0.18	-3.69	-0.82
B + H + 2F \rightarrow BH ₂ F ₂	-411.02	5.67	-4.17	0.49	-6.89	3.28	-21.38	-20.21	-17.06
2H + O \rightarrow H ₂ O	-230.63	3.29	1.04	2.74	-0.20	3.48	-2.45	-4.98	-3.89
H + F \rightarrow HF	-140.37	1.98	0.43	2.03	-0.88	6.22	-4.12	-5.26	-4.40
2C + 3H \rightarrow CH ₂ CH	-446.39	6.26	-2.31	-1.23	4.61	6.22	-0.03	-5.11	3.00
O + H \rightarrow OH	-106.00	1.56	0.50	0.94	0.69	1.59	0.37	-0.84	-0.21
3C + 4H \rightarrow propyne	-706.71	11.43	-3.25	0.28	-4.44	3.27	-5.15	-15.19	-12.14
2C + O + 4H \rightarrow acetaldehyde	-677.49	11.06	-1.68	2.69	-2.35	6.73	-9.28	-16.01	-11.43
3C + 4H \rightarrow allene	-706.21	11.76	-3.05	-0.32	-2.83	3.02	-2.31	-11.91	-8.68
Si + 4F \rightarrow SiF ₄	-565.82	9.26	-3.98	5.27	-10.90	9.68	-38.94	-36.65	-31.47
B + 3F \rightarrow BF ₃	-470.35	7.65	-5.83	1.17	-10.73	4.79	-31.89	-30.34	-26.26

Table C.1: (continued)

Reaction	CCSD(T)	$\Delta(\text{CCSD})$	$\Delta(\text{MP2.8:}\kappa\text{-OOMP2})$	$\Delta(\text{MP3:}\kappa\text{-OOMP2})$	$\Delta(\text{MP2.5})$	$\Delta(\text{MP3})$	$\Delta(\kappa\text{-OOMP2})$	$\Delta(\text{OOMP2})$	$\Delta(\text{MP2})$
$2\text{C} + \text{F} + 3\text{H} \rightarrow \text{C}_2\text{H}_3\text{F}$	-573.91	9.71	-2.48	1.12	-2.88	4.73	-8.59	-14.09	-10.49
$2\text{C} + \text{O} + 4\text{H} \rightarrow \text{oxirane}$	-651.46	11.17	-1.81	2.51	-3.26	5.91	-10.78	-16.23	-12.42
$\text{C} + 2\text{F} + 2\text{H} \rightarrow \text{CH}_2\text{F}_2$	-437.43	7.47	-1.70	2.79	-3.23	6.30	-14.76	-16.45	-12.77
$\text{Al} + 3\text{F} \rightarrow \text{AlF}_3$	-423.42	7.18	-3.06	4.53	-9.34	7.43	-31.88	-30.12	-26.11
$\text{Be} + 2\text{F} \rightarrow \text{BeF}_2$	-310.40	5.22	-4.87	0.30	-11.65	-0.42	-26.88	-23.42	-22.88
$2\text{C} + 2\text{H} \rightarrow \text{CH}_2\text{C}$	-359.99	6.61	-1.60	-0.40	3.10	5.28	1.82	-4.83	0.93
$4\text{H} + 2\text{N} \rightarrow \text{N}_2\text{H}_4$	-433.85	7.96	2.81	4.69	3.12	7.00	2.58	-3.06	-0.75
$\text{C} + \text{N} + 3\text{H} \rightarrow \text{CH}_2\text{NH}$	-437.60	8.09	0.63	2.78	1.38	5.84	0.70	-6.20	-3.08
$\text{Al} + \text{F} \rightarrow \text{AlF}$	-160.40	3.13	-0.47	2.29	-2.43	3.47	-8.96	-10.15	-8.34
$2\text{C} + 2\text{O} + 4\text{H} \rightarrow \text{acetic acid}$	-802.21	15.31	-2.77	4.73	-5.03	10.55	-19.98	-27.84	-20.61
$2\text{C} + 2\text{H} \rightarrow \text{C}_2\text{H}_2$	-405.33	8.01	-2.29	0.47	-3.25	2.86	-2.55	-11.67	-9.36
$2\text{H} + \text{C} + \text{O} \rightarrow \text{H}_2\text{CO}$	-373.20	7.51	-0.30	3.37	-1.33	6.40	-6.92	-12.51	-9.05
$2\text{H} + \text{C} + \text{N} \rightarrow \text{H}_2\text{CN}$	-342.06	6.81	-1.00	0.77	8.03	10.24	0.78	-5.49	5.82
$\text{B} + \text{F} \rightarrow \text{BF}$	-182.20	3.79	-1.63	1.08	-2.83	2.92	-9.65	-10.79	-8.58
$\text{Be} + 2\text{Cl} \rightarrow \text{BeCl}_2$	-227.19	4.66	-5.47	-3.26	-11.46	-6.43	-14.80	-14.37	-16.48
$\text{C} + \text{O} + 2\text{H} \rightarrow \text{trans-HCOH}$	-320.67	6.94	-0.08	2.70	4.45	10.10	-4.29	-9.05	-1.21
$\text{Al} + 3\text{Cl} \rightarrow \text{AlCl}_3$	-306.63	6.58	-4.00	-0.64	-9.33	-1.33	-14.15	-17.53	-17.34
$\text{C} + \text{O} + 2\text{H} \rightarrow \text{cis-HCOH}$	-315.91	7.07	-0.02	2.75	5.15	10.78	-3.94	-8.89	-0.47
$\text{Al} + \text{Cl} \rightarrow \text{AlCl}$	-120.00	2.86	-1.00	0.09	-2.69	-0.12	-2.03	-5.43	-5.25
$2\text{C} + \text{O} + 2\text{H} \rightarrow \text{ketene}$	-532.93	12.44	-3.17	2.86	-4.96	7.61	-14.11	-23.46	-17.53
$\text{Si} + \text{F} \rightarrow \text{SiF}$	-139.06	3.30	-0.15	2.64	-0.94	5.01	-9.17	-9.67	-6.89
$\text{C} + 2\text{O} + 2\text{H} \rightarrow \text{formic acid}$	-498.86	11.89	-1.60	5.33	-4.06	10.37	-17.89	-24.97	-18.48
$\text{C} + \text{N} + 2\text{H} \rightarrow \text{HCNH}$	-334.08	8.09	-0.58	2.34	4.38	9.48	-1.94	-9.84	-0.72
$2\text{C} + 2\text{O} + 2\text{H} \rightarrow \text{glyoxal}$	-632.90	16.23	-2.63	5.96	0.13	16.85	-20.40	-31.75	-16.60
$\text{C} + \text{O} + \text{F} + \text{H} \rightarrow \text{HCOF}$	-401.82	10.48	-2.12	4.67	-4.34	9.71	-19.07	-24.66	-18.38
$\text{N} + \text{Cl} + 2\text{H} \rightarrow \text{NH}_2\text{Cl}$	-244.42	6.53	1.50	3.38	1.19	5.10	1.16	-4.79	-2.72
$\text{C} + 4\text{F} \rightarrow \text{CF}_4$	-478.14	12.36	-4.76	4.51	-9.17	10.84	-34.62	-35.95	-29.18
$2\text{C} + \text{F} + \text{H} \rightarrow \text{HCCF}$	-398.03	10.54	-3.67	1.57	-5.99	5.45	-13.17	-21.55	-17.42
$\text{H} + \text{C} + \text{N} \rightarrow \text{HCN}$	-311.37	8.79	-0.10	4.17	-1.98	7.26	-4.76	-14.78	-11.21
$\text{H} + \text{C} + \text{N} \rightarrow \text{HNC}$	-296.11	8.43	-0.27	3.15	-1.12	6.19	-3.79	-11.79	-8.43
$2\text{C} + \text{H} \rightarrow \text{CCH}$	-265.01	6.92	-3.00	-0.29	8.10	12.32	-3.50	-11.92	3.88
$\text{H} + \text{C} + \text{O} \rightarrow \text{HCO}$	-277.78	7.74	-1.03	3.44	-1.52	7.78	-9.65	-15.85	-10.82
$\text{C} + \text{O} \rightarrow \text{CO}$	-257.54	7.63	-0.88	4.02	-3.06	7.35	-11.52	-17.57	-13.47
$2\text{C} + \text{O} + 2\text{H} \rightarrow \text{oxirene}$	-454.13	13.57	-2.26	3.48	3.84	15.20	-11.04	-21.83	-7.52
$\text{C} + \text{O} + 2\text{F} \rightarrow \text{F}_2\text{CO}$	-418.18	12.75	-3.84	5.20	-7.71	11.49	-29.53	-34.22	-26.90
$\text{C} + \text{O} + \text{N} + \text{H} \rightarrow \text{HOCN}$	-406.69	12.92	-0.98	6.14	-4.48	10.72	-14.46	-25.58	-19.68
$2\text{H} + 2\text{O} \rightarrow \text{HOOH}$	-265.74	8.43	1.72	5.81	0.52	9.06	-5.60	-11.96	-8.03
$2\text{H} + 2\text{N} \rightarrow \text{trans-N}_2\text{H}_2$	-291.95	9.36	2.54	5.60	12.63	17.18	1.62	-7.26	8.08
$\text{C} + \text{O} + \text{N} + \text{H} \rightarrow \text{HNCO}$	-431.49	13.93	-1.71	6.17	-4.44	11.89	-17.52	-28.44	-20.77
$2\text{N} + 2\text{H} \rightarrow \text{cis-N}_2\text{H}_2$	-286.23	9.55	2.56	5.62	13.28	17.75	2.02	-7.18	8.81
$\text{C} + 2\text{F} \rightarrow \text{CF}_2$	-257.31	8.67	-2.01	3.75	0.86	12.40	-16.82	-20.35	-10.68
$\text{C} + 2\text{O} \rightarrow \text{CO}_2$	-387.26	13.19	-2.57	6.67	-6.71	12.52	-25.10	-34.00	-25.94
$2\text{C} + 2\text{F} \rightarrow \text{FCCF}$	-385.08	12.97	-4.89	2.70	-8.52	7.99	-23.24	-30.82	-25.04

Table C.1: (continued)

Reaction	CCSD(T)	$\Delta(\text{CCSD})$	$\Delta(\text{MP2.8-}\kappa\text{-OOMP2})$	$\Delta(\text{MP3-}\kappa\text{-OOMP2})$	$\Delta(\text{MP2.5})$	$\Delta(\text{MP3})$	$\Delta(\kappa\text{-OOMP2})$	$\Delta(\text{OOMP2})$	$\Delta(\text{MP2})$
C + 2O + 2H → dioxirane	-407.73	13.86	-0.84	6.17	9.11	20.63	-13.46	-23.84	-2.41
C + F → CF	-131.92	4.70	-1.04	2.01	-0.21	5.80	-8.25	-10.35	-6.21
2S + H → SSH	-158.96	5.81	0.08	1.45	1.54	4.09	3.33	-4.92	-1.01
H + O + Cl → HOCl	-162.68	6.44	0.92	4.03	-0.42	6.00	-4.08	-9.80	-6.84
2N + 2C → NCCN	-498.43	19.60	-2.02	8.48	15.04	31.66	-16.57	-39.19	-1.58
2N → N ₂	-223.58	9.02	1.78	7.07	-0.87	10.50	-6.87	-16.33	-12.24
2N + H → N ₂ H	-220.12	8.61	1.00	4.83	9.16	14.72	-1.84	-10.81	3.60
O + C + S → OCS	-331.41	13.96	-1.89	5.86	-5.80	10.52	-14.40	-29.19	-22.11
Si + O → SiO	-186.90	8.13	1.85	7.66	-1.56	10.30	-8.83	-19.22	-13.42
Cl + C + N → ClCN	-282.06	11.93	-0.83	5.42	-4.65	8.91	-10.34	-23.05	-18.20
H + 2O → HOO	-172.37	7.45	-0.48	3.95	4.07	11.18	-7.60	-13.76	-3.05
C + O + N + H → HCNO	-362.44	16.54	0.18	9.90	-3.31	16.03	-15.04	-33.16	-22.65
C + O + N + H → HONC	-346.90	13.37	-0.16	6.31	-1.97	11.47	-10.57	-22.10	-15.41
H + N + O → HNO	-201.40	9.32	1.69	6.28	15.44	21.82	-4.51	-13.34	9.06
H + O + F → HOF	-156.38	7.65	1.12	5.03	1.25	9.17	-5.46	-11.30	-6.68
H + N + 2O → <i>cis</i> -HONO	-306.61	15.69	1.44	10.95	4.78	21.04	-15.82	-29.57	-11.49
H + N + 2O →	-307.09	15.75	1.50	11.07	6.63	22.48	-15.55	-29.82	-9.22
<i>trans</i> -HONO									
C + 2S → CS ₂	-274.02	15.33	-0.88	5.64	-5.44	8.77	-2.53	-25.25	-19.64
H + 3N → HN ₃	-325.51	17.81	3.16	12.91	-0.10	19.08	-10.07	-30.67	-19.29
C + S → CS	-167.69	9.49	-0.23	3.61	-0.62	6.93	2.03	-13.54	-8.16
C + N → CN	-177.09	9.10	-0.58	5.69	17.10	23.79	-6.16	-21.93	10.42
S + 3O → SO ₃	-320.43	19.29	-1.32	12.55	-7.25	20.91	-34.71	-48.81	-35.42
C + 2Cl → CCl ₂	-172.12	10.17	-2.13	1.82	4.31	11.64	-4.19	-15.86	-3.02
B + N → ³ BN	-103.84	5.94	-2.74	-0.50	0.08	4.55	-4.86	-10.26	-4.39
S + 2O → SO ₂	-242.81	15.18	0.94	11.92	-2.91	18.10	-21.83	-37.29	-23.92
N + O → NO	-148.93	8.55	0.86	6.23	2.59	12.71	-8.88	-16.60	-7.53
S + O → SO	-120.04	7.12	-0.42	4.49	-0.66	8.46	-9.36	-17.09	-9.79
2N + O → N ₂ O	-265.47	17.98	2.65	14.63	-2.15	21.08	-18.37	-38.24	-25.38
2S → S ₂	-97.71	6.59	-1.04	1.21	-1.05	3.58	1.05	-9.45	-5.68
4P → P ₄	-277.29	20.34	5.24	13.32	0.19	17.60	9.18	-26.41	-17.23
2Cl → Cl ₂	-55.39	4.31	-0.13	1.35	-1.45	1.85	-0.57	-5.75	-4.75
2O → O ₂	-118.26	7.70	-0.97	4.71	-0.80	10.12	-12.43	-19.33	-11.73
2F → F ₂	-37.02	7.34	-0.20	3.51	23.99	27.18	-5.28	-11.51	20.81
2S + O → S ₂ O	-191.58	15.50	-1.03	7.95	12.03	23.95	-9.96	-34.17	0.11
2P → P ₂	-108.52	9.03	1.19	3.77	19.02	21.08	12.47	-8.63	16.96
Cl + F → ClF	-60.01	5.01	0.32	3.23	-0.35	5.54	-5.47	-9.27	-6.24
N + 2O → NO ₂	-222.79	17.98	1.37	13.53	0.16	22.37	-20.91	-39.11	-22.06
Cl + O → ClO	-60.64	5.83	-1.84	1.83	4.62	9.11	-4.98	-12.58	0.13
H + ClO → HOCl	-102.04	0.61	2.76	2.20	-5.03	-3.10	0.90	2.78	-6.96
OH + Cl → HOCl	-56.69	4.88	0.42	3.09	-1.11	4.41	-4.45	-8.96	-6.63
OH + F → HOF	-50.39	6.09	0.62	4.09	0.56	7.59	-5.83	-10.46	-6.47
NO + O → NO ₂	-73.86	9.42	0.50	7.31	-2.43	9.67	-12.02	-22.51	-14.53
NO + N → N ₂ O	-116.54	9.42	1.78	8.40	-4.74	8.37	-9.49	-21.64	-17.85
N ₂ + O → N ₂ O	-41.89	8.96	0.87	7.56	-1.28	10.58	-11.50	-21.91	-13.14

Table C.1: (continued)

Reaction	CCSD(T)	$\Delta(\text{CCSD})$	$\Delta(\text{MP2.8:}\kappa\text{-OOMP2})$	$\Delta(\text{MP3:}\kappa\text{-OOMP2})$	$\Delta(\text{MP2.5})$	$\Delta(\text{MP3})$	$\Delta(\kappa\text{-OOMP2})$	$\Delta(\text{OOMP2})$	$\Delta(\text{MP2})$
H + NO ₂ → <i>trans</i> -HONO	-84.30	-2.22	0.14	-2.46	6.47	0.11	5.35	9.29	12.84
OH + NO → <i>trans</i> -HONO	-52.16	5.64	0.14	3.91	3.35	8.18	-7.04	-12.38	-1.48
H + CN → HNC	-119.02	-0.68	0.32	-2.54	-18.22	-17.60	2.37	10.14	-18.84
NH + C → HNC	-213.79	7.37	-1.21	2.50	-3.50	4.56	-7.25	-14.25	-11.56
OH + CN → HONC	-63.82	2.72	-0.07	-0.31	-19.76	-13.91	-4.78	0.66	-25.62
NH + CO → HNCO	-91.63	5.24	-1.77	1.50	-3.76	2.91	-9.46	-13.34	-10.43
CH + NO → HCNO	-128.74	7.05	-1.83	3.00	-11.81	-1.85	-10.35	-19.76	-21.77
H + NO → HNO	-52.47	0.77	-1.83	0.06	12.85	9.11	4.37	3.26	16.59
NH + O → HNO	-119.08	8.26	0.76	5.63	13.06	20.19	-7.97	-15.80	5.92
CH ₃ + OH → methanol	-97.95	3.16	-0.09	2.05	-2.18	2.60	-6.67	-7.85	-6.96
CH + OH → <i>trans</i> -HCOH	-129.90	4.44	-1.73	1.09	-2.16	3.34	-8.85	-11.41	-7.65
HCO + H → <i>trans</i> -HCOH	-42.89	-0.81	0.95	-0.74	5.96	2.31	5.36	6.80	9.61
HCO + OH → formic acid	-115.09	2.59	-1.06	0.95	-3.23	1.00	-8.61	-8.29	-7.46
CH ₂ C + O → ketene	-172.95	5.84	-1.57	3.26	-8.06	2.34	-15.93	-18.64	-18.47
³ CH ₂ + CO → ketene	-83.31	3.92	-1.29	0.07	-1.95	0.79	-2.79	-6.04	-4.69
2HCO → glyoxal	-77.34	0.75	-0.56	-0.92	3.16	1.29	-1.10	-0.05	5.03
CH ₃ + HCO → acetaldehyde	-91.46	1.55	-0.50	-0.15	-2.08	-1.10	-2.46	-2.12	-3.05
CF ₂ + O → F ₂ CO	-160.87	4.08	-1.83	1.45	-8.57	-0.91	-12.71	-13.87	-16.22
HCO + F → HCOF	-124.04	2.74	-1.08	1.23	-2.82	1.93	-9.42	-8.82	-7.57
HCO + H → H ₂ CO	-95.42	-0.23	0.74	-0.07	0.19	-1.38	2.73	3.34	1.76
³ CH ₂ + O → H ₂ CO	-181.12	6.62	0.71	4.60	-1.38	6.93	-7.12	-12.65	-9.68
H + CO → HCO	-20.24	0.11	-0.15	-0.58	1.54	0.43	1.87	1.72	2.65
CH + O → HCO	-193.00	6.80	-2.18	2.76	-7.43	2.61	-13.84	-19.05	-17.47
CS + S → CS ₂	-106.33	5.84	-0.65	2.03	-4.82	1.84	-4.57	-11.71	-11.48
CO + O → CO ₂	-129.72	5.56	-1.69	2.65	-3.65	5.17	-13.58	-16.43	-12.47
³ CH ₂ + NH ₂ → CH ₂ NH ₂	-107.44	3.26	-0.54	1.07	-1.28	2.21	-4.60	-6.24	-4.76
CH ₂ NH + H → CH ₂ NH ₂	-42.75	-1.61	-0.68	-1.54	0.30	-1.66	-0.52	2.51	2.26
CH ₃ + NH → CH ₃ NH	-82.94	2.98	-0.61	0.65	-0.69	1.89	-3.19	-4.70	-3.27
CH ₂ NH ₂ + H → CH ₃ NH	-35.90	-2.28	-0.44	-2.07	1.56	-2.27	2.40	5.91	5.38
CH ₂ NH ₂ + H → CH ₃ NH ₂	-100.20	0.45	1.10	0.87	0.20	-0.24	2.04	1.76	0.64
CH ₃ NH + H → CH ₃ NH ₂	-107.06	1.12	0.86	1.40	-1.06	0.36	-0.88	-1.64	-2.48
HCNH + H → CH ₂ NH	-103.53	0.00	1.21	0.44	-3.00	-3.64	2.64	3.64	-2.36
NH + CH → HCNH	-166.98	6.09	-2.67	1.01	-3.91	2.68	-9.59	-15.50	-10.51
HCN + H → HCNH	-22.71	-0.70	-0.48	-1.84	6.36	2.22	2.82	4.94	10.49
CN + H → HCN	-134.28	-0.31	0.48	-1.52	-19.08	-16.53	1.39	7.15	-21.63
CH + N → HCN	-226.59	7.85	-1.25	3.50	-7.89	2.09	-8.95	-17.98	-17.86
2CN → NCCN	-144.25	1.39	-0.85	-2.91	-19.17	-15.92	-4.26	4.67	-22.42
HS + H → H ₂ S	-95.32	1.23	0.51	0.51	0.44	0.37	2.38	0.51	0.52
HOO + O → <i>trans</i> -HOOO	-53.83	8.97	-0.84	6.08	20.06	24.11	-7.88	-27.26	16.00
OH + O ₂ → <i>trans</i> -HOOO	-1.96	7.17	-0.85	4.38	24.24	23.59	-3.42	-20.85	24.89
HOO + H → HOOH	-93.37	0.98	2.20	1.87	-3.55	-2.12	2.00	1.80	-4.98
2OH → HOOH	-53.75	5.32	0.73	3.94	-0.86	5.89	-6.34	-10.28	-7.62
HS + S → SSH	-72.40	4.73	-0.79	0.79	0.06	3.18	0.03	-6.72	-3.07
S ₂ + H → SSH	-61.25	-0.78	1.12	0.23	2.59	0.51	2.28	4.54	4.66

Table C.1: (continued)

Reaction	CCSD(T)	$\Delta(\text{CCSD})$	$\Delta(\text{MP2.8-}\kappa\text{-OOMP2})$	$\Delta(\text{MP3-}\kappa\text{-OOMP2})$	$\Delta(\text{MP2.5})$	$\Delta(\text{MP3})$	$\Delta(\kappa\text{-OOMP2})$	$\Delta(\text{OOMP2})$	$\Delta(\text{MP2})$
OH + O \rightarrow HOO	-66.38	5.89	-0.98	3.01	3.38	9.60	-7.97	-12.92	-2.84
O ₂ + H \rightarrow HOO	-54.12	-0.25	0.49	-0.76	4.87	1.06	4.83	5.58	8.68
OH + H \rightarrow H ₂ O	-124.64	1.73	0.54	1.80	-0.89	1.90	-2.82	-4.15	-3.68
N ₂ + NH \rightarrow HNHN	-19.61	7.74	0.44	5.19	-1.62	6.95	-6.66	-16.80	-10.19
2NH ₂ \rightarrow N ₂ H ₄	-72.18	3.30	-0.18	1.87	-2.68	2.01	-6.57	-7.89	-7.37
2NH \rightarrow <i>trans</i> -N ₂ H ₂	-127.31	7.25	0.66	4.29	7.87	13.92	-5.30	-12.18	1.81
NH + N \rightarrow N ₂ H	-137.80	7.56	0.06	4.18	6.77	13.08	-5.30	-13.27	0.46
NH ₂ + Cl \rightarrow NH ₂ Cl	-63.58	4.20	0.00	1.97	-1.71	2.61	-3.42	-7.20	-6.03
NH ₂ + H \rightarrow NH ₃	-114.64	1.34	0.36	1.00	-0.54	0.88	-0.94	-2.04	-1.96
NH + H \rightarrow NH ₂	-98.52	1.27	0.56	0.75	0.52	0.86	1.11	-0.04	0.17
CH ₂ C + ³ CH ₂ \rightarrow allene	-154.14	4.27	-0.44	1.31	-5.99	-1.73	-4.33	-7.22	-10.24
CCH + CH ₃ \rightarrow propyne	-133.45	2.74	-0.10	1.16	-13.77	-9.09	-4.49	-5.23	-18.46
CH ₂ CH + CH ₃ \rightarrow propene	-108.59	2.65	0.17	1.29	-7.24	-4.06	-3.41	-4.35	-10.42
CH ₂ CH + F \rightarrow C ₂ H ₃ F	-127.51	3.45	-0.17	2.35	-7.49	-1.49	-8.57	-8.98	-13.49
2CH ₃ \rightarrow C ₂ H ₆	-97.57	2.55	-0.29	0.73	-1.44	0.87	-2.82	-4.03	-3.75
2 ³ CH ₂ \rightarrow C ₂ H ₄	-180.21	5.31	0.82	2.28	-0.35	2.88	1.17	-4.27	-3.57
CH ₂ C + H \rightarrow CH ₂ CH	-86.41	-0.35	-0.71	-0.83	1.51	0.95	-1.85	-0.29	2.07
C ₂ H ₂ + H \rightarrow CH ₂ CH	-41.07	-1.75	-0.02	-1.70	7.86	3.37	2.52	6.55	12.36
³ CH ₂ + C \rightarrow CH ₂ C	-167.91	5.72	-0.60	0.82	3.05	5.80	1.62	-4.97	0.30
CCH + F \rightarrow HCCF	-133.02	3.62	-0.66	1.86	-14.08	-6.87	-9.67	-9.63	-21.30
CH + CF \rightarrow HCCF	-181.33	4.90	-3.78	-1.11	-11.69	-5.53	-9.12	-14.40	-17.86
CCH + H \rightarrow C ₂ H ₂	-140.31	1.08	0.71	0.75	-11.35	-9.46	0.94	0.26	-13.23
2CH \rightarrow C ₂ H ₂	-235.77	6.12	-4.59	-0.89	-15.07	-7.48	-10.94	-18.07	-22.66
CH ₃ + F \rightarrow CH ₃ F	-114.64	3.23	-0.24	2.14	-1.78	3.46	-7.62	-8.42	-7.02
CH ₃ + H \rightarrow CH ₄	-112.18	1.00	0.56	0.57	0.70	0.64	1.62	0.70	0.75
³ CH ₂ + H \rightarrow CH ₃	-116.17	0.88	0.86	0.64	1.19	0.57	2.63	1.82	1.81
CH + H \rightarrow ³ CH ₂	-107.30	-0.05	-2.15	-1.90	-5.86	-5.70	-3.99	-3.06	-6.02
CF + F \rightarrow CF ₂	-125.39	3.98	-0.97	1.74	1.06	6.60	-8.57	-10.01	-4.47
CN + Cl \rightarrow ClCN	-104.97	2.83	-0.25	-0.27	-21.75	-14.89	-4.19	-1.12	-28.61
2BH ₃ \rightarrow B ₂ H ₆	-46.08	2.73	-0.65	-0.20	-0.22	0.76	-0.25	-2.01	-1.19
S ₂ + O \rightarrow S ₂ O	-93.87	8.91	0.01	6.73	13.08	20.37	-11.01	-24.71	5.78
S + SO \rightarrow S ₂ O	-71.54	8.38	-0.61	3.45	12.69	15.49	-0.60	-17.08	9.90
SO ₂ + O \rightarrow SO ₃	-77.62	4.12	-2.26	0.63	-4.35	2.81	-12.88	-11.52	-11.50
SO + O \rightarrow SO ₂	-122.77	8.05	1.36	7.43	-2.25	9.64	-12.46	-20.21	-14.13
2P ₂ \rightarrow P ₄	-60.26	2.27	2.86	5.78	-37.84	-24.55	-15.75	-9.15	-51.14
HF + CH ₃ \rightarrow H + CH ₃ F	25.74	1.25	-0.68	0.11	-0.90	0.83	-3.51	-3.16	-2.62
OH + HCl \rightarrow H + HOCl	49.70	3.37	0.05	2.50	-1.02	4.02	-5.89	-8.42	-6.06
OH + HF \rightarrow H + HOF	89.99	4.11	0.19	2.07	1.44	4.95	-1.72	-5.21	-2.07
HCl + O \rightarrow H + ClO	45.75	4.31	-2.21	1.24	4.70	8.71	-6.42	-12.03	0.69
OH + Cl \rightarrow H + ClO	45.36	4.27	-2.34	0.89	3.93	7.52	-5.35	-11.74	0.33
OH + NO \rightarrow H + NO ₂	32.13	7.87	0.01	6.37	-3.12	8.08	-12.40	-21.68	-14.32
NH + O ₂ \rightarrow H + NO ₂	-22.21	9.22	1.40	8.17	-1.42	10.62	-11.94	-22.24	-13.47
OH + N ₂ \rightarrow H + N ₂ O	64.11	7.40	0.37	6.62	-1.97	8.99	-11.87	-21.08	-12.94
NH + NO \rightarrow H + N ₂ O	-34.22	8.37	0.85	7.75	-7.12	6.74	-12.95	-24.10	-20.98
OH + HNO \rightarrow H + <i>trans</i> -HONO	0.31	4.88	-0.69	3.85	-9.50	-0.93	-11.41	-15.64	-18.07

Table C.1: (continued)

Reaction	CCSD(T)	$\Delta(\text{CCSD})$	$\Delta(\text{MP2.8:}\kappa\text{-OOMP2})$	$\Delta(\text{MP3:}\kappa\text{-OOMP2})$	$\Delta(\text{MP2.5})$	$\Delta(\text{MP3})$	$\Delta(\kappa\text{-OOMP2})$	$\Delta(\text{OOMP2})$	$\Delta(\text{MP2})$
NH + HOO → H +	-52.39	7.25	1.04	6.47	0.18	9.66	-11.42	-18.53	-9.31
<i>trans</i> -HONO									
NH + HCO → H + HNCO	-71.39	5.13	-1.61	2.07	-5.30	2.48	-11.33	-15.06	-13.09
CH + HNO → H + HNCO	-145.31	3.67	-4.55	-0.79	-25.79	-15.10	-17.20	-18.31	-36.48
OH + HCN → H + HNCO	-14.12	3.59	-2.10	1.05	-3.15	3.05	-13.13	-12.83	-9.35
NH + OH → H + HNO	-13.08	6.71	0.26	4.69	12.37	18.60	-8.35	-14.96	6.13
NH + O → H + NO	-66.61	7.50	-0.07	5.57	0.20	11.08	-12.34	-19.06	-10.67
OH + N → H + NO	-42.93	7.00	0.37	5.29	1.90	11.12	-9.26	-15.76	-7.33
OH + C ₂ H ₂ → H +	57.20	4.01	-0.47	2.07	6.40	10.76	-8.86	-9.33	2.04
oxirene									
OH + C ₂ H ₄ → H +	18.90	2.53	-1.12	1.75	-3.70	2.50	-12.72	-11.41	-9.90
oxirane									
OH + CH ₄ → H +	14.23	2.16	-0.65	1.48	-2.87	1.96	-8.29	-8.55	-7.71
methanol									
CH + H ₂ O → H +	-5.26	2.70	-2.27	-0.71	-1.26	1.44	-6.03	-7.27	-3.97
<i>trans</i> -HCOH									
OH + ³ CH ₂ → H +	-22.60	4.49	0.42	3.00	3.70	9.04	-4.86	-8.35	-1.63
<i>trans</i> -HCOH									
OH + <i>trans</i> -HCOH →	-72.19	3.40	-2.01	1.69	-9.19	-1.32	-13.98	-15.09	-17.07
H + formic acid									
H ₂ O + HCO → H +	9.55	0.86	-1.60	-0.85	-2.34	-0.90	-5.79	-4.14	-3.77
formic acid									
CH + HOOH → H +	-148.34	2.52	-4.47	-1.16	-10.49	-3.87	-16.49	-16.22	-17.10
formic acid									
OH + CH ₂ C → H +	-66.95	4.28	-2.07	2.32	-8.75	0.75	-16.30	-17.80	-18.26
ketene									
CH + H ₂ CO → H +	-74.95	3.99	-4.03	-1.19	-9.55	-3.96	-11.38	-14.16	-15.13
ketene									
OH + oxirene → H +	-72.78	1.11	-0.87	1.54	-4.40	0.07	-9.73	-9.08	-8.87
glyoxal									
CH + formic acid → H +	-49.26	3.40	-2.18	-0.05	-1.73	1.32	-6.70	-9.98	-4.78
glyoxal									
CH + methanol → H +	-80.52	3.64	-3.09	-0.38	-8.01	-2.67	-10.01	-12.48	-13.35
acetaldehyde									
OH + C ₂ H ₄ → H +	-7.13	2.42	-0.99	1.94	-2.80	3.32	-11.22	-11.18	-8.91
acetaldehyde									
OH + CF ₂ → H + F ₂ CO	-54.88	2.53	-2.32	0.51	-9.26	-2.50	-13.08	-13.03	-16.02
HF + HCO → H + HCOF	16.33	0.76	-1.52	-0.80	-1.94	-0.71	-5.30	-3.56	-3.17
OH + ³ CH ₂ → H + H ₂ CO	-75.13	5.07	0.21	3.66	-2.07	5.34	-7.49	-11.81	-9.47
CH + H ₂ O → H + H ₂ CO	-57.79	3.28	-2.48	-0.04	-7.03	-2.25	-8.66	-10.73	-11.81
OH + CH → H + HCO	-87.00	5.24	-2.68	1.83	-8.12	1.03	-14.21	-18.21	-17.26
HS + CS → H + CS ₂	-19.77	4.76	-1.52	1.37	-6.30	0.93	-7.86	-13.51	-13.53
CH + S ₂ → H + CS ₂	-91.53	7.80	-0.99	3.75	-10.30	0.02	-7.78	-19.00	-20.62
OH + CS → H + OCS	-57.72	2.91	-2.15	1.31	-5.87	2.00	-16.81	-14.82	-13.75
CH + SO → H + OCS	-126.58	5.89	-2.62	0.69	-11.05	-3.12	-9.23	-15.31	-18.98

Table C.1: (continued)

Reaction	CCSD(T)	$\Delta(\text{CCSD})$	$\Delta(\text{MP2.8-}\kappa\text{-OOMP2})$	$\Delta(\text{MP3-}\kappa\text{-OOMP2})$	$\Delta(\text{MP2.5})$	$\Delta(\text{MP3})$	$\Delta(\kappa\text{-OOMP2})$	$\Delta(\text{OOMP2})$	$\Delta(\text{MP2})$
HS + CO \rightarrow H + OCS	12.70	5.25	-1.88	1.18	-4.22	2.25	-6.17	-13.42	-10.70
OH + CO \rightarrow H + CO ₂	-23.72	4.00	-2.19	1.72	-4.34	3.58	-13.95	-15.60	-12.27
CH + O ₂ \rightarrow H + CO ₂	-184.23	4.55	-2.75	1.29	-11.82	-2.77	-16.86	-17.87	-20.86
CH + S \rightarrow H + CS	-82.91	8.55	-1.38	2.93	-6.53	1.76	-2.16	-16.74	-14.81
HS + C \rightarrow H + CS	-81.12	8.42	-1.11	2.95	-2.10	6.02	-1.26	-15.34	-10.22
SiH + O \rightarrow H + SiO	-113.32	7.69	0.24	6.52	-4.97	7.98	-13.03	-22.77	-17.91
OH + Si \rightarrow H + SiO	-80.91	6.58	1.35	6.73	-2.25	8.72	-9.20	-18.38	-13.21
CH + O \rightarrow H + CO	-172.76	6.69	-2.03	3.34	-8.97	2.18	-15.71	-20.77	-20.12
OH + C \rightarrow H + CO	-151.54	6.08	-1.38	3.08	-3.75	5.77	-11.90	-16.73	-13.26
NH + CH \rightarrow H + HCN	-144.27	6.79	-2.19	2.84	-10.27	0.46	-12.41	-20.44	-21.00
CH + N \rightarrow H + CN	-92.31	8.16	-1.73	5.01	11.19	18.62	-10.35	-25.13	3.76
NH + C \rightarrow H + CN	-94.77	8.04	-1.52	5.04	14.72	22.16	-9.62	-24.39	7.28
HS + H ₂ \rightarrow H + H ₂ S	13.23	1.23	-1.39	-0.69	-2.60	-0.93	-3.26	-4.24	-4.26
AlH + Cl \rightarrow H + AlCl	-46.02	2.57	-2.42	-0.84	-7.66	-4.08	-6.68	-8.83	-11.24
HCl + Al \rightarrow H + AlCl	-13.61	1.34	-1.38	-0.50	-2.60	-0.52	-3.47	-4.88	-4.69
AlH + F \rightarrow H + AlF	-86.43	2.84	-1.89	1.36	-7.41	-0.49	-13.61	-13.55	-14.33
HF + Al \rightarrow H + AlF	-20.03	1.15	-0.90	0.26	-1.55	0.84	-4.84	-4.89	-3.95
OH + H ₂ O \rightarrow H + HOOH	70.88	3.58	0.19	2.14	0.03	4.00	-3.52	-6.13	-3.93
2HS \rightarrow H + SSH	14.16	3.65	-1.66	0.13	-1.43	2.27	-3.27	-8.51	-5.12
2OH \rightarrow H + HOO	39.62	4.34	-1.47	2.07	2.69	8.01	-8.34	-12.08	-2.64
OH + H ₂ \rightarrow H + H ₂ O	-16.08	1.73	-1.36	0.60	-3.94	0.60	-8.46	-8.89	-8.47
NH + NH ₂ \rightarrow H + <i>trans</i> -N ₂ H ₂	-28.79	5.98	0.10	3.54	7.35	13.06	-6.42	-12.14	1.64
CH + C ₂ H ₄ \rightarrow H + propyne	-57.57	3.40	-3.20	-0.22	-10.10	-3.73	-10.91	-14.41	-16.48
CH + C ₂ H ₆ \rightarrow H + propene	-64.39	3.64	-2.85	-0.76	-8.34	-3.92	-7.65	-10.59	-12.75
HF + CH ₂ CH \rightarrow H + C ₂ H ₃ F	12.86	1.48	-0.60	0.33	-6.61	-4.12	-4.45	-3.72	-9.09
CH + CH ₃ F \rightarrow H + C ₂ H ₃ F	-66.25	3.77	-3.24	-1.10	-8.25	-3.94	-8.00	-10.83	-12.56
CH + CH ₄ \rightarrow H + C ₂ H ₄	-59.16	3.38	-2.75	-0.83	-8.09	-4.02	-7.08	-9.84	-12.16
CH + CH ₃ \rightarrow H + CH ₂ CH	-53.37	3.55	-3.31	-1.32	-2.54	1.01	-7.06	-10.27	-6.09
CH + CF ₂ \rightarrow H + FCCF	-42.99	3.35	-4.03	-1.73	-15.29	-9.58	-10.61	-13.67	-21.01
HF + CCH \rightarrow H + HCCF	7.35	1.64	-1.10	-0.17	-13.20	-9.51	-5.56	-4.37	-16.90
CH + ³ CH ₂ \rightarrow H + C ₂ H ₂	-128.47	6.17	-2.43	1.02	-9.21	-1.79	-6.95	-15.01	-16.64
CH + Cl ₂ \rightarrow H + CCl ₂	-31.95	4.91	-3.15	-0.21	-0.15	4.62	-7.82	-13.32	-4.92
CH + F ₂ \rightarrow H + CF ₂	-135.51	0.39	-2.96	-0.44	-29.05	-19.95	-15.74	-12.05	-38.14
HF + CF \rightarrow H + CF ₂	14.99	2.00	-1.41	-0.29	1.95	3.96	-4.46	-4.75	-0.07
CH + H ₂ \rightarrow H + ³ CH ₂	1.25	-0.05	-4.05	-3.10	-8.90	-6.99	-9.63	-7.81	-10.81
HF + Si \rightarrow H + SiF	1.32	1.32	-0.58	0.62	-0.06	2.38	-5.05	-4.41	-2.49
SiH + F \rightarrow H + SiF	-65.47	2.86	-1.76	1.50	-4.35	2.69	-13.37	-13.22	-11.39
HCl + CN \rightarrow H + ClCN	1.41	1.31	-0.62	-0.86	-21.66	-15.28	-5.63	-0.57	-28.05
HF + C \rightarrow H + CF	8.45	2.72	-1.47	-0.02	0.68	3.17	-4.13	-5.09	-1.82
CH + F \rightarrow H + CF	-47.15	3.75	-2.18	1.33	-6.12	0.63	-12.44	-13.55	-12.86
HF + B \rightarrow H + BF	-41.83	1.81	-2.06	-0.94	-1.95	0.29	-5.53	-5.54	-4.18

Table C.1: (continued)

Reaction	CCSD(T)	$\Delta(\text{CCSD})$	$\Delta(\text{MP2.8-}\kappa\text{-OOMP2})$	$\Delta(\text{MP3-}\kappa\text{-OOMP2})$	$\Delta(\text{MP2.5})$	$\Delta(\text{MP3})$	$\Delta(\kappa\text{-OOMP2})$	$\Delta(\text{OOMP2})$	$\Delta(\text{MP2})$
BH + F \rightarrow H + BF	-96.39	3.23	-3.49	-0.34	-9.76	-3.65	-13.86	-14.13	-15.87
BH + N \rightarrow H + ³ BN	-18.03	5.39	-4.60	-1.92	-6.85	-2.03	-9.07	-13.60	-11.68
NH + B \rightarrow H + ³ BN	-21.52	4.89	-3.68	-1.15	-2.30	2.91	-8.32	-12.72	-7.52
HS + SO \rightarrow H + S ₂ O	15.03	7.30	-1.48	2.79	11.21	14.58	-3.90	-18.88	7.85
OH + S ₂ \rightarrow H + S ₂ O	12.12	7.36	-0.49	5.80	12.39	18.78	-11.39	-23.88	5.99
OH + SO ₂ \rightarrow H + SO ₃	28.38	2.56	-2.76	-0.31	-5.04	1.23	-13.26	-10.68	-11.30
OH + SO \rightarrow H + SO ₂	-16.77	6.50	0.87	6.49	-2.94	8.05	-12.84	-19.37	-13.92
HS + O ₂ \rightarrow H + SO ₂	-37.99	6.40	1.04	6.56	-3.59	7.07	-12.70	-19.76	-14.24
HS + O \rightarrow H + SO	-33.48	6.05	-1.29	3.83	-2.15	7.55	-12.66	-18.88	-11.84
OH + S \rightarrow H + SO	-14.05	5.57	-0.92	3.56	-1.35	6.88	-9.74	-16.25	-9.58
HS + S \rightarrow H + S ₂	-11.15	5.51	-1.91	0.55	-2.53	2.67	-2.25	-11.25	-7.73
HCl + Cl \rightarrow H + Cl ₂	51.00	2.80	-0.50	0.75	-1.37	1.46	-2.02	-5.20	-4.19
HCl + F \rightarrow H + ClF	46.37	3.50	-0.05	2.64	-0.26	5.14	-6.92	-8.73	-5.67
HF + Cl \rightarrow H + ClF	80.36	3.03	-0.11	1.21	0.53	2.90	-1.36	-4.02	-1.84
HF + F \rightarrow H + F ₂	103.35	5.37	-0.64	1.48	24.87	24.54	-1.16	-6.25	25.21
OH + O \rightarrow H + O ₂	-12.26	6.14	-1.47	3.77	-1.49	8.54	-12.80	-18.50	-11.52
NH + N \rightarrow H + N ₂	-141.26	7.96	0.84	6.41	-3.25	8.87	-10.33	-18.79	-15.37
CF + CH ₃ \rightarrow C + CH ₃ F	17.29	-1.46	0.79	0.13	-1.57	-2.34	0.62	1.93	-0.81
CO + HF \rightarrow C + HOF	241.53	-1.97	1.57	-1.01	5.19	-0.82	10.18	11.53	11.19
CO + Cl \rightarrow C + ClO	196.90	-1.81	-0.96	-2.19	7.67	1.75	6.54	4.99	13.59
CO + NO \rightarrow C + NO ₂	183.68	1.79	1.38	3.29	0.63	2.31	-0.50	-4.95	-1.06
CN + O ₂ \rightarrow C + NO ₂	72.56	1.17	2.92	3.14	-16.14	-11.54	-2.32	2.15	-20.75
CO + N ₂ \rightarrow C + N ₂ O	215.65	1.32	1.75	3.54	1.78	3.23	0.02	-4.35	0.32
CN + NO \rightarrow C + N ₂ O	60.55	0.32	2.37	2.71	-21.84	-15.42	-3.33	0.29	-28.26
CO + HNO \rightarrow C +	151.85	-1.20	0.69	0.77	-5.75	-6.69	0.48	1.09	-4.81
<i>trans</i> -HONO									
CN + HOO \rightarrow C +	42.38	-0.80	2.57	1.43	-14.54	-12.50	-1.80	5.87	-16.59
<i>trans</i> -HONO									
CN + HCO \rightarrow C + HNCO	23.38	-2.91	-0.09	-2.96	-20.02	-19.68	-1.72	9.33	-20.37
CO + HCN \rightarrow C + HNCO	137.42	-2.49	-0.73	-2.03	0.60	-2.72	-1.24	3.90	3.91
CN + OH \rightarrow C + HNO	81.69	-1.34	1.78	-0.34	-2.35	-3.56	1.27	9.43	-1.15
CN + O \rightarrow C + NO	28.16	-0.55	1.45	0.54	-14.52	-11.08	-2.73	5.33	-17.95
CO + N \rightarrow C + NO	108.61	0.92	1.74	2.21	5.65	5.36	2.64	0.97	5.94
CO + C ₂ H ₂ \rightarrow C +	208.74	-2.07	0.91	-1.01	10.15	4.99	3.03	7.40	15.30
oxirene									
CO + C ₂ H ₄ \rightarrow C +	170.44	-3.55	0.26	-1.33	0.05	-3.27	-0.83	5.32	3.36
oxirane									
CO + CH ₄ \rightarrow C +	165.78	-3.92	0.72	-1.60	0.87	-3.80	3.60	8.18	5.55
methanol									
CO + ³ CH ₂ \rightarrow C +	128.95	-1.59	1.80	-0.08	7.45	3.27	7.03	8.38	11.63
<i>trans</i> -HCOH									
CO + <i>trans</i> -HCOH \rightarrow	79.35	-2.68	-0.63	-1.39	-5.44	-7.08	-2.08	1.65	-3.80
C + formic acid									
CO + CH ₂ C \rightarrow C + ketene	84.59	-1.80	-0.69	-0.76	-5.01	-5.02	-4.41	-1.07	-5.00
CO + oxirene \rightarrow C + glyoxal	78.76	-4.97	0.51	-1.54	-0.65	-5.70	2.17	7.65	4.39

Table C.1: (continued)

Reaction	CCSD(T)	$\Delta(\text{CCSD})$	$\Delta(\text{MP2.8-}\kappa\text{-OOMP2})$	$\Delta(\text{MP3.}\kappa\text{-OOMP2})$	$\Delta(\text{MP2.5})$	$\Delta(\text{MP3})$	$\Delta(\kappa\text{-OOMP2})$	$\Delta(\text{OOMP2})$	$\Delta(\text{MP2})$
$\text{N}_2 + \text{HOO} \rightarrow \text{N} +$	88.87	-0.71	0.20	0.06	3.43	0.79	-1.09	0.26	6.06
<i>trans</i> -HONO									
$\text{N}_2 + \text{HCO} \rightarrow \text{N} + \text{HNCO}$	69.87	-2.83	-2.46	-4.34	-2.05	-6.39	-1.00	3.73	2.29
$\text{CN} + \text{HNO} \rightarrow \text{N} + \text{HNCO}$	-53.00	-4.49	-2.82	-5.81	-36.98	-33.72	-6.85	6.83	-40.24
$\text{NO} + \text{HCN} \rightarrow \text{N} + \text{HNCO}$	28.81	-3.41	-2.47	-4.24	-5.05	-8.07	-3.88	2.94	-2.02
$\text{N}_2 + \text{OH} \rightarrow \text{N} + \text{HNO}$	128.18	-1.26	-0.58	-1.72	15.62	9.73	1.98	3.83	21.50
$\text{N}_2 + \text{O} \rightarrow \text{N} + \text{NO}$	74.65	-0.47	-0.92	-0.84	3.46	2.21	-2.01	-0.27	4.70
$\text{NO} + \text{C}_2\text{H}_2 \rightarrow \text{N} +$	100.13	-2.99	-0.83	-3.22	4.50	-0.37	0.39	6.44	9.37
oxirene									
$\text{NO} + \text{C}_2\text{H}_4 \rightarrow \text{N} +$	61.83	-4.47	-1.48	-3.54	-5.60	-8.63	-3.47	4.36	-2.57
oxirane									
$\text{NO} + \text{CH}_4 \rightarrow \text{N} +$	57.16	-4.83	-1.02	-3.81	-4.77	-9.16	0.96	7.22	-0.39
methanol									
$\text{CN} + \text{H}_2\text{O} \rightarrow \text{N} +$	87.05	-5.46	-0.54	-5.72	-12.46	-17.18	4.32	17.87	-7.73
<i>trans</i> -HCOH									
$\text{NO} + {}^3\text{CH}_2 \rightarrow \text{N} +$	20.33	-2.51	0.06	-2.30	1.81	-2.09	4.39	7.41	5.70
<i>trans</i> -HCOH									
$\text{NO} + \text{trans-HCOH} \rightarrow$	-29.26	-3.60	-2.38	-3.60	-11.09	-12.44	-4.72	0.68	-9.74
$\text{N} + \text{formic acid}$									
$\text{CN} + \text{HOOH} \rightarrow \text{N} +$	-56.03	-5.64	-2.74	-6.18	-21.68	-22.49	-6.14	8.92	-20.87
formic acid									
$\text{NO} + \text{CH}_2\text{C} \rightarrow \text{N} +$	-24.02	-2.72	-2.44	-2.97	-10.65	-10.37	-7.05	-2.04	-10.93
ketene									
$\text{CN} + \text{H}_2\text{CO} \rightarrow \text{N} +$	17.36	-4.17	-2.29	-6.20	-20.74	-22.58	-1.03	10.98	-18.90
ketene									
$\text{NO} + \text{oxirene} \rightarrow \text{N} +$	-29.85	-5.89	-1.24	-3.75	-6.30	-11.05	-0.47	6.68	-1.55
glyoxal									
$\text{CN} + \text{formic acid} \rightarrow \text{N} +$	43.05	-4.76	-0.45	-5.06	-12.92	-17.31	3.65	15.16	-8.54
glyoxal									
$\text{CN} + \text{methanol} \rightarrow \text{N} +$	11.79	-4.52	-1.36	-5.39	-19.21	-21.30	0.34	12.65	-17.12
acetaldehyde									
$\text{NO} + \text{C}_2\text{H}_4 \rightarrow \text{N} +$	35.80	-4.58	-1.36	-3.35	-4.69	-7.81	-1.96	4.58	-1.58
acetaldehyde									
$\text{NO} + \text{CF}_2 \rightarrow \text{N} + \text{F}_2\text{CO}$	-11.95	-4.47	-2.69	-4.78	-11.16	-13.62	-3.83	2.73	-8.69
$\text{NO} + {}^3\text{CH}_2 \rightarrow \text{N} + \text{H}_2\text{CO}$	-32.20	-1.93	-0.15	-1.63	-3.97	-5.78	1.77	3.95	-2.15
$\text{CN} + \text{H}_2\text{O} \rightarrow \text{N} + \text{H}_2\text{CO}$	34.52	-4.88	-0.75	-5.06	-18.23	-20.88	1.69	14.41	-15.58
$\text{NO} + \text{CH} \rightarrow \text{N} + \text{HCO}$	-44.07	-1.75	-3.04	-3.46	-10.02	-10.10	-4.96	-2.45	-9.93
$\text{CN} + \text{S}_2 \rightarrow \text{N} + \text{CS}_2$	0.78	-0.36	0.74	-1.27	-21.49	-18.60	2.57	6.14	-24.38
$\text{NO} + \text{CS} \rightarrow \text{N} + \text{OCS}$	-14.79	-4.09	-2.52	-3.98	-7.77	-9.12	-7.55	0.95	-6.42
$\text{CN} + \text{SO} \rightarrow \text{N} + \text{OCS}$	-34.27	-2.27	-0.89	-4.33	-22.24	-21.74	1.12	9.83	-22.74
$\text{NO} + \text{CO} \rightarrow \text{N} + \text{CO}_2$	19.21	-3.00	-2.56	-3.57	-6.24	-7.54	-4.69	0.17	-4.94
$\text{CN} + \text{O}_2 \rightarrow \text{N} + \text{CO}_2$	-91.91	-3.61	-1.02	-3.72	-23.01	-21.39	-6.52	7.26	-24.63
$\text{CN} + \text{S} \rightarrow \text{N} + \text{CS}$	9.40	0.39	0.35	-2.08	-17.72	-16.86	8.19	8.39	-18.58
$\text{NO} + \text{Si} \rightarrow \text{N} + \text{SiO}$	-37.98	-0.42	0.99	1.44	-4.15	-2.41	0.05	-2.62	-5.88
$\text{CN} + \text{O} \rightarrow \text{N} + \text{CO}$	-80.45	-1.47	-0.30	-1.67	-20.16	-16.44	-5.37	4.36	-23.88

Table C.1: (continued)

Reaction	CCSD(T)	$\Delta(\text{CCSD})$	$\Delta(\text{MP2.8-}\kappa\text{-OOMP2})$	$\Delta(\text{MP3.}\kappa\text{-OOMP2})$	$\Delta(\text{MP2.5})$	$\Delta(\text{MP3})$	$\Delta(\kappa\text{-OOMP2})$	$\Delta(\text{OOMP2})$	$\Delta(\text{MP2})$
$\text{CO} + \text{C}_2\text{H}_6 \rightarrow \text{O} +$	108.37	-3.05	-0.83	-4.10	0.63	-6.11	8.06	10.18	7.37
propene									
$\text{CO} + \text{CH}_3\text{F} \rightarrow \text{O} + \text{C}_2\text{H}_3\text{F}$	106.51	-2.93	-1.21	-4.45	0.72	-6.12	7.72	9.94	7.56
$\text{CO} + \text{CH}_4 \rightarrow \text{O} + \text{C}_2\text{H}_4$	113.60	-3.31	-0.72	-4.17	0.88	-6.21	8.64	10.93	7.96
$\text{CO} + \text{CH}_3 \rightarrow \text{O} + \text{CH}_2\text{CH}$	119.39	-3.15	-1.28	-4.66	6.43	-1.18	8.66	10.50	14.03
$\text{CO} + \text{CF}_2 \rightarrow \text{O} + \text{FCCF}$	129.77	-3.34	-5.07	-5.07	-6.33	-11.76	5.10	7.10	-0.89
$\text{CO} + {}^3\text{CH}_2 \rightarrow \text{O} + \text{C}_2\text{H}_2$	44.29	-0.52	-0.41	-2.32	-0.24	-3.97	8.77	5.76	3.48
$\text{CO} + \text{Cl}_2 \rightarrow \text{O} + \text{CCl}_2$	140.81	-1.78	-1.13	-3.55	8.82	2.44	7.90	7.45	15.20
$\text{CO} + \text{F}_2 \rightarrow \text{O} + \text{CF}_2$	37.25	-6.31	-0.93	-3.78	-20.08	-22.13	-0.02	8.72	-18.02
$\text{CO} + \text{H}_2 \rightarrow \text{O} + {}^3\text{CH}_2$	174.02	-6.74	-2.03	-6.44	0.07	-9.18	6.09	12.96	9.31
$\text{SiO} + \text{F} \rightarrow \text{O} + \text{SiF}$	47.85	-4.84	-2.00	-5.02	0.62	-5.29	-0.34	9.55	6.53
$\text{ClO} + \text{CN} \rightarrow \text{O} + \text{ClCN}$	-44.33	-3.00	1.59	-2.10	-26.37	-23.99	0.79	11.46	-28.74
$\text{CO} + \text{F} \rightarrow \text{O} + \text{CF}$	125.61	-2.94	-0.16	-2.01	2.85	-1.55	3.28	7.22	7.26
$\text{NO} + \text{B} \rightarrow \text{O} + {}^3\text{BN}$	45.09	-2.61	-3.60	-6.73	-2.51	-8.16	4.02	6.34	3.14
$2\text{SO} \rightarrow \text{O} + \text{S}_2\text{O}$	48.51	1.25	-0.19	-1.04	13.36	7.03	8.76	0.00	19.69
$\text{O}_2 + \text{S}_2 \rightarrow \text{O} + \text{S}_2\text{O}$	24.38	1.21	0.98	-2.03	13.88	10.25	1.41	-5.38	17.51
$\text{O}_2 + \text{SO}_2 \rightarrow \text{O} + \text{SO}_3$	40.64	-3.58	-1.30	-4.08	-3.54	-7.31	-0.46	7.81	0.23
$\text{O}_2 + \text{SO} \rightarrow \text{O} + \text{SO}_2$	-4.51	0.35	2.33	2.72	-1.44	-0.48	-0.03	-0.87	-2.40
$\text{O}_2 + \text{S} \rightarrow \text{O} + \text{SO}$	-1.79	-0.58	0.55	-0.21	0.14	-1.66	3.06	2.25	1.94
$\text{SO} + \text{S} \rightarrow \text{O} + \text{S}_2$	22.33	-0.54	-0.62	-3.28	-0.38	-4.88	10.41	7.63	4.11
$\text{ClO} + \text{Cl} \rightarrow \text{O} + \text{Cl}_2$	5.25	-1.52	1.71	-0.48	-6.07	-7.25	4.41	6.83	-4.88
$\text{ClO} + \text{F} \rightarrow \text{O} + \text{ClF}$	0.63	-0.82	2.16	1.40	-4.97	-3.57	-0.50	3.31	-6.36
$\text{NO} + \text{N} \rightarrow \text{O} + \text{N}_2$	-74.65	0.47	0.92	0.84	-3.46	-2.21	2.01	0.27	-4.70
$\text{F}_2 + \text{CH}_3 \rightarrow \text{F} + \text{CH}_3\text{F}$	-77.61	-4.11	-0.04	-1.37	-25.77	-23.71	-2.35	3.09	-27.83
$\text{ClF} + \text{O} \rightarrow \text{F} + \text{ClO}$	-0.63	0.82	-2.16	-1.40	4.97	3.57	0.50	-3.31	6.36
$\text{CF} + \text{HNO} \rightarrow \text{F} + \text{HNCO}$	-98.17	-0.08	-2.37	-2.13	-19.67	-15.73	-4.76	-4.76	-23.61
$\text{CF} + \text{H}_2\text{O} \rightarrow \text{F} +$	41.88	-1.05	-0.09	-2.04	4.85	0.81	6.41	6.28	8.89
<i>trans</i> -HCOH									
$\text{CF} + \text{HOOH} \rightarrow \text{F} +$	-101.19	-1.23	-2.28	-2.49	-4.37	-4.50	-4.05	-2.67	-4.24
formic acid									
$\text{CF} + \text{H}_2\text{CO} \rightarrow \text{F} +$ ketene	-27.81	0.24	-1.84	-2.52	-3.43	-4.59	1.05	-0.61	-2.27
$\text{CF} +$ formic acid $\rightarrow \text{F} +$	-2.12	-0.35	0.00	-1.38	4.39	0.68	5.74	3.57	8.09
glyoxal									
$\text{CF} +$ methanol $\rightarrow \text{F} +$	-33.37	-0.12	-0.90	-1.71	-1.90	-3.31	2.43	1.07	-0.49
acetaldehyde									
$\text{F}_2 + \text{HCO} \rightarrow \text{F} + \text{HCOF}$	-87.01	-4.61	-0.88	-2.28	-26.81	-25.25	-4.14	2.69	-28.38
$\text{CF} + \text{H}_2\text{O} \rightarrow \text{F} + \text{H}_2\text{CO}$	-10.65	-0.47	-0.30	-1.37	-0.92	-2.88	3.78	2.82	1.05
$\text{CF} + \text{S}_2 \rightarrow \text{F} + \text{CS}_2$	-44.38	4.05	1.20	2.42	-4.18	-0.61	4.66	-5.45	-7.76
$\text{CF} + \text{SO} \rightarrow \text{F} + \text{OCS}$	-79.44	2.14	-0.64	-0.64	-4.93	-3.75	-1.76	-1.76	-6.11
$\text{CF} + \text{O}_2 \rightarrow \text{F} + \text{CO}_2$	-137.08	0.80	-0.57	-0.04	-5.70	-3.40	-4.43	-4.32	-8.00
$\text{CF} + \text{S} \rightarrow \text{F} + \text{CS}$	-35.76	4.80	0.80	1.60	-0.41	1.13	10.28	-3.19	-1.95
$\text{SiF} + \text{O} \rightarrow \text{F} + \text{SiO}$	-47.85	4.84	2.00	5.02	-0.62	5.29	0.34	-9.55	-6.53
$\text{CF} + \text{O} \rightarrow \text{F} + \text{CO}$	-125.61	2.94	0.16	2.01	-2.85	-7.22	-3.28	-7.22	-7.26
$\text{CF} + \text{N} \rightarrow \text{F} + \text{CN}$	-45.16	4.41	0.45	3.68	17.31	17.99	2.09	-11.59	16.63
$\text{AlF} + \text{Cl} \rightarrow \text{F} + \text{AlCl}$	40.41	-0.27	-0.53	-2.20	-0.25	-3.60	6.93	4.72	3.09

Table C.1: (continued)

Reaction	CCSD(T)	$\Delta(\text{CCSD})$	$\Delta(\text{MP2.8:k-OOMP2})$	$\Delta(\text{MP3:k-OOMP2})$	$\Delta(\text{MP2.5})$	$\Delta(\text{MP3})$	$\Delta(\kappa\text{-OOMP2})$	$\Delta(\text{OOMP2})$	$\Delta(\text{MP2})$
$\text{ClF} + \text{Al} \rightarrow \text{F} + \text{AlCl}$	-59.99	-2.16	-1.32	-3.14	-2.34	-5.66	3.44	3.85	0.99
$\text{F}_2 + \text{Al} \rightarrow \text{F} + \text{AlF}$	-123.38	-4.21	-0.27	-1.22	-26.43	-23.70	-3.68	1.36	-29.15
$\text{CF} + \text{C}_2\text{H}_4 \rightarrow \text{F} +$ propyne	-10.42	-0.36	-1.02	-1.55	-3.99	-4.36	1.52	-0.86	-3.62
$\text{CF} + \text{C}_2\text{H}_6 \rightarrow \text{F} +$ propene	-17.24	-0.11	-0.67	-2.09	-2.22	-4.56	4.79	2.96	0.11
$\text{F}_2 + \text{CH}_2\text{CH} \rightarrow$ $\text{F} + \text{C}_2\text{H}_3\text{F}$	-90.49	-3.89	0.03	-1.16	-31.48	-28.66	-3.29	2.53	-34.30
$\text{CF} + \text{CH}_3\text{F} \rightarrow \text{F} + \text{C}_2\text{H}_3\text{F}$	-19.10	0.01	-1.05	-2.44	-2.13	-4.57	4.44	2.72	0.31
$\text{CF} + \text{CH}_4 \rightarrow \text{F} + \text{C}_2\text{H}_4$	-12.01	-0.37	-0.57	-2.16	-1.98	-4.66	5.36	3.70	0.71
$\text{CF} + \text{CH}_3 \rightarrow \text{F} + \text{CH}_2\text{CH}$	-6.22	-0.21	-1.13	-2.65	3.58	0.37	5.38	3.28	6.78
$\text{CF} + \text{CF}_2 \rightarrow \text{F} + \text{FCCF}$	4.16	-0.40	-1.84	-3.06	-9.18	-10.21	1.82	-0.12	-8.15
$\text{F}_2 + \text{CCH} \rightarrow \text{F} + \text{HCCF}$	-96.00	-3.73	-0.46	-1.65	-38.08	-34.05	-4.40	1.88	-42.11
$\text{CF} + {}^3\text{CH}_2 \rightarrow \text{F} + \text{C}_2\text{H}_2$	-81.32	2.42	-0.25	-0.31	-3.10	-2.42	5.49	-1.46	-3.77
$\text{CF} + \text{Cl}_2 \rightarrow \text{F} + \text{CCl}_2$	15.20	1.16	-0.97	-1.54	5.97	3.99	4.62	0.23	7.95
$\text{F}_2 + \text{CF} \rightarrow \text{F} + \text{CF}_2$	-88.36	-3.37	-0.77	-1.77	-22.93	-20.58	-3.30	1.50	-25.28
$\text{CF} + \text{H}_2 \rightarrow \text{F} + {}^3\text{CH}_2$	48.40	-3.81	-1.87	-4.43	-2.79	-7.63	2.81	5.74	2.06
$\text{F}_2 + \text{Si} \rightarrow \text{F} + \text{SiF}$	-102.03	-4.05	0.05	-0.87	-24.93	-22.16	-3.89	1.84	-27.70
$\text{ClF} + \text{CN} \rightarrow \text{F} + \text{ClCN}$	-44.96	-2.18	-0.57	-3.50	-21.40	-20.43	1.29	8.16	-22.37
$\text{F}_2 + \text{C} \rightarrow \text{F} + \text{CF}$	-94.90	-2.65	-1.50	-2.43	-24.20	-21.37	-2.97	1.16	-27.02
$\text{F}_2 + \text{B} \rightarrow \text{F} + \text{BF}$	-145.17	3.56	-1.42	-2.43	-26.82	-24.25	-4.38	0.72	-29.39
$\text{BF} + \text{N} \rightarrow \text{F} + {}^3\text{BN}$	78.36	2.16	-1.11	-1.58	2.91	1.62	4.79	0.53	4.19
$\text{ClF} + \text{Cl} \rightarrow \text{F} + \text{Cl}_2$	4.62	-0.70	-0.45	-1.88	-1.10	-3.69	4.90	3.52	1.48
$\text{F}_2 + \text{Cl} \rightarrow \text{F} + \text{ClF}$	-22.99	-2.33	0.53	-0.28	-24.34	-21.64	-0.20	2.24	-27.05
$\text{SO} + \text{HCl} \rightarrow \text{S} + \text{HOCl}$	63.75	-2.20	0.97	-1.06	0.33	-2.86	3.84	7.83	3.52
$\text{SO} + \text{HF} \rightarrow \text{S} + \text{HOF}$	104.04	-1.46	1.11	-1.49	2.79	-1.93	8.02	11.04	7.51
$\text{SO} + \text{Cl} \rightarrow \text{S} + \text{ClO}$	59.41	-1.30	-1.42	-2.66	5.28	0.64	4.39	4.51	9.92
$\text{SO} + \text{NO} \rightarrow \text{S} + \text{NO}_2$	46.18	2.30	0.92	2.81	-1.77	1.20	-2.66	-5.43	-4.74
$\text{SO} + \text{N}_2 \rightarrow \text{S} + \text{N}_2\text{O}$	78.16	1.83	1.28	3.07	-0.62	2.11	-2.14	-4.83	-3.35
$\text{SO} + \text{HNO} \rightarrow \text{S} +$ <i>trans</i> -HONO	14.36	-0.69	0.23	0.29	-8.15	-7.80	-1.67	0.60	-8.49
$\text{CS} + \text{HNO} \rightarrow \text{S} + \text{HNCO}$	-62.41	-4.88	-3.17	-3.73	-19.26	-16.86	-15.04	-1.56	-21.66
$\text{SO} + \text{HCN} \rightarrow \text{S} + \text{HNCO}$	-0.07	-1.98	-1.19	-2.50	-1.80	-3.83	-3.40	3.42	0.23
$\text{SO} + \text{N} \rightarrow \text{S} + \text{NO}$	-28.88	1.43	1.28	1.73	3.25	4.25	0.48	0.48	2.26
$\text{SO} + \text{C}_2\text{H}_2 \rightarrow \text{S} +$ oxirene	71.25	-1.56	0.45	-1.48	7.75	3.88	0.87	6.92	11.62
$\text{SO} + \text{C}_2\text{H}_4 \rightarrow \text{S} +$ oxirane	32.95	-3.04	-0.20	-1.80	-2.35	-4.38	-2.99	4.84	-0.32
$\text{SO} + \text{CH}_4 \rightarrow \text{S} +$ methanol	28.28	-3.41	0.26	-2.08	-1.52	-4.91	1.44	7.70	1.87
$\text{CS} + \text{H}_2\text{O} \rightarrow \text{S} +$ <i>trans</i> -HCOH	77.64	-5.85	-0.89	-3.64	5.27	-0.31	-3.87	9.48	10.85
$\text{SO} + {}^3\text{CH}_2 \rightarrow \text{S} +$ <i>trans</i> -HCOH	-8.55	-1.08	1.34	-0.56	5.06	2.16	4.88	7.90	7.95
$\text{SO} + \text{trans-HCOH} \rightarrow$ $\text{S} +$ formic acid	-58.14	-2.17	-1.09	-1.87	-7.84	-8.20	-4.24	1.16	-7.48
$\text{CS} + \text{HOOH} \rightarrow \text{S} +$ formic acid	-65.43	-6.03	-3.08	-4.10	-3.96	-5.63	-14.33	0.53	-2.29

Table C.1: (continued)

Reaction	CCSD(T)	$\Delta(\text{CCSD})$	$\Delta(\text{MP2.8-}\kappa\text{-OOMP2})$	$\Delta(\text{MP3.}\kappa\text{-OOMP2})$	$\Delta(\text{MP2.5})$	$\Delta(\text{MP3})$	$\Delta(\kappa\text{-OOMP2})$	$\Delta(\text{OOMP2})$	$\Delta(\text{MP2})$
SO + CH ₂ C → S + ketene	-52.90	-1.29	-1.15	-1.23	-7.40	-6.13	-6.57	-1.55	-8.68
CS + H ₂ CO → S + ketene	7.96	-4.56	-2.64	-4.13	-3.02	-5.72	-9.22	2.58	-0.32
SO + oxirene → S + glyoxal	-58.73	-4.46	0.05	-2.01	-3.05	-6.81	0.01	7.17	0.71
CS + formic acid → S + glyoxal	33.65	-5.15	-0.80	-2.98	4.80	-0.44	-4.54	6.76	10.04
CS + methanol → S + acetaldehyde	2.39	-4.91	-1.71	-3.31	-1.49	-4.43	-7.85	4.26	1.46
SO + C ₂ H ₄ → S + acetaldehyde	6.92	-3.15	-0.07	-1.62	-1.44	-3.56	-1.48	5.07	0.68
SO + CF ₂ → S + F ₂ CO	-40.83	-3.04	-1.41	-3.05	-7.90	-9.38	-3.35	3.22	-6.43
SO + ³ CH ₂ → S + H ₂ CO	-61.08	-0.50	1.13	0.10	-0.71	-1.54	2.25	4.44	0.11
CS + H ₂ O → S + H ₂ CO	25.11	-5.27	-1.10	-2.98	-4.01	-4.01	-6.50	6.01	3.00
SO + CH → S + HCO	-72.96	-0.33	-1.76	-1.73	-6.76	-5.85	-4.48	-1.96	-7.68
CS + S ₂ → S + CS ₂	-8.62	-0.75	0.39	0.81	-3.77	-1.74	-5.62	-2.26	-5.81
SO + CS → S + OCS	-43.68	-2.66	-1.24	-2.25	-4.52	-4.88	-7.07	1.43	-4.16
S ₂ + CO → S + OCS	23.84	-0.26	0.03	0.63	-1.69	-0.42	-3.93	-2.17	-2.97
SO + CO → S + CO ₂	-9.67	-1.57	-1.28	-1.84	-2.99	-3.30	-4.21	0.65	-2.68
CS + O ₂ → S + CO ₂	-101.32	-4.00	-1.37	-1.64	-5.29	-4.53	-14.71	-1.13	-6.05
S ₂ + C → S + CS	-69.98	2.90	0.81	2.40	0.43	3.35	0.98	-4.08	-2.49
SO + Si → S + SiO	-66.86	1.01	2.27	3.17	-0.89	1.84	0.54	-2.13	-3.63
CS + O → S + CO	-89.85	-1.86	-0.65	0.41	-2.44	0.42	-13.56	-4.03	-5.31
SO + C → S + CO	-137.49	0.51	-0.46	-0.48	-2.39	-1.11	-2.16	-0.48	-3.68
CS + N → S + CN	-9.40	-0.39	-0.35	2.08	17.72	16.86	-8.19	-8.39	18.58
S ₂ + H ₂ → S + H ₂ S	24.38	-4.28	0.52	-1.24	-0.07	-3.60	-1.01	7.01	3.47
SO + H ₂ O → S + HOOH	84.93	-1.99	1.10	-1.42	1.39	-2.88	6.22	10.11	5.65
SO + H ₂ → S + H ₂ O	-2.03	-3.83	-0.44	-2.96	-2.58	-6.28	1.28	7.36	1.12
CS + C ₂ H ₄ → S + propyne	25.34	-5.15	-1.82	-3.15	-3.57	-5.48	-8.75	2.33	-1.67
CS + C ₂ H ₆ → S + propene	18.52	-4.91	-1.47	-3.70	-1.81	-5.68	-5.49	6.15	2.06
CS + CH ₃ F → S + C ₂ H ₃ F	16.66	-4.78	-1.85	-4.04	-1.72	-5.70	-5.84	5.91	2.26
CS + CH ₄ → S + C ₂ H ₄	23.75	-5.17	-1.37	-3.77	-1.56	-5.78	-4.92	6.90	2.66
CS + CH ₃ → S + CH ₃ CH	29.54	-5.01	-1.93	-4.25	3.99	-4.75	-4.90	6.47	8.73
CS + CF ₂ → S + FCF	39.92	-5.20	-2.65	-4.67	-8.77	-11.33	-8.46	3.07	-6.20
CS + ³ CH ₂ → S + C ₂ H ₂	-45.56	-2.38	-1.05	-1.92	-2.69	-3.55	-4.79	1.73	-1.82
CS + Cl ₂ → S + CCl ₂	50.96	-3.64	-1.77	-3.14	6.38	2.86	-5.66	3.42	9.90
CS + F ₂ → S + CF ₂	-52.60	-8.16	-1.57	-3.37	-22.52	-21.71	-13.58	4.69	-23.33
CS + H ₂ → S + ³ CH ₂	84.16	-8.60	-2.67	-6.04	-2.37	-8.75	-7.47	8.93	4.01
CS + F → S + CF	35.76	-4.80	-0.80	-1.60	0.41	-1.13	-10.28	3.19	1.95
S ₂ + SO → S + S ₂ O	26.17	1.79	0.43	2.24	13.74	11.91	-1.65	-7.63	15.57
SO + SO ₂ → S + SO ₃	42.42	-3.01	-1.85	-3.86	-3.68	-5.65	-3.52	5.56	-1.71
2SO → S + SO ₂	-2.72	0.93	1.78	2.93	-1.58	1.17	-3.10	-3.12	-4.34
S ₂ + O ₂ → S + SO ₂	-26.85	0.89	2.96	6.00	-1.06	4.40	-10.45	-8.50	-6.51
S ₂ + O → S + SO	-22.33	0.54	0.62	3.28	0.38	4.88	-10.41	-7.63	-4.11

Table C.1: (continued)

Reaction	CCSD(T)	$\Delta(\text{CCSD})$	$\Delta(\text{MP2.8-}\kappa\text{-OOMP2})$	$\Delta(\text{MP3-}\kappa\text{-OOMP2})$	$\Delta(\text{MP2.5})$	$\Delta(\text{MP3})$	$\Delta(\kappa\text{-OOMP2})$	$\Delta(\text{OOMP2})$	$\Delta(\text{MP2})$
SO + O \rightarrow S + O ₂	1.79	0.58	-0.55	0.21	-0.14	1.66	-3.06	-2.25	-1.94
ClF + CH ₃ \rightarrow Cl + CH ₃ F	-54.62	-1.78	-0.57	-1.10	-1.43	-2.08	-2.15	0.85	-0.78
ClO + HCl \rightarrow Cl + HOCl	4.34	-0.91	2.39	1.60	-4.95	-3.50	-0.54	3.33	-6.40
ClO + HF \rightarrow Cl + HOF	44.63	-0.16	2.53	1.17	-2.49	-2.57	3.64	6.54	-2.40
Cl ₂ + O \rightarrow Cl + ClO	-5.25	1.52	-1.71	0.48	6.07	7.25	-4.41	-6.83	4.88
ClO + NO \rightarrow Cl + NO ₂	-13.22	3.59	2.34	5.48	-7.05	0.56	-7.04	-9.94	-14.66
ClO + N ₂ \rightarrow Cl + N ₂ O	18.75	3.13	2.71	5.73	-5.90	1.47	-6.52	-9.33	-13.27
ClO + HNO \rightarrow Cl +	-45.05	0.60	1.65	2.96	-13.43	-8.45	-6.06	-3.90	-18.41
<i>trans</i> -HONO									
ClO + HCN \rightarrow Cl + HNCO	-59.48	-0.69	0.23	0.16	-7.08	-4.47	-7.78	-1.08	-9.68
ClO + N \rightarrow Cl + NO	-88.29	2.72	2.70	4.40	-2.03	3.60	-3.90	-4.02	-7.66
ClO + C ₂ H ₂ \rightarrow Cl +	11.84	-0.27	1.87	1.18	2.47	3.24	-3.51	2.41	1.71
oxirene									
ClO + C ₂ H ₄ \rightarrow Cl +	-26.46	-1.74	1.22	0.86	-7.63	-5.02	-7.37	0.34	-10.23
oxirane									
ClO + CH ₄ \rightarrow Cl +	-31.13	-2.11	1.68	0.59	-6.80	-5.56	-2.94	3.20	-8.05
methanol									
ClO + ³ CH ₂ \rightarrow Cl +	-67.96	0.22	2.76	2.10	-0.22	1.52	0.49	3.39	-1.96
<i>trans</i> -HCOH									
ClO + <i>trans</i> -HCOH \rightarrow	-117.55	-0.88	0.33	0.79	-13.12	-8.84	-8.62	-3.34	-17.40
Cl + formic acid									
ClO + CH ₂ C \rightarrow Cl +	-112.31	0.01	0.27	1.43	-12.68	-6.77	-10.95	-6.06	-18.59
ketene									
ClO + oxirene \rightarrow Cl +	-118.14	-3.16	1.47	0.65	-8.33	-7.45	-4.37	2.66	-9.21
glyoxal									
ClO + C ₂ H ₄ \rightarrow Cl +	-52.48	-1.86	1.35	1.04	-6.72	-4.20	-5.87	0.56	-9.24
acetaldehyde									
ClO + CF ₂ \rightarrow Cl + F ₂ CO	-100.24	-1.75	0.01	-0.39	-13.18	-10.02	-7.73	-1.29	-16.35
ClF + HCO \rightarrow Cl + HCOF	-64.03	-2.27	-1.41	-2.00	-2.47	-3.61	-3.94	0.46	-1.33
ClO + ³ CH ₂ \rightarrow Cl + H ₂ CO	-120.49	0.79	2.55	2.77	-5.99	-2.18	-2.14	-0.07	-9.81
ClO + CH \rightarrow Cl + HCO	-132.36	0.97	-0.34	0.93	-12.04	-6.49	-8.86	-6.47	-17.59
ClO + CS \rightarrow Cl + OCS	-103.08	-1.36	0.18	0.42	-9.80	-5.52	-11.45	-3.07	-14.08
ClO + CO \rightarrow Cl + CO ₂	-69.08	-0.27	0.14	0.82	-8.27	-3.94	-8.60	-3.85	-12.60
ClO + Si \rightarrow Cl + SiO	-126.27	2.31	3.69	5.83	-6.17	1.20	-3.85	-6.64	-13.54
ClO + C \rightarrow Cl + CO	-196.90	-1.46	0.96	2.19	-7.67	-1.75	-6.54	-4.99	-13.59
Cl ₂ + Al \rightarrow Cl + AlCl	-64.61	-1.46	-0.88	-1.26	-1.24	-1.98	-1.46	0.32	-0.50
AlCl + F \rightarrow Cl + AlF	-40.41	0.27	0.53	2.20	0.25	3.60	-6.93	-4.72	-3.09
ClF + Al \rightarrow Cl + AlF	-100.39	-1.88	-0.80	-0.94	-2.08	-2.07	-3.48	-0.87	-2.10
ClO + H ₂ O \rightarrow Cl + HOOH	25.53	-0.69	2.52	1.25	-3.89	-3.52	1.83	5.61	-4.26
OH + ClO \rightarrow Cl + HOO	-5.74	0.06	0.86	1.18	-1.24	0.92	-2.99	-0.34	-2.97
ClO + H ₂ \rightarrow Cl + H ₂ O	-61.44	-2.54	0.98	-0.29	-7.86	-6.92	-3.11	2.85	-8.80
ClF + CH ₂ CH \rightarrow	-67.50	-1.56	-0.49	-0.88	-7.14	-7.03	-3.09	0.30	-7.25
Cl + C ₂ H ₃ F									
ClF + CCH \rightarrow Cl + HCCF	-73.01	-1.39	-0.99	-1.37	-13.73	-12.41	-4.20	-0.35	-15.06
ClF + CF \rightarrow Cl + CF ₂	-65.37	-1.03	-1.30	-1.49	1.41	1.06	-3.10	-0.74	1.77

Table C.1: (continued)

Reaction	CCSD(T)	$\Delta(\text{CCSD})$	$\Delta(\text{MP2.8:}\kappa\text{-OOMP2})$	$\Delta(\text{MP3:}\kappa\text{-OOMP2})$	$\Delta(\text{MP2.5})$	$\Delta(\text{MP3})$	$\Delta(\kappa\text{-OOMP2})$	$\Delta(\text{OOMP2})$	$\Delta(\text{MP2})$
ClF + Si \rightarrow Cl + SiF	-79.04	-1.72	-0.47	-0.59	-0.59	-0.53	-3.69	-0.39	-0.65
Cl ₂ + CN \rightarrow Cl + ClCN	-49.58	-1.48	-0.12	-1.62	-20.30	-16.74	-3.61	4.63	-23.86
ClF + C \rightarrow Cl + CF	-71.91	-0.32	-1.36	-1.23	0.14	0.26	-2.77	-1.07	0.03
ClF + B \rightarrow Cl + BF	-122.19	-1.23	-1.95	-2.15	-2.48	-2.62	-4.18	-1.52	-2.34
ClO + S ₂ \rightarrow Cl + S ₂ O	-33.23	3.08	1.85	4.90	8.46	11.27	-6.04	-12.14	5.66
ClO + SO ₂ \rightarrow Cl + SO ₃	-16.98	-1.71	-0.42	-1.20	-8.96	-6.29	-7.90	1.06	-11.63
ClO + SO \rightarrow Cl + SO ₂	-62.13	2.22	3.20	5.60	-6.86	0.53	-7.48	-7.63	-14.25
ClO + S \rightarrow Cl + SO	-59.41	1.30	1.42	2.66	-4.38	-0.64	-4.39	-4.51	-9.92
Cl ₂ + F \rightarrow Cl + ClF	-4.62	0.70	0.45	1.88	1.10	3.69	-4.90	-3.52	-1.48
ClF + F \rightarrow Cl + F ₂	22.99	2.33	-0.53	0.28	24.34	21.64	0.20	-2.24	27.05
ClO + O \rightarrow Cl + O ₂	-57.62	1.87	0.87	2.87	-5.42	1.02	-7.45	-6.75	-11.86
HOF + CH ₃ \rightarrow OH + CH ₃ F	-64.25	-2.86	-0.87	-1.96	-2.34	-4.12	-1.79	2.04	-0.55
HOO + HCl \rightarrow OH + HOCl	10.08	-0.97	1.52	0.42	-3.71	-3.99	2.45	3.67	-3.43
HOO + HF \rightarrow OH + HOF	50.37	-0.22	1.66	-0.01	-1.25	-3.06	6.63	6.88	0.56
HOO + O \rightarrow OH + ClO	-3.95	0.95	-2.26	-1.26	5.72	4.69	-0.53	-3.62	6.76
HOO + Cl \rightarrow OH + ClO	5.74	-0.06	-0.86	-1.18	1.24	-0.49	2.99	0.34	2.97
HOO + NO \rightarrow OH + NO ₂	-7.48	3.53	1.48	4.30	-5.81	0.07	-4.06	-9.59	-11.69
HNO + O ₂ \rightarrow OH + NO ₂	-9.13	2.51	1.14	3.48	-13.79	-7.98	-3.59	-7.28	-19.60
HOO + N ₂ \rightarrow OH + N ₂ O	24.49	3.07	1.84	4.55	-4.66	0.98	-3.53	-8.99	-10.30
HNO + NO \rightarrow OH + N ₂ O	-21.14	1.66	0.59	3.05	-19.49	-11.86	-4.60	-9.14	-27.11
HOO + HNO \rightarrow OH + <i>trans</i> -HONO	-39.31	0.54	0.78	1.78	-12.19	-8.94	-3.07	-3.56	-15.44
HCO + HNO \rightarrow OH + HNCO	-58.31	-1.57	-1.87	-2.62	-17.67	-16.12	-2.99	-0.09	-19.22
HOO + HCN \rightarrow OH + HNCO	-53.74	-0.75	-0.63	-1.02	-5.84	-4.96	-4.79	-0.74	-6.71
HNO + O \rightarrow OH + NO	-53.52	0.79	-0.33	0.88	-12.16	-7.53	-4.00	-4.10	-16.80
HOO + N \rightarrow OH + NO	-82.55	2.66	1.84	3.22	-0.79	3.11	-0.91	-3.68	-4.69
HOO + C ₂ H ₂ \rightarrow OH + oxirene	17.58	-0.33	1.01	0.00	3.71	2.74	-0.52	2.75	4.68
HOO + C ₂ H ₄ \rightarrow OH + oxirane	-20.72	-1.81	0.36	-0.32	-6.39	-5.51	-4.38	0.68	-7.27
HOO + CH ₄ \rightarrow OH + methanol	-25.39	-2.17	0.82	-0.59	-5.56	-6.05	0.05	3.54	-5.08
HCO + H ₂ O \rightarrow OH + <i>trans</i> -HCOH	81.74	-2.54	0.41	-2.53	6.85	0.42	8.19	10.95	13.29
HOO + ³ CH ₂ \rightarrow OH + <i>trans</i> -HCOH	-62.22	0.15	1.90	0.92	1.02	1.03	3.48	3.73	1.01
HOO + <i>trans</i> -HCOH \rightarrow OH + formic acid	-111.81	-0.94	-0.54	-0.39	-11.88	-9.33	-5.63	-3.00	-14.43
HCO + HOOH \rightarrow OH + formic acid	-61.34	-2.72	-1.79	-2.99	-2.37	-4.90	-2.27	2.00	0.16
HOO + CH ₂ C \rightarrow OH + ketene	-106.57	-0.05	-0.60	0.25	-11.44	-7.26	-7.96	-5.72	-15.62

Table C.1: (continued)

Reaction	CCSD(T)	$\Delta(\text{CCSD})$	$\Delta(\text{MP2.8-}\kappa\text{-OOMP2})$	$\Delta(\text{MP3.}\kappa\text{-OOMP2})$	$\Delta(\text{MP2.5})$	$\Delta(\text{MP3})$	$\Delta(\kappa\text{-OOMP2})$	$\Delta(\text{OOMP2})$	$\Delta(\text{MP2})$
HCO + H ₂ CO → OH + ketene	12.05	-1.25	-1.35	-3.02	-1.43	-4.98	2.83	4.05	2.13
HOO + oxirene → OH + glyoxal	-112.40	-3.23	0.60	-0.53	-7.09	-7.94	-1.38	3.00	-6.24
HCO + formic acid → OH + glyoxal	37.74	-1.84	0.50	-1.87	6.39	0.29	7.52	8.23	12.49
HCO + methanol → OH + acetaldehyde	6.49	-1.61	-0.41	-2.20	0.10	-3.70	4.21	5.73	3.91
HOO + C ₂ H ₄ → OH + acetaldehyde	-46.74	-1.92	0.48	-0.14	-5.48	-4.70	-2.88	0.90	-6.27
HOO + CF ₂ → OH + F ₂ CO	-94.50	-1.81	-0.85	-1.57	-11.95	-10.51	-4.74	-0.95	-13.38
HOF + HCO → OH + HCOF	-73.65	-3.35	-1.71	-2.86	-3.38	-5.66	-3.58	1.64	-1.10
HOO + ³ CH ₂ → OH + H ₂ CO	-114.75	0.73	1.68	1.59	-4.76	-2.67	0.85	0.27	-6.84
HCO + H ₂ O → OH + H ₂ CO	29.21	-1.96	0.20	-1.87	1.08	-3.28	5.56	7.49	5.45
HOO + CH → OH + HCO	-126.62	0.91	-1.21	-0.25	-10.80	-6.98	-5.87	-6.13	-14.63
HCO + S ₂ → OH + CS ₂	-4.53	2.56	1.69	1.92	-2.18	-1.01	6.44	-0.79	-3.36
HOO + CS → OH + OCS	-97.34	-1.42	-0.68	-0.76	-8.56	-6.01	-8.46	-2.73	-11.11
HCO + SO → OH + OCS	-39.58	0.65	0.06	-1.14	-2.93	-4.14	4.99	2.90	-1.71
HOO + CO → OH + CO ₂	-63.34	-0.33	-0.72	-0.36	-7.03	-4.43	-5.61	-3.51	-9.63
HCO + O ₂ → OH + CO ₂	-97.22	-0.69	-0.07	-0.54	-3.70	-3.80	-2.65	0.34	-3.60
HCO + S → OH + CS	4.10	3.31	1.30	1.11	1.59	0.73	12.06	1.47	2.45
HOO + Si → OH + SiO	-120.53	2.24	2.83	4.65	-4.93	0.70	-0.86	-6.30	-10.57
HCO + O → OH + CO	-85.76	1.45	0.65	1.52	-0.85	1.16	-1.50	-2.56	-2.86
HOO + C → OH + CO	-191.16	1.74	0.10	1.01	-6.44	-2.25	-3.55	-4.65	-10.63
HNO + CH → OH + HCN	-131.19	0.08	-2.45	-1.85	-22.64	-18.15	-4.07	-5.48	-27.13
HCO + N → OH + CN	-5.31	2.92	0.95	3.19	19.31	17.60	3.87	-6.92	21.03
HNO + C → OH + CN	-81.69	1.34	-1.78	0.34	2.35	3.56	-1.27	-9.43	1.15
HOCI + Al → OH + AlCl	-63.31	-2.02	-1.43	-3.00	-1.58	-4.54	2.42	3.54	1.38
HOF + Al → OH + AlF	-110.02	-2.96	-1.09	-1.81	-2.99	-4.11	-3.13	0.32	-1.87
HOO + H ₂ O → OH + HOOH	31.27	-0.76	1.66	0.07	-2.66	-4.02	4.82	5.95	-1.29
HOO + H ₂ → OH + H ₂ O	-55.70	-2.60	0.11	-1.47	-6.62	-7.41	-0.12	3.19	-5.83
HNO + NH ₂ → OH + trans-N ₂ H ₂	-15.71	-0.73	-0.16	-1.15	-5.02	-5.54	1.93	2.82	-4.49
HCO + C ₂ H ₄ → OH + propyne	29.43	-1.85	-0.52	-2.04	-1.99	-4.75	3.30	3.80	0.78
HCO + C ₂ H ₆ → OH + propene	22.62	-1.60	-0.17	-2.59	-0.22	-4.95	6.56	7.62	4.51
HOF + CH ₂ CH → OH + C ₂ H ₃ F	-77.13	-2.63	-0.79	-1.74	-8.05	-9.07	-2.73	1.48	-7.02
HCO + CH ₃ F → OH + C ₂ H ₃ F	20.76	-1.48	-0.56	-2.93	-0.13	-4.97	6.22	7.38	4.70

Table C.1: (continued)

Reaction	CCSD(T)	$\Delta(\text{CCSD})$	$\Delta(\text{MP2.8:k-OOMP2})$	$\Delta(\text{MP3:k-OOMP2})$	$\Delta(\text{MP2.5})$	$\Delta(\text{MP3})$	$\Delta(\kappa\text{-OOMP2})$	$\Delta(\text{OOMP2})$	$\Delta(\text{MP2})$
<i>cis</i> -N ₂ H ₂ → <i>trans</i> -N ₂ H ₂	-5.72	-0.18	-0.02	-0.02	-0.65	-0.57	-0.40	-0.09	-0.73
allene → propyne	-0.51	-0.34	-0.20	0.60	-1.61	0.25	-2.84	-3.29	-3.46
dioxirane → formic acid	-91.13	-1.97	-0.75	-0.84	-13.17	-10.26	-4.43	-1.13	-16.07
oxirene → ketene	-78.81	-1.12	-0.91	-0.62	-8.80	-7.58	-3.06	-1.63	-10.01
oxirane → acetaldehyde	-26.02	-0.11	0.13	0.18	0.91	0.82	1.51	0.22	0.99
HCNH → H ₂ CN	-7.98	-1.28	-0.42	-1.57	3.65	0.76	2.72	4.35	6.54
CH ₃ NH → CH ₂ NH ₂	-6.86	0.67	-0.24	0.53	-1.26	0.61	-2.92	-3.40	-3.12
F + CH ₄ → CH ₃ F + H	-2.45	2.24	-0.81	1.57	-2.47	2.82	-9.25	-9.12	-7.77
F + CH ₃ F → CH ₂ F ₂ + H	-14.55	2.47	-1.31	1.24	-2.69	2.80	-9.97	-9.99	-8.18
F + C ₂ H ₆ → CH ₃ F + CH ₃	-17.07	0.68	0.05	1.41	-0.34	2.59	-4.81	-4.39	-3.27
F + C ₂ H ₅ F →	-22.97	0.75	-0.27	1.20	-0.63	2.43	-5.29	-5.01	-3.69
CH ₂ F ₂ + CH ₃									
F + propane →	-20.82	0.60	-0.14	1.17	-0.22	2.54	-4.84	-4.25	-2.99
C ₂ H ₅ F + CH ₃									
F + CH ₃ NH ₂ →	-23.16	0.40	0.06	0.84	0.49	2.06	-2.44	-2.12	-1.09
CH ₃ F + NH ₂									
F + CH ₃ NH →	-31.70	0.25	0.36	1.49	-1.09	1.57	-4.43	-3.72	-3.74
CH ₃ F + NH									
F + methanol →	-16.68	0.07	-0.15	0.09	0.40	0.86	-0.95	-0.57	-0.06
CH ₃ F + OH									
F + acetaldehyde →	-23.17	1.68	0.26	2.29	0.30	4.56	-5.16	-6.30	-3.97
CH ₃ F + HCO									
F + acetaldehyde →	-32.58	1.19	-0.58	1.39	-0.74	3.03	-6.96	-6.70	-4.52
CH ₃ + HCOF									
F + H ₂ CO → HCOF + H	-28.61	2.97	-1.82	1.30	-3.01	3.31	-12.15	-12.15	-9.33
F + HCOF → F ₂ CO + H	-16.37	2.27	-1.72	0.52	-3.37	1.77	-10.46	-9.56	-8.52
F + glyoxal →	-46.69	1.99	-0.52	2.15	-5.98	0.64	-8.32	-8.76	-12.60
HCOF + HCO									
RMSD		4.94	1.59	3.22	8.97	9.24	7.58	10.82	11.99
MSD		1.49	-0.45	0.33	-2.85	-0.80	-3.14	-3.50	-4.90
MIN		-8.60	-5.83	-8.12	-40.24	-38.57	-38.94	-48.81	-51.14
MAX		20.34	5.24	14.63	24.87	31.66	13.56	17.87	27.28

C.2 RSE43

Table C.2 presents CCSD(T) reaction energies for the RSE43 set in kcal mol⁻¹ and errors for other methods. All calculations were performed with the aVTZ basis set and the corresponding RI basis was used for the MP2, OOMP2, and κ -OOMP2 calculations. For this set, we did not use the RI approximation for the CCSD(T), CCSD, or MP3 contributions.

Table C.2: (continued)

Reaction	CCSD(T)	$\Delta(\text{CCSD})$	$\Delta(\text{MP2.8:k-OOMP2})$	$\Delta(\text{MP3:k-OOMP2})$	$\Delta(\text{MP2.5})$	$\Delta(\text{MP3})$	$\Delta(\text{k-OOMP2})$	$\Delta(\text{OOMP2})$	$\Delta(\text{MP2})$
$\text{N}(\text{CH}_3)_3 + \text{CH}_3 \rightarrow$	-12.75	0.67	-0.51	-0.26	0.99	1.32	-0.12	-1.07	0.66
$\text{N}(\text{CH}_3)_2\text{CH}_2\text{CH}_4$									
$\text{CH}_3\text{NO}_2 + \text{CH}_3 \rightarrow$	-2.49	0.34	-0.78	-0.64	2.17	1.38	0.08	-1.12	2.97
$\text{CH}_2\text{NO}_2 + \text{CH}_4$									
$\text{CH}_3\text{OCF}_3 + \text{CH}_3 \rightarrow$	-3.37	0.34	-0.41	-0.27	0.54	0.68	-0.14	-0.57	0.40
$\text{CH}_2\text{OCF}_3 + \text{CH}_4$									
$\text{CH}_3\text{OCH}_3 + \text{CH}_3 \rightarrow$	-2.67	0.20	-0.34	-0.26	0.37	0.42	-0.12	-0.37	0.32
$\text{CH}_2\text{OCH}_3 + \text{CH}_4$									
$\text{HCOOCH}_3 + \text{CH}_3 \rightarrow$	-5.54	0.46	-0.37	-0.25	0.58	0.75	-0.03	-0.53	0.42
$\text{HCOOCH}_2 + \text{CH}_4$									
$\text{CH}_3\text{COOCH}_3 + \text{CH}_3 \rightarrow$	-6.03	0.53	-0.41	-0.25	0.78	0.97	0.03	-0.65	0.60
$\text{CH}_3\text{COOCH}_2 + \text{CH}_4$									
$\text{CH}_3\text{OH} + \text{CH}_3 \rightarrow$	-4.02	0.19	-0.41	-0.30	0.16	0.28	-0.38	-0.53	0.04
$\text{CH}_2\text{OH} + \text{CH}_4$									
$\text{CH}_3\text{PH}_3 + \text{CH}_3 \rightarrow$	1.48	-0.06	-0.03	-0.11	0.41	0.20	0.34	0.40	0.61
$\text{CH}_2\text{PH}_3 + \text{CH}_4$									
$\text{CH}_3\text{SCH}_3 + \text{CH}_3 \rightarrow$	-10.29	0.63	-0.70	-0.42	1.30	1.55	-0.16	-1.26	1.05
$\text{CH}_2\text{SCH}_3 + \text{CH}_4$									
$\text{CH}_3\text{SCHO} + \text{CH}_3 \rightarrow$	-7.68	0.65	-0.61	-0.35	1.44	1.57	0.07	-1.13	1.32
$\text{CH}_2\text{SCHO} + \text{CH}_4$									
$\text{CH}_3\text{SH}_2 + \text{CH}_3 \rightarrow$	3.37	0.06	-0.24	-0.21	0.40	0.39	-0.09	-0.14	0.42
$\text{CH}_2\text{SH}_2 + \text{CH}_4$									
$\text{CH}_3\text{SH} + \text{CH}_3 \rightarrow$	-8.87	0.51	-0.63	-0.38	1.06	1.30	-0.27	-1.06	0.83
$\text{CH}_2\text{SH} + \text{CH}_4$									
$\text{CH}_3\text{SO}_2\text{CH}_3 + \text{CH}_3 \rightarrow$	0.60	0.31	-0.40	-0.21	1.07	1.02	0.34	-0.61	1.13
$\text{CH}_2\text{SO}_2\text{CH}_3 + \text{CH}_4$									
$\text{CH}_3\text{SOCH}_3 + \text{CH}_3 \rightarrow$	-2.16	0.29	-0.65	-0.58	1.19	1.02	0.21	-0.55	1.36
$\text{CH}_2\text{SOCH}_3 + \text{CH}_4$									
$\text{NH}_2\text{CH}_2\text{CN} + \text{CH}_3 \rightarrow$	-21.97	0.76	-1.25	-0.85	6.57	4.97	-0.42	-2.21	8.16
$\text{NH}_2\text{CHCN} + \text{CH}_4$									
$\text{NH}_2\text{CH}_2\text{CONH}_2 + \text{CH}_3$	-23.89	0.94	-0.85	-0.40	0.69	1.25	-0.77	-2.16	0.13
$\rightarrow \text{NH}_2\text{CHCONH}_2 + \text{CH}_4$									
$\text{NH}_2\text{CH}_2\text{COOH} + \text{CH}_3 \rightarrow$	-25.16	0.97	-0.90	-0.44	0.53	1.10	-0.96	-2.26	-0.03
$\text{NH}_2\text{CHCOOH} + \text{CH}_4$									
$\text{CH}_3\text{CCH} + \text{CH}_3 \rightarrow$	-12.85	0.30	-0.88	-0.94	7.09	5.25	0.92	-0.08	8.93
$\text{CH}_2\text{CCH} + \text{CH}_4$									
$\text{CH}(\text{CH}_3)_3 + \text{CH}_3 \rightarrow$	-5.98	0.06	-0.60	-0.68	0.76	0.37	0.42	0.17	1.14
$\text{C}(\text{CH}_3)_3 + \text{CH}_4$									
$\text{C}(\text{CH}_3)_4 + \text{CH}_3 \rightarrow$	-2.65	0.09	0.05	0.00	0.81	0.58	0.73	0.48	1.05
$\text{C}(\text{CH}_3)_3\text{CH}_2 + \text{CH}_4$									
RMSD		0.45	0.63	0.52	3.23	2.43	0.48	0.92	4.10
MSD		0.32	-0.54	-0.42	1.91	1.56	-0.61	-0.61	2.25
MIN		-0.82	-1.73	-1.55	0.06	0.11	-0.96	-2.26	-0.03
MAX		0.97	0.05	0.00	12.90	9.36	1.02	0.48	16.44

C.3 BH76RC

Table C.3 presents CCSD(T) reaction energies for the BH76RC set in kcal mol⁻¹ and errors for other methods. All calculations were performed with the aVTZ basis set and the corresponding RI basis was used for all methods.

Table C.3: CCSD(T)/aVTZ energies (in kcal/mol) for the BH76RC set and errors for other methods.

Reaction	CCSD(T)	$\Delta(\text{CCSD})$	$\Delta(\text{MP2.8:k- OOMP2})$	$\Delta(\text{MP3:k- OOMP2})$	$\Delta(\text{MP2.5})$	$\Delta(\text{MP3})$	$\Delta(\text{k- OOMP2})$	$\Delta(\text{OOMP2})$	$\Delta(\text{MP2})$
H + N ₂ O → OH + N ₂	-64.16	-7.18	-0.16	-6.21	2.00	-8.62	11.86	20.50	12.61
H + CH ₃ F → HF + CH ₃	-25.68	-1.26	0.68	-0.11	0.89	-0.84	3.51	3.16	2.62
H + F ₂ → HF + F	-103.25	-5.01	0.54	-1.50	-21.41	-21.60	1.43	5.94	-21.21
CH ₃ + ClF → CH ₃ F + Cl	-54.62	-1.78	-0.60	-1.12	-1.46	-2.09	-2.20	0.79	-0.82
F ⁻ + CH ₃ Cl → Cl ⁻ + CH ₃ F	-31.56	-1.67	-1.30	-3.02	-0.51	-3.71	2.45	4.67	2.69
CH ₃ Cl...F ⁻ → CH ₃ F...Cl ⁻	-25.41	-1.88	-0.83	-2.38	-0.93	-3.63	1.70	4.16	1.76
OH ⁻ + CH ₃ F → CH ₃ OH + F ⁻	-19.59	-0.48	-0.70	-0.97	-0.50	-1.06	-2.10	0.68	0.07
CH ₃ F...OH ⁻ → CH ₃ OH...F ⁻	-36.59	-0.05	-1.15	-1.54	-0.66	-1.34	-2.34	0.87	0.01
H + N ₂ → HN ₂	3.44	-0.35	-0.72	-2.13	9.90	4.23	5.03	5.41	15.58
H + CO → HCO	-20.24	0.10	-0.16	-0.58	1.54	0.43	1.84	1.71	2.64
H + C ₂ H ₄ → C ₂ H ₅	-40.86	-1.87	-0.17	-1.06	0.89	-1.27	-0.14	3.15	3.05
CH ₃ + C ₂ H ₄ → C ₃ H ₇	-28.20	-0.06	-1.03	-0.80	-1.19	-0.80	-4.68	-1.94	-1.58
HNC → HCN	-15.25	0.34	0.14	0.98	-0.86	1.02	-1.00	-2.94	-2.74
H + HCl → H ₂ + Cl	-2.18	-1.52	1.53	0.61	3.14	0.91	4.21	5.31	5.36
OH + H ₂ → H ₂ O + H	-16.07	1.73	-1.36	0.60	-3.94	0.60	-8.46	-8.89	-8.47
CH ₃ + H ₂ → CH ₄ + H	-3.62	1.00	-1.34	-0.63	-2.35	-0.66	-4.02	-4.05	-4.03
OH + CH ₄ → H ₂ O + CH ₃	-12.45	0.74	-0.02	1.23	-1.59	1.26	-4.44	-4.84	-4.44
OH + NH ₃ → H ₂ O + NH ₂	-9.99	0.40	0.18	0.81	-0.34	1.03	-1.86	-2.10	-1.71
HCl + CH ₃ → Cl + CH ₄	-5.81	-0.52	0.20	-0.02	0.79	0.25	0.19	1.25	1.33
OH + C ₂ H ₆ → H ₂ O + C ₂ H ₅	-15.80	0.83	-0.25	0.99	-1.31	1.46	-4.31	-4.87	-4.08
F + H ₂ → HF + H	-31.81	1.98	-1.47	0.83	-3.92	1.34	-9.76	-10.01	-9.19
O + CH ₄ → OH + CH ₃	6.18	0.56	-0.07	0.37	-0.01	0.94	-1.25	-1.53	-0.96
H + PH ₃ → H ₂ + PH ₂	-20.93	-0.78	1.22	0.75	2.13	1.04	2.70	3.12	3.23
H + OH → H ₂ + O	-2.56	-1.55	1.40	0.26	2.36	-0.28	5.27	5.58	4.99
H + H ₂ S → H ₂ + HS	-13.25	-1.23	1.39	0.69	2.60	0.94	3.28	4.24	4.27
O + HCl → OH + Cl	0.38	0.04	0.13	0.35	0.78	1.19	-1.06	-0.28	0.37
NH ₂ + CH ₃ → NH + CH ₄	-13.65	-0.27	0.00	-0.18	0.18	-0.22	0.51	0.73	0.58
NH ₂ + C ₂ H ₅ → NH + C ₂ H ₆	-10.30	-0.37	0.23	0.06	-0.10	-0.42	0.38	0.76	0.22
C ₂ H ₆ + NH ₂ → C ₂ H ₅ + NH ₃	-5.81	0.43	-0.44	0.18	-0.97	0.43	-2.45	-2.77	-2.37
NH ₂ + CH ₄ → NH ₃ + CH ₃	-2.46	0.34	-0.21	0.42	-1.25	0.23	-2.58	-2.74	-2.72
RMSD		1.90	0.84	1.57	4.62	4.51	4.22	5.52	6.34
MSD		-0.64	-0.14	-0.44	-0.54	-0.97	-0.28	0.84	-0.10
MIN		-7.18	-1.47	-6.21	-21.41	-21.60	-9.76	-10.01	-21.21
MAX		1.98	1.53	1.23	9.90	4.23	11.86	20.50	15.58

C.4 HTBH38

Table C.4 presents CCSD(T) barrier heights for the HTBH38 set in kcal mol⁻¹ and errors for other methods. All calculations were performed with the aVTZ basis set and the corresponding RI basis was used for all methods.

Table C.4: CCSD(T)/aVTZ barrier heights (in kcal/mol) for the HTHB38 set and errors for other methods.

Reaction	CCSD(T)	$\Delta(\text{CCSD})$	$\Delta(\text{MP2.8:\kappa- OOMP2})$	$\Delta(\text{MP3:\kappa- OOMP2})$	$\Delta(\text{MP2.5})$	$\Delta(\text{MP3})$	$\Delta(\kappa\text{- OOMP2})$	$\Delta(\text{OOMP2})$	$\Delta(\text{MP2})$
H + HCl \rightarrow TS1	5.21	0.10	1.18	0.60	3.61	2.11	4.39	3.84	5.11
H ₂ + Cl \rightarrow TS1	7.39	1.61	-0.36	-0.01	0.47	1.19	0.17	-1.47	-0.25
OH + H ₂ \rightarrow TS2	4.99	1.82	-0.69	0.43	3.10	4.33	-0.99	-3.29	1.88
H ₂ O + H \rightarrow TS2	21.06	0.09	0.67	-0.17	7.04	3.73	7.48	5.60	10.34
CH ₃ + H ₂ \rightarrow TS3	11.29	1.37	-0.03	0.23	1.29	1.78	0.79	-0.57	0.80
CH ₄ + H \rightarrow TS3	14.91	0.38	1.30	0.86	3.64	2.44	4.81	3.48	4.83
OH + CH ₄ \rightarrow TS4	5.64	2.61	-0.53	0.97	3.21	5.03	-1.42	-4.56	1.39
H ₂ O + CH ₃ \rightarrow TS4	18.09	1.87	-0.50	-0.26	4.80	3.77	3.02	0.28	5.83
H + H ₂ \rightarrow TS5	9.77	0.30	1.26	0.96	2.67	2.01	3.40	2.67	3.32
H ₂ + H \rightarrow TS5	9.77	0.30	1.26	0.96	2.67	2.01	3.40	2.67	3.32
OH + NH ₃ \rightarrow TS6	3.17	3.54	-0.51	1.54	5.06	7.21	-1.43	-6.42	2.91
H ₂ O + NH ₂ \rightarrow TS6	13.16	3.14	-0.70	0.74	5.40	6.18	0.43	-4.32	4.63
HCl + CH ₃ \rightarrow TS7	0.09	1.79	-0.15	0.22	1.39	2.03	0.81	-0.99	0.76
CH ₄ + Cl \rightarrow TS7	5.89	2.31	-0.35	0.24	0.60	1.77	0.62	-2.24	-0.57
OH + C ₂ H ₆ \rightarrow TS8	2.68	2.69	-0.83	0.71	3.63	5.32	-1.41	-4.80	1.94
H ₂ O + C ₂ H ₅ \rightarrow TS8	18.48	1.85	-0.58	-0.28	4.94	3.87	2.90	0.06	6.02
F + H ₂ \rightarrow TS9	1.14	1.20	-1.23	-0.58	3.40	3.84	-0.21	-1.44	2.95
HF + H \rightarrow TS9	32.95	-0.78	0.24	-1.41	7.32	2.50	9.56	8.57	12.14
O + CH ₄ \rightarrow TS10	13.61	2.37	-0.51	0.14	3.27	4.11	0.75	-1.58	2.43
OH + CH ₃ \rightarrow TS10	7.43	1.82	-0.45	-0.23	3.28	3.17	2.01	-0.05	3.39
H + PH ₃ \rightarrow TS11	2.29	0.59	0.97	0.80	2.16	1.73	2.90	1.84	2.59
H ₂ + PH ₂ \rightarrow TS11	23.21	1.37	-0.25	0.04	0.03	0.70	0.19	-1.28	-0.64
H + OH \rightarrow TS12	10.24	0.44	0.83	0.36	5.43	3.73	5.27	3.69	7.14
H ₂ + O \rightarrow TS12	12.80	1.99	-0.57	0.10	3.08	4.01	0.00	-1.89	2.14
H + H ₂ S \rightarrow TS13	3.16	0.65	0.97	0.79	2.33	1.88	3.06	1.87	2.78
H ₂ + HS \rightarrow TS13	16.41	1.88	-0.43	0.10	-0.27	0.94	-0.22	-2.38	-1.49
O + HCl \rightarrow TS14	9.73	3.58	-1.29	-0.44	5.89	6.88	1.97	-3.54	4.90
OH + Cl \rightarrow TS14	9.35	3.55	-1.42	-0.79	5.11	5.69	3.03	-3.27	4.53
CH ₃ + NH ₂ \rightarrow TS15	7.66	1.99	-0.27	0.05	2.62	2.94	1.81	-0.54	2.29
CH ₄ + NH \rightarrow TS15	21.31	2.26	-0.27	0.23	2.44	3.16	1.30	-1.27	1.72
C ₂ H ₅ + NH ₂ \rightarrow TS16	8.21	2.09	-0.21	0.20	2.50	2.98	1.53	-0.88	2.02
C ₂ H ₆ + NH \rightarrow TS16	18.51	2.46	-0.44	0.15	2.60	3.40	-0.35	-1.64	1.79
NH ₂ + C ₂ H ₆ \rightarrow TS17	10.39	2.73	-0.39	0.72	2.00	3.74	1.16	-3.59	0.26
NH ₃ + C ₂ H ₅ \rightarrow TS17	16.20	2.30	0.04	0.54	2.97	3.31	2.09	-0.83	2.63
NH ₂ + CH ₄ \rightarrow TS18	13.23	2.55	-0.23	0.77	1.81	3.46	-0.18	-3.17	0.16
NH ₃ + CH ₃ \rightarrow TS18	15.68	2.21	-0.03	0.36	3.06	3.23	2.40	-0.43	2.89
<i>s-trans</i> cis-C ₅ H ₈ \rightarrow TS19	40.42	4.15	-0.04	1.75	4.40	6.51	-1.02	-7.15	2.29
<i>s-trans</i> cis-C ₅ H ₈ \rightarrow TS19	40.42	4.15	-0.04	1.75	4.40	6.51	-1.02	-7.15	2.29
RMSD		2.21	0.71	0.73	3.69	3.88	2.92	3.48	4.04
MSD		1.88	-0.12	0.35	3.25	3.51	1.66	-0.95	2.99
MIN		-0.78	-1.42	-1.41	-0.27	0.70	-1.43	-7.15	-1.49
MAX		4.15	1.30	1.75	7.32	7.21	9.56	8.57	12.14

C.5 NHTBH38

Table C.5 presents CCSD(T) barrier heights for the NHTBH38 set in kcal mol⁻¹ and errors for other methods. All calculations were performed with the aVTZ basis set and the corresponding RI basis was used for all methods.

Table C.5: CCSD(T)/aVTZ barrier heights (in kcal/mol) for the NHTHB38 set and errors for other methods.

Reaction	CCSD(T)	$\Delta(\text{CCSD})$	$\Delta(\text{MP2.8:k- OOMP2})$	$\Delta(\text{MP3:k- OOMP2})$	$\Delta(\text{MP2.5})$	$\Delta(\text{MP3})$	$\Delta(\text{k- OOMP2})$	$\Delta(\text{OOMP2})$	$\Delta(\text{MP2})$
H + N ₂ O → TS1	17.97	0.47	1.22	0.96	12.59	7.35	4.25	2.00	17.83
OH + N ₂ → TS1	82.13	7.65	1.38	7.18	10.59	15.96	-7.61	-18.49	5.22
H + HF → TS2	41.25	1.40	1.31	1.34	3.91	3.63	3.59	1.86	4.20
HF + H → TS2	41.25	1.40	1.31	1.34	3.91	3.63	3.59	1.86	4.20
H + HCl → TS3	18.23	1.19	1.16	1.00	4.06	3.56	4.47	2.32	4.55
H + HCl → TS3	18.23	1.19	1.16	1.00	4.06	3.56	4.47	2.32	4.55
H + CH ₃ F → TS4	30.09	1.98	1.17	1.52	5.29	5.29	4.51	0.94	5.28
HF + CH ₃ → TS4	55.77	3.24	0.49	1.63	4.39	6.13	1.00	-2.22	2.66
H + F ₂ → TS5	1.34	0.35	-0.01	0.35	3.05	1.68	3.35	0.36	4.42
HF + F → TS5	104.60	5.36	-0.54	1.84	24.46	23.28	1.93	-5.58	25.63
CH ₃ + FCl → TS6	5.60	2.61	-0.31	0.45	11.64	10.43	1.97	-2.62	12.85
CH ₃ F + Cl → TS6	60.22	4.39	0.29	1.57	13.10	12.52	4.17	-3.41	13.67
F ⁻ + CH ₃ F → TS7	-1.37	2.66	-0.47	0.69	2.78	4.27	-0.08	-2.53	1.29
CH ₃ F + F ⁻ → TS7	-1.37	2.66	-0.47	0.69	2.78	4.27	-0.08	-2.53	1.29
F ⁻ ...CH ₃ F → TS7	13.15	2.22	-0.24	0.96	2.30	3.98	-0.26	-2.84	0.61
CH ₃ F...F ⁻ → TS7	13.15	2.22	-0.24	0.96	2.30	3.98	-0.26	-2.84	0.61
Cl ⁻ + CH ₃ Cl → TS8	1.48	2.43	-0.53	0.02	2.35	3.03	2.49	-1.69	1.67
CH ₃ Cl + Cl ⁻ → TS8	1.48	2.43	-0.53	0.02	2.35	3.03	2.49	-1.69	1.67
Cl ⁻ ...CH ₃ Cl → TS8	13.02	1.92	-0.47	-0.01	2.17	2.70	2.34	-1.42	1.64
CH ₃ Cl...Cl ⁻ → TS8	13.02	1.92	-0.47	-0.01	2.17	2.70	2.34	-1.42	1.64
F ⁻ + CH ₃ Cl → TS9	-13.19	1.78	-0.95	-0.72	2.23	2.03	1.99	-0.41	2.42
CH ₃ F + Cl ⁻ → TS9	18.37	3.45	0.35	2.30	2.74	5.74	-0.46	-5.07	-0.27
F ⁻ ...CH ₃ Cl → TS9	3.24	1.16	-0.52	-0.22	1.61	1.74	1.33	-0.68	1.49
CH ₃ F...Cl ⁻ → TS9	28.65	3.04	0.31	2.16	2.55	5.37	-0.37	-4.84	-0.28
OH ⁻ + CH ₃ F → TS10	-3.22	2.79	-0.56	0.61	2.64	4.10	-0.70	-2.76	1.17
CH ₃ OH + F ⁻ → TS10	16.37	3.27	0.14	1.58	3.13	5.16	1.40	-3.43	1.10
OH ⁻ ...CH ₃ F → TS10	11.06	2.38	-0.41	0.78	2.31	3.91	-0.60	-2.86	0.71
CH ₃ OH...F ⁻ → TS10	47.66	2.43	0.74	2.32	2.97	5.25	1.74	-3.73	0.69
H + N ₂ → TS11	14.47	0.53	0.86	0.73	9.58	6.25	3.59	1.99	12.90
HN ₂ → TS11	11.03	0.88	1.58	2.86	-0.33	2.02	-1.43	-3.42	-2.68
H + CO → TS12	3.11	0.52	0.84	0.78	2.09	1.80	1.92	1.33	2.37
HCO → TS12	23.35	0.42	1.00	1.35	0.55	1.37	0.09	-0.37	-0.27
H + C ₂ H ₄ → TS13	2.04	0.13	0.51	0.36	5.91	4.80	1.66	1.28	7.02
C ₂ H ₅ → TS13	42.90	2.01	0.68	1.42	5.02	6.07	1.80	-1.87	3.97
CH ₃ + C ₂ H ₄ → TS14	5.46	1.37	-0.28	0.01	6.01	5.69	0.54	-0.86	6.34
C ₃ H ₇ → TS14	33.66	1.43	0.80	0.80	7.20	6.48	5.22	1.07	7.92
HCN → TS15	48.24	0.45	-0.10	-0.34	2.72	1.10	1.82	1.25	4.34
HNC → TS15	32.99	0.79	0.04	0.64	1.85	2.12	0.82	-1.68	1.59
RMSD		2.53	0.76	1.67	6.59	6.65	2.77	3.90	7.03
MSD		2.07	0.27	1.08	4.76	5.16	1.55	-1.65	4.37
MIN		0.13	-0.95	-0.72	-0.33	1.10	-7.61	-18.49	-2.68
MAX		7.65	1.58	7.18	24.46	23.28	5.22	2.32	25.63

C.6 TA13

Table C.6 presents CCSD(T) interactions for the TA13 set in kcal mol⁻¹ and errors for other methods. All calculations were performed with the aVTZ basis set and the corresponding RI basis was used for all methods.

Table C.6: CCSD(T)/aVTZ interaction energies (in kcal/mol) for the TA13 set and errors for other methods.

Complex	CCSD(T)	$\Delta(\text{CCSD})$	$\Delta(\text{MP2.8:k- OOMP2})$	$\Delta(\text{MP3:k- OOMP2})$	$\Delta(\text{MP2.5})$	$\Delta(\text{MP3})$	$\Delta(\text{k- OOMP2})$	$\Delta(\text{OOMP2})$	$\Delta(\text{MP2})$
H ₂ O...Al	-6.50	0.79	-2.05	-2.46	0.49	0.65	-0.09	-0.33	0.33
H ₂ O...Be ⁺	-62.90	-0.26	-0.06	-0.47	0.29	-0.49	0.54	1.37	1.08
H ₂ O...Br	-2.62	0.71	-0.12	0.09	0.51	0.82	0.05	-0.67	0.21
H ₂ O...CH ₃	-1.64	0.24	-0.02	0.01	0.13	0.16	0.03	-0.06	0.09
H ₂ O...Cl	-2.79	0.78	-0.27	-0.03	0.71	1.00	0.04	-0.77	0.41
H ₂ O...F	-2.99	1.42	-2.01	-1.27	3.71	4.00	-0.34	-1.94	3.42
H ₂ O...Li	-11.72	0.14	-0.08	-0.22	0.63	0.35	0.65	0.53	0.91
H ₂ O...HNH ₂ ⁺	-24.67	0.29	-0.32	-0.36	-0.26	-0.31	-0.59	-0.14	-0.21
H ₂ O...NH ₃ ⁺	-17.88	0.65	-0.52	-0.35	1.06	1.16	-0.04	-0.41	0.96
FH...BH ₂	-4.03	0.25	-0.01	0.03	0.17	0.22	-0.01	-0.05	0.12
HF...CO ⁺	-29.07	1.47	-0.25	-0.52	-3.89	-2.61	0.25	0.87	-5.16
FH...NH ₂	-9.84	0.29	-0.15	-0.10	-0.03	0.07	-0.54	-0.25	-0.13
FH...OH	-5.73	0.23	-0.11	-0.09	0.06	0.08	-0.21	-0.06	0.05
RMSD		0.72	0.82	0.81	1.56	1.44	0.35	0.79	1.79
MSD		0.54	-0.46	-0.44	0.28	0.39	-0.02	-0.15	0.16
MIN		-0.26	-2.05	-2.46	-3.89	-2.61	-0.59	-1.94	-5.16
MAX		1.47	-0.01	0.09	3.71	4.00	0.65	1.37	3.42

C.7 A24

Table C.7 presents CCSD(T) interaction energies for the A24 set in kcal mol⁻¹ and errors for other methods. All calculations were performed with the aVTZ basis set and the corresponding RI basis was used for the MP2, OOMP2, and κ -OOMP2 calculations. For this set, we did not use the RI approximation for the CCSD(T), CCSD, or MP3 contributions.

Table C.7: CCSD(T)/aVTZ interaction energies (in kcal/mol) for the TA13 set and errors for other methods.

Complex	CCSD(T)	$\Delta(\text{CCSD})$	$\Delta(\text{MP2.8:k- OOMP2})$	$\Delta(\text{MP3:k- OOMP2})$	$\Delta(\text{MP2.5})$	$\Delta(\text{MP3})$	$\Delta(\text{k- OOMP2})$	$\Delta(\text{OOMP2})$	$\Delta(\text{MP2})$
H ₂ O...NH ₃	-6.26	0.33	-0.07	-0.02	0.02	0.12	-0.30	-0.21	-0.07
H ₂ O...H ₂ O	-4.78	0.22	-0.08	-0.07	0.04	0.05	-0.18	-0.06	0.03
HCN...HCN	-4.63	0.12	-0.02	0.02	-0.06	0.05	-0.37	-0.18	-0.17
HF...HF	-4.32	0.14	-0.09	-0.11	0.05	-0.01	-0.08	0.06	0.10
NH ₃ ...NH ₃	-3.01	0.25	0.00	0.03	0.04	0.09	-0.03	-0.08	-0.01
HF...CH ₄	-1.56	0.21	-0.02	-0.01	0.07	0.09	-0.02	-0.03	0.05
NH ₃ ...CH ₄	-0.72	0.12	0.01	0.01	0.05	0.04	0.05	0.01	0.06
H ₂ O...CH ₄	-0.62	0.10	0.01	0.01	0.04	0.03	0.04	0.01	0.04
CH ₂ O...CH ₂ O	-4.22	0.43	-0.17	-0.06	0.16	0.34	-0.63	-0.47	-0.01
H ₂ O...C ₂ H ₄	-2.44	0.28	-0.02	0.03	-0.08	0.02	-0.19	-0.22	-0.18
CH ₂ O...C ₂ H ₄	-1.52	0.25	-0.01	0.03	0.00	0.06	-0.07	-0.16	-0.07
C ₂ H ₂ ...C ₂ H ₂	-1.45	0.18	0.03	0.05	-0.07	-0.01	-0.07	-0.12	-0.13
NH ₃ ...C ₂ H ₄	-1.31	0.21	0.01	0.05	-0.06	0.01	-0.04	-0.14	-0.13
C ₂ H ₄ ...C ₂ H ₄	-1.03	0.31	0.03	0.08	-0.07	0.02	0.08	-0.20	-0.17
CH ₄ ...C ₂ H ₄	-0.48	0.13	0.02	0.03	-0.03	-0.01	0.05	-0.04	-0.05
BH ₃ ...CH ₄	-1.37	0.35	0.00	0.02	0.08	0.11	0.20	-0.06	0.05
CH ₄ ...C ₂ H ₆	-0.79	0.21	0.03	0.05	0.06	0.09	0.11	-0.03	0.04
CH ₄ ...C ₂ H ₆	-0.57	0.16	0.02	0.03	0.06	0.06	0.11	0.01	0.06
CH ₄ ...CH ₄	-0.50	0.13	0.02	0.03	0.05	0.05	0.09	0.00	0.04
Ar...CH ₄	-0.34	0.09	0.02	0.04	0.02	0.05	0.02	-0.04	-0.02
Ar...C ₂ H ₄	-0.30	0.10	0.04	0.06	-0.03	0.03	0.00	-0.08	-0.08
C ₂ H ₄ ...C ₂ H ₂	0.96	0.36	0.15	0.26	0.65	0.80	0.06	-0.35	0.49
C ₂ H ₄ ...C ₂ H ₄	1.15	0.41	0.04	0.13	2.30	2.20	0.06	-0.36	2.40
C ₂ H ₂ ...C ₂ H ₂	1.23	0.33	0.23	0.37	-0.11	0.21	0.04	-0.40	-0.44
RMSD		0.25	0.07	0.11	0.49	0.49	0.18	0.19	0.52
MSD		0.23	0.01	0.04	0.13	0.19	-0.05	-0.13	0.08
MIN		0.09	-0.17	-0.11	-0.11	-0.01	-0.63	-0.47	-0.44
MAX		0.43	0.23	0.37	2.30	2.20	0.20	0.06	2.40

Appendix D

Additional Information: Polishing the gold standard: The role of orbital choice in CCSD(T) frequency prediction

D.1 Equilibrium bond lengths

Table D.1: Root mean square deviations, mean signed deviations, most negative deviation, and most positive deviations in the equilibrium bond lengths for all species are presented for the CCSD(T) methods utilizing different molecular orbital references.

	$\Delta(\text{CCSD(T): UHF})$	$\Delta(\text{CCSD(T): } \kappa\text{-OOMP2})$	$\Delta(\text{CCSD(T): OOMP2})$	$\Delta(\text{CCSD(T): BLYP})$	$\Delta(\text{CCSD(T): B97M-rV})$	$\Delta(\text{CCSD(T): B97})$	$\Delta(\text{CCSD(T): } \omega\text{B97X-V})$	$\Delta(\text{CCSD(T): } \omega\text{B97M-V})$
RMSD	0.02258	0.01283	0.01772	0.01338	0.01328	0.01330	0.01328	0.01331
MSD	0.00676	0.00627	0.00468	0.00639	0.00617	0.00616	0.00604	0.00611
MIN	-0.01283	-0.01153	-0.08190	-0.02182	-0.02153	-0.02277	-0.02355	-0.02448
MAX	0.17325	0.08127	0.08457	0.08479	0.08477	0.08473	0.08472	0.08471

Table D.2: Experimental equilibrium bond lengths (in Å) and errors in the computed bond lengths (in Å) for the closed-shell species are presented for the CCSD(T) methods utilizing different molecular orbitals. Root mean square deviations, mean signed deviations, most negative deviations, and most positive deviations (all in Å) for the set of species and subsets are presented. Experimental values were compiled by Huber and Herzberg[346].

Row 2- Row 2	Dimer	State	Expt.	$\Delta(\text{CCSD(T)}; \text{UHF})$	$\Delta(\text{CCSD(T)}; \kappa\text{-OOMP2})$	$\Delta(\text{CCSD(T)}; \text{OOMP2})$	$\Delta(\text{CCSD(T)}; \text{BLYP})$	$\Delta(\text{CCSD(T)}; \text{B97M-rV})$	$\Delta(\text{CCSD(T)}; \text{B97})$	$\Delta(\text{CCSD(T)}; \omega\text{B97X-V})$	$\Delta(\text{CCSD(T)}; \omega\text{B97M-V})$
	LiH	X ¹ Σ ⁺	1.5957	0.00180	0.00181	0.00181	0.00182	0.00182	0.00182	0.00181	0.00181
	Li ₂	X ¹ Σ ⁺	2.6729	0.00462	0.00463	0.00463	0.00465	0.00466	0.00463	0.00462	0.00462
	LiF	X ¹ Σ ⁺	1.56386	0.00439	0.00462	0.00477	0.00511	0.00480	0.00478	0.00472	0.00476
	BeH ⁺	X ¹ Σ ⁺	1.3122	0.00028	0.00028	0.00028	0.00029	0.00029	0.00029	0.00029	0.00029
	BeO	X ¹ Σ ⁺	1.3309	0.00544	0.00556	0.00735	0.00676	0.00591	0.00598	0.00546	0.00560
	BH	X ¹ Σ ⁺	1.2324	-0.00038	-0.00047	-0.00080	-0.00065	-0.00075	-0.00081	-0.00082	-0.00081
	BF	X ¹ Σ ⁺	1.26259	0.00606	0.00642	0.00654	0.00687	0.00654	0.00658	0.00649	0.00651
	C ₂	X ¹ Σ ⁺	1.24253	-0.00631	0.00372	0.00464	-0.02182	-0.02153	-0.02277	-0.02355	-0.02448
	CO	X ¹ Σ ⁺	1.12832	0.00411	0.00429	0.00432	0.00445	0.00430	0.00433	0.00428	0.00428
	N ₂	X ¹ Σ ⁺	1.09769	0.00260	0.00268	0.00268	0.00275	0.00267	0.00270	0.00267	0.00268
	NO ⁺	X ¹ Σ ⁺	1.06322	0.00245	0.00258	0.00257	0.00270	0.00258	0.00261	0.00258	0.00258
	OH ⁻	X ¹ Σ ⁺	0.97	-0.00330	-0.00322	-0.00310	-0.00321	-0.00326	-0.00325	-0.00327	-0.00327
	HF	X ¹ Σ ⁺	0.91681	0.00349	0.00355	0.00356	0.00356	0.00351	0.00352	0.00352	0.00352
	F ₂	X ¹ Σ ⁺	1.41193	-0.01148	0.00452	0.00446	0.00447	0.00449	0.00452	0.00454	0.00456
	RMSD			0.00489	0.00385	0.00415	0.00706	0.00689	0.00718	0.00732	0.00755
	MSD			0.00098	0.00293	0.00312	0.00127	0.00115	0.00107	0.00095	0.00090
	MIN			-0.01148	-0.00322	-0.00310	-0.02182	-0.02153	-0.02277	-0.02355	-0.02448
	MAX			0.00606	0.00642	0.00735	0.00687	0.00654	0.00658	0.00649	0.00651
Row 2- Row 3	Dimer	State	Expt.	$\Delta(\text{CCSD(T)}; \text{UHF})$	$\Delta(\text{CCSD(T)}; \kappa\text{-OOMP2})$	$\Delta(\text{CCSD(T)}; \text{OOMP2})$	$\Delta(\text{CCSD(T)}; \text{BLYP})$	$\Delta(\text{CCSD(T)}; \text{B97M-rV})$	$\Delta(\text{CCSD(T)}; \text{B97})$	$\Delta(\text{CCSD(T)}; \omega\text{B97X-V})$	$\Delta(\text{CCSD(T)}; \omega\text{B97M-V})$
	NaH	X ¹ Σ ⁺	1.8874	0.00481	0.00481	0.00479	0.00498	0.00483	0.00490	0.00493	0.00487
	NaLi	X ¹ Σ ⁺	2.81	0.08249	0.08127	0.08457	0.08479	0.08477	0.08473	0.08472	0.08471
	NaF	X ¹ Σ ⁺	1.92595	0.00882	0.00904	0.00926	0.00968	0.00936	0.00930	0.00918	0.00919
	MgH ⁺	X ¹ Σ ⁺	1.6519	0.00387	0.00387	0.00384	0.00415	0.00386	0.00402	0.00400	0.00389
	AlH	X ¹ Σ ⁺	1.6478	0.00092	0.00039	0.00039	0.00043	0.00046	0.00041	0.00039	0.00040
	AlF	X ¹ Σ ⁺	1.65437	0.00577	0.00607	0.00623	0.00663	0.00625	0.00629	0.00617	0.00620
	SH ⁺	X ¹ Σ ⁺	1.5041	-0.00065	-0.00089	-0.00089	-0.00085	-0.00083	-0.00086	-0.00087	-0.00086
	SiO	X ¹ Σ ⁺	1.50974	0.00527	0.00548	0.00600	0.00597	0.00563	0.00563	0.00541	0.00541
	PN	X ¹ Σ ⁺	1.49087	-0.00451	0.00504	0.00523	0.00515	0.00496	0.00502	0.00497	0.00499
	BeS	X ¹ Σ ⁺	1.74153	0.17325	0.00814	0.00821	0.00832	0.00821	0.00815	0.00812	0.00800
	CS	X ¹ Σ ⁺	1.53494	0.00444	0.00471	0.00495	0.00504	0.00479	0.00481	0.00465	0.00468
	NS ⁺	X ¹ Σ ⁺	1.44	-0.00806	0.00120	0.00125	0.00135	0.00117	0.00125	0.00119	0.00122
	HCl	X ¹ Σ ⁺	1.27455	-0.00054	-0.00053	-0.00052	-0.00054	-0.00053	-0.00053	-0.00054	-0.00053
	LiCl	X ¹ Σ ⁺	2.02067	0.00775	0.00777	0.00779	0.00790	0.00784	0.00782	0.00778	0.00780
	BCl	X ¹ Σ ⁺	1.7159	0.00408	0.00429	0.00460	0.00511	0.00479	0.00470	0.00436	0.00445
	ClF	X ¹ Σ ⁺	1.62831	0.00677	0.00682	0.00686	0.00662	0.00647	0.00653	0.00658	0.00660
	RMSD			0.04824	0.02097	0.02180	0.02188	0.02183	0.02182	0.02180	0.02180
	MSD			0.01841	0.00922	0.00954	0.00967	0.00950	0.00951	0.00944	0.00944
	MIN			-0.00806	-0.00089	-0.00089	-0.00085	-0.00083	-0.00086	-0.00087	-0.00086

MAX	0.17325	0.08127	0.08457	0.08479	0.08477	0.08473	0.08472	0.08471
Row 3- Row 3	$\Delta(\text{CCSD(T)}; \text{UHF})$	$\Delta(\text{CCSD(T)}; \kappa\text{-OOMP2})$	$\Delta(\text{CCSD(T)}; \text{OOMP2})$	$\Delta(\text{CCSD(T)}; \text{BLYP})$	$\Delta(\text{CCSD(T)}; \text{B97M-rV})$	$\Delta(\text{CCSD(T)}; \text{B97})$	$\Delta(\text{CCSD(T)}; \omega\text{B97X-V})$	$\Delta(\text{CCSD(T)}; \omega\text{B97M-V})$
Dimer	Expt.	State						
NaCl	2.36079	$X^1\Sigma^+$	0.01381	0.01392	0.01389	0.01387	0.01386	0.01382
AlCl	2.13011	$X^1\Sigma^+$	0.01491	0.01508	0.01521	0.01520	0.01504	0.01505
SiS	1.92932	$X^1\Sigma^+$	0.01031	0.01057	0.01053	0.01051	0.01031	0.01033
P ₂	1.8934	$X^1\Sigma^+$	0.00874	0.00880	0.00871	0.00874	0.00873	0.00874
Cl ₂	1.9879	$X^1\Sigma^+_g$	0.01591	0.01586	0.01578	0.01575	0.01582	0.01582
RMSD	0.01280		0.01301	0.01311	0.01312	0.01310	0.01305	0.01305
MSD	0.00972		0.01272	0.01283	0.01282	0.01281	0.01275	0.01275
MIN	-0.00649		0.00874	0.00880	0.00871	0.00874	0.00873	0.00874
MAX	0.01591		0.01583	0.01586	0.01578	0.01575	0.01582	0.01582
Closed-shell	$\Delta(\text{CCSD(T)}; \text{UHF})$	$\Delta(\text{CCSD(T)}; \kappa\text{-OOMP2})$	$\Delta(\text{CCSD(T)}; \text{OOMP2})$	$\Delta(\text{CCSD(T)}; \text{BLYP})$	$\Delta(\text{CCSD(T)}; \text{B97M-rV})$	$\Delta(\text{CCSD(T)}; \text{B97})$	$\Delta(\text{CCSD(T)}; \omega\text{B97X-V})$	$\Delta(\text{CCSD(T)}; \omega\text{B97M-V})$
RMSD	0.03311	0.01520	0.01577	0.01624	0.01617	0.01621	0.01622	0.01626
MSD	0.01020	0.00720	0.00744	0.00678	0.00663	0.00660	0.00652	0.00650
MIN	-0.01148	-0.00322	-0.00310	-0.02182	-0.02153	-0.02277	-0.02355	-0.02448
MAX	0.17325	0.08127	0.08457	0.08479	0.08477	0.08473	0.08472	0.08471

Table D.3: Experimental equilibrium bond lengths (in Å) and errors in the computed bond lengths (in Å) for the open-shell species are presented for the CCSD(T) methods utilizing different molecular orbitals. Root mean square deviations, mean signed deviations, most negative deviations, and most positive deviations (all in Å) for the set of species and subsets are presented. Experimental values were compiled by Huber and Herzberg[346].

Closed-shell	Dimer	State	Expt.	$\Delta(\text{CCSD(T)}): \Delta(\text{CCSD(T)})$									
				UHF)	κ -OOMP2)	OOMP2)	BLYP)	B97M-rV)	B97)	ω B97X-V)	$\Delta(\text{CCSD(T)}): \Delta(\text{CCSD(T)})$	ω B97M-V)	
	LiO	$X^2\Pi_i$	1.695	-0.00222	-0.00218	-0.00209	-0.00173	-0.00199	-0.00203	-0.00211	-0.00207		
	BeH	$X^2\Sigma^+$	1.3426	0.00043	0.00043	0.00043	0.00047	0.00055	0.00046	0.00044	0.00048		
	BeF	$X^2\Sigma^+$	1.361	0.00378	0.00393	0.00400	0.00425	0.00404	0.00405	0.00399	0.00404		
	B ₂	$X^3\Sigma_g^-$	1.59	-0.00741	-0.00463	0.00106	0.00905	0.00398	0.00280	-0.00081	0.00335		
	BN	$X^3\Pi$	1.281	0.04824	0.04909	0.04915	0.04917	0.04909	0.04908	0.04912	0.04914		
	BO	$X^2\Sigma^+$	1.2045	0.00498	0.00561	0.00580	0.00600	0.00573	0.00586	0.00571	0.00571		
	CH	$X^2\Pi_r$	1.1199	0.00095	0.00016	0.00016	0.00015	0.00017	0.00015	0.00015	0.00016		
	C ₂ ⁻	$X^2\Sigma^+$	1.26821	0.04244	0.00393	0.00407	0.00407	0.00389	0.00394	0.00390	0.00591		
	CN	$X^2\Sigma^+$	1.17182	-0.00157	0.00328	0.00340	0.00338	0.00321	0.00324	0.00322	0.00325		
	CO ⁺	$X^2\Sigma^+$	1.11522	0.00023	0.00412	0.00441	0.00448	0.00399	0.00419	0.00413	0.00409		
	CF	$X^2\Pi_r$	1.2718	0.00518	0.00577	0.00598	0.00636	0.00588	0.00591	0.00578	0.00580		
	NH	$X^2\Sigma^-$	1.03621	0.00182	0.00181	0.00181	0.00180	0.00180	0.00181	0.00180	0.00180		
	N ₂ ⁺	$X^3\Sigma^+$	1.11642	-0.00207	0.00252	0.00254	0.00263	0.00248	0.00254	0.00249	0.00251		
	NO	$X^2\Pi_r$	1.15077	-0.00019	0.00288	0.00285	0.00298	0.00289	0.00291	0.00289	0.00289		
	NF	$X^3\Sigma^-$	1.31698	0.00503	0.00572	0.00605	0.00644	0.00566	0.00576	0.00566	0.00563		
	OH	$X^2\Pi_i$	0.96966	0.00247	0.00247	0.00247	0.00246	0.00245	0.00246	0.00246	0.00246		
	HO ⁺	$X^3\Sigma^-$	1.0289	0.00134	0.00133	0.00133	0.00132	0.00133	0.00132	0.00131	0.00132		
	O ₂	$X^3\Sigma_g^-$	1.20752	0.00340	0.00335	0.00336	0.00337	0.00333	0.00335	0.00333	0.00334		
	O ₂ ⁺	$X^2\Pi_g$	1.1164	-0.00158	0.00227	0.00226	0.00235	0.00227	0.00230	0.00228	0.00229		
	O ₂ ⁻	$X^2\Pi_{g,i}$	1.35	0.00396	0.00373	0.00374	0.00361	0.00365	0.00370	0.00371	0.00370		
	OF	$X^2\Pi$	1.35411	0.00324	0.00492	0.00508	0.00516	0.00459	0.00472	0.00466	0.00463		
	HF ⁺	$X^2\Pi_i$	1.00105	0.00302	0.00302	0.00302	0.00302	0.00299	0.00300	0.00300	0.00301		
	F ₂ ⁺	$X^2\Pi_{g,i}$	1.3119	-0.00197	-0.00024	-0.00058	-0.00024	-0.00014	-0.00014	0.00009	0.00011		
	F ₂ ⁻	$X^2\Sigma_u^+$	1.88	0.03882	0.04568	0.04590	0.04528	0.04553	0.04555	0.04553	0.04544		
	RMSD			0.01562	0.01410	0.01413	0.01419	0.01406	0.01406	0.01404	0.01408		
	MSD			0.00635	0.00621	0.00651	0.00691	0.00656	0.00654	0.00636	0.00662		
	MIN			-0.00741	-0.00463	-0.00209	-0.00173	-0.00199	-0.00203	-0.00211	-0.00207		
	MAX			0.04824	0.04909	0.04915	0.04917	0.04909	0.04908	0.04912	0.04914		
Row 2-	Dimer	State	Expt.	$\Delta(\text{CCSD(T)}): \Delta(\text{CCSD(T)})$									
Row 3				UHF)	κ -OOMP2)	OOMP2)	BLYP)	B97M-rV)	B97)	ω B97X-V)	$\Delta(\text{CCSD(T)}): \Delta(\text{CCSD(T)})$	ω B97M-V)	
	MgH	$X^2\Sigma^+$	1.7297	0.00203	0.00201	0.00201	0.00242	0.00209	0.00229	0.00220	0.00211	0.00211	
	MgF	$X^2\Sigma^+$	1.75	0.00585	0.00605	0.00618	0.00658	0.00628	0.00629	0.00617	0.00616	0.00616	
	AlH ⁺	$X^2\Sigma^+$	1.6018	0.00589	0.00583	0.00582	0.00586	0.00581	0.00582	0.00583	0.00582	0.00582	
	SiH	$X^2\Pi_r$	1.5201	0.00085	0.00030	0.00031	0.00035	0.00037	0.00033	0.00032	0.00035	0.00035	
	SiF	$X^2\Pi_r$	1.6011	0.00604	0.00638	0.00657	0.00700	0.00662	0.00662	0.00647	0.00650	0.00650	
	PH	$X^3\Sigma^-$	1.42234	-0.00007	-0.00006	-0.00006	-0.00004	-0.00004	-0.00005	-0.00006	-0.00005	-0.00005	
	PH ⁺	$X^2\Pi_r$	1.4352	-0.01149	-0.01153	-0.01153	-0.01149	-0.01149	-0.01151	-0.01151	-0.01150	-0.01150	
	PH ⁻	$X^2\Pi_i$	1.407	0.02776	0.02776	0.02776	0.02777	0.02777	0.02781	0.02778	0.02780	0.02780	
	CP	$X^2\Sigma^+$	1.5622	-0.00410	0.00333	0.00491	0.00447	0.00362	0.00385	0.00334	0.00368	0.00368	
	PO	$X^2\Pi_r$	1.4759	0.00602	0.00626	0.00649	0.00639	0.00619	0.00618	0.00608	0.00609	0.00609	

PO ⁻	X ³ Σ ⁻	1.54	0.00107	0.00158	0.00198	0.00159	0.00139	0.00134	0.00126	0.00133
PF	X ³ Σ ⁻	1.5897	0.00616	0.00652	0.00671	0.00711	0.00667	0.00670	0.00658	0.00660
PF ⁺	X ² Π _r	1.5003	0.00642	0.00685	0.00712	0.00754	0.00707	0.00707	0.00688	0.00691
HS	X ³ Π _i	1.3409	-0.00046	-0.00044	-0.00044	-0.00043	-0.00043	-0.00042	-0.00043	-0.00043
BS	X ² Σ ⁺	1.6092	0.00431	0.00519	0.00540	0.00559	0.00536	0.00542	0.00531	0.00532
CS ⁺	X ² Σ ⁺	1.4954	-0.00616	0.00048	0.00154	0.00137	0.00044	0.00078	0.00052	0.00067
NS	X ² Π _r	1.49402	-0.00140	0.00501	0.00512	0.00515	0.00500	0.00500	0.00492	0.00498
SO	X ³ Σ ⁻	1.48109	0.00498	0.00559	0.00578	0.00539	0.00519	0.00523	0.00520	0.00522
SO ⁺	X ² Π _r	1.424	-0.00047	0.00617	0.00629	0.00605	0.00588	0.00591	0.00586	0.00586
HCl ⁺	X ² Π _i	1.31468	-0.00149	-0.00147	-0.00147	-0.00147	-0.00146	-0.00147	-0.00147	-0.00147
BeCl	X ² Σ ⁺	1.7971	0.00604	0.00606	0.00609	0.00621	0.00618	0.00613	0.00607	0.00610
CCl	X ² Π	1.645	0.00576	0.00609	0.00672	0.00708	0.00655	0.00656	0.00614	0.00624
NCI	X ³ Σ ⁻	1.6144	0.00466	0.00475	0.00537	0.00568	0.00510	0.00516	0.00487	0.00487
OCl	X ² Π _i	1.56963	0.00581	0.00644	0.00647	0.00646	0.00654	0.00652	0.00649	0.00650
RMSD			0.00752	0.00770	0.00784	0.00790	0.00775	0.00776	0.00769	0.00771
MSD			0.00308	0.00438	0.00463	0.00469	0.00445	0.00448	0.00437	0.00440
MIN			-0.01149	-0.01153	-0.01153	-0.01149	-0.01149	-0.01151	-0.01151	-0.01150
MAX			0.02776	0.02776	0.02777	0.02781	0.02777	0.02780	0.02778	0.02780
Row 3- Row 3	Dimer	State	Expt.	Δ(CCSD(T); UHF)	Δ(CCSD(T); κ-OOMP2)	Δ(CCSD(T); OOMP2)	Δ(CCSD(T); BLYP)	Δ(CCSD(T); B97M-rV)	Δ(CCSD(T); ωB97X-V)	Δ(CCSD(T); ωB97M-V)
MgCl	X ² Σ ⁺	2.1991	0.00793	0.00792	0.00793	0.00806	0.00798	0.00800	0.00797	0.00790
AlS	X ² Σ ⁺	2.029	0.01279	0.01346	0.01411	0.01355	0.01368	0.01342	0.01305	0.01291
Si ₂	X ³ Σ ⁻	2.246	0.00857	0.00846	-0.07907	0.00844	0.00841	0.00840	0.00842	0.00839
SiCl	X ² Π _r	2.058	0.01415	0.01415	0.01432	0.01467	0.01444	0.01437	0.01417	0.01422
P ₂ ⁺	X ² Π _u	1.9859	-0.01283	-0.00204	-0.08190	-0.00214	-0.00220	-0.00216	-0.00207	-0.00206
PS	X ² Π _r	1.9009	-0.00514	0.00596	0.00606	0.00606	0.00601	0.00597	0.00597	0.00597
S ₂	X ³ Σ ⁻	1.8892	0.01018	0.01007	0.01019	0.01007	0.01004	0.01004	0.01004	0.01004
S ₂ ⁺	X ² Π _{g,r}	1.825	-0.00387	0.00687	0.00694	0.00685	0.00679	0.00681	0.00684	0.00684
RMSD			0.01006	0.00938	0.04125	0.00952	0.00947	0.00941	0.00931	0.00928
MSD			0.00397	0.00811	-0.01268	0.00820	0.00814	0.00811	0.00805	0.00803
MIN			-0.01283	-0.00204	-0.08190	-0.00214	-0.00220	-0.00216	-0.00207	-0.00206
MAX			0.01415	0.01415	0.01432	0.01467	0.01444	0.01437	0.01417	0.01422
Open- shell	Dimer	State	Expt.	Δ(CCSD(T); UHF)	Δ(CCSD(T); κ-OOMP2)	Δ(CCSD(T); OOMP2)	Δ(CCSD(T); BLYP)	Δ(CCSD(T); B97M-rV)	Δ(CCSD(T); ωB97X-V)	Δ(CCSD(T); ωB97M-V)
RMSD			0.01197	0.01110	0.01884	0.01122	0.01110	0.01110	0.01106	0.01108
MSD			0.00506	0.00611	0.00395	0.00655	0.00629	0.00629	0.00616	0.00629
MIN			-0.01283	-0.01153	-0.08190	-0.01149	-0.01149	-0.01151	-0.01151	-0.01150
MAX			0.04824	0.04909	0.04915	0.04917	0.04909	0.04908	0.04912	0.04914

Table D.4: Root mean square deviations, mean signed deviations, most negative deviation, and most positive deviations in the equilibrium bond lengths for all species are presented for the CCSD methods utilizing different molecular orbital references.

	$\Delta(\text{CCSD: UHF})$	$\Delta(\text{CCSD: } \kappa\text{-OOMP2})$	$\Delta(\text{CCSD: OOMP2})$	$\Delta(\text{CCSD: BLYP})$	$\Delta(\text{CCSD: B97M-rV})$	$\Delta(\text{CCSD: B97})$	$\Delta(\text{CCSD: } \omega\text{B97X-V})$	$\Delta(\text{CCSD: } \omega\text{B97M-V})$
RMSD	0.02276	0.01352	0.020060	0.01465	0.01442	0.01445	0.01435	0.01437
MSD	-0.00021	-0.00259	-0.00454	-0.00245	-0.00202	-0.00205	-0.00177	-0.00182
MIN	-0.03572	-0.02706	-0.10195	-0.02699	-0.02629	-0.02621	-0.02596	-0.02589
MAX	0.17058	0.08265	0.08996	0.08987	0.08983	0.09008	0.09041	0.08989

Table D.5: Experimental equilibrium bond lengths (in Å) and errors in the computed bond lengths (in Å) for the closed-shell species are presented for the CCSD methods utilizing different molecular orbitals. Root mean square deviations, most signed deviations, and most positive deviations (all in Å) for the set of species and subsets are presented. Experimental values were compiled by Huber and Herzberg[346].

Row 2-	Dimer	State	Expt.	$\Delta(\text{CCSD: UHF})$	$\Delta(\text{CCSD: } \kappa\text{-OOMP2})$	$\Delta(\text{CCSD: OOMP2})$	$\Delta(\text{CCSD: BLYP})$	$\Delta(\text{CCSD: B97M-rV})$	$\Delta(\text{CCSD: B97})$	$\Delta(\text{CCSD: } \omega\text{B97X-V})$	$\Delta(\text{CCSD: } \omega\text{B97M-V})$
Row 2	LiH	$X^1\Sigma^+$	1.5957	0.00203	0.00204	0.00203	0.00203	0.00201	0.00203	0.00204	0.00204
	Li ₂	$X^1\Sigma_g^+$	2.6729	0.00946	0.00748	0.00746	0.00735	0.00711	0.00737	0.00747	0.00743
	LiF	$X^1\Sigma^+$	1.56386	0.00041	-0.00048	-0.00073	-0.00097	-0.00059	-0.00060	-0.00054	-0.00061
	BeH ⁺	$X^1\Sigma^+$	1.3122	0.00001	0.00001	0.00000	0.00000	0.00002	0.00000	0.00000	0.00000
	BeO	$X^1\Sigma^+$	1.3309	-0.00998	-0.01298	-0.01468	-0.01405	-0.01310	-0.01331	-0.01256	-0.01281
	BH	$X^1\Sigma^+$	1.2324	-0.00180	-0.00168	-0.00215	-0.00211	-0.00210	-0.00226	-0.00221	-0.00220
	BF	$X^1\Sigma^+$	1.26259	0.00188	0.00081	0.00063	0.00028	0.00073	0.00063	0.00074	0.00070
	C ₂	$X^1\Sigma_g^+$	1.24253	-0.01475	-0.01391	-0.00579	0.03649	0.03668	0.03615	0.03636	0.03743
	CO	$X^1\Sigma^+$	1.12832	-0.00318	-0.00443	-0.00463	-0.00470	-0.00431	-0.00437	-0.00423	-0.00424
	N ₂	$X^1\Sigma_g^+$	1.09769	-0.00473	-0.00565	-0.00580	-0.00584	-0.00551	-0.00559	-0.00544	-0.00545
	NO ⁺	$X^1\Sigma^+$	1.06322	-0.00638	-0.00775	-0.00792	-0.00790	-0.00750	-0.00757	-0.00742	-0.00742
	OH ⁻	$X^1\Sigma^+$	0.97	-0.00732	-0.00821	-0.00854	-0.00826	-0.00803	-0.00793	-0.00796	-0.00796
	HF	$X^1\Sigma^+$	0.91681	0.00062	0.00019	0.00014	0.00005	0.00027	0.00022	0.00022	0.00020
	F ₂	$X^1\Sigma_g^+$	1.41193	-0.03572	-0.02017	-0.02067	-0.02037	-0.01982	-0.01987	-0.01972	-0.01969
	RMSD			0.01140	0.00850	0.00816	0.01252	0.01236	0.01229	0.01225	0.01249
	MSD			-0.00496	-0.00462	-0.00433	-0.00129	-0.00101	-0.00109	-0.00094	-0.00090
	MIN			-0.03572	-0.02017	-0.02067	-0.02037	-0.01982	-0.01987	-0.01972	-0.01969
	MAX			0.00946	0.00748	0.00746	0.03649	0.03668	0.03615	0.03636	0.03743
Row 2-	Dimer	State	Expt.	$\Delta(\text{CCSD: UHF})$	$\Delta(\text{CCSD: } \kappa\text{-OOMP2})$	$\Delta(\text{CCSD: OOMP2})$	$\Delta(\text{CCSD: BLYP})$	$\Delta(\text{CCSD: B97M-rV})$	$\Delta(\text{CCSD: B97})$	$\Delta(\text{CCSD: } \omega\text{B97X-V})$	$\Delta(\text{CCSD: } \omega\text{B97M-V})$
Row 3	NaH	$X^1\Sigma^+$	1.8874	0.00651	0.00674	0.00671	0.00700	0.00677	0.00685	0.00698	0.00694
	NaLi	$X^1\Sigma^+$	2.81	0.08327	0.08265	0.08996	0.08987	0.08983	0.09008	0.09041	0.08989
	NaF	$X^1\Sigma^+$	1.92595	0.00475	0.00380	0.00346	0.00338	0.00364	0.00369	0.00382	0.00373
	MgH ⁺	$X^1\Sigma^+$	1.6519	0.00236	0.00239	0.00233	0.00259	0.00236	0.00250	0.00254	0.00243
	AlH	$X^1\Sigma^+$	1.6478	-0.00022	-0.00130	-0.00136	-0.00150	-0.00131	-0.00145	-0.00132	-0.00133
	AlF	$X^1\Sigma^+$	1.65437	0.00093	-0.00018	-0.00044	-0.00083	-0.00029	-0.00041	-0.00027	-0.00032
	SH ⁺	$X^1\Sigma^+$	1.5041	-0.00247	-0.00290	-0.00293	-0.00299	-0.00293	-0.00295	-0.00289	-0.00289
	SiO	$X^1\Sigma^+$	1.50974	-0.00615	-0.00802	-0.00892	-0.00862	-0.00816	-0.00816	-0.00775	-0.00778
	PN	$X^1\Sigma^+$	1.49087	-0.01339	-0.01050	-0.01150	-0.01088	-0.01047	-0.01042	-0.01002	-0.01001
	BeS	$X^1\Sigma^+$	1.74153	0.17058	-0.00488	-0.00585	-0.00611	-0.00551	-0.00559	-0.00488	-0.00507
	CS	$X^1\Sigma^+$	1.53494	-0.00762	-0.00962	-0.01049	-0.01026	-0.00969	-0.00976	-0.00921	-0.00932
	NS ⁺	$X^1\Sigma^+$	1.44	-0.01821	-0.01577	-0.01669	-0.01611	-0.01558	-0.01560	-0.01519	-0.01523
	HCl	$X^1\Sigma^+$	1.27455	-0.00306	-0.00319	-0.00324	-0.00330	-0.00320	-0.00323	-0.00316	-0.00322
	LiCl	$X^1\Sigma^+$	2.02067	0.00558	0.00549	0.00538	0.00517	0.00536	0.00535	0.00542	0.00534
	BCl	$X^1\Sigma^+$	1.7159	0.00065	0.00024	-0.00024	-0.00090	-0.00046	-0.00041	0.00005	-0.00007
	ClF	$X^1\Sigma^+$	1.62831	-0.00640	-0.00772	-0.00807	-0.00799	-0.00748	-0.00756	-0.00739	-0.00742
	RMSD			0.04796	0.02172	0.02359	0.02352	0.02343	0.02350	0.02352	0.02340
	MSD			0.01357	0.00233	0.00238	0.00241	0.00268	0.00268	0.00295	0.00285
	MIN			-0.01821	-0.01577	-0.01669	-0.01611	-0.01558	-0.01560	-0.01519	-0.01523

MAX			0.17058	0.08265	0.08996	0.08987	0.08983	0.09008	0.09041	0.08989
Row 3-	Dimer	State	$\Delta(\text{CCSD: UHF})$	$\Delta(\text{CCSD: } \kappa\text{-OOMP2})$	$\Delta(\text{CCSD: OOMP2})$	$\Delta(\text{CCSD: BLYP})$	$\Delta(\text{CCSD: B97M-rV})$	$\Delta(\text{CCSD: B97})$	$\Delta(\text{CCSD: } \omega\text{B97X-V})$	$\Delta(\text{CCSD: } \omega\text{B97M-V})$
Row 3		Expt.								
	NaCl	$X^1\Sigma^+$	0.01274	0.01276	0.01265	0.01259	0.01265	0.01269	0.01281	0.01272
	AlCl	$X^1\Sigma^+$	0.01222	0.01200	0.01174	0.01126	0.01164	0.01158	0.01184	0.01178
	SiS	$X^1\Sigma^+$	-0.00253	-0.00378	-0.00481	-0.00500	-0.00447	-0.00448	-0.00376	-0.00390
	P ₂	$X^1\Sigma_g^+$	-0.01803	-0.00962	-0.01062	-0.01054	-0.01009	-0.01012	-0.00945	-0.00949
	Cl ₂	$X^1\Sigma_g^+$	0.00599	0.00566	0.00544	0.00526	0.00556	0.00556	0.00567	0.00563
	RMSD		0.01165	0.00944	0.00963	0.00948	0.00947	0.00947	0.00938	0.00935
	MSD		0.00208	0.00340	0.00288	0.00271	0.00306	0.00305	0.00342	0.00335
	MIN		-0.01803	-0.00962	-0.01062	-0.01054	-0.01009	-0.01012	-0.00945	-0.00949
	MAX		0.01274	0.01276	0.01265	0.01259	0.01265	0.01269	0.01281	0.01272
Closed-shell			$\Delta(\text{CCSD: UHF})$	$\Delta(\text{CCSD: } \kappa\text{-OOMP2})$	$\Delta(\text{CCSD: OOMP2})$	$\Delta(\text{CCSD: BLYP})$	$\Delta(\text{CCSD: B97M-rV})$	$\Delta(\text{CCSD: B97})$	$\Delta(\text{CCSD: } \omega\text{B97X-V})$	$\Delta(\text{CCSD: } \omega\text{B97M-V})$
	RMSD		0.03351	0.01604	0.01716	0.01812	0.01802	0.01805	0.01804	0.01803
	MSD		0.00452	-0.00030	-0.00023	0.00097	0.00126	0.00123	0.00146	0.00142
	MIN		-0.03572	-0.02017	-0.02067	-0.02037	-0.01982	-0.01987	-0.01972	-0.01969
	MAX		0.17058	0.08265	0.08996	0.08987	0.08983	0.09008	0.09041	0.08989

Table D.6: Experimental equilibrium bond lengths (in Å) and errors in the computed bond lengths (in Å) for the open-shell species are presented for the CCSD methods utilizing different molecular orbitals. Root mean square deviations, most negative deviations, and most positive deviations (all in Å) for the set of species and subsets are presented. Experimental values were compiled by Huber and Herzberg[346].

Row 2- Row 2	Dimer	State	Expt.	$\Delta(\text{CCSD: UHF})$	$\Delta(\text{CCSD: } \kappa\text{-OOMP2})$	$\Delta(\text{CCSD: OOMP2})$	$\Delta(\text{CCSD: BLYP})$	$\Delta(\text{CCSD: B97M-rV})$	$\Delta(\text{CCSD: B97})$	$\Delta(\text{CCSD: } \omega\text{B97X-V})$	$\Delta(\text{CCSD: } \omega\text{B97M-V})$
	LiO	$X^2\Pi_i$	1.695	-0.00729	-0.00808	-0.00846	-0.00889	-0.00844	-0.00844	-0.00828	-0.00842
	BeH	$X^2\Sigma^+$	1.3426	-0.00045	-0.00051	-0.00051	-0.00054	-0.00045	-0.00054	-0.00053	-0.00054
	BeF	$X^2\Sigma^+$	1.361	0.00033	-0.00042	-0.00056	-0.00085	-0.00049	-0.00054	-0.00048	-0.00054
	B ₂	$X^3\Sigma_g^-$	1.59	-0.02379	-0.02361	-0.00059	-0.02699	-0.02375	-0.02397	-0.02270	-0.02356
	BN	$X^3\Pi$	1.281	0.03714	0.03588	0.03526	0.03517	0.03575	0.03578	0.03600	0.03581
	BO	$X^2\Sigma^+$	1.2045	-0.00266	-0.00412	-0.00455	-0.00470	-0.00420	-0.00436	-0.00407	-0.00411
	CH	$X^2\Pi_r$	1.1199	-0.00108	-0.00185	-0.00187	-0.00200	-0.00186	-0.00193	-0.00187	-0.00192
	C ₂ ⁻	$X^2\Sigma^+$	1.26821	0.03456	-0.00645	-0.00720	-0.00663	-0.00613	-0.00624	-0.00608	-0.00579
	CN	$X^2\Sigma^+$	1.17182	-0.00895	-0.00851	-0.00865	-0.00830	-0.00805	-0.00816	-0.00805	-0.00825
	CO ⁺	$X^2\Sigma^+$	1.11522	-0.00599	-0.00804	-0.00855	-0.00849	-0.00771	-0.00793	-0.00774	-0.00773
	CF	$X^2\Pi_r$	1.2718	-0.00126	-0.00325	-0.00361	-0.00402	-0.00339	-0.00341	-0.00321	-0.00325
	NH	$X^3\Sigma^-$	1.03621	-0.00064	-0.00087	-0.00090	-0.00102	-0.00089	-0.00090	-0.00088	-0.00092
	N ₂ ⁺	$X^2\Sigma^+$	1.11642	-0.00980	-0.00828	-0.00899	-0.00819	-0.00764	-0.00773	-0.00745	-0.00752
	NO	$X^2\Pi_r$	1.15077	-0.00682	-0.00878	-0.00907	-0.00899	-0.00852	-0.00860	-0.00842	-0.00844
	NF	$X^3\Sigma^-$	1.31698	-0.00409	-0.00726	-0.00797	-0.00844	-0.00722	-0.00735	-0.00700	-0.00696
	OH	$X^2\Pi_i$	0.96966	-0.00029	-0.00061	-0.00066	-0.00075	-0.00061	-0.00061	-0.00060	-0.00063
	HO ⁺	$X^3\Sigma^-$	1.0289	-0.00101	-0.00117	-0.00118	-0.00133	-0.00126	-0.00122	-0.00124	-0.00126
	O ₂	$X^3\Sigma_g^-$	1.20752	-0.00845	-0.01060	-0.01101	-0.01075	-0.01022	-0.01023	-0.01006	-0.01009
	O ₂ ⁺	$X^2\Pi_g$	1.1164	-0.01172	-0.01209	-0.01243	-0.01216	-0.01167	-0.01172	-0.01152	-0.01154
	O ₂ ⁻	$X^2\Pi_{g,i}$	1.35	-0.01316	-0.01649	-0.01747	-0.01637	-0.01565	-0.01566	-0.01552	-0.01552
	OF	$X^2\Pi$	1.35411	-0.00842	-0.01446	-0.01657	-0.01550	-0.01338	-0.01356	-0.01296	-0.01283
	HF ⁺	$X^3\Pi_i$	1.00105	0.00023	-0.00003	-0.00005	-0.00025	-0.00005	-0.00011	-0.00013	-0.00013
	F ₂ ⁺	$X^2\Pi_{g,i}$	1.3119	-0.02617	-0.02706	-0.02809	-0.02695	-0.02629	-0.02621	-0.02596	-0.02589
	F ₂ ⁻	$X^2\Sigma_u^+$	1.88	0.00653	0.03413	0.03232	0.03358	0.03458	0.03461	0.03464	0.03463
	RMSD			0.01393	0.01437	0.01365	0.01461	0.01421	0.01425	0.01409	0.01413
	MSD			-0.00264	-0.00427	-0.00381	-0.00472	-0.00406	-0.00413	-0.00392	-0.00398
	MIN			-0.02617	-0.02706	-0.02809	-0.02699	-0.02629	-0.02621	-0.02596	-0.02589
	MAX			0.03714	0.03588	0.03526	0.03517	0.03575	0.03578	0.03600	0.03581
Row 2- Row 3	Dimer	State	Expt.	$\Delta(\text{CCSD: UHF})$	$\Delta(\text{CCSD: } \kappa\text{-OOMP2})$	$\Delta(\text{CCSD: OOMP2})$	$\Delta(\text{CCSD: BLYP})$	$\Delta(\text{CCSD: B97M-rV})$	$\Delta(\text{CCSD: B97})$	$\Delta(\text{CCSD: } \omega\text{B97X-V})$	$\Delta(\text{CCSD: } \omega\text{B97M-V})$
	MgH	$X^2\Sigma^+$	1.7297	0.00074	0.00060	0.00054	0.00089	0.00055	0.00082	0.00076	0.00064
	MgF	$X^2\Sigma^+$	1.75	0.00142	0.00045	0.00019	-0.00003	0.00024	0.00028	0.00041	0.00031
	AlH ⁺	$X^2\Sigma^+$	1.6018	0.00274	0.00223	0.00210	0.00194	0.00200	0.00198	0.00206	0.00206
	SiH	$X^2\Pi_r$	1.5201	-0.00073	-0.00200	-0.00206	-0.00217	-0.00209	-0.00211	-0.00200	-0.00203
	SiF	$X^2\Pi_r$	1.6011	0.00007	-0.00129	-0.00160	-0.00204	-0.00150	-0.00155	-0.00138	-0.00141
	PH	$X^3\Sigma^-$	1.42234	-0.00307	-0.00315	-0.00321	-0.00329	-0.00321	-0.00324	-0.00314	-0.00319
	PH ⁺	$X^2\Pi_r$	1.4352	-0.01396	-0.01406	-0.01409	-0.01414	-0.01409	-0.01412	-0.01405	-0.01409
	PH ⁻	$X^2\Pi_i$	1.407	0.02464	0.02448	0.02432	0.02420	0.02434	0.02431	0.02452	0.02441
	CP	$X^2\Sigma^+$	1.5622	-0.01089	-0.01033	-0.01147	-0.01147	-0.01050	-0.01059	-0.00990	-0.01018
	PO	$X^2\Pi_r$	1.4759	-0.00649	-0.00840	-0.00917	-0.00890	-0.00848	-0.00842	-0.00810	-0.00810

PO ⁻	X ³ Σ ⁻	1.54	-0.00968	-0.01166	-0.01253	-0.01222	-0.01182	-0.01167	-0.01136	-0.01144
PF	X ³ Σ ⁻	1.5897	-0.00123	-0.00281	-0.00319	-0.00372	-0.00307	-0.00311	-0.00291	-0.00291
PF ⁺	X ² Π _r	1.5003	-0.00140	-0.00341	-0.00386	-0.00423	-0.00363	-0.00365	-0.00340	-0.00341
HS	X ² Π _i	1.3409	-0.00320	-0.00333	-0.00339	-0.00346	-0.00339	-0.00341	-0.00330	-0.00337
BS	X ² Σ ⁺	1.6092	-0.00411	-0.00513	-0.00578	-0.00604	-0.00547	-0.00558	-0.00507	-0.00525
CS ⁺	X ² Σ ⁺	1.4954	-0.01279	-0.01351	-0.01497	-0.01452	-0.01346	-0.01370	-0.01313	-0.01335
NS	X ² Π _r	1.49402	-0.01009	-0.01066	-0.01193	-0.01096	-0.01033	-0.01031	-0.00982	-0.00993
SO	X ³ Σ ⁻	1.48109	-0.00657	-0.00856	-0.00929	-0.00873	-0.00831	-0.00821	-0.00794	-0.00799
SO ⁺	X ² Π _r	1.424	-0.01295	-0.01122	-0.01204	-0.01149	-0.01105	-0.01099	-0.00794	-0.01068
HCl ⁺	X ² Π _i	1.31468	-0.00421	-0.00426	-0.00427	-0.00430	-0.00427	-0.00425	-0.00422	-0.00428
BeCl	X ² Σ ⁺	1.7971	0.00404	0.00387	0.00373	0.00346	0.00365	0.00365	0.00380	0.00372
CCl	X ² Π	1.645	0.00099	-0.00037	-0.00139	-0.00184	-0.00116	-0.00120	-0.00044	-0.00064
NCI	X ³ Σ ⁻	1.6144	0.00039	-0.00092	-0.00249	-0.00311	-0.00186	-0.00204	-0.00120	-0.00125
OCl	X ² Π _i	1.56963	-0.00068	-0.00504	-0.00797	-0.00621	-0.00446	-0.00481	-0.00382	-0.00394
RMSD			0.00821	0.00852	0.00910	0.00883	0.00850	0.00851	0.00832	0.00836
MSD			-0.00279	-0.00369	-0.00438	-0.00427	-0.00381	-0.00383	-0.00351	-0.00360
MIN			-0.01396	-0.01406	-0.01497	-0.01452	-0.01409	-0.01412	-0.01405	-0.01409
MAX			0.02464	0.02448	0.02432	0.02420	0.02434	0.02431	0.02452	0.02441
Row 3-	State	Expt.	Δ(CCSD: UHF)	Δ(CCSD: κ-OOMP2)	Δ(CCSD: OOMP2)	Δ(CCSD: BLYP)	Δ(CCSD: B97M-rV)	Δ(CCSD: B97)	Δ(CCSD: ωB97X-V)	Δ(CCSD: ωB97M-V)
Row 3	Dimer									
MgCl	X ² Σ ⁺	2.1991	0.00554	0.00544	0.00530	0.00518	0.00524	0.00527	0.00542	0.00535
AlS	X ² Σ ⁺	2.029	0.00689	0.00444	0.00204	0.00352	0.00344	0.00404	0.00521	0.00518
Si ₂	X ³ Σ ⁻	2.246	-0.00635	-0.00697	-0.09502	-0.00848	-0.00771	-0.00788	-0.00715	-0.00724
SiCl	X ² Π _r	2.058	0.01053	0.01015	0.00973	0.00914	0.00958	0.00959	0.00997	0.00988
P ₂ ⁺	X ² Π _u	1.9859	-0.02823	-0.02187	-0.10195	-0.02310	-0.02252	-0.02263	-0.02187	-0.02196
PS	X ² Π _r	1.9009	-0.01566	-0.00996	-0.01114	-0.01116	-0.01059	-0.01063	-0.00998	-0.01009
S ₂	X ³ Σ ⁻	1.8892	-0.00251	-0.00351	-0.00423	-0.00422	-0.00385	-0.00386	-0.00339	-0.00350
S ₂ ⁺	X ² Π _{g,r}	1.825	-0.01718	-0.01185	-0.01283	-0.01262	-0.01219	-0.01222	-0.01162	-0.01171
RMSD			0.01402	0.01079	0.04982	0.01135	0.01103	0.01111	0.01079	0.01083
MSD			-0.00587	-0.00427	-0.02601	-0.00522	-0.00483	-0.00479	-0.00418	-0.00426
MIN			-0.02823	-0.02187	-0.10195	-0.02310	-0.02252	-0.02263	-0.02187	-0.02196
MAX			0.01053	0.01015	0.00973	0.00914	0.00958	0.00959	0.00997	0.00988
Open-shell			Δ(CCSD: UHF)	Δ(CCSD: κ-OOMP2)	Δ(CCSD: OOMP2)	Δ(CCSD: BLYP)	Δ(CCSD: B97M-rV)	Δ(CCSD: B97)	Δ(CCSD: ωB97X-V)	Δ(CCSD: ωB97M-V)
RMSD			0.01184	0.01167	0.02168	0.01197	0.01161	0.01165	0.01147	0.01150
MSD			-0.00317	-0.00402	-0.00723	-0.00460	-0.00406	-0.00409	-0.00378	-0.00385
MIN			-0.02823	-0.02706	-0.10195	-0.02699	-0.02629	-0.02621	-0.02596	-0.02589
MAX			0.03714	0.03588	0.03526	0.03517	0.03575	0.03578	0.03600	0.03581

Table D.7: Species and experimental vibrational frequencies (in cm^{-1}) for which we were unable to compute a continuous PES with one or more of the methods surveyed. Experimental values were compiled by Huber and Herzberg[346].

Dimer	State	Expt.
CH^-	$X^3\Sigma^-$	979.23
CN^+	$a^1\Sigma$	2033.05
N_2^-	$X^2\Pi_g$	1968
MgO	$X^1\Sigma^+$	785.0
AlN	$X^3\Pi_i$	746.93
AlO	$X^2\Sigma^+$	979.23
SiN	$X^2\Sigma^+$	1151.3
Na_2	$X^1\Sigma_g^+$	159.124
Na_2^+	$X^2\Sigma_g^+$	126
Mg_2	$X^1\Sigma_g^+$	51.12
MgS	$X^1\Sigma^+$	528.74
Al_2	$X^3\Sigma_g^-$	350.01
Cl_2^+	$X^2\Pi_g$	645.61

D.2 Species not included in the test set

Tab. D.7 presents the species for which we were not able to obtain a continuous potential energy surface. For some cases this breakdown occurred at the SCF level with the reference curve changing character near equilibrium, leading to a discontinuous change in the CCSD energy. In other cases the t -amplitude optimization of CCSD was found to converge to different roots for different points along the surface.

D.3 Mean-field $\langle S^2 \rangle$ values

Table D.8: Mean-field $\langle S^2 \rangle$ values for the reference methods at the CCSD(T) minimum energy points used in the fitting procedure.

Closed-shell	Row 2-	Dimer	State	CCSD(T):	CCSD(T):	CCSD(T):	CCSD(T):	CCSD(T):	CCSD(T):	CCSD(T):	CCSD(T):	CCSD(T):
				UHF	κ -OOMP2	OOMP2	BLYP	B97M-rV	B97	ω B97X-V	ω B97M-V	
	Row 2	LiH	$X^1\Sigma^+$	0.00000	0.00000	0.00000	0.00000	0.00000	0.00000	0.00000	0.00000	0.00000
		Li ₂	$X^1\Sigma_g^+$	0.31860	0.00000	0.00000	0.00000	0.01065	0.00000	0.00000	0.00000	0.00000
		LiF	$X^1\Sigma^+$	0.00000	0.00000	0.00000	0.00000	0.00000	0.00000	0.00000	0.00000	0.00000
		BeH ⁺	$X^1\Sigma^+$	0.00000	0.00000	0.00000	0.00000	0.00000	0.00000	0.00000	0.00000	0.00000
		BeO	$X^1\Sigma^+$	0.00000	0.00000	0.00000	0.00000	0.00000	0.00000	0.00000	0.00000	0.00000
		BH	$X^1\Sigma^+$	0.47646	0.04871	0.00000	0.03506	0.00000	0.00000	0.00000	0.00000	0.00000
		BF	$X^1\Sigma^+$	0.00000	0.00000	0.00000	0.00000	0.00000	0.00000	0.00000	0.00000	0.00000
		C ₂	$X^1\Sigma_g^+$	1.65493	0.89140	0.00000	0.85447	0.94029	0.93904	1.01320	0.97020	0.97020
		CO	$X^1\Sigma^+$	0.00000	0.00000	0.00000	0.00000	0.00000	0.00000	0.00000	0.00000	0.00000
		N ₂	$X^1\Sigma_g^+$	0.00000	0.00000	0.00000	0.00000	0.00000	0.00000	0.00000	0.00000	0.00000
		NO ⁺	$X^1\Sigma^+$	0.00000	0.00000	0.00000	0.00000	0.00000	0.00000	0.00000	0.00000	0.00000
		OH ⁻	$X^1\Sigma^+$	0.00000	0.00000	0.00000	0.00000	0.00000	0.00000	0.00000	0.00000	0.00000
		HF	$X^1\Sigma^+$	0.00000	0.00000	0.00000	0.00000	0.00000	0.00000	0.00000	0.00000	0.00000
		F ₂	$X^1\Sigma_g^+$	0.31922	0.00000	0.00000	0.00000	0.00000	0.00000	0.00000	0.00000	0.00000
	Row 2-	Dimer	State	CCSD(T):	CCSD(T):	CCSD(T):	CCSD(T):	CCSD(T):	CCSD(T):	CCSD(T):	CCSD(T):	CCSD(T):
	Row 3			UHF	κ -OOMP2	OOMP2	BLYP	B97M-rV	B97	ω B97X-V	ω B97M-V	
		NaH	$X^1\Sigma^+$	0.00000	0.00000	0.00000	0.00000	0.00000	0.00000	0.00000	0.00000	0.00000
		NaLi	$X^1\Sigma^+$	0.32431	0.03641	0.00000	0.00000	0.00000	0.00000	0.00000	0.00000	0.00000
		NaF	$X^1\Sigma^+$	0.00000	0.00000	0.00000	0.00000	0.00000	0.00000	0.00000	0.00000	0.00000
		MgH ⁺	$X^1\Sigma^+$	0.00000	0.00000	0.00000	0.00000	0.00000	0.00000	0.00000	0.00000	0.00000
		AlH	$X^1\Sigma^+$	0.17105	0.00000	0.00000	0.00000	0.00000	0.00000	0.00000	0.00000	0.00000
		AlF	$X^1\Sigma^+$	0.00000	0.00000	0.00000	0.00000	0.00000	0.00000	0.00000	0.00000	0.00000
		SiH ⁺	$X^1\Sigma^+$	0.06997	0.00000	0.00000	0.00000	0.00000	0.00000	0.00000	0.00000	0.00000
		SiO	$X^1\Sigma^+$	0.00000	0.00000	0.00000	0.00000	0.00000	0.00000	0.00000	0.00000	0.00000
		PN	$X^1\Sigma^+$	0.70716	0.00000	0.00000	0.00000	0.00000	0.00000	0.00000	0.00000	0.00000
		BeS	$X^1\Sigma^+$	1.01647	0.00000	0.00000	0.00000	0.00000	0.00000	0.00000	0.00000	0.00000
		CS	$X^1\Sigma^+$	0.00000	0.00000	0.00000	0.00000	0.00000	0.00000	0.00000	0.00000	0.00000
		NS ⁺	$X^1\Sigma^+$	0.69154	0.00000	0.00000	0.00000	0.00000	0.00000	0.00000	0.00000	0.00000
		HCl	$X^1\Sigma^+$	0.00000	0.00000	0.00000	0.00000	0.00000	0.00000	0.00000	0.00000	0.00000
		LiCl	$X^1\Sigma^+$	0.00000	0.00000	0.00000	0.00000	0.00000	0.00000	0.00000	0.00000	0.00000
		BCl	$X^1\Sigma^+$	0.17749	0.00000	0.00000	0.00000	0.00000	0.00000	0.00000	0.00000	0.00000
		CCl ⁺	$X^1\Sigma^+$	0.00000	0.00000	0.00000	0.00000	0.00000	0.00000	0.00000	0.00000	0.00000
		ClF	$X^1\Sigma^+$	0.00000	0.00000	0.00000	0.00000	0.00000	0.00000	0.00000	0.00000	0.00000
	Row 3-	Dimer	State	CCSD(T):	CCSD(T):	CCSD(T):	CCSD(T):	CCSD(T):	CCSD(T):	CCSD(T):	CCSD(T):	CCSD(T):
	Row 3			UHF	κ -OOMP2	OOMP2	BLYP	B97M-rV	B97	ω B97X-V	ω B97M-V	
		NaCl	$X^1\Sigma^+$	0.00000	0.00000	0.00000	0.00000	0.00000	0.00000	0.00000	0.00000	0.00000
		AlCl	$X^1\Sigma^+$	0.00000	0.00000	0.00000	0.00000	0.00000	0.00000	0.00000	0.00000	0.00000
		SiS	$X^1\Sigma^+$	0.00000	0.00000	0.00000	0.00000	0.00000	0.00000	0.00000	0.00000	0.00000
		P ₂	$X^1\Sigma_g^+$	0.67604	0.00000	0.00000	0.00000	0.00000	0.00000	0.00000	0.00000	0.00000
		Cl ₂	$X^1\Sigma_g^+$	0.00000	0.00000	0.00000	0.00000	0.00000	0.00000	0.00000	0.00000	0.00000
	Row 2-	Dimer	State	CCSD(T):	CCSD(T):	CCSD(T):	CCSD(T):	CCSD(T):	CCSD(T):	CCSD(T):	CCSD(T):	CCSD(T):
	Row2			UHF	κ -OOMP2	OOMP2	BLYP	B97M-rV	B97	ω B97X-V	ω B97M-V	
		LiO	$X^2\Pi_i$	0.75970	0.75603	0.75612	0.75371	0.75619	0.75480	0.75372	0.75439	0.75439

Dimer	State	CCSD(T)									
		UHF	κ -OOMP2	CCSD(T)	CCSD(T)	CCSD(T)	CCSD(T)	CCSD(T)	CCSD(T)	CCSD(T)	CCSD(T)
BeH	$X^2\Sigma^+$	0.75204	0.75136	0.75144	0.75100	0.75042	0.75068	0.75107	0.75052		
BeF	$X^2\Sigma^+$	0.75083	0.75096	0.75103	0.75058	0.75212	0.75065	0.75065	0.75050		
B ₂	$X^3\Sigma^-$	2.90778	2.81206	2.00956	2.35395	2.47622	2.51071	2.90525	2.57710		
BN	$X^3\Pi$	2.05171	2.00636	2.00510	2.00289	2.00644	2.00383	2.00361	2.00340		
BO	$X^2\Sigma^+$	0.80067	0.76145	0.75971	0.75571	0.76350	0.75698	0.75704	0.75832		
CH	$X^2\Pi_r$	1.10075	0.75579	0.75551	0.75270	0.75428	0.75326	0.75279	0.75210		
C ₂	$X^2\Sigma_g^+$	0.75627	0.75579	0.75337	0.75332	0.75519	0.75544	0.76265	0.75835		
CN	$X^2\Sigma^+$	1.15755	0.76257	0.75580	0.75447	0.76131	0.75958	0.76000	0.76049		
CO ⁺	$X^2\Sigma^+$	0.96970	0.76730	0.76261	0.75964	0.77442	0.76532	0.76466	0.76630		
CF	$X^2\Pi_r$	0.76275	0.75627	0.75584	0.75299	0.75435	0.75370	0.75333	0.75220		
NH	$X^3\Sigma^-$	2.01660	2.01005	2.00985	2.00481	2.01010	2.00706	2.00562	2.00603		
N ₂ ⁺	$X^2\Sigma_g^+$	1.23889	0.75334	0.75207	0.75241	0.75417	0.75392	0.75423	0.75330		
NO	$X^2\Pi_r$	0.79621	0.75407	0.75343	0.75215	0.75368	0.75347	0.75324	0.75279		
NF	$X^3\Sigma^-$	2.02283	2.01047	2.00989	2.00507	2.00948	2.00795	2.00687	2.00626		
OH	$X^2\Pi_i$	0.75710	0.75446	0.75442	0.75224	0.75419	0.75299	0.75252	0.75279		
HO ⁺	$X^3\Sigma^-$	2.01414	2.00868	2.00858	2.00419	2.00758	2.00594	2.00511	2.00583		
O ₂	$X^3\Sigma_g^-$	2.04908	2.00962	2.00751	2.00526	2.01025	2.00981	2.00954	2.00857		
O ₂ ⁺	$X^2\Pi_g$	1.12597	0.75272	0.75229	0.75154	0.75292	0.75263	0.75259	0.75221		
O ₂ ⁻	$X^2\Pi_{g,i}$	0.79527	0.75617	0.75395	0.75412	0.75787	0.75739	0.75710	0.75631		
OF	$X^2\Pi$	0.77257	0.75447	0.75390	0.75224	0.75436	0.75378	0.75348	0.75376		
HF ⁺	$X^2\Pi_i$	0.75515	0.75336	0.75334	0.75169	0.75306	0.75219	0.75191	0.75209		
F ₂ ⁺	$X^2\Pi_{g,i}$	0.82975	0.75265	0.75193	0.75152	0.75314	0.75303	0.75308	0.75292		
F ₂	$X^2\Sigma_u^+$	0.77276	0.75746	0.75533	0.75283	0.75568	0.75597	0.75578	0.75599		
NaO	$X^2\Pi$	0.76211	0.75797	0.75866	0.75946	0.76283	0.75888	0.75546	0.75688		
MgH	$X^2\Sigma^+$	0.75985	0.75613	0.75575	0.75320	0.75128	0.75330	0.75516	0.75388		
MgF	$X^2\Sigma^+$	0.75036	0.75048	0.75057	0.75025	0.75076	0.75062	0.75052	0.75049		
AlH ⁺	$X^2\Sigma^+$	0.77723	0.76616	0.76425	0.75539	0.75413	0.75545	0.75903	0.75678		
SiH	$X^2\Pi_r$	0.79747	0.76132	0.75871	0.75404	0.75455	0.75485	0.75548	0.75211		
SiF	$X^2\Pi_r$	0.77677	0.76186	0.75908	0.75400	0.75480	0.75510	0.75597	0.75174		
PH	$X^3\Sigma^-$	2.02909	2.01225	2.01010	2.00492	2.00850	2.00709	2.00641	2.00395		
PH ⁺	$X^2\Pi_r$	0.79438	0.75888	0.75781	0.75364	0.75465	0.75448	0.75437	0.75231		
PH ⁻	$X^2\Pi_i$	0.77186	0.76106	0.75950	0.75478	0.75708	0.75612	0.75523	0.75394		
CP	$X^2\Sigma^+$	1.61297	0.82118	0.76087	0.76599	0.80531	0.78991	0.80446	0.79607		
PO	$X^2\Pi_r$	0.77298	0.75758	0.75572	0.75301	0.75418	0.75438	0.75529	0.75258		
PO ⁻	$X^3\Sigma^-$	2.04447	2.00989	2.00729	2.00468	2.00812	2.00860	2.01013	2.00607		
PF	$X^3\Sigma^-$	2.03511	2.01047	2.00788	2.00410	2.00876	2.00662	2.00654	2.00285		
PF ⁺	$X^2\Pi_r$	0.77166	0.75909	0.75772	0.75350	0.75552	0.75464	0.75478	0.75208		
HS	$X^2\Pi_i$	0.76481	0.75738	0.75666	0.75337	0.75530	0.75420	0.75383	0.75266		
BS	$X^2\Sigma^+$	0.85482	0.77318	0.76520	0.75858	0.77086	0.76235	0.76101	0.76416		
CS ⁺	$X^2\Sigma^+$	1.47259	0.80770	0.76914	0.77031	0.80860	0.79111	0.79583	0.79312		
NS	$X^2\Pi_r$	1.18951	0.75758	0.75365	0.75377	0.75636	0.75751	0.75990	0.75736		
SO	$X^3\Sigma^-$	2.05909	2.01059	2.00667	2.00507	2.00929	2.00982	2.01195	2.00851		
SO ⁺	$X^2\Pi_r$	1.18709	0.75583	0.75422	0.75259	0.75398	0.75413	0.75513	0.75304		
HCl ⁺	$X^2\Pi_i$	0.76226	0.75633	0.75598	0.75301	0.75489	0.75373	0.75332	0.75257		
LiCl ⁻	$X^2\Sigma^+$	0.75014	0.75016	0.75019	0.75008	0.75219	0.75038	0.75016	0.75018		
BeCl	$X^2\Sigma^+$	0.75155	0.75140	0.75150	0.75094	0.75221	0.75078	0.75079	0.75078		

Row 2-
Row 3

Dimer	State	CCSD(T):	CCSD(T):	CCSD(T):	CCSD(T):	CCSD(T):	CCSD(T):	CCSD(T):	CCSD(T):	CCSD(T):	CCSD(T):
		UHF	κ -OOMP2	OOMP2	BLYP	B97M-rV	B97	ω B97X-V	ω B97M-V	ω B97M-V	
CCl	X ² Π	0.76579	0.75772	0.75656	0.75355	0.75543	0.75493	0.75486	0.75405		
NCl	X ³ Σ ⁻	2.03589	2.01532	2.01178	2.00654	2.01180	2.01122	2.01189	2.01037		
OCl	X ² Π _i	0.77010	0.75664	0.75405	0.75289	0.75543	0.75536	0.75629	0.75521		
FCl ⁺	X ² Π	0.76463	0.75541	0.75456	0.75221	0.75387	0.75348	0.75381	0.75267		
Dimer	State	CCSD(T):	CCSD(T):	CCSD(T):	CCSD(T):	CCSD(T):	CCSD(T):	CCSD(T):	CCSD(T):		
		UHF	κ -OOMP2	OOMP2	BLYP	B97M-rV	B97	ω B97X-V	ω B97M-V		
MgCl	X ² Σ ⁺	0.75092	0.75085	0.75093	0.75045	0.75059	0.75084	0.75094	0.75082		
AlS	X ² Σ ⁺	0.77492	0.76188	0.75923	0.75355	0.75466	0.75498	0.75917	0.75552		
Si ₂	X ³ Σ ⁻ _g	2.01897	2.00946	2.00560	2.00441	2.00890	2.00554	2.00422	2.00332		
SiCl	X ² Π _r	0.77631	0.76144	0.75850	0.75402	0.75541	0.75517	0.75601	0.75208		
P ₂ ⁺	X ² Π _u	1.16866	0.75476	0.75651	0.75262	0.75510	0.75289	0.75237	0.75166		
PS	X ² Π _r	1.05380	0.76119	0.75590	0.75340	0.75496	0.75557	0.75791	0.75445		
S ₂	X ³ Σ ⁻ _g	2.06163	2.01837	2.00876	2.00494	2.00775	2.00936	2.01559	2.00936		
S ₂ ⁺	X ² Π _{g,r}	1.23007	0.75862	0.75431	0.75285	0.75386	0.75457	0.75747	0.75392		

Table D.9: Mean-field (S^2) values for the reference methods at the CCSD minimum energy points used in the fitting procedure.

Closed-shell	Row 2- Row 2	Dimer	State	CCSD:	CCSD:	CCSD:	CCSD:	CCSD:	CCSD:	CCSD:	CCSD:	CCSD:	CCSD:
				UHF	κ -OOMP2	OOMP2	BLYP	B97M-rV	B97	ω B97X-V	ω B97M-V		
		LiH	$X^1\Sigma^+$	0.00000	0.00000	0.00000	0.00000	0.00000	0.00000	0.00000	0.00000	0.00000	0.00000
		Li ₂	$X^1\Sigma_g^+$	0.31690	0.00000	0.00000	0.00000	0.01065	0.00000	0.00000	0.00000	0.00000	0.00000
		LiF	$X^1\Sigma^+$	0.00000	0.00000	0.00000	0.00000	0.00000	0.00000	0.00000	0.00000	0.00000	0.00000
		BeH ⁺	$X^1\Sigma^+$	0.00000	0.00000	0.00000	0.00000	0.00000	0.00000	0.00000	0.00000	0.00000	0.00000
		BeO	$X^1\Sigma^+$	0.00000	0.00000	0.00000	0.00000	0.00000	0.00000	0.00000	0.00000	0.00000	0.00000
		BH	$X^1\Sigma^+$	0.47646	0.04871	0.00000	0.03506	0.00000	0.00000	0.00000	0.00000	0.00000	0.00000
		BF	$X^1\Sigma^+$	0.00000	0.00000	0.00000	0.00000	0.00000	0.00000	0.00000	0.00000	0.00000	0.00000
		C ₂	$X^1\Sigma_g^+$	1.62372	0.90291	0.00000	0.92892	1.00478	1.00057	1.05327	1.02472	1.02472	1.02472
		CO	$X^1\Sigma^+$	0.00000	0.00000	0.00000	0.00000	0.00000	0.00000	0.00000	0.00000	0.00000	0.00000
		N ₂	$X^1\Sigma_g^+$	0.00000	0.00000	0.00000	0.00000	0.00000	0.00000	0.00000	0.00000	0.00000	0.00000
		NO ⁺	$X^1\Sigma^+$	0.00000	0.00000	0.00000	0.00000	0.00000	0.00000	0.00000	0.00000	0.00000	0.00000
		OH ⁻	$X^1\Sigma^+$	0.00000	0.00000	0.00000	0.00000	0.00000	0.00000	0.00000	0.00000	0.00000	0.00000
		HF	$X^1\Sigma^+$	0.00000	0.00000	0.00000	0.00000	0.00000	0.00000	0.00000	0.00000	0.00000	0.00000
		F ₂	$X^1\Sigma_g^+$	0.21545	0.00000	0.00000	0.00000	0.00000	0.00000	0.00000	0.00000	0.00000	0.00000
	Row 2- Row 3	Dimer	State	CCSD:	CCSD:	CCSD:	CCSD:	CCSD:	CCSD:	CCSD:	CCSD:	CCSD:	CCSD:
		UHF	BLYP	OOMP2	BLYP	B97M-rV	B97	ω B97X-V	ω B97M-V				
		NaH	$X^1\Sigma^+$	0.00000	0.00000	0.00000	0.00000	0.00000	0.00000	0.00000	0.00000	0.00000	0.00000
		NaLi	$X^1\Sigma^+$	0.32702	0.03641	0.00000	0.00000	0.00000	0.00000	0.00000	0.00000	0.00000	0.00000
		NaF	$X^1\Sigma^+$	0.00000	0.00000	0.00000	0.00000	0.00000	0.00000	0.00000	0.00000	0.00000	0.00000
		MgH ⁺	$X^1\Sigma^+$	0.00000	0.00000	0.00000	0.00000	0.00000	0.00000	0.00000	0.00000	0.00000	0.00000
		AlH	$X^1\Sigma^+$	0.17105	0.00000	0.00000	0.00000	0.00000	0.00000	0.00000	0.00000	0.00000	0.00000
		AlF	$X^1\Sigma^+$	0.00000	0.00000	0.00000	0.00000	0.00000	0.00000	0.00000	0.00000	0.00000	0.00000
		SiH ⁺	$X^1\Sigma^+$	0.06997	0.00000	0.00000	0.00000	0.00000	0.00000	0.00000	0.00000	0.00000	0.00000
		SiO	$X^1\Sigma^+$	0.00000	0.00000	0.00000	0.00000	0.00000	0.00000	0.00000	0.00000	0.00000	0.00000
		PN	$X^1\Sigma^+$	0.65868	0.00000	0.00000	0.00000	0.00000	0.00000	0.00000	0.00000	0.00000	0.00000
		BeS	$X^1\Sigma^+$	1.01646	0.00000	0.00000	0.00000	0.00000	0.00000	0.00000	0.00000	0.00000	0.00000
		CS	$X^1\Sigma^+$	0.00000	0.00000	0.00000	0.00000	0.00000	0.00000	0.00000	0.00000	0.00000	0.00000
		NS ⁺	$X^1\Sigma^+$	0.64038	0.00000	0.00000	0.00000	0.00000	0.00000	0.00000	0.00000	0.00000	0.00000
		HCl	$X^1\Sigma^+$	0.00000	0.00000	0.00000	0.00000	0.00000	0.00000	0.00000	0.00000	0.00000	0.00000
		LiCl	$X^1\Sigma^+$	0.00000	0.00000	0.00000	0.00000	0.00000	0.00000	0.00000	0.00000	0.00000	0.00000
		BCl	$X^1\Sigma^+$	0.17638	0.00000	0.00000	0.00000	0.00000	0.00000	0.00000	0.00000	0.00000	0.00000
		CCl ⁺	$X^1\Sigma^+$	0.00000	0.00000	0.00000	0.00000	0.00000	0.00000	0.00000	0.00000	0.00000	0.00000
		ClF	$X^1\Sigma^+$	0.00000	0.00000	0.00000	0.00000	0.00000	0.00000	0.00000	0.00000	0.00000	0.00000
	Row 3- Row 3	Dimer	State	CCSD:	CCSD:	CCSD:	CCSD:	CCSD:	CCSD:	CCSD:	CCSD:	CCSD:	CCSD:
		UHF	BLYP	OOMP2	BLYP	B97M-rV	B97	ω B97X-V	ω B97M-V				
		NaCl	$X^1\Sigma^+$	0.00000	0.00000	0.00000	0.00000	0.00000	0.00000	0.00000	0.00000	0.00000	0.00000
		AlCl	$X^1\Sigma^+$	0.00000	0.00000	0.00000	0.00000	0.00000	0.00000	0.00000	0.00000	0.00000	0.00000
		SiS	$X^1\Sigma^+$	0.00000	0.00000	0.00000	0.00000	0.00000	0.00000	0.00000	0.00000	0.00000	0.00000
		P ₂	$X^1\Sigma^+$	0.60962	0.00000	0.00000	0.00000	0.00000	0.00000	0.00000	0.00000	0.00000	0.00000
		Cl ₂	$X^1\Sigma_g^+$	0.00000	0.00000	0.00000	0.00000	0.00000	0.00000	0.00000	0.00000	0.00000	0.00000
	Row 2- Row 2	Dimer	State	CCSD:	CCSD:	CCSD:	CCSD:	CCSD:	CCSD:	CCSD:	CCSD:	CCSD:	CCSD:
		UHF	BLYP	OOMP2	BLYP	B97M-rV	B97	ω B97X-V	ω B97M-V				
		Open-shell											

Dimer	State	CCSD:										CCSD:									
		UHF	κ -OOMP2	OOMP2	BLYP	B97M-rV	B97	ω B97X-V	ω B97M-V	B97	ω B97X-V	ω B97M-V	B97	ω B97X-V	ω B97M-V						
LiO	$X^2\Pi_i$	0.75966	0.75599	0.75607	0.75366	0.75613	0.75475	0.75369	0.75435												
BeH	$X^2\Sigma^+$	0.75204	0.75136	0.75144	0.75100	0.75042	0.75068	0.75107	0.75052												
BeF	$X^2\Sigma^+$	0.75084	0.75096	0.75103	0.75058	0.75212	0.75065	0.75065	0.75050												
B ₂	$X^3\Sigma^-_g$	2.91265	2.82216	2.00956	2.40515	2.50830	2.54165	2.69514	2.61548												
BN	$X^3\Pi$	2.04561	2.00633	2.00510	2.00286	2.00650	2.00377	2.00355	2.00337												
BO	$X^2\Sigma^+$	0.79782	0.76122	0.75955	0.75559	0.76313	0.75683	0.75689	0.75813												
CH	$X^2\Pi_r$	1.10075	0.75579	0.75551	0.75270	0.75428	0.75326	0.75279	0.75210												
C ₂ ⁻	$X^2\Sigma^+_g$	0.75628	0.75577	0.75338	0.75331	0.75516	0.75534	0.76049	0.75748												
CN	$X^2\Sigma^+$	1.11881	0.76253	0.75590	0.75441	0.76117	0.75942	0.75973	0.76030												
CO ⁺	$X^2\Sigma^+$	0.95712	0.76676	0.76253	0.75924	0.77298	0.76444	0.76379	0.76536												
CF	$X^2\Pi_r$	0.76271	0.75624	0.75582	0.75297	0.75432	0.75368	0.75331	0.75218												
NH	$X^3\Sigma^-$	2.01660	2.01005	2.00985	2.00481	2.01010	2.00706	2.00562	2.00603												
N ₂ ⁺	$X^2\Sigma^+_g$	1.19138	0.75333	0.75212	0.75232	0.75406	0.75377	0.75416	0.75316												
NO	$X^2\Pi_r$	0.78638	0.75402	0.75344	0.75209	0.75356	0.75333	0.75311	0.75265												
NF	$X^3\Sigma^-$	2.02281	2.01045	2.00989	2.00505	2.00944	2.00791	2.00683	2.00616												
OH	$X^2\Pi_i$	0.75710	0.75446	0.75442	0.75224	0.75419	0.75299	0.75252	0.75279												
HO ⁺	$X^3\Sigma^-$	2.01414	2.00868	2.00858	2.00419	2.00758	2.00594	2.00511	2.00583												
O ₂	$X^3\Sigma^-_g$	2.04740	2.00967	2.00772	2.00516	2.01004	2.00958	2.00927	2.00834												
O ₂ ⁺	$X^2\Pi_g$	1.08640	0.75274	0.75233	0.75153	0.75289	0.75259	0.75255	0.75217												
O ₂ ⁻	$X^2\Pi_{g,i}$	0.79295	0.75622	0.75417	0.75405	0.75767	0.75718	0.75684	0.75610												
OF	$X^2\Pi$	0.76696	0.75440	0.75391	0.75219	0.75425	0.75364	0.75335	0.75353												
HF ⁺	$X^2\Pi_i$	0.75510	0.75334	0.75332	0.75168	0.75304	0.75218	0.75189	0.75207												
F ₂ ⁺	$X^2\Pi_{g,i}$	0.79656	0.75276	0.75213	0.75150	0.75312	0.75298	0.75302	0.75285												
F ₂ ⁻	$X^2\Sigma^+_g$	0.77581	0.75739	0.75531	0.75281	0.75565	0.75591	0.75571	0.75592												
Dimer	State	CCSD:	CCSD:	CCSD:	CCSD:	CCSD:	CCSD:	CCSD:	CCSD:	CCSD:	CCSD:	CCSD:	CCSD:	CCSD:	CCSD:						
NaO	$X^2\Pi$	0.76205	0.75794	0.75863	0.75938	0.76271	0.75882	0.75544	0.75684												
MgH	$X^2\Sigma^+$	0.75985	0.75613	0.75575	0.75320	0.75128	0.75330	0.75516	0.75388												
MgF	$X^2\Sigma^+$	0.75036	0.75048	0.75057	0.75024	0.75076	0.75061	0.75051	0.75048												
AlH ⁺	$X^2\Sigma^+$	0.77723	0.76584	0.76400	0.75531	0.75403	0.75536	0.75887	0.75666												
SiH	$X^2\Pi_r$	0.79747	0.76132	0.75871	0.75404	0.75455	0.75485	0.75548	0.75211												
SiF	$X^2\Pi_r$	0.77677	0.76186	0.75908	0.75400	0.75479	0.75510	0.75597	0.75174												
PH	$X^3\Sigma^-$	2.02913	2.01224	2.01007	2.00492	2.00848	2.00709	2.00641	2.00394												
PH ⁺	$X^2\Pi_r$	0.79445	0.75887	0.75780	0.75364	0.75464	0.75447	0.75437	0.75231												
PH ⁻	$X^2\Pi_i$	0.77189	0.76106	0.75949	0.75478	0.75707	0.75612	0.75523	0.75394												
CP	$X^2\Sigma^+$	1.59712	0.81614	0.76132	0.76525	0.80179	0.78701	0.79906	0.79240												
PO	$X^2\Pi_r$	0.77267	0.75758	0.75576	0.75300	0.75413	0.75434	0.75522	0.75252												
PO ⁻	$X^3\Sigma^-$	2.04349	2.00978	2.00720	2.00460	2.00799	2.00841	2.00993	2.00591												
PF	$X^3\Sigma^-$	2.03511	2.01048	2.00788	2.00411	2.00875	2.00663	2.00655	2.00284												
PF ⁺	$X^2\Pi_r$	0.77166	0.75910	0.75772	0.75350	0.75550	0.75464	0.75478	0.75207												
HS	$X^2\Pi_i$	0.76481	0.75737	0.75664	0.75337	0.75530	0.75420	0.75383	0.75266												
BS	$X^2\Sigma^+$	0.85146	0.77281	0.76503	0.75844	0.77046	0.76215	0.76083	0.76394												
CS ⁺	$X^2\Sigma^+$	1.44109	0.80436	0.76927	0.76925	0.80472	0.78827	0.79187	0.78999												
NS	$X^2\Pi_r$	1.16463	0.75742	0.75364	0.75364	0.75599	0.75702	0.75917	0.75672												
SO	$X^3\Sigma^-$	2.05772	2.01052	2.00679	2.00498	2.00905	2.00958	2.01162	2.00823												
SO ⁺	$X^2\Pi_r$	1.12991	0.75587	0.75431	0.75259	0.75396	0.75408	0.75502	0.75297												
HCl ⁺	$X^2\Pi_i$	0.76225	0.75631	0.75597	0.75300	0.75488	0.75372	0.75332	0.75257												

Row 2-
Row 3

Dimer	State	CCSD:		CCSD:		CCSD:		CCSD:		CCSD:	
		UHF	κ -OOMP2	OOMP2	BLYP	B97M-rV	B97	ω B97X-V	ω B97M-V	ω B97M-V	ω B97M-V
LiCl ⁻	X ² Σ ⁺	0.75014	0.75016	0.75019	0.75008	0.75219	0.75038	0.75016	0.75018		
BeCl	X ² Σ ⁺	0.75155	0.75140	0.75150	0.75094	0.75221	0.75078	0.75079	0.75078		
CCl	X ² Π	0.76583	0.75771	0.75655	0.75354	0.75541	0.75492	0.75486	0.75403		
NCl	X ³ Σ ⁻	2.03586	2.01531	2.01178	2.00653	2.01177	2.01119	2.01188	2.01031		
OCl	X ² Π _i	0.77006	0.75662	0.75412	0.75287	0.75540	0.75531	0.75626	0.75515		
FCI ⁺	X ² Π	0.76481	0.75542	0.75461	0.75222	0.75388	0.75348	0.75380	0.75265		
Row 3-	State	CCSD:	CCSD:	CCSD:	CCSD:	CCSD:	CCSD:	CCSD:	CCSD:	CCSD:	CCSD:
Row 3	State	UHF	κ -OOMP2	OOMP2	BLYP	B97M-rV	B97	ω B97X-V	ω B97M-V	ω B97M-V	ω B97M-V
MgCl	X ² Σ ⁺	0.75092	0.75084	0.75093	0.75045	0.75059	0.75083	0.75093	0.75081		
AlS	X ² Σ ⁺	0.77348	0.76156	0.75911	0.75350	0.75457	0.75487	0.75886	0.75537		
Si ₂	X ³ Σ ⁻ _g	2.01899	2.00949	2.00565	2.00442	2.00891	2.00555	2.00423	2.00335		
SiCl	X ² Π _r	0.77634	0.76144	0.75850	0.75402	0.75540	0.75517	0.75602	0.75208		
P ₂ ⁺	X ² Π _u	1.13370	0.75477	0.75663	0.75262	0.75508	0.75289	0.75237	0.75167		
PS	X ² Π _r	1.02029	0.76093	0.75592	0.75338	0.75484	0.75545	0.75780	0.75429		
S ₂	X ³ Σ ⁻ _g	2.06113	2.01829	2.00891	2.00493	2.00775	2.00931	2.01545	2.00924		
S ₂ ⁺	X ² Π _{g,r}	1.20499	0.75864	0.75444	0.75286	0.75388	0.75456	0.75743	0.75388		

D.4 CCSD data

Table D.10: Experimental vibrational frequencies and errors in the corrected vibrational frequencies for the closed-shell species are presented in for the CCSD methods utilizing different molecular orbitals. Root mean square deviations, mean signed deviations, minimum deviations, and maximum deviations for the set of species and subsets are also presented.

Row 2- Row 2	Dimer	State	Expt.	$\Delta(\text{CCSD: UHF})$	$\Delta(\text{CCSD: } \kappa\text{-OOMP2})$	$\Delta(\text{CCSD: OOMP2})$	$\Delta(\text{CCSD: BLYP})$	$\Delta(\text{CCSD: B97M-rV})$	$\Delta(\text{CCSD: B97})$	$\Delta(\text{CCSD: } \omega\text{B97X-V})$	$\Delta(\text{CCSD: } \omega\text{B97M-V})$
	LiH	$X^1\Sigma^+$	1405.49805 ^a	-4.95	-5.93	-5.25	-3.96	-6.91	-7.45	-4.46	-5.49
	Li ₂	$X^1\Sigma^+$	351.4066 ^a	-4.86	-10.16	-3.10	-4.03	-1.75	-3.36	-26.61	-4.36
	LiF	$X^1\Sigma^+$	910.57272 ^a	4.40	6.56	7.19	7.72	6.80	6.80	6.57	6.45
	BeH ⁺	$X^1\Sigma^+$	2221.7 ^b	-10.75	-10.66	-8.80	-10.75	-16.01	-8.7694	-13.26	-8.97
	BeO	$X^1\Sigma^+$	1487.32 ^b	75.94	88.76	93.78	91.43	89.12	90.2704	86.98	87.69
	BH	$X^1\Sigma^+$	2366.7296 ^a	12.83	8.70	12.76	15.81	8.90	14.66	11.03	10.41
	BF	$X^1\Sigma^+$	1402.15865 ^a	9.33	15.33	16.66	18.28	16.10	16.28	15.51	15.68
	C ₂	$X^1\Sigma^+$	1855.0663 ^a	96.46	85.08	78.07	-385.19	-366.32	-362.08	-340.93	-356.99
	CO	$X^1\Sigma^+$	2169.75589 ^a	55.68	70.60	73.72	72.33	68.78	68.93	67.27	67.34
	N ₂	$X^1\Sigma^+$	2358.57 ^a	76.36	88.42	91.17	89.58	86.00	86.76	84.80	84.93
	NO ⁺	$X^1\Sigma^+$	2376.72 ^a	103.61	123.66	127.13	123.61	119.47	118.90	117.38	117.44
	OH ⁻	$X^1\Sigma^+$	3735.2 ^c	52.95	69.59	76.05	69.57	65.42	65.63	64.56	64.61
	HF	$X^1\Sigma^+$	4138.385 ^a	39.17	48.26	49.86	49.91	46.21	48.53	46.91	46.61
	F ₂	$X^1\Sigma^+$	916.929 ^d	170.29	104.70	107.50	104.74	103.50	103.32	102.90	102.84
	RMSD			69.95	66.52	68.26	120.82	115.37	114.54	109.40	112.80
	MSD			48.32	48.78	51.20	17.07	15.67	17.03	15.62	16.30
	MIN			-10.75	-10.66	-8.80	-385.19	-366.32	-362.08	-340.93	-356.99
	MAX			170.29	123.66	127.13	123.61	119.47	118.90	117.38	117.44
Row 2- Row 3	Dimer	State	Expt.	$\Delta(\text{CCSD: UHF})$	$\Delta(\text{CCSD: } \kappa\text{-OOMP2})$	$\Delta(\text{CCSD: OOMP2})$	$\Delta(\text{CCSD: BLYP})$	$\Delta(\text{CCSD: B97M-rV})$	$\Delta(\text{CCSD: B97})$	$\Delta(\text{CCSD: } \omega\text{B97X-V})$	$\Delta(\text{CCSD: } \omega\text{B97M-V})$
	NaH	$X^1\Sigma^+$	1171.968 ^a	-8.37	-8.55	-8.45	-10.03	-8.69	-9.60	-9.63	-9.82
	NaLi	$X^1\Sigma^+$	256.5412 ^a	2.01	2.11	-2.86	-0.47	-0.59	-15.03	-3.63	-2.49
	NaF	$X^1\Sigma^+$	535.65805 ^a	0.17	1.57	1.93	2.13	1.72	1.52	1.57	1.63
	MgH ⁺	$X^1\Sigma^+$	1699.1 ^b	-0.10	-0.17	1.38	-1.86	-3.39	0.23	-1.82	-3.41
	AlH	$X^1\Sigma^+$	1682.37474 ^a	-7.02	-2.63	-6.91	-3.94	-8.11	-1.94	-2.19	-4.07
	AlF	$X^1\Sigma^+$	802.32447 ^a	2.01	4.73	5.55	6.33	5.17	5.24	4.87	4.99
	SH ⁺	$X^1\Sigma^+$	2157.17 ^a	8.25	12.28	12.44	14.13	14.30	13.86	8.73	12.63
	SiO	$X^1\Sigma^+$	1241.54388 ^a	43.96	53.88	59.60	56.14	54.35	53.99	51.85	51.92
	PN	$X^1\Sigma^+$	1336.948 ^a	73.08	72.09	79.35	73.46	71.43	71.25	69.02	69.04
	BeS	$X^1\Sigma^+$	997.94 ^a	-234.21	27.17	30.29	30.00	28.94	28.73	26.82	26.97
	CS	$X^1\Sigma^+$	1285.08 ^b	51.17	62.22	68.15	65.08	62.36	62.60	59.60	60.19
	NS ⁺	$X^1\Sigma^+$	1415 ^b	100.80	102.09	109.97	103.13	100.22	100.32	97.92	98.31
	HCl	$X^1\Sigma^+$	2990.9248 ^a	43.02	44.49	43.89	44.69	46.48	44.55	44.46	46.52
	LiCl	$X^1\Sigma^+$	642.95453 ^a	-3.92	-3.82	-3.91	-3.63	-3.61	-3.68	-4.01	-3.62
	BCl	$X^1\Sigma^+$	840.29472 ^a	5.09	7.21	8.77	10.30	9.28	8.85	7.72	7.96
	CCl ⁺	$X^1\Sigma^+$	1175 ^b	44.47	58.67	66.11	63.50	60.07	60.05	56.25	57.15
	ClF	$X^1\Sigma^+$	783.4534 ^a	28.96	32.27	33.38	32.36	31.19	31.30	31.19	31.16
	RMSD			68.52	41.95	45.59	43.30	42.05	42.01	40.38	40.78
	MSD			8.79	27.39	29.34	28.31	27.13	26.60	25.81	26.18
	MIN			-234.21	-8.55	-8.45	-10.03	-8.69	-15.03	-9.63	-9.82

MAX	100.80	102.09	109.97	103.13	100.22	100.32	97.92	98.31
Row 3-								
Row 3								
Dimer	$\Delta(\text{CCSD: UHF})$	$\Delta(\text{CCSD: } \kappa\text{-OOMP2})$	$\Delta(\text{CCSD: OOMP2})$	$\Delta(\text{CCSD: BLYP})$	$\Delta(\text{CCSD: B97M-rV})$	$\Delta(\text{CCSD: B97})$	$\Delta(\text{CCSD: } \omega\text{B97X-V})$	$\Delta(\text{CCSD: } \omega\text{B97M-V})$
State	Expt.							
NaCl	364.6842 ^a	-3.88	-3.69	-3.55	-3.70	-3.67	-3.77	-3.76
AlCl	481.77466 ^a	-4.48	-4.13	-3.65	-4.00	-3.98	-4.33	-4.30
SiS	749.64559 ^a	21.34	24.75	28.00	27.66	26.39	24.47	24.83
P ₂	780.77 ^a	45.20	39.47	42.93	41.59	40.53	38.80	38.96
Cl ₂	559.751 ^a	7.82	8.43	8.85	9.01	8.74	8.46	8.46
RMSD	22.79	21.34	23.39	22.81	22.15	22.11	21.02	21.16
MSD	13.18	12.86	14.39	14.21	13.62	13.57	12.73	12.84
MIN	-4.67	-4.48	-4.13	-3.65	-4.00	-3.98	-4.33	-4.30
MAX	45.20	39.47	42.93	41.59	40.53	40.57	38.80	38.96
Closed-shell								
Dimer	$\Delta(\text{CCSD: UHF})$	$\Delta(\text{CCSD: } \kappa\text{-OOMP2})$	$\Delta(\text{CCSD: OOMP2})$	$\Delta(\text{CCSD: BLYP})$	$\Delta(\text{CCSD: B97M-rV})$	$\Delta(\text{CCSD: B97})$	$\Delta(\text{CCSD: } \omega\text{B97X-V})$	$\Delta(\text{CCSD: } \omega\text{B97M-V})$
State	Expt.							
RMSD	64.75	51.14	53.57	81.45	77.97	77.48	74.07	76.13
MSD	24.77	33.69	35.76	21.98	20.79	21.07	20.03	20.48
MIN	-234.21	-10.66	-8.80	-385.19	-366.32	-362.08	-340.93	-356.99
MAX	170.29	123.66	127.13	123.61	119.47	118.90	117.38	117.44

^a From Ref. 349.

^b From Ref. 346.

^c From Ref. 350.

Table D.11: Experimental vibrational frequencies and errors in the corrected vibrational frequencies for the open-shell species are presented in for the CCSD methods utilizing different molecular orbitals. Root mean square deviations, mean signed deviations, minimum deviations, and maximum deviations for the set of species and subsets are presented.

Row 2- Row 2	Dimer	State	Expt.	$\Delta(\text{CCSD: UHF})$	$\Delta(\text{CCSD: } \kappa\text{-OOMP2})$	$\Delta(\text{CCSD: OOMP2})$	$\Delta(\text{CCSD: BLYP})$	$\Delta(\text{CCSD: B97M-rV})$	$\Delta(\text{CCSD: B97})$	$\Delta(\text{CCSD: } \omega\text{B97X-V})$	$\Delta(\text{CCSD: } \omega\text{B97M-V})$
	LiO	$X^2\Pi_i$	814.62 ^a	3.94	5.61	6.08	7.31	6.48	6.51	5.95	5.91
	BeH	$X^2\Sigma^+$	2061.235 ^a	1.68	1.23	4.44	2.76	0.82	1.41	2.78	1.21
	BeF	$X^2\Sigma^+$	1247.36 ^b	22.61	25.70	26.43	27.35	26.14	26.17	25.81	26.03
	B ₂	$X^3\Sigma^-$	1051.3 ^b	44.59	40.38	3.78	35.49	33.05	31.27	32.03	32.73
	BN	$X^3\Pi$	1514.6 ^b	64.98	68.38	71.04	68.20	66.68	65.12	64.42	66.43
	BO	$X^2\Sigma^+$	1885.286 ^a	43.31	55.40	59.77	58.97	54.94	55.58	54.35	54.42
	CH	$X^2\Pi_r$	2860.7508 ^a	14.37	22.42	20.91	23.07	22.30	20.99	20.73	22.84
	C ₂ ⁻	$X^2\Sigma^+$	1781.189 ^a	-65.13	57.66	64.77	58.17	55.07	54.40	6.09	25.65
	CN	$X^2\Sigma^+$	2068.648 ^a	103.60	78.37	81.29	76.63	75.27	74.70	73.98	75.70
	CO ⁺	$X^2\Sigma^+$	2214.127 ^a	91.85	112.67	119.04	113.90	105.88	107.95	106.78	107.09
	CF	$X^2\Pi_r$	1307.93 ^a	28.27	39.55	42.36	43.55	40.34	40.11	38.60	38.82
	NH	$X^3\Sigma^-$	3282.72 ^a	28.52	34.79	32.86	36.15	33.80	34.03	30.57	32.40
	N ₂ ⁺	$X^2\Sigma^+$	2207.0115 ^a	116.78	101.46	112.23	97.51	92.54	92.63	90.12	90.71
	NO	$X^2\Pi_r$	1904.1346 ^a	89.82	104.51	108.95	105.22	100.93	101.24	99.29	99.51
	NF	$X^3\Sigma^-$	1141.37 ^a	28.52	42.43	47.39	47.22	41.43	41.84	39.87	39.49
	OH	$X^2\Pi_i$	3737.761 ^a	30.46	36.53	36.58	38.33	35.95	36.01	36.65	35.49
	OH ⁺	$X^3\Sigma^-$	3113.37 ^b	33.25	35.47	35.67	38.43	39.19	36.47	34.66	36.60
	O ₂	$X^3\Sigma^-$	1580.161 ^a	81.40	99.60	104.70	99.11	95.69	95.12	93.78	93.88
	O ₂ ⁺	$X^2\Pi_g$	1905.892 ^a	133.11	150.65	156.65	148.73	144.25	144.04	142.11	142.24
	O ₂ ⁻	$X^2\Pi_{g,i}$	1090 ^b	102.15	119.79	127.46	118.74	116.16	115.49	114.22	114.17
	OF	$X^2\Pi$	1053.0138 ^a	50.04	75.93	93.00	79.55	68.15	68.72	65.06	64.20
	HF ⁺	$X^2\Pi_i$	3090.5 ^b	57.35	59.59	59.35	66.31	60.95	62.06	61.75	61.82
	F ₂ ⁺	$X^2\Pi_{g,i}$	1091.5 ^d	153.52	152.75	161.40	150.43	148.16	147.68	146.35	145.97
	F ₂ ⁻	$X^2\Sigma^+$	510 ^b	-24.34	-49.85	-47.22	-49.21	-50.23	-50.31	-50.52	-50.67
	RMSD			71.63	77.25	81.44	77.39	74.18	74.08	72.10	72.54
	MSD			51.44	61.29	63.71	62.16	58.92	58.72	55.64	56.78
	MIN			-65.13	-49.85	-47.22	-49.21	-50.23	-50.31	-50.52	-50.67
	MAX			153.52	152.75	161.40	150.43	148.16	147.68	146.35	145.97
Row 2- Row 3	Dimer	State	Expt.	$\Delta(\text{CCSD: UHF})$	$\Delta(\text{CCSD: } \kappa\text{-OOMP2})$	$\Delta(\text{CCSD: OOMP2})$	$\Delta(\text{CCSD: BLYP})$	$\Delta(\text{CCSD: B97M-rV})$	$\Delta(\text{CCSD: B97})$	$\Delta(\text{CCSD: } \omega\text{B97X-V})$	$\Delta(\text{CCSD: } \omega\text{B97M-V})$
	NaO	$X^2\Pi$	526 ^b	-31.86	-30.77	-29.95	-30.34	-30.32	-30.43	-30.74	-30.43
	MgH	$X^2\Sigma^+$	1492.7763 ^a	5.71	5.65	2.85	6.38	5.07	4.69	6.68	4.41
	MgF	$X^2\Sigma^+$	711.69 ^b	8.65	10.70	11.32	11.61	11.24	11.14	10.76	10.96
	AlH ⁺	$X^2\Sigma^+$	1620 ^b	35.64	39.98	49.31	53.80	55.42	53.32	56.24	56.34
	SiH	$X^2\Pi_r$	2042.5229 ^a	3.70	10.43	9.01	8.12	9.23	8.72	5.85	8.80
	SiF	$X^2\Pi_r$	837.32507 ^a	25.35	29.11	30.25	31.16	29.92	29.82	29.22	29.28
	PH	$X^3\Sigma^-$	2363.774 ^a	22.73	20.77	24.52	28.98	25.38	25.99	26.01	25.42
	PH ⁺	$X^2\Pi_r$	2299.6 ^b	111.17	106.73	108.42	110.46	110.30	111.31	109.79	111.25
	PH ⁻	$X^2\Pi_i$	2230 ^b	51.52	53.38	52.00	57.70	55.47	55.64	51.35	55.97
	CP	$X^2\Sigma^+$	1239.79924 ^a	46.65	49.54	65.23	56.05	50.55	50.81	46.51	49.01
	PO	$X^2\Pi_r$	1233.34 ^a	56.82	66.22	71.61	68.09	66.12	65.76	64.09	64.08

PO ⁻	X ³ Σ ⁻	1000 ^b	74.82	82.86	87.48	84.47	82.98	82.61	81.41	81.48
PF	X ³ Σ ⁻	846.75 ^a	11.24	15.47	16.87	17.82	16.23	16.25	15.49	15.46
PF ⁺	X ² Π _r	1053.25 ^b	22.32	31.21	33.88	34.16	32.02	31.73	30.52	30.60
HS	X ³ Π _i	2696.2475 ^a	33.10	35.89	35.10	37.34	34.95	35.14	33.01	34.04
BS	X ² Σ ⁺	1179.91 ^a	31.87	35.92	39.48	39.23	37.17	37.24	34.95	35.84
CS ⁺	X ² Σ ⁺	1384 ^b	50.49	60.63	72.80	65.99	59.11	60.42	56.66	58.66
NS	X ² Π _r	1218.7 ^b	51.77	68.59	78.28	69.90	66.09	65.95	62.92	63.65
SO	X ³ Σ ⁻	1150.7913 ^a	50.36	59.71	64.42	59.59	57.70	57.53	56.15	56.34
SO ⁺	X ² Π _r	1306.778 ^e	87.10	95.50	102.29	95.92	93.69	93.44	91.67	91.58
HCl ⁺	X ² Π _i	2673.69 ^a	51.07	48.92	50.61	50.83	50.09	47.95	50.09	50.43
LiCl ⁻	X ² Σ ⁺	480 ^b	29.43	29.89	29.55	30.19	29.52	29.54	29.86	29.65
BeCl	X ² Σ ⁺	846.7 ^b	1.99	2.41	2.76	3.28	2.99	2.83	2.48	2.63
CCl	X ² Π	876.89749 ^a	5.41	8.46	11.95	12.79	10.97	10.78	8.66	9.10
ClF ⁺	X ² Π	870 ^b	82.04	101.77	109.34	106.86	102.63	102.89	100.22	100.43
NCI	X ³ Σ ⁻	827.95767 ^a	0.17	1.02	5.88	7.27	4.12	4.14	1.93	1.87
OCl	X ² Π _i	853.64268 ^a	8.61	19.08	35.08	25.96	19.09	20.11	15.72	16.02
RMSD			46.34	51.27	55.65	53.93	52.03	52.00	50.70	51.28
MSD			34.37	39.23	43.35	42.36	40.29	40.20	38.80	39.36
MIN			-31.86	-30.77	-29.95	-30.34	-30.32	-30.43	-30.74	-30.43
MAX			111.17	106.73	109.34	110.46	110.30	111.31	109.79	111.25
Row 3-	Dimer	State	Δ(CCSD: UHF)	Δ(CCSD: κ-OOMP2)	Δ(CCSD: OOMP2)	Δ(CCSD: BLYP)	Δ(CCSD: B97M-rV)	Δ(CCSD: B97)	Δ(CCSD: ωB97X-V)	Δ(CCSD: ωB97M-V)
Row 3		Expt.								
MgCl	X ² Σ ⁺	462.12 ^b	5.04	5.14	5.31	5.42	5.30	5.35	5.17	5.23
AlS	X ² Σ ⁺	617.1169 ^a	-19.95	-11.12	-2.64	-7.46	-6.96	-8.69	-12.30	-12.27
Si ₂	X ³ Σ ⁻	510.98 ^a	20.68	21.66	55.58	23.52	22.94	22.99	21.82	21.99
SiCl	X ² Π _r	535.59 ^a	-2.40	-1.99	-1.29	-0.52	-1.07	-1.13	-1.70	-1.57
P ₂ ⁺	X ² Π _u	672.2 ^a	49.78	49.27	106.91	51.80	50.71	50.83	49.06	49.28
PS	X ² Π _r	739.1 ^b	40.49	32.27	36.60	35.72	34.10	34.18	32.45	32.74
S ₂	X ³ Σ ⁻	725.7102 ^a	22.26	24.59	26.94	26.26	25.43	25.24	24.32	24.48
S ₂ ⁺	X ² Π _{g,r}	790 ^b	60.19	61.62	65.35	63.46	62.42	62.37	60.82	61.02
RMSD			33.71	32.59	51.10	34.12	33.32	33.38	32.42	32.57
MSD			22.01	22.68	36.59	24.78	24.11	23.89	22.46	22.61
MIN			-19.95	-11.12	-2.64	-7.46	-6.96	-8.69	-12.30	-12.27
MAX			60.19	61.62	106.91	63.46	62.42	62.37	60.82	61.02
Open-shell	Dimer	State	Δ(CCSD: UHF)	Δ(CCSD: κ-OOMP2)	Δ(CCSD: OOMP2)	Δ(CCSD: BLYP)	Δ(CCSD: B97M-rV)	Δ(CCSD: B97)	Δ(CCSD: ωB97X-V)	Δ(CCSD: ωB97M-V)
		Expt.								
RMSD			56.78	61.44	66.86	62.65	60.23	60.17	58.60	59.06
MSD			39.64	45.96	50.71	48.03	45.67	45.52	43.43	44.18
MIN			-65.13	-49.85	-47.22	-49.21	-50.23	-50.31	-50.52	-50.67
MAX			153.52	152.75	161.40	150.43	148.16	147.68	146.35	145.97

^a From Ref. 349.

^b From Ref. 346.

^d From Ref. 351.

^e From Ref. 352.

* Theoretical results.